



Gordon

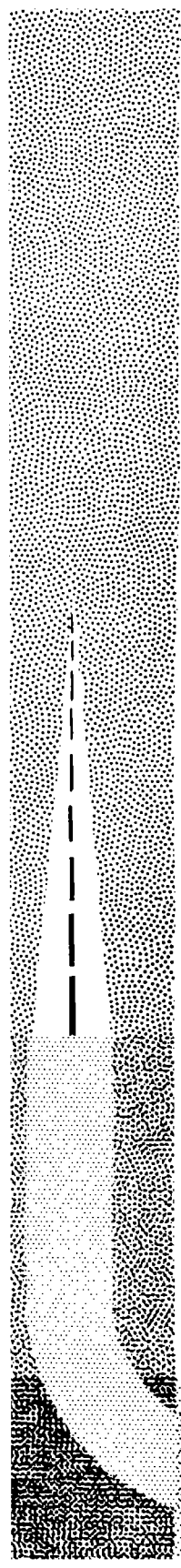
**Seventeenth Annual Conference
on Mass Spectrometry
and Allied Topics**

May 18-23, 1969

Dallas, Texas

Arranged by the Officers of

ASTM Committee E-14



**Seventeenth Annual Conference
on Mass Spectrometry
and Allied Topics**

**May 18-23, 1969
Dallas, Texas**

**Arranged by the Officers of
ASTM Committee E-14**



Preface

This volume is a collection of papers presented at the Seventeenth Annual Conference on Mass Spectrometry and Allied Topics, held in Dallas, Texas, May 18-23, 1969. It is intended that this volume be distributed only to registrants of the conference and, therefore, should not be considered as a publication.

It is suggested that any future references to individual reports be cited in the form: author(s), presented at the Seventeenth Annual Conference on Mass Spectrometry and Allied Topics, Dallas, Texas, May, 1969.

R. E. Honig, Program Chairman

Arranged by the officers of the ASTM Committee E-14

J. L. Franklin, Chairman
R. E. Honig, Vice-Chairman
C. E. Johannsen, Vice-Chairman
J. M. McCrea, Secretary
R. F. Porter, Member-at-Large
J. T. Herron, Member-at-Large

TABLE OF CONTENTS
 SEVENTEENTH ANNUAL CONFERENCE ON MASS SPECTROMETRY
 AND ALLIED TOPICS
 DALLAS, TEXAS, MAY 18-23, 1969

Paper No.		Page No.
SYMPOSIUM ON IONIZATION CROSS SECTIONS		
1.*	Accuracy and Reliability of Property Data or What's My Bag? L. J. Kieffer-----NO MANUSCRIPT RECEIVED	
2.*	Absolute Total Cross Sections for Ionization of Gases by Electron Impact. D. R. Rapp-----NO MANUSCRIPT RECEIVED	
3.*	Measurements of Cross Sections for Multiple Ionization by Electron Impact. J. T. Dowell-----NO MANUSCRIPT RECEIVED	
4.*	Crossed Beam Techniques for Measuring Ionization Cross Sections. G. H. Dunn-----NO MANUSCRIPT RECEIVED	
5.*	Electron Ionization Cross Sections for Hard-to-Vaporize Materials. C. K. Crawford-----	15
<u>DATA ACQUISITION AND PROCESSING</u>		
6.	Computer Controlled Data Acquisition and Isotopic Ratio Measurements in Real Time. C. A. Bailey, R. L. Peterson, P. D. Siemens, and R. J. Dupzyk-----	16
7.	MSYS - A General-Purpose Programming System for Mass Spectrometer Computations. D. R. McAdams-----	19
8.	Mass Spectrometers in a Time Shared Computer Environment. W. E. Reynolds, R. B. Tucker, R. A. Stillman, and J. C. Bridges-----	
9.	The Design of a Time-Shared Data Acquisition System for Quadrupole Mass Spectrometers. P. D. Olson and E. V. W. Zschau-----	20
10.	Use of a Computer as a Mass Marker. W. J. McMurray and S. R. Lipsky-----NO MANUSCRIPT RECEIVED-----	
11.	Development of Program for Plate Reader. M. A. Frisch-----NO MANUSCRIPT RECEIVED	
12.	Processing of Solids Mass Spectrographic Data Via Time-Sharing with Semi-Automatic Data Acquisition. J. R. Woolston and E. M. Botnick-----	25
13.	Computer Processing of Electronically Offset Multiple Exposures on Mass Spectrographic Plates. J. M. Ruth and D. L. Osheim-NO MANUSCRIPT RECEIVED-----	

*Invited Paper

Paper No.		Page No.
14.	A New, Remote On-Line Data Acquisition-Processing System for Low Resolution Combination Gas Chromatograph-Mass Spectrometer. H-Y. Li, J. Walden, R. Saunders, D. Simpson, L. Mills, K. Kinneberg and G. R. Waller-----	26
15.	Performance of a Computer-Coupled, Medium Resolution, Double-focusing Mass Spectrometer System. A. L. Burlingame, D. H. Smith, F. C. Walls, and R. W. Olsen-----	28
16.	Applications of a Small Digital Computer in the Mass Spectrometer Laboratory. R. Venkataraghavan, R. J. Klimowski, J. E. Coutant, and F. W. McLafferty-----	31
17.	Ab Initio Computer Programs for the Interpretation of Mass Spectral Data. J. D. Morrison-----	38
SOLIDS STUDIES		
18.*	Electrical Breakdown in Vacuum. A. S. Denholm-----	44
19.	Measurement of Sensitivity in a Secondary Ion Emission Microanalyser. C. M. Judson and R. K. Lewis-----	46
20.	WITHDRAWN	
21.	Mass Spectrometric Measurement of the Thermal Velocities of Various Species Evolved from Laser-Vaporized Materials. K. A. Lincoln and F. A. Wodley-----	51
22.	Mass Spectrometric Studies of Laser-Induced Vaporization of Solids. V. S. Van and B. E. Knox-----	57
23.	Electronic Configurations and the Spark-Source Mass Spectra of Some Elements. J. M. McCrea-----	58
24.	The Mass Spectrometric Analysis of a Series of Elements as Volatile Iodides. J. E. Delmore, Jr.-----	64
25.	Spark Source Mass Spectrographic Analysis of Smithonia Iron Meteorite. E. Berkey and G. H. Morrison----- NO MANUSCRIPT RECEIVED-----	
26.	On the Absolute Efficiency of Ion Bombardment Sources of Mass Spectrometers. J. M. Schroerer-----	65
METASTABLES		
27.	Experimental and Calculated Consecutive Metastable Peaks in Toluene. L. P. Hills, J. H. Futrell, and A. L. Wahrhaftig-----	71
28.	Energetic Metastable Transitions and Their Applications to the Dissociation Processes and Structural Transformations of Aromatic Molecules Under Electron Impact. P. Nounou-----	74

*Invited Paper

Paper No.		Page No.
29.	Consecutive Metastable Transitions. U. Lohle and Ch. Ottinger-----	80
30.	Metastable Ions in the Mass Spectra of N ₂ , NO, N ₂ O and NO ₂ . A. S. Newton and A. F. Sciamanna-----	83
31.	Structure Information from Metastable Spectra. F. W. McLafferty, D. J. McAdoo, H. D. R. Schuddemage, and J. S. Smith-NO MANUSCRIPT RECEIVED-----	
32.	Fast H(2S) Atoms Produced by Dissociative Excitation of Molecules. R. Clappitt-----	86
33.	Metastable Ion Intensities and Ionic Structure. J., L. Occolowitz-----	88
34.	Energetic Metastable Decompositions. K. C. Smyth and T. W. Shannon-----	89
35.	Structure in Broad Metastable Peaks. S. Jones and K. R. Jennings-----	95
36.	Enhanced Metastable Ion Measurement by Defocused Operation of Double Focusing Mass Spectrometers. A. H. Struck and H. W. Major, Jr.-----	102
	SYMPOSIUM ON COLLISIONS OF ELECTRONICALLY EXCITED ATOMS AND MOLECULES	
37. *	Penning Ionization Electron Spectroscopy. V. Cermak-----NO MANUSCRIPT RECEIVED	
38. *	Chemionization: Theories and Mechanism. R. Stephen Berry-----	107
39. *	Collisions of Fast Metastable Atoms. J. R. Peterson-----	112
40. *	Pulsed Mass Spectrometric Studies of Ionizing Collisions of Excited Atoms. F. W. Lampe-----	114
41. *	Reactions of Long-Lived Neutral Excited States in a Flowing Afterflow. F. C. Fehsenfeld---NO MANUSCRIPT RECEIVED	
	GAS CHROMATOGRAPHY; THERMAL ANALYSIS	
42.	Multiple Ion Detector Technique in Mass Spectrometry, a Device for Specific Analysis of GC-eluates. A. Linnarson----- NO MANUSCRIPT RECEIVED	
43.	An Investigation of the Carbohydrate Components of Glycoproteins Using a Gas Chromatograph-Mass Spectrometer-Computer System. V. N. Reinhold and K. Biemann-----	115
44.	An Improved Sample Enriching System. A. J. Luchte, D. C. Damoth and C. J. Moorman-----NO MANUSCRIPT RECEIVED	
45.	A Porous Stainless Steel Separator System for Gas Chromatography--Mass Spectrometry. P. M. Krueger and J. A. McCloskey-----	120

*Invited Paper

Paper No.		Page No.
46.	A Separator with Variable Conductance for GC/MS Analyses. C. Brunnee, H. J. Bultemann and G. Kappus-----	121
47.	Mass Spectra and Gas Chromatography of the ORMOSIA Alkaloids. K. L. Rinehart, Jr., K. J. Schilling, C. L. Brown and R. H. Heckendorn-----	127
48.	Flash Mass Thermal Analysis: A Method for Studying Pyrolysis of Solid Rocket Propellant Ingredients. W. G. Stapleton-----	128
49.	Mass Thermal Analysis of Hydroxylamine and Methoxyamine Perchlorates. B. B. Goshgarian-----	139
50.	Cyclic Oligomers Produced by Degrading Poly(Ethylene Terephthalate) in the Source of a Mass Spectrometer. J. S. Lewis, J. C. Gilland, Jr., and V. W. Goodlett-----	146
51.	The Use of Partial Pressure Mass Spectrometry in the Thermal Analysis Study of Carbons and Graphites. J. Dollimore, Clive M. Freedman, and B. H. Harrison-----	148
52.	Mass Spectrometric--Differential Thermal Analysis of Some Inorganic and Organic Materials. J. P. Redfern, B. L. Treherne, M. L. Aspinall, and W. A. Wolstenholme-----	158
MOLECULAR BEAMS		
53.*	Molecular Beams from Supersonic Jet Sources. J. B. Fenn-----NO MANUSCRIPT RECEIVED	
54.	Effects of Electric Fields and Sample Expansion on Ion Sampling at High Pressures. R. R. Burke and W. J. Miller-----	163
55.	Mass Spectrometry of Ions from Radio Frequency Plasmas. F. C. Kohout and D. D. Neiswender-----	170
56.	Mass Spectrometric Measurement of the Rates of Fast Association Reactions of Small Inorganic Species. T. P. Fehlner and G. W. Mappes-----	175
57.	The Reactions of Atomic Oxygen with Some Halo-Ethylenes. R. E. Huie, J. T. Herron and D. Davis-----	176
58.	Mass Spectrometric Studies of the Thermodynamics and Kinetics of Formation of Water Clusters. F. T. Green, A. E. Vandegrift, and T. A. Milne-----	177
59.	Molecular Beam Studies of the Temperature Dependence of n-Butane Fragmentation. T. A. Milne, J. Beachey and F. T. Greene-----	180
60.	The Ionization Properties of Water Clusters. J. Beachey, F. T. Green, and T. A. Milne-----	183

*Invited Paper

IONIZATION STUDIES; NEGATIVE IONS

61.	Monoenergetic Electron Impact Studies of Some Atoms and Small Molecules. C. E. Brion, L. A. R. Olsen and G. E. Thomas-	189
62.	Second Differential Ionization and Threshold Laws for Ionization by Electrons. B. G. Giessner and G. G. Meisels-----	190
63.	Total and Individual Cross Sections for the Production of Free Radicals, Positive Ions and Negative Ions from Water Vapor by 100eV Electrons. C. E. Melton-----	194
64.	Experimental Relative Electron Impact Ionization Cross Sections for Group III Metal Atoms and Comparison with Theories. K. A. Gingerich and G. D. Blue--NO MANUSCRIPT RECEIVED---	
65.	Relative Electron Impact Ionization Cross Section of Copper and Gold, and the Velocity of Evaporated Atoms. D. H. Gunduz, J. M. Schroeer, and S. Livingston-----	196
66.	Electron Impact Ionization Cross Sections by a Double Crossed Beam Technique. L. H. Rovner and J. H. Norman-----	201
67.	Negative Ion Mass Spectra of Some Cobalt and Manganese Carbonyl Derivatives. F. E. Saalfeld and M. V. McDowell-----	203
68.	Translational Energies of Some Negative Ions. A. L. Yergey and J. L. Franklin-----	204
69.	Negative Ions in Nitrous Oxide. F. Dale and J. F. Paulson-----	206
70.	Determination of Gas Phase Acidities from Negative Ion Impact Experiments. T. O. Tiernan and B. M. Hughes-----	208
71.	Negative Ion Processes in Nitrogen Dioxide. B. M. Hughes and T. O. Tiernan-----	212
SYMPOSIUM ON THERMAL ANALYSIS		
72.*	High-Temperature Gaseous Oxides, Halides and Oxyhalides. D. W. Muenow and J. L. Margrave-----	217
73.*	MTA--A Combination of Old Techniques or a New Method? H. G. Langer-----	219
74.*	The Application of Mass Spectrometric Thermal Analysis to Pyrolysis of Aliphatic Polyesters. H. L. Friedman-----NO MANUSCRIPT RECEIVED	
75.*	Advances in Simultaneous Thermogravimetric--Mass Spectrometric Measurements. H. P. Vaughan-----	223
76.*	Thermogravimetric--Mass Spectrometric Analysis. W. F. Haddon, A. H. DiEdwardo, and F. Zitomer-----NO MANUSCRIPT RECEIVED	

*Invited Paper

77.*	Thermal Degradation of Polymers using TGA-VPC-MS. A. H. DiEdwardo and F. Zitomer-----NO MANUSCRIPT RECEIVED-----	
	INSTRUMENTATION <i>DEFIN</i>	
78.	The Influence of Segmented Rods and Their Alignment on the Performance of a Quadrupole Mass Filter. W. Arnold-----	235 <i>JP</i>
79.	Operation of Quadrupole Mass Spectrometer at High Pressure. W. M. Brubaker and W. S. Chamberlin-----	243 <i>JP</i>
80.	A Mobile Quadrupole Mass Spectrometer System for Medical Applications. M. Mosharrafa, D. Witsoe, R. Patterson, and W. G. Kubicek-----NO MANUSCRIPT RECEIVED	<i>JP</i>
81.	A New Mass Spectrometer for Measurements of Very Small Isotopic Differences Between Two Uranium Samples. G. Nief, M. Lucas, and R. Bir-----	245
82.	WITHDRAWN	
83.	An Electronic Detection System Utilizing Integration Techniques for a Spark Source Mass Spectrometer. A. J. Socha, C. W. Baker, and E. M. Masumoto-----	251
84.	The Study of a Master Emulsion-Calibration Curve for Quantitative Spark Source Mass Spectrometric Analysis. Ping-Kay Hon-----	256
85.	Routine Analysis Using a Spark Source Mass Spectro- graph with Electrical Detection. C. A. Evans, R. J. Guidoboni and F. D. Leipziger-----	257
86.	Spark Source Mass Spectrometry Using "Autospark" Sample Control and On-Line Data Processing. R. A. Bingham, P. Powers, and W. A. Wolstenholme-----	261
87.	Multiple Specimen Holder for the Spark Source Mass Spectrometer. L. A. Ferguson, I. D. Dowdy, and E. D. Pierron-----	268
	PHOTOIONIZATION	
88.	Photoionization Yields and Cross-Sections of H ₂ O and D ₂ O. R. E. Huffman, D. H. Katayama, and C. L. O'Bryan-----	269
89.	A Study of Some Reactions of H ₂ ⁺ in Selected Vibrational States. W. A. Chupka, J. Berkowitz, and M. E. Russell-----	270
90.	Recent Experiments in Photoelectron Spectroscopy. G. R. Branton, D. C. Frost, T. Makita, C. A. McDowell, and I. Stenhouse-----	273
91.	The Energetics of Dissociative Photoionization. P. H. Doolittle and R. Schoen-NO MANUSCRIPT RECEIVED-----	

*Invited Paper

Paper No.		Page No.
92.	Photoionization of Cesium Halides: Chemical Shift of Autoionization. J. Berkowitz-----	274
93.	Chemical Ionization Mass Spectrometry Using a Modified Source with the MS-9. H. M. Fales, G. W. A. Milne and M. Vestal---	275
94.	Photoionization and Dissociation of Fluorine. V. H. Dibeler, J. A. Walker and K. E. McCulloh-----	276
95.	Mass Spectrometric Study of the Photoionization of Nitrogen Trifluoride and Trifluoramine Oxide. V. H. Dibeler and J. A. Walker-----	277
HIGH TEMPERATURE STUDIES		
96.	Thermochemistry with the Positive-Negative Ion Mass Spectrometer. H. J. Svec and G. D. Flesch-NO MANUSCRIPT RECEIVED-----	
97.	Molecular Beam Studies Using a Quadrupole Mass Spectrometer. T. C. Ehlert-----	281
98.	Stability of Gaseous Molecules in the As-P-System. G. D. Blue and K. A. Gingerich-NO MANUSCRIPT RECEIVED--	
99.	The Dissociation Energy and Ionization Potential of Silicon Monoxide. D. L. Hildenbrand and E. Murad-----	283
100.	Dissociation Energies of the Group IIA Metal Chlorides from Equilibrium and Electron Impact Measurements. D. L. Hildenbrand-----	284
101.	High Density Effects Associated with Pulse Vaporization in a Time-of-Flight Mass Spectrometer. Richard T. Meyer-----	286
102.	A Mass Spectrometric Study of the Positive and Negative Ions from Carbon Vapors. C. H. Williams-----	289
103.	A Mass Spectrometric Study of High Temperature Species in the W-O-I System. S. K. Gupta-----	291
SYMPOSIUM ON GEO- AND COSMO-APPLICATIONS I		
104.*	Mass Spectroscopy in Geo-and Cosmo-Chemistry-- and Overview. L. F. Herzog-----NO MANUSCRIPT RECEIVED	
105.*	Spark Source Mass Spectrometric Analysis of the Lunar Sample. G. H. Morrison and A. T. Kashuba-----	292
106.	Meteorite Dating with the Inert Gases. D. Heymann-----	293
107.*	Mass Spectrometry in Space Research (European Rocket Program). J. Zahringer-----NO MANUSCRIPT RECEIVED	

*Invited Paper

Paper No.		Page No.
108.*	Studies of the Composition of the Ionosphere with a Satellite-Mounted Mass Spectrometer. J. H. Hoffman-----	304
109.*	Isotopic Analysis of Lithium in Some Chondritic Meteorites and in Terrestrial Samples with a Sputtering Mass Spectrometer. E. Gradsztajan-----NO MANUSCRIPT RECEIVED	
HIGH RESOLUTION STUDIES		
110.	Precise Mass Determinations from High Resolution Spark Source Mass Spectra of Organic Substances. K. H. Maurer, C. Brunee and K. Habfast-----	310
111.	Highly Accurate Mass Measurement of Substances Having m/e Over 1000 by High Resolution Mattauch-Herzog Type Mass Spectrometer. E. Watanabe, M. Naito, M. Shino and Y. Itagaki NO MANUSCRIPT RECEIVED-----	
112.	Determination of Organic Contaminants in Air and Water by High-Resolution Mass Spectrometry. A. G. Sharkey, Jr., J. L. Shultz, T. Kessler, and R. A. Friedel-----	320
113.	On-Line Computer Analysis of High Resolution Mass Spectra: Mass Spectrometry of Medium Chain Length Compounds. S. R. Shrader, and A. M. Chalmers-----	323
114.	The Analysis of Some Mixtures Using Ultra High Resolution and Field Ionization Techniques. S. Evans, T. R. Kemp and W. A. Wolstenholme----	326
115.	Pyrolysis of Natural Products. IV. Identification of Products from Nucleotide Pyrolysis by Higher Resolution Mass Spectrometry. H. G. Boettger and A. M. Kelly-----	333
116.	Computer Analysis of High Resolution Mass Spectra IV. The Influence of Peak Model Parameters Upon Mass Measurement Accuracy and Multiplet Recognition. H. G. Boettger and A. M. Kelly-----	337
117.	WITHDRAWN	
118.	Analysis of Trimethylsilyl Derivatives of Carbohydrates by Mass Spectrometry. D. C. DeJongh and J. D. Hribar-----	342
119.	Mass Spectra of Polysubstituted Macrocyclic Lactones Derived from Macrolide Antibiotics. R. L. Foltz, L. A. Mitscher and M.I. Levenberg---	343
120.	Mass Spectrometry of the Branched-Cyclic Hydrocarbon Fraction of Green River Shale. E. J. Gallegos-----NO MANUSCRIPT RECEIVED	
SYMPOSIUM ON GEO- AND COSMO- APPLICATIONS II		
121.*	Contributions of Isotope Studies of Radiogenic Pb, Sr and Ar to the Understanding of Early History and Planetary Evolution. W. H. Pinson, Jr.--NO MANUSCRIPT RECEIVED	
122.*	Direct Dating of Fossil Carbonates by the Helium- Uranium Method. O. A. Schaeffer-----NO MANUSCRIPT RECEIVED	

*Invited Paper

123. *	High Precision Isotope Ratio Measurements Using a Programmable Magnetic Field, Thermionic Source Mass Spectrometer with On-Line Data Processing. G. J. Wasserburg---NO MANUSCRIPT RECEIVED	
124. *	Uses of C^{13}/C^{12} Ratios in Biological and Biogeochemical Research. P. L. Parker-----	349
125. *	Comparative Mass Spectrometric Studies on the Isoprenoids and Other Isomeric Alkanes in Terrestrial and Extraterrestrial Samples. E. Gelpi and J. Oro-----	350
126. *	Some Systematic Trends in C^{13} and O^{18} Concentration Variations in a Carbonatite. P. Deines-----	362
127. *	Isotope Ratio Mass Spectrometry at Phillips Petroleum Company. T. D. Morgan and R. S. Scanlan-----	371
CHEMICAL IONIZATION; ION MOLECULE REACTIONS I		
128.	Chemical Ionization Mass Spectrometry. IX. Temperature and Pressure Studies with Benzyl Acetate and t-Amyl Acetate. F. H. Field-----NO MANUSCRIPT RECEIVED	
129.	Chemical Ionization Mass Spectrometry of Bio-Organic Compounds. G. P. Arsenault-----	372
130.	Studies in Chemical Ionization Mass Spectrometry. J. Michnowicz, D. Schoengold, and B. Munson---	375
131.	Crossed Beam Study of the Ion-Molecule Reaction $N^+ + O_2 = NO^+ + O$. Z. Herman, J. C. Tully and R. Wolfgang-----	379
132.	Ion-Molecule Reactions in Methane-Ammonia Mixtures. W. T. Huntress, Jr., and D. D. Elleman-----	380
133.	Kinetic Analysis of Concurrent Ion-Molecule Reaction Systems Using Ion Ejection--Ion Cyclotron Resonance Techniques. M. T. Bowers and D. D. Elleman-----	381
134.	The Reactions of O_2^+ with Simple Alkanes and Ethylene. D. K. Bohme, R. A. Vane, F. C. Fehsenfeld, and E. E. Ferguson-----	383
135.	Ion-Cyclotron Resonance Study of the Kinetic Energy Dependence of Ion-Molecule Reaction Rates. R. P. Clow and J. H. Futrell-----	394
ORGANIC SPECTRA I		
136.	Compound Identification by Computer Matching of Mass Spectra. B. Knock, D. Wright, W. Kelly, and R. G. Ridley-----	398
137.	A Detailed Stereochemical Analysis of Electron Impact Induced 1, 3 Elimination in Cyclohexanol and Cyclohexyl Chloride. M. M. Green and R. J. Cook-----	402

*Invited Paper

Paper No.		Page No.
138.	Mass Spectra of Substituted Aromatic Anhydrides: Evidence for Reactions from Different Electronic States. N. Garcia and R. C. Dougherty-NO MANUSCRIPT RECEIVED-----	
139.	Naive Analysis of the Structure of Alkanes. R. I. Reed and D. H. Robertson-NO MANUSCRIPT RECEIVED-----	
140.	Mass Spectra of Some Organotin and Organosilicons. I. Lengyel, M. J. Aaronson and J. P. Dillon-----	403
141.	Stereoisomeric Effects on Mass Spectra. II. The Isomeric Methyldecalins. S. Meyerson and A. W. Weitkamp-----	406
142.	The (M-15) ⁺ Peak in the Mass Spectrum of Benzene. M. A. Baldwin, D. P. Craig and A. Maccoll----	407
143.	Carbon Skeletal Rearrangement of Butene-1 Ion. G. G. Meisels, J. Y. Park, and B. G. Giessner--	411
144.	Mass Spectral Studies of t-Butyl (Deuterated) Thiophenes. R. G. Fowler, N. G. Foster, and R. W. Higgins NO MANUSCRIPT RECEIVED-----	
145.	WITHDRAWN	
146.	WITHDRAWN	
ION MOLECULE REACTION II		
147.	Bimolecular Reactions of Ions Trapped in an Electron Space Charge. A. G. Harrison and A. A. Herod-----	414
148.	Identification of C ₂ H ₅ O ⁺ Structural Isomers by Ion Cyclotron Resonance Spectroscopy. J. L. Beachamp----NO MANUSCRIPT RECEIVED	
149.	Gas Phase Hydrations Studies of the Positive Alkali Ions and the Negative Halide Ions. S. K. Searles, I. Dzidic, M. Arshadi, R. Yamdagni and P. Kebarle-NO MANUSCRIPT RECEIVED-----	
150.	Mechanism and Rate Constants for the Thermal Ion Molecule Reactions Occurring in Oxygen which Contains Small Concentrations of Water Vapour. A. Good, D. A. Durden and P. Kebarle-----NO MANUSCRIPT RECEIVED-----	
151.	Time-of-Flight Analysis in Ion-Neutral Reactions. J. F. Paulson, S. A. Studniarz and F. Dale-- NO MANUSCRIPT RECEIVED-----	
152.	Mass Spectrometric Determination of the Proton Affinities of Various Molecules. M. A. Haney and J. L. Franklin-----	416
153.	Ion-Neutral Reactions in Carbon Dioxide. S. M. Schilderout and J. L. Franklin-----	419

Paper No.		Page No.
154.	Higher Ordeal Ion-Molecule Reactions II. Energy Dependency of Intermediate Complex Lifetimes. H. F. Tibbals and G. G. Meisels-----	421
155.	High-Resolution Chemical Ionization Mass Spectroscopy. L. Wojcik and J. H. Futrell-----	425
156.	Collision-Induced Dissociation of NO Ions at Low Kinetic Energies. R. E. Marcotte and T. O. Tiernan-----	426
157.	Ion-Polar Molecule Reactions: Energy Dependency of Hydrogen Atom and Ion Transfer in the Methanol-Acetaldehyde System. L. J. Leger, G. G. Meisels, and T. O. Tiernan--	431
ORGANIC SPECTRA II		
158.	Interaction of Functional Groups--The Loss of CH ₃ NO from o-Aminobenzophenones. W. Benz-----NO MANUSCRIPT RECEIVED	
159.	Fragmentation of Some Even-Electron Nitroaromatic Ions: The Question of the Nitrotropylium Ion. R. H. Shapiro and J. W. Serum-----	436
160.	Loss of Small and Large Radicals from Acetals and Ketones. R. G. Cooks, A. N. H. Yeo and D. H. Williams---	439
161.	Studies of the Mechanism of Decomposition of Acetophenone Azine Induced by Electron Impact. S. E. Scheppele R. D. Grigsby, D. Whitaker, S. Hinds and K. Kinneber-----NO MANUSCRIPT RECEIVED-----	
162.	Fragmentation Processes in the Mass Spectra of the Benzo (b) Thienylthiaalkanes. N. G. Foster, J. Pei-min Liao and R. W. Higgins--	441
163.	Mass Spectrometric Investigation of Substituted Diarylmethanes. W. M. Scott, M. E. Wacks, J. D. Fitzpatrick, and C. Steelink-----	442
164.	Elimination of Small Neutral Molecules in the Ionization-Dissociation of Salicylic Acid and Its Esters. C. D. Eskelson, J. C. Towne, C. Cazez, M. E. Wacks and W. M. Scott-----	445
165.	The Mass Spectra of Some Halogenated Phenols and Naphthols. T. L. Folk-----	447
166.	Quantitative Analysis of Triglyceride Mixtures by Mass Spectrometry. R. A. Hites-----	448
167.	Carbon-Heteroatom Bond Cleavage in the Fragmentation of n-Acetylpyrrolidine and Homologs. W. J. Ritcher, J. N. Tesarek and A. L. Burlingame-----	451
168.	Intramolecular Hydrogen Rearrangement in Molecular Ions Prior to Field Ionization. P. Schulze, W. J. Richter and A. L. Burlingame--	454

THEORY; THERMAL IONIZATION; FIELD IONIZATION		
169.	Mechanistic Studies in the Fragmentation of Substituted Benzyl Compounds. P. Brown-----	457
170.	Franck-Condon Factors for the Ionization of Nitrous Oxide. H. M. Rosenstock-----	458
171.	Peak Height Distribution of Organic Mass Spectra. S. L. Grotch-----	459
172.	Variations in U ²³⁴ Concentration of Natural Uranium. R. F. Smith and J. M. Jackson-----	467
173.	Mass Spectrometric Determinations of 2200 m/s Neutron Cross Sections of Fissile Nuclides. M. Lounsbury, R. W. Durham, and G. C. Hanna-----	468
174.	A Diffusion-Thermal Ionization Source for the Assay of Trace Metals. W. G. Meyers and F. A. White-----	470
175.	The Observation of UH ⁺ and PuH ⁺ Produced During the Thermal Ionization of Uranium and Plutonium. P. E. Moreland, Jr., D. J. Rokop, and C. M. Stevens-----	474
176.	Field Ionization Mass Spectrometry--Fragmentation and Mestables. E. M. Chait-----	475
177.	Electron Microscopic Study of the Surfaces of Wires Used in Field Ionization Mass Spectrometry. J. C. Tou, L. B. Westover and E. J. Sutton-----	478

ELECTRON IONIZATION CROSS SECTIONS FOR HARD TO VAPORIZE MATERIALS

C. K. Crawford

Massachusetts Institute of Technology

The accurate measurement of low energy electron ionization cross sections for low vapor pressure materials presents unusual experimental difficulties. In order to obtain neutral target particles, the use of a crossed beam geometry seems forced; a neutral beam is normally generated by vaporization of sample material under Knudsen or Langmuir conditions. Three serious problems arise: the identification of the chemical species actually present in the beam, the calibration of neutral beam flux density (including the flux of each species), and the identification of the specific reactions in the collision region which result in the ion species observed. Even pure elements frequently vaporize in a number of polyatomic species, and fragmentation commonly occurs (often with high fragment kinetic energies).

A comparison is made herein between the relative advantages of several techniques proposed by various groups to circumvent these difficulties. Included are simple methods such as Knudsen cell weight loss measurements (coupled with thermodynamic arguments), beam trap weight gain measurements, and more complicated methods such as the multiple crossed beam technique. A new (completely untried) exponential depletion method, which can measure cross sections without any knowledge of neutral flux density, is discussed.

The simpler techniques do not appear capable of providing adequate data. In using the more involved procedures however, the spectre of unexpected (and undetected) systematic errors is cause for serious concern.

COMPUTER CONTROLLED DATA ACQUISITION AND ISOTOPIC
RATIO MEASUREMENTS IN REAL TIME*

C. A. Bailey, R. L. Peterson, P. D. Siemens,
and R. J. Dupzyk

Lawrence Radiation Laboratory, University of California
Livermore, California

June 6, 1969

ABSTRACT

A computer program has been written on a 4K PDP-8 for on-line data acquisition from a multistage mass spectrometer. This system includes real time data acquisition, display, and data reduction. Data are obtained by pulse counting techniques (20 nano-second double pulse resolution) with the computer providing multisumming scaling over 256 channels.

A keyboard monitor provides the operator with complete control of the system. By typing control characters on the teletype various operations occur, such as: calling for real time data acquisition; storage of data on DECTape (magnetic tape); real time data display (log or linear); finding peaks in the spectrum; calculating atom ratios; or printing data on the teletype. By using program interrupt techniques several of these operations appear to go on at the same time.

*This work was performed under the auspices of the U. S. Atomic Energy Commission.

COMPUTER CONTROLLED DATA ACQUISITION AND ISOTOPIC
RATIO MEASUREMENTS IN REAL TIME

C. A. Bailey, R. L. Peterson, P. D. Siemens,
and R. J. Dupzyk

A computer controlled data acquisition and isotopic ratio measurement system has been developed by four people. Mr. Dupzyk was responsible for the overall design of the system, Mr. Peterson was responsible for the pulse counting and magnet sweep interfaces, Mr. Siemens was responsible for the data acquisition program, and Mrs. Bailey was responsible for the data reduction program.

At the heart of the system called MS-XL, which is a multistage, surface ionization mass spectrometer with electron multiplier detection in conjunction with pulse counting, lies a 4K PDP-8 computer. This small computer acts as a middle man between the Mass Spectrometer and its operator.

In designing the system the following important features were included:

- 1) The operator has complete control of the system, that is, he is able to start or stop any operation of his choice when he chooses.
- 2) If an error is made while typing an instruction, the system is able to recover from it without loss of time or information.
- 3) All commands are given over the teletype, with the exception of initial start up, so that an operator with little or no computer experience can operate the system.

For these reasons the entire system was written using the computer's interrupt service. This service gives the illusion that several operations occur at the same time.

In this system the magnetic field is swept over several hundred gauss. Just how fast the field is swept is under hardwire control and is interfaced to the computer. Each sweep is divided into 128 equal time segments or channels. A sweep is defined as the passing of the magnetic field from low gauss to high gauss. A free running clock in the computer is able to count to 4096 in equal time segments, thus allowing 32 clock counts per channel. Every 32nd clock count causes an interrupt signalling the computer that there is data for a channel in the pulse scaler to be transferred to the computer. When the clock interrupts the computer the pulse scaler is gated off until the data has been transferred to a temporary buffer. The scaler is then cleared and gated on to continue accumulating data. The data transfer time is less than 400 nanoseconds. Pulses are counted with a 20 nanosecond pulse resolution in a 12 bit scaler.

At any time the operator is free to do several things with the information stored in the temporary buffer.

He can -

- 1) cause the data to be stored in a single precision buffer and displayed on a scope as real time data. The operator can see what is occurring in each channel as the data are collected.
- 2) or cause the data to be added to a double precision buffer, channel by channel, to give what is called multi-summing-scaling. In using this technique data for the incoming channel are added to the previous data for that given channel giving an enhancement of signal to noise. Signal enhancement is proportional to the square

root of the number of sweeps.

Either of these operations can be displayed on a scope as a linear display with scaling available or as a logarithmic display with decade lines making it possible to estimate the number of counts in the peaks.

After the data have been collected, via the multi-summing-scaling technique, they are stored on dectape and the data reduction code is brought into core.

The following ideas were used in reducing the data.

- 1) A simple smoothing technique of a running sum is applied to the data.
- 2) The first and last $1/2$ mass unit of the spectrum are ignored when searching for peak heights. This blocks out tails from adjacent peaks not desired in the analysis.
- 3) Peak heights are found by searching the spectral array for the largest number which represents a peak.
- 4) Backgrounds are found by searching for the lowest number up to $3/4$ of a mass unit from the peak height on either side of the peak. They are averaged together and subtracted from the peak height to give a net count for the peak, which is then used to calculate the atom ratios.
- 5) When the peaks are found they are displayed upside down so the operator can observe where the backgrounds were taken.
- 6) An unweighted average of the atom ratios from any number of spectra can be calculated. Errors are calculated as one standard deviation assuming a Poisson distribution.

The interrupt service in this program has given the operator much more versatility in running his samples and collecting his information.

MSYS - A GENERAL-PURPOSE PROGRAMMING SYSTEM
FOR MASS-SPECTROMETER COMPUTATIONS

7

D. R. McAdams
Esso Research Laboratories
P. O. Box 2226
Baton Rouge, Louisiana 70821

The mass spectrometrists defines his computing procedures with versatile codes which control over forty mathematical, data input-output, logical, and library subroutines.

Applications have been spectral purification, multi-matrix assemblies, simple composition solutions, and complex compound-type analyses using custom assembled matrices.

Addition of other subroutines is readily allowed, but 1 1/2 years of use have shown few such needs. A desired computing plan may involve multiple use of each sub-routine regardless of sequence. The plan or "definition" is converted to a compact numerical map, named, filed for later use, or used immediately for a sequence of similar problems.

Established maps may be interrupted at any desired points in use for inclusion of additional computation steps. Temporary variations are convenient because neither language compiling nor core load building are ever required.

The system operates in "non-process" mode with 20K of 1800 core in the presence of process or on-line programs. The disk-file indices permit use of the entire library space for spectra, matrices, and maps without pre-designated boundaries.

Preparation of computing schemes usually requires less than one-fourth the time for conventional general languages. The system is available in simple Fortran.

THE DESIGN OF A TIME-SHARED DATA ACQUISITION
SYSTEM FOR QUADRUPOLE MASS SPECTROMETERS

by
Peter D. Olson
Edwin V.W. Zschau
Decision/Analysis Corporation
Palo Alto, California

Introduction

The advantages of a computer system for the acquisition and analysis of data from a mass spectrometer are well recognized, but the selection of the appropriate computer for such systems poses a dilemma. On one hand, economic considerations usually dictate that a computer dedicated to a mass spectrometer should be a small, low-priced one, but on the other hand, a small computer may not have the computational power to perform data analysis and machine interpretation of mass spectra using techniques that are currently being developed.¹

Ideally, a laboratory would like to get exactly the computing power it needs—where it needs it and when it needs it. In general, these requirements are (1) a minimal amount of computing power during the real-time data acquisition process, (2) the power of a small computer for data editing, data reduction, and presentation of results, and (3) the power of a medium or perhaps even large-scale computer system for sophisticated elucidation and interpretation of the spectra.

The problem of getting the right amount of computational power to the right place when it's needed has been solved in several application areas by a time-sharing approach. Using a time-sharing approach, a single computer system is used "simultaneously" by several users who are connected to it through telecommunications equipment and ordinary telephone lines. Since it could distribute the proper amount of computing power to many users—each user being charged for the amount of time he uses—we suggest that a commercial time-sharing system might be an economically efficient answer to the dilemma of computer selection for mass spectrometry.

Obviously, the question of whether or not a time-sharing approach is superior to a dedicated computer approach can't be answered by general, abstract arguments. Rather, specific designs for each approach must be compared along technical and economic dimensions. The purpose of this paper is to outline the design of a time-shared system for quadrupole mass spectrometers which we are currently evaluating in comparison to dedicated systems for such instruments. This paper should also acquaint you with a few of the important considerations used in designing real-time data acquisition systems for operation over regular telephone lines.

Computerized Data Acquisition Approaches

When you talk about applying a time-sharing approach to mass spectrometry you have to distinguish between two types of jobs that the computer can do: (1) Data Acquisition and reduction, and (2) Spectral data analysis, interpretation, and presentation. To make the distinction more precise, let's say that the first job is complete when the peak height for each integral mass unit² scanned is recorded and ready for presentation or further analysis. The second job consists of processing that spectral data.

This distinction is important because the second job can be done with current

time-sharing systems; it's just a regular data processing job requiring no new computer technology. However, to do the data acquisition job on a time-shared basis over ordinary telephone lines, new developments are required. This is because data acquisition is a real-time process. Whereas delays, perhaps even several seconds long, can easily be tolerated when the computer is analyzing and interpreting your spectral data or when it's presenting your results, such delays during data acquisition would either slow down the scan of the mass spectrometer or cause the system to lose some of the measurements that the spectrometer had made.

There are two approaches to computerizing the acquisition of data from a quadrupole mass spectrometer: data logging and computer control. Using the data logging approach, the mass spectrometer operates normally using the range of mass units and scan speed selected by the operator on the manual controls of the instrument. The computer system samples the ion intensities as they are generated at a rate specified to the computer by the operator. Next, these analog signals are converted to digital representations and those above a pre-set noise threshold are sent into the computer and stored. After the scan is complete, the computer retrieves the data points that have been stored, locates the peak centers, and stores the mass vs. intensity data for further analysis or presentation. Of course, with sufficient computing power, it is possible to do some or all of this peak identification "on the fly" as the data are being generated.

The computer control approach to data acquisition can be used with RF mass spectrometers only. Using it, the computer controls the operation of the mass spectrometer as well as recording the data from it. The user inputs to the computer what mass points he wants scanned and how long to integrate the ion intensity at each mass point. During a scan, the computer—based on the results of a previous calibration run—calculates the proper control voltage which when applied to the mass spectrometer (e.g. to the rods of the quadrupole) will allow ions at each desired mass point to be collected. These voltages in digital form are transmitted to a digital-to-analog converter which outputs the analog voltage to be applied to the mass spectrometer. At each mass setting, the ion intensity is integrated for the user-specified time, and the result is converted to a digital representation, sent to the computer, and stored. Since measurements are taken only at desired mass points, these data constitute the mass spectrum in digital form.

Because of the flexibility it gives the chemist in the ranges of the scan and the integration times he selects, we chose the computer control approach as the basis for our time-sharing system design.

Time-Sharing System Design

Our time-sharing system design consists of four components, illustrated in Fig. 1.

- (a) Interface Units
- (b) Communications Terminals
- (c) A Real-Time Data Acquisition Computer
- (d) A Central Time-Sharing Computer

Each of these components will be described below.

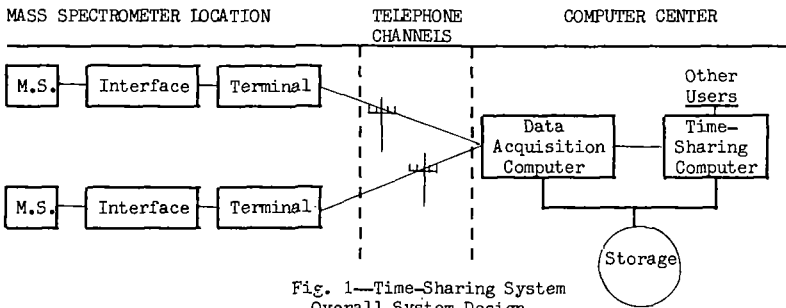


Fig. 1—Time-Sharing System
Overall System Design

Interface Units Design

To operate in a time-sharing system, the computer/mass spectrometer interface must contain its own timing and control circuitry to operate asynchronously from the computer on a request/response basis. For every digital voltage level and integration time input to the interface, the interface returns a digital representation of the ion intensity measured at that mass point for that time. Our design also includes the circuitry to automatically set the integration time as a function of the signal strength. The weaker the signal, the longer the integration time, so that weak signals, such as in the high mass ranges, are magnified while strong signals are recorded as they are produced.

Here's how the automatic integration time adjustment works. The operator specifies five parameters that are stored in registers in the interface.

- (a) A noise threshold level, N
- (b) A signal threshold level, S
- (c) A base integration time, T
- (d) An initial repeats number, R_1
- (e) A maximum repeats number, R_m

After the mass filter control voltage has been set, the interface begins integrating the ion current. It integrates the signal R_1 times for T seconds per integration; the integrator is not reset between integrations. After the R_1 integrations, the integrator is sampled, and the result is converted to a digital representation and compared to N . If it's below N , it's assumed to be noise; the ion intensity at that point is assumed to be zero. If it's above N but below S , the integrator is sampled T seconds again to see if the total signal is up to S yet. Integrations of T seconds duration are repeated (without resetting the integrator) until the signal reaches S or until the total number of repeats reaches R_m . Then the total signal level and the number of integration repeats are transmitted to the computer where they can be converted to a normalized signal for a standard integration time.

The effect of this automatic integration time adjusting mechanism is to produce spectral data with a nearly constant signal-to-noise ratio of about S/N . This is because the signal levels are nearly always up to S and the noise levels are nearly always below N .

Communications Terminal Design

The interface described above was designed to work directly with a computer in either a dedicated or a time-sharing mode. However, if it is to communicate with that computer over telephone lines, a communications terminal is needed to control the data flows, assemble received data inputs, and prepare data outputs for transmission.

Many of these tasks are standard in telecommunications equipment and will not be treated here. We'll discuss only the unique features of our communications terminal design.

If mass spectrometry data acquisition is to be done successfully over telephone lines, the telecommunications design must overcome the limitations on the sampling rate stemming from two sources: (a) the channel capacity of about 4800 baud and (b) the time required to prepare (synchronize) the sending and receiving modems for a data transmission.

Ignoring the effect of the channel capacity for a moment, let's look at the impact of the synchronization time on the sampling rate. Since the line preparation time is 8 milliseconds per transmission and since the interface, as designed, requires a minimum of 3.3 milliseconds per sample, the total time requirement per sample (ignoring the transmission time) using a standard request/response approach would be 19.3 milliseconds; 8 milliseconds to send the voltage, 3.3 milliseconds to sample, and 8 milliseconds to send the result back. Since this implies a maximum sampling rate of only about 50 samples per second, such a system would be too slow for many applications.

Our design solves the data rate problems from both sources by employing two concepts: (a) Two continuous-flow channels using "dummy" data words and (b) an input buffer in the communications terminal using the computer at the other end to monitor and regulate the data flow.

The dual line, continuous flow channel concept is based on the fact that once data transmission is initiated it can continue at the channel capacity without requiring another 8 milliseconds set-up. Our terminal design uses two telephone channels simultaneously; one for data flows out to the interface and the other for data flows back to the computer. Once the data flow begins, it is maintained by sending "dummy" data words whenever real data is not ready to send. The communications terminal generates these "dummy" data words for transmission back to the computer and the computer generates them for transmission to the interface. The "dummy" words are recognized at each end by the presence of a particular code bit and are ignored; only the real data is actually stored and used by the interface or the computer.

Although the dual line, continuous flow channel eliminates the channel preparation delays, the delays due to telephone channel capacities and data transmission times can still be significant. For instance, let's suppose that the system were designed such that after sending out to the interface a control voltage datum, the computer would wait for the ion intensity data at that mass to be sent back before sending out the next voltage level. The time requirement per sample would be as much as 15.6 milliseconds which would mean a maximum sampling rate of 64 samples per second.

Here's how this time per sample is calculated. The voltage level datum going out to the interface is represented by a 16-bit word, a 15-bit voltage level, and 1 control bit. This word, assuming a 4800 baud channel, requires 3.3 milliseconds to transmit. Adding these times to a "worst case" line delay of 2 milliseconds yields a total of 5.3 milliseconds to get the data word from the computer to the interface.

The same process is repeated for the intensity data that's sent back. A 24-bit data word is used, 12 bits for the intensity reading and 12 bits for the number of integration repeats. This requires 5 milliseconds to transmit which added to a 2 millisecond line delay is 7 milliseconds. Finally, taking the 3.3 millisecond

sampling time into account yields the 15.6 millisecond per sample figure.

By adding an input buffer to the communications terminal and by using the computer to monitor the number of data words in that buffer, all these transmission delays can be avoided once the scan is started. The idea is always to have stored in the buffer the next voltage level data word for the interface to use as soon as it's ready. The computer knows how many data words are "in the system" at any time—that's the difference between how many voltage data it sent out and how many intensity data it has received. Because of the transmission delays in both directions, the buffer must be large enough to avoid being depleted between the time a data word is taken from it by the interface and the time when that word's replacement reaches the buffer. That delay is about 12.3 milliseconds—7 milliseconds for the intensity data of the previous mass point to reach the computer, 5.3 milliseconds for the new voltage data word to reach the buffer, and negligible computer time (about 20 microseconds). During this delay no more than 4 samples can be taken (3.3 milliseconds per sample is the maximum sampling rate of the interface), so an input buffer of four 16-bit words is sufficient to maintain the maximum sampling rate of the interface.

The Data Acquisition and Time-Sharing Computers

The data acquisition computer is a small, general purpose computer devoted to the real-time handling of all the data streams coming over telephone lines from the several mass spectrometers. This machine is directly tied to the central time-sharing computer and to mass storage units (either disks or tapes) for spectral data storage. These storage units are also directly accessible by the central time-sharing computer. We estimate that a computer with the capabilities of a PDP-8/I, having 8000 12-bit words, could acquire and store data from about 15 mass spectrometers simultaneously. It appears that about 200 words of buffer in the computer would be needed for each user, but the actual processing time required per sample for each user would be only about 20 microseconds. The "dummy" data words would be handled—both peeled off of incoming signals and generated for outgoing signals—outside of the CPU by special hardware designed for that purpose.

Summary

A commercial time-sharing approach to computerizing mass spectrometers might be superior to dedicated systems, but specific designs must be compared. This paper presents a design with the following features.

- (1) Use of the computer control approach to data acquisition.
- (2) An interface that operates asynchronously on a request/response basis and can automatically adjust the integration time as a function of the signal strength.
- (3) A communications terminal that enables the interface to operate at its maximum rate by employing.
 - (a) A dual line continuous flow channel with "dummy" data to maintain flow.
 - (b) An input buffer, using the computer to monitor and regulate data flow.
- (4) A small, real-time data acquisition computer connected to the main time-sharing computer and a commonly-accessible storage unit.

We're currently evaluating this design in comparison to a technically equivalent dedicated system.

Footnotes

1. See, for example, R. Venkataraghavan, F. W. McLafferty, G. E. Van Lear, "Computer-Aided Interpretation of Mass Spectra" Organic Mass Spectrometry, 1969, Vol. 2, pp. 1-15

2. We'll assume, in this paper, that intensities of only the integral masses are recorded, although the approach can handle fractional mass data, too.

PROCESSING OF SOLIDS MASS SPECTROGRAPHIC DATA VIA
TIME-SHARING WITH SEMI-AUTOMATIC DATA ACQUISITION

12

J. R. Woolston and E. M. Botnick

RCA Laboratories
Princeton, N. J.

In processing solids mass spectrographic data, the primary need is to determine the intensity of the spectral lines. There is little, if any, problem in identifying them, in contrast to the case of high-resolution organic mass spectrographic data. The system described utilizes the RCA Time-Sharing System in spectral line-by-line, interactive fashion, and greatly facilitates the collection and processing of such data. A program has been written and a data acquisition system constructed that permits the following sequence: The selected line, which has been visually identified by the operator, is scanned on an optical microdensitometer and simultaneously displayed on a storage oscilloscope. A horizontal, non-storing cursor line is then positioned first at the peak level and subsequently at the background level of the displayed line profile. At each position, a digital voltmeter displays the percent blackening value. These two values, together with the line identification and exposure information, are then typed into the time-sharing terminal. The program then immediately calculates the parts per million atomic concentration and displays this result on the terminal. The program includes the following features: construction of the emulsion response curve from any number of available data via the Hull equation; geometric average of multiple analytical results; deletion of abnormal values; print-out of complete reports; suspension of partially processed analyses for later completion; and automatic billing to the customer for the analysis service. The system is designed for a planned enhancement that will transmit the complete peak profile, represented by 100 or so points, to the computer so that integrated peak intensity can be obtained. This will substantially improve analytical precision.

A NEW, REMOTE ON-LINE DATA ACQUISITION-PROCESSING
 SYSTEM FOR LOW RESOLUTION COMBINATION
 GAS CHROMATOGRAPH-MASS SPECTROMETER

H-Y, Li, J. Walden, R. Saunders, D. Simpson,
 L. Mills, K. Kinneberg and G.R. Waller

Departments of Biochemistry, Electrical Engineering, and Computer Center
 Oklahoma State University, Stillwater, Oklahoma 74074

A new, remote data acquisition-processing system has been put in operation for the LKB-9000 single-focusing fast-scanning low-resolution combination gas chromatograph-mass spectrometer. An IBM-360/50 is used to process the data. The system uses two private analog lines to transmit the ion-intensity signal and the Hall generator signal (mass marker) via two pairs of line isolation differential amplifiers to an IBM-1827 analog/digital control unit situated one-half mile from the mass-spectrometer. The digitized signals are stored temporarily in a 60 K-byte buffer which is composed of 30,000 alternating half-words of mass-spectrometer and mass-marker data. The gross core storage lay-out which provides for a total of 130 K-bytes of devoted core is shown below:

GROSS CORE STORAGE LAYOUT OF S/360-50 AT OSU

OS	MASS SPEC PROGRAM	.	.		
NUC	A	.	B	.OSUWAT.	C	.	D	HASP
MFT-II	130K DEVOTED CORE
.

Fast Core 40000_{16}
 Bytes (256 K)

Slow Core 100000_{16} Bytes
 (1024 K)

Digitized and reduced intensity-mass value pairs (up to 1,500 mass values) along with spectra labels are stored in the disk. The processed data (i.e., normalized by subtracting background) may be listed on the printer, punched on cards, stored on magnetic tape or plotted as a bar graph on a CalComp 565 digital incremental plotter upon request by the mass spectrometer operator. The plotter and an IBM-2741 Remote Communications Terminal are situated near the mass-spectrometer. A digital line is provided to handle the two-way communication from and to the IBM-2741 and to send the plotting signal from the IBM 360/50 to the plotter. The digital signals from the IBM-360 reach the mass spectrometry lab via an IBM-2701 data adapter, a Western Electric 103F data set, and a CalComp 211 data interface control unit.

(Supported in part by Research Grants, GB-3482 and GB-7731 from the National Science Foundation).

Intended for publication in Analytical Biochemistry.

A. L. Burlingame, D. H. Smith, F. C. Walls and R. W. Olsen
Space Sciences Laboratory, University of California, Berkeley, California 94720

Over the past five years considerable effort has been devoted to the development of computer techniques in high resolution mass spectrometry. Our laboratory has been concerned with the development of on-line, real-time acquisition, processing and presentation of high resolution mass spectra as an alternate approach to the recording and processing of high resolution mass spectrograms. Since our first report of the on-line acquisition of high resolution data in 1965 (1), great strides have been made in the techniques of computer-coupled acquisition, processing and display of high resolution mass spectra (2). The general goal has been to explore and define in detail the quality of high resolution mass spectral data both in terms of the accuracy of mass measurement and the accuracy of relative ion abundance measurement which can be obtained from rapid magnetic scanning of a double focusing mass spectrometer on-line to a high speed digital computer. The effect of the spectrometer scan rate, resolution, sensitivity, analog to digital converter digitization rate and multiple scan averaging techniques on the accuracy of mass and abundance measurements for real-time data we have discussed on previous occasions (3). The range of resolutions previously covered has been from 10,000 to 30,000 for both single magnetic scans as well as the averaging of multiple scans (3,4,5). Unresolved multiplet detection and identification has been based only on assumptions regarding the separation ($\Delta M/M$) of isobaric species, shifts in the measured centers of gravity and the fragmentation pattern of the molecule in question (4). The general conclusion from these studies has demonstrated that resolution must be sacrificed for sensitivity in order to obtain very high precision mass measurements which then will permit both unambiguous assignment of elemental composition to singlets and recognition and identification of unresolved multiplets based on "errors" in the centers of gravity measurements (6).

The range of mass measurement accuracy which has been demonstrated ranges from the order of 4 ppm down to 0.1 ppm, depending upon the instrument resolution scan and digitization rates and calibration techniques for a given sample flow rate into the ion source of the mass spectrometer (7).

At the previous E-14 meeting two groups presented data on accuracy of mass measurement for single focusing instruments: the AEI MS-12 and the Varian Atlas CH-5. Chapman, Evans and Holmes (8) reported a standard deviation of 14 ppm for a single scan, while Brunnee, Habfast, Markwardt, Meier and Wegner (9) reported 10 ppm on much fewer experimental data.

We wish to report and discuss the accuracy of mass measurements obtainable at resolutions between 2,500 and 10,000 from a modified AEI MS-902 mass spectrometer coupled to an SDS Sigma 7 digital computer (4) and then discuss external calibration of the Perkin-Elmer Model 270 mass spectrometer coupled to an SDS Sigma 2 computer.

The hardware configuration which has been employed in our laboratory for the past couple of years was utilized (3). The mass spectrometer scan rate is 16 sec per decade, digitization rate 24 KHz and the clocking controlled by a temperature controlled quartz crystal oscillator.

The software of the Sigma 7 computer for the data acquisition mode ("on the fly") under high resolution scanning conditions has been discussed previously (5). There is only one aspect of the system which is new, and that is a Tektronix 611 storage cathode ray display which has been added to the system. The quality of the line resolution is far superior to that which has been previously reported, although the system function is essentially the same (2). Previous results on the accuracy of mass measurement from single scan and averaged multiple scans from our system, at a resolution of 11,000, considered a dynamic range of 50:1 and yielded the majority of measurements in the 1 ppm range (4).

Complete 10-average data was taken as discussed previously (4) excepting that all peaks over dynamic range 200:1 were considered and the results are plotted as a histogram (Fig. 1). It should be noted that all the data in this histogram show mass measurements better than 3 ppm with 95% better than 2 ppm. In Figure 2 data is plotted in a histogram for scanning at a resolution of 5,000. This data is essentially the same quality as the 10,000 except that there is 5% scatter to 4 ppm. In Figure 3 data are plotted for the same experiment at a resolution of 2,500. It should be noted that the precision drops off an additional 1 ppm, although 80% of measurements are still 2 ppm or better. The distribution of mass measurement errors in the histogram for a single scan of the spectrum at 2,500 resolution is shown in Figure 4. Sixty percent of the mass measurements for a single scan are still better than 3 ppm. The rest of this spread is out to 6 or 7 ppm, which one might expect, but 80% are still better than 5 ppm. It should be pointed out that even at 2,500 the distribution of errors on a single scan for this dynamic range shows spectra of higher quality than has been reported in the literature for recording of mass spectra on photographic plates at any routine instrument resolution (10,11,12).

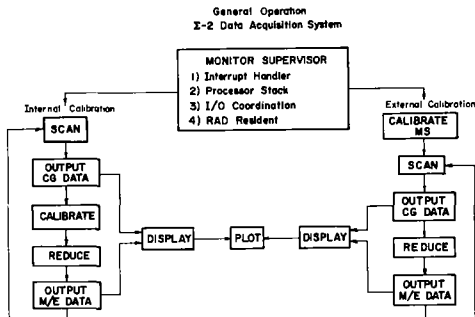
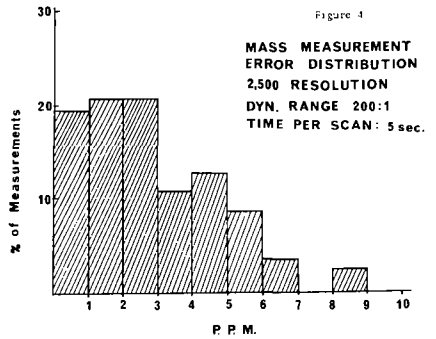
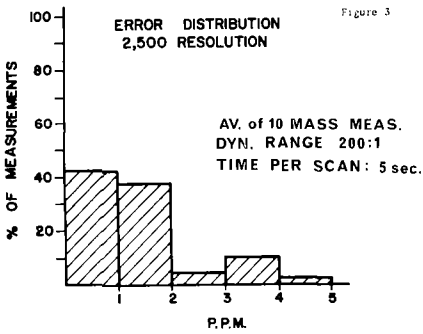
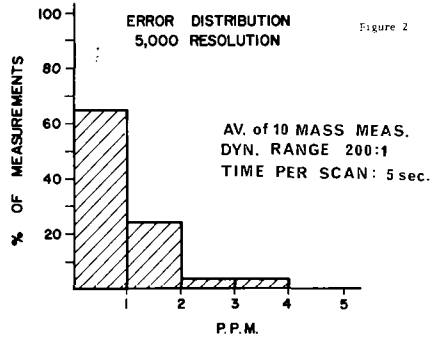
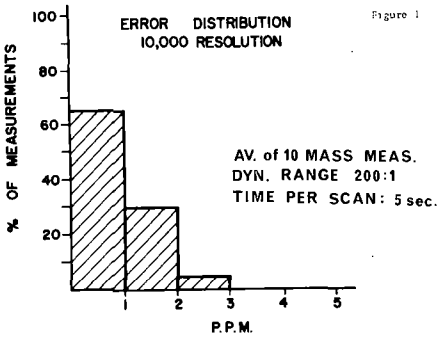


Figure 5

It was of some interest to determine whether techniques discussed previously for resolution of unresolved multiplets (4,6) based on the shift of center of gravity applicable to data taken at this lower resolution. Working at this lower resolution, of course, means that one will encounter many more unresolved multiplets than at higher resolutions. To determine the applicability of the center of gravity resolution technique several spectra of the compound discussed previously (4), methyl arachidate, were recorded at a resolution of 2,500. The following results are representative of the data obtained and the study of doublets of the type ^{13}C vs. CH in the spectra of this ester. For mass 70 (C_5H_{10} vs. $\text{C}_4^{13}\text{CH}_9$) the observed error for the CH species was 10.4 ppm. The predicted error on the basis of the center of gravity technique was 12.1 ppm, a difference of 1.7 ppm. Similarly for doublets the mass at 88 ($\text{C}_4\text{H}_8\text{O}_2$ vs. $\text{C}_3^{13}\text{CH}_7\text{O}_2$) and the mass at 130 ($\text{C}_7\text{H}_{14}\text{O}_2$ vs. $\text{C}_6^{13}\text{C}^{13}\text{H}_{12}\text{O}_2$) had observed errors of 27.6 and 12.7 ppm with predicted errors of 27.0 and 10.7 ppm, a difference of 0.6 and 2.0 ppm, respectively. As can be seen, the differences between the observed and predicted errors indicate that the center of gravity resolution technique is applicable to data taken at relatively low resolution. It yields mass measurement errors of the same order as errors on measurements of single peaks.

This discussion may be concluded by pointing out that the performance of a double focusing mass spectrometer of smaller ion optical dimensions than the MS-902 should in principle yield similar quality data. It should be anticipated that in the very near future this will be routinely obtainable. If such accuracy is coupled with evaluation of multiplets from mass measurement errors, it would appear that the amount of information which is extractable from an on-line double focusing, medium resolution mass spectrometer would far exceed the normal utilization of any mass spectrometer in research laboratories of organic chemistry throughout the world today.

Finally, we wish to discuss briefly the results of on-line operation of the Perkin-Elmer Model 270 gas chromatographic-mass spectrometer system with an SDS Sigma 2 computer using "external" calibration for nominal mass and pattern normalization during gas chromatographic runs. The software logic of this system is shown in Figure 5. Operating the mass spectrometer at a resolution of 400, digitizing at 8 KHz and scanning at 3 sec/decade in mass, the peak width is approximately 2,500 ppm. The mass accuracy is better than 12% of the peak width during a 24-hour period of operation subsequent to one calibration run with PFK. This corresponds to a long term stability of approximately 300 ppm in mass measurement, i.e., 0.03 amu at m/e 100 and 0.15 amu at m/e 500. The salient feature of taking advantage of this accuracy is in the use of accurate masses in calibration routines rather than the nominal masses such as described in the systems by Hites and Biemann for the Hitachi RMU-6 mass spectrometer (13).

Acknowledgement. The authors are indebted for financial support of this research to the National Aeronautics and Space Administration, Contracts NAS 9-7889 and NAS 9-7381.

References

1. R. W. Olsen and A. L. Burlingame, Proc. 13th Ann. Conf. on Mass Spectrometry and Allied Topics, St. Louis, Mo., May 16-21, 1965, p. 192.
2. A. L. Burlingame, D. H. Smith and R. W. Olsen, Anal. Chem. 40, 13 (1968).
3. A. L. Burlingame, in Advances in Mass Spectrometry Vol. 4 (E. Kendrick, Ed.), The Institute of Petroleum, London, 1968, p. 15.
4. A. L. Burlingame, D. H. Smith, R. W. Olsen and T. O. Merren, Proc. 16th Ann. Conf. on Mass Spectrometry and Allied Topics, Pittsburgh, Pa., May 13-17, 1968, p. 109.
5. D. H. Smith, R. W. Olsen and A. L. Burlingame, Proc. 16th Ann. Conf. on Mass Spectrometry and Allied Topics, Pittsburgh, Pa., May 13-17, 1968, p. 101.
6. A. L. Burlingame, D. H. Smith, T. O. Merren and R. W. Olsen, in Computers in Analytical Chemistry (C. H. Orr and J. Norris, Eds.), Plenum Press, New York, in press.
7. A. L. Burlingame, Proc. International Chromato-Mass Spectrometry Symposium, Moscow, May 21-28, 1968.
8. J. R. Chapman, S. Evans and J. M. Holmes, Proc. 16th Ann. Conf. on Mass Spectrometry and Allied Topics, Pittsburgh, Pa., May 13-17, 1968, p. 313.
9. C. Brunnée, K. Habfast, U. Markwardt, S. U. Meier and E. Wegner, Proc. 16th Ann. Conf. on Mass Spectrometry and Allied Topics, Pittsburgh, Pa., May 13-17, 1968, p. 85.
10. K. Biemann, Proc. 11th Ann. Conf. on Mass Spectrometry and Allied Topics, San Francisco May 19-24, 1963, p. 235.
11. R. Venkataraghavan, R. D. Board, R. Klimowski, J. W. Amy and F. W. McLafferty, in Advances in Mass Spectrometry Vol. 4 (E. Kendrick, Ed.), The Institute of Petroleum, London, 1968, p. 65.
12. D. D. Tunnicliff and P. A. Wadsworth, Anal. Chem. 40, 1826 (1968).
13. R. A. Hites and K. Biemann, in Advances in Mass Spectrometry Vol. 4 (E. Kendrick, Ed.), The Institute of Petroleum, London, 1968, p. 37; Anal. Chem. 40, 1217 (1968).

Applications of a Small Digital Computer
in the Mass Spectrometer Laboratory

R. Venkataraghavan, R.J. Klimowski, J.E. Coutant, and F.W. McLafferty
Department of Chemistry, Cornell University, Ithaca, New York 14850

ABSTRACT: We have found that a fast small digital computer (PDP-8, Digital Equipment Corporation) can perform many important tasks of data acquisition, reduction, and interpretation in the mass spectrometry laboratory. A computer memory of only 4096 words can be used by employing fast-access disc storage for both data acquisition and program swapping, and by coding routine programs in machine language. Special design considerations of hardware and organization of software are necessary to optimize the time required for both data acquisition and reduction. The final data needed by the mass spectrometrists can be obtained nearly in real-time, the main limitation being in the speed of data print-out. Complete elemental composition data can be obtained from exact mass measurements within 5 minutes after the start of the mass spectrometer scan. The system is also applicable to several other important data problems.

INTRODUCTION: There are several reports in the literature describing real-time data acquisition and processing systems for high resolution mass spectrometers. Such systems have utilized computers costing up to a quarter of a million dollars. Our experience in this area shows that a small dedicated computer satisfactorily produces significant information for the mass spectrometrists. This fact combined with the low cost of the computer and associated interface (about \$50,000) makes such a systems approach very attractive.

The inherent speed of the processor and memory subsystems may be effectively retained through the utilization of a low cost random access bulk storage device and other high speed peripherals. This is especially true in applications of large data volumes and high data rates. Under such conditions, the small, dedicated computer can be more efficient and valuable than other data acquisition approaches such as a time-sharing terminal and necessary instrument interface. With sufficient care in the initial installation design, such a system can find multiple usage in many diverse areas of chemical instrumentation.

At the last E-14 meeting in Pittsburgh we briefly reported on an approach using a PDP-8 computer.¹ Since that time, a second generation hardware and software design has been developed. We would like to discuss some of the essential features of the present system and several of its current applications at Cornell.

SYSTEM APPROACH: Figure 1 shows a block diagram of the basic instrument-computer system, in this case utilizing a Hitachi RMU-7 mass spectrometer. The essential point of this diagram is the interface region in the center. The interface has the following functions.

- (1) to present the instrument analog output to the computer
- (2) to provide hardware control of the A/D converter and its synchronization to a frequency established by an external crystal clock.
- (3) to provide hardware thresholding of the digitized analog signal, allowing data compression of up to 97%.
- (4) to provide a continuous time base during an instrument cycle.
- (5) to provide a direct line of communication between the instrument and computer for control purposes, which at present includes the START/STOP function and electric sector potential of the mass spectrometer.

The small 4096 word memory unit is completely adequate for all operations when the software system is designed along modular lines and the full potential of the disc system is utilized. The high resolution software system is constructed along such lines and the five phases (or sections) of the mass spectrometer software are referred to as:

- | | |
|------|-----------------------------------|
| I. | data acquisition |
| II. | peak center calculation |
| III. | reference peak identification |
| IV. | exact mass calculation |
| V. | elemental composition calculation |

At the beginning of a scan, an operator-computer conversational dialogue takes place. The information supplied to the computer results in the desired operating parameters being set in the interface. Phase I then acquires the data and stores the resultant compressed spectrum on the disc system. A logarithmic amplifier is used between the mass spectrometer and A/D converter to allow representation of a linear dynamic range of at least 20,000 in a 12 bit computer word. An optional data dump may be produced by

MASS SPECTROMETER — COMPUTER

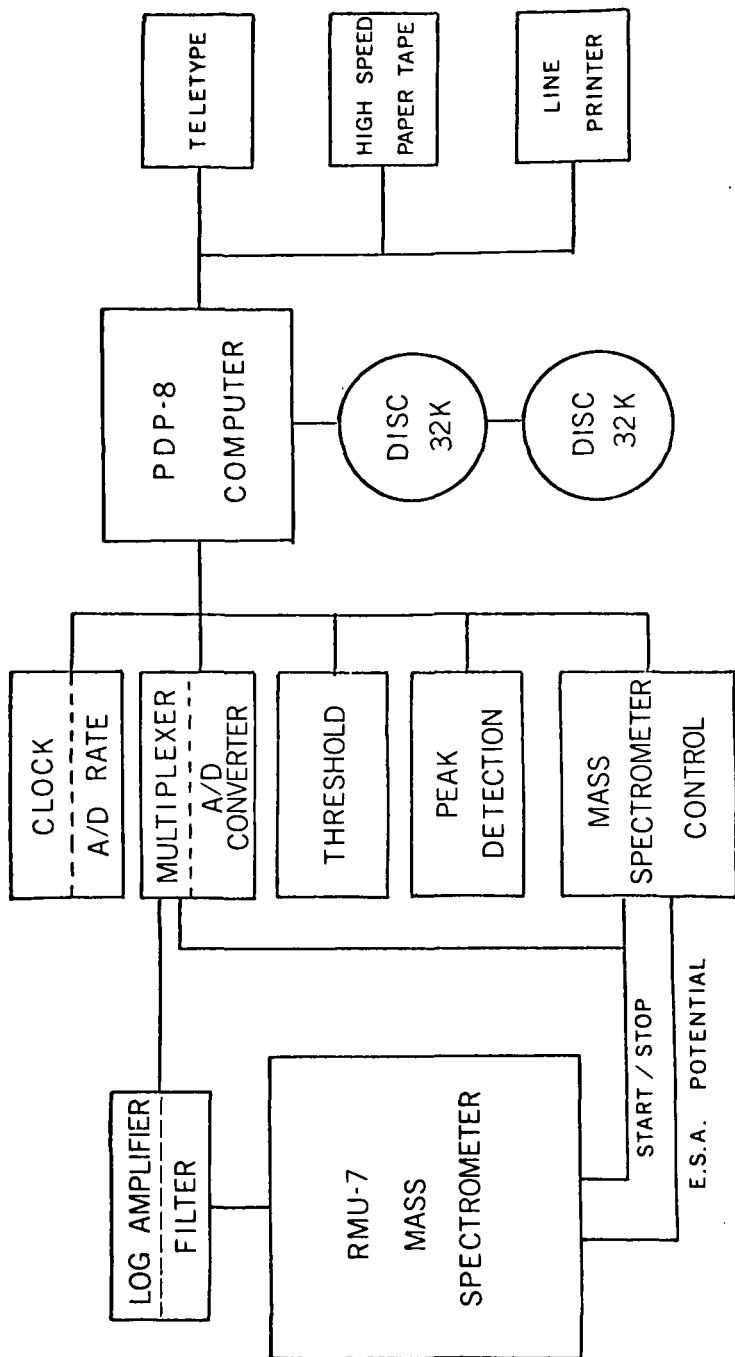


FIGURE 1.

PHASE 5. TYPICAL PRINTOUT

	+185.9695	NO HIT					
	+185.9752	NO HIT					
	+186.9858	NO HIT					
+ 1.1	+193.0711	+193.0725	-1.41	+ 8/0	+ 9	4	2
	+193.0773	NO HIT					
+ .0	+193.0816	+193.0805	+1.09	+ 8/1	+10	3	2
+100.0	+194.0811	+194.0803	+ .74	+ 8/0	+10	4	2
+ 5.4	+195.0829	+195.0836	+ .75	+ 7/1	+10	4	2
	+200.9898	NO HIT					
	+200.9989	NO HIT					

molecular ion region

CAFFEINE: $C_8H_{10}N_4O_2$

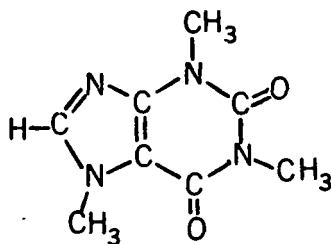


FIGURE 2.

BENZENE - PYRIDINE DBLT.

R > 10,000

REL. AB.	MASS	CALC.	ERR.	C12/C13	H	N	O
+ 6.5	+ 78.0345	+ 78.0343	+ .14	+ 5/0	+ 4	1	0
+ 5.2	+ 78.0456	+ 78.0469	-1.24	+ 6/0	+ 6	0	0
+100.0	+ 79.0425	+ 79.0421	+ .33	+ 5/0	+ 5	1	0
+ .6	+ 79.0503	+ 79.0502	+ .14	+ 5/1	+ 6	0	0
+ 1.7	+ 80.0466	+ 80.0454	+1.14	+ 4/1	+ 5	1	0
	+ 92.9996	NO HIT					

ELEMENTAL COMPOSITION PROGRAM COMPLETED.

WOULD YOU LIKE TO TRY DIFFERENT LIMITS ?
IF SO, PRESS 'CONTINUE' AND WE'LL TRY AGAIN !

FIGURE 3.

Phase I. This output contains all of the original data collected by the computer and is grouped into digital values describing the peak profile followed by a time count identifying the position of this peak from the beginning of the scan.

Upon completion of PHASE I, PHASE II is swapped into core from the disc and begins execution, the entire operation requiring about 20 milliseconds and no operator intervention. This phase calculates the centroid of each peak and integrates the peak profile, after rescaling the logarithmic raw data. An optional listing is also available from PHASE II. Such an output contains the area of each peak and the time associated with the center of each peak. Centroid calculations of this type require less than 60 sec. for an entire typical spectrum.

PHASE III is then automatically swapped into core. This phase automatically identifies the reference lines contained in the centroid data and produces a listing of those reference lines found and absent. This output is always produced and serves as an indication of the overall performance of the system. Again, in this case, no operator intervention is required to locate the reference lines - a time consuming operation compared to the speed of the computer. Instead, the computer uses a basic pattern algorithm to find the reference lines, quite similar to the approach of the mass spectrometrists himself.

PHASE IV then begins execution. The exact masses are calculated using four reference lines and a Legendre polynomial equation, and requires about 5 seconds of time for the whole spectrum. An optional output is available from this phase giving the normalized area and exact calculated mass for each sample line.

PHASE V then begins execution and calculates elemental compositions for each sample mass. The operator may select various criteria to be used by the computer in performing such calculations. Figure 2 shows the output available from PHASE V. This particular example shows the region in the vicinity of the molecular ion of caffeine. Various pertinent information is given in tabular form for each ion fragment.

RESULTS: The ability of the entire system to maintain a working resolution of 10,000 was verified by running a mixture of benzene- and pyridine. Figure 3 shows the 78-79 region of the elemental composition listing for such a scan. The mixture used produced approximately equally abundant ions at mass 78. A centroid method of determining peak centers was employed which required the dynamic resolution of the whole system to be at least 10,000 to produce the mass 79 doublet shown.

We have investigated the system's accuracy for mass measurements under low resolution conditions of about 2,200, which are desirable for fast scan-GC operations. Figure 4 shows the random nature of the resultant errors of the C_7H_{15} hydrocarbon ion for successive scans. The ordered convergence limits for such error occurrence as well as the natural average error are shown as a function of the number of samples. We have also noted a net improvement in overall mass measuring accuracy using successive scan averaging at a resolution of 10,000. Table 1 shows the average errors for 10 successive scans for several hydrocarbon ion fragments. Such error convergence appears to be independent of the region of the spectrum investigated and the resulting accuracy may justify making several repetitive scans.

Table 1. AVERAGE ERRORS FOR 10 CONSECUTIVE SCANS AT R = 10,000

ION TYPE	AVG. ERROR (MMU)
C_5H_{11}	-0.62
C_6H_{13}	-0.17
C_7H_{15}	0.11
C_8H_{17}	0.24

In addition to high resolution data processing, this system can also be utilized (in the low resolution mode) for the fully automatic processing and acquisition of metastable ion information. The availability of such information to the chemist is a valuable tool in elucidating structures, especially if a great expense of time or human interaction is not necessary.

Ions formed in the source of a mass spectrometer and not undergoing decompositions before reaching the detector appear as the normal sharp peaks of a mass spectrum, while those ions decomposing in the second field free region appear as the familiar diffuse metastable peaks. In addition, decompositions also occur in the first field-free region and are not normally seen because of discrimination by the electrostatic analyzer. If, however the magnetic field is set for detection of a metastable produced in the second

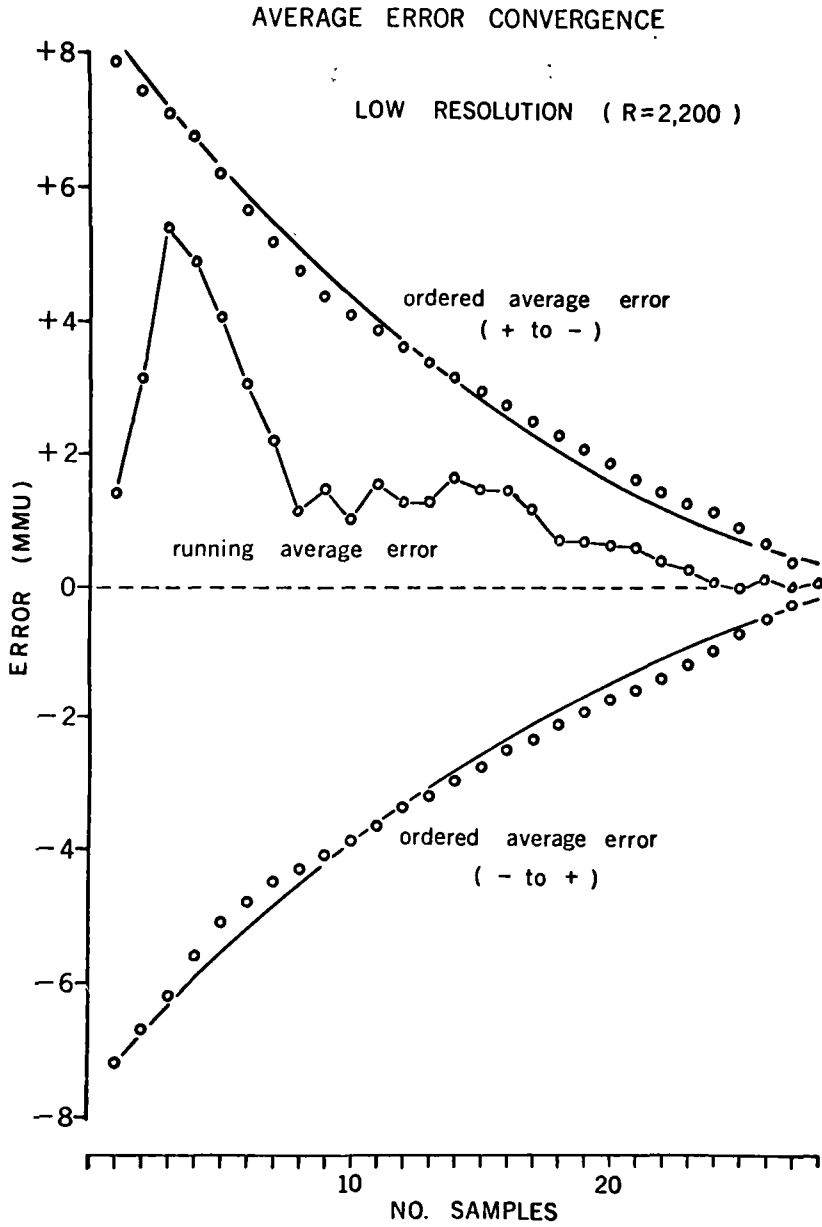


FIGURE 4.

FIGURE 5.
THREE-DIMENSIONAL MASS SPECTRUM

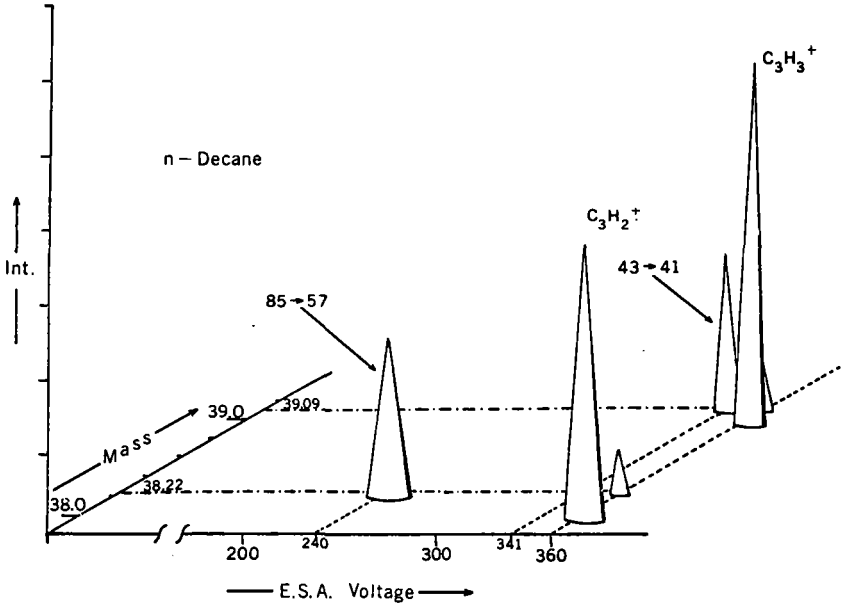
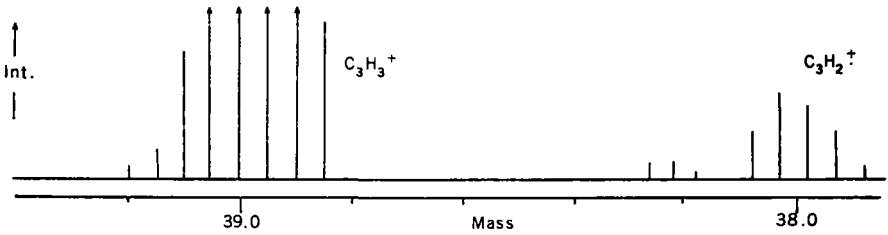


FIGURE 6.
DIGITAL OUTPUT OF THREE-DIMENSIONAL SCAN - n-DECANE

a. "Focused"

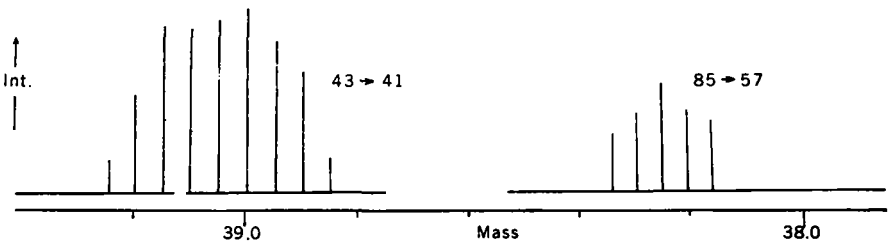
(E.S.A. = 360v.)



b. "Defocused"

(E.S.A. = 341v.)

(E.S.A. = 240v.)



field-free region and the potential of the electric-sector is lowered, the corresponding metastable produced in the first field-free region may be detected. Such 'defocused' metastables, as shown in Figure 5, appear at a unique mass and electric sector potential combination and are generally more abundant than the corresponding metastables observed in the normal spectrum. This then represents a three-dimensional mass spectrum with the new axis being the electric sector potential. To reiterate, all ion cones intersecting the line representing the 360 volt electric sector potential correspond to peaks seen in the normal mass spectrum. All other ion cones can only be seen using lower electric sector potentials.

In practice, the computer acquires such three-dimensional spectra by sweeping the electric sector voltage of the mass spectrometer at a high rate compared to the sweep of the magnetic field while digitizing the electron multiplier output, 50 electric sector scans being acquired per amu of mass scan. On each electric sector scan, peaks are digitized and values of the electric sector potential and mass position are stored for later calculations. Successive sweeps in the vicinity of an ion cone result in acquiring sufficient data to define the mass and voltage centroid of each ion cone.

Figure 6 shows the digitized peak profiles of both "focused" and "defocused" ions in the mass 38-39 region of n-decane. The upper digital display is the normal "focused" spectrum occurring at an electric sector potential of 360 volts. The lower digital displays are the "defocused" metastables in the same mass region but occurring at different electric sector potentials. The increased sensitivity and lack of interference from other ions is evident. The final data output is a tabular listing of the abundance and mass of all ions observed and, in the case of metastable ions, the transitions which occurred, based on the unique electric sector potential and mass observed for each.

The reduction of the amount of time required to obtain such data and the ability to make a correct and unique transition assignment for each metastable are primary assets of this technique.

The previous applications have suggested the usefulness of the small dedicated computer in the laboratory, but realistically such a small computer need not be dedicated always to one instrument or type of application. At Cornell we are attempting to incorporate such small computers into larger data systems allowing both dedicated and non dedicated usage of any part of the whole system, with the emphasis on the small computer as a primary data processor. One such approach is the incorporation of a PDP-8 into a larger PDP-9 configuration. The net result of such interaction is the ability to produce a system capable of allowing operator-computer interaction of a sophisticated nature such as that utilizing a CRT display. Operator demand based on such a display can force the computer into various options that it might not ordinarily select, particularly in the case of poorly defined information such as that with a low signal to noise ratio.

In conclusion, the small computer has achieved a very real place in today's laboratory and is limited in operation and application only by the imagination of its users.

ACKNOWLEDGMENT: The generous support of the National Institutes of Health (grant GM-16609) is sincerely appreciated.

Reference

1. R. Venkataraghavan, J.W. Amy, R.D. Board, R.D. Brown, R.J. Klimowski and F.W. McLafferty, Sixteenth Annual Conference on Mass Spectrometry (ASTM E-14), Pittsburgh (1968).

AB INITIO COMPUTER PROGRAMS FOR THE INTERPRETATION
OF MASS SPECTRAL DATA.

by

James D. Morrison
La Trobe University,
Bundoora 3083, Victoria, Australia.

The combination of the gas chromatograph and mass spectrometer gives us the capability of recording the mass spectra of the individual components of complicated mixtures, from microscopic amounts of sample, and with a minimal requirement for chemical isolation of these samples. This capability produces a very real flood of data, and leads us in self-defence to attempt to mechanize its processing and interpretation. This data processing can take several forms.

Firstly, there is the problem of recording the mass spectra, digitizing them, fixing on a mass scale, and producing a record of peak heights and mass numbers. This problem has been fairly adequately solved in different ways, by Biemann, McLafferty, and by Bowen, and their collaborators.

The second type of processing is the visual presentation of the information contained in the mass spectrum in as accessible a manner as possible. This may take the simple form of logarithmic plots of peaks, the removal of isotope peaks, or may involve the assignation of exact formulae to each ion peak and its display on an element map.^{1,2}

The third type of processing involves the comparison of the measured spectrum with a catalogue of mass spectra. This can be readily carried out. It is not necessary to compare all the peaks, the six strongest alone being quite adequate. To compare an unknown spectrum with 3000-odd catalogued spectra requires only seconds.³

The fourth step is to make a detailed study of the processes of reasoning by which a mass spectrometrists deduces a structure from a mass spectrum, and on the basis of this to attempt to program a computer to carry out the same processes, that is, the deduction of a chemical structure ab initio.

Parts of this process can fairly easily be systematised, and as such are readily amenable to programming. A computer can be made to trace out the McLafferty rearrangement in a spectrum explicitly, and to identify not only the groupings on both sides of the double bonded atom, but also the α -substituents. Another process of ion fragmentation which has been automated in this way is the sequencing of amino acid residues in a polypeptide.

A great part of the interpretation of a mass spectrum is by no means so systematic. One proceeds by interrogating the mass spectrum using a series of questions, and it is seldom that one gets a completely unequivocal answer in return to any one of them.

Let us look at a typical interrogation scheme in simplified form. (Fig. 1). Interest has been restricted for our purposes to a limited class of relatively simple molecules of molecular weight less than 250. One of the first questions one puts is what is the molecular weight. When one breaks down the logic of this question, it turns out to involve a surprisingly complex set of decisions. A variety of consistency checks can be applied to verify the correctness of the assignment.

- e.g.,
- a). Greater abundance of even-electron over odd-electron fragment ions.
 - b). No significant peaks at $p - 2$ to $p - 13$?
 - c). Is there a significant $p - 3$?

The parent isotope peaks can be used to set upper and lower limits to the elemental composition. Estimates can be made of the number of unsaturations, and of the oxygen, and nitrogen atom contents, by calculating a Δ value from the postulated molecular formula.

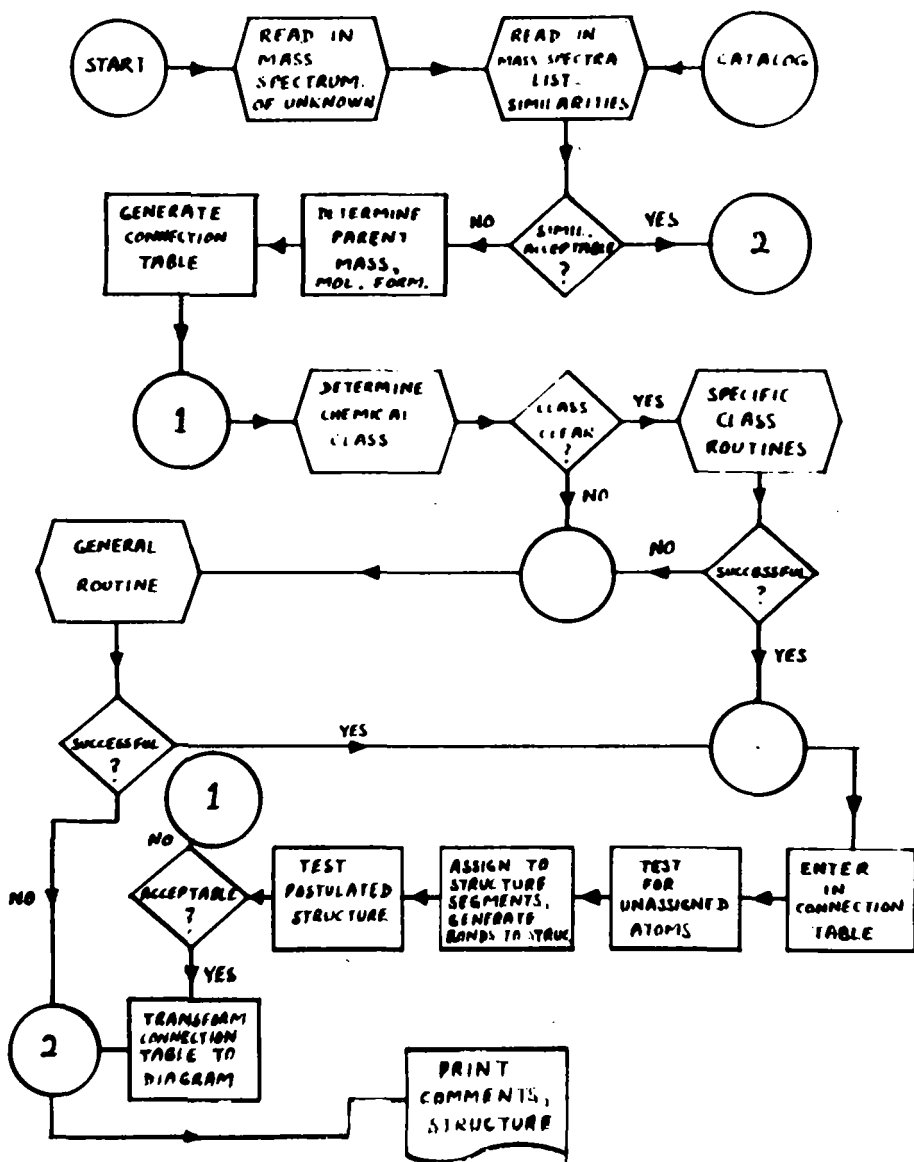


FIGURE 1

Given :-
(1-Heptenal)

MOLECULAR WEIGHT
114

MAIN FRAGMENTS

29 44 55 70 81 96 114

MOST PROBABLE FUNCTIONAL GROUPS OR TYPES AND RELATIVE PROBABILITIES.

ALDEHYDE 22.9% ALKANE 13.5% ALCOHOL 12.3%

ANALYSIS ROUTINE USED: GENERAL.

MOLECULAR FORMULAE

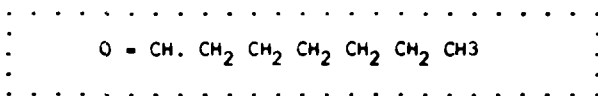
R = RINGS + UNSATURATIONS

C	O	N	R VALUE	H
7	1	0	1	14
6	2	0	2	10
5	1	2	2	10
5	3	0	3	6

GROUP COMBINATIONS

CONSISTENT WITH MOLECULAR WT

ALDEHYDE
ALDEHYDE ALCOHOL
ALDEHYDE ALCOHOL ALKENE



Given :-
(1-3 Diethyl Benzene)

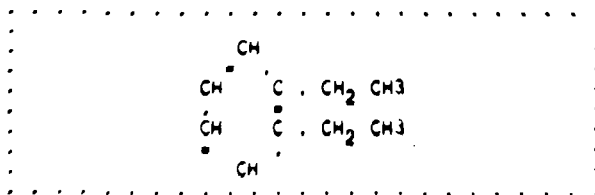
MOLECULAR WEIGHT
134

MAIN FRAGMENTS
UNDETERMINED.

MOST PROBABLE FUNCTIONAL GROUPS OR TYPES AND RELATIVE PROBABILITIES.

AROMATIC 61.1% ALCOHOL 5.3% ESTER 4.9%

ANALYSIS ROUTINE USED: SPECIAL.



TIME FOR ANALYSIS 7.627 SECONDS

FIGURE 2

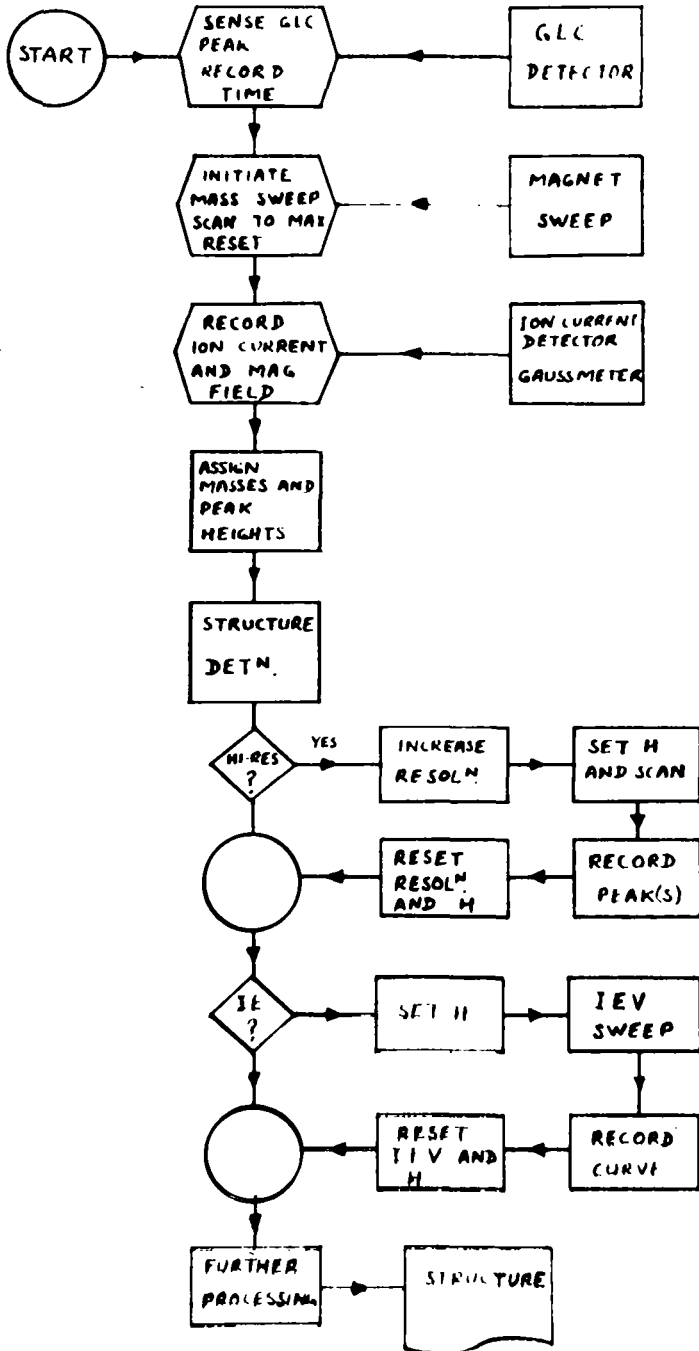


FIGURE 3

appearance potential data on certain ions. The whole time for this processing should be of the order of five seconds, so that a given GLC peak will be present throughout the time required.

This whole process of attempting to program "intelligence" is fascinating, and has involved us in a much more general study of the thought processes of a chemist, and other aspects of mechanized chemical education. I believe that in the not too distant future, programs of 100000 words and more will be in use, with immediate capabilities for special purposes far exceeding any human operator.

REFERENCES

1. R. Venkataraghavan & F.W. McLafferty,
Anal. Chem., Vol. 39, No.2, 278-279, (1967).
2. D. Desiderio, P. Bommer, & K. Biemann,
Tetrahedron Letters, (1964), 1725.
3. L. Crawford & J.D. Morrison, Paper I,
Anal. Chem., Vol. 40, No. 10, 1464-1469, (1968).
4. L. Crawford & J.D. Morrison, Paper II,
Anal. Chem., Vol. 40, No. 10, 1469-1474, (1968).
5. L. Crawford & J.D. Morrison,
Anal. Chem., In process of publication, (1969).

A. S. Denholm

Ion Physics Corporation
Burlington, Massachusetts

Vacuum as a dielectric has limitations initiated by superficial action. Loss of insulation strength can occur both across simple gaps and along dielectric surfaces, and is influenced by the quality of vacuum, the electrode material, and the amplitude and temporal form of the applied voltage. Three recent symposia have served to clarify the several processes which can lead to discharges in vacuum. (1, 2, 3)

With direct voltage or low frequency, there are essentially two breakdown conduction phenomena across vacuum gaps. One form is known as the microdischarge and is an incomplete conduction, whereas the other is a complete spark breakdown. Microdischarges are related to the organic contamination consistent with an unbaked vacuum system. These start at a threshold voltage and take the form of a pulse of current, perhaps lasting milliseconds. The pulse characteristics are strongly related to the surface condition. It is this phenomenon which gives current loading in accelerator tubes and velocity separators. Arnal⁽⁴⁾ and others⁽⁵⁾ have provided good evidence that the effect is related to a chain mechanism involving hydrogen ions of both signs; although most of the current appears to be electronic. By raising the pressure in a system, microdischarge thresholds can be immediately increased, apparently by gas scattering.

Spark breakdown is initiated by either a field emission process or by small 'clumps' of material detached from one electrode surface and accelerated across the gap to strike the other. Field emission occurs at microprotrusions on the cathode surface, and breakdown can be either cathode or anode initiated, depending on the geometry of the protrusions. Protrusions giving high field intensification lead to an instability at the protrusion and cathode initiated breakdown. Protrusions of smaller intensification lead to an anode instability through the power density of the bombarding electron beam. These processes have been discussed at considerable length by several authors.^(1, 2, 3) Field emission can be reduced and breakdown voltages raised, by increasing pressure in a system. Here, field emission electrons produce positive ions which sputter away the emitting tip and reduce field intensification. The improvement is not immediate but takes a specific time for significant sputtering.

For the designer wishing to prevent vacuum breakdown, titanium or some of its alloys are interesting electrode materials. Dielectric coatings on negative surfaces have also proven valuable; for example, anodized aluminum has been used with success on large velocity analyzers.

With regard to insulator breakdown under low frequency or direct voltage, the mechanisms are not well understood. However, end effects are critical as might be expected from the field intensification which can occur at the triple point. Stresses up to 250 kV/inch have been obtained in experiments, and accelerator tube structures can operate at 100 kV/inch. In general, where insulator surfaces have to operate at high gradients and voltages, grading techniques using equipotential planes at fixed potential interposed along the dielectric surface are necessary.

At the other end of the time spectrum, it has been shown that with very fast pulses, breakdown is initiated by the explosion of cathode micro-projections, and that complete breakdown is not accomplished until a plasma has bridged the gap. Studies in this area have been made by Mesyats and his colleagues.⁽⁶⁾ In this same time regime, breakdown across insulators is an electronic process involving avalanching down the dielectric surface.⁽⁷⁾

In summary, there appear to be three mechanisms which can account for breakdown in vacuum. One is field emission dependent where instabilities can develop either at the cathode or at the anode. There is also a 'clump' mechanism whereby particles from one electrode surface are accelerated across the gap to produce vaporization at the opposing surface. Finally, there is the hydrogen ion exchange mechanism which initiates the microdischarge.

REFERENCES

1. Proc. Symposium on Insulation of High Voltage in Vacuum, Boston 1964.
2. Proc. Symposium on Insulation of High Voltage in Vacuum, Boston 1966.
3. Proc. Symposium on Discharges and Electrical Insulation in Vacuum, Paris 1968.
4. Arnal, R., *Annales de Physique*, 10, p. 830, 1955.
5. Mansfield, W.K., et al, *Brit. J. Appl. Phys.* 8, p. 73, 1957.
6. Mesyats, G. A., et al, *Symposium on Discharges and Electrical Insulation in Vacuum*, p. 212, Paris, 1968.
7. Watson, A., *J. Applied Physics*, 38, No. 5, p. 2019 (1967).

Measurement of Sensitivity in a Secondary Ion Emission Microanalyzer

by C. M. Judson and R. K. Lewis
CEC/Analytical Instruments Division
Bell & Howell Company
Monrovia, California 91016

The Ion Microanalyzer was first described by Castaing in 1962.⁽¹⁾ A second version with energy filtering added to improve resolution was described in 1965.⁽²⁾ Last year at this meeting a paper prepared by Rouberol and his co-workers at Cameca described the design and performance of the commercial instrument being manufactured by Cameca.⁽³⁾

We have had one of these instruments in our laboratory in Monrovia since January. The main subject of this paper is to describe our experience in using this instrument, and in particular to report on measurements of relative sensitivities under various conditions. Some changes in the design of the optical system which have been incorporated since last year, one of which appears to involve a significant addition to the understanding of the optical system used will also be reported.

This instrument combines a secondary ion emission microscope with a mass spectrometer to obtain a magnified surface distribution map of the components of a sample. The optical system was described in the paper by Rouberol presented last year. A primary beam strikes the sample and secondary ions are formed and accelerated by an immersion lens, forming a magnified image of the surface. Ions of a specified mass are selected by the mass analyzer. A mass analysis is made using two deflections in a magnetic prism and one reflection in an electrostatic mirror. The ions leaving the analyzer are projected onto an image converter and the electron image formed is detected in one of several ways which will be discussed below.

This prism-mirror-prism system was selected as a convenient way to build a stigmatic analyzer. The theory of Cotte⁽⁴⁾, recently reviewed by Septier⁽⁵⁾, showed that with a properly selected entrance angle, a magnetic prism has four stigmatic points such that if the crossover and initial virtual image are placed at the first two points, a new crossover and virtual image are formed at the second two points. The mirror is designed so as to cause a symmetrical second passage through the magnetic field with the final virtual image and crossover symmetrical to the first image and crossover.

It is now recognized that the virtual image formed by the immersion lens and constituting the object for the prism-mirror-prism analyzer does not have to be at the first stigmatic point. If the mirror is located with its center and apex at the second two stigmatic points of the prism, an image at any point along the axis of the analyzer is reproduced as an image at another point, with magnification or demagnification depending on the location of the image with respect to the first stigmatic point.

The demonstration of this property of the prism-mirror-prism system is easily made in the Ion Microanalyzer by changing the focus on the immersion lens which precedes the mass analyzer, and observing that good images are maintained while the total magnification of the analyzer is changed.

The practical use of this capability which has been made in the Ion Microanalyzer is to somewhat simplify the lens system following the mass analyzer which was required in order to operate with either positive or negative secondary ions. The power supply required for the image converter is now symmetric for both positive and negative ions. The same physical lenses which were described last year are used, but with different potentials applied. The basic discovery that the prism-mirror-prism system can operate with variable magnification seems to be more important than the particular application which has been made of this principle.

Two other changes in design have been made from that described last year. A rectangular aperture has been placed in front of the circular aperture at the intermediate crossover, designed so as to minimize aberrations and resulting in an improvement in the compromise between mass resolution and sensitivity.

An astigmatism corrector has also been provided for the primary beam.

It should also be noted that the optical design which was shown last year does not show the field aperture located just before the entrance to the prism. This field aperture acts to limit the sample area seen by the analyzer.

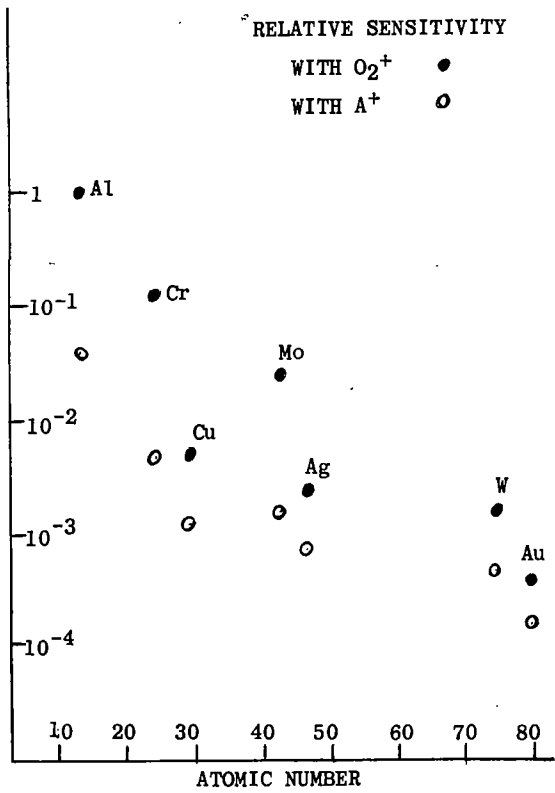


FIGURE 2

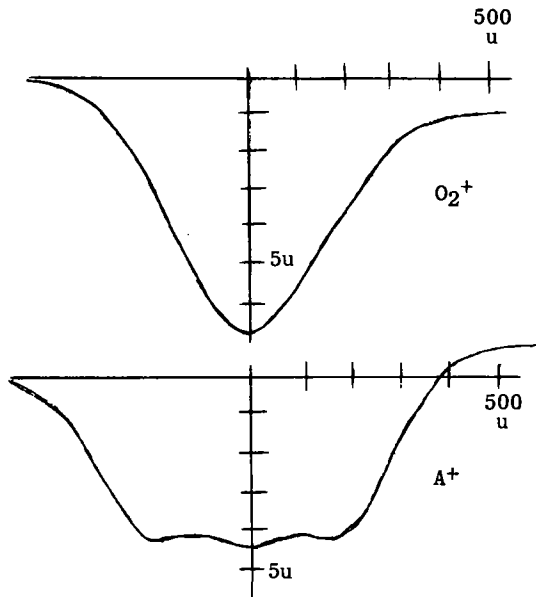


FIGURE 1

DEPRESSION IN SILICON 111
AFTER ION BOMBARDMENT

The primary beam current is of the order of 25 uA and has an area of the order of several hundred microns. The spatial resolution is obtained by recording a stigmatic image and not by use of a small primary beam spot. The primary beam is generally either argon or oxygen.

Using a cylindrical condenser to deflect the primary beam into the mass analyzer, the composition of the primary beam can be determined. Except for about 5% mass 16 for oxygen and the same amount of mass 20 for argon, the beams are found to be essentially pure mass 32 and mass 40, the largest impurity peaks being of the order of 0.1%.

Figure 1 shows the shape of the depression formed in a sample by the primary beam as measured with an interference microscope. A flatter bottom appears to be formed with argon, but we have not established that this is true under all conditions. What we do know is that with either a flat or rounded bottom, we can adjust the field aperture so that only ions from the center are seen and we can eliminate any ions from the edges. This represents an inherent advantage of the microscope approach over any method which measures the total secondary ion beam formed, in that it permits obtaining measurements which represent entirely the signal from a specified depth.

The ion beam is projected onto an image converter which is essentially a Daly detector and is converted into an electron beam. There are three possible methods of observing the image. (1) The reflected electron beam can be imaged onto photographic film, (2) it can be deflected onto a scintillator for visual operation or (3) a part of the beam selected by a diaphragm in the image plane can be passed to a scintillator-photomultiplier for current measurement.

This instrument was designed with the primary objective of forming images representing the composition of the sample, and particularly of forming a series of images at successive depths within the sample. Examples of such images were shown last year. Images can be obtained in very much shorter times than are required with an electron microprobe. One can also obtain images for the very light elements and for specific isotopes which cannot possibly be obtained with the electron microprobe.

In order to fully understand the capabilities of the instrument, we have to know something about the concentrations which must be present and the time of exposure or depth of sample erosion required to obtain an image at a particular concentration of a particular element. We have carried out a series of measurements of the relative sensitivities for various elements being bombarded with either argon or oxygen.

The same measurements of relative sensitivities which are needed to evaluate sensitivity for forming images are also required for comparing sensitivities for detection of trace quantities by measurement of the total secondary current observed. We will first consider the question of sensitivity for current measurements and then come back to the question of sensitivity for image formation.

The detection limit for current measurement for a given element is the ratio of the noise in the measurement system to the current obtained with a pure sample. The next slide shows that for aluminum, the most sensitive element, using O_2^+ primary ions, this limit is

$$\frac{5 \times 10^{-17}}{5 \times 10^{-9}} = 10^{-8} \text{ or } 10 \text{ ppb}$$

This is for a system with one second time response, with the mirror adjusted for 50% valley at mass 200, and using the full 350 micron sample area. With 10% valleys at mass 350, the detection limit is about 3 fold higher. When a complete spectrum is scanned, the time constant will generally be somewhat lower and the detection limit higher. When a single element is being measured the time constant can easily be greater than 1 second, and the detection limit lower. Using longer measurement times and counting ions or using a digital memory oscilloscope, an improvement of at least one and possible two orders of magnitude can be expected.

The detection limit for any element can be calculated by multiplying the detection limit for aluminum by the relative sensitivity compared to aluminum.

$$\text{Det. Limit} = 10^{-8} \frac{K_x}{K_{Al}}$$

where K is the yield of the most abundant secondary ion as a ratio to the number of primary ions.

The depth of sample consumed in the time required for a measurement can be calculated from three factors; the erosion rate for Aluminum, approximately 100 Angstroms per second, the time of the experiment, and the relative sputtering rate compared to aluminum.

$$\text{depth} = 100 \frac{\text{\AA}}{\text{SEC}} \cdot \text{TIME} \cdot \frac{S_{Mx}}{S_{Al}}$$

The relative sputtering rates under more or less similar conditions are available in the literature and are in the range of 1 to 10 times that for aluminum. In typical experiments involving a few seconds to a few minutes, one consumes of the order of 10^4 Angstroms or 1 micron.

The time required to form an image for pure aluminum is 4 milliseconds, and the concentration which can be detected in a specified time can be calculated by the following equation:

$$C_x = \frac{0.004}{\text{TIME}} \cdot \frac{1}{K_x/K_{Al}}$$

This time may be limited by the time available or by the depth of penetration which can be allowed. Assuming maximum values are about 100 seconds or 1 micron, the limit of detection for an image with pure aluminum is 4.0×10^{-5} or 40 ppm. This is considerably higher than the detection limit for current measurement from a large area, but very much less than the detection limit for current measurement from an area equal to the spatial resolution. The presence of a particular concentration in a sample area of micron size can be detected more easily from an image than from an attempt to measure current.

Figure 2 shows a plot of relative sensitivity against atomic number. The closed circles with the higher sensitivities are for oxygen bombardment, the open circles with somewhat lower sensitivities for argon bombardment. Previous workers have shown that there is a change in atom sputtering yield and in secondary ion yield within a period of the periodic table. This variation appears to be related at least in part to the number of d electrons. At any rate we selected Cr, Mo and W to represent elements near the beginning of the period, all in a single group, and Cu, Ag and Au as subgroup elements which represent approximately the lowest sensitivity. Elements between Cr and Cu in the periodic table might be expected to have sensitivities between the figures measured for Cr and Cu.

The data shown are sensitivities for the most abundant isotopes. Similar but slightly different plots can be obtained for the total yield of all isotopes.

The data for O_2^+ are generally similar to those which have been reported by Anderson for negative O_16^- .⁽⁶⁾ To our knowledge, however, there has not previously been presented any systematic comparison across the periodic table of sensitivities for argon and oxygen under similar conditions.

The sensitivities for argon are less, but the reduction between oxygen and argon is less for the low sensitivity than for the high sensitivity elements. On the average the sensitivity for argon is about one order of magnitude lower, but the variation in sensitivity with element is less with argon.

We have since measured four other elements (Mg, Si, Ti and Sn) and the results are consistent. We have obtained spectra for each of the elements studied which we are in the process of correlating. The most significant observations are that oxygen produces lower yields of dimers and higher polymers than argon but provides the additional complexity of forming many compound ions with one or more oxygen atoms and one or more metal atoms.

Finally it is interesting to consider what we know about the relation of sensitivity to the three factors which determine sensitivity; the yield of sputtered atoms, the yield of ions from these atoms, and the transmission of the instrument. Experiments have been carried out with aluminum to measure the number of collected ions per sputtered atom. This was done by integrating the aluminum ion current while sputtering through a film of known thickness. The yields for oxygen and argon, respectively, were 1.0×10^{-3} and 1.4×10^{-5} Al^+ ions per sputtered atom. The instrument transmission is mainly limited by the number of ions eliminated by the aperture of the immersion lens because of the lateral component of energy. For aluminum the distribution of secondary ion energies has been measured by Hennequin and the transmission can be calculated. The estimated value is 0.058. On this basis the ionization yields are 1.7×10^{-2} and 2.4×10^{-4} for oxygen and argon respectively.

References

- (1) Castaing and Slodzian, *J. Microscopie* 1, 395, 1962a.
- (2) Castaing. 4th International Congress on X-ray Optics and Microanalysis, 1965, Hermann, Paris.
- (3) Rouberol, Guernet, Deschamps, Dagnot and Guyon de la Berge, *ASTM E-14 Proceedings*, 1968, p. 216.
- (4) Cotte, *Ann. Phys.*, (11), 10, 333, 1938.
- (5) *Focusing of Charged Particles*, Vol. 2, Septier, Academic Press, 1967, p.265.
- (6) Anderson, *Int. Jour. Mass Spec. and Ion Phys.* 2, 61, 1969.

MASS SPECTROMETRIC MEASUREMENT OF THE THERMAL VELOCITIES
OF VARIOUS SPECIES EVOLVED FROM LASER-VAPORIZED MATERIALS

K. A. Lincoln, F. A. Wodley
Naval Radiological Defense Laboratory, San Francisco, California 94135

INTRODUCTION

The mass spectrometer, by acting as a selective detector, serves as an effective instrument for measuring the velocities of molecular species vaporized from refractory materials. In these measurements the spectrometer functions essentially to establish the time of arrival of specific molecules at a measured distance from the sample. For full realization of this potential, however, such an instrument must have the capability of time resolving mass spectra obtained from short events in the submillisecond regime. The technique described here is applicable to gases which emanate from a common point and have long mean-free-paths (i.e., in a vacuum).

We have employed a pulsed laser of moderate energy (about one joule per pulse) to bring very small amounts of sample material quickly to a high temperature inside the ion source of the mass spectrometer. A complete description of the laser system, the mass spectrometer and technique for time resolving spectra have been reported previously.¹

The chief reason for using a TOF instrument is its ability to detect and time resolve, simultaneously, several molecular species produced by individual laser bursts; the resultant output of the instrument is an intensity versus time record of the preselected mass peaks. This has provided us with an effective tool for determining the thermal velocities attained by individual molecular species, and at the same time learn something of the vaporization characteristics of some refractory-type materials under high thermal loadings. It has also provided us with a technique for quantitative measurement of the components comprising these vapor plumes which exist for only a millisecond or less.

EXPERIMENTAL

The lasers employed for vaporizing samples are Nd-doped glass operated in the normal burst mode. Their output pulse widths can be varied from 100 μ s to nearly a millisecond, and the energy delivered to the sample is approximately 0.1 - 1.0 joule. Figure 1 shows schematically how the laser is coupled to the mass spectrometer so that the beam from the laser is focused on the sample which is located within the ion source on the end of the inlet probe. The He-Ne laser merely facilitates aligning the optics and indicates where the pulsed laser beam will strike the target. The probe can be rotated and moved vertically to position the sample material at measured distances from the electron beam in the ion gun. It should be pointed out that the laser optics moves with the sample to insure that the material is subjected to identical thermal loadings when the vapor path is varied, i.e., the distance between lens and sample remains constant.

Although the mass spectrometer and the method we use for time resolving mass spectra has been fully described in the earlier publication, a brief resume is necessary for an understanding of the applications described here. The instrument is a Bendix TOF mass spectrometer with a multichannel multiplier at the output and operates at a repetition rate of up to 65 kHz. To record the intensities of individual mass peaks as a function of time, each gating pulse to the multiplier is positioned (in delay time from

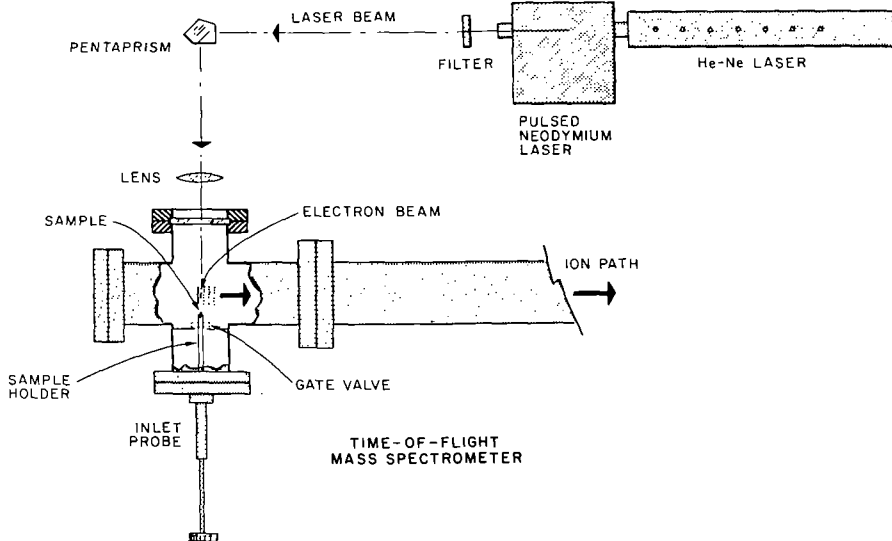


Fig. 1. Laser coupled to TOF Mass Spectrometer

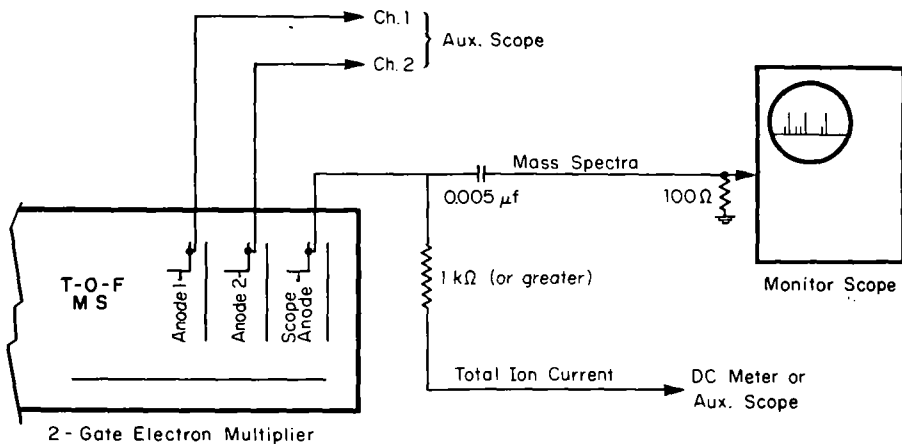
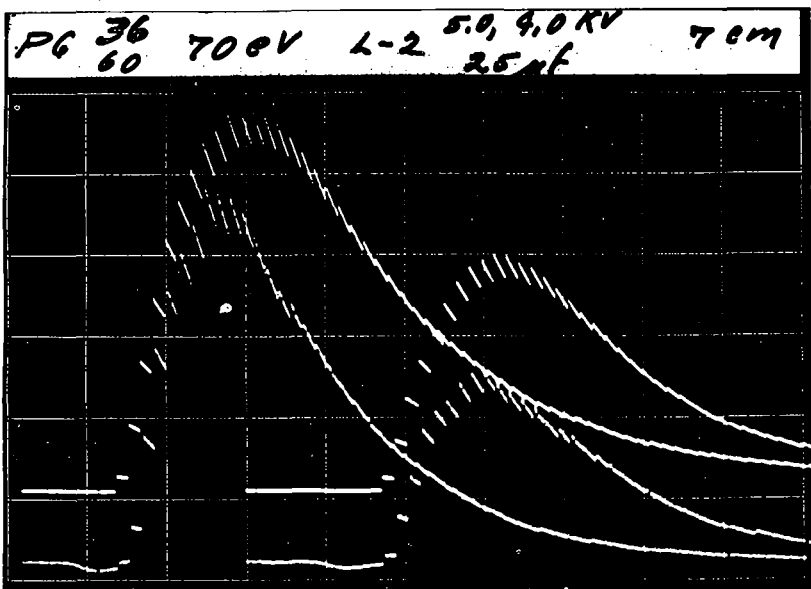


Fig. 2. Schematic of circuitry for measuring individual m/e intensities



Upper: 0.5V/cm Lower: .05V/cm 0.1 ms/cm

Fig. 3. C_3 and C_5 from graphite (two laser shots)

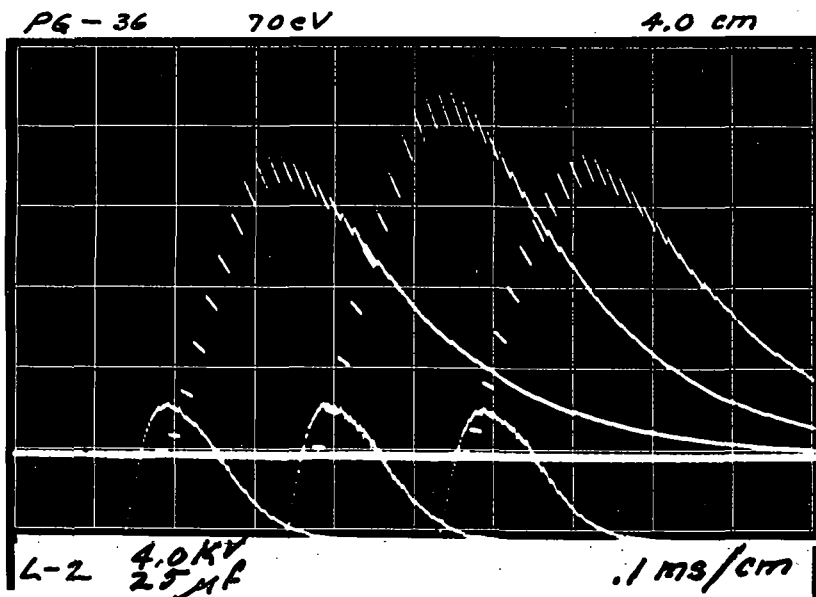
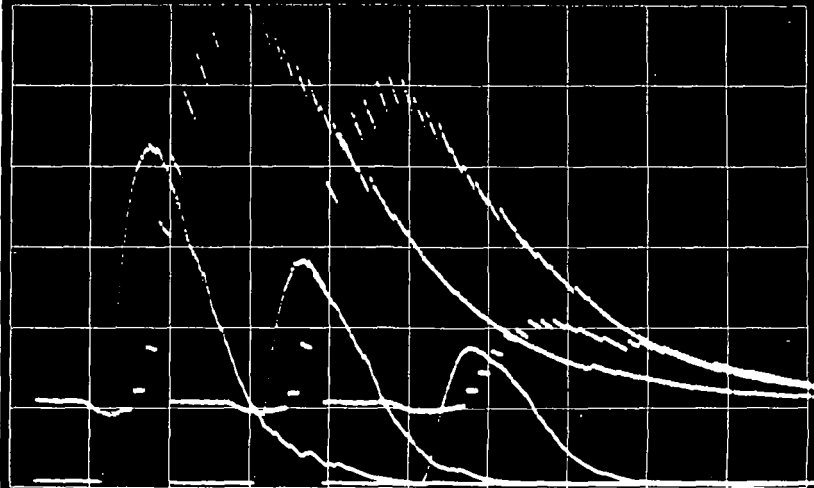


Fig. 4. Laser pulse and resulting C_3 from graphite (three laser shots).

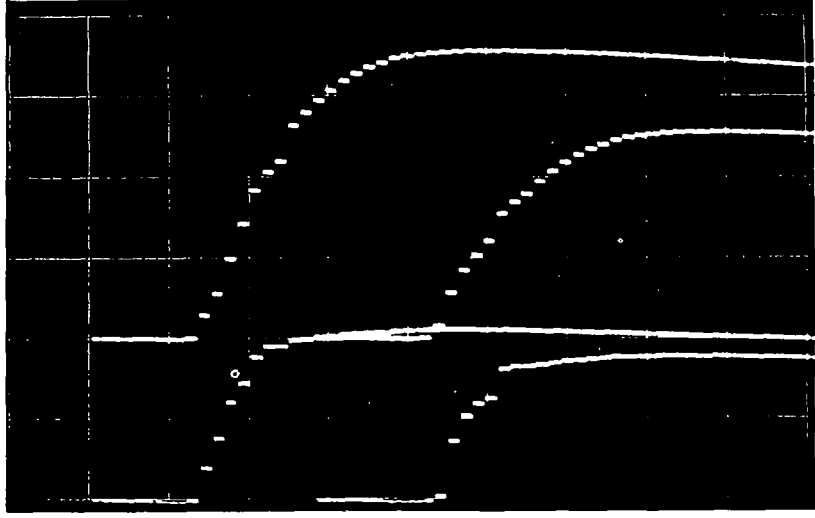
PG-60 70 eV 7.0 cm



L-2 $\begin{matrix} 5.0 \\ 4.5 \\ 4.0 \end{matrix}$ KV 25 μ F .1 ms/cm

Fig. 5. Laser pulses and resulting C_5 from graphite (three laser shots).

PG 36 70 eV 2.5 cm 4.5 KV 25 μ F
60



Up: .05V/cm Ir: .02V/cm 0.1 ms/cm

Fig. 6. Simultaneous integration of C_3 and C_5 from graphite (two laser shots).

the beginning of each cycle) to coincide with a mass peak of interest. Each is adjusted wide enough in time to divert the entire mass peak to the corresponding anode (see Figure 2). The outputs from the anodes are fed directly to the vertical inputs of the multitrace auxiliary oscilloscope (not shown) with its horizontal sweep triggered by the laser. Thus with each laser burst we get a complete, simultaneous time record of the intensity of each mass peak which has been selected for observation for that event. Note that it is not necessary to synchronize the mass spectrometer with the laser; it runs freely and only the oscilloscope sweep is triggered by the laser. Figure 3 was recorded from a dual-trace oscilloscope via a two-gate multiplier and shows the time history of two mass peaks. (Up to six mass peaks can be recorded simultaneously by utilizing a six-gate multiplier available from the manufacturer.) The traces are made up of segments, because they are composed of contributions from successive cycles of the spectrometer operating at 65,000 cycles/sec (i.e. every mass peak occurs at 16 μ sec intervals). It is also evident that these two species are free radicals or condensibles, because their intensity drops to zero immediately after the vapor plume has surged past the ion gun.

Two types of time measurements are possible with this technique: As already shown, the difference in arrival time between two or more molecular species at the ion gun can be measured directly (Figure 3). Secondly, the time lapse between laser pulse and arrival of vapor species at the ion gun can be measured by monitoring the laser beam with a photosensitive device and including that output on the oscilloscope presentation. This is shown in Figures 4 and 5 for identical laser energies and for varied laser energies. It also provides a comparison between laser pulse and resulting vapor pulse shape.

Another useful contribution this technique makes to analytical measurement is in the determination of the relative concentrations of vapor species produced by individual laser bursts. This is most easily accomplished by integrating the previously shown mass pulses electrically; the outputs from the multiplier are fed to the oscilloscope via an integrating circuit (or integrating amplifier). Figure 6 is the result of integrating two masses in this manner, and the vertical displacement of the trace is the integrated value of each one. However, no correction has been included for relative sensitivities or ionization cross-sections.

RESULTS

There are several instrumental factors which need to be considered in applying this time-resolving technique to measuring the velocities of vapor components.

(1) The time duration of the laser pulse (or actually the vapor pulses) must not be too long compared to the travel time of the vapors. Otherwise it is difficult to actually ascertain the travel time.

(2) The repetition rate of the TOF mass spectrometer must be fast enough so that the time between cycles is short compared to the event under study. This is necessary to adequately describe the intensity-time curve of the vapor species. The figures shown here resulted from a repetition rate fast enough so that each mass peak in the spectrum occurred every 16 μ sec during these vapor plumes which lasted two or three hundred μ sec.

(3) If the vaporization occurs at short range to the ion gun or if the vapor molecules travel quite fast, the time of flight in the drift tube between ion gun and multiplier must be subtracted from the overall time. This is also true when

measuring time differences between species of widely separated m/e values. Usually this correction amounts to less than 20 μsec .

(4) In a high vacuum the laser-induced vapors leave the surface at essentially a 2π angle; therefore, there is a trade off between sample distance from the ion gun and detection sensitivity.

Most of the applications of this instrumentation have been related to the study of graphite vaporization at several hundred joules/ cm^2 per laser pulse. We have found the major vapor component to be C_3 and have used this as a basis for comparing the other species. Our tentative conclusions are that C_5 vaporization occurs during a shorter time span than C_3 , but it occurs somewhat sooner, although its thermal velocity is less than C_3 . At increased thermal loadings the time difference between C_5 and C_3 is increased and the ratio C_5 and C_3 is increased and the ratio C_5/C_3 is also increased. The experimental verification that all the vapors do not leave the surfaces simultaneously is important in this work. It means that velocities cannot be calculated by using the time between laser pulse and vapor pulse; instead, the difference in arrival times at two different sample distances must be used: $\text{velocity} = \Delta d/\Delta t$.

So far nothing has been said about thermally-produced ions. We have detected some such ions from graphite at short sample distances, but the spectral resolution has been poor. Furthermore, detection of ions produced at long sample distances requires that they be shielded from stray electric fields, otherwise, they do not reach that critical zone within the ion gun which permits them to be accelerated down the drift tube to the multiplier.

REFERENCE

1. K. A. Lincoln, "Improved Instrumentation for Time-Resolved Mass Spectrometry with Application to Laser-Vaporization of Solid Materials," J. Mass Spectrometry and Ion Physics, 2:75-83 (1969).

V. S. Ban^{*} and B. E. Knox[†]
Materials Research Laboratory
The Pennsylvania State University
University Park, Pa. 16801

Various inorganic substances were vaporized in the ion source of a time-of-flight mass spectrometer by means of a focused laser beam. Substances with relatively low melting points ($T_m < 1000^\circ\text{C}$), such as the elements of groups V-A and VI-A, various compounds consisting of these elements and some V-A - VI-A binary and ternary systems have been studied (1,2). The conditions of laser-solid interaction have been investigated, and a phenomenological model for the laser-induced vaporization has been proposed.

It has been shown that laser-induced vaporization proceeds under conditions significantly different from vaporization produced by other heating methods. Laser-solid interactions can result in surface temperatures of several thousand degrees and pressures of several thousand atmospheres. For many substances the critical temperature and pressure can be reached in the laser-solid interaction, thus providing new possibilities for the study of the behavior of the substances under extreme temperature and pressure conditions, not experimentally achievable before (3). Mass spectrometric analyses of the laser-produced vapor revealed the existence of new and unusual vapor species not discovered previously in vaporization experiments (4). Furthermore, it was shown that in some systems one can correlate the laser-produced vapor species with the structure of the condensed phase. For instance, in the case of As_2O_3 polymorphs, the ionic spectra of arsenolite did not show presence of species containing less than four arsenic atoms; this is consistent with the presence of As_4O_6 molecules in solid arsenolite. On the other hand, lower species were abundant in the ionic spectra of claudetite indicating fracturing of the sheet-like structure of this compound.

In the case of various organic materials, large unfragmented molecules dominate laser-produced vapor (5). The simplicity of the observed mass spectra suggests interesting analytical possibilities for the laser-mass spectrometer.

^{*}Current address: RCA Laboratories, Princeton, N. J. 08540

[†]Also with the Department of Material Science

- (1) Knox, B.E., V.S. Ban and J. Schottmiller, Mat. Res. Bull. 3, 337 (1968).
- (2) Knox, B.E. and V.S. Ban, Mat. Res. Bull. 3, 885 (1968).
- (3) These aspects of laser-solid interaction will be discussed in more details in an article accepted for publication in the Journal of Chemical Physics.
- (4) Paper containing an extensive list of laser-produced vapor species of various substances is accepted for publication in the International Journal of Mass Spectrometry and Ion Physics.
- (5) Vastola, F.J., A.J. Pirone and R.O. Mumma, 16th Conf. on Mass Spect. (ASTM E-14) Pittsburgh, Pa. (1968), pp. 299-301.

ELECTRONIC CONFIGURATIONS AND THE SPARK-SOURCE
MASS SPECTRA OF SOME ELEMENTS

J. M. McCrea
 Applied Research Laboratory
 United States Steel Corporation
 Monroeville, Pennsylvania 15146

Abstract

In spark-source mass spectra of elements, all ions of Li, Be, Na, Mg, Al, and Si that must be produced by ionizing beyond helium-like ($1s^2$) or neon-like ($1s^2, 2s^2, 2p^6$) configurations are much scarcer than would be expected in a regular gradation. The very low values for the Na^{2+}/Na^{1+} and Mg^{3+}/Mg^{1+} intensity ratios show that use of typical $2+/1+$ and $3+/1+$ ratios for iron and many other elements will produce enormous errors in determining sodium and magnesium from the Na^{2+} and Mg^{3+} ion intensities.

Introduction

In the mass spectrometric analysis of solids, the spectra are influenced by the instrumentation and particularly by the ion source used.¹⁾ Craig, Errock, and Waldron described the spectrum of iron as the main example of spectra produced in the radio-frequency spark source.²⁾ They reported that the intensity of multiply charged ions decreased rapidly, approximately by a factor of five, with each ionization. Owens mentions consecutive ionizations up to 16, with the rate of decrease in number of ions with increasing charge quite variable.³⁾ His examples indicate variation with both sample type and instrumental factors. This report is based on the distinctive spectra observed for various elements.

Experiments and Data Acquisition

Spectra were obtained with instrumental factors as constant as possible by the techniques described for analysis of high-purity irons.⁴⁾ As a precaution against misidentification of lines in quantitative analysis, the progression of intensity with charge level was visually inspected on all analytical plates. Photometric data were taken only as required for quantitative analysis, or if the spectra appeared to have unusual intensity progressions.

Visual Results

All spectra obtained for iron samples showed a regular progression of intensity in the series Fe^{1+} to Fe^{n+} where n was typically 7 or more. The estimated factor for decrease in the progression ranged from 2.5 to 3.0, and was smaller than the 5 suggested for different instrumentation.²⁾ Similar progressions were observed for C, Cu, Zn, Nb, Sn, Pt, and Pb.

Samples of aluminum and silicon did not yield regular progressions. The aluminum spectra had three strong lines followed by weak lines for more highly charged ions. Silicon spectra had four lines in a strong progression, followed by two weak lines. The sharp drop in intensity corresponds to ionization beyond the valence shell, and was also noted in special runs with Mg, Be, Na, and Li. Fig. 1 shows several spectra of magnesium. The lines at the $1+$ and $2+$ positions are strong; those at $3+$ and $4+$ positions are much weaker or not even recorded. Divalent beryllium like magnesium gave two strong lines. Only one strong charge level was noted for monovalent Li and Na. Lines for charge exchange processes, such as $Al^{3+}+2+$, $Si^{3+}+2+$, and $Si^{4+}+3+$ were observed only if the initial charge level also gave a strong line.

FIG. 1 MASS SPECTRA OF MAGNESIUM. PLATE EXPOSURES WERE GRADED FROM 50 TO 0.056 NANOCOULOMBS IN 9 APPROXIMATELY GEOMETRIC STEPS AND THEN RANDOMIZED AT 8 LEVELS BETWEEN 1.7 AND 14 PICOCOULOMBS

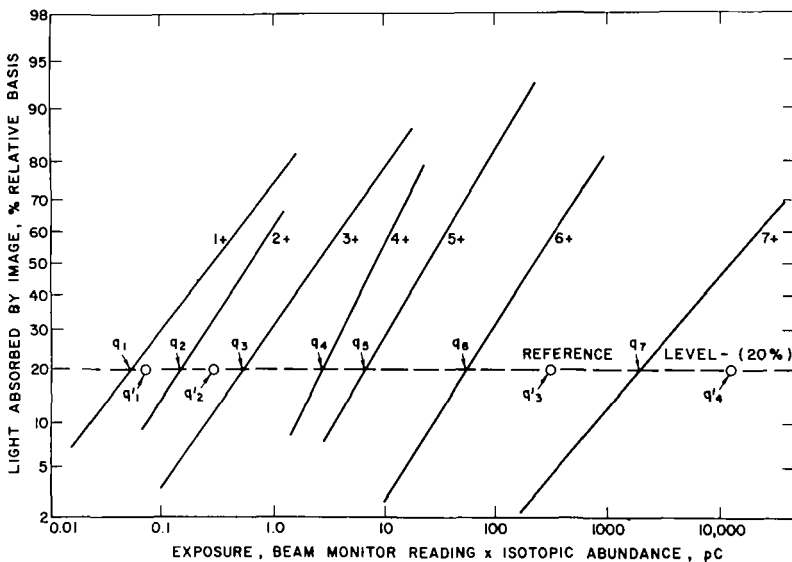


FIG. 2 LOGARITHMIC-PROBABILITY PLOT OF PHOTOMETRIC DATA FOR VARIOUSLY CHARGED IRON IONS (SEE TEXT FOR EXPLANATION OF Q'S)

Results From Photometric Measurements

The data were interpreted by logarithmic-probability plots as in the analysis of high-purity irons.⁴⁾ The relationship of the plots for the iron is conveniently illustrated on a composite plot, Fig. 2. The visually regular progression corresponds to the crudely equal separation of roughly parallel lines on Fig. 2.

Because the slopes differ, exposure comparisons are made at a selected ordinate. The 20% ordinate was selected as a compromise for reducing extrapolations and yet keeping close to the 10% level where Fe^{1+} data for various Q2 plates showed reduced variations.⁵⁾ Let q_1 , q_n denote exposures at which lines plotted for the $1+$ and $n+$ ions cross the 20% ordinate. A plate given an exposure q_1 also receives q_1/q_n times the number of $n+$ ions necessary to produce a 20% level at the $n+$ spectral line. If $n+$ ions are measured by the number of $1+$ ions producing an equivalent response, q_1/q_n is an effective ratio for $n+$ and $1+$ ions in the spectrum.

Effective ratios for the light metals correspond to uneven spacing on a composite plot. The points q_1' , q_2' , q_3' , and q_4' on Fig. 2 show the spacing for the $1+$ to $4+$ magnesium similar to the q_1 , q_2 , q_6 , and q_7 for iron. The difference in ionization between Mg^{2+} and Mg^{3+} corresponds to about four extra steps for Fe^{2+} and is reflected in a sharp drop in intensity on Fig. 1.

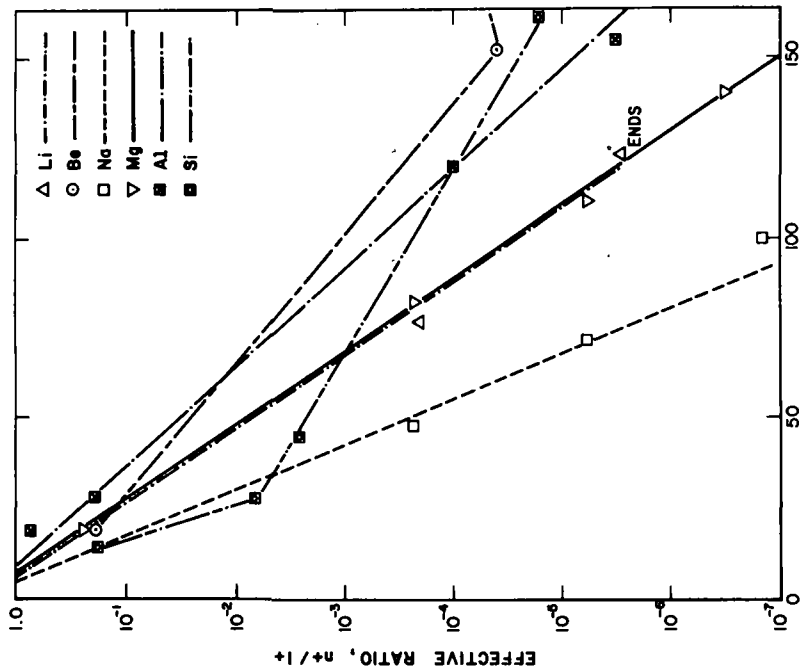
Discussion

Observations on light elements and Table I are consistent with independent measurements and with the periodic table and electronic configurations. Nicholls found that $2+$ ions of the alkali metals from a nonmetallic matrix never account for more than 2% of the total ionization.⁵⁾ Berkey, Sweeney, and Hickam report a rather variable ratio around 3000 for $\text{Na}^{1+}/\text{Na}^{2+}$ that agrees with the reciprocal quantity in Table I.⁷⁾ The trend of Owens' results is different from that in Table I, but different parts of the periodic table are emphasized and no essential inconsistency is present.⁸⁾

Calculations made from Table I show that the intensity of multiply charged ions for several light elements does not decrease by a constant factor with each ionization. Semilog plots of ion charge and effective ratio, Fig. 3, illustrate this behavior. Iron ions from Fe^{1+} to Fe^{6+} show the nearly linear relation typical of a roughly constant factor, but other elements show distinct breaks. The breaks correspond to ions that must be formed by ionization beyond a helium-like ($1s^2$) structure in the case of Li and Be, or beyond a neon-like ($1s^2, 2s^2, 2p^6$) structure for the third period elements. Nicholls' data on the $1+/2+$ ratio for the alkali metals as a class show that the effect of the inert gas structure is present for the heavier alkali metals as well.⁶⁾

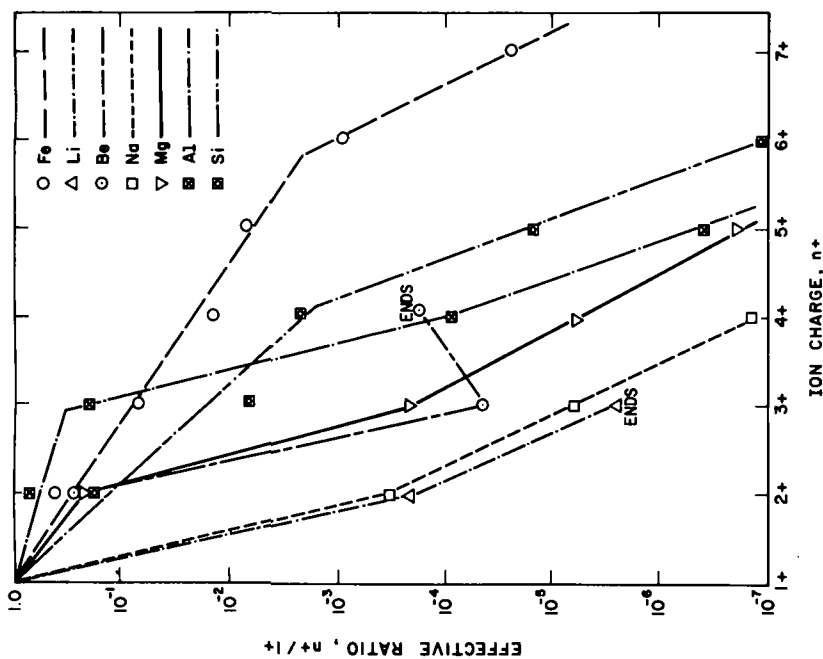
Mechanisms such as electron bombardment, thermal ionization, and field ionization compete in spark-source ionization, and correlations rather than explicit formulas must currently be used to interpret spectra in terms of atomic properties.⁹⁾ Energies of ionization offer an alternative to charge level for correlation with effective ratios. The energy E_n required to convert a $1+$ ion to an $n+$ ion is the sum of $(n-1)$ ionization potentials from the second to the n th. Some third period data are listed in Table II. Ions were observed up to E_n values of 350 volts with the exposures used.

Semilog plots of E_n and the effective ratio $n+/1+$ are distinctly curved; they do not show breaks because a break in E_n through a rare gas configuration compensates for a similar break in effective ratio. On empirical criteria of compensation and linearity, semilog plots of the



n^{th} IONIZATION POTENTIAL, ELECTRON VOLTS

FIG. 4 SEMILOGARITHMIC PLOT OF IONIZATION POTENTIAL AND EFFECTIVE RATIO. POINTS FOR RATIO 1.0 BETWEEN 5.1 AND 9.3 ELECTRON VOLTS NOT SHOWN TO AVOID OVERLAPPING



ION CHARGE, n^+

FIG. 3 SEMILOGARITHMIC PLOT OF ION CHARGE AND EFFECTIVE RATIO. IONIZATION OF LI AND Be IS COMPLETE AT END INDICATED ON THEIR PLOTS

Table I Effective Ratio for n+/l+ Ions

n	Element						
	Li	Be	Na	Mg	Al	Si	Fe
	Effective Ratio						
1+	1.00	1.00	1.00	1.00	1.00	1.00	1.00
2+	2.0 x10 ⁻⁴	2.0 x10 ⁻¹	3.3 x10 ⁻⁴	2.3 x10 ⁻¹	7.7 x10 ⁻¹	1.7 x10 ⁻¹	3.4 x10 ⁻¹
3+	2.7 x10 ⁻⁶	3.7 x10 ⁻⁵	5.5 x10 ⁻⁶	2.2 x10 ⁻⁴	1.1 x10 ⁻¹	7.0 x10 ⁻³	7.5 x10 ⁻²
4+	*	1.8 x10 ⁻⁴	1.5 x10 ⁻⁷	5.3 x10 ⁻⁶	9.6 x10 ⁻⁵	2.6 x10 ⁻³	1.6 x10 ⁻²
5+	*	*	<10 ⁻⁷	3x10 ⁻⁷	3.0 x10 ⁻⁶	1.7 x10 ⁻⁵	7.2 x10 ⁻³
6+	*	*	<10 ⁻⁷	<10 ⁻⁷	<10 ⁻⁷	<10 ⁻⁷	9.3 x10 ⁻⁴
7+	*	*	*	*	*	*	2.5 x10 ⁻⁵
8+	*	*	*	*	*	*	<10 ⁻⁷

* Ions with charge greater than atomic number not allowed.

Table II

Cumulative Ionization Energy E_n of Singly Charged Ions to Higher Ionization

To n Level	Na+	Mg+	Al+	Si+
	E _n , electron volts			
2+	47.29	<u>15.03</u>	<u>18.82</u>	<u>16.34</u>
3+	118.94	95.15	<u>47.26</u>	<u>49.80</u>
4+	217.82	204.44	167.22	<u>94.93</u>
5+	(356.19)	345.67	320.99	261.66
6+	(528.28)	(532.16)	(511.41)	466.77

NOTE: Entries underlined correspond to strong progression ions, regular entries to observed ions in weak progressions, and entries in parentheses to ions detected very weakly or not at all.

nth ionization potential and the $n^+/1^+$ ratio are more satisfactory, in spite of an inconsistency in referring ratios to a 1^+ level and energies to an $(n-1)^+$ level. Several straight-line relationships for light metals can be seen in Fig. 4, along with relations for beryllium and silicon that are not straight. Owens has used similar plots for his data.⁸⁾

Although electronic configurations and ionization potentials explain the effective ion ratios, two points remain to be mentioned: conversion of effective ratios to number ratios and the effect of uneven progressions on analytical results. In the ion-optics used, the energy of the n^+ ion is n times that of a 1^+ ion and the width of the spectral lines may be different. Available data, such as Owens',¹⁰⁾ on the energy variation of the Q2 plate are for energies well below the normal energies of multiply charged ions in the spectrometer, and correction involves extended extrapolation not yet subjected to experimental check. Both energy and width factors act to make the number ratio substantially less than the effective ratio; quantitative evaluation should await data on ion beams of different charge by simultaneous current measurement or particle counting methods.

No analytical problems arise if results are based on 1^+ ions, but some techniques for avoiding interferences use lines for 2^+ and 3^+ ions. One is the use of Na^{2+} for Na, presumably with the assumption of a "normal" ratio for $1^+/2^+$ near five.²⁾ Although data from the Na^{1+} line may be high as a result of surface ionization of sodium impurity, the sodium from Na^{2+} lines could be low by a factor of several hundred. Similar use of Mg^{3+} to avoid interferences of $^{24}\text{Mg}^{2+}$ with $^{12}\text{Cl}^{1+}$ and $^{24}\text{Mg}^{1+}$ with $^{12}\text{C}_2^{1+}$ would also introduce vast errors if ratios for the spectrum of magnesium were not used. Ideally, data for a matrix of similar work function and composition should be obtained for calibration of these analyses.

Summary

Spark-source spectra of some light elements have a sharp break in the progression of intensity with the ion charge. They correspond to ionization of a rare-gas-like configuration and to similar irregularities in ionization potentials. If ions such as Na^{2+} and Mg^{3+} with charge levels above the break are used for analytical determinations, correct data for the spectrum are necessary. Very large errors result from an assumption of a regular progression such as that for iron.

Literature Cited

1. Mass Spectrometric Analysis of Solids, A. J. Ahearn, ed., Elsevier Publishing Co., Amsterdam (1966).
2. R. D. Craig, G. A. Errock, and J. D. Waldron, in *Advances in Mass Spectrometry*, (Pergamon 1959), pp. 136-155.
3. E. B. Owens, in Ref. 1, pp. 90-92.
4. J. M. McCrea, *Appl. Spectry*, 23, 55 (1969).
5. J. M. McCrea, *Appl. Spectry*, 21, 305 (1967).
6. G. D. Nicholls, Eastern Analytical Symposium, New York, Nov., 1968.
7. E. Berkey, G. G. Sweeney, and W. M. Hickam, *Nuclear Applns.* 5, 344 (1968).
8. E. B. Owens, in *Advances in Mass Spectrometry*, Vol. 3, (Institute of Petroleum, London, 1966), pp. 200-204.
9. R. E. Honig, in Ref. 1, pp. 27-34.
10. E. B. Owens, *Appl. Spectry*, 16, 148 (1962).

THE MASS SPECTROMETRIC ANALYSIS OF A SERIES
OF ELEMENTS AS VOLATILE IODIDES

James E. Delmore, Jr.
Idaho Nuclear Corporation
Idaho Falls, Idaho 83401

A series of elements has been evaluated as to suitability for mass spectrometric analysis as volatile iodides in a crucible source mass spectrometer (Hitachi RMU-6E). Particular attention was paid to the practicability of applying isotope dilution techniques to submicrogram quantities of the element. In this paper, four aspects of this type of analysis will be discussed: (1) The practicability of synthesizing the desired iodide from submicrogram quantities of the starting material. (2) The conditions under which the compounds have been analyzed. (3) The sensitivities of the individual iodides. (4) The forms of memory exhibited in the mass spectrometer. These four aspects will be discussed for six elements, the II-B series and the three heaviest of the V-A series.

Of these six elements, only those of the II-B series (Zn, Cd, Hg) have proven to meet the stringent requirements for isotope dilution and are quite practical to analyze by the method. The method could be extended to several other elements if the memory problem could be overcome. It has been shown that the element must be baked from the ion source for memory to be eliminated; hence, an extension of the bakeout temperature to much higher levels would open new possibilities.

ON THE ABSOLUTE EFFICIENCY OF ION BOMBARDMENT SOURCES OF MASS SPECTROMETERS

Juergen M. Schroerer

Department of Physics, University of Wyoming, Laramie, Wyoming 82070

INTRODUCTION

When mass analyzing solid samples, the problem is always how to produce ions of the different elements composing the solid. One technique for doing this is to bombard the sample with inert gas ions, and then to utilize the sputtered particles. Most of them are neutral atoms, but a small fraction, of the order of 10^{-5} to 10^{-3} consists of ions. A mass spectrometer might use the sputtered ions directly for the analysis of the mass to charge ratio, or ionize the sputtered neutral atoms by an electron beam. This latter technique is rather inefficient because of the high velocity of the sputtered atoms. Using the ions directly is more efficient, but requires a knowledge of the probability with which sputtered atoms become ionized as they leave the surface.

I will present here an equation for the probability of ionization, the theoretical justification for it, and experimental evidence in support of it.

The total sputtering yield S for a pure element is defined as the ratio of the number of sputtered atoms to the number of bombarding ions,

$$S = \frac{[M^0] + [M^+]}{[A^+]} = \frac{[M^0]}{[A^+]}, \quad (1)$$

where $[M^0]$, $[M^+]$, and $[A^+]$ are the numbers of sputtered neutrals, sputtered ions, and incident ions, respectively.

Similarly, we can define the sputtering yield for ions

$$S^+ = \frac{[M^+]}{[A^+]}. \quad (2)$$

The probability of ionization is

$$R = \frac{[M^+]}{[M^+] + [M^0]} = \frac{S^+}{S} = \frac{[M^+]}{[M^0]}. \quad (3)$$

In practice, the mass spectroscopist would measure the apparent sputtering yield for ions,

$$Y^+ = cS^+, \quad (4)$$

where c is the concentration of the element of interest in the sample. In fact, he measures Y^+ and would like to deduce c from it, i.e.,

$$c = Y^+/S^+ = Y^+/SR. \quad (5)$$

Thus in any particular determination of c , in addition to Y^+ , S and R need also be known.

In this paper we are concerned primarily with R .

THEORY

Past attempts at the interpretation of the ionization of sputtered atoms considered

the Langmuir-Saha equation,

$$R = \exp - (I-\phi)/kT, \quad (6)$$

where I is the ionization energy of the sputtered atom, ϕ the work function and T the temperature of the surface. Since Eq. (6) was derived under the assumption of thermal equilibrium between the surface and an evaporated atom, Eq. (6) is not expected to be applicable to sputtering which is not an equilibrium process. In fact, the temperature dependence predicted by Eq. (6) is not observed.⁽¹⁾

A quantum mechanical calculation of the probability of ionization R is more fruitful.⁽¹⁾ Fig. 1 shows a simple energy level diagram at the metal surface. Initially, the valence electron belonging to the sputtered atom is in the conduction band. As the sputtered atom slowly leaves the surface, the wave function of its valence electron slowly changes from that appropriate to the conduction band, to that of an electron in the ground state of the free atom. But since the potential seen by the electron changes, even if slowly, there is a small chance of a transition to a state different from the ground state of the free atom. The nearest and most dense states are those at the top of the conduction band.

The so-called adiabatic approximation⁽²⁾ gives the probability of such a transition,

$$R = \left| \int_{-\infty}^{\infty} \langle \psi_f^* | \partial H / \partial t | \psi_i \rangle (I-\phi)^{-1} \exp [i(I-\phi)t/\hbar] dt \right|^2. \quad (7)$$

ψ_i and ψ_f are the initial and final wavefunctions of the electron, and $\partial H / \partial t$ is the rate of change of the potential as seen by the electron.

It is difficult at best to evaluate the matrix element

$$Z(t) = \langle \psi_f^* | \partial H / \partial t | \psi_i \rangle \quad (8)$$

exactly. But we do know that a plot of $Z(t)$ versus time t must have the following characteristics: $Z(t) \rightarrow 0$ as $t \rightarrow \pm \infty$; $Z_{\max} = A/\Delta t$, where A is the binding energy of a surface atom and Δt the time it takes the sputtered atom to penetrate the surface; and $Z(t)$ has a width at half maximum of Δt . Also, $\Delta t = a/v$, where " a " is the thickness of the surface, and v the velocity of the sputtered atoms.

For simplicity's sake, we assumed two reasonable, alternative expressions for $Z(t)$, which satisfy the above conditions, and which make Eq. (7) integrable:

$$Z_1(t) = \frac{A}{\Delta t} \exp - |t|/\Delta t, \quad \text{and} \quad Z_2(t) = \frac{A}{\Delta t} \frac{1}{1 + 4(t/\Delta t)^2}.$$

Substituting Z_1 and Z_2 into Eq. (7) yields

$$R_1 = \left(\frac{A}{I-\phi} \right)^2 \left[\frac{\hbar v}{a(I-\phi)} \right]^4, \quad (9)$$

and

$$R_2 = \left(\frac{A}{I-\phi} \right)^2 \frac{\pi^2}{4} \exp - \frac{(I-\phi)a}{\hbar v}. \quad (10)$$

Since the choices of Z were somewhat arbitrary, it was decided to generalize Equations

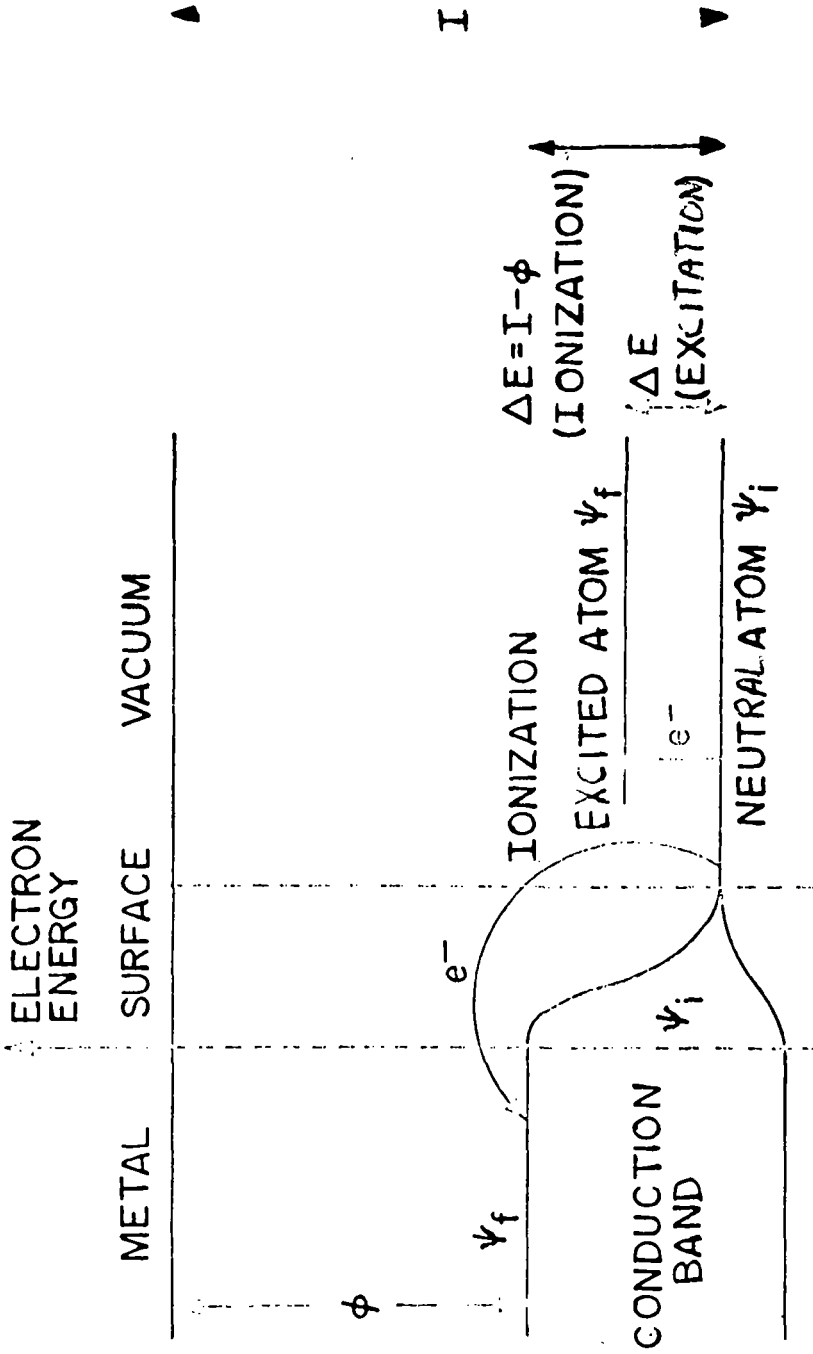


Fig. 1. Energies and wavefunctions of an atomic electron as a sputtered atom leaves the surface.

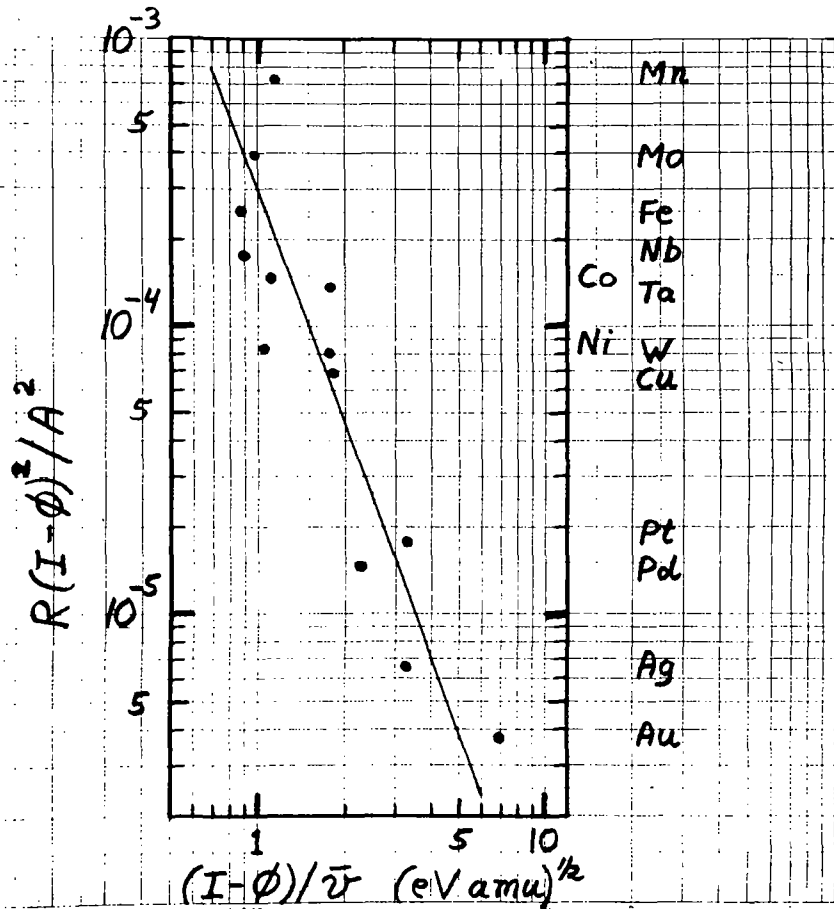


Fig. 2. Probability P of ionization of an atom during sputtering of different metals, under bombardment with 12 keV argon ions. I is the ionization potential, \bar{v} the average velocity, and A the binding energy of the sputtered atom; ϕ is the work function of the surface.

(9) and (10) to

$$R_3 = \left(\frac{A}{I-\phi} \right)^2 \left[\frac{h\nu}{a(I-\phi)} \right]^n \quad (11)$$

Eq. (11) will be fitted to available experimental data, with n and "a" as the adjustable parameters.

EXPERIMENTAL DATA

Fig. 2 shows the fitting of available experimental data to Eq. (11). Various metals were bombarded by 12 keV argon ions. R was measured by Beske⁽³⁾, the values for \bar{v} were derived from the data of Kopitzki and Stier,⁽⁴⁾ for A the bulk sublimation energy was used,⁽⁵⁾ and I and ϕ were obtained from a standard handbook.⁽⁶⁾

Values of $n = 2.7$ and $a = 1.4 \text{ \AA}$ gave the best fit to the data points, which all lie within a factor of three of the solid line. It is impossible to say right now to what extent the scatter of the experimental points is due to inaccurate data and to what extent to inadequacies in Eq. (11). By looking at the shape of $Z_1(t)$ and $Z_2(t)$, together with the definition of $\Delta t = a/v$, it is seen that the actual thickness of the surface is at least $2a = 2.8 \text{ \AA}$. This is what one would expect on the grounds that the thickness of the surface should be about one lattice constant, which for most metals is of the order 3 to 5 \AA .

PRACTICAL CONSIDERATIONS

Equations (5) and (11) can be combined into

$$c = \frac{Y^+}{S} \left(\frac{I-\phi}{A} \right)^2 \left[\frac{a(I-\phi)}{h\nu} \right]^n \quad (12)$$

For the case of a sample consisting of a basic metal with some impurities in it, Eq. (12) can be simplified. We assume for the velocity \bar{v} of the sputtered impurity atoms of mass m_2 that

$$\bar{v} = v_0 \frac{2m_1}{m_1 + m_2}, \quad (13)$$

where v_0 is the velocity of a sputtered basic metal atom of mass m_1 . Eq. (13) holds exactly for head-on elastic collisions. Substituting Eq. (13) into Eq. (12), and combining various constants into a new constant K , we obtain

$$c = KY^+ \left(\frac{m_1 + m_2}{2m_1} \right)^n (I-\phi)^{n+2} \quad (14)$$

I applied Eq. (15) to data⁽³⁾ on the sputtering of Fe samples which had impurities of either Mn, Cr, V, C, Cu, Ni, or Mo in it with concentrations between 10^{-4} and 10^{-1} (100 to 100,000 ppm). The agreement between Eq. (14) and the experimental values was within a factor of 3 to 4.

REFERENCES

1. J. Schroer, T. N. Rhodin, and R. C. Bradley, to be published.
2. L. I. Schiff, Quantum Mechanics, 2nd Ed., (McGraw-Hill, New York, 1955), p. 213.

3. H. Beske, Z. Naturforschung 22a, 459 (1967).
4. K. Kopitzki and H. E. Stier, Z. Naturforschung 17a, 346 (1962).
5. Handbook of Chemistry, 10th Ed.
6. Handbook of Chemistry and Physics, 49th Ed.

EXPERIMENTAL AND CALCULATED CONSECUTIVE
METASTABLE PEAKS IN TOLUENE

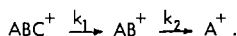
Lorin P. Hills, Jean H. Futrell, Austin L. Wahrhaftig
University of Utah, Salt Lake City

Introduction.

Unimolecular dissociations which are observed in a mass spectrometer as metastable peaks occur around a microsecond after formation of parent ion. They result normally from parents having internal energy only slightly above the activation energy. The resulting primary ionic fragment, sharing the small amount of available energy with the neutral fragment, is unlikely to undergo further dissociation. Examples have recently been found,¹⁻⁴ however, of ions dissociating in the first field free region of a double focusing mass spectrometer (region I) with the resulting primary fragment dissociating further in the second field free region (region II). The occurrence of such a delayed consecutive process seems likely to require rather special conditions under the framework of the quasi-equilibrium theory of mass spectra.⁵ An experimental study of such a consecutive system combined with extensive theoretical calculations provides an interesting test for the statistical approach.

Fractional Abundance Expressions.

Consecutive dissociations of the type described above require that the primary and secondary rates be competitive in the metastable range. It is necessary, therefore, that both rates be included in the expressions for peak intensities. Consider the general reaction:



Solution of the normal rate expressions gives for fractions of ions leaving the source (source residence time = τ_1):

$$ABC^+ = e^{-k_1 \tau_1} \quad (1)$$

$$AB^+ = \frac{k_1}{k_1 - k_2} [e^{-k_2 \tau_1} - e^{-k_1 \tau_1}] \quad (2)$$

$$A^+ = 1 - \frac{k_1 e^{-k_2 \tau_1} - k_2 e^{-k_1 \tau_1}}{k_1 - k_2} \quad (3)$$

ABC^+ and AB^+ are subject, however, to further dissociation in flight. For some time $t > \tau_1$ we have

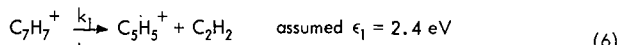
$$ABC^+(t, \tau_1) = e^{-k_1 t} \quad (4)$$

$$AB^+(t, \tau_1) = \frac{k_1 e^{-k_2 t}}{k_1 - k_2} [1 - e^{-(k_1 - k_2) \tau_1}] \quad (5)$$

A normal peak or metastable intensity is obtained by substituting the proper value(s) of residence time(s). A more complete derivation and the full list of functions for all peaks calculated may be found in the formal publication.⁶

Calculations.

We selected for calculations and experimental study the toluene consecutive reactions:



This system is of special interest due to the observation of a very small metastable peak corresponding to a dissociation in the first field free region (region I):



This may be entirely due to fast consecutive reactions (6) and (7) occurring within a single region. We therefore wished to compare the calculated consecutive -1,1 peak with this observed peak.

The rates were calculated using the method of Vestal, Wahrhaftig and Johnston.⁷ The first activated state was assumed to be preceded by tropylium ring cleavage. The

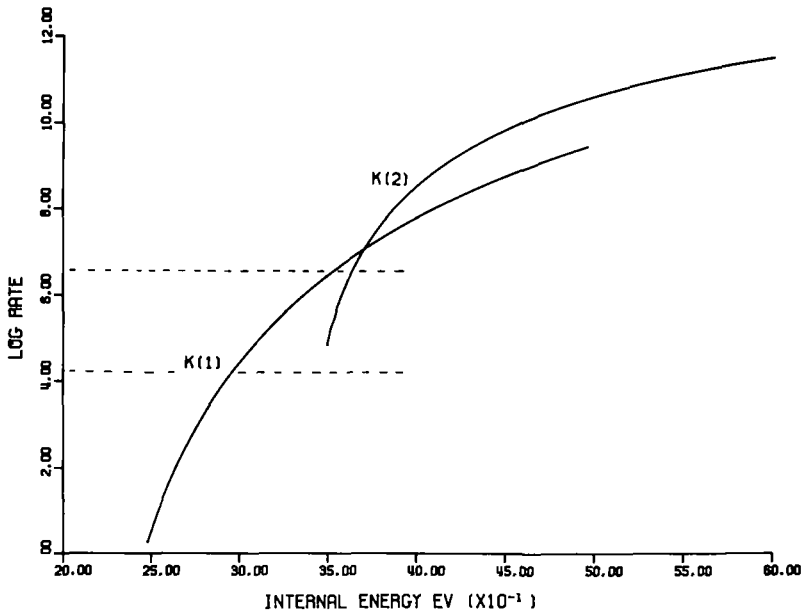


Figure 1. Calculated Primary and Secondary Rates.

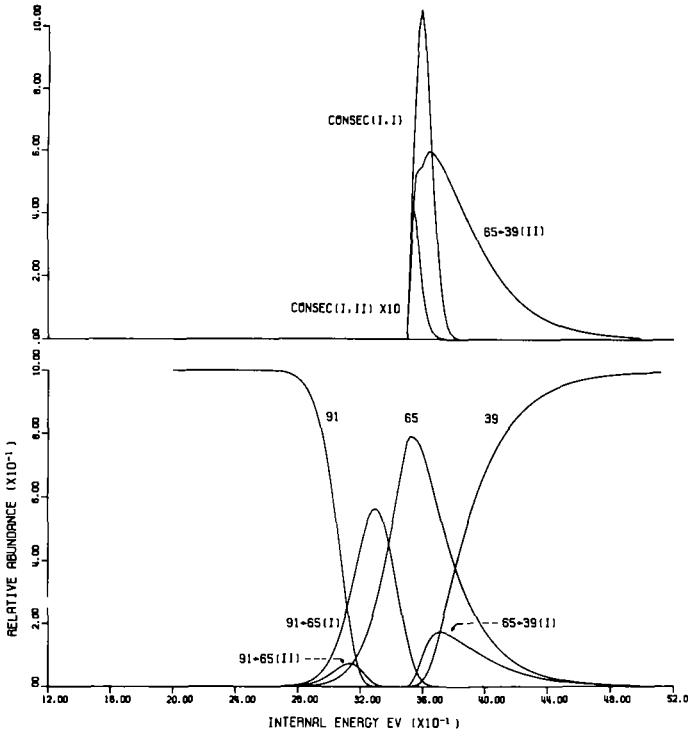


Figure 2. Breakdown Curves for Tropylum Ion.

rates (Figure 1) are plotted as $k_1(E)$, where E = energy in $C_7H_7^+$, and $k_2(E - \epsilon_1)$, i.e., no energy lost to neutral primary fragment or reaction coordinate. The actual breakdown curves (Figure 2) include a distribution of energies given to the neutral. They are calculated using the proper fractional abundance expressions (for example, Eq. 5) and are not normalized to unity.

The breakdown curves as a function of internal energy can be compared with experiment by assuming an energy transfer function which is constant over the energy range 2.8 to 4.8 eV and normalizing the peak areas to the known intensity $65^+ = 14.0$. The results are shown in Table I. The experiments were done on a CEC 21-110 mass spectrometer with the usual voltage control modifications.

TABLE I
Experimental Relative Abundance vs. Calculated Peak Areas
($65^+ = 14$)

Species	Exp. R. A.	Calculated
65^+	14.	14.
$91 \rightarrow 65(I)$	2.2	5.9
$91 \rightarrow 65(II)$	0.20	0.52
$65 \rightarrow 39(I)$	0.25	2.0
$65 \rightarrow 39(II)$	0.010	0.094
Consec. (I, I)	0.013	0.043
Consec. (II, II)	Not Observed	9.3×10^{-14}
Consec. (I, II)	$\sim 6 \times 10^{-4}$	1.1×10^{-3}

Discussion and Conclusions.

We found, as expected, that consecutive metastable peaks will not be observed unless primary and secondary rates compete over some portion of the region corresponding to metastable formation. This range is approximately defined by the dotted line in Figure 1. This places an upper limit on ϵ_2 the secondary activation energy. A lower limit for ϵ_2 is indicated by the very high initial secondary rate. This rate rises rapidly with decreasing ϵ_2 and a value only about 0.3 eV smaller would result in a rate too high for metastable observation.

While the calculated metastable peaks are all larger than experiment, we feel the relative agreement is quite satisfactory. The study indicates strongly that the process $C_7H_7^+ \rightarrow C_3H_3^+ + C_4H_4$ does not occur as a single-step reaction.

References.

1. K. R. Jennings, Chem. Commun. (London), 1966, 283.
2. J. Seibl, Helv. Chim. Acta, 50, 263 (1967).
3. R. A. Koob, L. P. Hills, J. H. Futrell, submitted to J. Phys. Chem. (1969).
4. C. H. Ottinger, presented Seventeenth Annual Conference on Mass Spectrometry, Dallas, Texas, 1969.
5. H. M. Rosenstock, M. B. Wallenstein, A. L. Wahrhaftig and H. Eyring, Proc. Natl. Acad. Sci. U. S., 38, 667 (1952).
6. L. P. Hills, J. H. Futrell and A. L. Wahrhaftig, submitted to J. Chem. Phys., 1969.
7. M. Vestal, A. L. Wahrhaftig and W. H. Johnston, J. Chem. Phys., 37, 1276 (1962).

Energetic metastable transitions and their applications to the dissociation processes and structural transformations of aromatic molecules under electron impact (*)

Pierre Nounou
Laboratoire d'Applications THOMSON-CSF
51 Bd de la République - 78 Chatou
France

Introduction

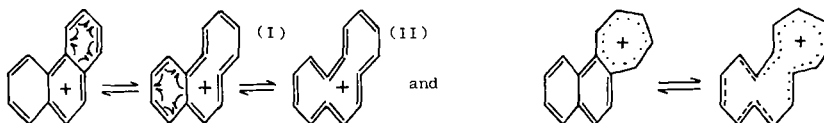
The so called metastable peaks of a mass spectrum are essentially due to decompositions of "metastable" ions occurring during their flight from the source to the collector of a mass spectrometer. As such, they can provide a direct, and, consequently, accurate information on the cracking pattern of a molecule under electron impact, but also on the structures of its resulting fragments. The purpose of this paper is to describe the study of metastable peaks applied to phenanthrenic ions, as an attempt to verify fundamental hypotheses concerning skeletal rearrangements of the molecular ions and drawn from preceding studies of their ionization processes (1) and mass spectra (2). These two studies constitute with the present one an interpretation method of the dissociation processes under electron impact of large aromatic molecules. We have previously applied this method to the phenanthrenes and methyl-phenanthrenes (3) which are studied here.

Experimental

All experiments were carried out both on double and single focusing mass spectrometers operating in the same conditions. The results obtained by means of the double focusing apparatus have been previously described elsewhere (3). Some of them are presented in Fig. 1. More accurate and complete experiments were subsequently carried out on a 30 cm radius of curvature, 60° sector field simple focusing THOMSON-CSF THN 206 mass spectrometer; its 52 cm distance between the ion source exit slit and the entrance boundary of the magnetic field represents a quite suitable condition for the occurrence of metastable peaks. All measurements were made using 70 Volt ionizing electrons with a controlled trap current of 120 μ A. The source temperature was 220°C; the source pressure was of the order of $5 \cdot 10^{-6}$ Torr while the pressure in the analyser tube was of the order of 10^{-8} Torr.

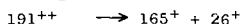
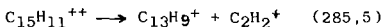
Results and discussion

The principal metastable peaks observed and assigned to specific decompositions are listed in table I. They are quite consistent with similar reactions studied for other smaller aromatic molecules such as benzene and naphthalene. In Fig. 1 is presented the peak corresponding to the loss of an ethylenic fragment by the phenanthrenic ion ($178^+ \rightarrow 152^+$) first obtained by the double focusing apparatus (a) and then by the single focusing one (b). Under the same operating conditions, the peak shapes observed are quite identical and roughly gaussian for this reaction type. The kinetic energy determined from the width of this peak is, within experimental error, in good agreement with the results of Eland (4). Other similar peaks corresponding to the loss of C_2 and C_2H fragments expected and observed for the phenanthrenic and diphenylic ions, but not for the anthracenic or naphthalenic ions, seem to attest the existence of electron impact induced rearrangements pointed out by the ionization processes study and giving rise to the mesomeric phenanthrenic or "pseudo-tropylic" ions :



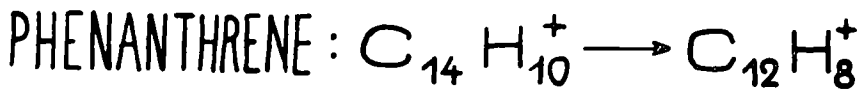
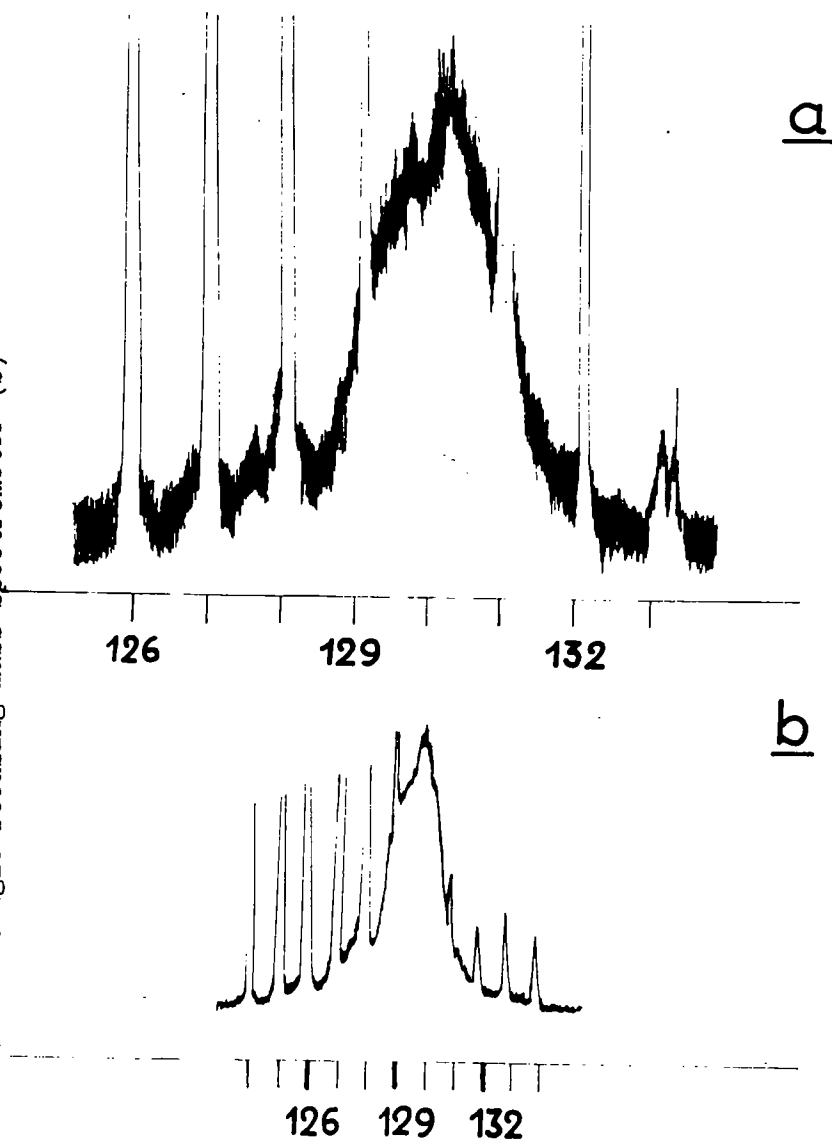
These could also be radical ions (3). The portions of methyl-phenanthrene mass spectra represented in Fig. 2, 3 and 4 exhibit three groups of broadened metastable peaks occurring at masses higher than the molecular mass. Pressure versus ion current plots for the most of them indicated that the contribution of collision induced dissociation were not significant.

a) The first of these broad metastable peaks observed in the range $m/e = 280$ to $m/e \approx 290$ can easily be ascribed to the decomposition of a doubly-charged ion into two singly-charged ions :



(*) a more detailed account of this work has been submitted to the "Journal of mass spectrometry and ion physics".

Fig. 1 - Metastable peaks corresponding to the transition $178^+ \rightarrow 152^+ + 26$ obtained by means of a double focusing mass spectrometer (a) and by means of a single focusing mass spectrometer (b)



a) Me.9.Ph.

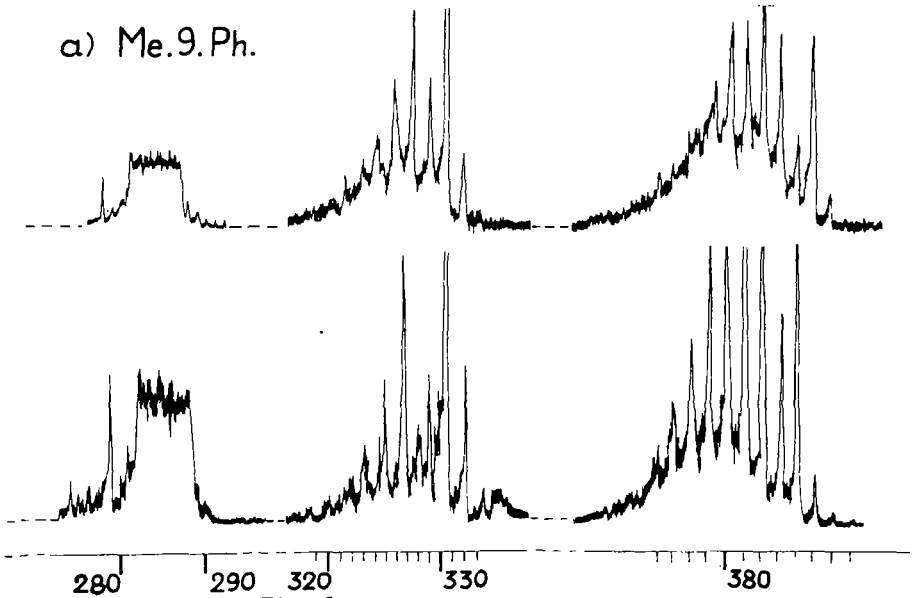


Fig. 2 -

Mass spectra of the 9-methyl-phenanthrene (a) and the 1-methyl-phenanthrene (b) obtained by means of a single focusing mass spectrometer THN 206 and recorded at masses higher than $m/e = 192$

b) Me.1.Ph.

Me.9. Anth.

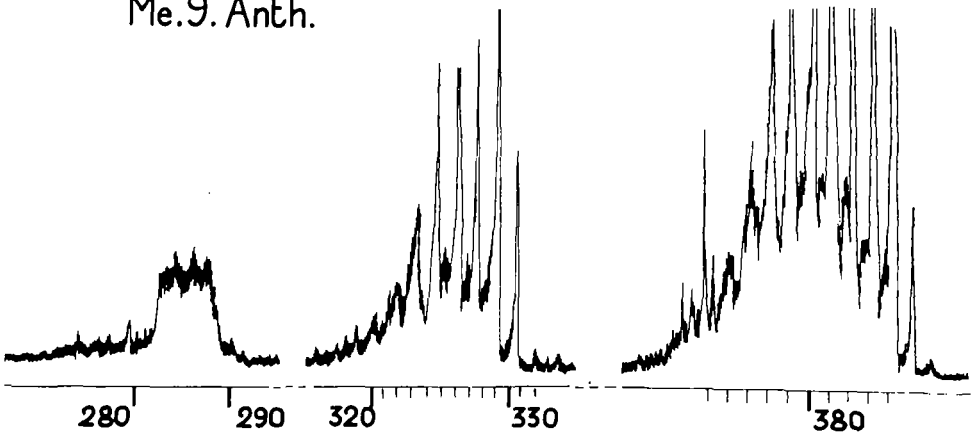
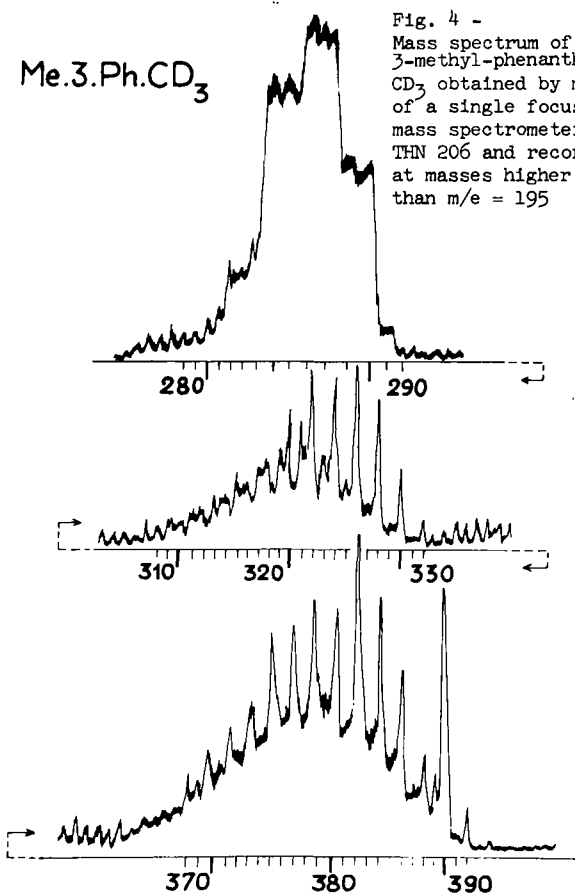


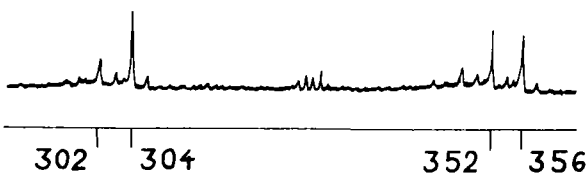
Fig. 3 - Mass spectrum of the 9-methyl-anthracene obtained by means of a single focusing mass spectrometer THN 206 and recorded at masses higher than $m/e = 192$

Me.3.Ph.CD₃

Fig. 4 -
Mass spectrum of the
3-methyl-phenanthrene
CD₃ obtained by means
of a single focusing
mass spectrometer
THN 206 and recorded
at masses higher
than m/e = 195



Phenanthrene



Anthracene

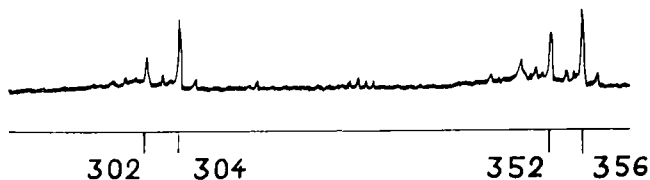
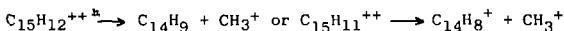


Fig. 5 -
Mass spectra of the phenanthrene (a) and anthracene (b)
obtained by a single focusing mass spectrometer THN 206
and recorded at masses higher than m/e = 178

In fig. 2 and 3 the great intensity of these peaks outlines the important contribution of the polycharged ions to the total ionization of aromatic molecules. The metastable peak shown in fig. 4 and assigned to the similar dissociation reaction of the methyl-1-phenanthrene-CD₃ is splitted into three ones at least; these are well resolved and their mid points correspond closely to the expected losses of C₂H₂⁺, C₂HD⁺ or C₂D₂ by the C₁₅H₉D₂⁺⁺ or C₁₅H₈D₃⁺⁺ pseudo-tropylic deuterated ions, the relative intensities of each peak being proportional to the probability of each reaction. The accurate widths of the metastable peaks enable us to find a very strong kinetic energy released by the preceding reactions, of the order of 5 to 6 eV. If all this energy is, according to Beynon (5), the result of repulsion between two positive charges in the doubly-charged parent ion, it can be equalled to the work required to bring two unit charges from infinity to their distance in the doubly-charged ion, which would then be of 2,6 = 2 x 1,3 Å²; this inter-charge distance would be equal to the diameter of a tropylic ring, which each 191⁺ ion was assumed to contain. Actually part only of the energy released in the reaction arises from the charge separation, so that the inter-charge distance is surely shorter than the above calculated one, which seems to assert the skeletal rearrangement we have assumed. Furthermore the identity of the shape of each peak and the equality of the kinetic energy released by each reaction seem to involve an identity of structure for each (M-26)⁺ fragment ion. This consequence, giving by the way an information about the activation energies calculations (7), is quite consistent with the fundamental hypothesis of the quasi-equilibrium theory which can thus be reasonably extended to large aromatic molecules. In fact, the peak shapes being the same only depend on the kinetic energy distribution; this means that the unimolecular decomposition of excited ions depends only on its excitation energy and not on the way in which this energy may be transferred.

b) The second group of metastable peaks consists in metastable peaks masked by normal peaks. The metastable peaks observed in the range of m/e = 320 to m/e = 332 can be ascribed to the reactions :



leading to fragment ions of fluorenic structure by loss of CH₃⁺ groups.

c) The third group of peaks in the range of m/e = 376 to m/e = 384 arises from the loss of H⁺ or H₂⁺ respectively by the molecular doubly charged or by the pseudo-tropylic 191⁺⁺ ions; correspondently the peaks 1⁺ and 2⁺ have been observed in each mass spectrum as well as the peaks 3⁺ and 4⁺ in the mass spectra of the deuterated compounds.

As regards the normal peaks masked by the two preceding groups of metastable peaks, they can be due to duplicated ions of the molecular ions, or of the most intense fragment ions; these dimerized ions can then dissociate according to the same cracking pattern of their monomer. Such processes can even be seen for the phenanthrenic and anthracenic ions on the mass spectra shown in fig. 5; the photosensitized dimerization of the anthracene molecule was already well known (6). Among the many possible structures which can be assigned to these dimerizations, the most probable seem correspond to bridges between the different carbon atoms of phenanthrenic radical ions having the structures I and II or by means of -CH₂- groups of methyl-phenanthrenic radical ions. These would be "head to tail" dimerized ions and would represent a significant consequence of the skeletal rearrangements postulated at the beginning. However, "head to head" dimerized compounds of essentially fluorenic fragment ions can be taken in account and responsible for the normal peaks observed in the second group. But these peaks can also be due to fragment ions arising from the decomposition of the first ones observed close to the double molecular mass m/e = 384. The expected dimerized ions arising from the dimerization processes of the 1-methyl-phenanthrene-CD₃ can be found in the mass spectrum shown in fig. 4.

References

- (1) - P. Nounou - J.Chim.Phys. 40, 914 (1966)
- (2) - P. Nounou - J.Chim.Phys. 65, 700 (1968)
- (3) - P. Nounou - Ph.D. Thesis, University of Grenoble (1968)
- (4) - J.H.D. Eland - Private communication
- (5) - J.H. Beynon and A.E. Fontaine - Chem. Comm. 717 (1966)
- (6) - See for example R. Calas, P. Mauret and R. Lalonde - C.R. Ac. Sc. 247, 2146 (1958)
- (7) - P. Nounou - Advances in Mass Spectrometry, Vol. 4, 551 (1968)

Acknowledgment

The author is indebted to Miss B. Renahy for assistance in this work.

Table I
Observed metastable transitions (***)

1) Phenanthrene

$178^+ \longrightarrow 177^+$	m = 176
$178^+ \longrightarrow 176^+$	174
$178^+ \longrightarrow 163^+$	149,26
$178^+ \longrightarrow 152^+$	129,8
$178^+ \longrightarrow 154^+$	133,24
$178^+ \longrightarrow 126^+$	89,20 (*)
$178^{++} \longrightarrow 163^{++}$	74,6
$178^{++} \longrightarrow 152^{++}$	64,90
$178^{++} \longrightarrow 154^{++}$	66,60
$178^{++} \longrightarrow 139^{++}$	54,27
$178^{++} \longrightarrow 126^{++}$	44,52
$178^{++} \longrightarrow 153^{++}$	65,60
$152^+ \longrightarrow 126^+$	104,43
$152^{++} \longrightarrow 126^{++}$	52,22
$126^+ \longrightarrow 100^+$	79,40

2) 1-methyl-phenanthrene

$192^+ \longrightarrow 191^+$	190
$192^+ \longrightarrow 190^+$	188
$192^+ \longrightarrow 177^+$	163,17
$192^+ \longrightarrow 166^+$	143,52
$192^{++} \longrightarrow 191^+ + H$	380 (**)
$192^{++} \longrightarrow 177^+ + 15^+$	326,34(**) and 2,34
$192^{++} \longrightarrow 166^+ + 26^+$	287,04(**) and 7,04
$191^+ \longrightarrow 165^+$	142,53
$191^+ \longrightarrow 176^+$	162,18
$191^+ \longrightarrow 152^+$	120,96
$191^{++} \longrightarrow 190^+ + H^+$	378 (**)
$191^{++} \longrightarrow 166^{++}$	71,80
$191^{++} \longrightarrow 166^+ + 25^+$	289 (**) and 6,53
$191^{++} \longrightarrow 165^+ + 26^+$	285 (**) and 7,08
$166^{++} \longrightarrow 140^{++}$	59

(*) - represented in fig. 1

(**)- represented in fig. 2 and 3

(***) m is the observed centre of each peak

U. Löhle and Ch. Ottinger
 Physikalisches Institut der Universität Freiburg, Germany

We have studied consecutive metastable decompositions of the type first reported by Jennings¹ and at this meeting by Hills, Futrell and Wahrhaftig. In ethane, propane, butane, heptane, cyclohexane and cycloheptane we have found about 50 of these processes, in which an ion A decomposes into B and then into C, each step occurring with a delay of several μ secs.

A conventional 60° 8" radius instrument was used which was equipped with an electrostatic ion energy analyzer between the exit slit and the detector. In this arrangement, the first metastable transition, occurring between ion source and magnet, is detected in the conventional manner by the non-integral mass. The second decomposition step, occurring between the magnet and the electrostatic analyzer, is detected by a further reduction of the kinetic energy of the ions.

Careful checks on the pressure dependence of the decompositions were made. The analyzer tube was differentially pumped, and through a special gas inlet krypton gas was admitted to raise the pressure from 6×10^{-8} to about 1×10^{-6} Torr. This permitted a clear evaluation of the pressure-independent contribution, which was done in every case.

The following examples illustrate various aspects of these consecutive metastables. In heptane 17 processes were found. Their intensities ranged between 10^{-5} and 8×10^{-4} percent of the intensity of the base peak. With few exceptions a two-step process is intense if and only if the individual steps $A \rightarrow B$ and $B \rightarrow C$, measured as normal metastables, are sufficiently intense. This can be best illustrated by cases where the intermediate ion B decomposes in several competing ways:

n-heptane	I	I _{BC}	cyclo-hexane	I	I _{BC}	
	55 ⁺	0.00080	0.090	41 ⁺	0.00039	0.51
100 ⁺ → 70 ⁺ → 42 ⁺	0.00065	0.075	84 ⁺ → 56 ⁺ → 40 ⁺	0.00005	0.09	
	28 ⁺	0.00002	0.005	28 ⁺	0.00003	0.072

The first column gives the intensities of the three consecutive processes, the second those of the second decomposition steps occurring as normal metastable transitions. As would be expected, the first column is roughly proportional to the second. There are also examples for the inverse situation, where several ions A decompose into the same intermediate B, and this into C:

n-heptane	I	I _{AB}
57 ⁺	0.00017	0.41
43 ⁺ ↘ 41 ⁺ + 39 ⁺	0.00050	0.56
42 ⁺ ↗	0.00001	0.031

Again, the consecutive metastable intensities are about proportional to the intensities of the first step AB occurring as a normal metastable.

On the whole it appears that in the case of heptane the consecutive metastables can be described simply as a succession of two normal metastables. For a molecule as large as heptane the rate constant for the first step $A \rightarrow B$ rises rather slowly with the internal energy, so that this step can still occur as a metastable at excitation energies large enough for a secondary decomposition to occur. We know experimentally the dependence of the heptane decomposition rate constant on the internal energy.² It rises quite slowly, from 10^5 to 10^6 sec^{-1} over an energy interval as large as 0.5 eV. The width of this energy band may be sufficient to explain the consecutive metastables in heptane on the basis of the statistical theory alone, without invoking any special mechanism.

However, this is not true for the other gases we studied. In ethane, propane and butane we found analogous consecutive metastables consisting of the loss of an H atom from the parent ion followed by the loss of an H₂ molecule. These are compared in the following table with the intensities normalized to the respective total ionizations.

		I _{AB}	I _{BC}	I	E _{act} (eV)
ethane	30 ⁺ → 29 ⁺ → 27 ⁺	0.0045	0.059	$4.5 \cdot 10^{-5}$	2.5
propane	44 ⁺ → 43 ⁺ → 41 ⁺	0.25	0.05	$6.8 \cdot 10^{-5}$	~1.8
butane	58 ⁺ → 57 ⁺ → 55 ⁺	0.00022	0.00045	$1.9 \cdot 10^{-5}$	0.8

Here it is obvious that the consecutive metastables have nothing to do with the normal metastables. The first step $A \rightarrow B$ as a normal metastable shows a very strong intensity variation among the three gases. This is well understood; the breakdown curves given by Chupka & Berkowitz³ demonstrate why propane should have a very intense transition, ethane much weaker and butane extremely weak. By contrast, the observed intensities I for the consecutive processes are all quite similar. This suggests that a specific mechanism is operative, possibly even the same in the three gases, which delays the loss of the H atom from some highly excited parent ions. The last column of the table gives the activation energy for the H₂ loss; it seems impossible to explain by the usual

statistical theory how a parent ion whose internal energy exceeds the threshold for H loss by this much could live for several microseconds. It is especially surprising that this failure of the statistical theory occurs at excitation energies rather high above the threshold, where one would expect a particularly good coupling between the internal modes.

There are also examples where the second decomposition step is not governed by the principles of the statistical theory.

		cyclo-hexane		cyclo-heptane	
		I	I _{BC}	I	I _{BC}
$69^+ + 41^+ \rightarrow$	39^+	0.0001	0.04	0.00004	0.38
	15^+	0.000017		0.00002	
		0.000023		0.00015	
$56^+ + 41^+ \rightarrow$	39^+	0.0006	0.000023	0.00002	0.00001
	15^+	0.000012		0.00001	

The mass 41 ion can decompose into mass 39 and also into mass 15, after it itself has been formed by a metastable transition from either a mass 69 or a mass 56 ion. It is very clear that the ratio of the consecutive metastable intensities I has nothing to do with the ratio of the normal metastable intensities I_{BC}.

Some of the mass 41 ions are prepared by the preceding metastable transition from 69 or 56 in such a state, that their further decomposition to mass 15 is not in competition with the decomposition to mass 39. This particular state may be distinguished by a special persistent isomeric structure or alternatively by certain excited energy levels which do not couple with other states.

REFERENCES

- 1) K. R. Jennings, Chem. Comm. (London) 283 (1966).
- 2) I. Hertel und Ch. Ottinger, Z. Naturf. 22a, 1141 (1967).
- 3) W. A. Chupka and J. Berkowitz, J. Chem. Phys. 47, 2921 (1967).

METASTABLE IONS IN THE MASS SPECTRA OF N_2 , NO, N_2O , AND NO_2 ^{1,2}

Amos S. Newton and A. F. Sciamanna

Lawrence Radiation Laboratory
University of California
Berkeley, California 94720

Except for a report by Kupriyanov³ on the existence of a metastable dissociation in CO^{++} , no metastable ions have been reported in the mass spectra of diatomic molecules. Metastable ions have been studied in the mass spectra of the triatomic species CO_2 ,⁴ N_2O ,^{5,6} NO_2 ,⁶ and H_2S .⁷

Using a CEC Model 21-103B mass spectrometer which was modified to increase the pumping speed in the analyzer tube, to increase the sensitivity of the D. C. amplifier, and to accurately measure potentials applied to the metastable suppressor, metastable ions have been observed in the mass spectra of N_2 and NO. In N_2O and NO_2 metastable dissociation of N_2^+ and NO^+ were also observed.

Metastable peaks which have been observed in these molecules are:

- 1) $N_2^+ \rightarrow N^+ + N$ $(M/q)^* = 7.00$ from N_2 and N_2O
- 2) $NO^+ \rightarrow O^+ + N$ $(M/q)^* = 8.53$ from N_2 , N_2O , and NO_2
- 3) $N_2O^{++} \rightarrow N^+ + NO^+$ $(M/q)^* = 8.91$
- 4) $N_2O^+ \rightarrow NO^+ + N$ $(M/q)^* = 20.45$
- 5) $NO_2^+ \rightarrow NO^+ + O$ $(M/q)^* = 19.57$

Each of these transitions has been shown to proceed by a unimolecular mechanism.

Half lives for the metastable dissociations have been studied by various methods. For reaction (3), studies on an AEI-MS9 high resolution instrument with an ion transit time from source to collector of about 7 μsec , showed that no N_2O^{++} ions exist ($<10^{-4}\%$ of N_2O^+ intensity) at that time after formation.⁸ Therefore $M/q = 22$ in N_2O represents N_2O^{++} plus CO^{++} background and a half life of N_2O^{++} is obtainable from an ion-accelerating voltage discrimination curve of the intensity of $M/q = 22$. A value of $t_{1/2} = 0.46 \pm 0.05$ μsec was found. For the other transitions, especially those in Eqs. (1) and (2), the method of Hipple⁹ could not be applied owing to the low intensity of these peaks even under the best conditions of focus. Therefore accelerating voltage discrimination curves of the intensity of the metastable peak were compared to computer calculated curves in assessing the half lives.

Kinetic energy release in the metastable dissociation was evaluated from the width of the metastable suppressor cutoff curves of the metastable ion peak.

The Tables I, II, and III give data on these transitions as a function of the source of the metastable ion.

Table I. Data for the transition $N_2^+ \rightarrow N^+ + N$, $(M/q)^* = 7.00$, with source of N_2^+ .

Source	N_2	N_2O
$t_{1/2}$ (μsec)	≥ 0.15	≥ 0.15
T (eV)	0.55 ± 0.10	0.20 ± 0.05
AP (eV, obs.)	24.9 ± 0.3	27.5 ± 0.5
AP (eV, calc.)	24.85	26.18
ΔAP (obs. - calc.)	---	~ 1.3

Table II. Data for the transition $\text{NO}^+ \rightarrow \text{O}^+ + \text{N}$, $(M/q)^* = 8.53$, with source of NO^+ .

Source	NO	N_2O	NO_2
$t_{1/2}$ (μsec)	≥ 0.18	≥ 0.18	≥ 0.18
T (eV)	0.04 ± 0.02	0.13 ± 0.03	0.13 ± 0.13
AP (eV, obs.)	20.2 ± 0.2	27.5 ± 0.5	24.6 ± 0.5
AP (eV, calc.)	20.14	25.16	23.35
ΔAP (obs. - calc.)	---	~ 2.3	~ 1.3

Table III. Data for miscellaneous transitions in N_2O and NO_2 .

Transition	$\text{N}_2\text{O}^{++} + \text{N}^+ + \text{NO}^+$	$\text{N}_2\text{O}^+ + \text{NO}^+ + \text{N}$	$\text{NO}_2^+ + \text{NO}^+ + \text{O}$
$(M/q)^*$	8.91	20.45	19.57
$t_{1/2}$ (μsec)	0.46 ± 0.05	0.09 ± 0.01	$[0.7]^a$
T (eV)	6.5 ± 0.5	> 0.3	$[2.5]$
AP (eV, obs.)	36.5 ± 0.5	$[1.05 \pm 0.05]$	$[1.1]$
AP (eV, calc.)	35.2	15.23	$[0.5]$
ΔAP (obs. - calc.)	~ 1.3	~ 0.5	---

^aBracketed figures are from Ref. 6.

In Table I, for $\text{N}_2^+ \rightarrow \text{N}^+ + \text{N}$, the half life is seen to be independent of source but the kinetic energy release changes from 0.55 eV from N_2 as a source to 0.20 eV from N_2O as a source. From N_2 the observed AP equals that calculated from the dissociation limits, but from N_2O as a source, about 1.3 eV of energy is unaccounted for. It is assumed that this is kinetic energy released in the initial fast fragmentation of $\text{N}_2\text{O}^+ \rightarrow (\text{N}_2^+)^* + \text{O}$. A similar situation exists in the metastable dissociation $\text{NO}^+ \rightarrow \text{O}^+ + \text{N}$, in the mass spectra of N_2O and NO_2 .

In regard to the mechanism of the metastable dissociation, three mechanisms are considered. 1) A slow radiation from a higher bound state to a dissociative state. The half life is then the radiation lifetime. This is impossible in Eqs. (1) and (2) since with N_2 and NO as sources, the calc. and obs. AP's are equal, leaving no energy for radiation. 2) A tunneling mechanism through a low barrier to dissociation. In $\text{N}_2^+ \rightarrow \text{N}^+ + \text{N}$ from N_2 and N_2O sources, the difference in T would imply a difference in half life of at least a factor of 100 for tunneling. Since the half lives are essentially equal, this mechanism can be discarded. 3) A predissociation mechanism in which a bound state is crossed by a repulsive state. The crossing must be a forbidden one. In $\text{NO}^+ \rightarrow \text{O}^+ + \text{N}$, the state in NO^+ is probably an unknown higher triplet which is crossed by the ${}^5\Sigma$ state to the dissociation limit at 20.101 eV. In $\text{N}_2^+ \rightarrow \text{N}^+ + \text{N}$, possible states of N_2^+ are the ${}^2\Sigma_u^-$, ${}^2\Delta_u$, and ${}^2\Pi_u$ states with a forbidden crossing of the ${}^4\Pi_u$ state to the 24.301 eV dissociation limit. All of the bound states radiate to the $D\ {}^2\Pi_g$ state by allowed transitions but the radiation would be of low energy (< 3 eV) hence have a long half life.

The dissociation of N_2O^{++} may proceed by mechanism 1), with the half life being determined by the radiation lifetime of ~ 1.3 eV radiation from a bound state to a repulsive state of N_2O^{++} .

Footnotes and References

1. This work was performed under the auspices of the U. S. Atomic Energy Commission.
2. Long abstract combining results of two papers to be published in *J. Chem. Phys.*
3. S. E. Kupriyanov, *Soviet Physics-Technical Physics* 9, 659 (1964).
4. A. S. Newton and A. F. Sciamanna, *J. Chem. Phys.* 37, 2167 (1962).
5. G. M. Begun and L. Landau, *J. Chem. Phys.* 35, 547 (1961).
6. A. S. Newton and A. F. Sciamanna, *J. Chem. Phys.* 44, 4327 (1966).
7. V. H. Dibeler and H. Rosenstock, *J. Chem. Phys.* 39, 3016 (1963).
8. The authors thank Dr. R. M. Teeter of Chevron Research Company for this determination.
9. J. A. Hipple, *Phys. Rev.* 71, 594 (1947).

FAST H(2S) ATOMS PRODUCED BY DISSOCIATIVE
EXCITATION OF MOLECULES

R. Clampitt

U.K.A.E.A., Culham Laboratory, Abingdon,
Berkshire, England.

A B S T R A C T

The detection and time-of-flight resolution of fast H(2S) atoms from dissociative excitation of H₂ by electron impact has been reported^(1,2). These atoms were studied by detecting Lyman- α photons arising from Stark-effect quenching of the atoms in an electric field⁽¹⁾ and by counting electrons ejected on de-excitation at a metal surface⁽²⁾. In the latter method, photons and H₂(c³ff) molecules are also detected. Time-of-flight resolution of H(2S) atoms from electron impact on H₂O, NH₃, and other molecules has been reported recently⁽³⁾. The method is as follows. A molecular beam is formed by effusion through a honeycomb array of glass capillaries and intersects a pulsed electron beam (~ 10 μ A) of 200 ns duration and 5 kHz repetition rate. Charged particles are removed from the beam by a combination of weak electric and magnetic fields. Metastable atoms are detected by electron ejection from the earthed cathode of an 18-stage electron multiplier. Pulses from the anode, operating at + 3 kV, are amplified and processed by a time-to-height converter and pulse-height analyser to produce a time-of-flight spectrum [P(t)] of excited particles. It can be shown that the observed excited species are H(2S) atoms by quenching them in a localised electric field (~ 100 V/cm) beyond the excitation region whereupon the spectrum disappears. Furthermore, if a lithium fluoride window is moved into the path of the beam to ensure that no excited particles reach the detector, P(t) distributions of the electric field-induced photons from the 1S \leftrightarrow 2P transition can be obtained.

In the hydrogen halides two metastable excited fragments are produced⁽⁴⁾: one is a fast H(2S) atom; the other cannot be quenched and has a time-of-flight corresponding to the parent molecule. The slow fragment could be an excited parent molecule but could also be an excited halogen atom since, on dissociation, the unexcited H atom would

carry away almost all of the kinetic energy. Electron excitation and time-of-flight analysis of the halogen molecules, viz. I_2 , Br_2 , etc., shows that excited atoms are produced in considerable abundance⁽⁴⁾. Therefore it seems not unreasonable to suggest that the thermal metastable species from the halogen halides might be a halogen atom.

It is significant that every one of the two dozen or so molecules examined so far gives electronically excited neutral fragments of one sort or another. These excited atoms probably result from super-excited states of the molecule such as those predicted by Platzman⁽⁵⁾. At electron impact energies greater than the ionisation energy of the molecules a process of dissociative excitation into excited atoms can occur in addition to dissociative excitation.

REFERENCES

1. Leventhal, M., Robiscoe, R.T. and Lea, K.R., Phys. Rev. 158, 49, 1967.
2. Clampitt, R., and Newton, Amos S., J. Chem. Phys. 50, 1997, 1969.
3. Clampitt, R., Physics Letters, 28A, 581, 1969.
4. Clampitt, R. (to be published).
5. Platzman, R.L., Radiation Res., 17, 419, 1962.

METASTABLE ION INTENSITIES AND IONIC STRUCTURE

J. L. Occolowitz

Lilly Research Laboratories, Indianapolis, Indiana, 46206

Expressions are derived which relate the relative intensities of metastable ions resulting from reactions of an ionic species to the energy distribution of progenitor molecular ions and the rate constants for the reactions involved. Two cases are considered, viz., where all reactions of the ion occur from a single state and where the reactions arise from different states.

For the case where all reactions arise from a single state, the derived expression shows that there may be some variation in the metastable intensity ratio for reactions of ions of identical structure derived from different origins. This variation arises because of differences in the energy distribution of molecular ions and differences in the rate of formation of the ions whose reactions lead to the metastable ions considered. It is estimated that in these cases variations of 30-50% are not unusual.

The relative intensity of metastable ions arising from reactions of more than one state of an ion are much more dependent on the molecular ion energy distribution. If more than one reacting state is involved, the determination of two or more metastable intensity ratios can show which reactions occur from states common to all origins.

Experimental results are presented for $C_2H_4O_2$ ions derived from acetic and substituted acetic acids, C_6H_{10} ions derived from cyclohexene and cyclohexyl acetate, and C_8H_6O ions derived from coumarin, benzofuran, and *o*-ethynylphenol.

Scheduled for publication in full in the September, 1969, issue of the Journal of the American Chemical Society.

ENERGETIC METASTABLE DECOMPOSITIONS*

K. C. Smyth and T. W. Shannon

The Dow Chemical Company
Eastern Research Laboratory
Wayland, Massachusetts 01778

The observation of flat-topped metastable peaks¹ has prompted a renewed interest in the shape of metastable peaks. The flat-topped nature of certain metastable peaks is attributed to the release of internal energy in the decomposing ion as relative translational energy of the products.¹ A comprehensive study of the shape of metastable peaks has been carried out² considering the effects of instrument discrimination, finite beam dimensions angular spreading and kinetic energy released during the decomposition. These calculations revealed that it was not possible to match experimental and computed peak shapes using a discrete value of the kinetic energy released. As the distribution of kinetic energy released in any such transition may be a sensitive indicator of the nature of the reaction involved, we have extended the original calculations in an effort to obtain the distribution of kinetic energies released in a metastable decomposition.

The basic equations used in this work have been developed previously² for a decomposition occurring in the field-free region according to the reaction,



where T is the total amount of kinetic energy released as kinetic energy of the products, the apparent mass of the metastable ion is given by

$$m^* = m_2 \frac{E_\alpha R^2}{E_0 R_2^2} = \frac{m_2^2}{m_1} \frac{R_2}{R_2^2} \left[1 + \frac{\mu T}{E_0} \cos^2 \theta \pm 2 \cos \theta \cos \theta \sqrt{\frac{\mu T}{E_0}} \right] \quad (2)$$

E_0 is the initial energy of m_1^+ and E_α is the energy of m_2^+ entering the magnetic field at an angle α to the normal ion direction and traversing a path of radius R_2 through the magnetic field. A collector slit discrimination term is included in the calculations which takes into account the finite dimensions of the ion beam.

The $31^+ \rightarrow 29^+$ Transition: This metastable transition occurs in methanol and gives a flat-topped metastable peak at m/e 27.13. The observed peak shape is shown in figure 1 and corresponds to the reaction



The width W of the top of the peak gives a measure of the energy released and the slopes of the sides of the peak equals $(W_{max} - W)/2$. The observed energy release in the transition is 1.5 eV.

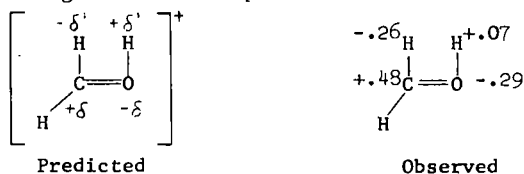
Attempts to match the experimental peak using various distributions of energy released indicated that the true energy distribution involves a greater probability of high energy values. The calculated energy release (corresponding to W) was set equal to the average energy \bar{E} . The distribution shown in figure 2, constructed through a process of trial and error results in a calculated metastable peak shape in excellent agreement with the observed peak. The release of such a large amount of kinetic energy in the transition and the distribution of the energy raises the possibility that excited as well as ground electronic states may be involved in the reaction.

The Reaction Mechanism: To test the importance of electronic states in the reaction, molecular orbital calculations were performed in which the effect of removing the elements of hydrogen from the reacting ion was studied. The method used has been amply discussed and documented.³⁻⁵

The $m/e=31$ is considered as protonated formaldehyde and calculations indicated that the ground state of the system is totally planar. The C-H and O-H distances were set equal to 1.09 Å and 0.96 Å respectively while both the HCH and COH angles were put equal to 120° . The C-O distance used was 1.32 Å, intermediate between the single and double bonds in methanol and formaldehyde. The CH_2OH^+ ion in this configuration is a member of the C_s point group. Of the seven in-plane normal modes only the one which is a combination of an HCH wag and COH bend brings the hydroxyl hydrogen close to a carbonyl hydrogen. The course of the reaction used for the

Calculations is shown in figure 3 and approximates the normal mode motion. The reaction distance is defined as the distance from the mid-point of a line joining the two hydrogen atoms to the center of the C-O bond. This distance was varied from 0.83 to 2.20 Å with a corresponding change of 2.35 to 0.74 Å in the H-H distance.

The reaction considered is a 1-2 elimination of hydrogen requiring the formation of a 4-center transition state, and may be discussed in terms of Benson and Bose's semi-ion pair model.^{6,7} In order to pass from the ground state of the reactants to the products, a concerted polarization of the O-H and C-H bonds in opposite directions must occur. This state is an association of two semi-ion pairs with a formal charge on each atom equal to half the electron charge. Energy is required to polarize the bonds and this accounts for most of the activation energy for the reaction. Once this is accomplished, charge transfer will proceed smoothly with the resulting formation of products.



The calculated net charges of the system indicate initially a high net positive charge on the oxygen atom in accord with the oxonium structure. As the reaction proceeds the change in the net charges is very pronounced with a maximum change occurring at a reaction distance of about 1.4 Å. The corresponding dipolar structure, shown above, has resulted in the reversal of the relative magnitudes of the charges on carbon and oxygen. Similar effects on the hydroxyl and carbonyl hydrogens are observed. With further extension of the reaction distance the charges on the oxygen and carbon reverse and the hydrogens become neutral.

The relative bond orders between the four atoms involved also undergo significant changes. At a distance of about 1.4 Å the bond orders of the OH, CH and HH bonds are approximately equal. No significant H-H bonding occurs until the reaction distance is approximately 1.3 Å and at this distance the major changes in the net charge distribution have already occurred. It appears that formation of the semi-ion pairs is necessary before any significant bonding can occur in the transition state.

An interesting picture is revealed on examination of the wavefunctions for the molecular orbitals involved in the reaction. Of major interest are the two highest filled and two lowest vacant orbitals. The highest vacant orbital considered involves mainly in-plane p_z orbitals on the carbon and oxygen atoms and 1s orbitals on the hydrogen atoms. The relative signs are such that the H atoms are bonding to each other, the p_z orbitals are bonding and the 1s-2p interaction is antibonding. This molecular orbital is thus very characteristic of the products, and we have given it the designation $\sigma^* \sigma$ indicating anti-bonding between H-C and O-H and bonding between the hydrogens.

The lowest vacant orbital involves two out-of-plane p_y atomic orbitals on the oxygen and carbon atoms. These orbitals are of opposite sign and thus antibonding so that this molecular orbital is designated π_y^* . Due to its out-of-plane nature it is not involved during the course of the reaction.

The highest occupied molecular orbital again involves 2p_z orbitals on the carbon and oxygen and 1s orbitals on the hydrogens. In this case it resembles the reactants in that it is bonding for the hydrogens to the carbon and oxygen and anti-bonding between the hydrogens. The orbital is designated $\sigma \sigma^*$. The last orbital considered is designated σ_x and involves bonding 2p_x orbitals on the carbon and oxygen and a 1s orbital on the third hydrogen atom.

The changes in the energy of these four orbitals during the course of the reaction is shown in figure 4. The $\sigma \sigma^*$ orbital, which resembles the reactants, becomes destabilized during the course of the reaction. As may be expected, the $\sigma^* \sigma$ orbital becomes increasingly more stable as the reaction proceeds. These two orbitals appear to cross. The crossing

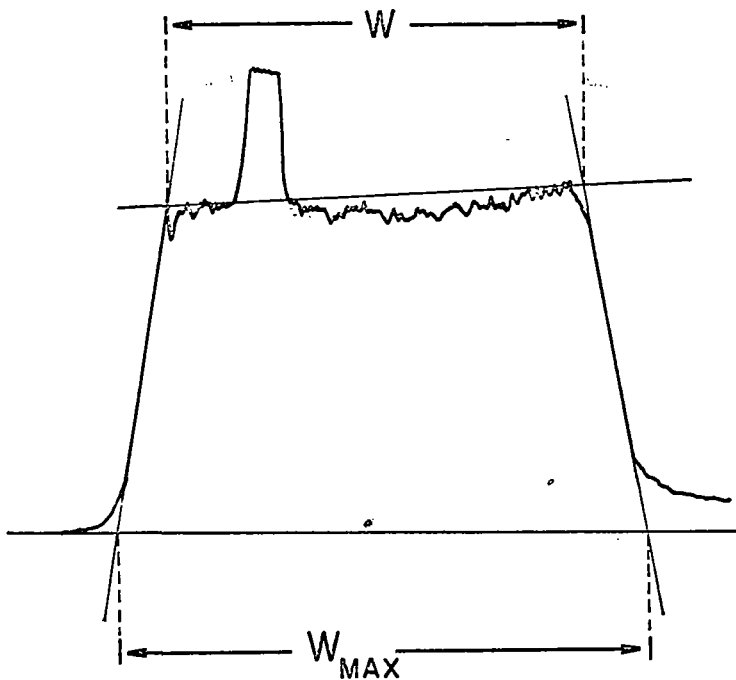


Figure 1. Observed peak shape for the transition $\text{CH}_2\text{OH}^+ \rightarrow \text{HCO}^+ + \text{H}_2$ in methanol.

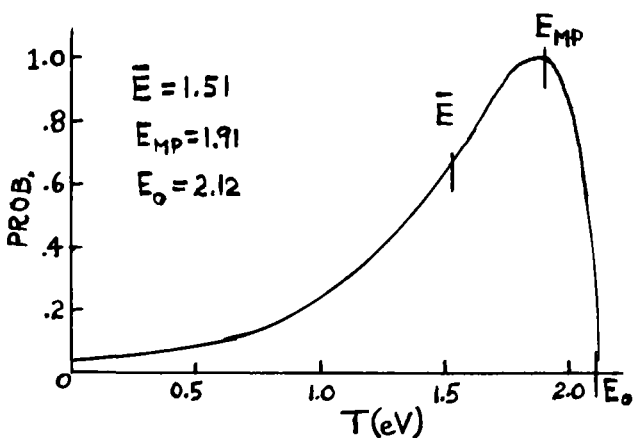


Figure 2. Calculated distribution of kinetic energy release.

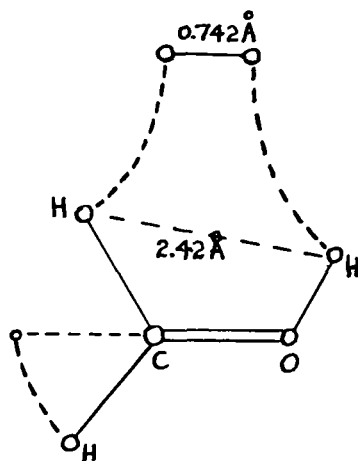


Figure 3. Atomic motions during the course of the elimination reaction.

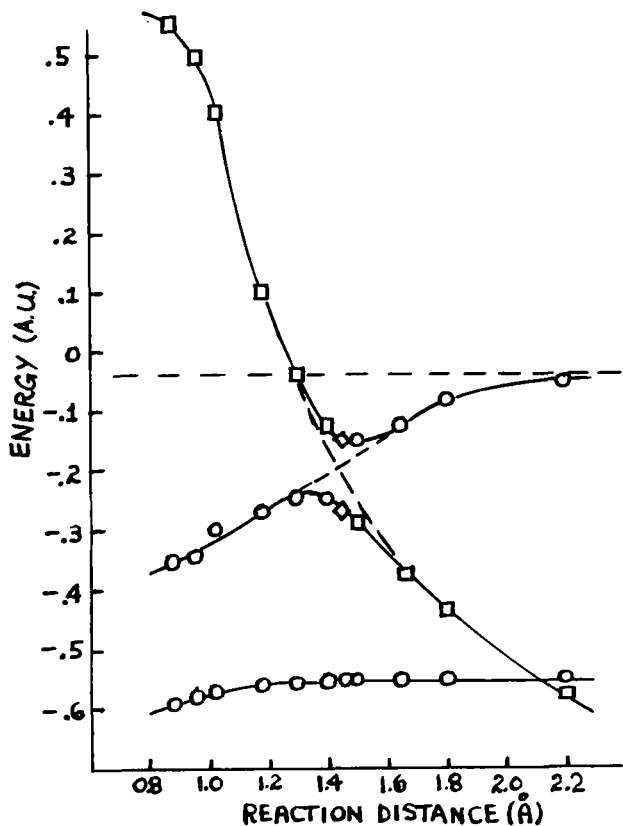


Figure 4. Orbital energy changes occurring during the elimination reaction.

point for these two orbitals occurs almost exactly at a reaction distance equal to 1.45 Å, i.e. at the transition state. The system however possesses very low symmetry, the only element of symmetry being the plane of the system. As the $\sigma\sigma^*$ and $\sigma^*\sigma$ orbitals involve pz, px and 1s orbitals both molecular orbitals are symmetric with respect to the plane and thus may not cross. At the transition state the system is degenerate since the two orbitals have the same energy. This introduces a resonance energy which separates the surfaces so that they never actually intersect but only approach each other closely.

Although all the planar orbitals of the system change as a function of the reaction distance, the most severe changes in energy occur in the $\sigma\sigma^*$ and $\sigma^*\sigma$ orbitals. Thus figure 4 mirrors the crossing of the electronic states of the system where the $\sigma\sigma^*$ orbital represents the ground electronic state and the $\sigma^*\sigma$ orbital represents a repulsive excited electronic state. If the reactant ion possesses sufficient internal energy so that the reaction distance will change with a finite rate, there is a finite probability that the ion will change from the ground electronic state to the excited electronic state. Once this has occurred, the ion will immediately decompose into HCO^+ and H_2 and the products will separate with an amount of translational energy approximately equal to the energy difference between the crossing point and the asymptote of the repulsive state. Thus a mechanism exists for the conversion of internal energy into translational energy of the products and the states involved are identified.

Discussion

The transfer of the system to a repulsive electronic state, although permitting a large energy release to occur, would also result in immediate dissociation. However, metastable peaks in a mass spectrometer are the result of decompositions in the first drift region proceeding with a rate of 10^5 to 10^6 sec^{-1} . Dissociations from a repulsive state are usually of the order of 10^{12} to 10^{13} sec^{-1} so we must add a further requirement that if the dissociation does occur from a repulsive state the process of getting to that state must be slow enough to allow appreciable decomposition in the first drift region.

A mechanism has been proposed⁸ to account for such a slow dissociation rate. The ions are formed by electron impact of relatively high energy electrons and thus possesses considerable internal energy. The reaction requires a certain activation energy (i.e. the system must overcome an energy barrier) in order to transfer to the repulsive state. If the internal energy of the system is greater than the barrier height the ions will pass smoothly over the barrier and dissociate in the ion source itself. These decompositions will not be observed as metastable ions. The ions present in the drift tube thus do not have sufficient energy to decompose by passing over the barrier. However, if the barrier is narrow enough the system may tunnel through it, and such a mechanism would proceed with a rate more likely in the order of 10^5 to 10^6 sec^{-1} and thus observable as a metastable peak in the mass spectrometer.

The assumption of funnelling can also explain the distribution of kinetic energy released (figure 2). The barrier is formed by the cross-over of the states whose highest occupied molecular orbitals are $\sigma\sigma^*$ and $\sigma^*\sigma$. The system, initially in the ground state, $\sigma\sigma^*$ doubly occupied, has vibrational energy to reach the transition state at which point it is more appropriately described by the repulsive state with $\sigma^*\sigma$. It immediately decomposes. If the initial vibrational energy distribution was fairly uniform over the lower vibrational states the reacting system in the $\sigma\sigma^*$ state has its vibrational population cut off at the level corresponding to the barrier height. Further leakage of the system into the repulsive state may now occur by a tunnelling mechanism. It is difficult to judge the exact shape and height of the barrier in terms of the orbital energies as the energy values have not been minimized. However, if we assume that the barrier is parabolic and associated with the transition state, then an estimate of its shape can be made by observation of the changes in the net charge distribution of the system. The estimated barrier has a half-height of approximately 0.25 Å and a height of the order of 2 volts. The calculated probability⁹ of passing through the barrier mirrors the distribution shown in figure 2. However, the probability of tunnelling is very sensitive to the mass of the particle passing through the barrier. For reactions involving elimination of neutral

species from higher mass ions the tunnelling probability will be too low to explain the distribution of energy release. A possible alternate mechanism could involve predissociation to the repulsive state via some type of forbidden transition which would allow the reaction to proceed at a slow enough rate to be observed as a metastable transition.

References

* Submitted for publication to the Journal of Chemical Physics

1. J. H. Beynon, R. A. Saunders, and A. E. Williams Z. Naturforsch., 20a, 180 (1965).
2. J. H. Beynon and A. E. Fontaine Z. Naturforsch., 22a, 334 (1967).
3. M. D. Newton, F. P. Boer, and W. N. Lipscomb, J. Am. Chem. Soc. 88, 2353 (1966).
4. F. P. Boer, M. D. Newton and W. N. Lipscomb, ibid., 88, 2361 (1966).
5. M. D. Newton, F. P. Boer and W. N. Lipscomb, ibid., 88, 2367 (1966).
6. S. W. Benson and A. N. Bose, J. Chem. Phys., 39, 3463 (1963).
7. S. W. Benson and G. R. Haugen, J. Am. Chem. Soc., 87, 4036 (1965).
8. J. H. Beynon, A. E. Fontaine and G. R. Lester, Int. J. Mass. Spec. and Ion Phys., 1, 1 (1968).

Structure in Broad Metastable Peaks

by S. Jones and K.R. Jennings

(Department of Chemistry, The University, Sheffield S3 7HF England)

Introduction

Because of the release of kinetic energy during the fragmentation process, peaks arising from metastable transitions are always broader than those arising from ions formed in the source.¹ If the fragmentation occurs in the field-free region before the magnetic analyser, the kinetic energy release is readily evaluated from the width of the peak.² If a double-focusing instrument of Nier-Roberts geometry is operated in the "defocussed mode", the widths of peaks arising from metastable transitions in the field-free region before the electrostatic analyser lead to values of kinetic energy release which are less than the true values.³ For a given fragmentation, both the peak shape and the apparent kinetic energy release are markedly dependent on the accelerating voltage and this has been ascribed to the use of a relatively wide monitor slit which allows the passage of ions with a range of component energies perpendicular to the direction of the ion beam. The present work was undertaken to investigate the effect of reducing the monitor slit width on the peak shape and apparent kinetic energy release associated with a number of metastable transitions occurring in the field-free region before the electrostatic analyser.

Experimental

The work was carried out on an MS9 double-focusing mass spectrometer (CEC-ABI Ltd.). For initial exploratory work, the standard monitor slit of width 0.28" was replaced by a fixed slit of width 0.10", but for later work, a variable monitor slit was fitted, each edge of which could be adjusted independently, and which could be used at slit widths from zero up to over 0.2". Because of the reduction in signal intensity, a minimum slit-width of 0.02" was used for most work.

In order to improve the signal-to-noise ratio, the peaks were scanned repeatedly and the output fed into a CAT (Biomac 1000), the output of which was displayed on a strip-chart recorder. The scanning voltage was derived from the magnet sweep coil supply and was incorporated into the reference voltage supplied to the 8kV stabilizing

Effect of monitor slit width on peak shape

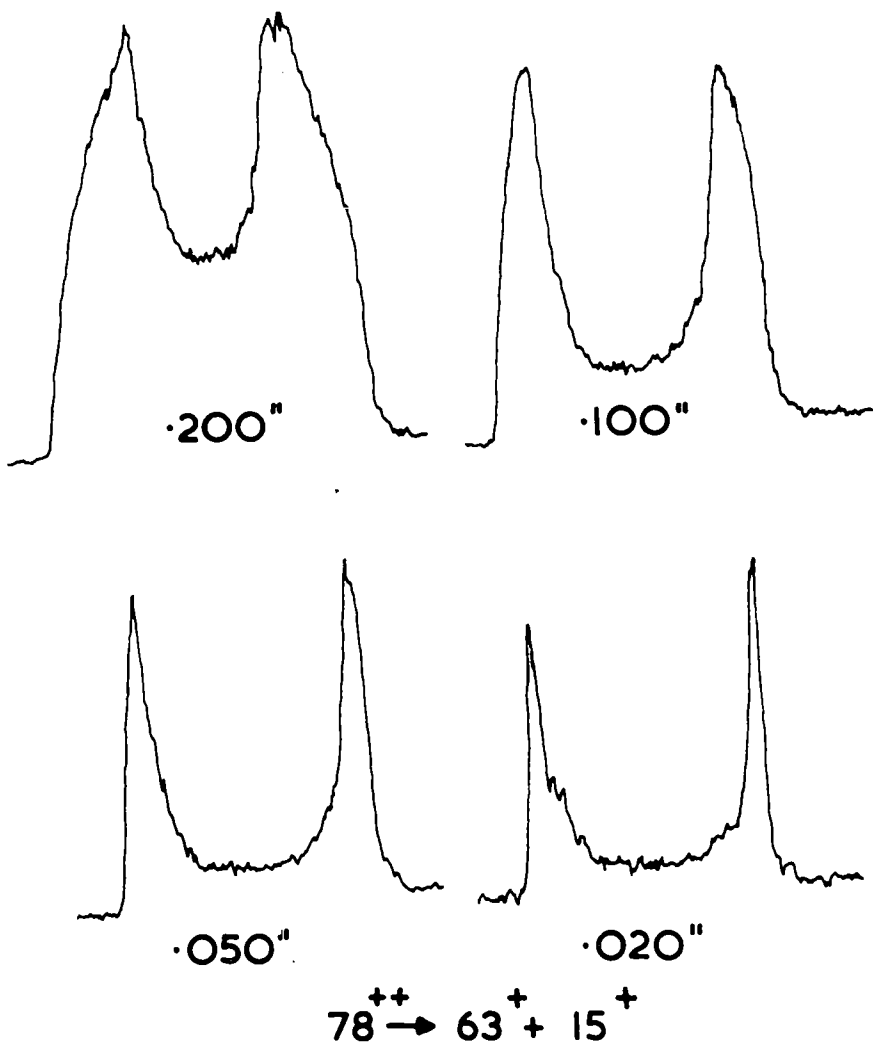
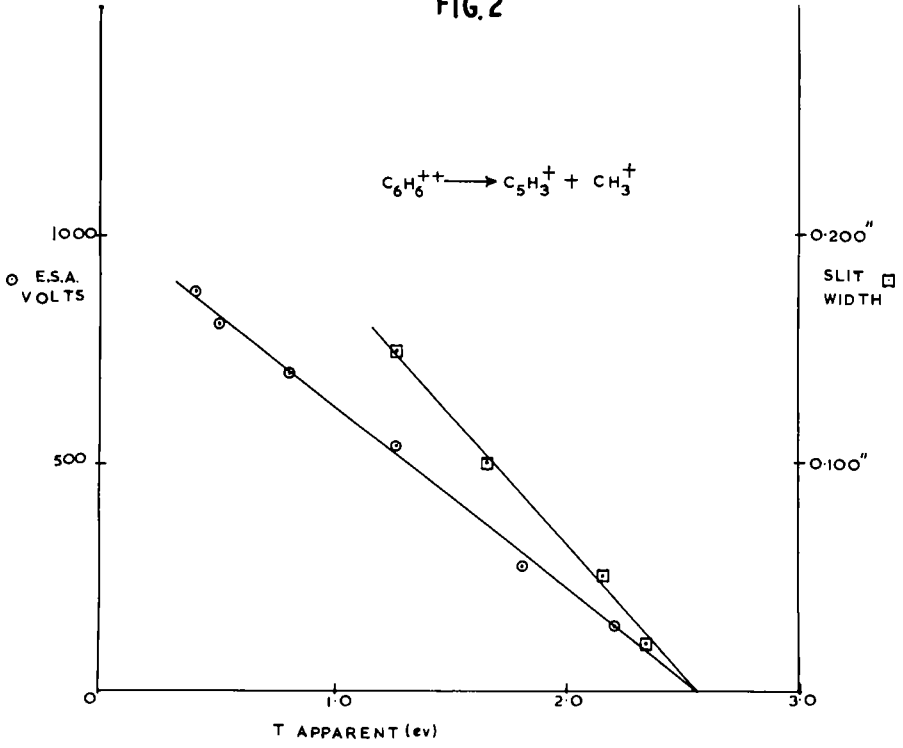


FIG.1

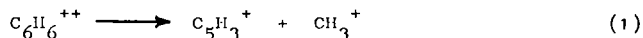
FIG. 2



amplifier. In this way, scanning rates up to about ten per second could be obtained, enabling one to obtain satisfactory peak shapes in 1-2 min. in most cases. During these scans, the magnet sweep coil was removed from the analyser tube so that the magnetic field remained constant.

Results and Discussion.

Since a careful study had already been made of the variation of peak shape with accelerating voltage for the metastable transition



in the mass spectrum of benzene, the variation of the shape of the peak given by the C_5H_3^+ ions was investigated as a function of monitor slit width. Peak shapes at four different monitor slit widths are shown in Fig. 1, and it can be seen that as the slit width is reduced, the "wings" of the peak become much sharper and move further apart. The intensity in the centre of the peak is much reduced since the narrow slit transmits relatively few ions having components of velocity perpendicular to the direction of the ion beam. A plot of the apparent kinetic energy release as a function of monitor slit width for a constant electrostatic analyser voltage of 540 volts is shown in Fig. 2 and is compared with the variation with electrostatic analyser voltage using a constant monitor slit width of 0.28". It is seen that the two plots lead, as expected, to the same limiting value of about 2.6 eV for the energy released in (1), in good agreement with the value of 2.67eV obtained from observations on metastable transitions which occur in the field-free region between the electrostatic and magnetic analysers.⁴ In view of the ease with which the monitor slit width can be varied, the evaluation of kinetic energy release from the variation of peak shape with slit width provides a rapid method of general applicability.

Peaks which arise from metastable transitions in which HF is lost by a singly-charged ion are frequently broad and approximately "flat-topped" or slightly concave due to the release of 0.4 - 0.7 eV during the fragmentation. Several of these have been found to exhibit interesting structure when observed at narrow monitor slit widths, examples of which are discussed below.

In the mass spectrum of $\text{CF}_3\text{CH}(\text{OH})\text{CH}_3$, the metastable transition $64^+ \longrightarrow 44^+ + \text{HF}$ gives rise to a broad metastable peak which when observed

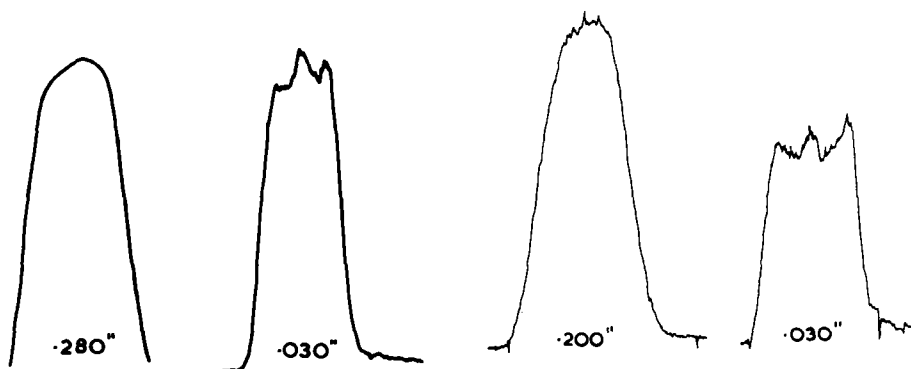
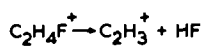
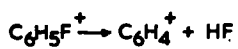


FIG.3a

FIG.3b

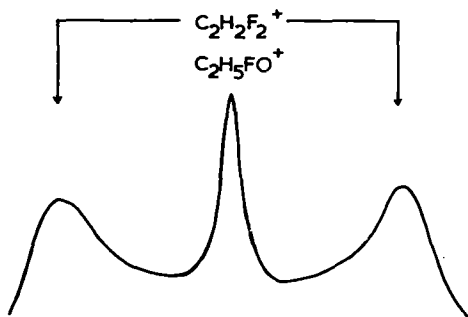
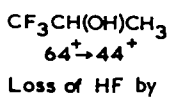


FIG.4

with a standard monitor slit (0.28") is approximately flat-topped with a slight increase in intensity at the centre of the peak. At a slit width of 0.10", this peak is resolved into three maxima, made up of a broad peak with two "wings" with a gaussian peak superimposed on it in the centre. At lower slit widths, the "wings" become sharper and their separation increases; in addition, their intensity relative to the central peak drops. An examination of the high resolution mass spectrum of the compound shows that both $m/e = 64$ and $m/e = 44$ are doublets, and the two processes responsible for the metastable transitions are:



This is supported by the fact that reaction (3) can be observed to occur in the mass spectrum of $\text{CH}_2=\text{CF}_2$, giving rise to a peak with "wings" but with no central component.

When observed with a standard monitor slit, the peaks arising from the two metastable transitions



in the mass spectra of fluorobenzene and ethyl fluoride respectively are broad with more or less flat tops. At higher gain, the peaks are approximately gaussian with flattened tops. When the monitor slit width is reduced, however, structure is observed in each peak, indicating that they are composed of a broad peak with two "wings" together with a central gaussian component, (Fig. 3). (a & b)

In the case of reaction (4), it was possible that the central component was an isotope peak of the reaction



which gives rise to an intense gaussian metastable peak. At a nominal electron energy of 16eV, however, the intensity of the metastable transition due to reaction (6) is very low, but the structure in the peak arising from reaction (4) is still present. The structure in the peak arising from reaction (5) cannot be explained in terms of isotope peak contributions.

The structure in the peaks suggests that at least two different

fragmentation processes are occurring in each case, in only one of which kinetic energy is released. It is possible that ions of similar structure in different energy levels may account for the observation; alternatively, it is possible that isomeric ions of different structures fragment with and without the release of kinetic energy.

A more detailed account of this work will be submitted for publication to the "International Journal of Mass Spectrometry and Ion Physics".

References.

- (1) J.H. Beynon and A.F. Fontaine *Z. Naturforsch.* 22a 334 (1967)
- (2) " , R.A. Saunders and A.F. Williams *Z. Nat.* 21a 180 (1966)
- (3) M. Barber, K.R. Jennings and R. Rhodes *Z. Nat.* 22a 15 (1967)

Column 3 of the data in Fig. 1 gives the measured values for the peaks obtained. These values were read from an index coupled to the potentiometers and which could be set to read 1.000 for the normal ion beam and which then read the ratio for $E_1/E_0 = m_1^+/m_0^+$ directly. The values obtained agreed with the calculated values to better than 1% and no attempt was made to improve the precision. It is possible to read the actual voltages with a digital voltmeter and improve the precision if necessary.

Columns 1 and 2 of Fig. 1 give the transitions occurring and the calculated values. All the data obtained using the RMU-7 was done at an ion accelerating voltage of 3600 volts and 1 mm slit openings.

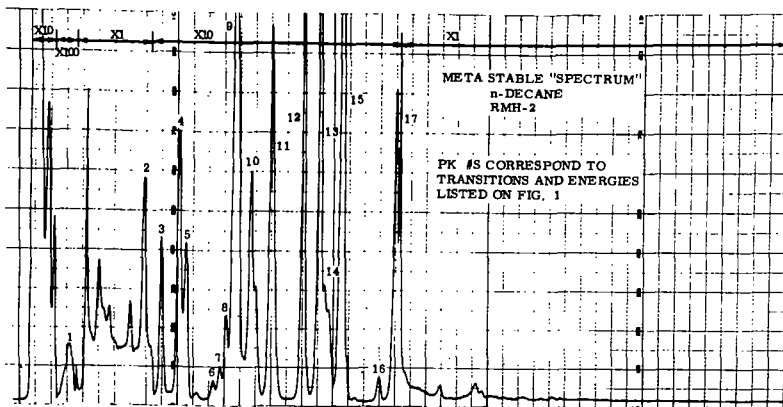


FIGURE 2

Fig. 2 shows a metastable "spectrum" of n-decane run by the same technique but obtained on a Hitachi Perkin-Elmer Model RMH-2 double focussing mass spectrometer. The energy spectrum obtained in this case is basically the same as for the RMU-7 but since it was run at higher acceleration voltage and smaller slits were used, the energy resolution is better, especially at the higher ratios of E_1/E_0 . The peaks have been assigned the same numbers as used in Fig. 1 and a comparison of the region of high E_1/E_0 ratios shows the better energy resolution obtained for the RMH-2 scan. The scan in Fig. 1 was run at constant attenuation while that in Fig. 2 was attenuated and the attenuation factors are given on the record.

Having determined the ratio m_1^+/m_0^+ for which metastable transitions are occurring, it then is necessary to determine the masses of m_0^+ and m_1^+ .

If the electric sector voltage is then set at a value corresponding to one of the maxima in an energy spectrum obtained as described above and a magnetic scan performed, a peak will be obtained for the m_1^+ ion from the transition $m_0^+ \rightarrow m_1^+ + (m_0 - m_1)$. This peak will occur at the same M/e position on the record as the metastable peak for this transition in a normal spectrum. Since the following relationship is true:

$$E_1/E_0 = m_1^+/m_0^+ = m^*/m_1 \quad \text{where } m^* = m_1^2/m_0$$

we can calculate m_1^+ and m_0^+ .

Also, because of the focussing properties of the electric sector, the divergence of the path of the metastable daughter ion will be energy corrected and thus the peak will be much narrower and thus considerably more intense than for the metastables occurring after the electric sector. In addition, under this "defocussed" condition the normal ion beam will not be transmitted to magnetic sector, thus the signal amplification can be increased and a considerable real gain in sensitivity will be realized.

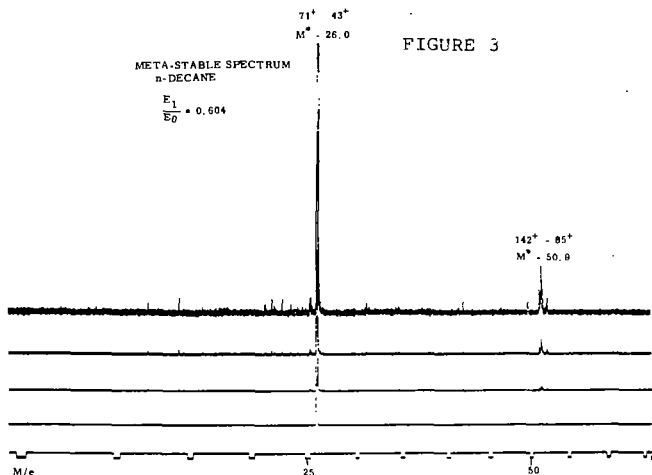


FIGURE 3

Fig. 3 shows such a magnetic scan with the electric sector voltage set at a relative value of 0.604 compared to 1.000 for the normal beam. A sharp intense peak at $M/e = 26.0$ corresponding to the $71^+ \rightarrow 43^+$ is observed. A much smaller peak at $M/e = 50.9$ due to the transition $142^+ \rightarrow 85^+$ is also observed. The m_1^+/m_0^+ value for this peak is 0.587, and if the sector voltage is adjusted to this ratio the intensity of the peak at $M/e = 50.9$ increases while the one at $M/e = 26.0$ decreases. As the system was operated, the energy resolution was more than sufficient to assign these transitions and no attempt was made to improve the energy resolution. In future work this will be investigated.

Because of scarcity of peaks in such a scan it is not possible to determine the mass of the peaks from the scan itself. Therefore it is necessary to either run part of the normal spectrum so that it can be overlaid to obtain the mass of the metastable peak or as in the case demonstrated, use a mass marker.

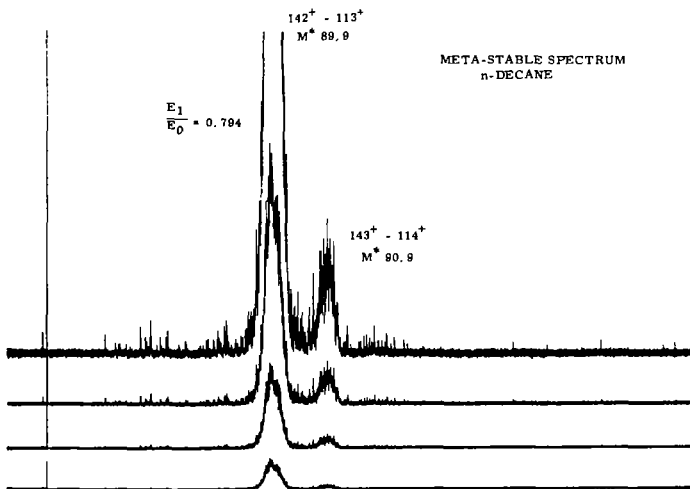


FIGURE 4

Fig. 4 is a magnetic scan with the ratio set at 0.794. The peaks observed are due to the transitions $142^+ \rightarrow 113^+$ and the $P + 1$ peak at 143^+ going to 114^+ . The 144 to 115 transition is also easily detectable.

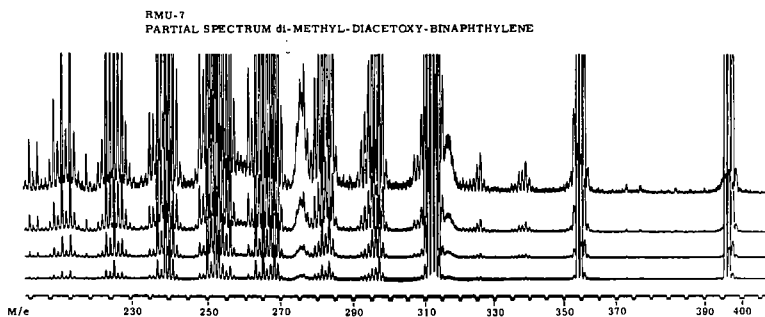


FIGURE 5

Fig. 5 is the partial mass spectrum of dimethyl diacetoxy-binaphthalene. Two metastable peaks due to the transitions $396^+ \rightarrow 354^+ \rightarrow 312^+$ can be observed. Fig. 6 is a partial energy spectrum of this compound showing the observed maxima for these transitions.

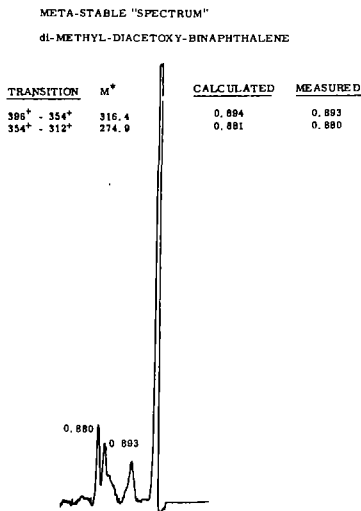


FIGURE 6

FIGURE 6

Figure 7 is a magnetic scan for this compound with the electric sector voltage set at a value of 0.893. A very intense, sharp peak is observed at M/e 316.4 for the transition $396^+ \rightarrow 354^+$ as well as peaks for the accompanying isotopic fragments $397^+ \rightarrow 355^+$, etc. Also observed is a diffuse peak at M/e 274.9. This peak is due to the m_1 peak of the $396^+ \rightarrow 354^+$ transition occurring before the electric sector now going through a second metastable transition $354^+ \rightarrow 312^+$ after the electric sector. In addition the scan shows a number of other peaks which can

which can also be easily assigned.

Many of these transitions could not be observed in the normal spectrum due to the intensity of the fragment peaks in the same mass regions. This data demonstrates the potential of the method for observing metastable transitions that would be difficult if not impossible to detect in normal spectra and also an unambiguous and accurate method of assigning daughter - precursor ion pairs.

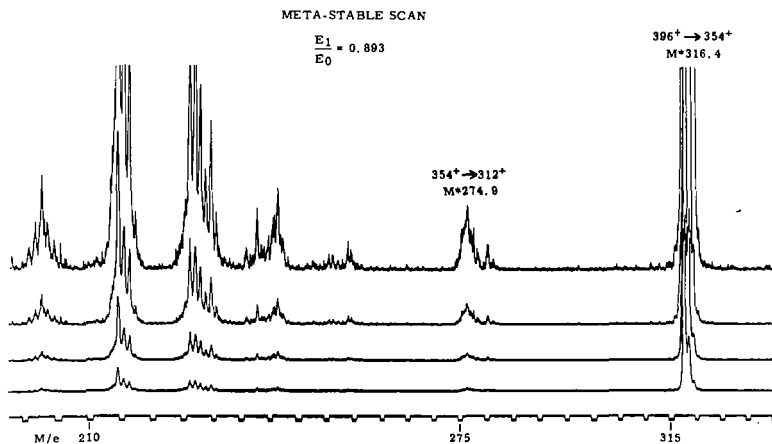


FIGURE 7

- [1] M. Barber, R. M. Elliot. ASTM E-14, 1964. Paper No. 22.
- [2] H. W. Major patent application docket No. 1185.
- [3] M. L. Gross, R. B. Fairweather, W. E. Haddon, F. W. McLafferty, and H. W. Major. ASTM E-14, 1968. Paper No. 53.
- [4] We wish to thank Dr. John Beynon of Purdue University for the data shown in Fig. 2.

CHEMIIONIZATION: THEORIES AND MECHANISMS

R. Stephen Berry
 Department of Chemistry and The James Franck Institute
 University of Chicago, Chicago, Illinois

We mean, by the term "chemiionization", those ionizing processes that occur in systems at "chemical" temperatures, corresponding to mean kinetic energies of no more than a few electron volts, at very most. We shall find it useful to consider other very closely related processes such as autoionization and predissociation. Thus the principal processes of chemi-ionization are

- a) associative ionization, e.g. $H^+ + H \rightarrow H_2^+ + e$ or $H + CO \rightarrow HCO^+ + e$;
- b) Penning ionization, e.g. $He^* + Hg \rightarrow He + Hg^+ + e$, and
- c) the rearrangement process attributed to Kuprianov, e.g. $Ar^* + H_2 \rightarrow ArH^+ + H + e$.

Under some circumstances, electron impact ionization may be considered a chemiionization process, and a high concentration of ions can be generated by thermally-induced collisions in some systems,¹ e.g. $CsBr(g) + Ar \rightarrow Cs^+ + Br^- + Ar$.

We shall not try to survey all the theories of chemi-ionization here. This writer has recently reviewed the subject, albeit with an intent to be didactic rather than comprehensive.² We shall merely review briefly what others have done, summarize briefly work of our own which has been published or is now in press or in preparation, and expand a little on some of the ideas which may not appear elsewhere.

It seems that the theory of chemi-ionization is in a state of rapid transition. We can expect the next two or three years to carry the subject from the level of phenomenological theories like the critical reaction radius models of Gioumousis and Stevenson,³ Ferguson⁴ or Bell, Dalgarno and Kingston,⁵ to a new plateau in which our understanding is based on microscopic considerations.

All microscopic theories of chemi-ionization have as their basis the idea that the nuclei are slow and heavy, and electrons are light and wave-like. One line of development has been that of Mori, Katsuura and Watanabe.⁶⁻¹⁰ This formulation is based on the model of relatively unperturbed atoms following classical trajectories, with the energy transfer occurring via simultaneous dipole transitions in both of the colliding partners. Until the most recent work of Mori,¹⁰ the method was restricted to situations in which the initially excited species was in a state connected to the ground state by an optically allowed transition. A related formulation was also given by Smirnov and Firsov.¹¹ No direct evidence is available about experimental values of these cross sections because of the short lifetimes of the required excited states. Sheldon¹² has calculated a number of cross sections for ionization of alkalis by excited rare gas atoms. At first sight the results may seem a little hard to accept because the values are only 10-100 times the observed cross sections for processes involving metastable rare gas atoms, and if the optical transition probabilities of the free atoms were the crucial factors, we would expect cross sections for allowed transitions to be $10^4 - 10^8$ times those involving transfer of energy from

a metastable state. However we must remember that the collision of $A^* + B$ does perturb both A and B, and that both optically allowed and optically forbidden transitions are perturbed. If an optically allowed state is perturbed and loses a few percent of its transition probability, this change would not have much effect on the cross section for Penning or associative ionization in the Mori-Katsuura-Watanabe model. However if this transition probability were all stolen by a normally forbidden transition, then the probability of this transition in the perturbed system would be enormously larger than its forbidden counterpart in free atoms. It therefore seems quite possible that the theoretical cross sections involving optically allowed states are compatible with the observed cross sections involving metastables. We look eagerly for the application of Mori's model for metastables¹⁰ to specific systems.

A very fruitful direction has been taken by Bardsley,¹³ who has developed the problem of associative ionization from the viewpoint of the formation of a resonance state. The cross section for associative ionization is then the product of the cross section for formation of this resonance state, multiplied by a survival probability toward ionization. The method seems very readily applicable to systems for which a moderate amount of spectroscopic data is available. Bardsley has already considered processes involving NO and N_2 .

S. E. Nielsen and this writer have developed a general near-adiabatic quantum-mechanical formulation in which one uses initial and final state functions $\Psi_{i,f}$ of the Born-Oppenheimer form,

$$\Psi(r, R, \omega) = \mathcal{Y}(r, R) \chi(R) \Theta(\omega)$$

in which $\mathcal{Y}(r, R)$ is the electronic function, dependent on electronic coordinates r and nuclear coordinates R ; $\chi(R)$ is a vibrational function, and Θ is a rotational function. If one can compute these functions for all the bound and free electronic states and vibrational states of interest, one can put large variety of processes on a common basis. The only distinction among them is in which states are bound and which are free. The processes include interactions among excited bound states, autoionization, predissociation, associative ionization, dissociative recombination, Penning ionization, electronic energy transfer and vibrational or rotational relaxation by electron collisions. This is discussed, together with the full development and consequences of the theory as applied to H_2 , in a series of papers by Nielsen and this author.¹⁴⁻¹⁸

Another formulation, falling roughly between that of Mori, Katsuura and Watanabe and that of Nielsen and Berry, is one developed by Warke¹⁹ and elaborated by Chan.²⁰ This model introduces some perturbation of the electrons in the form of an effective potential which varies during the collision. Applications to $e-O_2^+$, $e-N_2^+$ and $e-H_2^+$ have been quite successful.

We should point out that using the Born-Oppenheimer or adiabatic basis functions to represent the states solves only half of the problem of introducing the physics of the problem. The other half is solved when one decides what the important forces are that couple the basis functions and introduce transitions. Naturally this has its mathematical expression in one's choice of operator. There are apparently two operators (at least) that are important for this coupling. One is the electron correlation operator, which is strictly the difference between the real electron-electron interaction potential $\sum \frac{1}{r_{ij}}$ and the effective Hartree-Fock potential,

but which can be represented by $\sum v_{ij}^{-1}$; this operator introduces mixing among electronic configurations, and among these configurations we must include those with one or more free electrons, if they are energetically accessible. The other operator is the nuclear kinetic energy, which makes the Born-Oppenheimer basis functions into nonstationary states. Examples are now known which exhibit the action of each of these operators.

Certain general ideas have come out of our work concerning the classification of all the related coupling processes, on a microscopic basis, which is quite different from the classification on an observational basis, to which we previously referred. The microscopic classification puts coupling processes roughly into three groups, according to the internuclear distance range in which the transition occurs. These are:

- a) crossing-point cases, associated largely with transitions between states whose potential curves intersect quite sharply;
- b) turning-point cases, in which transitions in a given collisional-rotational state occur near the classical turning point of the effective potential curve (including the centrifugal potential) for the initial state, and
- c) broad-range cases, in which transition amplitude accumulates over a wide range of internuclear distance.

Both Case (a) and Case (b) occur when the asymptotic nuclear kinetic energy is relatively large and rather different for the initial and final states. Case (c) occurs when the initial and final states have rather similar potential curves. Case (a) leads to cross sections that are relatively independent of angular momentum but are sensitive functions of vibrational state and final electron energy. Case (b) leads to cross sections that are sensitive to vibrational state and may give a broad distribution of final electron energies, and is sensitive to rotational state (or impact parameter) as well. Case (c) is rather insensitive to rotational or vibrational state, but tends to put outgoing electrons in energy states that are sharply determined by the relative kinetic energy of the colliding partners. These cases are illustrated in Figures 1, 2a, b and 3.

The line of reasoning that seeks to interpret chemi-ionization in terms of potential curves has been developed recently by Čermák and Herman²¹⁻²³ and by Hotop and Niehaus.²⁴ It is hoped that the application of their work on energy analysis of electrons from Penning ionization will eventually allow the elucidation of potential curves.

REFERENCES

1. R. S. Berry, T. Cernoch, M. Coplan and J. J. Ewing, *J. Chem. Phys.* 49, 127 (1968).
2. R. S. Berry, "Chemionization", to be published in the Proceedings of the International School of Physics "Enrico Fermi", XLIV Course, Molecular Beams and Reaction Kinetics (Academic Press. to be published).
3. G. Gioumousis and D. P. Stevenson, *J. Chem. Phys.* 29, 299 (1958).
4. E. E. Ferguson, *Phys. Rev.* 128, 210 (1962).
5. K. L. Bell, A. Dalgarno and A. E. Kingston, *J. Phys. B (Proc. Phys. Soc.)* 1, 18 (1968).
6. M. Mori, T. Watanabe and K. Katsuura, *J. Phys. Soc. Japan* 19, 380 (1964).
7. K. Katsuura, *J. Chem. Phys.* 42, 3771 (1965).
8. T. Watanabe, *J. Chem. Phys.* 46, 3741 (1967).
9. T. Watanabe and K. Katsuura, *J. Chem. Phys.* 47, 800 (1967).
10. M. Mori, *J. Phys. Soc. Japan* 26, 773 (1969).
11. B. M. Smirnov and O. B. Firsov, *JETP Letters* 2, 297 (1965).
12. J. W. Sheldon, *J. Appl. Phys.* 37, 2928 (1966).
13. J. N. Bardsley, *J. Phys. B (Proc. Phys. Soc.)* 1, 349, 365 (1968).
14. R. S. Berry and S. E. Nielsen, *J. Chem. Phys.* 49, 116 (1968).
15. S. E. Nielsen and R. S. Berry, *Chem. Phys. Letters* 2, 503 (1968).
16. R. S. Berry and S. E. Nielsen, "Dynamic Coupling Phenomena in Molecular Excited States. I. General Formulation and Vibronic Coupling in H_2 " (to be submitted to *J. Chem. Phys.*)
17. R. S. Berry and S. E. Nielsen, "Dynamic Coupling Phenomena in Molecular Excited States. II. Autoionization and Predissociation in H_2 " (to be submitted to *J. Chem. Phys.*.)
18. S. E. Nielsen and R. S. Berry, "Dynamic Coupling Phenomena in Molecular Excited States. III. Associative Ionization and Dissociative Recombination in H_2 " (to be submitted to *J. Chem. Phys.*.)
19. C. S. Warke, *Phys. Rev.* 144, 120 (1966).
20. F. T. Chan, *J. Chem. Phys.* 49, 2533 (1968).

21. V. Čermák and Z. Herman, Chem. Phys. Letters 2, 359 (1968).
22. Z. Herman and V. Čermák, Coll. Czech. Chem. Comm. 31, 649 (1966).
23. V. Čermák, Coll. Czech. Chem. Comm. 33, 2739 (1968).
24. H. Hotop and A. Niehaus, Zeit. Physik 215, 395 (1968).

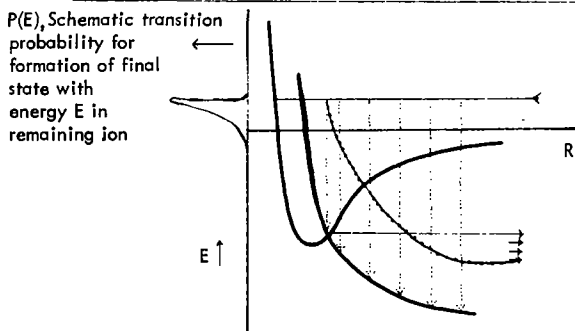


Figure 1

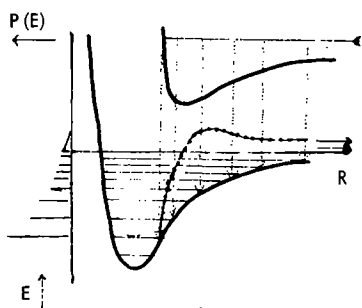


Figure 2 a

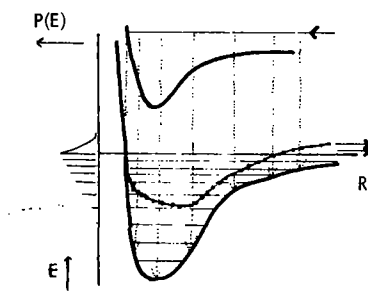


Figure 2 b

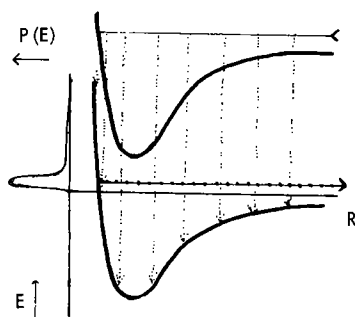
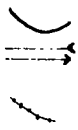


Figure 3



 Potential curve
 Energy levels of incoming and outgoing states
 Energy of remaining ion, as a function of inter-nuclear distance, if transition is vertical and nuclear kinetic energy is preserved

(ABSTRACT)

COLLISIONS OF FAST METASTABLE ATOMS

James R. Peterson

Stanford Research Institute
Menlo Park, California 94025

Various deexciting collisions of metastable species have been studied at thermal energies for some time. Recently developed techniques of producing fast, monoenergetic, excited neutral beams (by neutralizing ion beams with selected charge transfer reactions) have made studies possible over an extended range of higher energies. More stringent tests of collision theories are thus possible, and information can be gathered on intermolecular potential energies.

Several methods of detection of fast metastables are possible, but each is of limited usefulness and must be selected according to the characteristics of a specific experiment. Using charge transfer of He^+ and Ar^+ beams in alkali atom vapors to produce beams of metastable He and Ar, we have obtained Penning ionization cross sections for several reactant pairs by measuring the spatial decay of slow ions produced as the excited beam traverses a target gas.¹

A more recent set of experiments has used certain optical emissions as measures of the metastable content in the beams. As the fast metastable atoms traverse a gas, some undergo collisions in which they are excited to higher energy levels. Since these levels are not easily excited from the ground state, emissions from them can be used to monitor the metastable concentrations in the beam. Deexcitation cross sections for $\text{N}_2(\text{A}^3\Sigma_u^+)$ in N_2 and NO have been measured² from 250 to 2200 eV by detecting 2nd positive band emissions from $\text{N}_2(\text{C}^3\Pi_u)$. The metastable N_2 beam was formed by N_2^+ charge transfer in NO. Using an excited He beam obtained by charge transfer of He^+ in Cs or Rb, individual cross sections have been measured³ for the symmetric energy transfer reactions between the ground state $\text{He}(1^1\text{S})$ and each of the metastables $\text{He}(2^1\text{S})$ and $\text{He}(2^3\text{S})$ over a range of beam energies between 150 and 2200 eV. Spin conservation selection rules governing the collisions that produce the monitored emissions permit detection of the 2^1S component of the beam by monitoring the 6678 Å radiations from the 3^1D state, and similarly the 2^3S component was detected by measuring the 5876 Å emission from $\text{He}(3^3\text{D})$. The total energy transfer cross sections obtained permit a fairly accurate estimate to be made of the difference between the potentials of the Σ_g and Σ_u He_2 molecular states at internuclear separations inside the repulsive barriers in these potentials, which are not effectively penetrated at thermal energies. A recent calculation⁴ based on calculated and semi-empirical potentials gives a fair comparison with the experimental results but indicates the need for some modifications of the potentials.

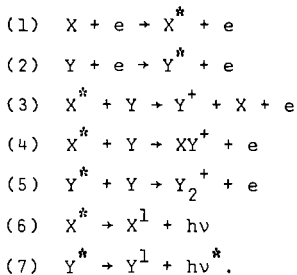
REFERENCES

1. M. Hollstein, D. C. Lorents, and J. R. Peterson, *Bull. Am. Phys. Soc.* 13, 197 (1968).
2. J. R. Sheridan and J. R. Peterson, *Phys. Rev.*, to be published, 1969.
3. M. Hollstein, D. C. Lorents, and J. R. Peterson, *Bull. Am. Phys. Soc.* 14, 262 (1969);
J. R. Sheridan, J. R. Peterson, M. Hollstein, and D. C. Lorents, submitted to
Phys. Rev., 1969.
4. S. A. Evans and N. F. Lane, *Bull. Am. Phys. Soc.* 14, 262 (1969).

Pulsed Mass Spectrometric Studies of Ionizing Collisions
of Excited Atoms^{*}

F. W. Lampe
Department of Chemistry
Pennsylvania State University

The use of pulsed mass spectrometry in kinetic studies of associative ionization and Penning ionization is discussed for several systems. It is shown that in a binary system X-Y, the reactions are in accord with the scheme



In (6) and (7) the numerical superscript indicates a lower energy state incapable of reactions (3)-(5). The determination of the kinetic parameters for a few systems are discussed.

^{*} This work will appear soon as an article in The Journal of Chemical Physics.

An Investigation of the Carbohydrate Components
of Glycoproteins Using a Gas Chromatograph-
Mass Spectrometer-Computer System

V. Reinhold* and K. Biemann

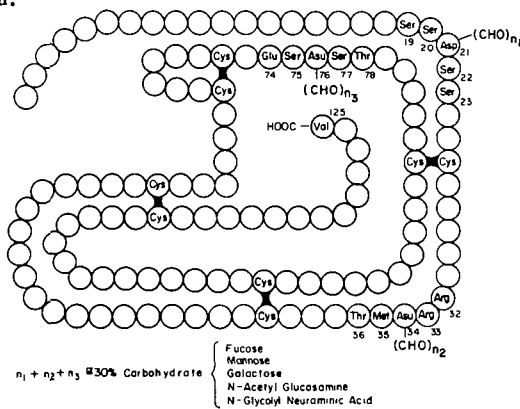
Department of Chemistry

Massachusetts Institute of Technology

Cambridge, Massachusetts 02139

As part of the continued use of gas chromatography-mass spectrometry and computer assisted analysis to biomedical problems, we have undertaken the investigation of glycoproteins.

As a typical example of a glycoprotein, figure 1 shows the primary and secondary structure of porcine ribonuclease. (1) The 125 amino acid enzyme possess approximately 30% carbohydrate consisting of fucose, mannose, galactose, N-acetyl glucosamine and N-glycolylneuraminic acid.



Ribonuclease, Porcine

Figure 1

Glycoproteins, implicated with many diseases, associated with hormonal, blood coagulation, viral inhibitor, and immune reactions have long neglected the careful investigative characterization subjected to many proteins. The neglect is obviously associated with the difficulty in carbohydrate chemistry. A great diversity of structural analogs are present in carbohydrate moieties bound to glycoproteins, from the basic amino sugars to the neuraminic acid components, but yet an even greater structural homogeneity within each class; that is, anomers and positional isomers as with mannose, galactose, and glucose.

The past developments in the gas chromatography-mass spectrometry of carbohydrates (2-4) have shown that much could be gained by application of these techniques to glycoproteins.

We have chosen to approach the problem in the following manner: First, by quantitative and qualitative determination of each carbohydrate monomer; second, by the identification of sequential or primary structure of these oligomers [(CHO)_n in Fig. 1], and thirdly, by characterization of the linkage points of the carbohydrate oligomers to the protein backbone. In ribonuclease (Fig. 1), the carbohydrate moieties are attached to amino acids 20, 34, and 76. If one assumes a tertiary structure analogous to the bovine enzyme it can be concluded that the carbohydrate is bound to the periphery of the enzyme.

Briefly, the experimental approach consists of methanolysis and silylation. For

* Helen Hay Whitney Fellow

quantitative studies, methanolysis was carried out for 16 hours followed by reacetylation, silylation and extraction. For qualitative work, methanolysis was limited from one to three hours followed directly by silylation. This latter procedure had the obvious advantage of shorter time, but more importantly, provided mass spectra of the free amines related to the acetamido sugars.

The analytical system (5) includes an IBM 1800 computer which handles raw data generated by a single focussing magnetic scanning mass spectrometer (Hitachi: P.E. RMU 6) interfaced with a gas chromatograph, (Aerograph, Hy-FI). Precise times for starting and stopping the magnetic scan provides the reproducibility necessary for accurate conversion of time units to masses. A mass spectrum is recorded and stored on magnetic disks every four seconds during the entire course of the gas chromatogram. The digitized signals are summed for each scan producing a plot analogous to a beam monitor recording and, ideally, identical to the gas chromatogram produced by the flame-ionization detector.

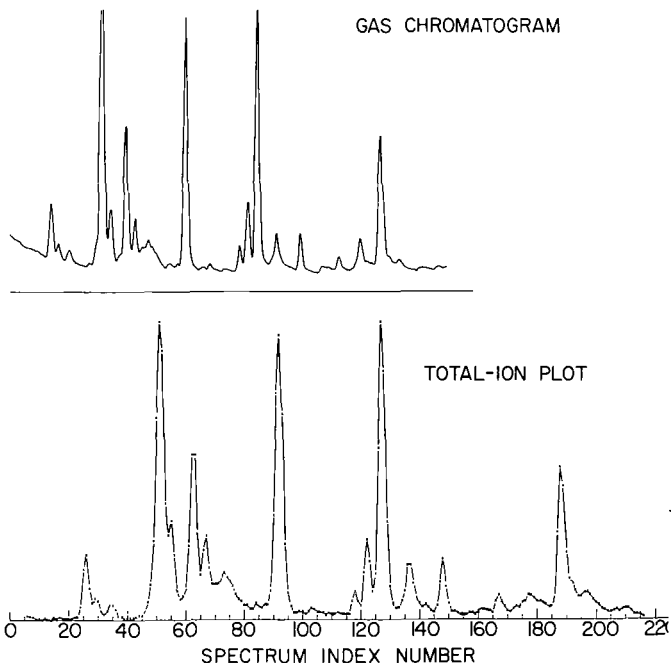


Figure 2

A comparison of total-ion plot with the gas-chromatograph flame-detector output, shown in figure 2, (bottom and top respectively) provides a careful check on sample elution, and loss of resolution or discrimination, if any. Although the time scales (abscissas) are not identical, it is easy to see the scan identity. It has been our experience in these studies to note that all components pass the separator with great facility and with essentially no loss in resolution. This is especially noteworthy since neuraminic acid derivatives, the last peak in figure 2, are classically very labile components.

Identification of each of these sugars was suggested by relative retention-time data this, combined with mass spectra, compared to a standard mixture of methyl glycosides, allowed positive identification.

Porcine ribonuclease, α_1 -acid glycoprotein, α_2 -(Zn)-glycoprotein, human and calf thyroglobulin, and fetuin were analyzed and found to consist of the expected components, fucose, mannose, galactose, N-acetyl glucosamine neuraminic acid, with the total qualitative analysis complete in a fraction of the time required with previous techniques. Mass-intensity plots are available for all components for the several glycoproteins. Figure 3 shows the mass spectrum of N-Acetyl neuraminic acid methyl ester, the sugar moiety obtained from most of these glycoproteins, which was eluted as the

B-N-ACETYLNEURAMINATE METHYL GLYCOSIDE

183

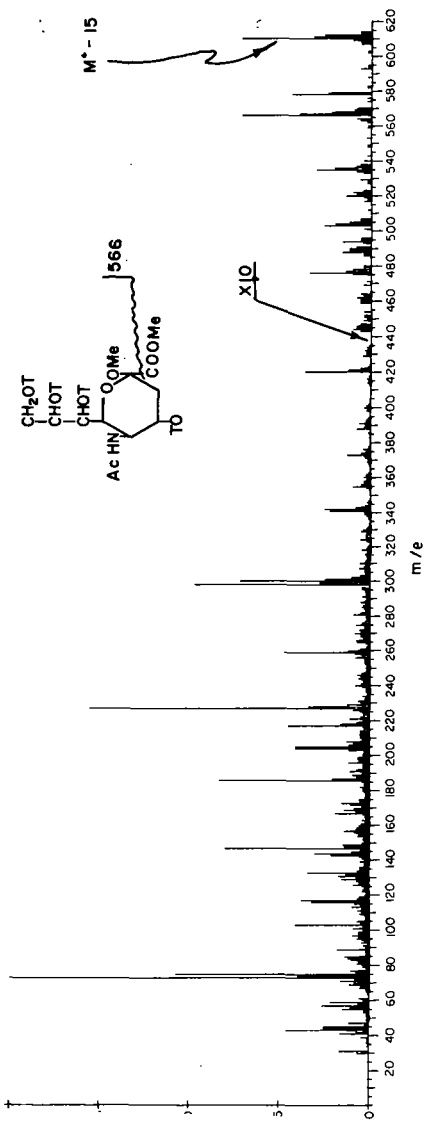
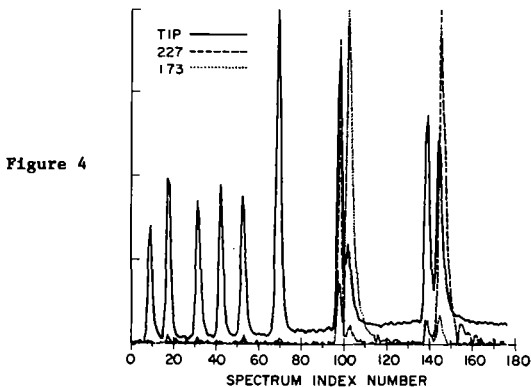


Figure 3

last peak from the gas chromatograph. The higher mass peaks can all be rationalized by the loss of methyl, methoxyl, carboxymethyl, or a combination of these.

In the mass spectra, it has been of considerable interest to observe fragmentation variation with subtle changes in structure, as exemplified in the α and β configurations of the methyl glycosides of N-acetyl glucosamine and N-acetyl neuraminate esters. This is best illustrated by an overplot of the total-ion curve with the relative abundance of a single mass as shown in Figure 4. This is one of the subroutines available (6)

STANDARD METHYL GLYCOSIDE MIXTURE
TOTAL ION PLOT
PLOT OF MASS 227+173



and is analogous to having the spectrometer set to resolve one specified mass and comparing this to the beam monitor recording. Any mass can be plotted even on samples run months ago. As can be seen mass 227 is found to occur in β -methyl-N-acetyl glucosamine and β -methyl-N-acetylneuraminate, but not in the other anomer. While mass 173, is significant only in the α anomer of N-acetylglucosamine.

Overplots of this type with highly specific but yet low intensity masses have been extremely helpful in locating sugars found only in trace amounts or incompletely resolved by the gas chromatograph.

Lastly, we would like to present some preliminary studies on disacchrides.

The dimer of fucose and glucosamine associated with blood group typing phenomenon is one example and its silyl derivative has a mass of 726. Consideration of the monomer of fucose which shows a strong 191 peak probably representing the number one carbon and two TMS groups, one due to rearrangement analogous to the pertrimethyl silylated glucose work presented recently by deJongh et al. (3) In the mass spectrum of N-acetylglucosamine, the prominent feature was the 173 peak associated with the second and third carbon of amino sugars.

A consideration of the low mass region of the disaccharide shows the absence of both a 191 and a 173 peak, suggesting a fucosyl (1-3) N-acetyl glucosamine linkage. Detailed interpretation of this structure must await the determination of the mass spectra of a series of disaccharides presently being considered.

Thus in summary one can conclude that using the present continuous scanning GC-MS-data acquisition system it is possible to approach a very complex area routinely and evaluate in a quantitative manner, as in this case, the carbohydrates bound to glycoproteins. Furthermore, indications are that much structural information can be gained from this systematic analysis of disaccharides and, hopefully, higher oligomers.

Probably of equal significance is the fact that these GC-MS-runs are permanently stored on tape to continuously reevaluate at the whim of the investigator with the different subroutines available, whether it be varying mass plots, library search, or just mass intensity grids.

References

1. R. L. Jackson and C. H. W. Hirs. Federation Proceedings 28, 344 (1969).
2. H. K. Kochekov, O. S. Shizhov, and N. N. Molsdtaov, Tetrahedron 24, 5587: (1969).

3. D. C. deJongh, T. Radford, J. D. Hribar, S. Hanessian, M. Bieber, G. Dawson, and C. C. Sweeley, *J. Am. Chem. Soc.*, 91, 1728 (1969).
4. C. C. Sweeley, R. Bently, M. Makita, and W. W. Wells, *J. Am. Chem. Soc.*, 85, 2497 (1963).
5. R. A. Hites, and K. Biemann, *Anal. Chem.* 40, 1217 (1968).
6. R. A. Hites, Ph.D. Thesis, Massachusetts Institute of Technology, Cambridge, Mass., 1968.

Acknowledgement

The authors would like to thank Mr. James Biller for valuable assistance with the computer aspects of this work, and the National Institutes of Health (Grants GM01523 and FR00317) for financial support.

Many carbohydrate samples used in this work have been kindly provided by Dr. R. Jeanloz, Harvard Medical School, Boston, Mass.

A POROUS STAINLESS STEEL SEPARATOR SYSTEM FOR
GAS CHROMATOGRAPHY-MASS SPECTROMETRY

P. M. Krueger and J. A. McCloskey

Baylor College of Medicine, Houston, Texas 77025

The use of silanized porous stainless steel tubing has been investigated as a separator interface for gas chromatography-mass spectrometry. Two versions were designed and tested for a CEC 21-110 mass spectrometer: (1) a temporary system in which the effluent is introduced through a direct inlet probe assembly, and (2) a compact, permanently mounted assembly with ion source entry through the shutter flange. The probe version produced an efficiency of 40% (cholestane) and separation factor of 108 at a column flow rate of 35 cc He/minute, resulting in an (uncorrected) ion source pressure of 1.8×10^{-5} mm Hg. The mounted assembly produced an efficiency of 48%, separation factor of 10 at a flow rate of 7 atmospheric cc/min (with the column under vacuum) and 3×10^{-5} mm Hg source pressure.

Comparison of the beam monitor chromatograms of cholestane and a compound of high polarity, 2',3'-O-isopropylidene adenosine, showed only slightly increased tailing in the latter compound. The M-18 peak of cholesterol increased from 28% using the direct introduction probe (ion source 190°) to 34% using the GLC inlet system (source 190° , separator 250°), indicating low tendency for thermal decomposition in the GLC system.

The porous stainless steel separator system is of rugged construction, heatable to high temperatures and is suitable for high molecular weight, polar compounds. Since the porous tubing can be obtained in a variety of physical dimensions and porosities, considerable flexibility and ingenuity can be exercised in the design of a separator system for a particular instrumental configuration.

(To be submitted to Analytical Chemistry)

A SEPARATOR WITH VARIABLE CONDUCTANCE FOR
GC/MS ANALYSES

C. Brunnée, H.J. Bültemann and G. Kappus
VARIAN MAT GmbH, Bremen, Germany

Abstract

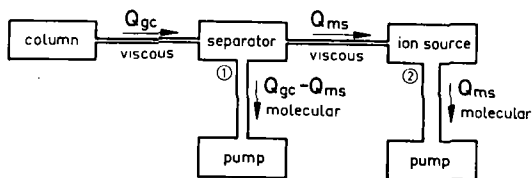
To obtain maximum separator efficiency in GC/MS analyses it is necessary to cope with the varying flow rates of the gas chromatographic column. A new type of separator is described whose conductance can be adapted during operation. Thus flow rates from below 1 up to 100 ml/min can be handled. No tailing effects could be observed due to the small volume and inner surface of the separator. Results obtained with this type of separator are reported.

The efficiency of a GC/MS combination is determined by the enrichment N and the yield Y of the separator interfacing the two instruments. Fig. 1 shows the relation between these two quantities, using the same designations as Grayson and Wolf ¹). Enrichment N is defined as the ratio of the concentration of the sample in the carrier gas at the inlet of the mass spectrometer to the concentration at the outlet of the gas chromatograph. Neglecting sample flow rate Q_S against carrier gas flow rate Q_C , N becomes the product of the ratio Q_{GC}/Q_{MS} of the carrier gas flow rates, and the ratio $(Q_S)_{MS}/(Q_S)_{GC}$ of the corresponding sample flow rates. The second factor is the separator yield, Y . The yield determines how many per cent of a sample will finally be available for analysis in the mass spectrometer. The magnitude of the enrichment N alone is not decisive: It is possible to make the enrichment very large, for example by using multi-stage separators. However, in this case the amount of gas, Q_{MS} , entering the mass spectrometer has to be reduced. Thus it may well happen that the separator yield Y does not increase, as desired, but decreases.

For separation of the samples by molecular effusion - a principle utilized in the separators of Biemann and Watson ²), Cree ³), Blumer ⁴), and Lawson, Leemans and McCloskey ⁵) - the theoretical enrichment can be calculated. One obtains equation (3).

There are three special cases :

1. If the amount of gas Q_{MS} flowing into the mass spectrometer is made much smaller than Q_{GC} so that Q_{GC}/Q_{MS} is considerably larger than $\sqrt{M_S/M_C}$ then N approaches the optimum value $N_{MOL} = \sqrt{M_S/M_C}$, equation (3a).
2. With indefinitely increasing molecular weight ratio M_S/M_C the enrichment tends towards a maximum value $N_{MAX} = Q_{GC}/Q_{MS}$, equation (3b) as follows immediately from (3). This maximum value is attained, when the total amount of the sample enters the mass spectrometer, the separator yield thus being 1. With $Y = 1$, equation (3b) also follows from (2). Like the other equations marked with an asterisk, (3b) is independent of the



$$N = \frac{\left(\frac{Q_S}{Q_C}\right)_{ms}}{\left(\frac{Q_S}{Q_C}\right)_{gc}}$$

$$Q_S \ll Q_C :$$

$$(Q_C)_{gc} \approx Q_{gc}, (Q_C)_{ms} \approx Q_{ms}$$

$$(1) N = \frac{Q_{gc}}{Q_{ms}} \cdot \frac{(Q_S)_{ms}}{(Q_S)_{gc}}$$

$$(2) Y = N \cdot \frac{Q_{ms}}{Q_{gc}}$$

$$(3) N = \sqrt{\frac{M_S}{M_C}} \cdot \frac{Q_{gc}}{Q_{ms}} \cdot \frac{Q_{gc} + \sqrt{\frac{M_S}{M_C}}}{Q_{ms} + \sqrt{\frac{M_S}{M_C}}}$$

$$(3a) N_{MOL} = \sqrt{\frac{M_S}{M_C}}$$

$$(3b) N_{MAX} = \frac{Q_{gc}}{Q_{ms}}$$

$$(4) N_{TOT} = \frac{M_S}{M_C}$$

Fig. 1

Basic formulae.

S * sample, C * carrier gas,

ms * mass spectrometer, gc * gas chromatograph,

Q * flow rate, N * enrichment,

Y * yield, M * molecular weight.

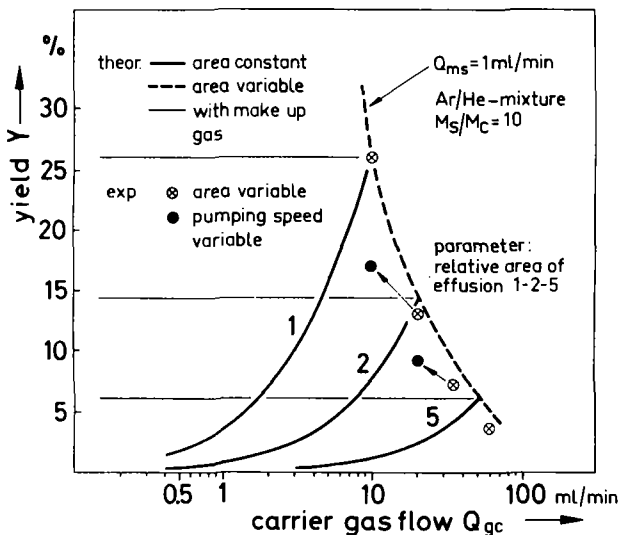


Fig. 2 Relationship between yield Y and carrier gas flow Q_{gc} .

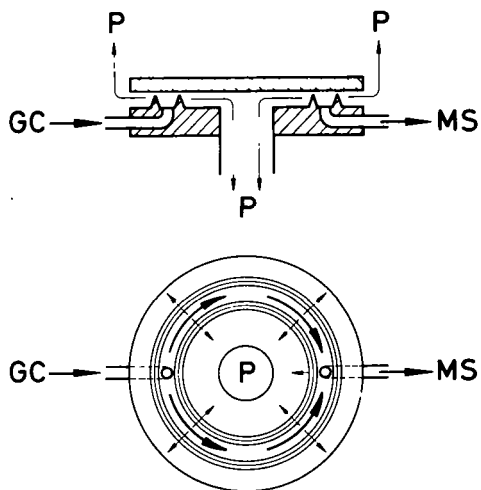


Fig. 3 Principle of the slit separator.

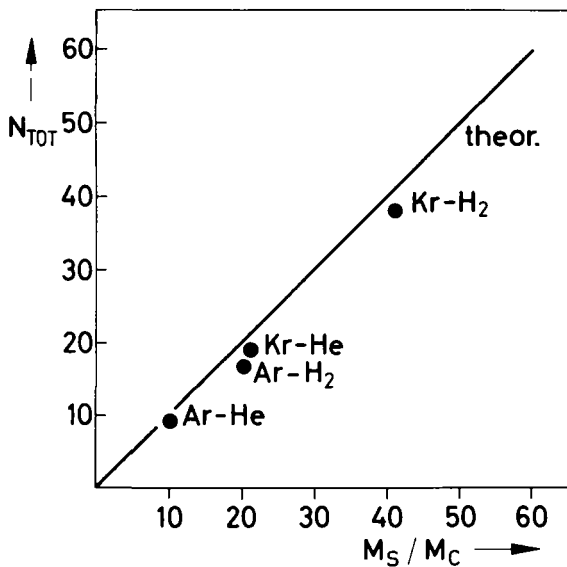


Fig. 4

Plot of the total enrichment N_{TOT} against the molecular weight ratio M_S/M_C of sample and carrier gas.

separation principle used.

Special case no. 3 corresponds to the direct CC/MS connection without gas flow reduction with a separator, for instance, when using capillary columns. Then $Q_{MS} = Q_{GC}$ and the enrichment N becomes 1 according to the equation (3), the yield Y also being 1, that is, 100 %.

It follows from the given formulae that the ratio of the flow rates Q_{MS}/Q_{GC} is of great influence on the yield Y . Let us assume that a single-stage separator working according to the molecular effusion principle is designed for an optimum flow rate Q_{GC} of, for instance, 50 ml/min. Then under optimum conditions the flow rate Q_{MS} may have the maximum permissible value for the mass spectrometer of 1 ml/min. If we use columns with a smaller flow rate instead, e. g. SCOT columns with 10 ml/min only, the yield Y decreases, because Q_{MS} decreases not linearly, but quadratically with Q_{GC} . The reason for this: If possible, the flow into the ion source should be *v i s c o u s*, because then at the ion source another separation by effusion occurs, due to the molecular flow always found in the mass spectrometer. The total enrichment N_{TOT} is then given by the product of the two enrichments at the points (1) and (2) of fig. 1 that is to say by N_C/N_{ig} in the ideal case, equation (4). However, in the case of viscous flow, the flow rate Q_{MS} does not decrease linearly but quadratically with pressure, that is, with Q_{GC} , which results in the drop in yield Y mentioned before. This relation can be seen from fig. 2, showing the calculated yield Y as a function of Q_{GC} . The parameter is the size of the effusion area, i. e. the area of the fritted glass tube or membrane which increases towards the right. As can be seen, a separator with an effusion area of a given size obtains optimum results only at a single point. At this point, Q_{MS} has the maximum permissible value. At higher flow rates Q_{GC} the gas flow into the mass spectrometer becomes unduly high; at lower flow rates the yield Y decreases.

The drop in yield with decreasing carrier gas flow can be eliminated by adding a make-up gas at the outlet of the column, keeping the gas flow into the mass spectrometer constant. Thus the yield remains constant too (thin line), but it can never reach the optimum values lying on the dashed line of fig. 2.

An effusion separator producing optimum results in the entire range of Q_{GC} can be realized, apparently, by making the effusion area variable. A separator of this type is shown on fig. 3. Here, effusion does not occur at a glass frit or porous membrane, but at two sharp circular edges about 20 mm in diameter. The carrier gas is pumped away outside and inside the two circular edges. The distance between the cover plate and the edges is continuously variable from zero to 50 μ m by means of a spindle. When the slit is closed, gas flow reduction is smaller than 1 ml/min, with a medium slit opening of 30 μ m it is about 60 ml/min. Therefore, the separator is suitable for all types of columns. The flow rates Q_{GC} of the columns can be varied, whereas the amount Q_{MS} entering the mass

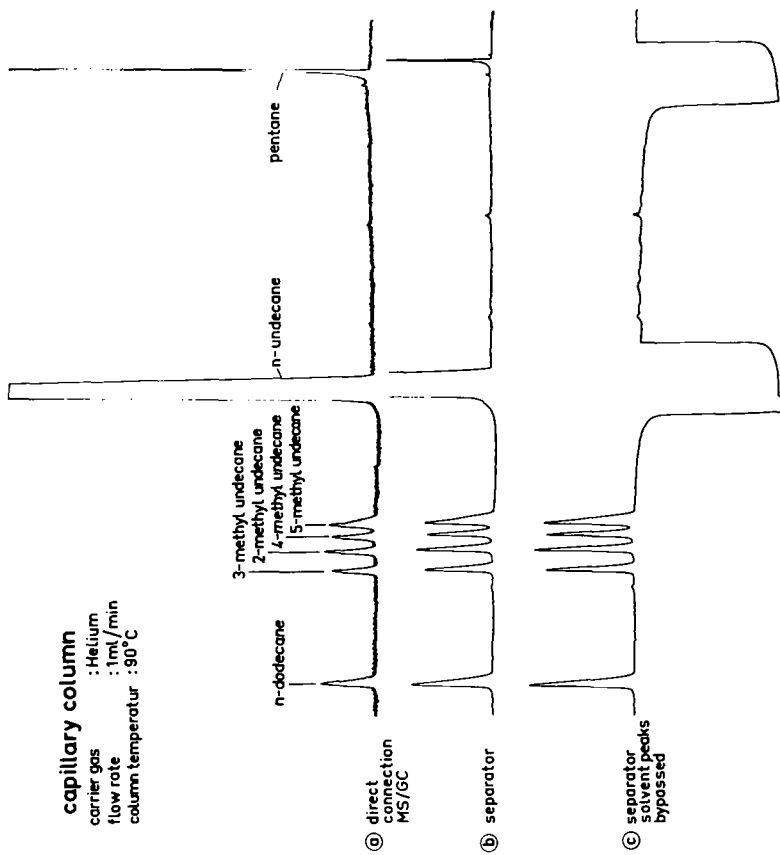


Fig. 5 Gas chromatograms

spectrometer can be set to any required value during operation. The outer diameter of the whole device is 6 cm only.

The dashed line in fig. 2 represents the calculated yield Y . The points \odot represent the yield obtained with the separator experimentally. They are absolute values which have not been matched to the theoretical curve. In each case the size of the circular slit had been set such that Q_{MS} had the maximum permissible value. Theory and experiment agree rather well. At very high flow rates, the yields obtained are slightly lower, because, due to the great distance between edge and plate, the condition for molecular flow is no longer exactly met. This effect can be utilized to reduce the height of the solvent peak: for this purpose, the separator is opened completely and then practically acts as a bypass. Thus the dynamic range of the GC/MS - combination is increased considerably. The curves apply to a mixture of argon and helium. At a higher molecular weight the yield is accordingly higher. For cholesterol with $M = 386$ we measured a yield of 32 % at a flow rate of 30 ml/min.

The diagram fig. 2 also shows that varying the area is resulting in a considerably higher yield than varying the pumping speed at the separator by means of a throttling valve in the by pass line (points \bullet).

According to the given formulae, the total enrichment N_{TOT} should increase linearly with increasing molecular weight. This was confirmed by experiment, as shown in fig. 4. At a molecular weight of 250 the total enrichment N_{TOT} is about 60.

Due to the very small interior surface of the separator, decomposition, adsorption and tailing effects are reduced to a minimum. The observed differences between the chromatograms, recorded without and with the separator, were negligible. As an example in fig. 5, the chromatograms of a mixture of methylated undecanes in undecane are shown.

References

- 1) M.A. Grayson, and C.J. Wolf
Anal. Chem. 39, 1438 (1967).
- 2) J.T. Watson, and K. Biemann
Anal. Chem. 36, 1135 (1964), Anal. Chem. 37, 844 (1965).
- 3) R.F. Cree
Pittsburgh Conf. on Anal. Chem. and Appl. Spectr., March 1967,
Abstr. of Papers, p. 96, No. 188.
- 4) M. Blumer
Anal. Chem. 40, 1590 (1968).
- 5) A.M. Lawson, F.A.J.M. Leemans, and J.A. McCloskey
ASTM Committee E-14, Denver (1967).
- 6) P.M. Llewellyn, and D.P. Littlejohn
Pittsburgh Conf. on Anal. Chem. and Appl. Spectr., Febr. 1966.

Mass Spectra and Gas Chromatography of the ORMOSIA Alkaloids, K. L. Rinehart, Jr., K. J. Schilling, C. L. Brown and R. H. Heckendorn, Department of Chemistry, University of Illinois, Urbana, Illinois 61801.

Species of the Ormosia plant genus are widely distributed in tropical regions. Their seeds usually contain several closely related pentacyclic and hexacyclic aliphatic alkaloids of molecular formula $C_{20-21}H_{31-35}N_3$. Some of these alkaloids have been shown to contain marked pharmacological activity. Mass spectra of alkaloids of known structures in this series and of their derivatives have been studied in detail. From these studies it is possible to make reasonable structural assignments, in part including stereochemistry, to a number of new alkaloids from the seeds.

All of the alkaloids pass readily through a gas chromatographic column and mixtures can be separated especially well by the temperature programming procedure. Coupling of the gas chromatograph with a Varian-MAT CH4B mass spectrometer was investigated by a number of methods. Direct introduction through the probe was generally unsuccessful as was the use of a Teflon separator, in which the alkaloids were generally retained. Spectra of some of the alkaloids could be obtained by employing a standard glass frit separator, while use of a shortened glass frit was more successful. Spectra of all of the alkaloids could be recorded via a commercial enrichment device (MAT) employing a glass frit separator and capillaries to restrict helium flow.

Flash Mass Thermal Analysis: A Method for Studying Pyrolysis of Solid Rocket Propellant Ingredients*

W. G. Stapleton**

Introduction

The molecular basis of initiation and propagation of burning solid rocket propellants and detonation of explosives is not well understood. Some constituents of these materials have seemingly unexplainable correlations of thermal stability and sensitivity to impact, friction or spark. Inability to rationalize the behavior of these materials arises from lack of knowledge as to the molecular events occurring during the detonation process. The usual picture of impact detonation, for example, assumes localization of the impact energy within microscopic volume elements, with consequent initiation of thermal decomposition. Exothermic reactions in the decomposition process produce further localized adiabatic heating and very rapid escalation of reaction rate to the point of detonation. A complete understanding of detonation sensitivity requires a detailed understanding of the thermal decomposition kinetics and mechanism at temperatures and times corresponding to detonation processes, i. e., at temperatures of several hundreds of degrees centigrade and times approximately between 0.05 and 50 milliseconds. The dependence of sensitivity upon molecular structure, for example, can be expected to differ if the explosive chain set up in the "hot spot" is strictly a thermal one or is additionally complicated by chemical chains, e. g., free radicals.

A method of mass spectral thermal analysis has been developed to determine the energetics and kinetics of the initiating reactions in the decomposition of solid propellant ingredients and explosives. This method is called Flash Mass Thermal Analysis (FMTA) and is an outgrowth of thermogravimetric and differential thermal analysis techniques. The term "flash" is used to denote that this method utilizes a very fast rate of energy input to the sample. A Bendix Time-of-Flight mass spectrometer, Model 12-101, was used as the instrument to detect the gaseous products from the decomposing/reacting materials. The sampling rate of 10 KHz permits adequate data acquisition at the rapid pyrolysis rates encountered with fast heating. The method developed for this type of study is herein described.

Method Development

Sample Preparation

A critical step in this analysis technique is insuring that the sample is uniformly distributed over the surface of the pyrolyzing heat source. From the standpoint of heat transfer to the sample, source heat capacity and low pressure requirement of the mass spectrometer vacuum, the sample must be on the order of 1-5 μ g to achieve the best results. Samples of solid oxidizers or fuels were dissolved in suitable solvents and were deposited on a platinum ribbon, the dimensions of which are 1.5 cm x 1 mm x 0.025 mm. Polymeric materials were successfully coated onto the ribbon by spreading a measured volume of solution along the length of the ribbon with a microsyringe. This technique was not useful for crystalline materials, however, since very large crystals form on the surface as the solvent evaporates. This difficulty was circumvented by spraying the solution onto the ribbon with an artist's air brush set to produce a very fine spray. The result was an evenly distributed pattern of microscopic crystals, 5-25 μ in size, over the entire surface.

Sample Introduction System

A Bendix Direct Inlet Probe, Model 843A, which permits access to the mass spectrometer ionization chamber by means of a pumped vacuum lock, was adapted to support the platinum ribbon which bears the sample. (Figure 1). When the probe is positioned in the mass spectrometer, the sample is approximately 2 mm from the ionizing electron beam. (Figure 2). This arrangement results in a higher intensity spectrum than would be possible for a system in which the sample were located at greater distances from the electron beam. Also, products which are short-lived may be detected before decay to secondary species.

* This work was performed under the auspices of the U. S. Air Force Rocket Propulsion Laboratory, Edwards Air Force Base, California under Air Force Contract No. AF 04(611)-11385.

** Lockheed Propulsion Company, Redlands, California

The ionization chamber is cryogenically pumped with two specially designed liquid nitrogen cold traps. (Figures 3 and 4). Their function is two-fold; (a) the residual H₂O background is reduced to practically zero and (b) pyrolysis products which escape from the ionization region are trapped before they can rebound from the walls and re-enter the ionization region. This insures that most of the products which are being analyzed are detected while in a high energy state and have not collided with sampling system walls.

Sample Heating System

In our experiments, the sample may be heated in two different modes: (1) very rapid temperature increase (1×10^6 °C/sec) to an isothermal condition and (2) a slower temperature rate of increase which may be varied from 50-200 °C/sec. In either case, the platinum filament constitutes one arm of a wheatstone bridge. Just prior to each sample run the bridge is nulled. As the ribbon is heated, its resistance changes and the bridge becomes unbalanced. The output signal of the bridge is fed to an oscilloscope and recorded photographically. (Figure 5).

The "slow heating" of the ribbon is produced by a 24 volt battery connected in series with the bridge. The rate of heating may be varied with a rheostat also in series with the bridge.

Rapid heating of the sample to an isothermal condition is accomplished by discharging a high voltage from a capacitor through the platinum ribbon. (Figure 6). The capacitor is charged by a high voltage power supply and the discharge is effected by energizing the hydrogen thyratron. A constant low voltage from a 24 volt battery serves as the bridge power supply which enables the temperature to be measured after the current surge from the capacitor has subsided. The duration of the capacitor discharge is less than 10 μ seconds. As in the slow heating, the bridge output is fed to an oscilloscope and is recorded photographically. The resistance of the platinum ribbon is calculated from the equation

$$R_f = \frac{ER_3 + 2VR_s + 2VR_3 + R_s R_3 V/R_1}{E - 2V - VR_s/R_1}$$

in which R_f is the ribbon resistance, E is the source voltage, R_3 is the variable arm of the bridge, R_s is the series resistance, R_1 and R_2 are the remaining known arms of the bridge and V is the bridge output voltage. The temperature of the ribbon is in turn calculated

$$T_{pt} = \frac{R_{ft} - R_{fi}}{3.89 \times 10^{-4}} + T_i$$

in which T_{pt} is the temperature at time t, R_{ft} is the resistance of the ribbon at time t, R_{fi} is the initial resistance of the ribbon and T_i is the room temperature.

In the fast heating experiments, the question of ribbon surface temperature profile arose. From considerations of the physical properties of the platinum ribbon and its stainless steel supports, radiant and conductive heat loss paths and applied current, an expression was developed which, when solved, could define temperature gradients with respect to time. A computer program was written for the solution and the result was that the temperature was shown to be constant over the middle two-thirds of the ribbon up to 10 milliseconds, for temperatures lying between 100 and 500 °C. (Figure 6).

Data Recording Techniques

Time-of-Flight mass spectrometry lends itself well to fast pyrolysis studies because of its rapid sampling rate (10 KHz) over the spectrum of 0-250 mass units. This rapid rate permits the use of very small samples and small heat sources which characteristically possess low heat capacities and therefore require less energy for a given temperature increase.

Rapid analysis coupled with extremely short periods in which the pyrolysis products are available for detection present some stringent requirements for recording data. In these experiments, the time range of interest may be as short as fifty microseconds or, at most, two seconds. Obviously, the data must be recorded photographically from an oscilloscope trace.

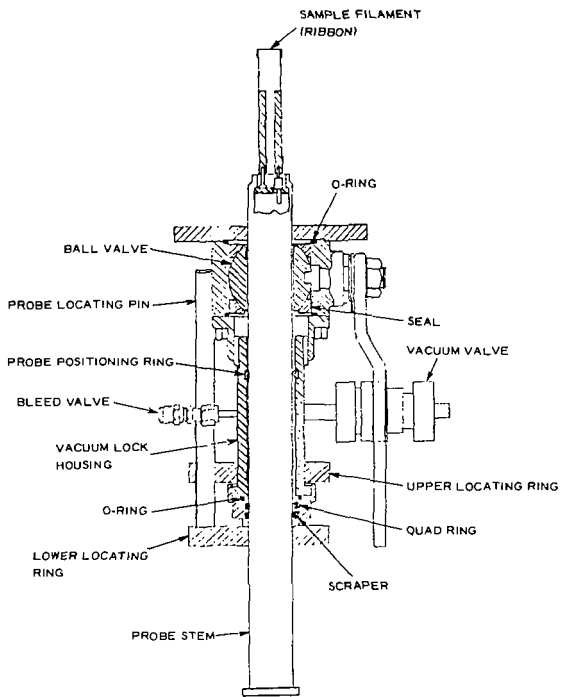


Figure 1 Bendix Direct Inlet Sample Probe

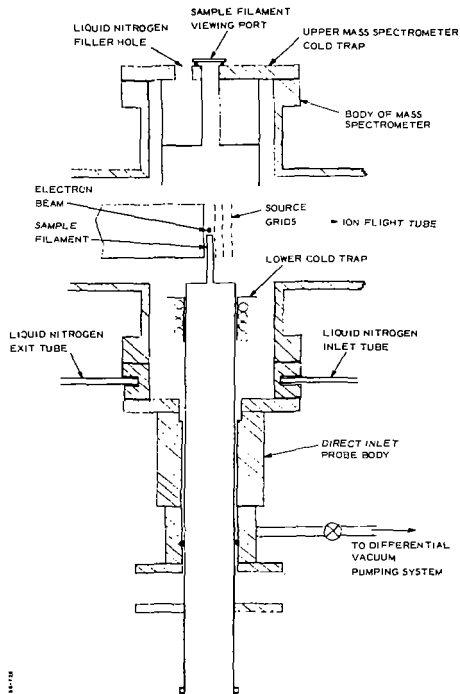


Figure 2 Complete Sample Probe and Trap Assembly

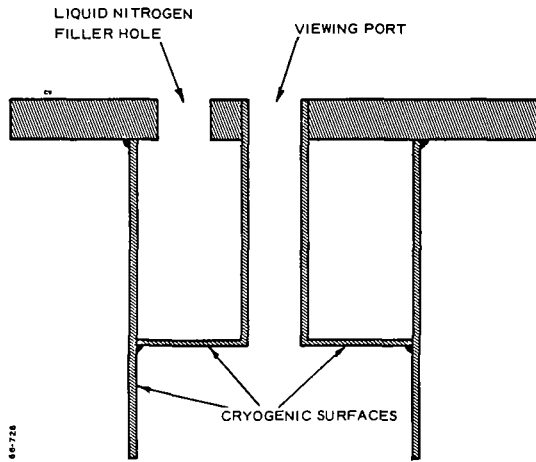


Figure 3 Upper Cold Trap for Ionization Region

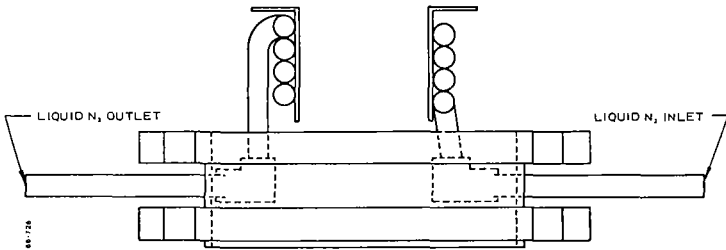


Figure 4 Lower Cold Trap for Ionization Region

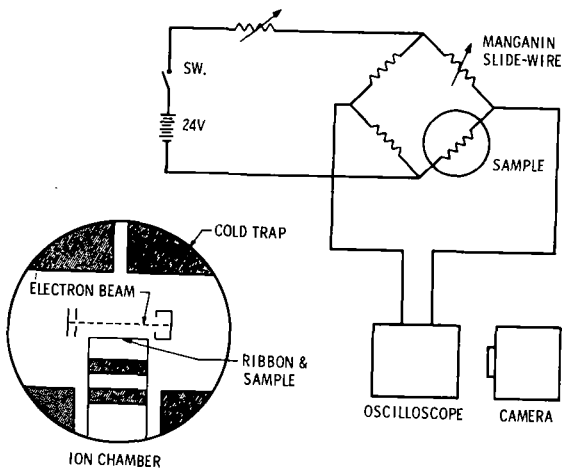


Figure 5 Dynamic FMTA Schematic

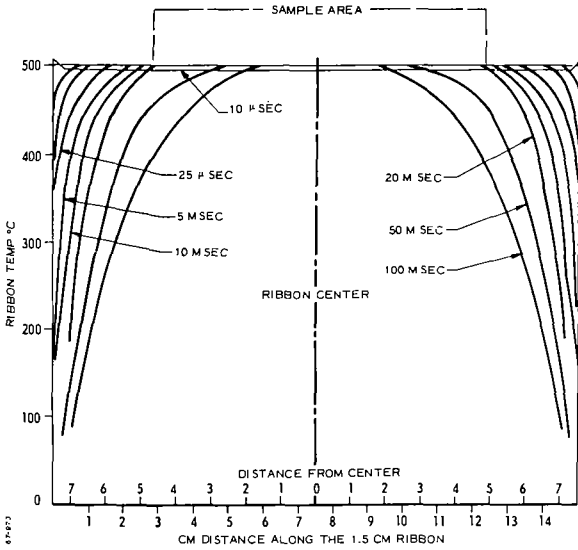


Figure 6 Computer-Predicted Ribbon Temperature Profile

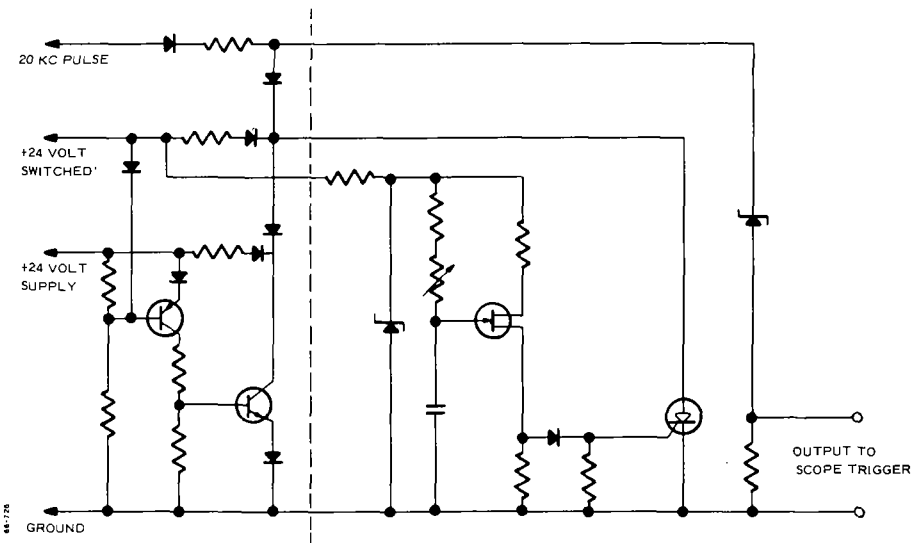


Figure 7 Variable Delay Oscilloscope Blanking Circuit

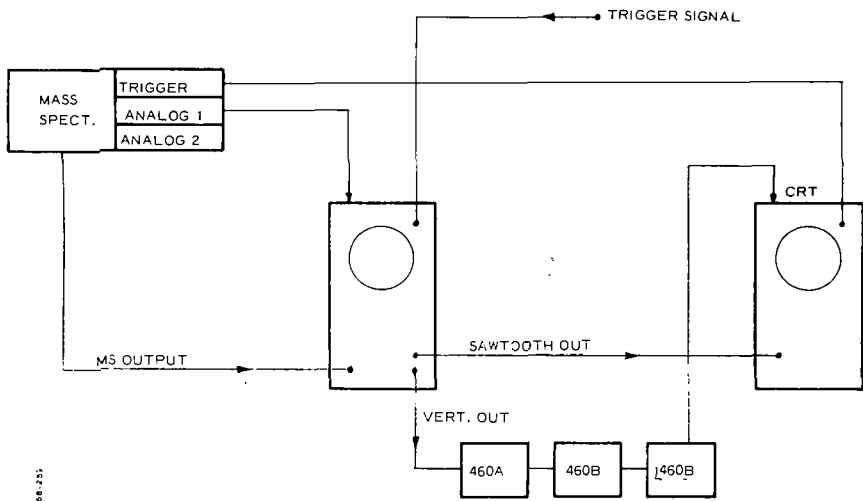


Figure 8 Z-Axis Experimental Arrangement

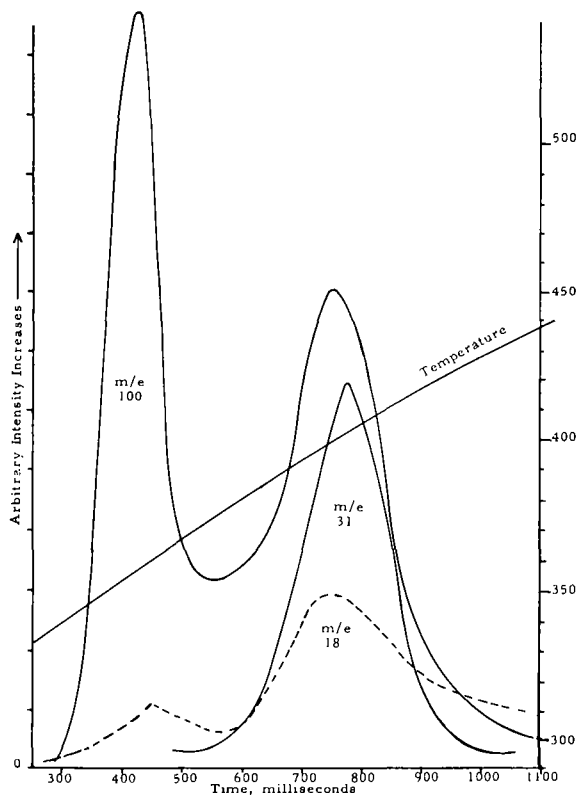


Figure 9 History of Fragments from Flash MTA of HP_2

For the slow heating experiments, a Milliken DBM-5C high speed framing camera was employed to photograph the spectrum oscilloscope trace at a speed of 200 frames/second (5 milliseconds/frame). In general, the heating rate was 100°C/sec. With the small sample, the pyrolysis event was usually completed within 2 seconds. To synchronize the temperature trace oscilloscope with the spectrum oscilloscope, a flashlamp was triggered simultaneously with the beginning of current input to the ribbon. The flash over-exposes the first few frames of the spectrum oscilloscope, thereby marking the beginning of the heating. The same trigger pulse that fires the flashlamp is also used to trigger the sweep of the temperature trace oscilloscope.

With the rapid heating method, two techniques of data acquisition were used. In the first method, the spectrum is recorded on a single exposure with a Polaroid camera. Since the mass species of interest are generated in the first 2 milliseconds after rapid heating is begun, it is necessary to blank out the oscilloscope trace after that period so that the build-up of gaseous products are not superimposed over the species of interest. Another reason for doing this is that, even though the sample is small, the ion concentration is high enough to saturate the multiplier electronic circuit which makes the resultant spectrum useless. The circuitry for blanking out the oscilloscope is given in Figure 7. The 10 KHz recurrent mass spectrometer trigger pulse is fed continuously to the spectrum oscilloscope causing the trace to sweep continuously. When the sample firing switch is activated, the positive 24 volt DC source is applied to the anode of the SCR. At the same time, the capacitor in the emitter circuit becomes charged through the variable resistor. At the peak emitter voltage, the UJT* conducts and the voltage is applied at the gate of the SCR, causing it to conduct. The 10 KHz trigger signal voltage then falls sharply to a value which will no longer trigger the spectrum oscilloscope. An advantage of this method over mechanical camera shutters is that the blanking time can be continuously varied and also precisely synchronized with the beginning of the rapid heating.

In the second method, a roughly semiquantitative technique which has been described by Lincoln^(1,2) was used. The method is termed Z-axis data display. The data is displayed on an oscilloscope in which each sweep is sufficiently displaced vertically upward from the preceding sweep. The mass units are displayed as a series of dots along each sweep, and the dot intensity is a function of the signal strength of each mass peak. The experimental arrangement, which requires two oscilloscopes and three amplifiers is given in Figure 8.

Oscilloscope No. 1 is triggered externally from the sample firing switch and is set for single sweep operation. Any single peak of interest in the spectrum may be selected to be displayed on this oscilloscope by feeding the time variable analogue gate pulse from the mass spectrometer to the CRT* input. Since the sweep speed of this oscilloscope is slow compared to the analogue pulse sampling rate, as many as 500 samples of the selected mass peak may be displayed during the single sweep.

Oscilloscope No. 2 is triggered as in the usual method for observing the mass spectrum. The vertical input is a linearly increasing ramp voltage which is derived from the sweep generator of oscilloscope No. 1. The sweep rate of oscilloscope No. 2 is 500 times faster than oscilloscope No. 1, and consequently the ramp voltage is sampled stepwise and is displayed as a series of nearly horizontal lines starting in time at the bottom of the CRT and progressing to the top. The mass spectrum signal which is originally fed into oscilloscope No. 1 is taken from the "vertical signal out" terminal of oscilloscope No. 1, amplified and inverted by three wide-band amplifiers and is fed into the CRT terminal of oscilloscope No. 2. The trace of oscilloscope No. 2 is brightened by the mass peak pulses and appears as a series of dots rather than vertically deflected peaks. The intensity of the dots is roughly proportional to the mass peak height. Since the vertical axis now represents time, the appearance and growth rate of mass fragments with respect to each other may be observed. Although the method can be considered only semi-quantitative, it affords a convenient means of time resolution which can elucidate the order of appearance of mass fragments. For a more detailed description, see References 1 and 2.

Flash mass thermal analysis as described above has been used extensively to detect the early thermal decomposition species in such materials as nitrocellulose (NC), ammonium perchlorate (AP), hydroxylamine perchlorate (HAP) and hydrazinium diperchlorate (HP₂). As examples of the types of phenomena that are observed by means of FMTA, nitrocellulose and hydrazinium diperchlorate time-intensity histories shall be presented here.

* SCR Silicon Controlled Rectifier
UJT Uni Junction Transistor
CRT Cathode Ray Tube

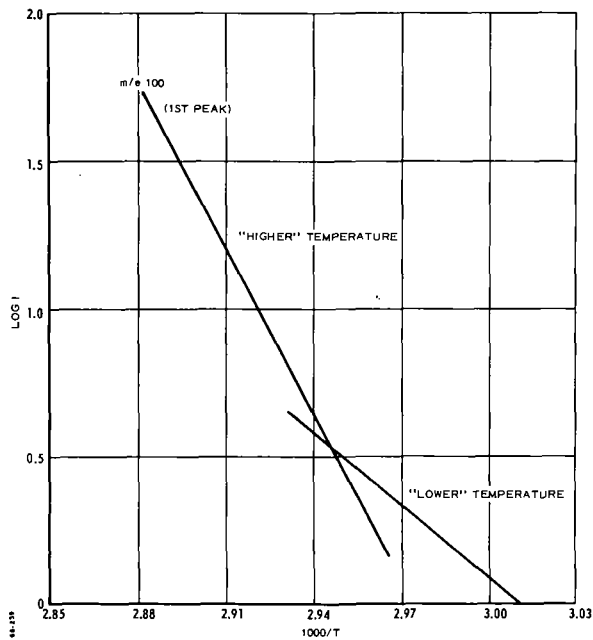


Figure 10 Arrhenius Plot of HClO_4 from Flash MTA of HP_2

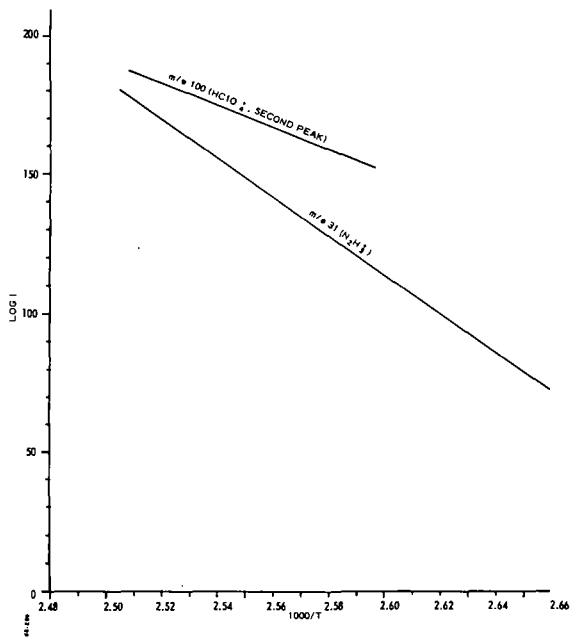


Figure 11 Arrhenius Plots for HClO_4^+ and N_2H_3^+ from the Flash FMTA of HP_2

Preliminary analysis of the films from the FMTA of HP_2 shows that the decomposition occurs in two distinct stages. The time-intensity curves, shown in Figure 9 illustrate the double peaks which are typical of all ion fragments associated with the perchloric acid parent thermal decomposition fragment. The single peaks which occur at later times are typical of all ion fragments associated with the hydrazine thermal fragment. This behavior indicates that the first process involves splitting off $HClO_4$, followed by complete disruption of the molecule at still higher temperatures.

Arrhenius plots for the $HClO_4$ (m/e 100) fragment and the hydrazine fragment $N_2H_3^+$ (m/e 31) are presented in Figures 10 and 11. The activation energies calculated from these plots are presented below.

Species	m/e	Activation Energies (Kcal/mole)		
		First Peak		Second Peak
		"Low T"	"High T"	
$HClO_4^+$	100	23	86	18
$N_2H_3^+$ (from $N_2H_4^+$)	31		32	

The activation energies and the Arrhenius plots show that the initial loss of $HClO_4$ begins with a low energy requirement, and converts to a high energy requirement⁴ at higher temperatures. Subsequent production of $HClO_4$ at the second peak then proceeds with an activation energy approximately the same as that for the low temperature stage of the initial decomposition. Production of m/e 31 overlaps the first and second $HClO_4$ peaks and seems to require an intermediate constant activation energy. This activation energy of 23 Kcal/mole compares well with that obtained at RMD³. The mass spectral data obtained from the dynamic FMTA also is consistent with the reaction mechanism postulated by the RMD workers - the initial peak is most likely because of the loss of one $HClO_4$ moiety, leaving hydrazinium monoperchlorate (HP). The HP then vaporizes at the higher temperature, and yields its characteristic mass spectral cracking pattern.

The FMTA of nitrocellulose shows similarities with that of HP_2 . The Arrhenius-type data treatment has been applied to the initial decomposition species. Figure 12 shows the intensity/time history of nitrocellulose. The two-stage reaction mechanism is evident, as is the transposition of the roles of the ions at m/e 46 and 30. The portions of the curves labeled "A" are obtained at early times (low temperature) and the portions labeled "B" are obtained at later times (higher temperatures). These portions are for the first peak only and do not describe the activation energy requirements for the second peak.

Figure 13 shows the results of the Arrhenius plot for portions A and B of the NC decomposition curve. The activation energies of 95 ± 5 Kcal/mole for the A portion and 16 ± 2 Kcal/mole for the B portion are in excellent agreement with the values of 100 Kcal/mole and 14 Kcal/mole reported by R. Musso⁽⁴⁾ of Hercules (ABL) for these same portions. This agreement with other data confirms the correctness of the experimental approach and the validity of the assumptions made in the calculation of the activation energies.

In summary, the FMTA technique provides an insight to early decomposition products which no other method has been able to demonstrate. The small sample, heated at a rapid rate, permits only a small amount of interaction in the gaseous phase. This condition enables detection of initial decomposition products which can be masked in larger samples heated at slower rates. Agreement of kinetic parameters using FMTA with those of other methods serves to confirm the validity of the FMTA technique.

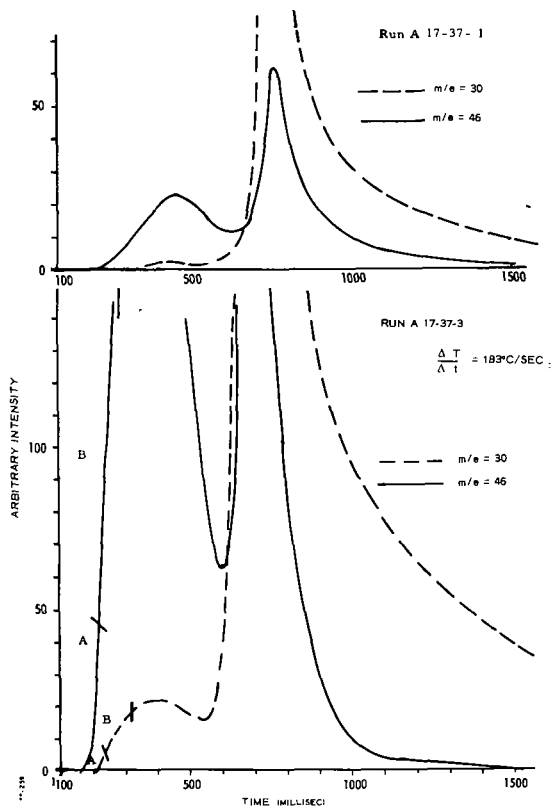


Figure 12 Flash MTA of Nitrocellulose, Showing m/e 30 and 46

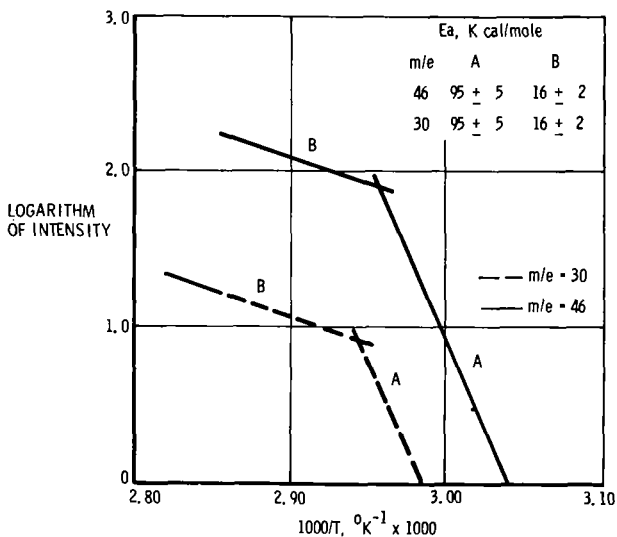


Figure 13 Arrhenius Plots for m/e 46 and 30 from Nitrocellulose Pyrolysis

References

- (1) Lincoln, K. A. USNRDL Report No. TR-731, March, 1964
- (2) Lincoln, K. A., "Improved Instrumentation for Time-Resolved Mass Spectrometry with Application to LASER-Vaporization of Solid Materials", Int. J. of Mass Spect. and Ion Phys., 2 (1969) 75-83
- (3) Grelecki, C. J. and Cruice, W., "Thermal Decomposition of Hydrazinium Mono-perchlorate and Hydrazinium Diperchlorate", Advanced Propellant Chemistry, ACS Advances in Chemistry Series 54, pp 73-81, Washington, D. C., 1966
- (4) Musso, R. (Hercules, ABL), private communication, 10 October 1967

MASS THERMAL ANALYSIS OF HYDROXYLAMINE AND METHOXYAMINE PERCHLORATES

Berge B. Goshgarian
Air Force Rocket Propulsion Laboratory
Edwards, California

ABSTRACT

Mass thermal analysis was used to study the thermal decomposition of hydroxylamine and methoxyamine perchlorates. The first step in the thermal decomposition of these salts is the proton transfer from the substituted ammonium ion to the perchlorate anion to form the free substituted amine and perchloric acid. Activation energies were determined to be 20.7 ± 2 kcal/mole ($65^\circ - 77^\circ\text{C}$) for the dissociation of hydroxylamine perchlorate, and 30 ± 2 kcal/mole ($53^\circ - 77^\circ\text{C}$) for the dissociation of methoxyamine perchlorate.

INTRODUCTION

The use of a mass spectrometer to identify the gaseous species formed during controlled thermal degradation of a solid has been termed mass thermal analysis (MTA). This technique may be used in conjunction with differential thermal analysis [1,2] thermogravimetric analysis [3] and thermal decomposition analysis [4,5] to provide insight into both the physical and chemical processes involved in phase changes, weight loss, and decomposition resulting from the thermal environment of a particular system.

The ion intensities of the gases liberated from the heated samples, and the temperature at which the gases are liberated can be plotted by the Arrhenius method to obtain activation energies for the processes occurring.

MTA techniques was chosen for our studies to determine the activation energies necessary for dissociation of hydroxylamine and methoxyamine perchlorates, and to identify the dissociation and oxidation products occurring during thermal decomposition.

EXPERIMENTAL PROCEDURE

A self-contained solids sample probe fabricated in our laboratory for these studies is shown in Figure 1. The probe head is made by wrapping five inches of #28 gauge nichrome resistance heater wire around the 30 mm long x 3 mm OD alumina tube shield. Two copper lead wires, cemented into the alumina probe body and used as electrical feed throughs for the heater, provided mechanical strength for the probe head.

Sample holders were made by fusing the centers of 25 mm x 2 mm OD glass melting point tubes and fit tightly into the alumina tube shield. A chromal-alumel thermocouple extending from the probe rod, fit tightly against the bottom of the sample holder to provide accurate measurement of the sample temperature.

The probe was inserted horizontally through a vacuum seal to within 10 mm of the electron beam in the ion source of a Consolidated Electrodynamics Corporation Model 21-110A mass spectrograph. The source was then evacuated to less than 2×10^{-7} torr prior to run.

The heating rate of the sample during a run was controlled by a Hewlett-Packard temperature programmer, and was limited to $0.5^\circ\text{C}/\text{minute}$. This permitted the pumping rate to maintain the total source pressure in the low 10^{-8} torr range during maximum gas evolution.

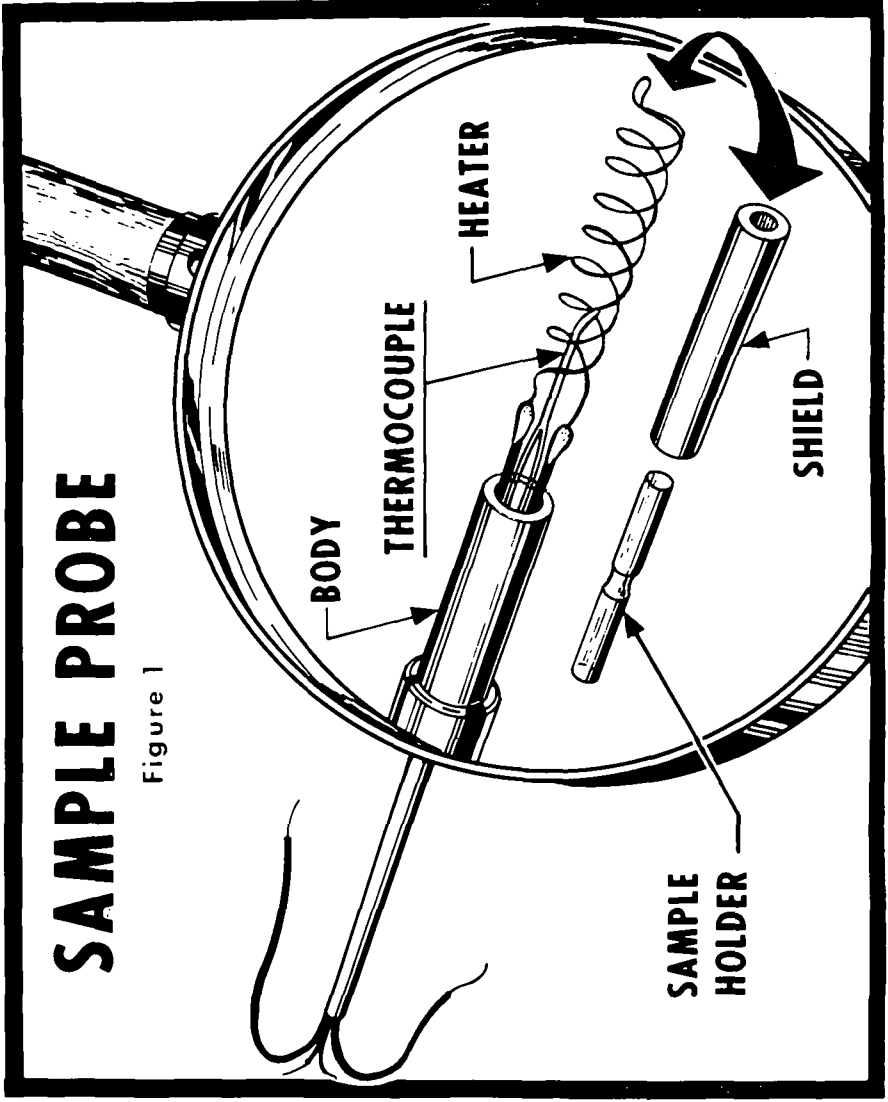
Spectra were collected on Ilford 0-2 photo plates using a constant exposure value of 7×10^{-12} coulombs. Obtaining this exposure value required from two minutes at the beginning of dissociation to less than one second during maximum dissociation and re- action. A constant exposure value was used to integrate and identify small quantities of dissociated products during initial stages of thermal dissociation.

Densities of the ion lines on the photoplates were obtained from a microphotometer trace and were reduced by computer. Line width and mass position corrections were made, however, no relative sensitivity corrections were made.

Reduced ion line density data were divided by the time required to obtain the constant exposure at a specific temperature, to yield an ion intensity-time relationship. The logarithm of the ion intensity-time relationship was plotted versus the inverse absolute temperature and the resultant slope value was inserted in the Arrhenius equation to obtain activation energies.

SAMPLE PROBE

Figure 1



RESULTS AND DISCUSSION

A. Hydroxylamine Perchlorate

An Arrhenius plot of the hydroxylamine (NH_2OH) and chlorate (ClO_3) ion intensities resulting from controlled thermal dissociation of hydroxylamine perchlorate ($\text{NH}_3\text{OHCIO}_4$) and the resulting perchloric acid (HOClO_3) are shown in Figure 2. A change in slope of the ion intensity lines is evident at 64°C ; this may be the result of a crystalline phase transition for hydroxylamine perchlorate which has been reported [6] to occur between $57^\circ - 62^\circ\text{C}$. An activation energy of 57.7 ± 2 kcal/mole was calculated for the transition from the slope of the line below 64°C .

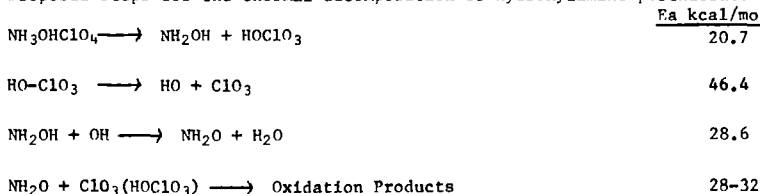
Once the crystalline phase transition is complete, dissociation of the solid hydroxylamine perchlorate continues smoothly to its melting point at 80°C . Melting was noted by a variation in relative peak intensities from the slope as well as by momentary cooling of the sample temperature, as would be expected for the endothermic melting process.

The activation energy for the dissociation of hydroxylamine perchlorate to hydroxylamine and perchloric acid between $65^\circ - 77^\circ\text{C}$, calculated from the slope of the hydroxylamine ion intensity line, is 20.7 ± 2 kcal/mole.

The calculated activation energy obtained from the slope of the chlorate ion intensity line, resulting from perchloric acid dissociation was 46.4 ± 2 kcal/mole. This value compares favorably with the value of 45.1 kcal/mole obtained by Levy [7] for the activation energy of the homogeneous thermal decomposition of perchloric acid vapor to HO and ClO_3 . The activation energy thus corresponds to the HO- ClO_3 bond strength of 45 kcal. This value was used as an internal standard in our studies.

Arrhenius plots for the NH_2O ion and N_2O oxidation product ion are shown in Figure 3. An increase in activation energy of 8 kcal/mole is required to dissociate the hydroxylamine after the hydroxylamine perchlorate has begun to dissociate. Once the hydroxylamine dissociates, oxidation of the dissociation products by perchloric acid proceeds.

Proposed steps for the thermal decomposition of hydroxylamine perchlorate are:



The initial reaction is the dissociation of the hydroxylamine perchlorate to the free amine and perchloric acid. Once dissociation occurs, further energy is required to dissociate the free amine and to oxidize the dissociation products.

Products identified during the oxidation of dissociated hydroxylamine by perchloric acid include water, oxides of nitrogen, oxygen, and hydrogen chloride, all formed by processes exhibiting activation energies between 28-32 kcal/mole.

B. Methoxyamine Perchlorate

An Arrhenius plot of the methoxyamine (CH_3ONH_2) and chlorate (ClO_3) ion intensities resulting from the thermal dissociation of methoxyamine perchlorate ($\text{CH}_3\text{ONH}_2\text{ClO}_4$) and the resulting perchloric acid (HOClO_3) are shown in Figure 4. No crystalline phase transitions for methoxyamine perchlorate occur in the temperature range studied, consequently, no changes in slope are observed.

The activation energy for the dissociation of methoxyamine perchlorate to methoxyamine and perchloric acid between $53^\circ - 77^\circ\text{C}$, as calculated from the slope of the methoxyamine ion intensity line, is 30 ± 2 kcal/mole.

The slope of the chlorate ion, representing the dissociation of perchloric acid, yields an activation energy of 44.2 ± 2 kcal/mole. This value is similar to the previous activation energy calculated for the perchloric acid dissociation in the hydroxylamine perchlorate case.

Arrhenius plots for some of the products of methoxyamine and perchloric acid inter-reactions are shown in Figure 5. The activation energies for these products lie in the

Figure 2

HYDROXYLAMINE PERCHLORATE DISSOCIATION

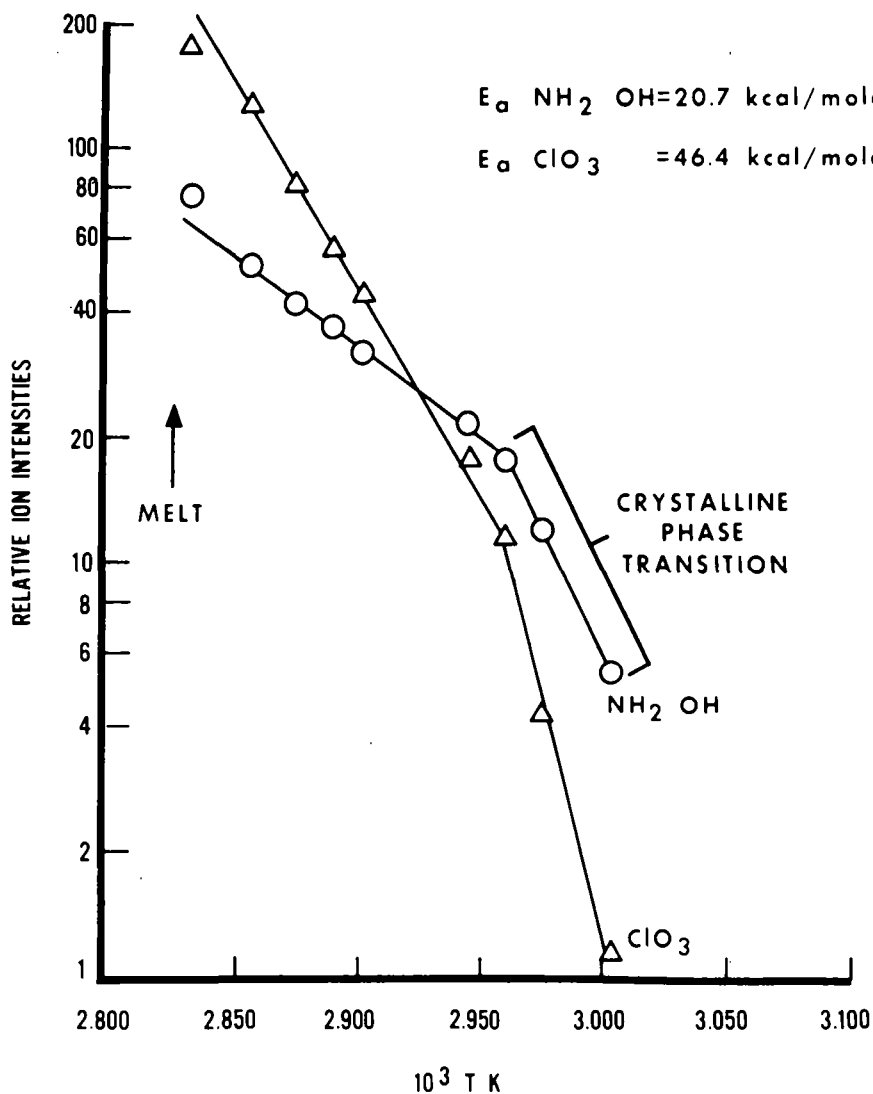


Figure 3

HYDROXYLAMINE PERCHLORATE DECOMPOSITION & REACTION PRODUCTS

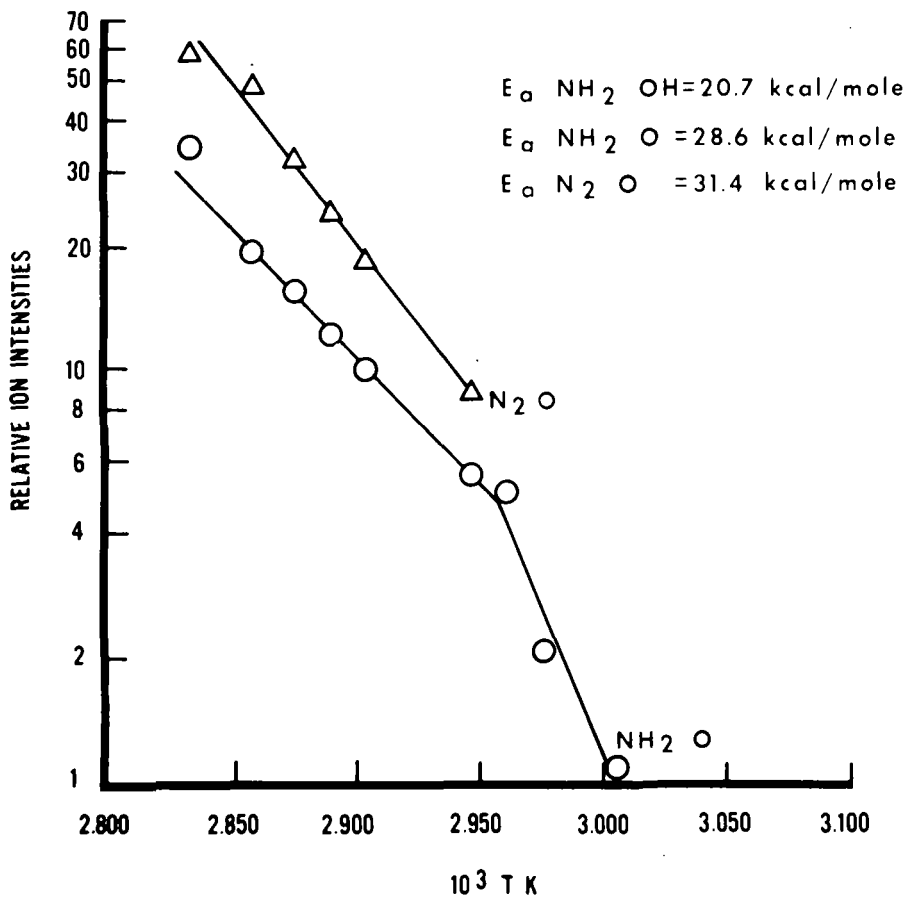


Figure 4

METHOXYAMINE PERCHLORATE DISSOCIATION

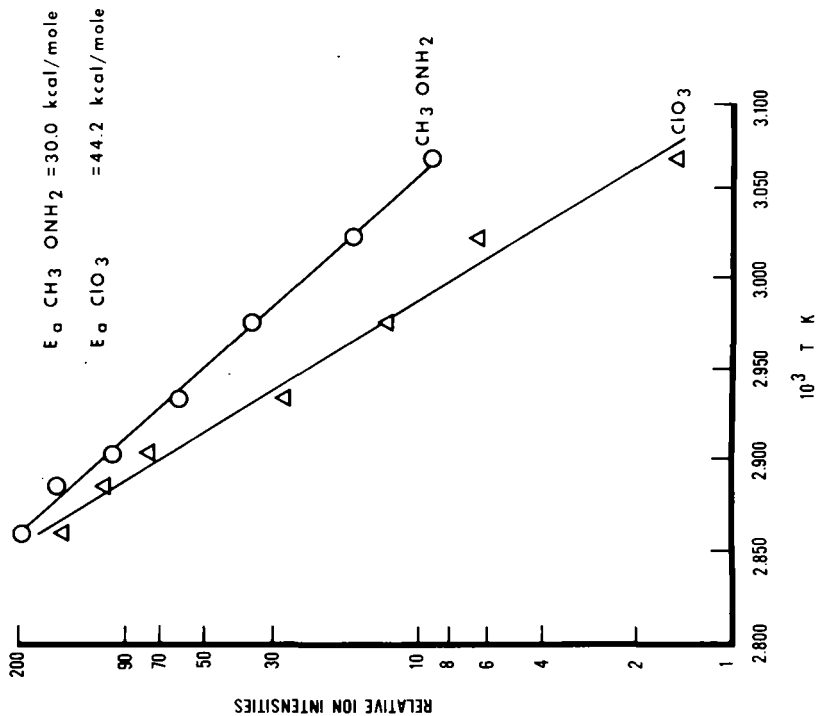
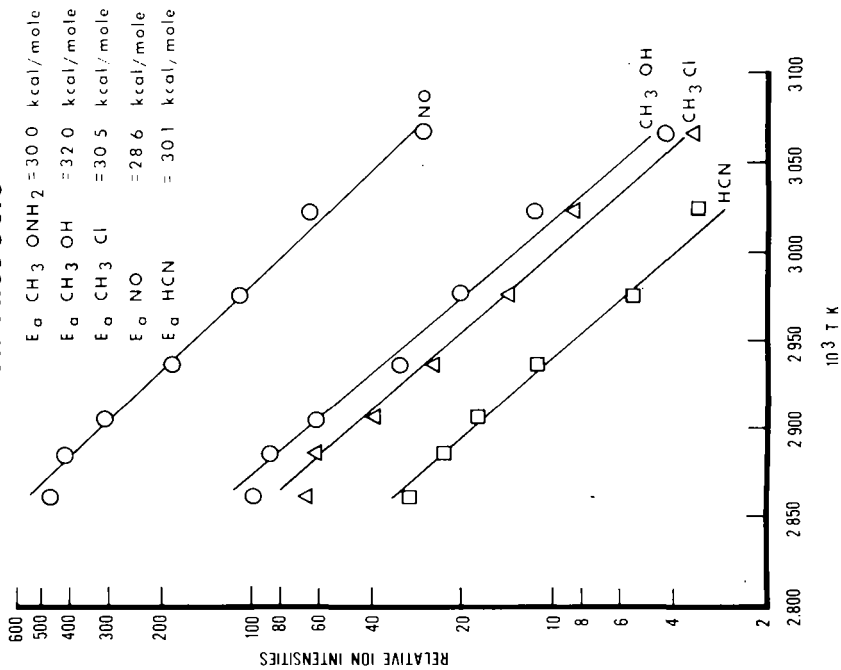


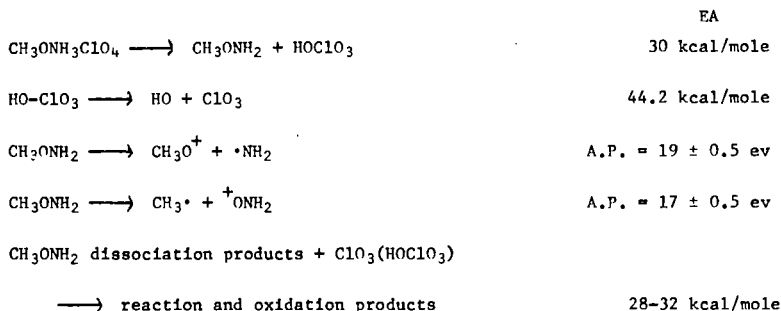
Figure 5

METHOXYAMINE DECOMPOSITION & REACTION PRODUCTS



range 28-32 kcal/mole, as with that calculated for the dissociation of methoxyamine perchlorate. Therefore, once methoxyamine perchlorate dissociates, sufficient energy is available in the system for the dissociation and reaction of the amine with perchloric acid to proceed.

Proposed steps for the thermal decomposition of methoxyamine perchlorate are:



The rate limiting reaction is the thermal dissociation of the methoxyamine perchlorate. Once this dissociation occurs, the methoxyamine immediately decomposes, forming either CH_3O and NH_2 or CH_3 and NH_2O . Appearance potential data for methoxyamine indicate that the $\text{CH}_3\text{-O}$ bond is weaker than the O-NH_2 bond. Therefore, preferential fragmentation will be CH_3 and NH_2O , with the methyl radical reacting further to form methylated compounds and oxides of carbon. The NH_2O radical will readily oxidize to nitrogen oxides and water.

Reaction and oxidation products include methyl chloride, methyl alcohol, hydrogen chloride, hydrogen cyanide, methyl perchlorate, water, and the oxides of carbon and nitrogen. All products exhibited activation energies between 28-32 kcal/mole.

SUMMARY

In summary, the mass thermal analysis of hydroxylamine and methoxyamine perchlorates indicate that the first step in thermal decomposition is the proton transfer dissociation of the amine perchlorate salt to the free amine and perchloric acid. The perchloric acid then undergoes decomposition, forming reactive ClO_3 radicals, which attack the amine or its dissociation products to form addition and oxidation products.

Since the thermal dissociation of methoxyamine perchlorate requires an activation energy approximately 9 kcal/mole greater than that for the hydroxylamine perchlorate, the methoxyamine can be concluded to be a stronger base than the hydroxylamine.

REFERENCES

1. Langer, H. G. and Karle, F. J., Paper #17, Fifteenth Annual Conference on Mass Spectrometry and Allied Topics, Denver, Colorado, May, 1967.
2. Gohlke, R. S., Paper #73, Fourteenth Annual Conference on Mass Spectrometry and Allied Topics, Dallas, Texas, May 1966.
3. Haddon, W. F., DiEdwardo, A. H., Zitomer, F., "Thermogravimetric - Mass Spectrometric Analysis", Seventeenth Annual Conference, ASTM E-14, Paper No. 76.
4. Friedman, H. L., Goldstein, H. W., and Giffith, G. A., Paper #8, Fifteenth Annual Conference on Mass Spectrometry and Allied Topics, Denver, Colorado, May 1967.
5. Gaulin, C. A., Gilmartin, D. F., Wachi, F. M., "A Mass-Thermal Method for Studying Ablative Polymer Degradation Mechanisms", Aerospace Corp. Report #N68-31794, March 1968.
6. Dickins, B., "Crystal Structure of Hydroxylamine Perchlorate", Unpublished Results, Naval Ordnance Station, Indian Head, Md.
7. Levy, J. P., "Thermal Decomposition of Perchloric Acid Vapor", J. Phy. Chem. 66, 1092, 1962.

CYCLIC OLIGOMERS PRODUCED BY DEGRADING POLY(ETHYLENE TEREPHTHALATE)
IN THE SOURCE OF A MASS SPECTROMETER*

J. S. Lewis, J. C. Gilland, Jr., and V. W. Goodlett

Research Laboratories, Tennessee Eastman Company,
Division of Eastman Kodak Company, Kingsport, Tennessee 37662

Abstract

When poly(ethylene terephthalate) is heated in the direct insertion probe of a mass spectrometer, degradation products are formed. Some of the degradation products and low molecular weight oligomers present in the polymer are volatile enough to give a useful mass spectrum. Our objective was to use both high- and low-resolution mass spectrometry to identify the vaporizable components present and those produced thermally and to elucidate the mechanism of formation of these species.

Since approximately 90% of the solvent-extractable oligomers present in poly(ethylene terephthalate) is the cyclic trimer of ethylene glycol and terephthalic acid (molecular weight 576), a thorough investigation was made of the m/e peaks from this molecule, with associated metastable ions, to determine the mechanism of ion fragmentation. The molecular ion undergoes fragmentation via a McLafferty rearrangement to yield an ion at m/e 533 which is quite characteristic of the cyclic trimer. Intense peaks were found at m/e 725, 917, and 1109, which are the strong peaks expected from the cyclic tetramer, pentamer, and hexamer, respectively, assuming a similar rearrangement.

Two questions arise concerning the origin of the cyclic oligomers:

1. Are the cyclic oligomers due to thermal degradation in the mass spectrometer or are they present before heating?
2. If the cyclic oligomers are thermal degradation products, what is the mechanism for their formation?

A sample of poly(ethylene terephthalate) was dialyzed to remove the cyclic and linear oligomers. The mass spectra of the degradation products from this sample are very similar to the spectra of the normally prepared polymer, which is evidence that the cyclic oligomers are produced during the thermal degradation of the polymer.

Two experiments were carried out to determine the effect of hydroxyl end group participation in the formation of cyclic oligomers. In the first experiment, poly(ethylene terephthalate) model compounds were heated in the inlet system of the mass spectrometer. We found that cyclic trimer is produced in the inlet of the mass spectrometer by heating hydroxyl-terminated monomer, dimer, or trimer at approximately 200°C. The formation of the cyclic trimer was not observed when a methyl ester terminated sample was heated.

A further study of the formation of cyclic oligomers involved the examination of dialyzed poly(ethylene terephthalate) and poly(ethylene terephthalate) with benzoate-capped end groups. The capped sample had been reacted with benzoyl chloride to form benzoate end groups from the hydroxyl end groups. Analysis of the end groups showed only 15% hydroxyethyl. Essentially all of the cyclic and linear oligomers had been removed from both samples. The spectra for the dialyzed sample and the capped sample are very similar, which indicates that decreasing the hydroxyl end groups does not prevent reequilibration.

We conclude from the first experiment that the presence of hydroxyl end groups is necessary for cyclic oligomer formation. However, the second experiment shows that the reduction of hydroxyl end groups in the polymer does not reduce the amount of cyclic oligomers produced by thermal degradation.

*This paper will be submitted for publication in the Journal of Polymer Science.

Poly(1,4-cyclohexylenedimethylene terephthalate) was also heated in the direct insertion probe. An intense peak was observed at m/e 423, presumably arising from a McLafferty rearrangement of the cyclic dimer.

THE USE OF PARTIAL PRESSURE MASS SPECTROMETRY IN THE THERMAL ANALYSIS STUDY
OF CARBONS AND GRAPHITE

By

John Dollimore, Clive M Freedman and Brian H Harrison
Department of Pure and Applied Physics
University of Salford
Salford 5
Lancashire
UK

ABSTRACT

A versatile partial pressure mass spectrometer system is described for measuring thermally desorbed species from solid surfaces. The system evaluates not only the ratio of masses quantitatively present in the gaseous phase but also relates the specific mass (mg per g of solid) desorbed or decomposed during thermal treatment. The extension of the method to oxidation studies is also described.

A study has been made of the evolution of gases from graphitic and non-graphitic carbons. These range in properties from a ground graphite of specific surface 102 square metres/gm to a nuclear type graphite of 0.6 square metres/gm. A study of a non-graphitic carbon, Saran Charcoal, of molecular sieve type is also included.

The formation of surface oxide on a clean surface at pressures of the order 0.2 mm Hg is evaluated along with the resultant thermal decomposition of the surface oxide. The data from this paper along with other published work on graphites is reviewed and used to illustrate the application of the thermal desorption results to oxidation studies on carbons and graphites.

1. Introduction

The reaction of molecular oxygen with graphite is primarily associated with the peripheral atoms of the basal planes¹. A study of graphite-oxygen reactivity is therefore closely aligned to the extent of the graphite edge planes. Low temperature oxidation of graphites at temperatures below 1000°C is markedly influenced by the presence of stable surface oxide².

It has now been established that the oxidation of graphite proceeds by the formation of stable surface oxide and the production of gaseous CO and CO₂³. At a given temperature the reaction between oxygen and a clean graphite surface has an initial transient period of surface oxide formation followed by a steady state reaction of the oxygen with the remaining uncovered part of the reactive surface. The steady state rate of oxidation is thus dependent on the proportion of exposed reactive surface.

The above mechanism has led us to investigate the proportion of the total surface which can be covered with surface oxide and its stability with temperature. The use of a partial pressure mass spectrometer allows us to follow the formation of surface oxide during the transient period of oxidation. The subsequent thermal decomposition of the surface oxide allows us to measure both its extent and thermal stability, thereby gaining an insight into the heterogeneity of the reactive surface⁴.

2. Experimental

2.1 Apparatus

The apparatus employed (Figure 1) was a static reaction system which consisted basically of a 40 cc's high purity silica reaction chamber leading into a 5.5 litre reservoir. The reservoir was connected to an AEI MS10 mass spectrometer via a fixed 10 lusec molecular leak valve, which allowed partial pressures of 0.1 to 600 microns in the reservoir to be measured with 1% accuracy on the mass spectrometer. The MS10 is a 2" radius, 180° deflection instrument employing electrostatic scanning. The mass spectrometer pumping system comprised of a 3" oil diffusion pump, cold trap and an orifice plate with a 1 litre/sec conductance. This arrangement allows continuous monitoring of the gaseous components in the reservoir with a sample loss of less than 2% over a period of 1 hour. A calibrated McLeod gauge was used to obtain conversion factors for ion current readings of CO, CO₂ and O₂ etc on the mass spectrometer to partial pressures in the reservoir chamber. Typical sensitivity-calibration plots are shown in Figure 2, which are carried out at the beginning and end of each experimental run. The reaction chamber and the reservoir could be evacuated to 10⁻⁶ mm's mercury

using two cold traps and an oil diffusion pump. High vacuum PTFE greaseless stopcocks were employed throughout the reaction system.

2.2 Design Considerations

The present experimental arrangement has been based on experience gained from the usage and interpretation of results obtained on a previous design⁵ which employed a 'batch' type sampling system. Certain disadvantages in the use of a 'batch' sampling system were encountered for this type of investigation which can be categorised as :-

- (a) The secondary reactions occurring between gaseous products and the sample when accumulating them over the sample.
- (b) The procedure of taking doses for analysis leads to a complicated mathematical correction⁵ to obtain quantitative results.
- (c) When the majority of the evolved gas is contained in the reaction chamber a large correction is necessary to allow for the difference in gas density in the hot and cold reaction zones⁵.
- (d) The restriction imposed on its versatility through being unable to directly monitor a continuous process.

The present system employs a direct sampling technique in which the majority of the evolved gas is collected in a 5.5 litre reservoir. The correction for about 30 cc's of the gas in the hot reaction zone is negligible relative to large reservoir volume. By a method employing an incremental desorption programme the problem of secondary gaseous reactions is reduced to a minimum by removing the desorbed gas at the temperature of desorption (c.f. section 2.3). This system has eliminated all the previous difficulties and allows direct monitoring of the reaction process.

2.3 General Procedure

The graphitic and non-graphitic samples were first cleaned by evacuating them to 10^{-6} mm's of mercury for 3 hours at 950°C. After cooling to the reaction temperature, the sample was isolated in the reaction chamber and a pre-determined oxygen pressure set in the reservoir. Initial pressures of oxygen were measured with the McLeod Gauge and on exposing the sample to the oxygen, the increase in the 28 (CO^+) and 44 (CO_2^+) mass peaks and the decrease in the 32 (O_2^+) mass peak were monitored with time. The depletion of oxygen in the gas phase gives the amount of surface oxide formed with time. To minimise the loss of sample gas, the leak valve was opened 2 minutes before a reading was required (allowing for dynamic equilibrium conditions to be obtained before taking the reading). At the end of an oxidation the oxygen and 'burn off' products above the sample were removed by evacuation. The reaction chamber and the reservoir were isolated from the diffusion pump and the sample temperature raised in given increments. During desorption studies the evolved CO and CO_2 resulting from the decomposition of surface oxide were monitored with time. At the end of each desorption run the reaction chamber was isolated from the reservoir, which was then quickly evacuated. This method prevented loss by isothermal desorption of the surface oxide during evacuation. Once evacuated the reservoir and reaction chamber were re-connected and the residual gas in the reaction chamber allowed to expand into the reservoir. This contribution to the reservoir background was usually found to be small and could easily be corrected for. By accurately calibrating the volume of the reservoir and by using the General Gas Law, $PV = nRT$, the mass of evolved gas at each stage could be determined.

3. Results and Discussion

3.1 Non-graphitic Carbon

This material was a polyvinylidene chloride carbon⁶ which has been the subject of a recent study. The versatility of the present system is illustrated in part by Figure 3 which shows the progressive formation of surface oxide on the clean surface of the P.V.D.C. carbon of total specific surface 1000 metres² gram⁻¹. Also shown is the accompanying depletion of oxygen and the production of 'burn off' products CO and CO_2 . It is noteworthy that one can see from Figure 3 a desorption of part of the surface oxide indicating that some of the oxide is unstable at the formation temperature. The amount of chemisorbed oxygen can be obtained directly from Figure 3 or by subsequent decomposition of the surface oxide and analysis of the oxygen present in the CO and CO_2 gaseous products.

The extent of surface oxide coverage can be determined from the number of carbon atoms desorbed on the basis of an assigned cross sectional area of 8.3\AA^2 for a carbon atom on the edge plane of graphite. The extent of surface oxide coverage on this non-graphitic

THERMAL DESORPTION APPARATUS

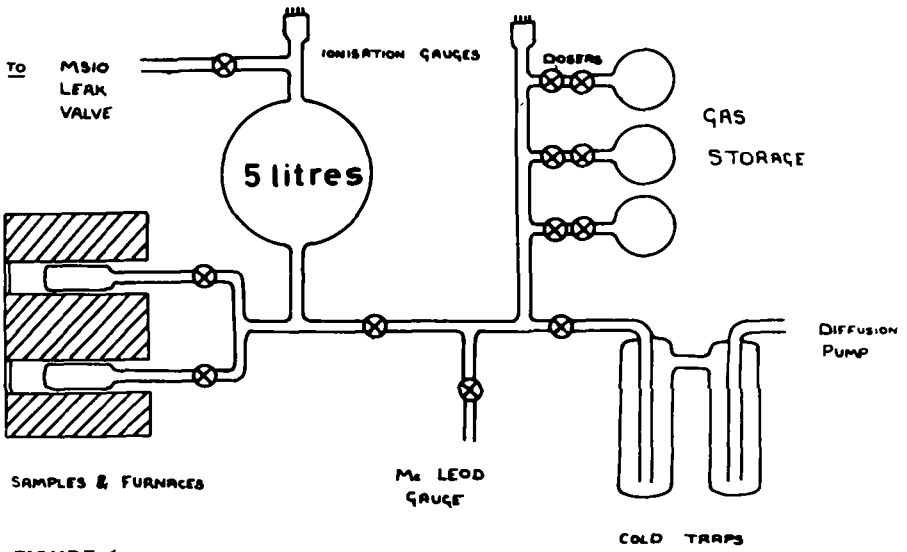


FIGURE 1

TYPICAL PRESSURE CALIBRATION RUN

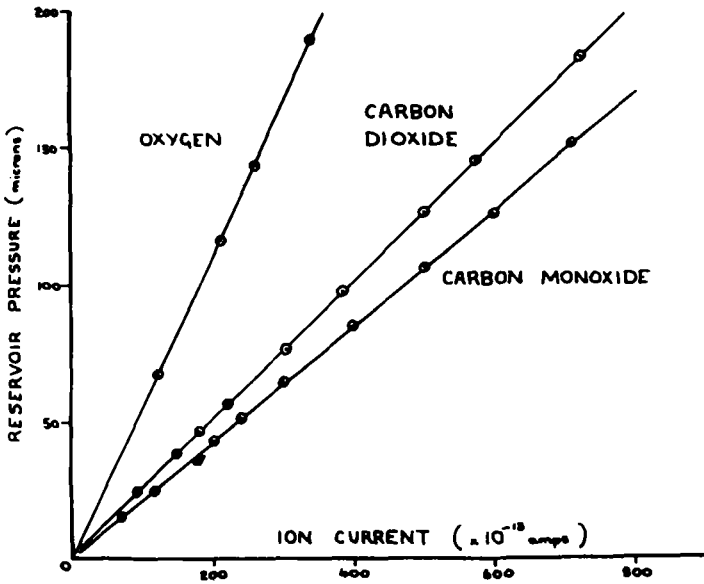


FIGURE 2

REACTION OF OXYGEN WITH SARAN CHARCOAL
AT 300°C PREVIOUSLY CLEANED AT 900°C

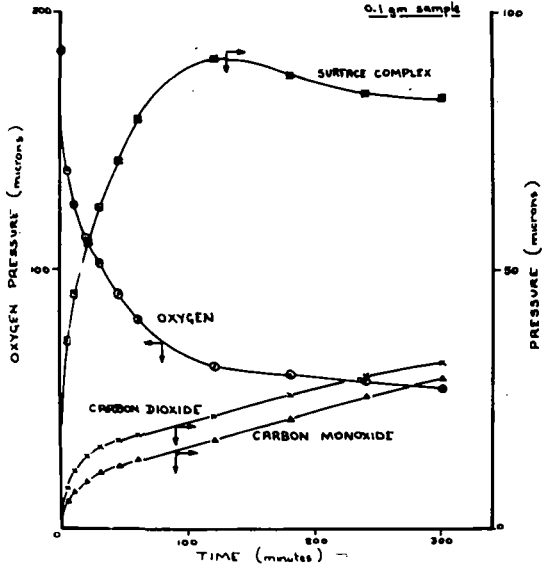


FIGURE 3

EFFECT OF TIME ON THE THERMAL DESORPTION OF GAS FROM SARAN CHARCOAL
AFTER OXYGEN CHEMISORPTION AT 300°C

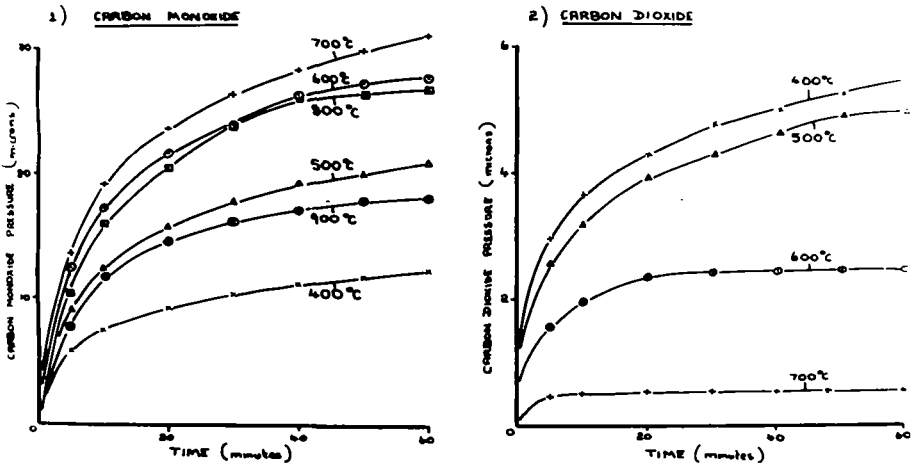


FIGURE 4

PLOTS OF LOG (RATE OF EVOLUTION) VS. ACCUMULATIVE EVOLVED CARBON MONOXIDE FROM SARAN CHAR USED IN DETERMINING ACTIVATION ENERGIES OF DESORPTION

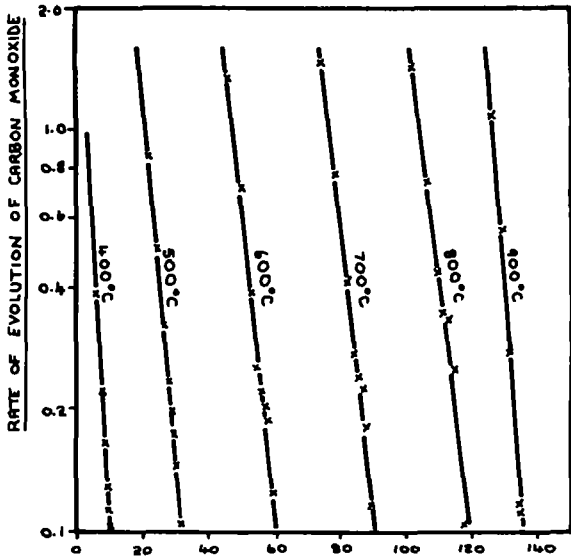


FIGURE 5 ACCUMULATIVE EVOLVED CARBON MONOXIDE (microns)

PLOTS OF ACTIVATION ENERGY vs COVERAGE ON SARAN CHAR

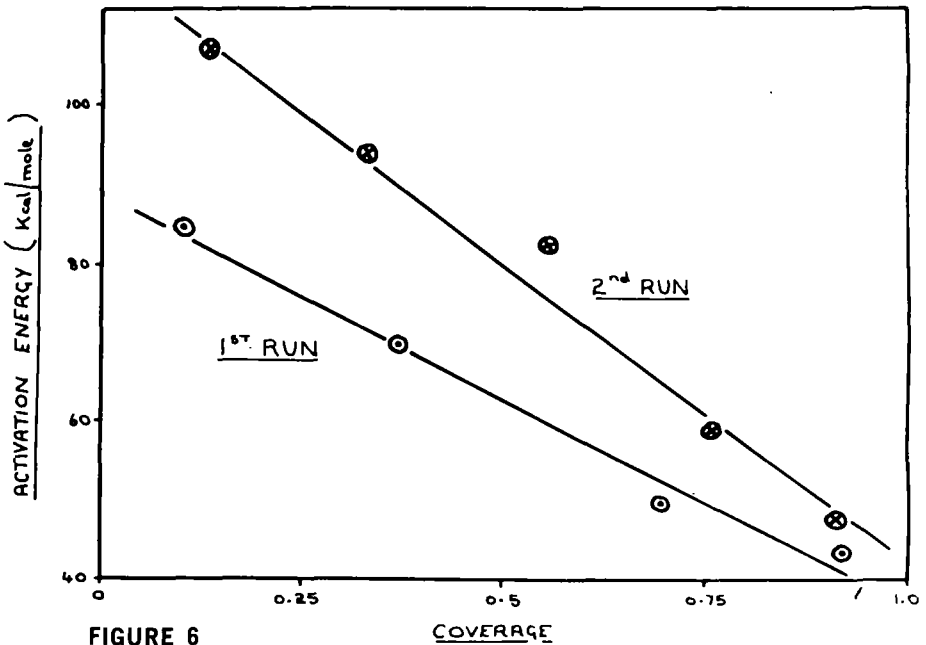


FIGURE 6

COVERAGE

carbon was found to be about 30 metres² gram⁻¹ or about 3% of the total surface.

The technique of isothermal desorption of the surface oxide can yield valuable information as to the energetic nature of the oxide on the surface. By using the isothermal pressure versus time curves shown in Figure 4 it is possible to obtain accurate isothermal desorption rate data. A computer programme has been developed which will fit each curve to an nth degree polynomial obtaining the best fit. This programme has the facility to differentiate the curves thus giving accurate rate data. Plots of log (desorption rate) versus total amount desorbed yield straight lines corresponding to each incremental desorption range.

From these plots it is possible to obtain two values for the rate of desorption at two consecutive temperature increments, both rates corresponding to one value of surface coverage. The Activation Energy of desorption (E) is then given by :-

$$\log_{10} \left(\frac{\text{desorption rate at } T_2}{\text{desorption rate at } T_1} \right) = \frac{E}{2.3 R} \left(\frac{1}{T_1} - \frac{1}{T_2} \right)$$

where R is the gas constant.

Figure 5 shows a typical plot of log (desorption rate) versus amount desorbed for CO desorbed from the P.V.D.C. carbon. The results obtained for the relationship between the activation energy of desorption with surface coverage of CO is shown in Figure 6 for two successive chemisorption-desorption cycles. This type of result might well be expected for an active carbon. These carbons are adsorbents with energy-heterogeneous surfaces resulting from both the random arrangement of elementary carbon crystallites on the surface of the adsorbent and the effect of the increase in energy of adsorption in very fine pores of carbon due to the superposition of forces of the opposite capillary walls⁷.

3.2 A Graphitic Carbon

This material was a ground Acheson's graphite with a total specific surface of 102 metres² gram⁻¹. It has been the basis of extensive desorption studies⁸, using a combined vacuum microbalance and mass spectrometer system, to compare the extents of graphite edge planes by X-ray line broadening techniques with the result obtained from a study of the desorbed surface oxide. The present discussion is therefore confined to the use of the mass spectrometer to determine the oxidation behaviour of this particular graphite. A series of experiments have been carried out on the cleaned surface of this graphite over a range of increasing temperatures. The interaction of oxygen at 400°C and 600°C is illustrated in Figures 7 and 8. Plots of the type shown in Figures 7 and 8 show the relationship between the various gaseous products during the course of an oxidation. However for a more detailed insight into the rate controlling mechanism for the oxidation it is necessary to plot Figures similar to 9 and 10 where the log of oxygen pressure is plotted with time.

The straight lines obtained indicate that there is a 1st order reaction where the rate controlling process is the dissociation of the oxygen molecule at the graphite surface. The initial deviations from a 1st order reaction are illustrated in the 300 and 400°C oxidation plots (but not at 600°C) and are due to the extra depletion of oxygen pressure to form the surface oxide in the initial transient period.

At the lower temperatures the rate controlling process in the transient period is the formation of surface oxide, whilst at higher temperatures the rate of production of gaseous products is becoming comparable in magnitude.

3.3 Nuclear Type Graphite

This was an improved nuclear graphite with a total specific surface of 0.62 metres² gram⁻¹ obtained by low temperature Krypton adsorption and showing the characteristic stepped adsorption isotherms of graphites. It is interesting to show how the present system can be used to study the initial degassing of such a low surface area material. Tables 1 and 2 show the masses of evolved species desorbed from the surface during the initial degassing and after exposure to the atmosphere for 15 days.

Using 10 grams of sample, sensitivities down to 0.01 micrograms have been obtained which favourably compare with the most advanced microbalances. The extent of surface oxide coverage after atmospheric exposure was 0.099 and 0.037 metres² gram⁻¹ before and after treatment to 950°C respectively.

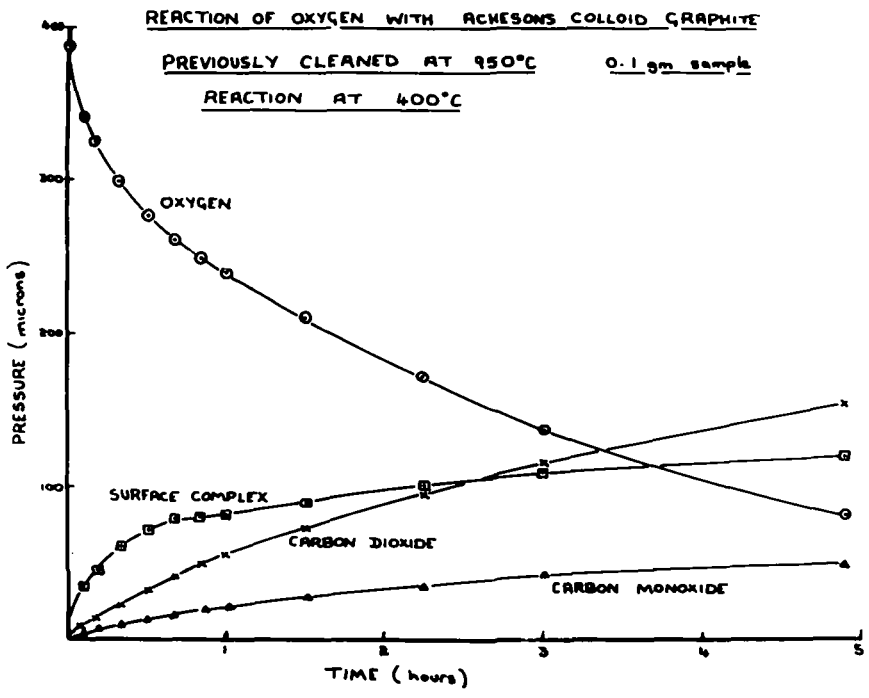


FIGURE 7

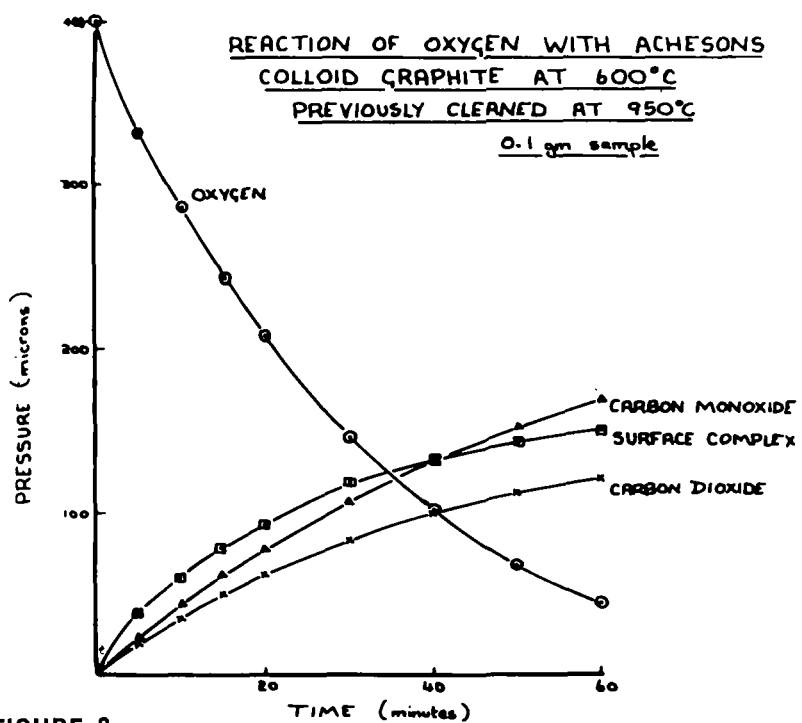
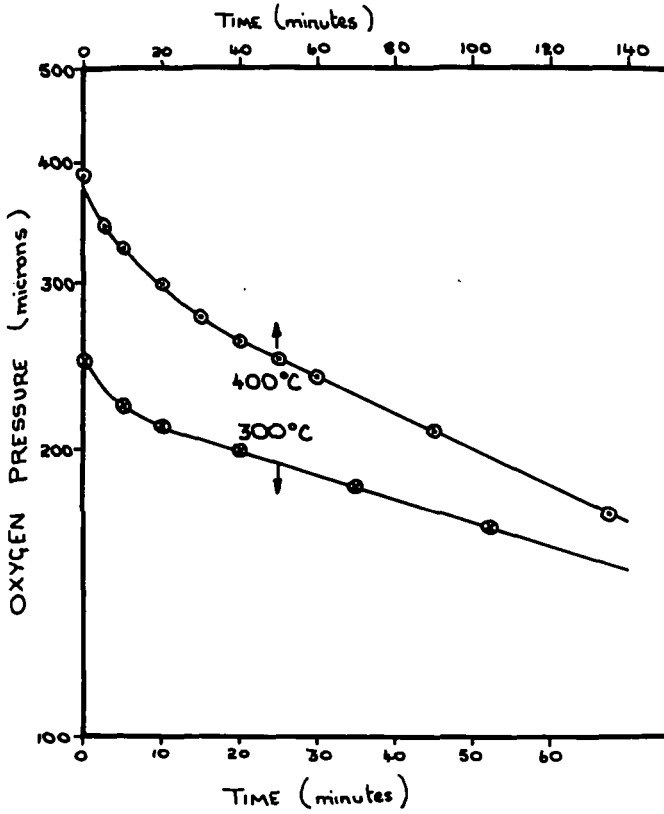


FIGURE 8

DEVIATION FROM FIRST ORDER RELATIONSHIP
OF OXYGEN CONSUMPTION ON ACHESONS COLLOID
GRAPHITE AT 300°C AND 400°C



FIRST ORDER RELATIONSHIP OF OXYGEN CONSUMPTION
ON ACHESON COLLOIDS GRAPHITE AT 600°C

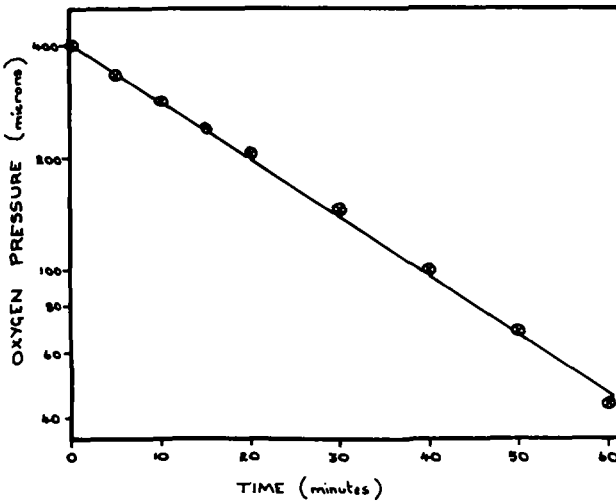


TABLE 1

Cumulative Thermal Desorption from Original Nuclear Graphite
quantities expressed in micrograms per gram of sample

Temperature Range °C	H ₂	CO	CO ₂	H ₂ O	N ₂	Hydro-carbons
0 - 200	0.04	0.57	5.66	1.08	1.58	0.31
0 - 400	0.10	6.75	14.98	2.45	5.33	1.12
0 - 600	0.55	8.25	48.69	2.45	7.62	2.01
0 - 800	1.27	14.74	54.19	2.45	8.09	2.01
0 - 900	1.78	20.12	56.34	2.45	8.66	2.01

TABLE 2

Cumulative Thermal Desorption from Nuclear Graphite Pre-degassed at 950°C for 3 hours and exposed to Atmosphere for 15 days.
quantities expressed in micrograms per gram of sample

Temperature Range °C	H ₂	CO	CO ₂	H ₂ O	N ₂	Hydro-carbons
0 - 200	-	-	-	-	-	-
0 - 300	-	-	-	-	-	-
0 - 400	0.01	0.21	0.51	0.18	0.42	0.06
0 - 600	0.02	1.67	21.97	0.43	0.62	0.13
0 - 800	0.10	3.71	23.52	0.51	0.82	0.16
0 - 900	0.22	6.13	23.52	0.51	0.91	0.16

Discussion

The application of mass spectrometry to the study of carbon and graphite reactivity has provided a technique for studying the fundamental processes involved at the surface of a wide range of these materials. The present system allows accurate adsorption-desorption phenomena to be determined with at least the same accuracy as a conventional microbalance but yielding far more discriminate information. The additional information obtained from this type of system is clearly demonstrated in Figures 7 and 8, during the production of surface oxide on the clean graphite surface. The weight changes involved, if this process was monitored thermogravimetrically, would be a complex function of at least two independent processes. Both the weight increase due to chemisorption of oxygen to produce surface oxide and the weight loss due to the removal of carbon atoms as CO and CO₂ are contributing to the net measured weight change. Normally in thermogravimetric studies this period is usually by-passed and the process is monitored after the steady state has been reached where only the gaseous products CO and CO₂ are being formed. With the mass spectrometer system the initial transient period can be broken down into the various competing processes. It is hoped that a detailed study of the transient period will lead to more fundamental ideas about the relevant mechanisms. The direct monitoring of oxidation at different temperatures can be seen to produce varying ratios of CO and CO₂. These can be easily followed with the aid of a mass spectrometer and compared with those ratios that are predicted by theoretical thermodynamic considerations.

The combined use of a mass spectrometer and microbalance has provided a direct correlation between the two methods of study for the desorbed species from graphite⁸. A direct agreement has been obtained independently by using the two methods simultaneously. The present system described in this paper has been improved for the study of much smaller surface area materials by using a variable leak valve and ultra high vacuum components. This improved system will produce a well cleaned surface prior to chemisorption experiments. In the range of pressures which the system normally encounters, degassing

from the walls and leaks are relatively undetectable, but development of the system to work at pressures below 10^{-5} mm's mercury requires a careful evaluation of leak rates, degassing and adsorption onto the walls.

One of the main aspects of work which is currently in progress on carbon and graphites is associated with nuclear graphites. Initial degassing and subsequent chemisorption and oxidation studies are of value in ascertaining reactivity and the amounts of occluded gases present in the graphite. These occluded gases if desorbed by the graphite moderator in a reactor at working temperature can embrittle fuel elements. A prior knowledge of the quantities of these occluded gases and the temperatures at which they are released is therefore important.

References

1. Hennig G R, Proceedings of the Fifth Conference on Carbon, Vol. I, p.143, Pergamon Press, Oxford, (1963).
2. Laine N R, Vastola F J and Walker P L Jr., J. Phys. Chem., 67, 2030, (1963).
3. Laine N R, Vastola F J and Walker P L Jr., Proceedings of the Fifth Conference on Carbon, Vol. II, p.211, Pergamon Press, Oxford, (1963).
4. Dollimore J, Freedman C M and Harrison B H, Ninth Biennial Conference on Carbon, Boston, USA, (1969).
5. Austin F E, Dollimore J and Harrison B H, Second International Conference on Thermal Analysis, Worcester, USA, (1968).
6. Dacey J R, Frohnsdorff G J C and Gallagher J T, Carbon, 2, 41, (1964).
7. Dubinin M M, Catalysis and Chemical Kinetics, p. 17, Academic Press, (1964).
8. Dollimore J, Freedman C M and Harrison B H, Seventh Conference on Vacuum Microbalance Techniques, Wakefield, USA, (1969).

Acknowledgements

B H Harrison and C M Freedman would like to acknowledge financial assistance from the National Gas Council and the University of Salford respectively.

MASS SPECTROMETRIC-DIFFERENTIAL THERMAL ANALYSIS OF SOLID
INORGANIC AND ORGANIC MATERIALS

J.P. Redfern and B.L. Treherne, Stanton Instruments Limited, England.

M.L. Aspinall and W.A. Wolstenholme, Consultant Laboratory,
AEI Scientific Apparatus Division, Manchester, England.

Introduction

Differential thermal analysis (DTA) is the technique of measurement of temperature change of a sample relative to a standard as both are heated at a uniform rate. The difference between the sample temperature and that of the standard is due to exothermic or endothermic processes occurring during heating. These may be phase changes, melting, or decomposition of the sample involving the evolution of volatile products. The thermogram gives information as to when and at what temperature these changes occur but does not give any information as to what the more volatile decomposition products evolved may be. The mass spectrometer is ideally suited to the identification of such volatile species. In a DTA unit, the cell is generally swept by a carrier gas such as helium or air, so that the main problem involved in the link up is the provision of a suitable representative sampling system of short time response. Some initial work has been done on such a system by Langer and co-workers¹ and Wenlandt². In this paper, we wish to present some results obtained on a new DTA-MS unit, the main feature of which is the relative simplicity of the mass spectrometer and its link to the DTA unit. A block diagram of the system is shown in Fig.1. The link between the mass spectrometer and the DTA unit is a capillary system which allows the mass spectrometer to sample at pressures up to atmospheric. This capillary is heated electrically and enters the DTA cell directly above the sample cup. The mass spectrometer tube is also heated to about 150°C. The cell is swept, usually with helium, at a flow rate of about 25ml per minute. The recording of the DTA curves and the mass spectra may be achieved using separate recorders, or alternatively, the two traces may be fed onto the same chart.

Results

Fig.2 shows the differential thermogram for copper sulphate pentahydrate which was chosen for the initial tests on the combined system. In this case, the mass spectrometer must sample water and follow the variation in its concentration above the sample. Fig.3 shows the recorder chart on which are displayed the DTA curve and the mass spectrometer trace for m/e 18. It can be seen that the mass spectrometer trace reflects quite faithfully the thermogram beginning with the relatively wide initial peak which includes the shoulder due to the formation of a saturated solution after the first loss of water which occurs at about 95°C. The rate of temperature rise across the first two endotherms was 6°/minute and this was then increased to 8°/minute for completion of the run. This result indicates that the sampling system used for the mass spectrometer link is quite satisfactory, in that no problems due to adsorption of the water vapour were encountered.

Fig.4 shows a further run on copper sulphate, this time using a sample of 1 mgm. Using this trace, it can be estimated that a further reduction in sample size of a factor three would still give a useful trace. In this particular case, due to extra amplifier ranges which are available, the mass spectrometer detection limit is at least three times better than that for the DTA unit alone.

One alternative method of operation of the apparatus is to scan the mass spectrum when a peak is detected on the DTA trace. Fig.5 shows an example of this type of operation, again for copper sulphate. The mass range covered in this case was m/e 45 \rightarrow m/e 12. The peaks at m/e 17 and 18 show the expected increased intensities for the endotherms. Note that the m/e 28 and 32 peaks are due to the sampling of air in the cell along with the helium carrier gas. Thus these peaks have the same intensities between the second and final endotherms as before the start of the run. Their lower intensity in the endotherm region reflects the lower relative concentration of air above the sample during the emission of water vapour.

Another hydrate studied was calcium oxalate monohydrate. Fig.6 shows the recorder trace giving the thermogram and the mass spectrometer traces for m/e 18 and m/e 44. Note that the m/e 44 trace confirms the presence of the small peak preceding the main exotherm at the end of the trace.

Fig.7 shows another run on the same compound with the mass spectrometer operated in the scanning mode. The large increase in m/e 18 and 17 confirms the loss of water for the first endotherm. In the case of the two exotherms, the peaks at masses 44 and 28 have increased in intensity. The peak at m/e 32 is at this point much lower relative

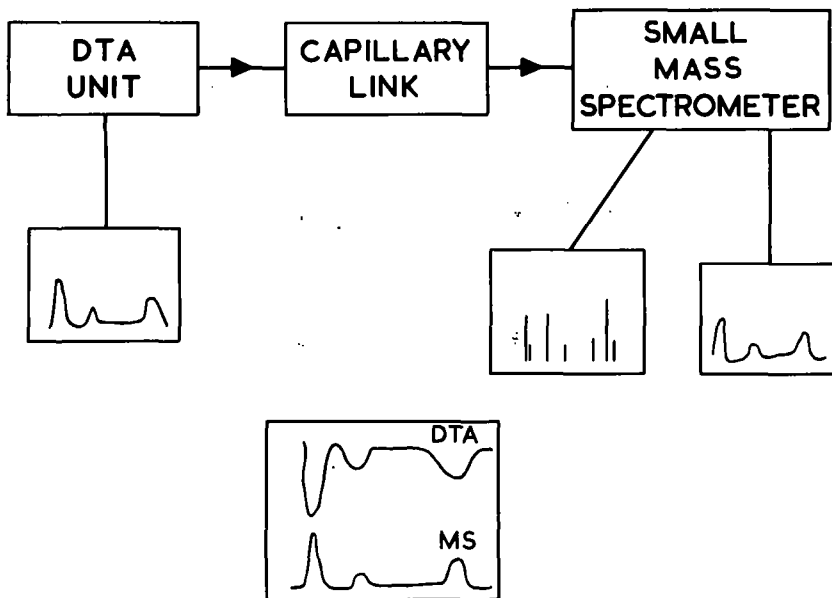


Fig.1 Block diagram of DTA-MS system

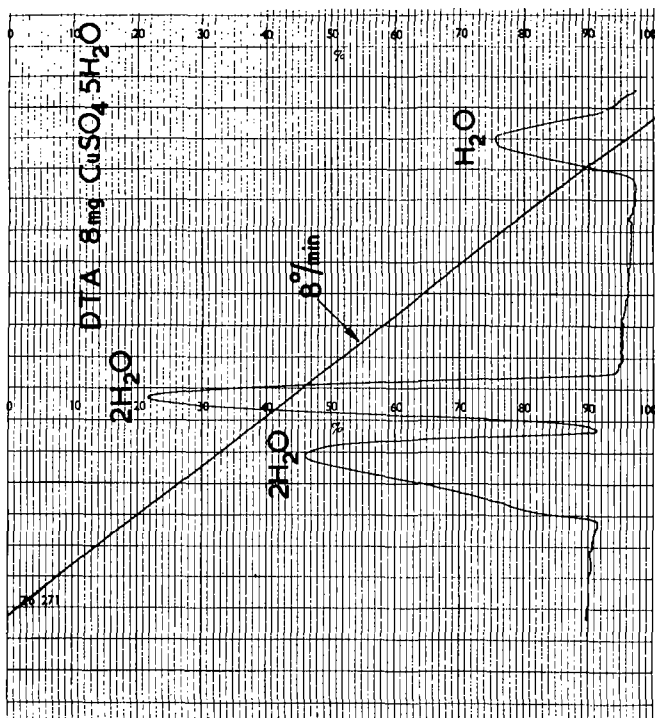


Fig.2 Differential thermogram for copper sulphate pentahydrate

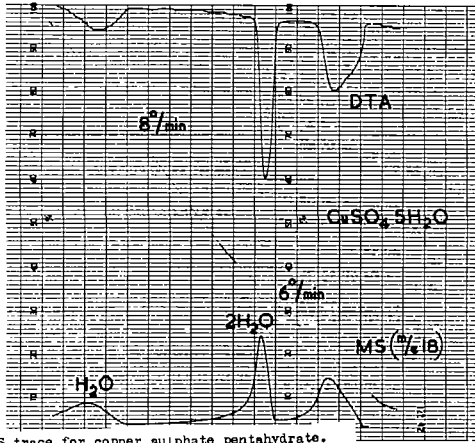


Fig. 3 DTA-MS trace for copper sulphate pentahydrate. Mass spectrometer tuned on m/e 18

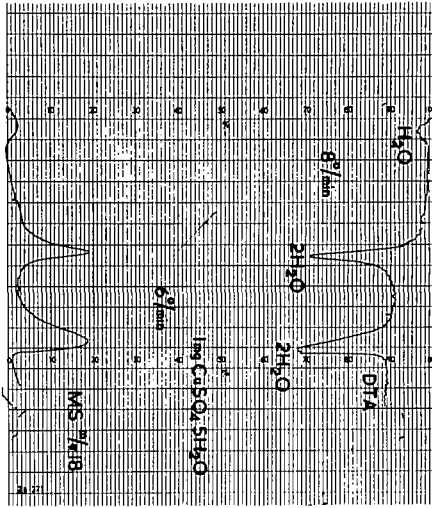


Fig. 4 DTA-MS trace for copper sulphate pentahydrate 1 mgm sample

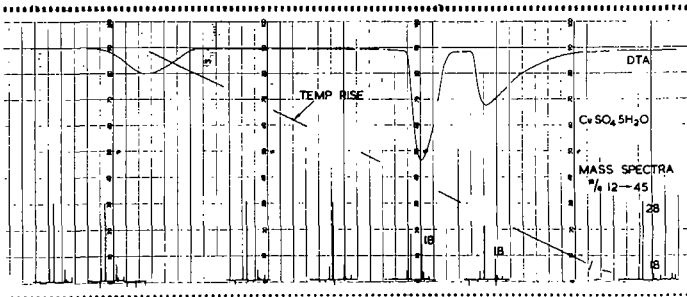


Fig. 5 DTA-MS trace for copper sulphate pentahydrate. mass spectrum scanned over mass 12 — 45.

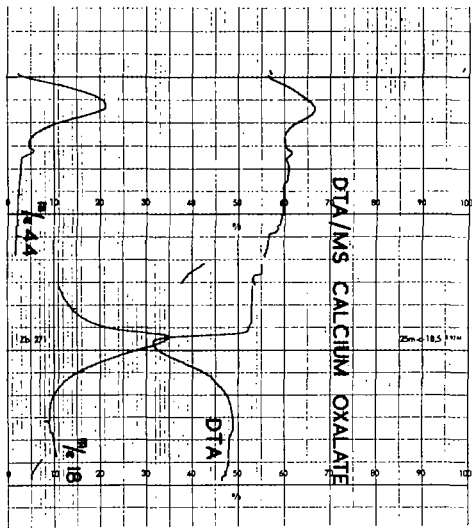


Fig.6 DTA-MS trace for calcium oxalate. Mass spectrometer tuned on m/e 18 and m/e 44.

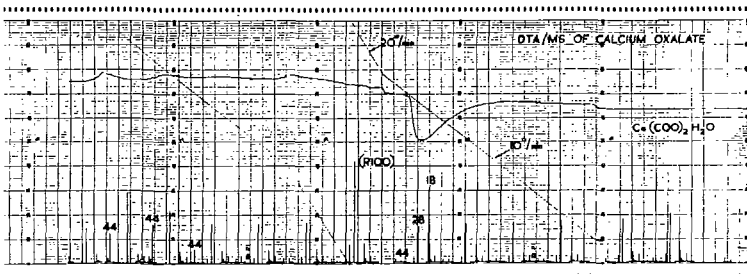


Fig.7 DTA-MS trace for calcium oxalate. Mass spectrum scanned.

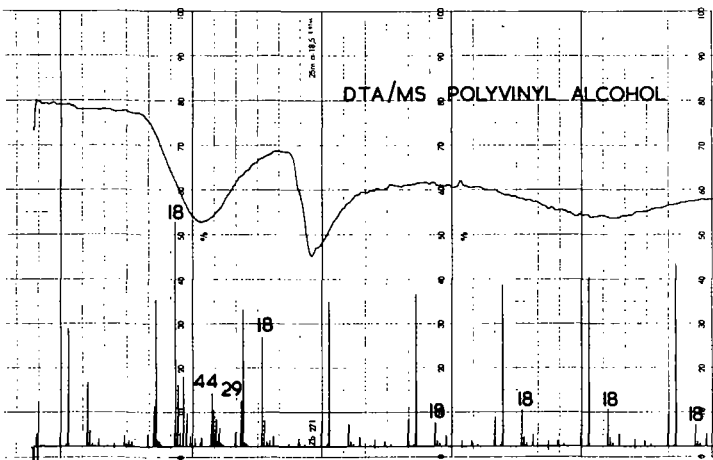


Fig.8 DTA-MS for polyvinyl alcohol.

to m/e 28 indicating that m/e 28 is due to carbon monoxide rather than nitrogen from air. Also the relative intensities of m/e 28 and 44 indicate that the increased m/e 28 intensity is not due solely to contribution from the spectrum of carbon dioxide, but rather that the mass spectrometer is at this point sampling a mixture of carbon dioxide and carbon monoxide.

Another major application of thermal analysis techniques is the study of the decomposition of organic compounds including polymers. Here again, the DTA-mass spectrometer system can give valuable information regarding the identity of degradation products. Considerable ambiguity may exist in the case of high molecular weight organic compounds or polymers and the interest lies in the identification of products and their order of evolution from the heated material.

An example of polymer degradation is shown in Fig.8. This gives the thermogram and associated mass spectra for polyvinyl alcohol. The DTA trace shows three endotherms and the mass spectrum was scanned repetitively between m/e 45 and m/e 12. The results show that the first shallow peak is due to the loss of water. The second peak shows no real change in the mass spectrum from background, and indicates the melting point of the polymer. The final endotherm involves a 1n of water, indicated by the intense m/e 18 peak, and other peaks with increased intensity are m/e 44, 29 and 15. These results can be correlated with the loss of acetaldehyde.

The results obtained have demonstrated the ability of the apparatus described to detect and identify the species evolved in the thermal degradation of a variety of compounds. The mass spectrometer and its link to the DTA unit are basically very simple but obviously adequate to provide valuable extra information for thermal analysis studies.

References

- (1) H.G. Langer, R.S. Gohlke and D.H. Smith, Mass Spectrometric Differential Thermal Analysis, Anal.Chem. 37, 433 (1965).
- (2) W.W. Wenlandt, T.M. Southern and S.R. Williams, Anal.Chim.Acta, 35, 254 (1965).

Acknowledgment

The authors wish to thank Dr. J.D. Waldron, Director and General Manager, AEE Scientific Apparatus Division, for permission to publish this paper.

EFFECTS OF ELECTRIC FIELDS AND SAMPLE EXPANSION
ON ION SAMPLING AT HIGH PRESSURES*†

Rudolf R. Burke and William J. Miller

AeroChem Research Laboratories, Inc.
 Princeton, New Jersey.
 a subsidiary of Sybron Corporation

INTRODUCTION

Experiments have been performed in which ions were sampled from two different reacting gas streams: (i) supersonic jets of combustion plasma at ≈ 1 Torr and (ii) streams below corona discharges in air at 1 atm. In both these systems, the dominant ions observed mass spectrometrically are $H^+(H_2O)_n$ where $1 \leq n < 10$ depending on the prevailing temperature and H_2O concentration. The results indicate that the apparent relative concentrations of the various hydrates are sensitive not only to the chemistry of the reacting system, but also to electrostatic field effects which tend to break up the ions, and to clustering processes which have the opposite effect. Both phenomena can occur during mass spectrometric sampling.

EXPERIMENTAL

1. Supersonic Jets of Combustion Plasma

Partially ionized gas is produced in the reservoir section of a previously described¹ plasma jet facility by hydrocarbon combustion and then expanded into a test section through a supersonic nozzle contoured to produce a shock-free Mach ≈ 3 free jet. The nozzle exit and mass spectrometer sampling system are shown in Fig. 1. The sampling system consists of a cylindrical probe with a protruding conical section. The sampling orifice, located at the tip of the cone, is designed to penetrate the detached shock formed by the supersonic gas stream impinging on the end surface of the probe. By placing plates of different thicknesses on the cylinder surface around the conical section of the sampling probe, the shock can be moved upstream of the cone tip, and the shock (front)-to-sampling orifice distance D can be easily adjusted.

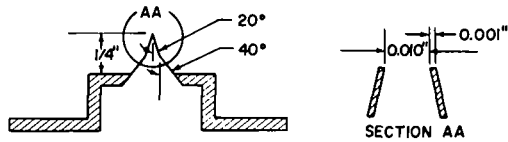
To study the effects of electric fields on ion sampling, the combustion plasma is biased with respect to the grounded sampling probe. This is achieved by floating both the burner and supersonic nozzle (Fig. 1).

Measured and estimated characteristics of the combustion plasma produced by a lean H_2/O_2 flame (mixture ratio 0.17) containing 1% of CH_4 are shown in Table I. Since one ion is produced per $\approx 10^6$ carbon atoms,² the ion mole fraction in the flame is $\approx 10^{-8}$. Ion recombination before and during expansion of the combustion plasma reduces the ion mole fraction in the free jet to the order of 10^{-9} .

Profiles of the total ion current sampled from the supersonic gas stream ahead of the shock wave (negative D) and through the subsonic gas stream behind the bow shock (positive D) are shown in Fig. 2. Figure 2 also contains total ion current data observed with various combustion plasma bias voltages (0 to 40 V). Figures 3 and 4 show total ion current and mass-analyzed ion currents, respectively, as functions of plasma bias for $D = 0$. The H_3O^+ and $H_5O_2^+$ ions dominate the ion spectrum. Mass-analyzed ion current data as functions of D at zero plasma bias are shown in Fig. 5.

* This research was sponsored in part by, but does not necessarily constitute the opinion of, the Air Force Systems Command and the Air Force Cambridge Research Laboratories, Office of Aerospace Research, under Contract No. F19628-67-C-0325. Funding for this research was supplied by DASA under Subtask No. 11BHAX 504 (07.504).

† This research was sponsored in part by the Department of the Army, Edgewood Arsenal Research Laboratories, under Contract No. DAAA 15-68-C-0469.



SAMPLING PROBE

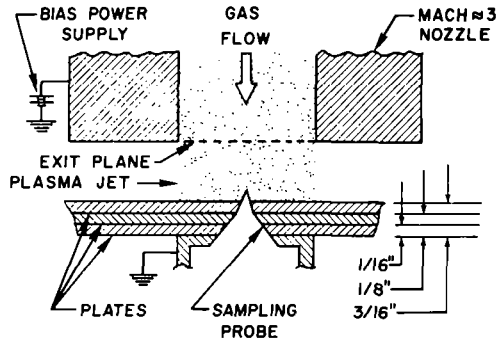


FIG. 1 SAMPLING PROBE AND PLATES FOR SUPER-SONIC JET SAMPLING

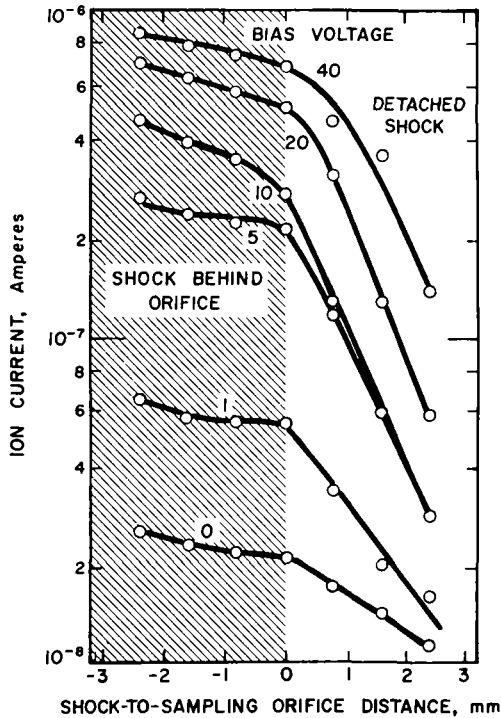


FIG. 2 TOTAL ION CURRENT AS A FUNCTION OF SHOCK-TO-SAMPLING ORIFICE DISTANCE AND PLASMA BIAS

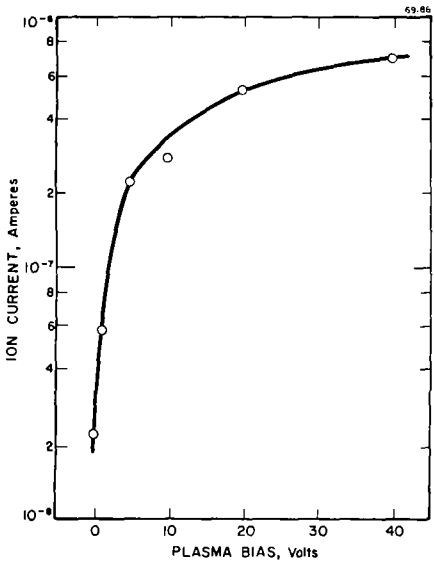


FIG. 3 TOTAL ION CURRENT AS A FUNCTION OF PLASMA BIAS AT ZERO SHOCK-TO-SAMPLING ORIFICE DISTANCE

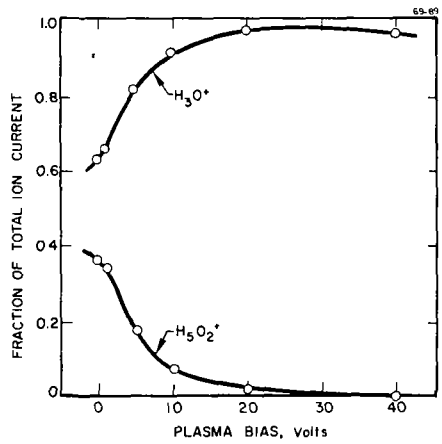


FIG. 4 MASS ANALYZED ION CURRENTS AS FUNCTIONS OF PLASMA BIAS AT ZERO SHOCK-TO-SAMPLING ORIFICE DISTANCE

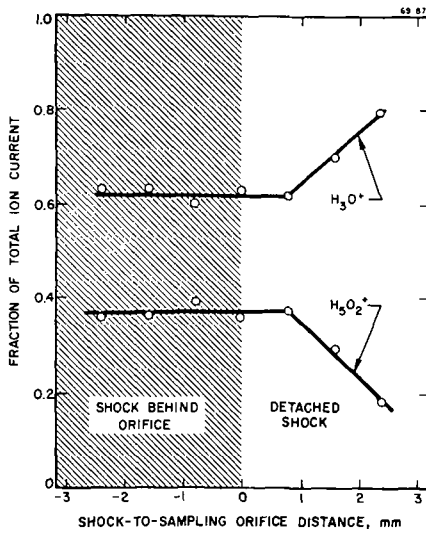


FIG. 5 MASS ANALYZED ION CURRENTS AS FUNCTIONS OF SHOCK-TO-SAMPLING ORIFICE DISTANCE AT ZERO PLASMA BIAS

TABLE I
EXPERIMENTAL CONDITIONS OF THE COMBUSTION PLASMA*

<p><u>A. Reservoir Section</u></p> <p>Unburned gas composition (mole fractions)</p> <table border="0" style="width: 100%;"> <tr><td>H₂</td><td>0.25</td></tr> <tr><td>O₂</td><td>0.74</td></tr> <tr><td>CH₄</td><td>0.01</td></tr> </table> <p>Adiabatic flame temperature (K) 2150 Stagnation pressure (Torr) 10 Number density (cm⁻³) 4.5 × 10¹⁶ Flow velocity (cm sec⁻¹) 15</p>	H ₂	0.25	O ₂	0.74	CH ₄	0.01	<p><u>B. Free Plasma Jet</u></p> <p>Burned gas composition (mole fractions)</p> <table border="0" style="width: 100%;"> <tr><td>H₂O</td><td>0.32</td></tr> <tr><td>O₂</td><td>0.67</td></tr> <tr><td>CO₂</td><td>0.01</td></tr> </table> <p>Mach number 2.7 Static pressure (Torr) 0.435 Static temperature (K) 1275/730 † Number density (cm⁻³) 3 × 10¹⁵ Jet velocity (cm sec⁻¹) 2 × 10⁵</p>	H ₂ O	0.32	O ₂	0.67	CO ₂	0.01
H ₂	0.25												
O ₂	0.74												
CH ₄	0.01												
H ₂ O	0.32												
O ₂	0.67												
CO ₂	0.01												
<p><u>C. Subsonic Flow Behind the Bow Shock</u></p> <table border="0" style="width: 100%;"> <tr><td>Pressure (Torr)</td><td>3.6</td></tr> <tr><td>Temperature (K)</td><td>2100</td></tr> <tr><td>Number density (cm⁻³)</td><td>1.5 × 10¹⁶</td></tr> <tr><td>Flow velocity (cm sec⁻¹)</td><td>4 × 10⁴</td></tr> <tr><td>Mach number</td><td>0.47</td></tr> </table>		Pressure (Torr)	3.6	Temperature (K)	2100	Number density (cm ⁻³)	1.5 × 10 ¹⁶	Flow velocity (cm sec ⁻¹)	4 × 10 ⁴	Mach number	0.47		
Pressure (Torr)	3.6												
Temperature (K)	2100												
Number density (cm ⁻³)	1.5 × 10 ¹⁶												
Flow velocity (cm sec ⁻¹)	4 × 10 ⁴												
Mach number	0.47												

* Unburned gas composition, stagnation pressure and static pressure were measured. Local equilibrium in flame and jet were assumed to compute the other parameters.

† Computed from the H₃O⁺/H₃O₂⁺ intensity ratio.

2. Corona Discharges in Flowing Air

The ionized sample in these experiments is obtained by flowing air at 1 atm with a linear velocity of ≈ 50 cm sec⁻¹ through a ≈ 5 kV, 10 μA point-to-point corona. To sample positive ions into the grounded sampling probe, the negative corona point is connected to ground. After sampling, the ions are focused and mass analyzed, as in the supersonic jet experiments. Two different sampling systems are used: (1) a system with direct expansion from atmospheric pressure to ≈ 10⁻⁴ Torr, and (2) a system with expansion to ≈ 10⁻⁴ Torr through an intermediate pumping stage at ≈ 10⁻¹ Torr.

The obtained ion spectra are again dominated by the oxonium (H₃O⁺) and hydronium (H₃O⁺·nH₂O) ions. The intensities of the ions observed in air with different water concentrations and using the direct sampling system are reported in Table II. The mole fraction of water (X_{H₂O}) in "cylinder dry" air is ≈ 10⁻⁴. To obtain "wet" air with X_{H₂O} ≈ 10⁻², cylinder air was saturated with water. "Very dry" air (estimated X_{H₂O} ≈ 10⁻⁶) was obtained by passing cylinder air through a P₂O₅ trap. In Table III the observed ion intensity ratios are compared with ratios computed from available thermodynamic data for H₃O⁺(H₂O)_n ions.³ Finally, an ion spectrum obtained in cylinder dry air with the two-stage sampling system is given in Table IV.

TABLE II
OXONIUM AND HYDRONIUM ION INTENSITIES IN WET AIR, CYLINDER DRY AIR AND VERY DRY AIR (DIRECT SAMPLING SYSTEM) (Intensities in 10⁻¹³ Ampere Units)

<u>Ion</u>	<u>Wet Air</u>	<u>Cylinder Dry Air</u>	<u>Very Dry Air</u>
H ₃ O ⁺	---	50	14
H ₃ O ⁺ (H ₂ O)	2	865	240
H ₃ O ⁺ (H ₂ O) ₂	20	1200	270
H ₃ O ⁺ (H ₂ O) ₃	40	440	100
H ₃ O ⁺ (H ₂ O) ₄	16	42	5
H ₃ O ⁺ (H ₂ O) ₅	6	2	--
H ₃ O ⁺ (H ₂ O) ₆	6	--	--
H ₃ O ⁺ (H ₂ O) ₇	3	--	--

TABLE III
COMPUTED AND OBSERVED RATIOS OF H_3O^+ HYDRATE INTENSITIES

$X_{\text{H}_2\text{O}}$: molar fraction of water; $a(b) \equiv a \times 10^b$

Air	$X_{\text{H}_2\text{O}}$	$\frac{\text{H}_3\text{O}^+(\text{H}_2\text{O})}{\text{H}_3\text{O}^+}$		$\frac{\text{H}_3\text{O}^+(\text{H}_2\text{O})_2}{\text{H}_3\text{O}^+(\text{H}_2\text{O})}$		$\frac{\text{H}_3\text{O}^+(\text{H}_2\text{O})_3}{\text{H}_3\text{O}^+(\text{H}_2\text{O})_2}$		$\frac{\text{H}_3\text{O}^+(\text{H}_2\text{O})_4}{\text{H}_3\text{O}^+(\text{H}_2\text{O})_3}$	
		Comp	Obs.	Comp	Obs.	Comp	Obs.	Comp	Obs.
Wet	10^{-2}	1.1(16)	--	5 (7)	10	1.3(4)	2	9.6(1)	4(-1)
Cylinder Dry	10^{-4}	1.1(14)	17	5 (5)	1.4	1.3(2)	4(-1)	9.6(-1)	1(-1)
Very Dry	10^{-6}	1.1(12)	17	5 (3)	1.1	1.3	4(-1)	9.6(-3)	5(-2)

Air	$X_{\text{H}_2\text{O}}$	$\frac{\text{H}_3\text{O}^+(\text{H}_2\text{O})_5}{\text{H}_3\text{O}^+(\text{H}_2\text{O})_4}$		$\frac{\text{H}_3\text{O}^+(\text{H}_2\text{O})_6}{\text{H}_3\text{O}^+(\text{H}_2\text{O})_5}$		$\frac{\text{H}_3\text{O}^+(\text{H}_2\text{O})_7}{\text{H}_3\text{O}^+(\text{H}_2\text{O})_6}$	
		Comp	Obs.	Comp	Obs.	Comp	Obs.
Wet	10^{-2}	7.6	4(-1)	1.2	1	4(-1)	5(-1)
Cylinder Dry	10^{-4}	7.6(-2)	5(-2)	1.2(-2)	---	4(-3)	---
Very Dry	10^{-6}	7.6(-4)	---	1.2(-4)	---	4(-5)	---

TABLE IV
ION SPECTRUM FROM A CORONA DISCHARGE IN CYLINDER DRY AIR,
OBSERVED WITH A TWO-STAGE SAMPLING SYSTEM*

(Intensities in 10^{-12} A Units)

Ion	Intensity	Ion	Intensity
H_3O^+	0	$\text{H}_3\text{O}^+(\text{H}_2\text{O})_{10}$	141
$\text{H}_3\text{O}^+(\text{H}_2\text{O})$	0	$\text{H}_3\text{O}^+(\text{H}_2\text{O})_{11}$	174
$\text{H}_3\text{O}^+(\text{H}_2\text{O})_2$	0	$\text{H}_3\text{O}^+(\text{H}_2\text{O})_{12}$	210
$\text{H}_3\text{O}^+(\text{H}_2\text{O})_3$	5	$\text{H}_3\text{O}^+(\text{H}_2\text{O})_{13}$	245
$\text{H}_3\text{O}^+(\text{H}_2\text{O})_4$	13	$\text{H}_3\text{O}^+(\text{H}_2\text{O})_{14}$	260
$\text{H}_3\text{O}^+(\text{H}_2\text{O})_5$	23	$\text{H}_3\text{O}^+(\text{H}_2\text{O})_{15}$	275
$\text{H}_3\text{O}^+(\text{H}_2\text{O})_6$	33	$\text{H}_3\text{O}^+(\text{H}_2\text{O})_{16}$	265
$\text{H}_3\text{O}^+(\text{H}_2\text{O})_7$	48	$\text{H}_3\text{O}^+(\text{H}_2\text{O})_{17}$	255
$\text{H}_3\text{O}^+(\text{H}_2\text{O})_8$	62	$\text{H}_3\text{O}^+(\text{H}_2\text{O})_{18}$	235
$\text{H}_3\text{O}^+(\text{H}_2\text{O})_9$	99	$\text{H}_3\text{O}^+(\text{H}_2\text{O})_{19}$	225

* $\text{H}_3\text{O}^+(\text{H}_2\text{O})_{19}$ is the largest cluster that can be observed with our mass filter.

DISCUSSION

A. Supersonic Jets of Combustion Plasma

1. Influence of Bias Potentials - When a bias potential is applied, the total ion current increases, and the gradients behind the shock become steeper (Figs. 2 and 3). The electric fields resulting from the applied bias increase the ion collection efficiency; any field effect in the plasma is furthermore enhanced by the conical structure of the sampling probe. The effect is more pronounced as the (neutral) density decreases since the ion transport is mobility controlled. The field effect is therefore highest when the shock is behind the cone tip; it gradually decreases as the shock is moved upstream.

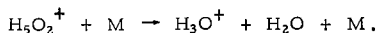
The bias potentials also induce conversion of H_5O_2^+ into H_3O^+ (Fig. 4). This conversion can be made nearly complete at high potentials, which indicates that H_5O_2^+ is a genuine ion in the free jet and is not produced by clustering effects after sampling.

2. Ion Recombination - When no bias potential is applied, interfering field effects are small. The ion decay slope behind the shock at zero plasma bias (Fig. 2) may therefore be used to compute the product of post-shock ion density (n_{t_0}) with recombination coefficient (α):

$$n_{t_0} \alpha \approx 10^5 \text{ sec}^{-1}.$$

With $\alpha(\text{H}_3\text{O}^+) \approx 2 \times 10^{-7} \text{ cm}^3 \text{ sec}^{-1}$ (Ref. 4), one computes $n_{t_0} \approx 5 \times 10^{11} \text{ cm}^{-3}$, or an ion mole fraction of $\approx 10^{-5}$. The actual ion mole fraction based on the CH_4 ion yield is approximately 10^{-9} . The four-orders-of-magnitude discrepancy is apparently due to the non-neutrality of the plasma jet (the negative charge is carried by electrons, which more easily diffuse out of the plasma, leaving the plasma slightly positive). The discrepancy shows the appreciable effect of even a small interfering field. The apparent ion decay is therefore due to a decrease in ion collection efficiency and is not due to ion recombination.

3. Ion Conversion - Unlike the ion decay, the ion composition shift behind the shock (Fig. 5) is kinetically controlled. Again, data at zero plasma bias is used to minimize interfering field effects. Although at zero plasma bias the total ion current is extremely sensitive to small changes in plasma bias (Fig. 3), the relative mass analyzed ion currents show only a weak dependence on plasma bias (Fig. 4). In the free jet (negative D in Fig. 5) H_3O^+ and H_5O_2^+ are apparently in equilibrium. This is indicated by the reasonable value for the temperature (730 K)* computed from the $\text{H}_5\text{O}_2^+/\text{H}_3\text{O}^+$ intensity ratio.³ Behind the shock, the composition starts evolving towards its new equilibrium (no detectable H_5O_2^+ at the post-shock temperature). The data lead to a rate constant of $\approx 10^{-11} \text{ cm}^3 \text{ molecule}^{-1} \text{ sec}^{-1}$ for the collisional break-up of H_5O_2^+ at $\approx 2000 \text{ K}$:



B. Corona Discharges in Flowing Air

The effect of electric fields on ion sampling are also extremely important in the corona experiments at 1 atm. Again, the potential of the sampling system relative to the two corona points has been observed to have a strong influence on the number of ions sampled.

The ratios of observed currents for specific ions, when coupled with known temperature, composition, and equilibrium constants, provide a convenient measure of the degree of prevalent disequilibrium. Equilibrium ratios of various hydrates are given in Table III together with the experimentally measured ratios. It may be seen that the data is very heavily weighted in favor of low mass ions. Ion breakup due to the strong fields induced by the corona is almost certainly responsible for the overabundance of the lower hydrates.

* The calculated value, 1275 K, given in Table I is unrealistically high for two reasons: i) due to heat losses and disequilibrium the adiabatic temperature will not be attained in the reservoir, and ii) overall local equilibrium of bulk species will not obtain in the jet; radical concentrations are much above equilibrium and heat release rates due to recombination are correspondingly lower than at equilibrium.

Ion clustering in the sampling process is almost surely occurring also, but the effect is imperceptible with the one-stage sampling system. However, this is not true when a sampling system with an intermediate pumping stage is used. From the data in Table IV, it is obvious that the combination of high pressure and low temperature in the first expansion section induces extensive cluster formation and shifts the mass spectrum toward high masses not representative of the pre-sampling ambient distributions.

REFERENCES

1. Burke, R.R., "Ion Sampling from Supersonic Gas Streams," AeroChem TN-123, June 1968; presented at the Sixteenth Annual Conference on Mass Spectrometry and Allied Topics, Pittsburgh, Pennsylvania, May 1968.
2. Sternberg, J.C., Gallaway, W.S. and Jones, D.T.L., "The Mechanism of Response of Flame Ionization Detectors," Gas Chromatography, eds. Brenner, N., Culler, J.E. and Weiss, M.D., (Academic Press, N.Y., 1962) pp. 231-267.
3. Kebarle, P., Searles, S.K., Zolla, A., Scarborough, J. and Arshadi, M., "The Solvation of the Hydrogen Ion by Water Molecules in the Gas Phase. Heats and Entropies of Solvation of Individual Reactions: $H^+(H_2O)_{n-1} + H_2O \rightarrow H^+(H_2O)_n$," J. Am. Chem. Soc. 89, 6393 (1967).
4. Calcote, H.F., Kurzius, S.C. and Miller, W.J., "Negative and Secondary Ion Formation in Low-Pressure Flames," Tenth Symposium (International) on Combustion (The Combustion Institute, Pittsburgh, 1965), pp. 605-619.

MASS SPECTROMETRY OF IONS FROM RADIO FREQUENCY PLASMAS

F. C. Kohout and D. D. Neiswender
 Mobil Research and Development Corporation
 Central Research Division Laboratories
 P. O. Box 1025, Princeton, New Jersey 08540

As a result of some interesting chemical conversions obtained from benzene RF discharges, (1) a program has been initiated to study the details of these discharges. This paper describes an apparatus designed to identify the plasma ions (+) and neutral species and to measure their relative densities. In addition, the results of some preliminary experiments with xenon will be included.

The apparatus consisted of a quadrupole mass analyzer (EAI Quad 250) equipped with a discharge-ion focusing system, crossed electron beam ion source, and electron multiplier detector. The electron impact ion source could be used to ionize plasma neutrals but in these initial rare gas experiments it was only employed to obtain reference spectra for the assignment of masses and comparison of resolutions. The signal from the multiplier was fed into a high gain (Tektronix 1A7A) scope preamplifier which was used in lieu of an electrometer. With this system ion currents of $\sim 10^{-17}$ amps (multiplier gain $\sim 10^6$) could easily be detected. The discharge tube was constructed of 1" square pyrex tubing into which a stainless steel disk electrode had been sealed. The voltage applied to the electrode served to control the plasma potential at the sampling position. The RF power at 3.69 MHz was capacitively coupled into the gas via external parallel plate electrodes. The total power dissipated in the gas was estimated by measuring the RMS current and voltage and then correcting for the capacitive component of the reactor current. The plasma particles effused through an orifice that had been sparked in the apex of a glass cone. This cone projected ~ 1 cm. into the discharge. The pinhole used was $\sim 30\mu$ in diameter. The inside of the cone was coated with a thin film of gold in order to establish the potential beyond the orifice. The effusing ions were focused onto the entrance aperture of the quadrupole with a cylindrical electrostatic lens system. (2) The potentials applied to this system were established experimentally to give the best sensitivity and resolution. A typical set of focusing voltages is illustrated in fig. 1. The quadrupole mass filter is inherently insensitive to a spread in axial ion energies; however, to obtain optimum resolution, the ions must remain in the field for a certain minimum number of RF oscillations. (3) Therefore, it is important to control the plasma potential (relative to the quadrupole entrance aperture) in order to maintain a low discharge-ion energy.

An example of a RF discharge-ion spectrum from a Xe sample containing a trace (<.5%) of Ne has been reproduced in fig. 2. The spectrum was taken on the high mass range under low resolution conditions (increased sensitivity). The three major peaks correspond to the unresolved isotopes of Xe^{++} , Xe^+ , and Xe_2^+ . The major ion in the spectrum was Xe^+ , which generally constituted at least 90% of the total ion intensity. A resolved spectrum of the dimer ion isotopes has been illustrated in the inset. The observed ion intensities agreed well with those calculated from the natural isotopic abundance of xenon. The initial part of this spectrum has been repeated in fig. 3 on the medium mass range at higher resolution. The observed resolution is very comparable to that obtained under normal operating conditions of the electron impact ion source. As can be seen from the high resolution inset the group of peaks at $\sim m/e$ 45 must correspond in part to Xe^{+++} ions. Note also the presence of Ne^+ together with many other ions (4) presumably due to traces of air, water, and organics that had not been eliminated during bakeout. It is apparent from the presence of Xe^{+++} , Xe^{++} , and Ne^+ that some electrons with energies in excess of ~ 30 eV must be present. These high energy electrons, together with Xe^+ charge exchange on low ionization potential organics, produce the observed contaminant ions. It is interesting to note that XeH^+ ions have never been detected, in contrast to observations on Ne, Ar, and Kr.

The effects of power and pressure on the relative intensities of the three major ions Xe^+ , Xe^{++} , and Xe_2^+ have been investigated. The experimental procedure consisted of initially setting the ion focusing potentials for a maximum in the Xe^+ intensity and thereafter maximizing

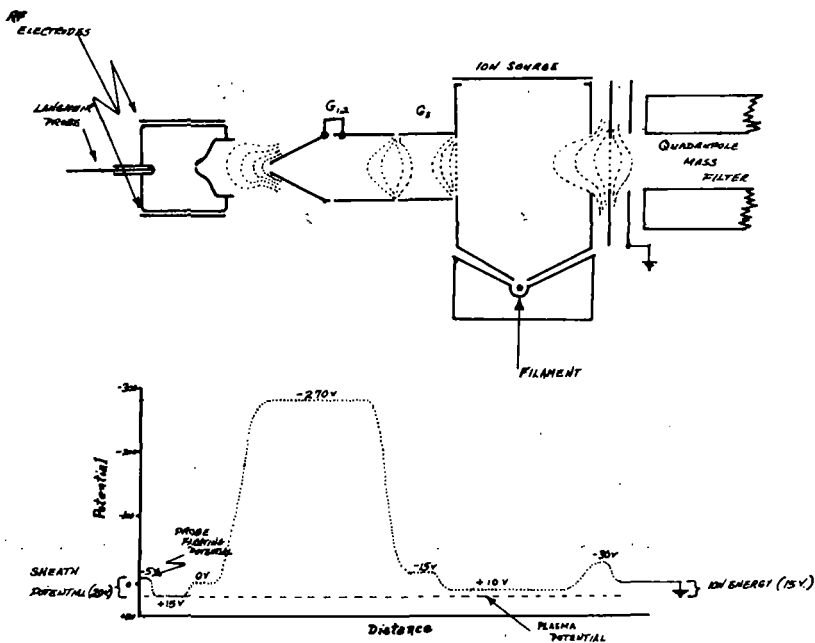


Fig. 1 ION LENS SCHEMATIC AND FOCUSING POTENTIALS

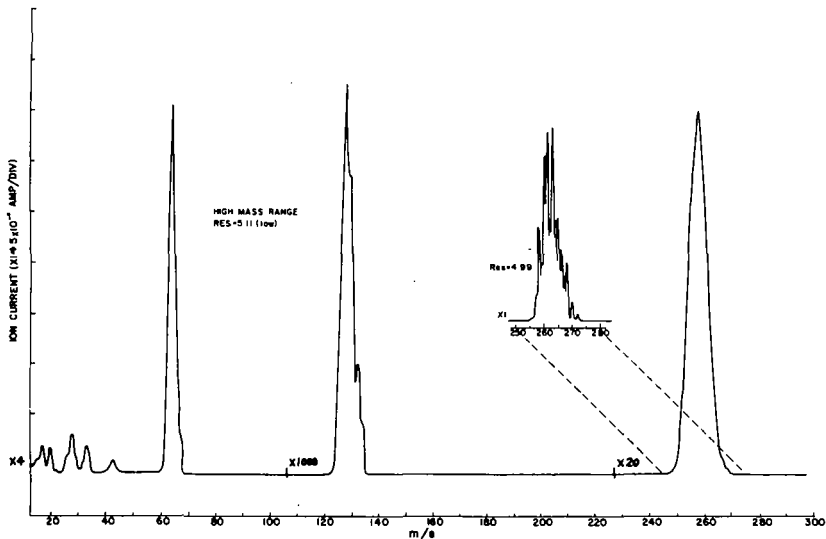


Fig. 2 Xenon RF DISCHARGE SPECTRUM (Power = 58 watts ; PRESSURE = .18 torr ; trace of Ne = .5%)

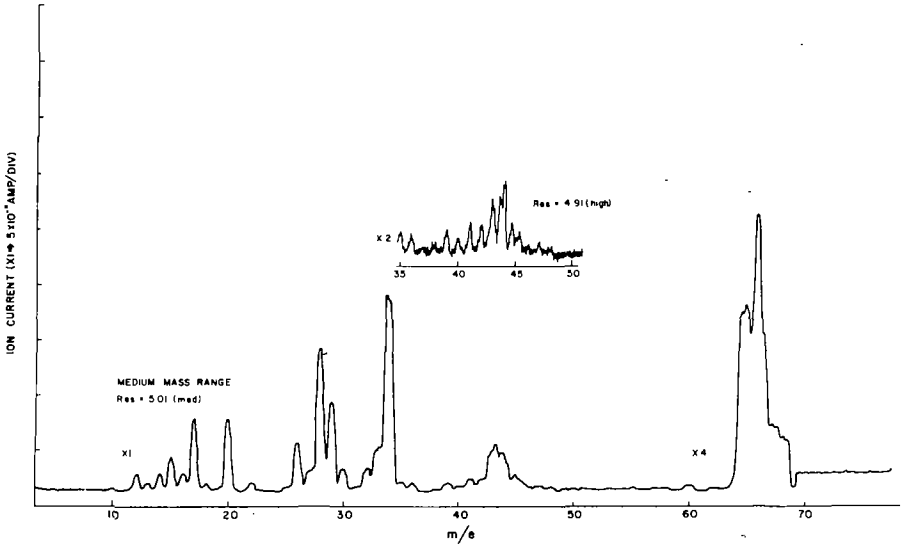


Fig. 3 XENON RF DISCHARGE SPECTRUM (Medium Mass Range)

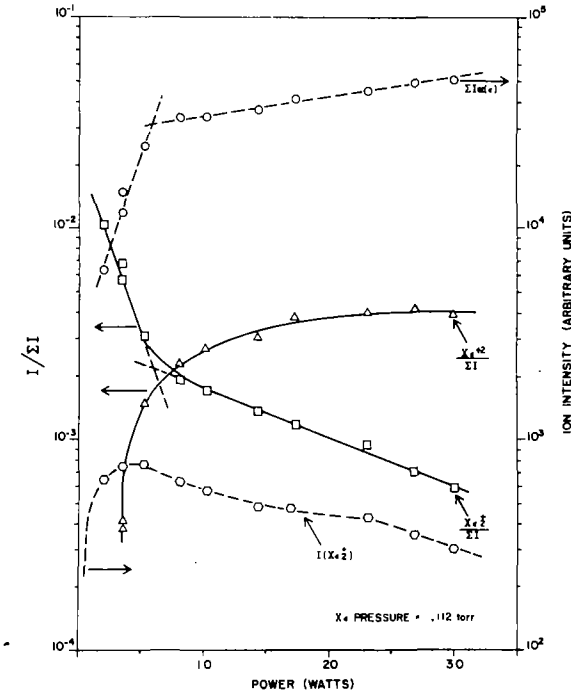


Fig. 4 ION INTENSITY VS. POWER
(Constant Pressure)

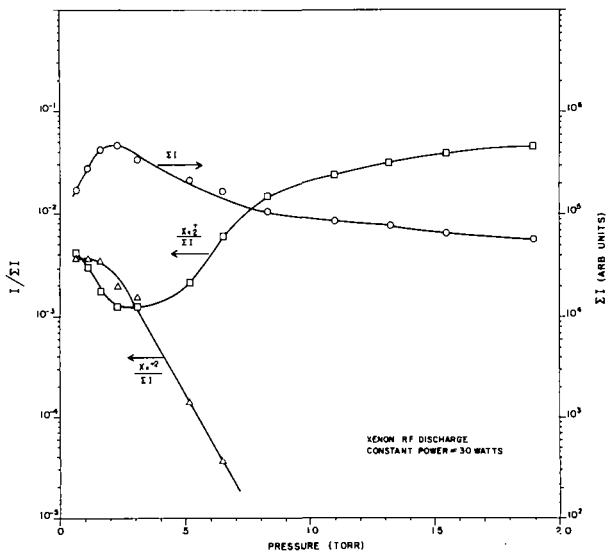


Fig. 5 ION INTENSITY VS. PRESSURE
(Constant Power)

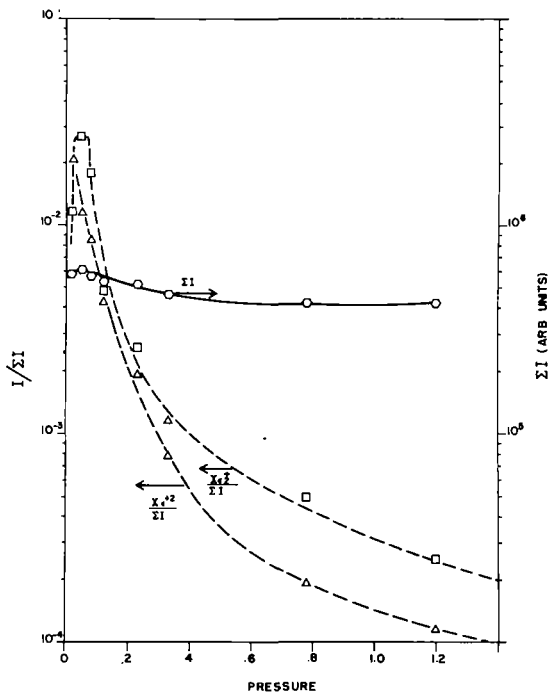


Fig. 6 ION INTENSITY VS. PRESSURE
(Constant Total Ion Intensity)

this peak via the internal plasma potential control electrode each time the power or pressure was varied. In addition, the axial ion energy was maintained to within ~ 13 ev of its initial value by checking the potential (applied to ion source chamber) necessary to retard all ions from entering the quadrupole filter.

The effect of power (up to a total of ~ 35 watts) on the ion densities in a xenon plasma at .11 torr can be seen in fig. 4. It is apparent that the onset of the process producing Xe^{++} occurs at a higher power than that forming Xe^+ and Xe_2^+ . As expected when the pressure is increased the entire Xe^{++} curve shifts to higher power reflecting the decrease in E/P and the lower electron temperature at equivalent fields.(5) At the same time, the dimer ion density always appears to inversely follow the total ion density (ΣI). Since the total ion density must be approximately equivalent to the electron density this behavior may be attributed to the predominance of a dissociative recombination process which destroys Xe_2^+ ions.

In experiments where the total power is held constant while the pressure is varied, the dimer ion density continues to follow inversely the total ion density. However, as indicated in fig. 5, the Xe^{++} ion density generally decreased very rapidly below our minimum detectable limit. This may be a result of a rapid decrease in electron temperature as E/P is decreased and/or to the increased importance of the energetically feasible charge-exchange reaction $Xe^{++} + Xe \rightarrow 2Xe^+ \quad \Delta H \cong -8$ ev.

Quantitative interpretation of the data has been obscured by apparent changes in the plasma power density as the pressure and total power were varied. The inhomogeneity of the power density was suggested from an observed concentration of the emitted radiation toward the RF electrodes and variation of the total ion density during an experiment.

Experiments have been conducted in which the total ion density at the plasma sampling orifice was held constant while the pressure was increased. The results of one of these experiments are indicated in fig. 6. There, instead of the relative dimer ion density increasing with pressure (as would be expected from a Hornbeck-Molnar or termolecular formation process) it decreases very dramatically. In fact, its decay is almost parallel to that of the Xe^{++} . During this experiment a concentration of the emitted plasma radiation toward the RF electrode was again observed as the pressure was increased. These observations may be explained considering the fact that because of the increased importance of the resonant charge exchange reaction, the mobility of Xe^+ ions through xenon will be much lower than that of the other ions present.(7) Therefore, the diffusion rate (loss rate) of Xe^+ to the walls would be lower than that for the other ions. In the extreme case (high pressures) there is little or no light being emitted from the sampled plane centered between the electrodes. It may be possible that there is no excitation or ionization occurring in this region and the electron temperature is very low. In this case all of the observed ions would have diffused into the sampling region and must be predominantly Xe^+ . Therefore, the total ion density must not be a good measure of the power density in these discharges and caution must be employed in interpreting plasma ion and electron density data. In fact, the overwhelming importance of the diffusion term observed in this system may also predominate in inductively coupled discharges where a variation in the power density would not be as apparent.

References:

- (1) D. D. Neiswender, *Advan. Chem. Series*, **80**, 338 (1969).
- (2) O. Klemperer and W. D. Wright, *Proc. Phys. Soc.*, **51**, 296 (1939).
- (3) C. E. Woodward and C. K. Crawford, M.I.T. Technical Report #194 (1964).
- (4) P. F. Knewstubb and A. W. Tickner, *J. Chem. Phys.*, **36**, 674 (1962); A. N. Hayhurst and P. J. Padley, *Trans. Faraday Soc.*, **63**, 1620 (1967).
- (5) W. L. Fite, *Advan. Chem. Series*, **80**, 1 (1969).
- (6) R. S. Mulliken, *Phys. Rev.*, **136**, A926 (1964); E. W. McDaniel, *Collision Phenomena in Ionized Gases*, p. 588, J. Wiley & Sons, New York, 1964.
- (7) R. N. Varney, *Phys. Rev.*, **88** 362 (1952).

Mass Spectrometric Measurement of the Rates of Fast
Association Reactions of Small Inorganic Species*

T. P. Fehlner and C. W. Mappes
Department of Chemistry
University of Notre Dame
Notre Dame, Indiana 46556

A fast tubular flow reactor utilizing helium as a carrier gas has been constructed and made operational. This reactor and flow system has been designed to allow precise control over the temperature, length of the reaction zone, position of the reaction zone, temperature gradients, pressure and flow rate. It has been operated in the temperature range 300-800° K, pressure range 1-10 torr and linear flow rate range of 1-10 x 10³ cm/sec. The composition of the efflux of the reactor is analyzed mass spectrometrically using modulated molecular beam sampling.

The apparatus described has been used to produce from BH₃CO substantially pure streams of BH₃ in helium (ca 70% BH₃, 20% BH₃CO and <3% D₂H₆; considering boron containing species alone). The production of BH₃ has been examined as a function of BH₃CO partial pressure, temperature and flow rate. The loss of BH₃ in a wall reaction to yield B and H₂ limits the usefulness of this thermal source of BH₃ to short (ca 10⁻³ sec) flow times. Consequently only the fast reactions of BH₃ can be examined.

Preliminary measurements on the fast reactions of this "orbitally unsaturated" molecule have been carried out. Our measurements on the self association of BH₃ at 560° K and 5 torr total pressure yield an upper limit of 10⁹ M⁻¹ sec⁻¹ for the second order rate constant. The second order rate constant for the association of BH₃ with CO under similar conditions is 3 x 10⁷ M⁻¹ sec⁻¹. The latter reaction is in the third order region.

* Supported by the National Science Foundation.

The Reaction of Atomic Oxygen with some Halo-Ethylenes

by

Robert E. Huie and John T. Herron
National Bureau of Standards

and

Douglas Davis
University of Maryland

The reaction of atomic oxygen with various halogen substituted ethylenes has been studied by a mass spectrometric technique. Rate constants at 307K, for these reactions, have been determined, and a limited amount of product analysis has been performed.

The apparatus consists of a discharge flow system connected to a mass spectrometer. A mixture of several percent oxygen in an argon carrier, at a total pressure of about two torr, is subjected to a microwave discharge, producing about 1μ of oxygen atoms. This stream, at a linear flow velocity of about 6 m/s, is then passed thru a 40 cm long, 20 mm diameter Pyrex reaction tube, which is surrounded by a thermostated water jacket. The organic reactant is introduced into the reactor thru a movable, multi-holed, central inlet. The inlet defines the start of the reaction zone. The end of the reaction zone is defined by a 30μ diameter glass leak, located at the base of the reactor, and directly above the electron beam in an open-type ion source. The ion source is part of a conventional mass spectrometer.

For a simple bimolecular reaction, the integrated rate expression is:

$$k = \ln(R_0/R) / \int_0^t [O] dt$$

where R_0 and R are the concentrations of the organic reactant at times zero and t , and O is the oxygen atom concentration.

The concentration of the organic reactant was generally about 10 percent that of the atomic oxygen, and the degree of its reaction was about 10-20 percent. Under these conditions, the integral may be replaced by the average value of the atomic oxygen concentration, times the reaction time. When a larger amount of reactant was used the integral was evaluated by graphical means.

The reaction time is determined from the length of the reaction zone, and the flow rate. R_0/R is determined as the ratio of the ion currents in the mass spectrometer, at the appropriate mass to charge ratio, with the discharge off and on. The oxygen atom concentration is determined at mass 16 at a reduced electron energy. This relative concentration is then put on an absolute basis by titration with nitrogen dioxide.

A major assumption in this derivation of the rate expression is that secondary reactions make a negligible contribution to the observed rate. This will be true if the apparent rate is, over a reasonable range, independent of the reactant concentration. The condition was not met for the reaction of atomic oxygen with C_2F_2H , C_2F_4 , and 1,1,2,2- $C_2F_2Cl_2$. For these compounds, we cannot measure the rate constant.

The other compounds were well behaved in this respect. C_2Cl_4 showed evidence of a wall reaction, which manifests itself in somewhat erratic rate data. Therefore, only an approximate value for its rate constant is reported. It did not, however, show evidence of secondary reaction.

Shown in the table are the results of this study. The rates are given both as absolute rate constants, in cc/mol sec, and relative to the rate of the ethylene reaction. The relative rates for 1,1,2,2- $C_2F_2Cl_2$, and C_2F_2Cl are from the recent paper by Tyerman¹, that for C_2F_4 is from both Tyerman and Heicklen². Also listed are upper limits for the rate constants for the reactions of CF_2O and CCl_2O with atomic oxygen.

The aldehydic products for the reactions were determined by mass spectrometric analysis during reaction. In general, where they overlap, these results agree with those of Mitchell and Simmons³ on the reactions of atomic oxygen with 1,1-difluoro-olefins. The major difference is our observation of CH_2O and CF_2O as products for 1,1- C_2F_2H . They saw little CF_2O , and postulated that the CH_2O , which they expected but did not observe, was formed with sufficient vibrational energy to dissociate. The products

listed for 1,1,2,2-C₂F₂Cl₂, and C₂F₃Cl were not observed by Tyerman, but were by both us and Mitchell and Simmons. For C₂F₃Cl, the CF₂O peak corresponds to a major fragment ion of the reactant, so its identification is less certain. CHClO, which might have been expected from the C₂H₃Cl reaction, is known to be unstable to disassociation. CHBrO is probably the same.

Rate Constants for the Reaction of Atomic Oxygen with some Halo-olefins at 307K.

Reactant	Aldehydic Products	10^{-11} cm ³ mol ⁻¹ s ⁻¹	k/k(C ₂ H ₄)
C ₂ H ₄	CH ₂ O	5.6	1.0
C ₂ H ₃ F	CHFO, CH ₂ O	2.6	.46
C ₂ H ₃ Cl	CH ₂ O	5.6	1.0
C ₂ H ₃ Br		5.1	.91
1,1-C ₂ H ₂ F ₂	CF ₂ O, CH ₂ O	2.2	.39
1,2-C ₂ H ₂ F ₂	CHFO	2.7	.48
1,1,2,2-C ₂ F ₂ Cl ₂	CF ₂ O		.67(T)
1,2,1,2-C ₂ F ₂ Cl ₂	CFClO	5.3	.95
C ₂ HF ₃	CF ₂ O, CHFO		
C ₂ F ₃ Cl	CFClO, (CF ₂ O?)		.51(T)
C ₂ F ₄	CF ₂ O		1.05(T,H)
C ₂ HCl ₃	-	2.5	.45
C ₂ Cl ₄	-	~1.0	~.2
CF ₂ O		<0.2	
CCl ₂ O		<0.2	

(T) W. J. R. Tyerman, *Trans. Faraday Soc.*, 65, 163 (1969).

(H) D. Saunders and J. Hecklen, *J. Phys. Chem.*, 70, 1950 (1966).
J. Hecklen and V. Knight, *J. Phys. Chem.*, 70, 3893 (1966).

References

1. W. J. R. Tyerman, *Trans. Faraday Soc.*, 65, 163 (1969).
2. D. Saunders and J. Hecklen, *J. Am. Chem. Soc.*, 87, 2088 (1965), and *J. Phys. Chem.*, 70, 1950 (1966).
J. Hecklen and V. Knight, *Ibid.* 3893.
3. R. C. Mitchell and J. P. Simons, *J. Chem. Soc.*, 1005 (1968).

MASS SPECTROMETRIC STUDIES OF THE THERMODYNAMICS AND KINETICS
OF FORMATION OF WATER CLUSTERS

By Frank T. Greene, A.E. Vandegrift, and Thomas A. Milne
Midwest Research Institute
Kansas City, Missouri 64110

A combination of mass spectrometric and molecular beam techniques is being used to study the equilibrium thermochemistry and kinetics of formation of water clusters. By measuring the equilibrium concentration of water clusters as a function of temperature, one can obtain their heats and entropies of formation. The heats are directly related to the strength of hydrogen bonds in water. Both thermodynamic quantities may give some insight into the "structure" of liquid water. Kinetic measurements, which are also being made, are of importance to an understanding of homogeneous nucleation.

In both the equilibrium and kinetic studies, water clusters are introduced as a molecular beam into the ion source of a Bendix TOF mass spectrometer. The general features of the apparatus have been discussed previously.^{1,2} The beam is modulated and phase sensitive detection has been included in the output circuitry in order to discriminate against background in the ion source and to enhance the signal-to-noise ratio. A double cell was used as the vapor source in order that the pressure and temperature of the water vapor could be varied independently.

The equilibrium studies utilized both molecular effusion (or near molecular effusion) and high pressure (free-jet) sampling techniques.³ The molecular effusion experiments were limited to water dimer. Several series of these measurements were made holding either temperature or pressure constant. The measurements in which pressure was held constant and temperature varied gave a heat of dimerization which was independent of the pressure to within experimental error. However, there was substantial inconsistency between the constant pressure and temperature experiments, suggesting that cluster formation during beam formation may be very important. Consequently, more extensive studies of dimer concentration as a function of Knudsen number are in progress.

High-pressure sampling techniques were also employed to determine equilibrium cluster concentrations. The dimer, trimer, and tetramer concentrations were measured using expansion orifices ranging from 0.0005 to 0.016 in. and initial conditions of 0.2 and 0.8 atmospheres at 150°C. The measured dimer concentrations were clearly dominated by cluster formation during the expansion and a meaningful extrapolation to zero orifice diameter was not possible. The measured trimer concentrations, however, when plotted against orifice diameter, approached an asymptotic value at small orifice diameters for the 0.2 atmosphere data. The trimer observed at 0.8 atmospheres was dominated by cluster formation during the expansion, and no extrapolation was possible. The tetramer concentrations did appear to approach an asymptotic value at small orifices but the curve was too poorly defined to permit an extrapolation. These results are very encouraging. It appears that it is possible to measure the concentrations of a number of higher water polymers using high-pressure sampling techniques.

It is of interest to note that the free-jet results cited above include implicit data on the rates of formation of water clusters. Since the temperature-pressure history of an ideal free-jet expansion is known, it is possible to fit rate equations to the observed polymer concentrations. Such a treatment has been carried out for argon dimer, and a similar treatment is in progress for water dimer.

This work was supported by the Chemical Physics Branch, Office of Saline Water.

References

1. Greene, F.T., and T.A. Milne, "Mass Spectrometric Sampling of High Pressure - High Temperature Sources," *Adv. in Mass Spec.*, Vol. III, p. 841, The Institute of Petroleum, London, 1966.

2. Milne, T.A., and F.T. Greene, "Direct Mass-Spectrometric Sampling of High-Pressure Systems," Adv. in Chemistry Series, No. 72, p. 68, the American Chemical Society, Washington, 1968.
3. Milne, T.A., and F.T. Greene, J. Chem. Phys., 47, 4095 (1967).
4. Milne, T.A., A.E. Vandegrift, and F.T. Greene, Mass Spectrometric Observations of Argon Clusters in Nozzle Beams. II. The Kinetics of Dimer Growth, to be published.

MOLECULAR BEAM STUDIES OF THE TEMPERATURE DEPENDENCE OF
n-BUTANE FRAGMENTATION

By Thomas A. Milne, J.E. Beachey, and Frank T. Greene
Midwest Research Institute
Kansas City, Missouri 64110

I. Introduction

Our work with the techniques and phenomena accompanying the direct molecular beam sampling of high pressure systems^{1/} has led us to consider the information that can be gained from the temperature dependence of fragmentation patterns determined in beam experiments. Using a three-stage, high-pressure modulated molecular beam system previously described^{2/} we have studied the temperature-dependent fragmentation of n-butane under a number of conditions. The results and implications of such studies are discussed in this paper.

II. Molecular Beams from Effusive Sources

The use of modulated molecular beams from effusive sources in studies of the temperature dependence of fragmentation patterns has a number of advantages over conventional methods. The principal advantages are as follows:

1. Gas temperatures can be more accurately determined since the entire mass spectrometer ion source does not need to be heated.
2. Reactions with the source filament are avoided.
3. The onset of thermal decomposition may be detected by beam diagnostic techniques.
4. Velocity analysis may be used to indicate the parents of ions.

The difficulties most likely to be encountered when using the molecular beam technique are:

1. Signals will be weak as a result of the molecular beam path length. However, by employing beam modulation techniques, the signal-to-noise ratio may not be greatly reduced.
2. Due to the longer residence time of the sample in the heated cell, required for thermal equilibrium at the higher pressures, thermal decomposition problems may be more severe.

With pure n-butane heated in a nickel effusion cell at pressures such that molecular flow occurred through the orifice, we determined the fragmentation pattern as a function of temperature. The results agreed very well with those reported by Ehrhardt and Osberghaus^{3/} using a heated ion source.

III. Free-Jet Vibrational Relaxation Studied through Cracking Pattern Measurements

With beams formed under continuum flow conditions, new possibilities for using fragmentation patterns occur. In this case, the temperature-dependent fragmentation pattern of molecules in the beam can be a useful tool for studying the internal energy relaxation in free jets. Since the fragmentation pattern is independent of the translational and rotational energy but is determined by the average vibrational energy content of the ion,^{4/} we can use the fragmentation pattern as a convenient "vibrational thermometer."

Shown in Figure 1 is the fragmentation ratio $58^+/43^+$ from n-butane, under both effusive and continuum flow conditions, as a function of temperature from 25 to 500°C when sampled through a 0.003 in. orifice. As mentioned above, the low pressure data agree quite well with Ehrhardt and Osberghaus^{3/} whose data were taken using a heated ion source designed to provide an average of 40 wall collisions per molecule. The baffle values, in both the effusive and one-atmosphere case, represent data taken with a water-cooled baffle placed directly above the sampling orifice. This allows the n-butane to adjust to the

temperature of the beam system and to be sampled effusively from stage one. The constancy of the baffle values of $58^+/43^+$ with temperature indicates very little chemical reaction up to 500°C .

The $58^+/43^+$ ratio for the one-atmosphere free-jet beam, at all temperatures, is higher than for the effusive case. Thus, at 500°C , the free-jet value of $58^+/43^+$ is equal to that of the effusive gas at about 350°C . This we interpret as indicating about 150°C of vibrational cooling of n-butane during expansion in the free jet. Data from several other ions from n-butane show similar cooling effects. The degree of cooling as ascertained from four different ion ratios varied from 150° to 170°C . It was further found that by increasing the orifice diameter from 0.003 to 0.006 in., the apparent vibrational cooling in n-butane, initially at one atmosphere and 500°C , was approximately 240°C .

IV. Fragmentation of Clusters

The one-atmosphere, room temperature ratio of $58^+/43^+$ of ~ 0.3 is equal to or very slightly higher than the effusive or baffle value, and is believed to be the highest value attainable by simply cooling the monomer gas. However, we found that by diluting the room temperature n-butane with argon, the $58^+/43^+$ ratio increased significantly, reaching a value of almost 2 at one percent n-butane in argon. Upon further dilution, the $58^+/43^+$ ratio again returns to the 0.3 value, indicating that cooling was not responsible for the observed changes.

The explanation to the above behavior is apparently that the $58^+/43^+$ ratio is being dominated, in the intermediate dilution case, by contributions from dimer or higher clusters. That n-butane nucleation would be promoted by initial dilution with argon is expected due to the effect of the argon on the free-jet expansion history. The fragmentation ratios from the clusters seem to be significantly different from the monomer value. To verify this, we measured the n-butane dimer ($m/e = 116$) ion concentration at several argon dilution levels. At one atmosphere, with a 0.006 in. sampling orifice, a search for dimer produced only an upper limit of the ratio $116^+/58^+$ of 1.25×10^{-4} . However, upon dilution with argon, the dimer and higher clusters became prominent. At 1% n-butane in argon, the 116^+ and 58^+ were approximately equal, and clusters giving ions up to $(\text{C}_4\text{H}_{10})_{10}^+$ were easily observable. Upon further dilution, $116^+/58^+$ again became quite small, confirming the above explanation for the high $58^+/43^+$ ratio.

A cluster ion like $(\text{C}_4\text{H}_{10})_2^+$ is possibly representative of the intermediate collision complexes which are involved in some ion-molecule reactions.^{5/} A mass spectrometric study of these clusters and their fragmentation behavior has potential usefulness in elucidating the properties of such intermediate complexes.

V. Conclusions

1. The use of direct molecular beam-sampling (under effusive conditions to avoid relaxation effects) to determine the temperature-dependence of electron-impact fragmentation appears to offer advantages in versatility and diagnostic ability over the conventional process of heating the ion sources to the desired temperature.
2. The use of mass spectrometrically determined temperature dependencies of fragmentation behavior in free jets makes possible a direct study of average internal-energy relaxation in expanding gases.
3. In high-pressure molecular beam mass spectrometry, careful attention must be given to the fragmentation pattern changes which may result from clusters formed as a result of the free-jet expansion as well as from relaxation effects.

This work was supported by the Office of Naval Research.

References

1. Milne, T.A., and F.T. Greene, Advances in Chemistry Series, No. 72, 68 (1968), American Chemical Society.
2. Milne, T.A., and F.T. Greene, J. Chem. Phys., 47, 4095 (1967).
3. Ehrhardt, H., and O. Osberghaus, Z. Naturforsch., 15A, 575 (1960).
4. Rosenstock, A.M., Adv. in Mass Spectrometry, 4, 523 (1968).
5. Futrell, J.H., and T.O. Tiernan, Science, 162, 415 (1968).

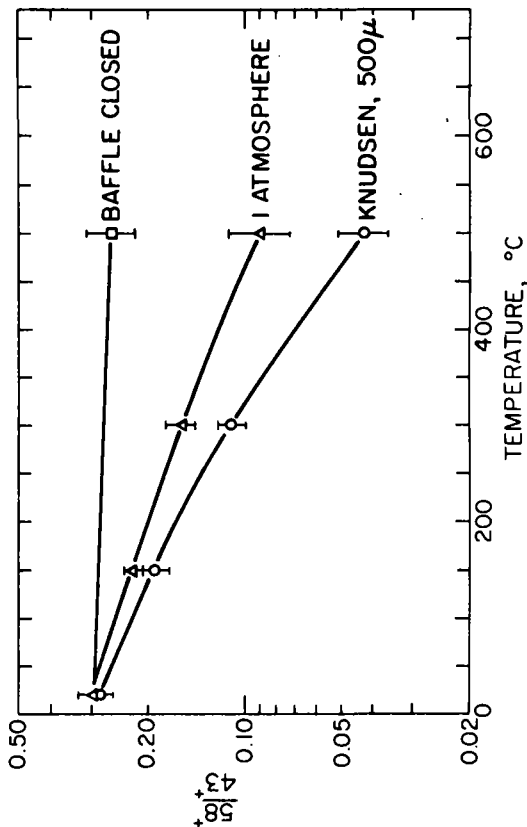


Figure 1 - Fragmentation of n-Butane under Various Sampling Conditions

THE IONIZATION PROPERTIES OF WATER CLUSTERS

by J. Beachey, F.T. Greene and T.A. Milne
Midwest Research Institute
Kansas City, Missouri

I. Introduction

The series of ions, $H^+(H_2O)_n$, are a prominent component of the D-region of the atmosphere, as revealed by recent rocket-borne mass spectrometer flights.^{1/} There is uncertainty as to the origin of such ions, one postulate being that they may be formed by photoionization of large water clusters. To provide information as to possible methods of formation, we have measured the appearance potentials of these ions by electron impact of neutral water clusters generated in supersonic expansions of water vapor. Such a study also supplies information about the nature of ionization processes in weakly bound hydrogen-bonded systems. In the case of water clusters, ionization is predominantly through loss of an OH, whereas in methanol, for example, predominantly parent ions are formed. Ionization efficiency curves for ions through $H^+(H_2O)_{10}$ are presented below, and appearance potentials determined by a log-matching procedure are compared with values deduced through a thermochemical cycle involving ion solvation energies. Evidence that the mass spectrum of highly nucleated water involves complex dissociative ionization is then presented.

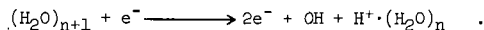
II. Source of Neutral Water Clusters

The observation of quite large neutral water clusters ionizing by loss of OH to form the series $H^+(H_2O)_n$ was made during direct sampling studies for ONR^{2/} and OSW.^{3/} The circumstances for formation of the clusters involve homogeneous nucleation during a rapid, nearly isentropic, free-jet expansion of water or its mixtures into a high vacuum, with subsequent collimation into a modulated molecular beam followed by mass spectrometric detection. The extent of nucleation is governed principally by the molecular nature and specific heat ratio of the gas being expanded, the partial pressure of water, the total initial pressure, the initial temperature and the expansion orifice diameter.

A particularly favorable circumstance for nucleation of water involves passing argon gas at 1 to 5 atmospheres over liquid water. Table I shows a typical cluster distribution for 5 atmospheres of argon over liquid water held at room temperature. It is assumed at this point that mass 19⁺ comes from the dimer, 37⁺ from the trimer, etc. In Figure 1 is shown the behavior of some of these clusters with argon pressure. It can be seen that quite large water clusters can readily be generated, even with rather limited pumping (6 in. diffusion pump in stage one).

III. Predicted Appearance Potentials for Water Clusters

We are presuming that the observed positive ions, $H^+(H_2O)_n$, come from the dissociative ionization of the neutral clusters $(H_2O)_{n+1}$ via the reaction



A variety of evidence indicates that ion-molecule reactions are unimportant under the short residence times (a few microseconds) and low pressures ($< 10^{-7}$ torr) that typically exist in the Bendix TOF ion source.

Data exist to allow predictions to be made of the minimum energy for such processes.

The appearance potential of H_3O^+ from dimer is just the sum of four energy terms involving the proton affinity of water, the hydrogen bond energy of the dimer, the H-OH bond energy and the ionization potential of H. Choosing $PA(H_2O)$, the proton affinity of water, as either 7.0 eV^{4,5,6/} or as 7.9 eV,^{7/} and taking $E(H\text{-bond})$ as about 0.25 eV, $D_0(H\text{-OH})$ as 5.2 eV and I.P. (H) as 13.6 eV gives $AP(H_3O^+)$ as 12.1 or 11.2 eV as shown in Table II.

TABLE I

ION INTENSITIES OBSERVED WHEN ARGON AT 5 ATMOSPHERES IS PASSED
THROUGH WATER AT ROOM TEMPERATURE AND EXPANDED AS A
FREE JET THROUGH A 0.003 IN. DIAMETER ORIFICE

$(\text{H}_2\text{O})_n$	Water Peaks	Argon Peaks	Relative Intensity	
			Water Peaks	Argon Peaks
	18		8.0	
2	19		15.0	
3	37	40	12.0	1000.0
4	55		8.5	
5	73	80	6.0	22.5
6	91		4.0	
7	109	120	3.1	5.8
8	127		2.4	
9	145		1.9	
10	163	160	1.4	1.4
11	181		1.3	
12	199	200		
13			0.9	
14	235	240	0.6	0.5
15	253		0.5	
16	271	280	0.45	0.3
17	299		0.4	
18	307		0.2	

TABLE II

PREDICTED AND OBSERVED APPEARANCE POTENTIALS FOR NEUTRAL WATER CLUSTERS
(Expansion from Ar Saturated with Water at 25°C)

Ion	Proposed Neutral	Appearance Potentials				
		Predicted		Observed Relative to Ar ⁺ at 15.8 ev		
		Kebarle ^{7/}	Friedman ^{8/}	5 Atm. Ar	1 Atm. Ar	3 Atm. He
H ₂ O ⁺	H ₂ O ⁺		12.6	14.1 ± 0.3	12.8 ± 0.3	12.4 ± 0.3
H ₃ O ⁺	(H ₂ O) ₂	12.1	11.2	14.6 ± 0.3	12.3 ± 0.3	11.9 ± 0.3
H ₅ O ₂ ⁺	(H ₂ O) ₃	10.9	10.5	14.3 ± 0.3		
H ₇ O ₃ ⁺	(H ₂ O) ₄	10.2	10.0	13.8 ± 0.5		
H ₉ O ₄ ⁺	(H ₂ O) ₅	9.8	-	13.1 ± 0.5		
H ₁₁ O ₅ ⁺	(H ₂ O) ₆	9.4	-	13.1 ± 0.5		
H ₁₇ O ₉ ⁺	(H ₂ O) ₉	8.9	-	12.8 ± 0.5		
H ₂₁ O ₁₀	(H ₂ O) ₁₁	-	-	12.8 ± 0.5		
H ₃₁ O ₁₅	(H ₂ O) ₁₆	-	-	12.6 ± 0.5		
.						
.						
H _{2n-1} O _n			7.9			

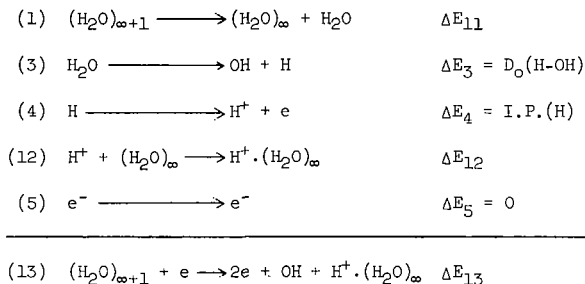
Estimates of higher cluster-ion appearance potentials can be made using a set of reactions which employ ion association energies. From these reactions it follows that in general:

$$\text{AP}[\text{H}^+ \cdot (\text{H}_2\text{O})_n] = \text{AP}[\text{H}^+ \cdot (\text{H}_2\text{O})_{n-1}] + \Delta E_{n,n+1}(\text{H-Bond}) \\ + \Delta E_{n-1,n} \text{ (Ion Association)}$$

That is, the appearance potential of successively higher clusters is lowered to the extent that the ion association energy exceeds the hydrogen bond energy. Table II presents

the results of such predictions based on the ion association energies of Kebarle *et al.*^{8/} or De Pas *et al.*,^{1/} and on estimated H-bond energies in the clusters involved. (Enthalpies and energies are used indiscriminately at this point, the error being of order RT, or about 0.03 ev.) Both the ion association energies and the H-bond energies should approach the energy of evaporation of water, about 0.42 ev, although the ion-association values may actually fall below this value at some intermediate small cluster size.

There is one further thermochemical cycle that can be used to predict the limit of the appearance potential for an infinitely large cluster, liquid water, to produce $H^+ \cdot (H_2O)_\infty$.



Taking the previously cited values for ΔE_3 and ΔE_4 , taking ΔE_{11} as the evaporation energy of liquid water, and taking ΔE_{12} , the total enthalpy of solvation of the gaseous proton in liquid water, as equal to -261 Kcal/mole (11.3 ev),^{9,10/} yields $\Delta E_{13} = 7.9$ ev.

At some point, parent water cluster ions may become important and these appearance potentials should approach the work function of liquid water or ice.

IV. Electron-Impact Appearance Potential Results

The first determinations of $H^+ \cdot (H_2O)_n$ appearance potentials have been made using the Bendix TOF mass spectrometer and an ordinary hot-filament source of electrons. The variation of ion intensity with electron energy was determined manually. Measurements were made on known species, as well as the water clusters, to calibrate the electron energy scale in terms of the voltage applied. A log-matching method was used to determine relative appearance potentials of knowns and unknowns. The semi-log plots of intensity versus electron energy were of different shape for the water cluster ions and argon.

The results shown in Table II were determined by carrying out the log matching at about 3 orders of magnitude intensity diminution from the 50 ev value. Indications are that comparison at lower intensity would yield lower appearance potentials for the water cluster ions.

V. Evidence for Complex Fragmentation of Neutral Water Cluster

The results in Table II indicate that the observed appearance potentials for the series $H^+ \cdot (H_2O)_n$, at high degrees of nucleation, are considerably higher than minimum possible values. The dependence of 18^+ and 19^+ appearance potentials on expansion conditions, the behavior of 18^+ and $18^+/17^+$ ratios in Figure 1 and the indication that the lower the electron energy, the lower the apparent appearance potentials, all add to the conclusion that the ionization behavior of partly nucleated water is more complex than the simple loss of OH from a series of neutral clusters.

To provide additional evidence as to the fragmentation behavior and energetics, we have applied the ion-peak-shape scheme of Franklin *et al.*^{11/} to a determination of the kinetic energy of the observed ions and to indicate complexities in cluster fragmentation behavior.

These workers have developed a relation between the ion peak shape in the Bendix and the amount of kinetic energy the ion possessed in the ion source. In the case of parent ions from species in thermal equilibrium at the ion source effective temperature

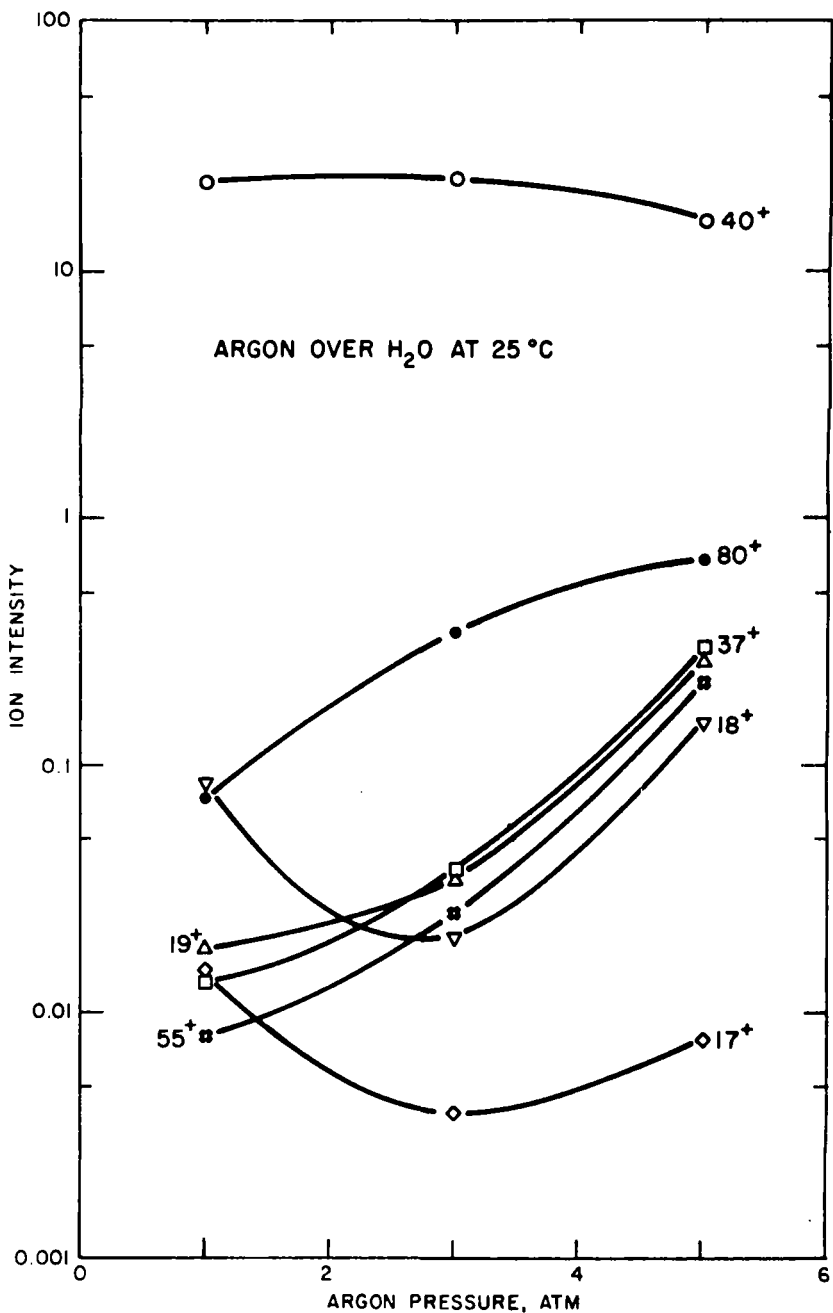


Figure 1 - Variation of Ion Intensities with Free-Jet Source Conditions

(random gas in the ion source), it was shown that the half-width of the approximately gaussian ion peak shape was proportional to the square root of the molecular weight (after correction for the finite width of the gate pulse). In the case of well collimated molecular beam sources of gas, the thermal spread of the beam molecules along the axis of the flight tube is very small, and hence all parent ions should exhibit the same peak shape, according to the model and assumptions of Franklin *et al.*¹¹ This was found to be the case, at least for parent ions of mass up to 150.

Our first results from peak shape analysis are shown in Table III. The widths of these ion peaks have not yet been interpreted in terms of kinetic energies of the fragment ion, but several observations can be drawn from the half-width behavior at 50 ev. For the background gas parent ions, the data shown, and other similar data, indicate a variation in half-width with molecular weight close to that expected from Franklin's work. For beam parent ions such as 2^+ , 18^+ , 40^+ , 44^+ and 80^+ from 1 atmosphere beams, the peak half-widths are all about 14 ± 1 nanoseconds, apparently the minimum width possible with our electronic gate width and optimum space focusing. The fragment ions from the beam, 15^+ from propane, and 19^+ , 37^+ , 55^+ , and 181^+ from water clusters, are broadened, presumably due to kinetic energy acquired during dissociative ionization. Not expected were the broadened peaks for the argon gas cluster ions 80^+ and 360^+ (and presumably intermediate Ar_n ions). Likewise, 18^+ is broad from 5 atmosphere Ar gas over H_2O . These results are consistent with the postulate of complex fragmentation of highly nucleated water (and argon as well).

If it is true, as we hope to verify, that a significantly broadened ion peak originating from a beam species can only arise from a dissociative ionization process, then such peak shape analysis can serve an extremely valuable role in analyzing mass spectra by molecular beam techniques.

TABLE III

ION PEAK SHAPES FROM ELECTRON IMPACT (at 50 ev) OF
VARIOUS BEAMS AND BACKGROUND GASES

<u>Beam and Source</u> <u>Conditions</u>	<u>Supposed</u> <u>Neutral</u>	<u>Ion</u>	<u>Beam or</u> <u>Background</u>	<u>Peak Half-</u> <u>Width</u> <u>(± 1 n sec.)</u> <u>(n sec.)</u>
Background Gases	H_2	2^+	Background	14
" "	N_2	28^+	"	21
" "	Ar	40^+	"	21
" "	C_3H_8	44^+	"	21
" "	Hg	204^+	"	34
" "	C_3H_8	15^+	"	20
1 atm. H_2	H_2	2^+	Beam	13
1 atm. Propane	C_3H_8	44^+	"	15
1 atm. Propane	C_3H_8	15^+	"	24 *
1 atm. Ar	Ar	40^+	"	14
	Ar_2	80^+	"	14
1 atm. Ar over H_2O	H_2O	18^+	"	14
	Ar	40^+	"	14
	$(H_2O)_2$	19^+	"	21 *
	$(H_2O)_3$	37^+	"	20 *
	Ar_2	80^+	"	13
5 atm. Ar over H_2O	H_2O	18^+	"	22 *
	$(H_2O)_2$	19^+	"	19 *
	$(H_2O)_3$	37^+	"	19 *
	$(H_2O)_4$	55^+	"	26 *
	$(H_2O)_{10}$	181^+	"	36 *
	Ar	40^+	"	14
	Ar_2	80^+	"	29 *
	Ar_9	360^+	"	33 *

* Very broad-base ion peak. Not gaussian.

VI. Future Studies Required

From the standpoint of attempting to verify the predictions of Table II, further measurement of appearance potentials of water clusters will be attempted using less nucleated water, using electron impact and the vanishing current method, using resonance-line photoionization and using very large water clusters.

This work was supported by the Air Force Cambridge Research Laboratories and the Defense Atomic Support Agency.

References

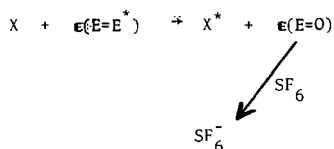
1. Narcisi, R.S., "On Water Cluster Ions in the Ionospheric D-Region," in press, Space Research, IX (1969).
2. Milne, T.A., and F.T. Greene, "Mass Spectrometry of Metal-Containing Flames," Final Technical Summary Report, 1 September 1961 - 30 November 1967, Contract No. Nonr-3599(00).
3. Greene, F.T., A.E. Vandegrift, and T.A. Milne, "An Experimental Study of the Structure, Thermodynamics and Kinetic Behavior of Water," Quarterly Progress Reports, 1 July 1967 - 1 July 1968, Office of Saline Water, Contract No. 14-01-0001-1479.
4. Beuchamp, J.L., and S.E. Buttrell, Jr., J. Chem. Phys., 48, 1783 (1968).
5. Chupka, W.A., and M.E. Russell, J. Chem. Phys., 48, 1527 (1968).
6. Haney, M., and J.L. Franklin, J. Chem. Phys., 50, 2028 (1969).
7. De Pas, M., J.J. Leventhal, and L. Friedman, J. Chem. Phys., 49, 5543 (1968).
8. Kebarle, P., S.K. Searles, A. Zolla, J. Scarborough, and M. Arshadi, J. Am. Chem. Soc., 89, 6393 (1967).
9. Noyes, R.M., J. Am. Chem. Soc., 84, 513 (1962).
10. Halliwell, H.F., and S.C. Nyburg, Trans. Far. Soc., 59, 1126 (1963).
11. Franklin, J.L., P.M. Hierl, and D.A. Whan, J. Chem. Phys., 47, 3148 (1967).

"MONOENERGETIC" ELECTRON IMPACT STUDIES OF SOME
ATOMS AND SMALL MOLECULES

BY C.E. Brion, L.A.R. Olsen and G.E. Thomas
Department of Chemistry
The University of British Columbia
Vancouver 8, B.C., Canada

ABSTRACT

A system consisting of a double 127 degree electron monochromator and a monopole mass filter (1) has been used to study threshold electron impact excitation and ionization. Sulphur hexafluoride was used to scavenge the near zero energy electrons ejected at the excitation thresholds.



Studies of He, Ne, Ar, Kr and Xe below the first ionization potential (2,3) show a high probability for optically forbidden transitions. Xenon also shows interesting structure above the first ionization potential due to excitation of the 5s electron (4), Xe⁺ and Xe⁺⁺ formation (3). Interesting structure is also observed in the scavenging spectra of CO₂, COS and CS₂. (5)

REFERENCES

- (1) C.E. Brion and G.E. Thomas, Internat. J. Mass Spectry Ion Phys. 1,25 (1968)
- (2) C.E. Brion and C.R. Eaton, Internat. J. Mass Spectry Ion Phys. 1,102 (1968)
- (3) C.E. Brion, C.R. Eaton, L.A.R. Olsen and G.E. Thomas - to be published, Chem. Phys. Letters.
- (4) C.E. Brion and L.A.R. Olsen submitted for publication.
- (5) C.E. Brion and G.E. Thomas to be published.

by

B. G. Giessner and G. G. Meisels
 Chemical Physics Program
 Department of Chemistry
 University of Houston
 Houston, Texas 77004

ABSTRACT

Second differential ionization efficiencies of helium and xenon are compared with calculated curves obtained from linear and nonlinear threshold laws convoluted with an experimentally determined electron energy distribution. The method is sensitive to a 10% deviation from a linear threshold law over more than ca. 0.5 eV above threshold. When proper allowance is made for autoionizing states of xenon, all results appear consistent with linear dependence of ionization cross sections on excess electron energy.

The use of the maximum in the second differential ionization efficiency curve to assess appearance potentials leads to an error less than kT_{electron} (typically ca. 0.16 eV) for exponents between 1.0 and 1.9 in the power law for a single state.

INTRODUCTION

The dependence of electron impact ionization cross sections on energy above threshold has been of considerable interest in the past few years and is a controversial subject. A theoretical treatment by Wannier (1) suggested that ionization cross sections should obey a 1.127 power dependence; Geltman subsequently derived a threshold law linear in excess electron energy (2). Recently, Kang and Foland (3) removed certain shortcomings of Geltman's approach but confirmed his conclusion.

Experimental evidence exists for both the 1.0 and 1.127 power dependencies. The broad electron energy distribution, typically of the order of 0.5 eV wide at half height, causes difficulty in the assessment of the energy dependency of the cross section. Electron energy selectors or quasimonoeenergetic sources are therefore used to reduce the smearing of the ionization efficiency curve and to permit an assessment of the power dependency of the ionization cross section. The RPD results of Fox *et. al.* (4) are perhaps the most widely cited evidence for the linear threshold law, and were supported by Foner and Nall (5) using velocity selected electrons. Brion, using a 127° electrostatic electron energy selector, later obtained an ionization efficiency curve for helium which was consistent with a 1.127 power law over some 8 volts above threshold (6), while McGowan and Clarke (7), also using a 127° electrostatic-velocity selector, suggested that ionization of atomic and molecular hydrogen exhibited a 1.127 power dependency for about 0.4 eV above threshold, although a linear power dependency best described their data between 0.4 to 3.0 eV.

Ionization efficiency curves can be described (8) by the equation

$$i(V) = \int_{E_C}^{\infty} P(E - V)(E - E_C)^{\beta} dE \quad (1)$$

where $i(V)$ is the ion current at an electron accelerating potential V , $P(U) = P(E - V)$ the initial energy distribution function of the ionizing electrons, and β is the power dependency of ionization above the threshold energy, E_C .

It has been customary to derive the electron energy distribution $P(U)$ from the second differential of the electron impact ionization efficiency curves (9,10): when a linear threshold law applies, the second differential is simply a reflection of the energy distribution with the energy axis reversed (8). Conversely it should be possible to obtain the power dependency β if the electron energy distribution is known a-priori. The results of a study in which the electron energy distribution was determined directly, convoluted with various power laws, and compared to experimental second differential ionization efficiency curves for helium and xenon are reported here.

EXPERIMENTAL

A plastic junction box was inserted between the ion source and the power supply cable of an Atlas Ch-4 mass spectrometer equipped with a standard AN 4 ion source. The filament power supply was isolated and the ionizing voltage was supplied from mercury batteries and a ten-turn 0.1% linear potentiometer. This potentiometer was ganged with a second potentiometer which was employed to drive the x-axis of a Hewlett-Packard model 203 x-y recorder. A retarding potential could be supplied between the ionization chamber and the electron trap from 2 ten-turn ganged potentiometers and mercury batteries. D. C. potentials in reproducible steps of 0.07 eV and the output from a Hewlett-Packard model 3300A function generator could be superimposed on the ionizing voltage. The modulation voltage from the function generator was maintained at 0.08 eV for all experiments. A

FIGURES

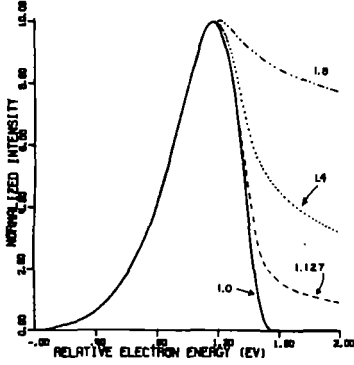


Fig. 1. Second derivative ionization efficiency curves obtained by folding a quasi-Boltzman distribution (2000°K) into various threshold laws as indicated.

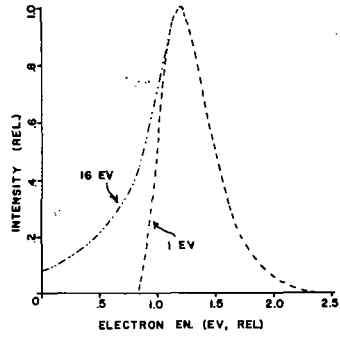


Fig. 2. Variation of experimentally determined electron energy distributions with electron accelerating potential.

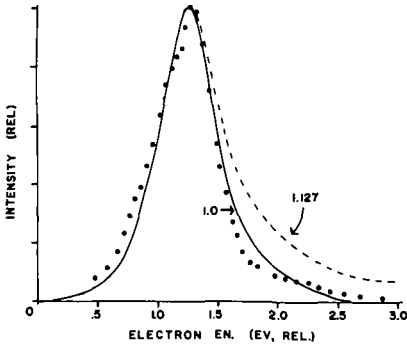


Fig. 3. Comparison of experimental second differential ionization efficiency curve for helium with those calculated from an energy distribution at 23 V and two threshold laws.

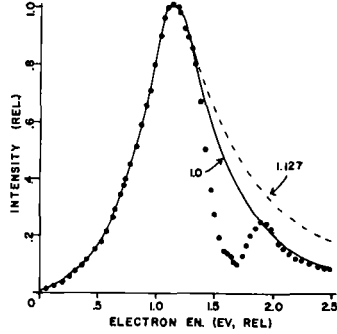


Fig. 4. Second derivative ionization efficiency curve for xenon and calculated curves assuming 1.0 and 1.127 power laws without allowance for autoionization.

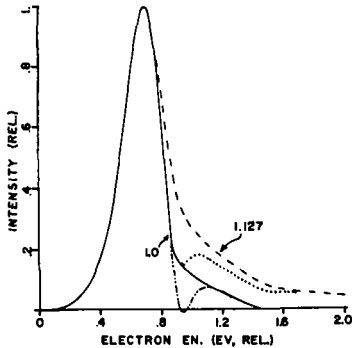


Fig. 5. Effect of an autoionizing state on the second derivative curve calculated for a 1.0 and a 1.127 power threshold law.

Trimetrics 4000-400M digital voltmeter with 0.01% accuracy (0.01 eV), powered from an isolation transformer, permitted direct measurement of the electron accelerating potential during each run. The filament shield was maintained at -0.6 volts with respect to the filament, and drawout potentials were maintained at -0.6 volts with respect to the ionization chamber.

The ion beam was defined by a 0.1 mm source slit and a 0.9 mm collector slit in order to obtain optimum peak flatness. The output of the electron multiplier, after one stage of amplification, was fed to a model 121 Princeton Applied Research lock-in amplifier, referenced by the function generator. The synchronously detected ion current output from the lock-in amplifier (the first differential of the ionization efficiency curve) was plotted directly. Second derivatives of the ionization efficiency curve were obtained experimentally using a constant step voltage of 0.07V, or could be calculated from the first derivative ionization efficiency curve using an IBM 7094 computer. Electron energy distributions were obtained as a function of retarding potential directly from the synchronously amplified electron current. Trap currents were maintained at 1 μ A in all experiments.

RESULTS AND DISCUSSION

Calculated second derivatives of the convolution of an electron energy distribution with threshold laws having an exponent β (equation 1) equal to 1.00, 1.127, 1.4 and 1.8 are shown in Figure 1. The maximum in the second derivative curve is retained even when the threshold law deviates substantially from linearity. For $\beta = 1$ and a thermal distribution, the maximum is displaced by kT_{electron} from the threshold electron energy if the scale is defined by V , the electron gun potential after corrections for contact potentials, etc. For $\beta = 2$, the second derivative becomes constant at the threshold without displacement. The maximum systematic error in the assessment of differences in the maxima of two second differential curves arising from single states but obeying different threshold laws is therefore less than kT_{electron} or 0.16 eV under typical conditions.

As shown by Morrison (8), the second differential ionization efficiency curve for the linear case is the original electron energy distribution, inverted on the energy scale. The tailing of the high energy side of the second derivative (beyond the maximum), corresponds to ionization from the low energy portion of the electron energy distribution. As the power law is increased, this tailing becomes more prominent. Figure 1 demonstrates clearly that the high energy portion of the second differential ionization efficiency curves can be used as a sensitive probe for the power dependency of the ionization cross section above threshold provided that the electron energy distribution is known accurately.

Figure 2 shows experimentally measured electron energy distributions for several nominal electron energies. These distributions were not affected by the pressure of gas in the ionization chamber, and were not significantly dependent on electron current below ca. 3 μ A. The low energy side of the electron energy distributions changes as a function of nominal accelerating energies even though all measurements were made at the same filament temperature. A valid comparison with experimentally obtained second differential ionization efficiency curves requires use of the electron energy distributions appropriate to the energy range covered since knowledge of the low energy tail of the distribution is crucial to the determination of the power dependency of the ionization cross sections.

Figure 3 shows the second derivative ionization efficiency curve of helium and two computed second derivatives resulting from convolution of a 1.0 and 1.127 power dependency with the appropriate experimental electron energy distribution. Our results for helium are in agreement with those reported earlier (8,9) and are consistent with a linear threshold power dependency, or a value of unity for β in equation 1.

The second derivative ionization efficiency curve for xenon is given in Figure 4, and is again similar to results reported earlier (8). Before a comparison can be made with the appropriate distribution, the effect of the known autoionizing state approximately 0.3 eV above onset (11,12) has to be evaluated.

A cross section following a linear and a 1.127 power law with an added step function were convoluted with an assumed electron energy distribution. The inverted distribution, or second differential ionization efficiency curve for a linear power dependence without autoionization, is shown in Figure 5. The effect of autoionization is clearly demonstrated by a second maximum in both calculated cases, but the magnitude of this second peak depends on the threshold law. In the region before the second culmination, the second differential for the linear case with added autoionization falls below the inverted distribution whereas beyond this peak it superimposes on the inverted distribution. However, the second differential calculated on the basis of $\beta = 1.127$ and an added autoionizing state shows a positive deviation with respect to the inverted electron energy distribution in the region preceding the second crest, beyond which it follows the high energy portion of the second differential calculated for a 1.127 power dependency and no autoionization, and is substantially above the inverted distribution.

A precise match of calculated and experimental curves is not expected because the step height associated with the cross section for autoionization is uncertain, and because higher autoionizing states may be expected to contribute (9). The comparison of the second differential ionization efficiency curve of xenon with the inverted distributions assuming $\beta = 1$ or 1.127 (Figure 4) suggests that our results for xenon are also consistent with a threshold law for ionization linear with excess energy.

ACKNOWLEDGEMENTS

This investigation was supported in part by the Robert A. Welch Foundation, and by an equipment grant from the National Science Foundation. We are greatly indebted for this assistance. The computing facilities were those of the Texas Medical Center (IBM 7094), supported by the Robert A. Welch Foundation and by the United States Public Health Service under grant FR-00254.

LITERATURE CITED

1. G. Wannier, Phys. Rev. 90, 817 (1953).
2. S. Geltman, Phys. Rev. 102, 171 (1956).
3. I. Kang and W. D. Foland, Phys. Rev. 164, 122 (1967).
4. R. E. Fox, W. M. Hickam, D. J. Grove, and T. Kjeldass, Rev. Scien. Inst. 26, 1101 (1955).
5. S. N. Foner and B. H. Nall, Phys. Rev. 122, 512 (1961).
6. C. E. Brion and G. E. Thomas, J. M. S. and I. P. 1, 25 (1963).
7. J. W. McGowan and E. M. Clarke, Phys. Rev. 167, 43 (1968).
8. J. D. Morrison, J. Chem. Phys., 21, 1767 (1953).
9. J. D. Morrison, J. Chem. Phys. 40, 2488 (1964).
10. J. H. Collins, R. E. Winters, and G. G. Engerholm, J. Chem. Phys. 49, 2469 (1968).
11. H. Beutler, Z. Physik 93, 177 (1935).
12. R. E. Huffman, Y. Tanaka, and J. C. Larrabee, J. Chem. Phys. 39, 902 (1963).

Total and Individual Cross Sections for the Production of Free Radicals, Positive Ions
and Negative Ions from Water Vapor by 100 eV Electrons^{a,b}

Charles E. Melton
Department of Chemistry
University of Georgia
Athens, Georgia 30601

Abstract

The abundances of, and the total and individual cross section for, primary products (positive ions, neutral species, and negative ions) resulting from elementary reactions induced by the absorption of energy from ionizing radiation (100 eV electrons) by H₂O have been measured. This was accomplished by means of the dual beam and high transmission ion sources¹ attached to the Georgia research mass spectrometer (see acknowledgement). Positive ions are produced in much greater abundance than free radicals 67.2% vs. 32.1%. Negative ions, on the other hand, are about two orders of magnitude less abundant than the other primary products. Results are shown in Table I.

Table I

Individual cross section for primary products resulting from the irradiation of H₂O with 100 eV electrons at a pressure of 6×10^{-6} torr.

Neutral Species		
Neutral	% of Total Products	$\sigma \times 10^{16} \text{cm}^2$
H	17.38	0.57
H ₂	4.27	0.14
O	2.87	0.094
OH	7.57	0.248
Total	32.09	1.052
Positive Ions		
Ion	% of Total Products	$\sigma \times 10^{16} \text{cm}^2$
H ⁺	4.57	0.15
H ₂ ⁺	0.34	0.011
O ⁺	1.62	0.053
OH ⁺	13.12	0.43
H ₂ O ⁺	47.58	1.56
Total	67.23	2.204
Negative Ions		
Ion	% of Total Products	$\sigma \times 10^{16} \text{cm}^2$
H ⁻	0.64	0.021
O ⁻	0.034	0.0011
OH ⁻	0.003	0.0001
Total	0.677	0.0222

Values for the specific cross sections are actually sums of cross sections for all reactions that produce a specific product. Cross sections for ionization of free radicals were necessary but not available to obtain the results for the neutral species given in Table I. The cross sections for ionization of oxygen and hydrogen atoms was assumed to be one-half that for ionization of the corresponding neutral diatomic molecules for the same values of $(E-I)$, where E is the electron energy and I is the ionization potential. Results for the OH radical are perhaps more uncertain. The cross section was assumed to be equal to 70% of that for H₂O at equal values of $(E-I)$. This assumption probably gives the lower limit for the cross sections for ionization of OH.

a. This research was supported by the U. S. Atomic Energy Commission under Contract No. AT(40-1)-3729 with the University of Georgia.

b. To be published in the Journal of Chemical Physics.

A comparison of this work with previous results is restricted to the positive ions because no data are available for neutral species. Mann et al² reported a much lower abundance for all of the fragment ions than that observed in the present study. Schutten et al³ also reported a lower abundance for all fragment ions except H⁺ which is higher by a factor of three. Total cross section, on the other hand, reported by Schutten et al² agree to within 5% with that measured in this study 2.1×10^{-16} cm² molecule⁻¹. Furthermore, individual cross sections reported by these workers agree with the present results to within 25% for the fragment ions with the exception of that for H⁺ which differs by a factor of three. This large discrepancy has not been resolved.

Acknowledgement

The author is deeply indebted to W. D. Harmon and W. Rice of the Y-12 Mass Spectrometer Laboratory, Oak Ridge, Tennessee for providing surplus components from which the research mass spectrometer was constructed.

Bibliography

- 1) C. E. Melton, J. Chem. Phys. 45, 4414 (1966).
- 2) M. M. Mann, A. Hustrulid, and J. T. Tate, Phys. Rev. 58, 340 (1940).
- 3) J. Schutten, F. J. DeHeer, H. R. Maustafa, A. J. H. Boerboom, and J. Kistemaker, J. Chem. Phys. 44, 3924 (1966).

RELATIVE ELECTRON IMPACT IONIZATION CROSS SECTIONS OF COPPER AND GOLD,
AND THE VELOCITY OF EVAPORATED ATOMS*

Dinçer H. Gündüz, Juergen M. Schroeder, and Spencer Livingston[†]

Department of Physics, University of Wyoming, Laramie, Wyoming 82070

INTRODUCTION

We present here the variation of the total ionization cross section by electron impact of evaporated Cu and Au atoms as a function of the electron energy between 40 and 250 eV. We will also make a few remarks about the velocity of evaporated atoms.

So far, the cross sections of only a few metals have been measured. In the thirties, mercury and some of the alkali metals were investigated. More recently, Pottier¹ measured the cross sections of Zn, Te, and Cd, McFarland² the cross sections of Cs, and Crawford³ those of Ag and Cu.

EXPERIMENTAL METHOD

For the measurement of ionization cross sections by electron impact of low vapor pressure materials, the so-called crossed-beam technique is used. A beam of electrons and of evaporated atoms intersect, as shown in Fig. 1, producing ions. Unless a mass spectrometer is used, it is not possible to distinguish between the ions of different charge states.

The ion current i_I detected at the ion collector is proportional to the electron current i_E , the total cross section σ , the density n of the metal atoms, and the path length λ of the electrons through the beam of evaporated atoms,

$$i_I = i_E n \sigma \lambda. \quad (1)$$

In practice, the number N of the evaporated atoms arriving at the beam collector during a time interval t with average velocity \bar{v} is measured, together with the diameter d of the electron beam,

$$i_I = \frac{i_E \sigma N}{t \bar{v} d}. \quad (2)$$

As the source of the evaporated atoms we used an evaporation boat. The velocity of atoms evaporated from an open liquid has never been measured before. Other investigators always used a Knudsen cell for which the velocity of the escaping atoms is well known. We assume that the average velocity of the atoms evaporating from the boat can be expressed as

$$\bar{v} = \beta \sqrt{2kT/m}, \quad (3)$$

where k is Boltzman's constant, T the surface temperature of the molten metal in the boat, and m the mass of the evaporating atoms. β is a constant, which depends on the details of the evaporating process, but is assumed to be independent of the material being evaporated.

Solving Eq. (2) for σ , and using the expression in Eq. (3) for \bar{v} , we obtain,

$$\sigma = \frac{i_1 \text{tdB}}{i_E N} \sqrt{\frac{2kT}{m}} \quad (4)$$

A schematic diagram of the apparatus is shown in Fig. 2. Most of it was constructed from a commercially available kit,⁴ which consists of prepunched stainless steel parts and alumina rods.

RESULTS

Fig. 3 shows the relative cross sections for Cu and Au as measured by us, together with Crawford's³ absolute cross section for Cu as a solid line. We selected $\beta = 0.72$ for plotting our Cu and Au data, so as to give best agreement in the graph between our copper data and Crawford's. The error bars represent the random uncertainties in our measurements. In addition, all our data points are subject to a possible systematic error of $\pm 9\%$, and Crawford's data to $\pm 25\%$. The inclusion of these systematic errors leads to $\beta = 0.72 \pm 0.25$.

The results can be summarized as follows:

- (a) Our curve of the cross section of Cu versus the electron energy agrees well with Crawford's data.
- (b) Between 40 and 180 eV the ratio of the cross sections is

$$\sigma(\text{Au})/\sigma(\text{Cu}) = 2.0 \pm 0.1 \quad (5)$$

This value agrees with Ackerman et al's value of 1.9 at 75 eV.⁵ Both experimental measurements are in disagreement with Mann's⁶ theoretical ratio of 1.6 at about 90 eV.

- (c) If we assume that the average velocity of evaporated atoms is given by Eq. (3), then for Cu evaporating from an evaporation boat filled with liquid copper at 1730°K,

$$\beta = 0.72 \pm 0.25 \quad (6)$$

Thermal equilibrium between the liquid surface and the evaporating atoms predicts $\beta = 1.33$. Thus, on the basis of presently available experimental evidence, copper atoms evaporating from an open surface of liquid copper are not in thermal equilibrium with the surface. This contrasts with the findings of Mar and Searcy⁷ and of Rothberg et al.⁸ who found that atoms sublimating from solid surfaces of gallium nitride and of alkali halides, respectively, are in thermal equilibrium with the solid surface.

EVAPORATION MODEL

Thermal equilibrium between the evaporated atoms and the liquid surface means that the velocity distribution, both in magnitude and in direction, of the evaporated atoms is the same as if we had a perfect gas in a large container at the temperature of the liquid surface, with atoms diffusing out of the container through a hole. Such a container is called a Knudsen cell, for which the velocity distribution and average velocity of the diffusing atoms is well known,⁹ i.e.

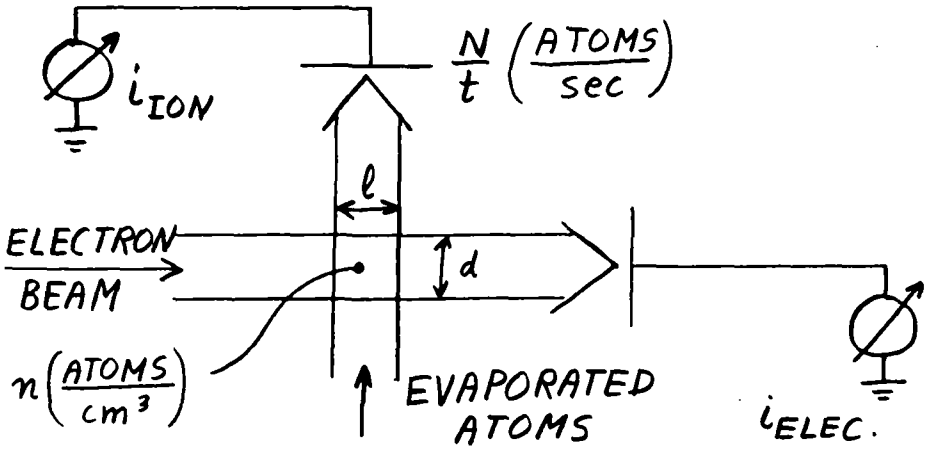


Fig. 1. Crossed beam experiment for the measurement of the ionization cross section by electron impact of evaporated metal atoms.

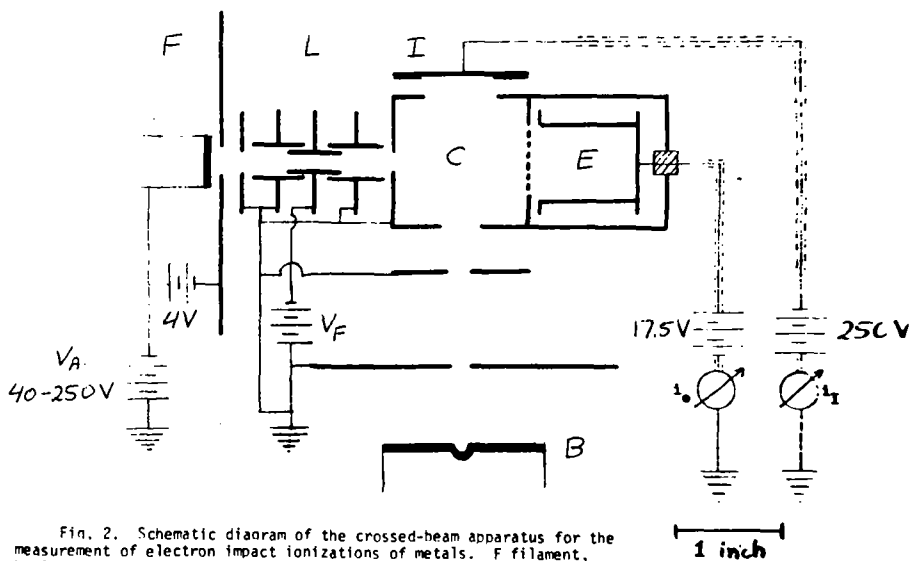


Fig. 2. Schematic diagram of the crossed-beam apparatus for the measurement of electron impact ionizations of metals. F filament, L electrostatic lens, B atomic beam source, C collision chamber, I ion and atomic beam collector, E electron collector, V_A accelerating voltage, V_F focussing voltage, i_e electron current, i_1 ion current.

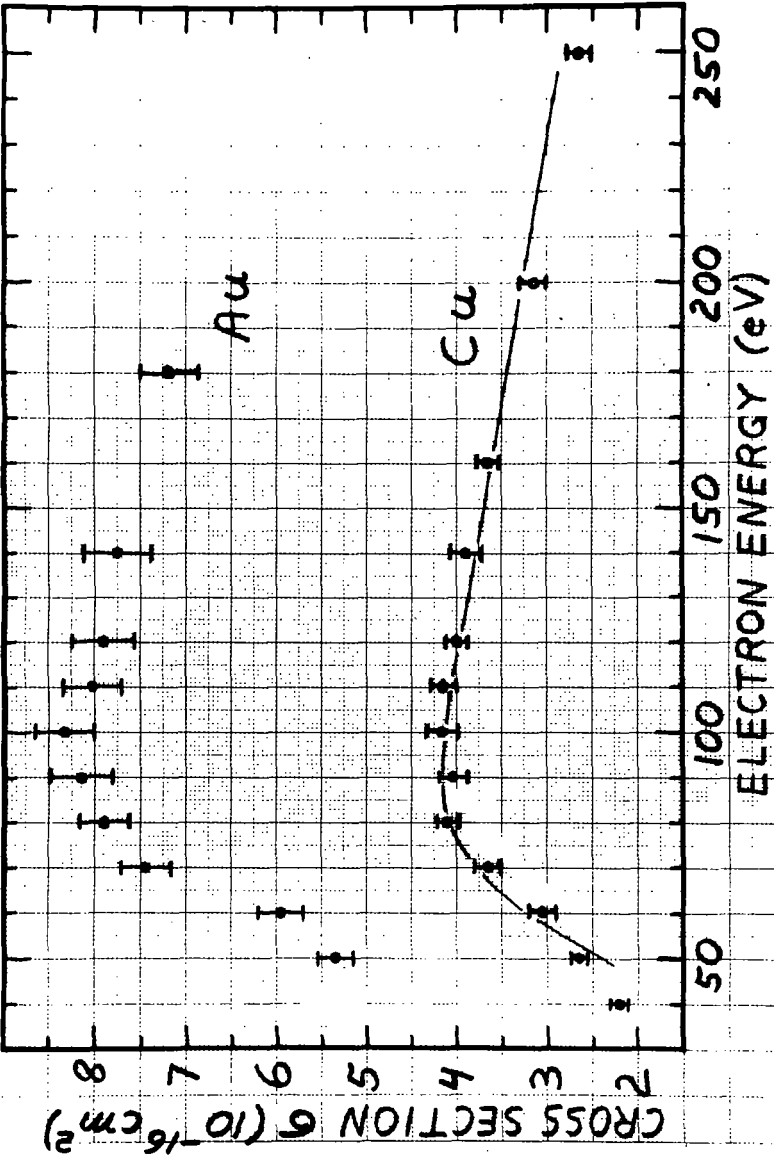


Fig. 3. The total relative ionization cross sections of copper and gold as a function of the bombarding electron energy. The solid line represents Crawford's absolute cross section of copper.

$$\bar{v} = \frac{\int_0^{\infty} v^4 \exp - (mv^2/2kT) dv}{\int_0^{\infty} v^3 \exp - (mv^2/2kT) dv} \quad (6)$$

$$= \frac{3}{4} \sqrt{\pi} \sqrt{2kT/m} = 1.33 \sqrt{2kT/m} \quad (7)$$

REFERENCES

*Supported in part by a grant from the Society of the Sigma Xi.

†Participant in a program of Research Participation for High School Teachers sponsored by the National Science Foundation.

1. R. F. Pottie, *J. Chem. Phys.* 44, 916 (1966).
2. R. H. McFarland, The Fourth International Conference on the Physics of Electronic and Atomic Collisions, Quebec, Canada, August 1965 (Science Bookcrafters, Hastings-on-Hudson, New York, 1965), p. 416.
3. C. K. Crawford, "Electron Impact Ionization Cross Sections," Technical Report #1, Particle Optics Laboratory, Massachusetts Institute of Technology, Cambridge, Massachusetts, 1967. AFML-TR-67-376. Also, C. K. Crawford and K. I. Wang, *J. Chem. Phys.* 47, 4667 (1967).
4. EAI Kit 606 from Nuclide Corp., AGV Division, 914 Main Street, Acton, Mass. 01720.
5. M. Ackerman, F. E. Stafford, and J. Drowart, *J. Chem. Phys.* 33, 1784 (1960).
6. J. B. Mann, *J. Chem. Phys.* 46, 1646 (1967).
7. R. W. Mar and A. W. Searcy, *J. Chem. Phys.* 49, 182 (1968).
8. G. M. Rothberg, M. Eisenstadt, and P. Kusch, *J. Chem. Phys.* 30, 517 (1959).
9. E. H. Kennard, Kinetic Theory of Gases, McGraw-Hill (New York, 1938), Chapter III.

ELECTRON IMPACT IONIZATION CROSS SECTIONS
BY A DOUBLE CROSSED BEAM TECHNIQUE

Lee H. Rovner and John H. Norman

GULF GENERAL ATOMIC INCORPORATED
San Diego, California 92112

A simple method of accurately measuring relative electron impact ionization cross sections of low vapor pressure materials is extremely desirable. We are in the process of developing a technique whereby the measurements are made on a molecular beam which is crossed by two successive electron beams. This idea is similar to that mentioned by Crawford.¹ The additional electron beam, which is modulated, is interposed between the Knudsen cell and the entrance slit to the source region of a mass spectrometer. The effect of the consequent modulation in intensity of the molecular beam, ΔI_2 , is observed for each of the component species of the beam on the output of the mass spectrometer, I_2 .

The attenuation of the molecular beam flux, $\Delta \dot{n}$, due to the first ionizer is

$$\Delta \dot{n} = K \dot{n} i (\Sigma Q) \left(\frac{M}{T} \right)^{1/2}$$

where i is electron current, M molecular weight, T temperature, and K a geometric constant. As written, ΣQ is a collision probability and not the normal cross section as defined in terms of an equivalent ion current. The value of $\Delta \dot{n}$ therefore is related to, but not equal to, the ion current that would be collected in an experiment designed to measure absolute ionization cross sections. In such an experiment, several precautions are necessary relevant to the accuracy of defining the effective electron and molecular beam densities and their effective mutual volume of intersection. Secondary electron emissions must be suppressed and ions formed from background gases must be eliminated. These requirements are difficult to achieve in practice.

For our measurements, we are interested only in the relative attenuation

$$\frac{\Delta \dot{n}}{\dot{n}} = \frac{\Delta I_2}{I_2} .$$

Eliminating $\Delta \dot{n}$,

$$\frac{\Delta I_2}{I_2} = K i \Sigma Q \left(\frac{M}{T} \right)^{1/2}$$

and if the measurement is limited to a comparison of the relative attenuations of two different species in the molecular beam,

$$\frac{\Sigma Q_M \left(\frac{M T_{M'}}{M' T_M} \right)^{1/2}}{\Sigma Q_{M'} \left(\frac{M' T_M}{M T_{M'}} \right)^{1/2}} = \left(\frac{\Delta I_2}{I_2} \right)_M / \left(\frac{\Delta I_2}{I_2} \right)_{M'}$$

The constant K as well as the electron current cancel and, therefore, the stringent requirements for absolute measurements are greatly relaxed for these relative measurements. Only the necessity for time constancy remains, and this is easily achieved. In addition, the method may be applied to condensed systems vaporizing in a complex fashion as well as to minor components of the vapor phase. These applications are of much interest to the study of the thermochemistry of high temperature systems.

It must be noted that the collision probability, ΣQ , includes all processes which will remove molecules from the beam. This certainly includes ionization since the entrance slit to the mass spectrometer is operated at about 6 KV positive with respect to the first ionizer, but may also include other inelastic as well as elastic collision processes. The apparent cross sections for these processes are dependent on the momentum transfer relative to the width of the molecular beam and the acceptance angle of the mass spectrometer.

The uniform density portion of the molecular beam presents a $1/2^\circ$ half-angle to the mass spectrometer entrance slit and this, then, is the angular deviation required in a collision before the collision probability measured will be affected by other than ionization processes. We had some concern that elastic collisions might possibly contribute measurably to the collision probability. Therefore, in checking out this technique by comparison with some of the literature values for ionization cross sections, atoms having large differences in mass were chosen to see if the values obtained would show deviations appropriate to these other processes.

The relative magnitude of the attenuation caused by the first ionizer, of the order of 0.1%, required use of phase sensitive detection in order to facilitate the measurement. The same square wave with which the electron current was modulated provided the reference

phasing of the lock-in amplifier. The intensities, I_2 and ΔI_2 , were recorded simultaneously. Their ratio for our present setup showed an experimental spread of about 15%.

The experimental results are shown in Table 1. The total experimental collision probability is ΣQ and the collision probabilities for formation of the indicated ions are Q_{M+} and Q_{M++} . The relative probability for formation of the doubly charged ions was obtained from the relative intensities given by the mass spectrometer which were corrected for the relative yields of the multiplier.

By using the Q_{M++}/Q_{M+} ratios, the data were converted to total cross sections, σ , (assuming only ionization) or to cross sections for production of single ions in order to enable comparison with the available literature values as shown in Table 2. The generally good agreement gives experimental verification of this technique for measuring relative ionization cross sections. For atomic vapors, other collision processes do not appear to have been important in those cases designed to test this question.

Table 1
Experimental Results (50 eV)

	$\Sigma Q_M / \Sigma Q_{M'}$		Q_{M++} / Q_{M+}
Tl/Ca	1.10	Tl	0.055
Ag/Ca	0.63	Ca	0.20
Ag/Pb	0.70	Ag	0.023
W_2O_6/Ag	2.4	Pb	0.18
W_3O_9/W_2O_6	1.25		

Table 2
Comparison with Literature (50 eV)

Quantity	Value	Literature
$\sigma_{Tl} / \sigma_{Ca}$	0.99	1.02 ²
Q_{Ag+} / Q_{Pb+}	0.81	0.70 (60 eV) ³ 0.68 ^{1, 4}
$\sigma_{Ag} / \sigma_{Pb}$	0.61	0.35 ⁵

- 1 C. K. Crawford, "Electron Ionization Cross Sections for Hard-to-Vaporize Materials," presented at the 17th Annual Conference on Mass Spectrometry and Allied Topics, Dallas, Texas, 1969; Technical Report AFML-TR-69-5, January 1969, Particle Optics Laboratory, Massachusetts Institute of Technology.
- 2 R. H. McFarland, Phys. Rev. 159, 20 (1967).
- 3 S-S Lin and F. E. Stafford, J. Chem. Phys. 47, 4664 (1967).
- 4 C. K. Crawford and K. I. Wang, J. Chem. Phys. 47, 4667 (1967).
- 5 S. I. Pavlov, V. I. Rakhovskii and G. M. Fedorova, Soviet Physics JETP 25, 12 (1967).

(This paper will be submitted for publication in the Journal of Chemical Physics.)

Negative Ion Mass Spectra of Some Cobalt and Manganese Carbonyl Derivatives

F. E. Saalfeld and M. V. McDowell
Naval Research Laboratory
Washington, D. C. 20390

The negative ion mass spectra of several cobalt and manganese carbonyl derivatives ($\text{Cl}_3\text{SiCo}(\text{CO})_4$; $(\text{CH}_3)_3\text{SiMn}(\text{CO})_5$; $(\text{CH}_3)_3\text{SiMn}(\text{CO})_4(\text{PF}_3)$ and $(\text{CH}_3)_3\text{SiMn}(\text{CO})_3(\text{PF}_3)_2$ have been investigated. These compounds exhibit interesting negative spectra in that several metastable ion transitions are observed. The kinetic energy released in these transitions ranges from 0 to 0.3 e.v.

The appearance potentials of selected ions from these spectra have been measured and from these data the electron affinities have been estimated. In addition, the formation of a parent negative ion in the 70-volt spectrum of $(\text{CH}_3)_3\text{SiMn}(\text{CO})_5$ was shown to be due to electron scatter inside the ion source. The parent ion was eliminated by coating the inside of the source with an electron velvet (Aquadag); after this precaution, the largest m/e ion observed was the parent-CO. These results indicate caution must be employed when negative ion spectra are investigated because secondary electron scatter in the ion chamber can produce significant ion currents.

A. L. Yergey and J. L. Franklin
Department of Chemistry
Rice University
Houston, Texas 77001

The purpose of this work is to devise a method to obtain reliable values for energetic distribution in negative ions formed by dissociative resonance attachment. We hope to relate in a general way the measurement of the translational energy of a fragment ion to the total excess energy involved in an electron attachment process with a system analogous to that already in use for positive ions.¹ We have investigated several triatomic molecules and their various fragment ions thus far and we have encountered some difficulty in explaining the mechanisms of electron attachment and ion decomposition.

A Model 12 Bendix time-of-flight mass spectrometer coupled with a Bendix Model 3015 Output Scanner and Electrometer and a Model MPL-153 Voltage Divider has been used in this work. The gated anode signal was lead through the vacuum flange with a shielded connection because of the presence of large leakage currents without this shielding. It was necessary to operate the electron gun at very low trap current levels in order to observe attachment process in the appropriate energy range and with the resonance peaks having appropriate widths.

Due to low ion intensities, appearance potentials were obtained by using a very simple electron gun with no attempted use of monoenergetic electron methods. The appearance potentials obtained were in excellent internal agreement with those observed by Kraus² and his calibration of the energy scale for the initial onset was taken as correct after it was confirmed early in this work. Average translational energies of fragment ions were measured by the method of Franklin, Hierl and Whan³ by which the width at half height of an ion peak at a series of electron energies is measured and related to the average ionic translational energy and thence to the total average translational energy of the fragments.

A molecule may dissociatively capture an electron to form a particular ion at more than one electron energy. These captures are separated by 2 to 4 eV and have associated with them translational energies that are horizontal in the regions where the captures do not overlap. The lower energy resonance capture is associated with the lower level of the translational energy. When ions result from any process other than multiple resonance capture, plateaus are not observed. Any explanation of these plateaus is unsatisfactory in some respect and their origin is not understood at this time. We have several suggestions to advance for possible mechanisms of electron attachment but at this time we cannot positively eliminate or choose any one of these suggestions. We can propose mechanisms that require that the electron energy distribution changes as the electron energy varies, that there is anisotropic dissociation of the parent negative ion, that there are two different but nevertheless narrow energy cross sections for electron attachment or that all excess energy above a certain level is converted into excitation of internal modes of the fragments.

In the dissociation process, the distribution of excess energy among the products of the higher energy dissociative attachment process is not completely understood at this time. In the cases where translational energy is associated with a particular ion, we

observe that the total average translational energy of the fragments of the system amounts to about 15% of the total excess energy for the dissociative attachment process. The total excess energy is the difference between an appearance potential and the ground state heats of formation of the fragments and precursor. The portion of total excess energy other than translation must be distributed somehow among internal modes of the fragments. The observation of excited electronic states of negative fragment ions is unlikely because they would probably be too short-lived to observe. We do, however, have some cause to suggest that the neutral sulfur atom resulting from the higher energy dissociative attachment to CS_2 is formed in an excited electronic state. In the higher energy dissociative attachment to CO_2 or SO_2 to form O^- , we can suggest that the non-translational portion of excess energy is distributed into vibration - rotation of the diatomic fragment and not into electronic excitation of this fragment.

Further work is underway in this area to characterize more fully the behavior cited here. We will extend this work to a larger number of systems to see if the behavior noted here is observed in larger molecules.

References

1. M. A. Haney and J. L. Franklin, J. Chem. Phys. 48, 4093 (1968).
2. V. K. Kraus, Z. Naturforschg 16a, 1378 (1961).
3. J. L. Franklin, P. M. Hierl and D. A. Whan, J. Chem. Phys. 47, 3148 (1967).

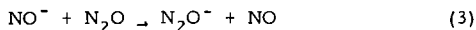
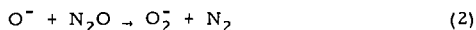
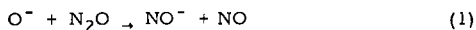
A complete paper will be submitted for publication later.

NEGATIVE IONS IN NITROUS OXIDE

Fred Dale and John F. Paulson
 Air Force Cambridge Research Laboratories (OAR)
 L. G. Hanscom Field, Bedford, Massachusetts 01730

Negative ions produced in N_2O , either by dissociative attachment or by ion-neutral reactions, have been studied by several workers. The production of ions at m/e 44 is of particular interest. Using a high pressure ion source, we have confirmed our earlier observation of a negative ion at m/e 44 in $^{14}N^{14}NO$, shifting to m/e 45 in $^{14}N^{15}NO$, and therefore assigned as N_2O^- . The reaction producing N_2O^- is found to be third order in N_2O pressure, in conflict with our earlier result. Studies using a double mass spectrometer have shown conclusively that the N_2O^- is produced by charge transfer between NO^- and N_2O . This result explains the third order pressure dependence in the ion source, since NO^- is itself a secondary ion.

Reactions observed with the double mass spectrometer system are:



Use of isotopically labeled reactants has shown that, in the kinetic energy range from 0.3 to 10 eV, reaction (1) proceeds through both dissociative charge transfer and N-atom transfer mechanisms, whereas reaction (3) is almost entirely a charge transfer process.

TIME-of-FLIGHT ANALYSIS IN ION-NEUTRAL REACTIONS

John F. Paulson, Stanley A. Studniarz*, and Fred Dale
Air Force Cambridge Research Laboratories (OAR)
L. G. Hanscom Field, Bedford, Massachusetts 01730

A double mass spectrometer system, consisting of a magnetic sector ion selector, a collision chamber, and a quadrupole mass filter, has been adapted for use in measuring time-of-flight (TOF) distributions of reactant and product ions in ion-neutral reactions. A 0.1 to 1 microsecond pulse applied to an electron control grid produces an ion bunch which, after mass analysis, enters the collision chamber, produces a product ion bunch, and passes through the mass filter. Times-of-flight of reactant and product ions through the mass filter are measured using a multichannel analyzer and a clock rate of 50 to 200 nanoseconds per channel. The TOF of reactant ions from formation in the ion source to the collision chamber is measured by applying a suitably delayed pulse at a retarding grid just downstream from the collision chamber. The mass filter is frequently operated as a high pass filter, the mass resolution required being obtained from the TOF principle alone.

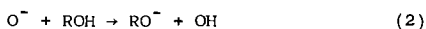
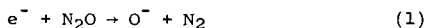
The TOF-quadrupole system described has been used to obtain velocity distributions of ions in symmetric and asymmetric charge transfer, atom and ion transfer, and collisional ion dissociation and dissociative charge transfer reactions, in the range of product ion kinetic energies from thermal to 150 eV. Emphasis in this paper will be placed on symmetric and asymmetric charge transfer and atom transfer reactions.

*NAS-NRC Postdoctoral Research Associate

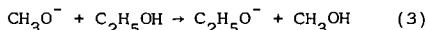
Thomas O. Tiernan and B. Mason Hughes[†]
Aerospace Research Laboratories
Office of Aerospace Research
Wright-Patterson Air Force Base, Ohio 45433

Recent studies in our laboratory have been concerned with negative ion-molecule reactions¹. It has been demonstrated that O⁻ ions react with various alcohols primarily by abstracting a proton from the alcohol, forming the alkoxide ion. The present investigation deals with the reactions of various alkoxide ions generated in this manner with a series of alcohols. As will be shown, these experiments yield some quite interesting chemical information.

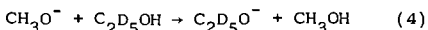
The instrument utilized in these studies was a tandem mass spectrometer which has been described in detail previously². Except where otherwise indicated, all experiments reported here were conducted with impacting ions of 0.3 eV kinetic energy. The collision chamber temperature was maintained at 190°C, and the collision chamber pressure held constant at 5 microns, which is sufficiently low to ensure that only single collision events occur. The impacting alkoxide ions were produced in the first stage ion source by electron impact on a mixture of N₂O and the appropriate alcohol. Under the operating conditions of the experiment³, the N₂O molecules undergo dissociative electron capture, forming O⁻ ions and these then abstract a proton from the alcohol producing the alkoxide ion. The latter species is the impacting ion which is accelerated into the collision chamber.



The only detectable reaction between alkoxide ions and alcohols also involves transfer of a proton from the neutral molecule to the ion. Thus, in the tandem spectrometer, the observed reaction of CH₃O⁻ ions with ethanol is,

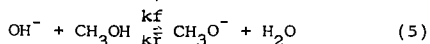


In one sense, these reactions may be regarded as simple acid-base reactions in which the alcohol, of course, is the acid or proton donor. By making comparisons between a series of such reactions for various alcohols, one can establish a scale of relative acidities or acid strengths for the alcohols. In using such reactions to determine relative acidities, it is assumed, of course, that the proton transferred in all cases comes from the hydroxyl group. That this is true at least for the case of ethanol is shown by the isotopic experiment in which deuterated ethanol is introduced into the collision chamber,



Here C₂D₅O⁻ is the only product ion detected and the transfer is clearly from the hydroxyl group. For the low kinetic energy experiments reported here, only transfer from the hydroxyl group is expected for the other alcohols as well, although the lack of availability of the remaining deuterated alcohols prevented our actually establishing this experimentally.

In a mixture of two alcohols, processes such as reaction 3 might be regarded as equilibrium processes in which the equilibrium constant is a measure of the relative acidity of the two alcohols. Thus in a water-methanol mixture, the equilibrium established may be represented as,



Since the equilibrium constant, to a good approximation is given by the ratio,

$$K_{eq} = \frac{k_f}{k_r} \quad (6)$$

it is apparent that these constants can be obtained by measuring k_f and k_r . Using the tandem spectrometer, the rate constants for both forward and reverse reactions of such equilibria have been independently measured for a series of alkoxide ion-alcohol interactions and these are reported in Table I along with the calculated

* A more detailed account of this investigation will be submitted for publication in the Journal of the American Chemical Society.

† Research performed at the U. S. A. F. Aerospace Research Laboratories while in the capacity of an Ohio State University Research Foundation Visiting Research Associate under Contract F33615-67-C-1758.

equilibrium constants.

Table I
Rate Constants for Alkoxide Ion-Alcohol Reactions Determined in
the Tandem Mass Spectrometer and Calculated Equilibrium Constants

			$(10^{-9} \text{ cm}^3 \text{ molecule}^{-1} \text{ sec}^{-1})$		
<u>Reaction</u>			<u>k_f</u>	<u>k_r</u>	<u>$K_{eq}(\bar{E} \sim 0.3 \text{ eV})$</u>
OH^-	+ CH_3OH	$\rightleftharpoons \text{CH}_3\text{O}^- + \text{H}_2\text{O}$	1.3	0.016	80.0
CH_3O^-	+ $\text{C}_2\text{H}_5\text{OH}$	$\rightleftharpoons \text{C}_2\text{H}_5\text{O}^- + \text{CH}_3\text{OH}$	1.09	0.10	10.9
$\text{C}_2\text{H}_5\text{O}^-$	+ $n\text{-C}_3\text{H}_7\text{OH}$	$\rightleftharpoons \text{C}_3\text{H}_7\text{O}^- + \text{C}_2\text{H}_5\text{OH}$	0.92	0.35	2.6
$\text{C}_3\text{H}_7\text{O}^-$	+ $n\text{-C}_4\text{H}_9\text{OH}$	$\rightleftharpoons \text{C}_4\text{H}_9\text{O}^- + \text{C}_3\text{H}_7\text{OH}$	0.48	0.34	1.4
$\text{C}_4\text{H}_9\text{O}^-$	+ $n\text{-C}_5\text{H}_{11}\text{OH}$	$\rightleftharpoons \text{C}_5\text{H}_{11}\text{O}^- + \text{C}_4\text{H}_9\text{OH}$	0.39	0.28	1.4
$\text{C}_5\text{H}_{11}\text{O}^-$	+ $n\text{-C}_6\text{H}_{13}\text{OH}$	$\rightleftharpoons \text{C}_6\text{H}_{13}\text{O}^- + \text{C}_5\text{H}_{11}\text{OH}$	0.25	0.15	1.7

On the basis of this data and similar measurements for various isomeric alcohols, the order of relative gas phase acidities established is, $\text{H}_2\text{O} < \text{CH}_3\text{OH} < \text{C}_2\text{H}_5\text{OH} < n\text{-C}_3\text{H}_7\text{OH} < n\text{-C}_4\text{H}_9\text{OH} < t\text{-C}_4\text{H}_9\text{OH} < n\text{-C}_5\text{H}_{11}\text{OH} < t\text{-C}_5\text{H}_{11}\text{OH}$ and, $n\text{-C}_5\text{H}_{11}\text{OH} < n\text{-C}_6\text{H}_{13}\text{OH}$. It will be realized that this order of acidities is essentially the reverse of the so-called "inductive" order determined from solution studies, which has been presumed to result from the electron donating properties of alkyl group substituents. In view of our data, it seems likely that the order observed in solution is actually the result of solvent effects, possibly hydrogen bonding or dipole interactions between the solvent and alkoxide ions which are subject to strong steric effects.

It may also be noted that the results obtained in the present study are essentially in agreement with those reported recently from ion-cyclotron resonance studies⁴. The latter studies which involve single reaction chamber experiments, reportedly evaluated the relative acidities by determining the "sign" of ΔH_R for the alkoxide ion-alcohol processes. Our data, however raise some interesting points regarding the energetics of these reactions and some questions about the general meaning of the "sign" of the reaction enthalpy. For example, it can be seen in Table I that the equilibrium constants for the first two systems are quite large while the remaining K_{eq} are somewhat greater than unity. A reasonable interpretation of this behavior is that the reverse reactions for the first two systems, (water-methanol and methanol-ethanol) are actually endothermic. The reason for our observation of even a small rate constant for the reverse reactions in these cases is probably due to a small fraction of internally excited ions in the beam or to the 0.3 eV translational energy of the impacting ions, either of which may supply the necessary heat of reaction. On the other hand, the rather large reverse reactions observed for the other systems shown in Table I dictates that these processes must be very nearly thermoneutral. One must therefore be especially concerned about the measurements of the sign of ΔH_R in the cyclotron resonance instrument, since very little is currently known about energy effects such as those described above in such experiments.

Energy dependence studies conducted with the tandem spectrometer support the above conclusions regarding the energetics of the alkoxide ion-alcohol reactions. In Table II, the relative cross sections for the forward and reverse steps of reaction 5 are shown as a function of kinetic energy of the impacting ion. As expected from the above considerations, the cross section for the forward reaction falls off rapidly with increasing energy, behavior typical of an exothermic reaction. The reverse reaction, however exhibits an apparent energy threshold followed by a rapid rise in cross section, similar to behavior observed for many endothermic ion-molecule processes.

The energy dependence of the cross section for both forward and reverse reactions in the propanol-butanol system, which has an equilibrium constant of 1.4, is shown in Table III. Here both reactions exhibit behavior characteristic of exothermic or thermoneutral processes.

Recent spectroscopic studies⁵ have pointed to the effect of alkyl groups in stabilizing negatively charged groups. In an effort to probe such possibilities for alkoxide ion reactions, the reactions of CH_3O^- with isomeric C_4 and C_5 alcohols were studied. Rate constants for these reactions are reported in Table IV. At first glance, these results would seem to indicate that there are no substantial differences between the normal, iso- and tertiary structures as far as anion stability is concerned, if it can be assumed that the rates of these

reactions provide a measure of such stability.

Table II
Relative Cross Sections for Alkoxide Ion-Alcohol Reactions as a Function of Kinetic Energy of the Impacting Ion

$$\text{OH}^- + \text{CH}_3\text{OH} \rightleftharpoons \text{CH}_3\text{O}^- + \text{H}_2\text{O}$$

$\text{OH}^- + \text{CH}_3\text{OH} \rightarrow \text{CH}_3\text{O}^- + \text{H}_2\text{O}$		$\text{CH}_3\text{O}^- + \text{H}_2\text{O} \rightarrow \text{OH}^- + \text{CH}_3\text{OH}$	
$\bar{E} (\text{OH}^-)$	Relative σ	$\bar{E} (\text{CH}_3\text{O}^-)$	Relative σ
0.3 eV	1.00	0.3 eV	1.00
0.6	0.50	0.5	1.19
0.8	0.27	0.7	1.05
1.0	0.15	1.1	1.83
1.4	0.08	1.5	2.24
1.8	0.05	1.9	2.76
2.8	0.04	2.9	2.29
4.8	0.03	4.9	1.65

Table III
Relative Cross Sections for Alkoxide Ion-Alcohol Reactions as a Function of Kinetic Energy of the Impacting Ion

$$\text{n-C}_3\text{H}_7\text{O}^- + \text{n-C}_4\text{H}_9\text{OH} \rightleftharpoons \text{n-C}_4\text{H}_9\text{O}^- + \text{n-C}_3\text{H}_7\text{OH}$$

$\text{C}_3\text{H}_7\text{O}^- + \text{n-C}_4\text{H}_9\text{OH} \rightarrow \text{C}_4\text{H}_9\text{O}^- + \text{C}_3\text{H}_7\text{OH}$		$\text{C}_4\text{H}_9\text{O}^- + \text{n-C}_3\text{H}_7\text{OH} \rightarrow \text{C}_3\text{H}_7\text{O}^- + \text{C}_4\text{H}_9\text{OH}$	
$\bar{E} (\text{C}_3\text{H}_7\text{O}^-)$	Relative σ	$\bar{E} (\text{C}_4\text{H}_9\text{O}^-)$	Relative σ
0.3 eV	1.00	0.3 eV	1.00
0.6	0.46	0.6	0.43
0.8	0.29	0.8	0.31
1.0	0.21	1.0	0.22
1.4	0.14	1.4	0.17
1.8	0.08	1.8	0.11
2.8	0.04		

Table IV
Structural Effects on the Rate Constants of Alkoxide Ion Reactions

Reaction	$k(10^{-9} \text{ cm}^3 \text{ molecule}^{-1} \text{ sec}^{-1})$
$\text{CH}_3\text{O}^- + \text{n-C}_4\text{H}_9\text{OH} \rightarrow \text{C}_4\text{H}_9\text{O}^- + \text{CH}_3\text{OH}$	0.61
" + i-C ₄ H ₉ OH → " + "	0.55
" + t-C ₄ H ₉ OH → " + "	0.59
$\text{CH}_3\text{O}^- + \text{n-C}_5\text{H}_{11}\text{OH} \rightarrow \text{C}_5\text{H}_{11}\text{O}^- + \text{CH}_3\text{OH}$	0.52
" + i-C ₅ H ₁₁ OH → " + "	0.55
" + t-C ₅ H ₁₁ OH → " + "	0.52

However, since the butanols and amyl alcohols are substantially more acidic than methanol, that is, these reactions are exothermic by a substantial amount, these factors may mask any possible structural effects. Thus, the reactions in these cases, may be controlled simply by the ion-induced dipole forces and the reaction rates therefore proportional to the polarizabilities of the neutral species which are essentially the same for the isomers in question. This reasoning is apparently confirmed by trends observed in the reactions of CH_3O^- with a series of normal alcohols (not shown here), in which the observed reaction rates fall off smoothly with increasing molecular weights of the alcohol, that is with decreasing polarizability.

Somewhat more evidence for structural effects can be obtained from some of the less exothermic reactions such as shown in Table V. It can be concluded from the reactions shown here that production of the tertiary ionic structure is more favorable than production of the primary structure. These results therefore seem to be consistent with the idea of increasing anion stability with increasing alkyl substitution around the charge center. Further studies are in progress to assess temperature effects on these reactions.

Table V
Structural Effects in Alkoxide Reactions

Reaction	$(10^{-9} \text{ cm}^3 \text{ molecule}^{-1} \text{ sec}^{-1})$		
	k_f	k_r	$K_{eq}(E^{\circ} 0.3\text{eV})$
$n\text{-C}_4\text{H}_9\text{O}^- + n\text{-C}_5\text{H}_{11}\text{OH} \rightleftharpoons n\text{-C}_5\text{H}_{11}\text{O}^- + n\text{-C}_4\text{H}_9\text{OH}$	0.39	0.28	1.4
$t\text{-C}_4\text{H}_9\text{O}^- + t\text{-C}_5\text{H}_{11}\text{OH} \rightleftharpoons t\text{-C}_5\text{H}_{11}\text{O}^- + t\text{-C}_4\text{H}_9\text{OH}$	0.35	0.12	2.9
$t\text{-C}_4\text{H}_9\text{O}^- + n\text{-C}_5\text{H}_{11}\text{OH} \rightleftharpoons n\text{-C}_5\text{H}_{11}\text{O}^- + t\text{-C}_4\text{H}_9\text{OH}$	0.17	0.42	0.4
$n\text{-C}_4\text{H}_9\text{O}^- + t\text{-C}_5\text{H}_{11}\text{OH} \rightleftharpoons t\text{-C}_5\text{H}_{11}\text{O}^- + n\text{-C}_4\text{H}_9\text{OH}$	0.50	0.057	8.8

References:

1. B. M. Hughes and T. O. Tiernan, Proceedings of the 16th Annual Conference on Mass Spectrometry and Allied Topics, Pgh., Pa., 1968, p. 28.
2. J. H. Futrell and C. D. Miller, Rev. Sci. Instr. 37, 1521 (1966).
3. A brief description of the high efficiency negative ion source is given by T. O. Tiernan and B. M. Hughes, Proceedings of the 16th Annual Conference on Mass Spectrometry and Allied Topics, Pgh., Pa., 1968, p. 24; submitted for publication in Rev. Sci. Instr.
4. J. I. Brauman and L. K. Blair, J. Am. Chem. Soc. 90, 6561(1968).
5. W. M. Schubert, R. B. Murphy and J. Robins, Tetrahedron 17, 199 (1962).

B. Mason Hughes⁺ and Thomas O. TiernanAerospace Research Laboratories
Office of Aerospace Research
Wright-Patterson Air Force Base, Ohio 45433

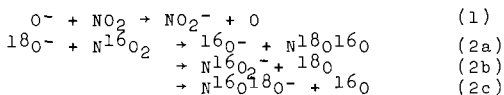
The presence of negative ions in the upper atmosphere¹ and in flames² has been well established and the stabilities of such species as O^- , OH^- , NO_2^- , CO_3^- and C_2H^- in such environments indicate relatively large electron affinities for the corresponding neutral molecules or radicals. While negative ions such as these can be studied by mass spectrometric techniques, the generally low abundances of these species create sensitivity problems which make accurate determinations of electron affinities quite difficult. The studies reported here are aimed in part at the estimation of approximate electron affinities for several radicals and molecules from the observation of appropriate negative ion-molecule reactions in a tandem mass spectrometer³. Negative ion experiments with the beam instrument are facilitated by a high efficiency negative ion source and a mode of operation which was developed in our laboratory⁴. The assumptions required in deriving electron affinity data from experiments such as those described here, and the limitations imposed by the rather small number of reactions which could be observed for any given species, dictates that these determinations are rather crude. Thus it is possible from experiments of this type to establish at best only limits for the electron affinity values. For many radicals and molecules, however, not even limits for electron affinities are currently available.

In the first part of the present study, a more detailed examination of the negative ion reactions in nitrogen dioxide has been accomplished. Mixtures of nitrogen dioxide and water have also been investigated at higher pressures in order to assess possible reactions of significance to the upper atmosphere. Also, since there has previously been considerable controversy regarding the value of the electron affinity of NO_2 , attempts have been made to assign this quantity within rather narrow limits.

Ionic Reactions in Pure NO_2 .

Negative ion intensities in nitrogen dioxide were measured as a function of pressure using a modified high pressure source fitted to a time-of-flight mass spectrometer⁵. Figure 1 shows the relative intensities at pressures up to 600 microns. It is apparent that $N_2O_6^-$ and $N_3O_9^-$ are not formed by simple bimolecular processes involving NO_2 . These products are possibly the result of three-body collisions of NO_3^- and $N_2O_6^-$ respectively with two molecules of NO_2 . However, since N_2O_4 , the dimer, is a stable entity at higher pressures in gaseous NO_2 , these reactions might also be considered to occur in bimolecular processes in which the neutral species is N_2O_4 *. The lifetime of this dimer is probably of sufficient duration for reaction to occur at pressures of several hundred microns.

The pressure dependence data of Figure 1 suggests that NO_2^- reacts with NO_2 to yield NO_3^- . However, when NO_2^- ions were impacted on NO_2 at 5 microns collision chamber pressure in the ARL tandem mass spectrometer, no product could be detected. Since at this pressure only single collision events occur in the tandem instrument, this observation indicates that NO_3^- is also produced by a process greater than second order in the high pressure spectrometer. Although not shown in Figure 1, O^- is also produced at very low pressures in the single source instrument (5 microns). The reaction of O^- with NO_2 yielding NO_2^- is known to be fast, a rate constant of $\sim 1.0 \times 10^{-9} \text{ cm}^3 \text{ molecule}^{-1} \text{ sec}^{-1}$ having been reported for this reaction^{6,7}. The O^-/NO_2 reaction was examined in detail in the tandem mass spectrometer using isotopic techniques to explore the reaction mechanism. The reactions observed in these experiments are as follows:



⁺ Research performed at the U.S.A.F. Aerospace Research Laboratories while in the capacity of an OSURF Visiting Research Associate.

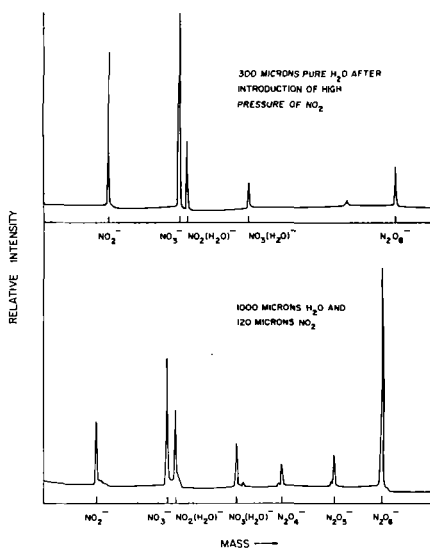
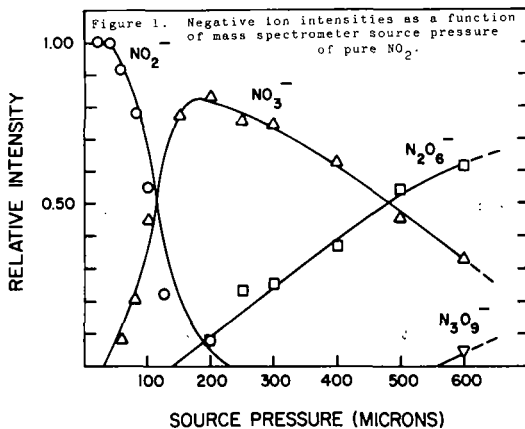
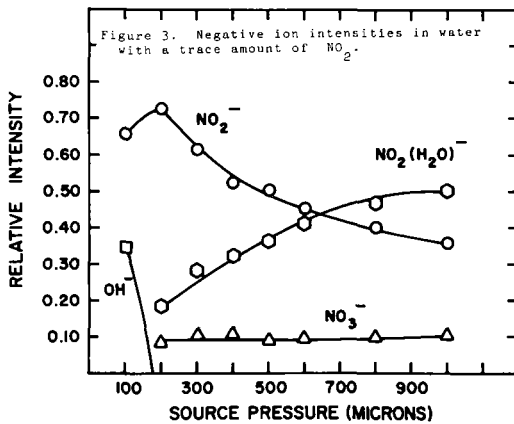


Figure 2. Mass spectra of water with various amounts of NO_2 in the spectrometer source.



Rate constants for reactions 2a-2c were determined by comparing the measured cross-sections to that for reaction 1 and using the rate constant for the latter process cited above. The values determined are $k_{2a} = 0.13 \times 10^{-9} \text{ cm}^3 \text{ molecule}^{-1} \text{ sec}^{-1}$, $k_{2b} = 1.08 \times 10^{-9} \text{ cm}^3 \text{ molecule}^{-1} \text{ sec}^{-1}$ and $k_{2c} = 0.09 \times 10^{-9} \text{ cm}^3 \text{ molecule}^{-1} \text{ sec}^{-1}$. The production of 16O^- and $\text{N}^{16}\text{O}^{18}\text{O}^-$ from the $18\text{O}^-/\text{N}^{16}\text{O}_2$ interaction suggests that the mechanism involves in part a more intimate collision complex than would be expected for a simple long range charge transfer. The collisional stabilization of this complex at higher pressures could also yield the NO_3^- product. Such a mechanism involving two successive bimolecular steps would be indistinguishable in our studies from a termolecular reaction as mentioned above.

Ionic Reactions in Mixtures of Nitrogen Dioxide and Water.

Ionic reactions involving NO_2 and H_2O are of some interest because the NO_2^- ion has been detected in the upper atmosphere. In Figure 2, two mass spectra are shown resulting from the introduction of 300 microns water into the mass spectrometer after a high pressure of NO_2 had been present, and from a water- NO_2 mixture. Although O^- and OH^- are initially produced from water at lower pressures, at the pressures shown in Figure 2 these ions have already reacted with NO_2 by the fast charge exchange reaction to form NO_2^- . The additional products observed in the mass spectrum are results of further reaction of NO_2^- with NO_2 or with water. The NO_3^- and N_2O_6^- probably are formed, as was discussed in the pure NO_2 system, as a result of three body collisions. The solvation of NO_2^- and NO_3^- are the only observable reactions of these ions with water. When a higher pressure of NO_2 is present (the lower mass spectrum of Figure 2) the additional products, N_2O_4^- and N_2O_5^- , are produced, probably as a result of reaction of the solvated NO_2^- and NO_3^- ions with NO_2 . Since the hydration of NO_2^- could be studied as a function of water pressure using the trace NO_2 impurity as is shown in Figure 2, it was of interest to examine the pressure dependence of negative ions in this system. Figure 3 shows these results. As can be seen, the pressure studies suggest that OH^- , formed initially in water, charge exchanges with NO_2 to form NO_2^- and that this ion either reacts with water to form $\text{NO}_2(\text{H}_2\text{O})^-$ or with NO_2 to form NO_3^- . The formation of NO_3^- in this case could also be due to either a three-body collision of NO_2^- with 2NO_2 , or of stabilization of $(\text{NO}_3^-)^*$ as was suggested in the pure NO_2 case.

Estimation of Limits for Electron Affinities.

The observation of a negative ion-molecule reaction of the type,

$$\text{O}^- + \text{RH} \rightarrow \text{OH} + \text{R}^- \quad (3)$$

can be used to calculate limits for the heat of formation of one of the species if the remaining heats of formation are known and if the energetics of the reaction are known or can be assumed. Obviously, electron affinities can also be derived from such data. For reactions observed in the tandem mass spectrometer at low kinetic energies, a large rate constant of the order of $10^{-10} \text{ cm}^3 \text{ molecule}^{-1} \text{ sec}^{-1}$ or larger, may be taken as an indication that the reaction is exothermic or at least thermoneutral. However since the energy spread and average energy of the ion beam is 0.3 eV (usually 0.2 eV in the center-of-mass system) in our experiments, reactions which are as much as 0.2 eV endothermic may actually occur with substantial rate constants. Realizing these limitations, a number of reactions such as noted above were used to estimate limits of electron affinities for a number of organic and inorganic radicals. While the observation of a large rate constant for a given reaction can determine the upper limit for the heat of formation of the product ion, failure to observe a reaction does not necessarily establish a lower limit. For this reason no lower limits of heats of formation are calculated for reactions more complicated than charge exchange.

In the reaction of HS^- with NO_2 , a rate constant of $0.65 \times 10^{-9} \text{ cm}^3 \text{ molecule}^{-1} \text{ sec}^{-1}$ was observed for the formation of NO_2^- . On the other hand, charge exchange from C_2H^- to NO_2 was not observed to occur. From these facts, it can be determined that $3.1 > \text{EA}(\text{NO}_2) > 2.5$. This is consistent with a value of 2.8 for $\text{EA}(\text{NO}_2)$ which has been reported previously⁷. The latter value will be used in our subsequent considerations. From the C_2H^- reaction with NO_2 , which occurs with a very low rate constant at our lowest energy and increases as the C_2H^- energy is increased, it can be estimated that $\text{EA}(\text{C}_2\text{H}) \sim \text{EA}(\text{NO}_2)$. In a similar series of ex-

experiments, the following rate constants were measured:

	$k(10^{-9} \text{cm}^3 \text{molecule}^{-1} \text{sec}^{-1})$
(4a) $\text{O}^- + \text{CH}_3\text{OH} \rightarrow \text{OH}^- + \text{CH}_3\text{O}$	0.366
(4b) $\quad \quad \quad + \text{CH}_3\text{O}^- + \text{OH}$	0.142
(5a) $\text{O}^- + \text{C}_2\text{H}_5\text{OH} \rightarrow \text{OH}^- + \text{C}_2\text{H}_5\text{O}$	0.298
(5b) $\quad \quad \quad + \text{C}_2\text{H}_5\text{O}^- + \text{H}_2 + \text{OH}$	0.144
(5c) $\quad \quad \quad + \text{C}_2\text{H}_5\text{O}^- + \text{OH}$	0.165
(6) $\text{OH}^- + \text{CH}_3\text{OH} \rightarrow \text{CH}_3\text{O}^- + \text{H}_2\text{O}$	1.35
(7) $\text{OH}^- + \text{C}_2\text{H}_5\text{OH} \rightarrow \text{C}_2\text{H}_5\text{O}^- + 2\text{H}_2\text{O}$	1.00
(8) $\text{NH}_2^- + \text{CH}_3\text{OH} \rightarrow \text{CH}_3\text{O}^- + \text{NH}_3$	large
(9) $\text{NH}_2^- + \text{C}_2\text{H}_5\text{OH} \rightarrow \text{C}_2\text{H}_5\text{O}^- + \text{NH}_3$	"
(10) $\text{CH}_3\text{O}^- + \text{NO}_2 \rightarrow \text{NO}_2^- + \text{CH}_3\text{O}$	0.515
(11) $\text{C}_2\text{H}_5\text{O}^- + \text{NO}_2 \rightarrow \text{NO}_2^- + \text{C}_2\text{H}_5\text{O}$	0.478
(12) $\text{C}_2\text{H}_3\text{O}^- + \text{NO}_2 \rightarrow \text{NO}_2^- + \text{C}_2\text{H}_3\text{O}$	1.37

From reactions 14-16, it can be deduced that $\text{EA}(\text{CH}_3\text{O})$, $\text{EA}(\text{C}_2\text{H}_5\text{O})$ and $\text{EA}(\text{C}_2\text{H}_5\text{O}^-) < 2.8 \text{ eV}$. In a similar manner, upper limits for the heats of formation can be assigned to $\Delta H_f(\text{CH}_3\text{O})$, $\Delta H_f(\text{C}_2\text{H}_5\text{O})$, $\Delta H_f(\text{CH}_3\text{O}^-)$ and $\Delta H_f(\text{C}_2\text{H}_5\text{O}^-)$ if $\Delta H_f < 0$ is assumed for reactions 5-13. Table I gives these limits, along with known heats of formation of CH_3O and $\text{C}_2\text{H}_5\text{O}$. The three

Table I. Upper Limits for Heats of Formation in the Reactions of O^- , OH^- and NH_2^- with Alcohols.

X	Upper Limit Value for	
	$\Delta H_f(X)$ in kcal/mole	Previous Values for $\Delta H_f(X)$
CH_3O	11.9	-0.5 ^a
$\text{C}_2\text{H}_5\text{O}$	3.8	-8.5 ^a
CH_3O^-	-31.9	-
"	-24.7	-
"	-32.8	-
$\text{C}_2\text{H}_5\text{O}^-$	-40.0	-
"	-32.8	-
"	-29.8	-

^a Reference 9.

values of $\Delta H_f(\text{CH}_3\text{O}^-)$ and $\Delta H_f(\text{C}_2\text{H}_5\text{O}^-)$ arise from reactions 6, 10 and 12 and 9, 11 and 13, respectively. Using these heats of formation along with the heats of formation of the radicals shown in Table I, the lower limits of the electron affinities of CH_3O and $\text{C}_2\text{H}_5\text{O}$ are calculated to be 1.4 eV. A summary of these data along with limits of electron affinities for other radicals obtained in the same manner are given in table II. It is recognized that the precision of these results is not very great, but it is anticipated that further studies will lead to the establishment of much narrower brackets for some of these values. These experiments are in progress.

Table II. Lower Limits for Electron Affinities of Several Radicals

Reaction	Radical	Lower Limit for	
		Electron Affinity(eV)	Reported Electron Affinities(eV)
O^-/HCl	Cl	1.5	3.8 ^a
$\text{O}^-/\text{CH}_2\text{Cl}$	"	1.0	"
$\text{OH}^-/\text{CH}_2\text{Cl}$	"	1.5	"
NH_2^-/HCl	"	1.1	"
$\text{NH}_2^-/\text{CH}_2\text{Cl}$	"	1.2	"
$\text{O}^-/\text{C}_2\text{H}_5$	C_2H_5	1.8	2.8 ^b
$\text{OH}^-/\text{C}_2\text{H}_5$	"	1.5	"
$\text{NH}_2^-/\text{C}_2\text{H}_5$	"	1.4	"
$\text{O}^-/\text{CH}_2\text{OH}$	CH_2O	1.4	
$\text{OH}^-/\text{CH}_2\text{OH}$	"	1.1	
$\text{NH}_2^-/\text{CH}_2\text{OH}$	"	1.4	
$\text{O}^-/\text{C}_2\text{H}_5\text{OH}$	$\text{C}_2\text{H}_5\text{O}$	1.4	
$\text{O}^-/\text{C}_2\text{H}_5$	C_2H_5	0.5	2.1 ^a
$\text{O}^-/\text{CH}_2\text{Cl}$	CH_2Cl	0.7	

^aReference 9.

^bIon impact studies discussed in the text.

References:

1. C. Y. Johnson, E. B. Meadows and J. C. Holmes, J. Geophys. Res. 63, 443 (1958).
2. H. F. Calcotte and D. E. Jensen, Advances in Chemistry Series 58, 291 (1966).
3. J. H. Futrell and C. D. Miller, Rev. Sci. Instr. 37, 1521 (1966).
4. T. O. Tiernan and B. M. Hughes, Proceedings of the 16th Annual Conference on Mass Spectrometry and Allied Topics, Pgh., Pa., 1968; submitted to Rev. Sci. Instr.
5. J. H. Futrell, T. O. Tiernan, F. P. Abramson and C. D. Miller, Rev. Sci. Instr. 39, 340 (1968).
6. A. Henglein and G. A. Muccini, J. Chem. Phys. 31, 1426 (1959).
7. R. K. Curran, Phys. Rev. 125, 910 (1962).
8. L. M. Branscomb, Ann. Geophys. 20, 88 (1964).
9. V. I. Vedeneyev, L. V. Gurvich, V. N. Kondrat'yev, V. A. Medvedev and Ye. L. Frankevich, "Bond Energies, Ionization Potentials and Electron Affinities", St. Martin's Press, New York (1966).

High Temperature Gaseous Oxides,
Halides and Oxyhalides

D. W. Muenow and J. L. Margrave

Department of Chemistry
Rice University

The evolution of gaseous species from a variety of solids, including binary oxides and halides, ternary oxides and halides, as well as more complex systems, can be followed conveniently by mass spectrometric techniques.

A high-temperature mass spectrometric analysis of a philippinite tektite, for example, indicates the presence of small amounts of benzene, polynuclear aromatics and other hydrocarbons. Benzene appears to have been embedded within the tektite matrix as well as the trapped gases O_2 , CO and CO_2 (to be published in Science).

The polymorphic nature of tetraphosphorus decaoxide has also been demonstrated by examination of the vapor species above its various crystalline modifications. At temperatures below $150^\circ C$, the equilibrium vapor consists primarily of $P_4O_{10}(g)$ with small amounts of $P_4O_9(g)$. Between $175^\circ C$ and approximately $350^\circ C$, the vapor contains $P_4O_{10}(g)$, $P_4O_9(g)$ and $P_4O_8(g)$, while at temperatures greater than $400^\circ C$, the molecular species $P_4O_7(g)$ is observed as well. Second-law heats of reaction for equilibria among the gaseous molecular species have been obtained. Also, free evaporation studies of both solid and liquid P_4O_6 indicate that the vapor consists primarily of $P_4O_6(g)$. Average values for the (P-O) and (P=O)-bond energy have been calculated. (to be published in J. Inorg. and Nucl. Chem.)

Fluorinated samples of reagent grade P_4O_{10} have also revealed the existence of of high molecular weight phosphorus oxyfluorides. Ionic species of mass greater than 1000 have been observed. The ions, formed by impact with 15-volt electrons, can be classified into three groups. Group I consists of ions of the type $P_n O_{2n-1} F_{n+2}^+$, for $n = 1-13$. The neutral molecular precursors for the first two members of this series are the well characterized molecules, POF_3 and $P_2O_3F_4$. Group II consists of ions of the type $P_n O_{2n} F_{n+2}^+$, $n = 2-11$, and Group III includes ions of the type $P_n O_{2n+1} F_{n+2}^+$, $n = 2-10$. It is suggested that the parent ions of Group I result from the simple ionization of a linear polymer with the general formula, $(PO_2F)_n$, where each of the terminal phosphorus atoms of the chain is bonded to two oxygen atoms, one of which is a bridging atom, and to two fluorine atoms. (to be published, J. Inorg. and Nucl. Chem.)

Investigations of the equilibrium vapors over crystalline tellurium dioxide have shown the existence of the molecular species $(\text{TeO}_2)_n$ and $(\text{TeO})_n$, where $n = 1, 2, 3, 4$ as well as Te_2 and O_2 . Under neutral conditions the most abundant species are $\text{TeO}_2(\text{g})$ and $\text{TeO}(\text{g})$. Second and third-law heats of reaction and entropies for the various equilibria among these species have been obtained. Fundamental frequencies obtained from infrared absorption studies of the species isolated in rare gas matrices were used for calculations of thermodynamic functions at various temperatures. Heats of atomization for $(\text{TeO}_2)_2$ and $(\text{TeO})_2$ were obtained. Using the average of the second and third-law heats, $\Delta H_{298}^\circ = 2.5 \pm 2 \text{ kcal. mole}^{-1}$, for the reaction $\text{TeO}(\text{g}) = \frac{1}{2} \text{Te}_2(\text{g}) + \frac{1}{2} \text{O}_2(\text{g})$ one obtains the dissociation energy for $\text{TeO}(\text{g})$, $D_{\text{O}}^\circ = 89.4 \pm 2 \text{ kcal. mole}^{-1}$. A bent geometry (110°) is indicated for TeO_2 and evidence for cyclic structures of $(\text{TeO}_2)_2$ and $(\text{TeO})_2$ is given. (to be published, Trans. Faraday Soc.)

MTA - A COMBINATION OF OLD TECHNIQUES OR A NEW METHOD?

H. G. Langer
The Dow Chemical Company
Eastern Research Laboratory
Wayland, Massachusetts 01778

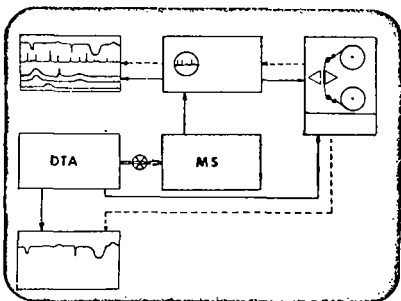
Recently, at the IUPAC Committee on Nomenclature and Thermal Analysis it was recommended that terms such as MTA and MDTA should not be used. Instead a full description of the method should be used when this technique is employed. Today, I would like to stand up in defense of the term MTA coined by Roland Gohlke and myself years ago, but have it describe in broader terms an analytical method instead of an instrumental technique. What then is the definition of MTA and why is it a new method?

If we define MTA as the method of obtaining complete mass spectra as a function of temperature, we operate in a three-dimensional system where the result is represented as the change in the complete mass spectrum as a function of linearly increasing temperature. It is also obvious that a new technique and instrumentation is required to obtain this information for different sample imposed conditions and also record the changes in heat capacity of the test sample (which of course is defined as differential thermal analysis) as well as changes in decomposition patterns caused by reduced operating pressure inherent in mass spectrometry.

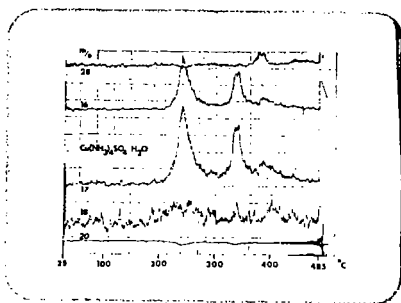
Different instrumental approaches have been used by various investigators as this Symposium today really shows, each one adapted for a specific need and each one producing specific results. For our suggested universal use of the term MTA, however, let me refer to the schematic we introduced a year ago. (Figure 1) Even though we use a specific instrument, any system would be complete if it contained the following functions:

- #1 - Sample environment control of pressure, atmosphere, gas flow
- #2 - Sample temperature program (in most cases, linear temperature increase)
- #3 - Mass analyzer
- #4 - Data storage capacity
- #5 - Data retrieval and display functions

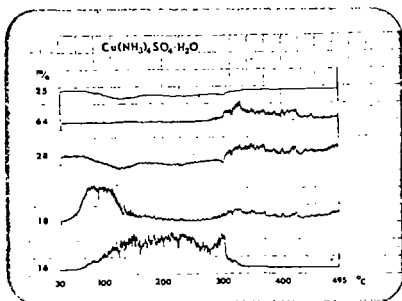
Other papers in this Symposium and at this meeting in general have shown a variety of applications of this general principle and thus for the following examples, I will restrict myself to the system used in our laboratory.



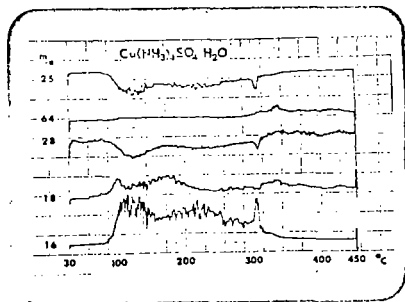
1 MTA Schematic



2 Decomposition of Tetrammine-copper sulfate monohydrate at atmospheric pressure

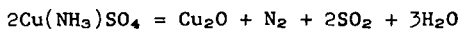


3 Decomposition of Tetrammine-copper sulfate monohydrate in vacuo



4 Decomposition of Tetrammine-copper sulfate monohydrate in vacuo after 24 h.

The first example shows the effect of time and pressure on diffusion-controlled decomposition reactions. At atmospheric pressure the monohydrate of tetramminecopper sulfate releases water and ammonia in clearly defined steps before a complicated final decomposition occurs according to the following equation -

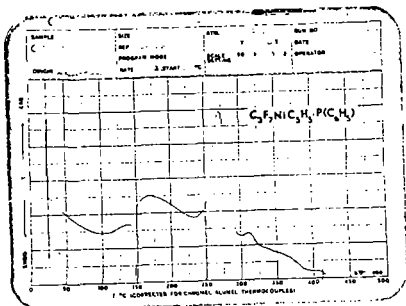


as shown in Figure 2. This was carried out with an external DTA cell sampling from atmospheric pressure through a capillary and valve into the ion source of the mass spectrometer. With an internal cell at 10^{-7} torr the loss of water and ammonia occurs at considerably lower temperatures whereas the chemical decomposition is much less affected (Figure 3). The next figure (Figure 4) was obtained after a 24-hour evacuation in the mass spectrometer and shows clearly the loss of most water and a measurable amount of ammonia. No effect on the thermodynamically controlled high temperature reaction was detected.

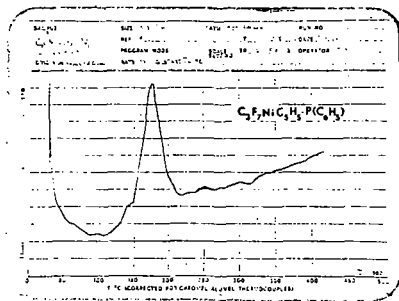
For the decomposition of perfluoropropylcyclopentadienyl nickel triphenyl phosphine we have demonstrated the effect of pressure changes on chemical decompositions. As shown on figure 5 the exothermic decomposition is clearly separated from the melting process even though a change in slope after the melting point indicates a change in heat capacity of the sample. In vacuum (Figure 6), the melting process is no longer separated from the decomposition so that even for a complicated chemical reaction as demonstrated on figure 7 the rate of diffusion or that of vaporization of reaction products determines the rate of the overall reaction. This MTA trace at the same time explains the change in slope on the DTA curve which is most likely due to vaporization of solvent after the sample had melted.

In summary, no matter which instrumentation or which environmental control over the sample is used, I would strongly urge that the term "mass spectrometric thermal analysis" or even its abbreviation "MTA" - is used whenever a changing mass spectrum is observed or recorded as a function of temperature which in turn is changing in a controlled fashion. Even though additional information such as changes in physical properties of the test sample, weight changes, changes in heat capacity, etc., are valuable information, the only direct result is the change of the mass spectrum as a

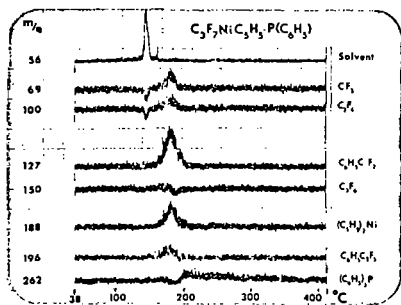
function of temperature; as simple as this relationship is, as general it is, and thus indeed constitutes a new analytical method and not a combination of instrumental techniques.



5 DTA of a Nickel Complex



6. MTA of a Nickel Complex
(Internal DTA)



7 MTA of a Nickel Complex
(Intensity Traces)

ADVANCES IN SIMULTANEOUS THERMOGRAVIMETRIC -
MASS SPECTROMETRIC MEASUREMENTS

H. P. Vaughan
Mettler Instrument Corporation
Princeton, NJ 08540

Summary

The combination of the mass spectrometer and the vacuum thermobalance is a logical step in the further study of gas-solid reaction systems. Both measurements are complementary -- thermogravimetry on one hand providing quantitative data on sample mass changes, the mass spectrometer on the other hand providing data on the identity, order of evolution and relative concentration of effluent gases. Gas analysis is useful not only in identifying reaction products but equally important in many cases, it is used to establish purity or concentration of reactive components in gas atmospheres prior to and during thermogravimetric studies of reversible reaction systems.

Introduction: Thermogravimetry

At some temperature and pressure all solid or liquid compounds will either undergo a chemical conversion involving release or absorption of a gas, or they will vaporize. If a sample can be placed on a mass measurement instrument at the required temperatures and pressures, it will be possible to directly measure the temperature at which the phenomenon occurs, the total amount of mass change and the rate of mass change. This latter value in a carefully designed experiment -- and this careful experiment design must be emphasized -- can be related to the reaction rate. [1]

This is the basis of the technique of thermogravimetry -- which can be defined as the measurement of changes in mass of a sample as a function of controlled temperatures in specified gas atmospheres and pressures.

The range of conditions in which these measurements can be performed is quite wide as is shown in Table I.

It can be quickly seen from this table that there is very little limitation on the environmental conditions under which an experiment can be carried out and that the measurement is quite sensitive.

Thermogravimetry is generally broken down into two classes: Dynamic thermogravimetry, in which the temperature is changed at a linear rate (usually 0.5 - 15°/min); and Isothermal thermogravimetry, in which the temperature is held constant. Heating in isothermal steps is also another common mode of temperature control.

Fig. 1 shows an example of dynamic heating of a sample of calcium oxalate in He at 0.5°/min. The TG curve on top is the integral weight loss curve showing loss of water, CO and finally CO₂ at temperatures characteristic for these reactions under the experimental conditions used.

The lower two curves are superimposed curves of the DTG or first derivative of the weight loss curve and a gas chromatography curve made simultaneously by leading a series of samples of the effluent gas through a GC column and then to a thermal conductivity detector. Each point on the GC curve represents a measured peak area value at the corresponding temperature. [2]

This comparison gives a quick idea of the type of information available

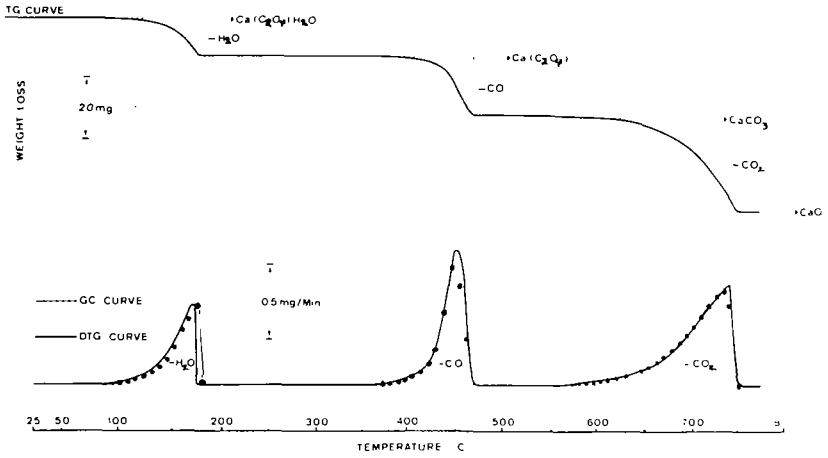
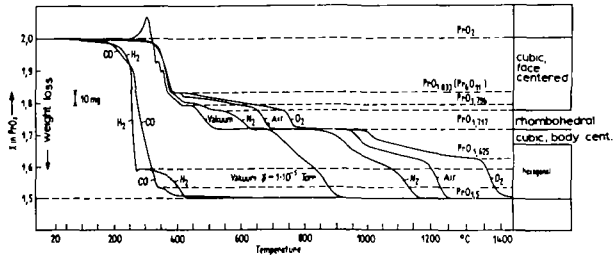


Fig. 1 Simultaneous TG, DTG and GC of calcium oxalate in He at 0.5°C/min. showing thermal separation of reactions.



OXIDE SYSTEM OF PRASEODYMIUM
 weight: 2.95586 g, gas flow rate 10 l/h, heating rate 8°C/min

Fig. 2 TG measurements of PrO₂ in different gases, showing characteristic differences in the weight loss curves.

DECOMPOSITION OF CaCO₃ UNDER VARIOUS CONDITIONS
 weight 19.00 mg, heating rate 8°C/min

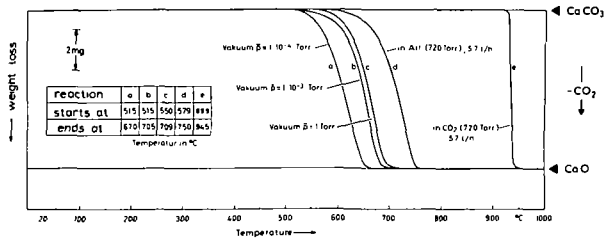


Fig. 3 Decomposition of CaCO₃ at various pressures showing the lowering of apparent decomposition temperature -- characteristic of reversible gas-solid reaction systems.

and its relationship to methods of gas analysis. A second example is shown in Fig. 2 of the decomposition of praseodymium oxide in various gas atmospheres. The various oxidation steps characteristic of the material at various temperatures are also here, clearly characteristic of the gas atmosphere used. [3] A further example can be seen in Fig. 3 of the decomposition of calcium carbonate as a function of various pressures. [4] The relationship between the equilibrium decomposition temperature of this material and the partial pressure of CO_2 is well known. Equilibrium conditions are, by no means, obtained in a simple dynamic heating test and, as a result, these apparent decomposition temperature values are somewhat higher than the true values. [5]

In another example in Fig. 4 we can see just how much information can be obtained from a single test using techniques of simultaneous measurement of weight, DTA and pressure changes caused by evolved gases under vacuum conditions. This example shows the decomposition of asbestos which, in addition to dehydroxilation, also shows a solid state transformation at about 800° which is clearly shown by the DTA exotherm. The sudden rise of temperature and/or the crystal lattice re-arrangement also causes a sudden loss of adsorbed gas, presumably H_2O , which can be seen on the weight curve as well as on the DTG and pressure curve.

Simultaneous Mass Spectrometric Analysis

We have seen so far how, in a dynamically programmed experiment, characteristic reaction steps can be separated by thermal methods, analagous to the separation of gas components in a chromatographic column. No direct information, however, has been obtained on the identification of these gases or on whether or not the various gases evolved are single gases or gas mixtures. This would be very useful information and furthermore, when gas mixtures are being evolved a combination of total mass measurement and gas analysis is a basis for determining the different rates at which the various gas components may evolve.

This is the main reason why the combination of the mass spectrometer and the thermobalance is one which is of increasing usefulness.

The combination of the two techniques is not difficult, particularly when one can use the relatively small, compact, low resolution type mass analyzer, such as the various types of quadrupoles which are now on the market.

Fig. 5 shows a typical capillary inlet system which can be connected to most thermobalances operating above high vacuum pressures. A capillary of 0.2 - 0.15mm diameter is chosen since it:

a) Creates a pressure drop from atmospheric pressure to rough vacuum, while drawing only about 5 liters of gas per hour. This flow is compatible with the achievement of high weighing sensitivity with most thermobalances, and this flow also limits the extent of dilution of the unknown gas by the carrier gas. Often only very small rates of gas evolution are available when slow dynamic or isothermal heating is used.

b) Achieves a maximum rate of transfer of the sample gas from the thermobalance reaction chamber to the mass spectrometer. The time delay with this system is on the order of 30 sec., which is insignificant compared to the normal slow recording speeds and heating rates used in thermogravimetry.

The capillary is shown here equipped with a heating mantle to prevent condensation of gases.

With this general type of system, it is possible to have the sample at various pressures down to rough vacuum, since the mean free path of the gas

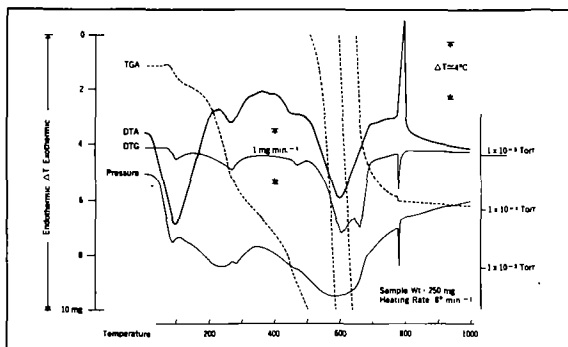


Fig. 4 Decomposition of chrysotile asbestos under vacuum showing loss of water, dehydroxylation and finally conversion to forsterite at about 800°C.

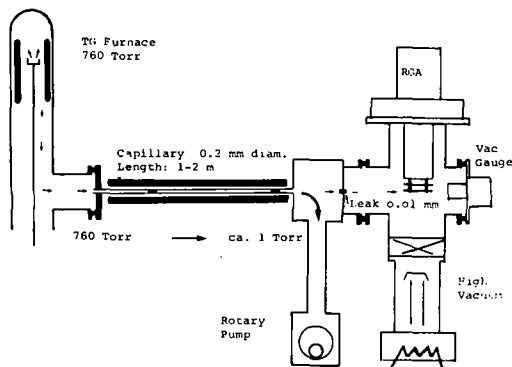


Fig. 5 A typical capillary inlet system for a mass spectrometer-thermobalance combination.

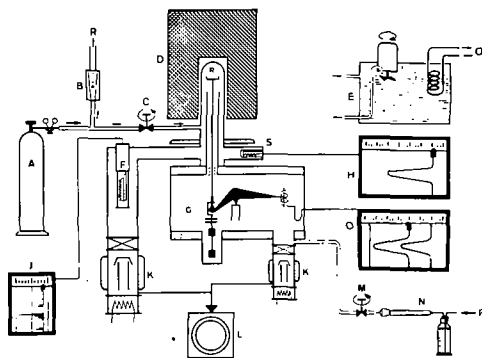


Fig. 6 High vacuum thermobalance connection for a mass spectrometer. (R) sample holder, (D) furnace, (G) balance, (F) mass analyzer, (S) ionization gauge, (C) calibration gas inlet.

molecules is still short compared to the capillary diameter.

In many cases, however, it is very desirable to have the sample at high vacuum. An arrangement showing this possibility is shown in Fig. 6. First of all, a double diffusion pumping system is used, which is separated by a diffusion baffle at the base of the sample holder. This prevents unwanted diffusion of condensable gases into the balance mechanism chamber. The sample gases move from the sample crucible through approximately 1 3/4" tubes to the ionizing portion of the mass analyzer and thence to the diffusion pump. A separate cold cathode gauge is used to measure total pressure. A, B and C is a calibration gas inlet system in order to measure, with the help of the cold cathode gauge, the mass spectrometer peak height in amps/torr. The gas inlet, M, N, P can be used for pressure control in the system. [6]

Normal working vacuum with this system is 10^{-6} torr to $\approx 5 \times 10^{-5}$ torr, well within the range of the quadrupole mass analyzer.

Aside from extending the range of conditions under which one can work, some other advantages of the high vacuum thermogravimetry/mass spectrometer combination as opposed to the normal pressure system are:

- a) Less possibility of condensation,
- b) Nearly no measurable time delay between the balance and mass spectrometer,
- c) No dilution of the sample gas with carrier gas,
- d) All of the sample gases pass by the mass analyzer with no loss through the rough pumping system, as is the case with the capillary inlet.

Examples of Recent Applications

Simultaneous thermogravimetry and mass spectrometric gas analysis have been used recently to solve a number of interesting problems. Fig. 7 shows the oxidation and decomposition of very finely powdered palladium used as a catalyst. According to the stoichiometric formula, the end weight after loss of O_2 should be exactly equal to the beginning weight. This was not the case, as can be seen on the weight curve. X-ray analysis, run in parallel on the same sample lot, showed no presence of PdO before or after the thermal treatment. Fig. 8 shows the results of a high vacuum TG/MS test on the palladium after considerable vacuum treatment at room temperature. Adsorbed gases released at higher temperatures were identified by the mass spectrometer as mostly H_2O , O_2 and CO_2 , and were closely equal in weight to the difference noted in the previous slide. [7]

As shown in fig. 9, this combined technique was used to show the vacuum decomposition behavior of zinc oxalate, which first loses 2 moles of water and then decomposes directly to zinc oxide, simultaneously giving off CO and CO_2 . The partial pressures of the three gases along with total pressure are shown at the top of the slide; TG and DTA are shown at the bottom. The evolution of CO_2 is about the same as CO , taking into consideration the logarithmic scale of the partial pressure curves. Measurement of CO , of course, was made more difficult by the N_2 background. [8]

Another example is given in Fig. 10 of the decomposition of dawsonite [$NaAl(OH)_2CO_3$] in an oil shale sample possibly containing other minerals such as, dolomite, nahcolite or analcite, all of which contain CO_2 and analcite containing Al, which would confuse any chemical analysis based on measurement of either of these constituents. By running a combined MS/TG/DTA experiment it was possible to separate the various reaction steps due to other minerals and due to oil contained in the shale. Loss of CO_2 due to decomposition of dawsonite occurs at approximately 395° , while the next

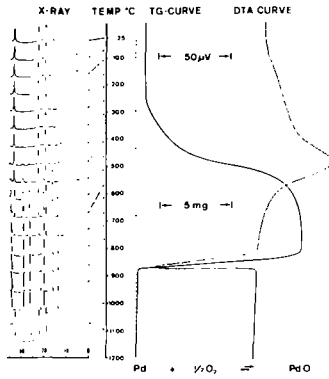


Fig. 7 Oxidation and decomposition of palladium in air along with parallel x-ray measurements. Difference in weight of palladium at beginning and end of test is due to adsorbed gases as shown in fig. 8.

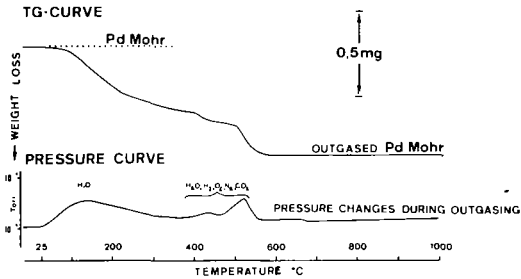


Fig. 8 Vacuum TG of palladium in fig. 7, showing temperature of release and identification of adsorbed gases. The total weight loss was almost identical to that shown in fig. 7.

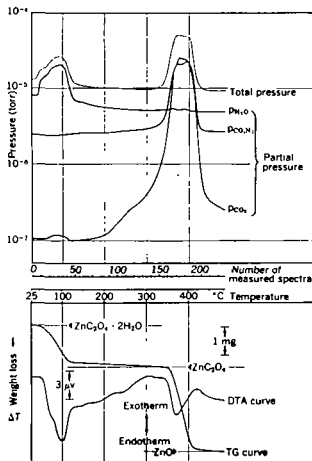


Fig. 9 Simultaneous TG, DTA and mass spec of zinc oxalate dihydrate, showing dehydration followed by decomposition of the oxalate.

step beginning just after 400° is due to loss of oil cracking products. By this thermal separation in vacuum of reaction steps and by identification of the evolved gases, it was possible to make an estimate of the dawsonite content of about 10% which agreed well with an estimate by chemical analysis of 10.3% which, until this time, had been in some doubt. [9]

Fig. 11 shows some of the mass spectra actually taken from this measurement at 45°, 360° and 490°C.

Measurements on Reversible Reaction Systems

It had been briefly mentioned earlier that true equilibrium conditions were rarely achieved in a dynamically temperature programmed experiment. Constantly changing temperatures may cause thermal gradients of some sort within samples of nearly all sizes. Thermal equilibrium conditions are approached as the heating rate is lowered. When the heating rate is lowered to 0°/min or isothermal, there is a good chance with good sample holder design that a very close approach to thermal equilibrium can be reached. Thermal equilibrium alone is not sufficient, however, whenever one is dealing with a reversible reaction whose reaction rate is not only dependent on a function of temperature but also on the partial pressure of the surrounding reaction gas.

In thermogravimetry, the researcher very quickly becomes aware of the effects of sample geometry and gas atmosphere around his sample. We have already seen these effects on the decomposition of calcium carbonate. Fig. 12 shows the effect of sample shape on mass spectrometric measurements of water evolution from calcium oxalate monohydrate decomposed in high vacuum. The material at the bottom of the slide is in an ill-defined pile and, since this is a reversible decomposition, the gas evolution rate is dependent on the water partial pressures built up within the sample which, in this case, are also ill-defined. The flat sample layer arrangement shown in (A) or (B) gives an obviously better result. [10]

This same effect by TG can be seen in Fig. 13 of the dehydration of two equal masses of calcium oxalate monohydrate; the one to the right is a 6mg single crystal, while the curve to the left is 6mg of finely divided powder. Similar geometric effects can be expected with any reversible decomposition and will also affect apparent reaction rates with non-reversible reactions which depend on exposed surface area or other geometric considerations.

A close approach to both chemical and thermal equilibrium under vacuum conditions up to approximately 1 torr can be reached using a Knudsen Cell, such as shown in Fig. 14. This particular cell, made of aluminum, is suitable for low or medium temperature work. Pressure outside the cell must be some degree of high vacuum to allow Knudsen effusion through the cell orifice. The orifice diameter must always be somewhat smaller than the mean free path of the molecules at the given pressure -- which means a diameter of $\approx 0.01\text{mm}$ to 2-3mm, at pressures from 10^{-2} torr $\rightarrow 10^{-6}$ torr.

The partial pressure of the reaction gas inside the cell is calculated from the rate of weight loss of the vaporizing or decomposing product by means of the ideal Knudsen equation. It can be assumed that equilibrium conditions are achieved when, at constant temperature, the rate of weight loss is constant over a long period of time, usually many hours. An example is shown in Fig. 15 of the sublimation of benzoic acid at 17°C. The rate of weight loss is 2.25mg over a period of 5 hours, or $1.24 \times 10^{-7}\text{g/sec}$. Temperature is shown to be constant within 0.1°C. Outside pressure was maintained constant at $\sim 1.5 \times 10^{-5}$ torr. The resulting vapor pressure at this temperature was 4.6×10^{-4} torr.

Fig. 16 shows a plot of log vapor pressure vs. $1/T$ for a series of measurements on benzoic acid. The shape of the curve is calculated by re-

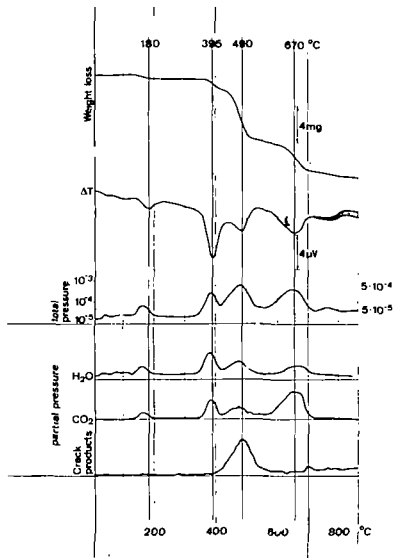


Fig.10 Simultaneous TG, DTA and mass spec of an oil shale containing dawsonite. The DTA peak at 395° is due to dawsonite. The DTA peak at 670° is due to dolomite. Oil products are evolved between 400° and 550°.

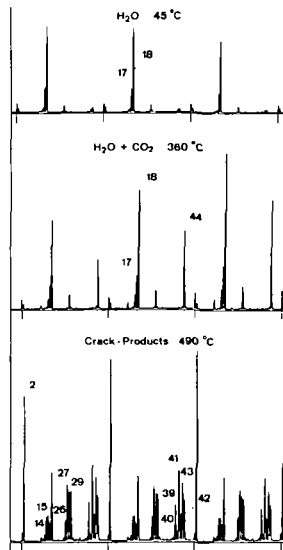


Fig.11 Individual spectra taken from the test shown in fig.10. Three spectra are shown at each temperature.

gression analysis; in this case, using a CDC-3600 computer. The latent heat of sublimation can be directly calculated from this slope using the expression $\log P = -A/T + B$, where $A \times 4.574$ corresponds to the heat of sublimation. The values in these tests of benzoic acid show excellent agreement with known values in the literature down to 10^{-2} torr. Values below this were not given in the literature. [11]

It can be noted in the vapor pressure curve that there is a break in the curve below $290^{\circ}\text{K}(17^{\circ}\text{C})$, which is suspected to be caused by a possible dimerization of the benzoic acid molecule. The mass spectrometer is currently being used to investigate this irregularity. [12]

Fig. 17 shows the instrument arrangement used for these tests. The molecules leaving the Knudsen Cell form a molecular beam which condenses mostly on the cold trap, B. This helps maintain a constant pressure within the apparatus. This is also a possibly excellent location for the mass analyzer.

The combination of a mass spectrometer with a Knudsen Cell source can also be used to measure vapor pressures in the range below $\approx 10^{-4}$ torr, where the ion current is equal to the vapor pressure times a proportionality constant. A plot of $\log(\text{ion current}) \times \sqrt{T}$ vs. $1/T$ will give a straight line paralleling the plot of $\log p$ vs. $1/T$. Complications occur, however, in determining absolute values due to cracking of the parent molecule in the ionizing field and a number of other factors. [13] Gravimetry in combination with the mass spectrometer will possibly yield the best data.

Monitoring Gas Compositions

So far, all the examples of application given have been in identification of unknown gases or in separation of multi-component effluents. Another very important area of use for the mass spectrometer is in checking the purity of inert gases or composition of reaction gas mixtures, when these gases are used in such common DTA and TGA applications as:

- a) Melting points and phase diagrams of metals subject to oxidation,
- b) Oxidation/reduction or reaction phase diagrams, etc. as a function of the partial pressure of various gases or gas mixtures.

In these cases, the mass spectrometer is used as an accessory control device rather than as a primary analytical tool; it is very useful, nonetheless.

Conclusion

Although only relatively simple examples have been shown to demonstrate the feasibility of the combination of the thermobalance with the mass spectrometer, its application to more complex chemical problems such as polymer decomposition has already been undertaken. [14]

Information obtained by both types of analysis is complementary in that, except in rare instances, it would be very difficult to obtain the same data by either method alone.

Combined measurement methods can be used for all substances which evolve gases with a sufficiently high vapor pressure to be transported the short distance from the thermobalance to the mass spectrometer, at temperatures ranging from 25° to a maximum of about 150°C .

Experience gained from thermal analysis on the effects of sample configuration and temperature control on apparent reaction rates, can also be put to good use in the design of sample holders and means of temperature control and programming for solid sample probes directly introduced into

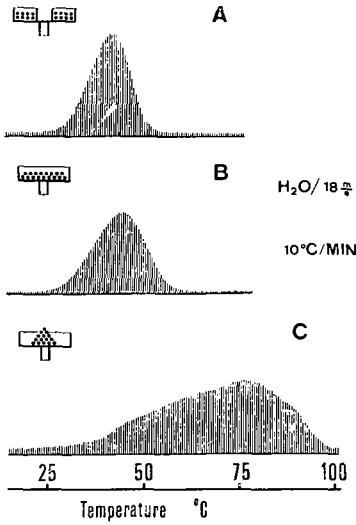


Fig.12 Mass spec measurements of the dehydration of calcium oxalate monohydrate, showing differences in rate of water evolution with different sample shapes.

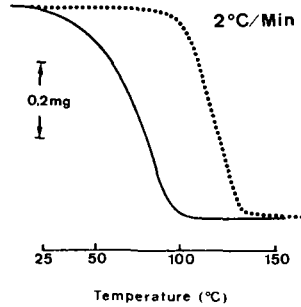


Fig.13 TG measurements of the dehydration of calcium oxalate monohydrate, showing the difference between a 6mg single crystal (dotted line) and an equal mass of powder (solid line).

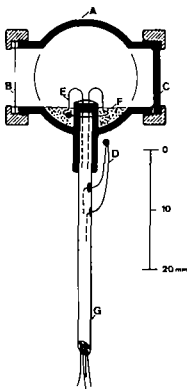


Fig.14 Knudsen effusion cell used for vapor pressure measurements. Thermocouple (D) is used to control furnace temperature. Thermocouple (E) can be used to either measure the temperature of the substance (F) or of the vapor in the cell. A threaded cover (C) can be removed for insertion of the sample.

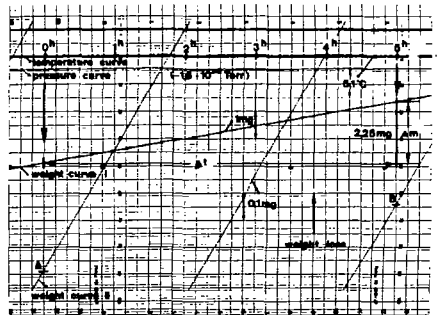


Fig.15 A representative test curve (original size 10" wide), showing the sublimation of benzoic acid at 17°C. Temperature, pressure and weight loss in two sensitivities, 1:10, are shown recorded simultaneously.

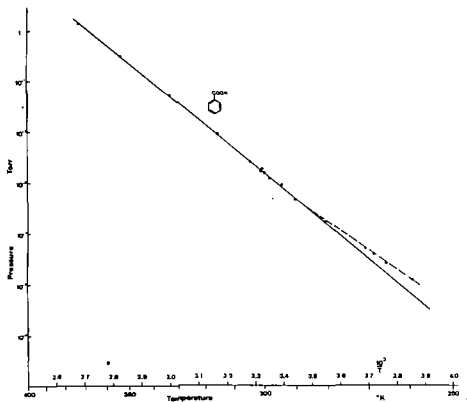


Fig.16 The vapor pressure curve of benzoic acid between 380K and 260K. The break in the curve below 290K is believed to be due to a possible dimerization.

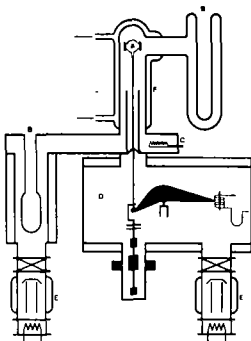


Fig.17 Schematic of vacuum TG apparatus suitable for middle and low temperature vapor pressure measurements.

Table I

Approximate Measurement Ranges in Thermogravimetry

	Normal Range	Extreme Range
Pressure	10^{-6} torr \rightarrow 760 torr	10^{-10} torr \rightarrow 10^4 torr
Type of gas	Nearly all, incl. corrosive	
Temperature	-150°C \rightarrow 1600°C	\rightarrow $>2500^{\circ}\text{C}$
Sample mass	\approx 1mg \rightarrow 500mg	\approx 1 μg \rightarrow 2-3 kg
Rate of weight change	\rightarrow 1×10^{-10} g/sec.	
Detectable Δw	5 - 10 μg	0.1 μg
Δw /sample weight	$\geq 1 \times 10^{-7}$	

the mass spectrometer. The use of separate measurements on the thermobalance and the mass spectrometer under the same temperature conditions would be required for materials with very high vaporization temperatures, such as many of the metals or metal oxides, where the only means of transport to the ionization sector of the mass spectrometer is by short molecular beams.

ACKNOWLEDGEMENT

Grateful acknowledgement is given to H. G. Wiedemann, of the Mettler Research and Development Laboratory in Greifensee, Switzerland, for providing much of the experimental data shown here and for his helpful discussions in areas of application.

References

1. P. D. Garn, "Thermoanalytical Methods of Investigation," Academic Press, N.Y. (1965)
2. H. G. Wiedemann, Paper, "Thermal Analysis '68," Proc. of the 2nd Int. Conf. on Thermal Analysis, Academic Press, N.Y. (1969)
3. H. G. Wiedemann, Chemie-Ingenieur-Technik, 36, 1105 (1964)
4. H. Jucker, H. G. Wiedemann, H. P. Vaughan, Paper, Pittsburgh Conference on Analytical Chemistry and Applied Spectroscopy, March 1965
5. R. L. Stone, J. American Ceramic Society, 35(4) 91 (1952)
6. H. G. Wiedemann, Paper, "Thermal Analysis '68," Proc. of the 2nd Int. Conf. on Thermal Analysis, Academic Press, N.Y. (1969)
7. R. Maurer, H. G. Wiedemann, Paper, "Thermal Analysis '68," Proc. of the 2nd Int. Conf. on Thermal Analysis, Academic Press, N.Y. (1969)
8. R. Giovanoli, H. G. Wiedemann, H. Chimica Acta, 51(4) 1134 (1968)
9. M. Müller-Vonmoos, Paper, "Thermal Analysis '68," Proc. of the 2nd Int. Conf. on Thermal Analysis, Academic Press, N.Y. (1969)
10. S. Klosky, L. P. L. Woo, R. J. Flannigan, J. Am. Chem. Soc. 49, 1280 (1927)
11. H. G. Wiedemann, H. P. Vaughan, Proc. 3rd Toronto Symposium on Thermal Analysis, H. G. McAdie, Ontario Res. Foundation, Toronto, ed. (1969)
12. A. N. Nesmeyanov, "Vapor Pressure of the Chemical Elements," Elsevier, N.Y. (1963)
13. H. G. Wiedemann, Paper, 7th Annual Conf. on Vacuum Microbalance Techniques, Eindhoven (1968)
14. F. Zitomer, Anal. Chem. 40(7) 1091 (1968)

The Influence of Segmented Rods and Their Alignment
on the Performance of a Quadrupole Mass Filter

by W. Arnold
CEC/Analytical Instruments Division
Bell and Howell Company
Monrovia, California

We have found in our work with quadrupole mass filters that an improvement over the performance of conventional quadrupoles could be achieved by three modifications of conventional design. These modifications are (1) use of segmented rods, (2) control of DC/AC ratio to maintain unit resolution, and (3) maintenance of very precise alignment.

Figure 1 shows a quadrupole mass filter.

A two dimensional quadrupole field is established between four electrodes of cylindrical cross-section with the two opposite rods connected together electrically. RF and DC potentials are applied to the two electrode pairs according to the formula.

$$\bar{V} = \pm (U + V_0 \cos \omega t)$$

Ions entering the quadrupole field start oscillating in the X and Y directions. Depending on the ratio between RF and DC voltage, only ions that have stable oscillations can pass through the filter without striking the rods.

1. Segmented Rods.

We will first describe the results obtained from the use of segmented rods. Performance of the filter is affected by the fringing electric field in the region between the exit of the ion source and the uniform field region of the filter assembly. Brubaker, at this meeting two years ago, described the use of segmented rods to minimize the effects of this problem.

By segmenting the rods used in a quadrupole mass filter at the entrance to the filter assembly, transmission of ions from the source to the filter can be improved. The segments are only AC coupled to the main rods so oscillations for ions in both X and Y directions are stable. See Figure 2. Ions can pass through this section without colliding with the segments.

The resulting advantage is that the instrument can be operated with lower ion energy thus allowing the ions to stay in the resolving fields longer, as reported by Brubaker, the result is that better resolving power and transmission are obtained.

The use of segmented rods also has another advantage. In a conventional quadrupole filter, good peak shape at low mass is obtained only with low ion energies. Higher ion energies are required to get good transmission at higher masses. The result is that for optimum performance, ion energy should be varied with the mass range. Figure 3.

2. D.C./A.C. Ratio.

We will next consider the way in which it is desirable to vary the DC/AC ratio as we vary the mass. Optimum sensitivity at all masses will be obtained if we maintain unit mass resolution at all masses.

Near the apex of the stability diagram where the boundaries can be approximated by straight lines, the relationship between resolution and DC/AC ratio follows the function:

Figure 4

$$\frac{U}{V} \approx .16784 - .126 \frac{\Delta m}{m} \quad (I)$$

The RF peak voltage is proportional to m , in our case,

$$V \approx .538 m^2 \quad (II)$$

calc
 $f = 2\pi C$

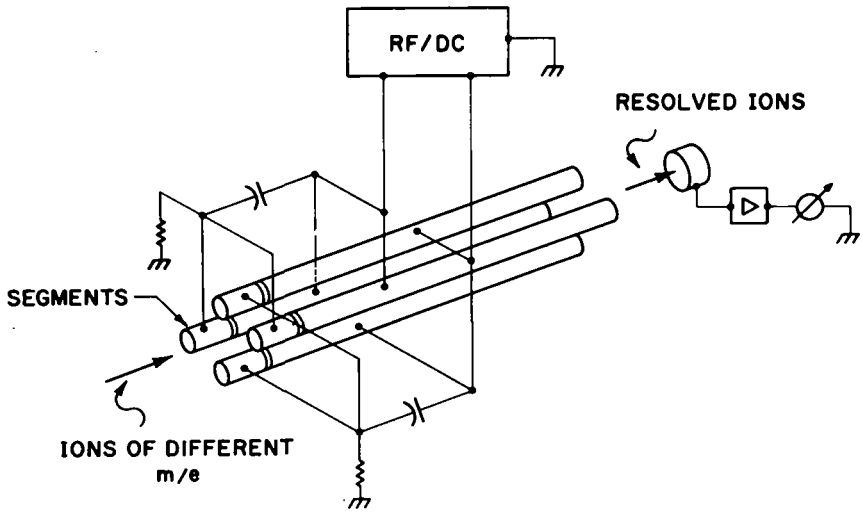


FIG. 1. QUADRUPOLE MASS FILTER

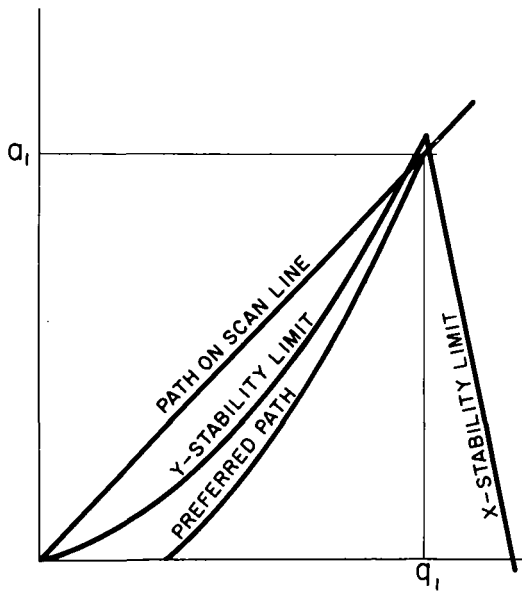


FIGURE 2.

STABILITY DIAGRAM, SHOWING TWO PATHS OF WORKING POINT DURING TRAVERSAL OF FRINGING FIELD.

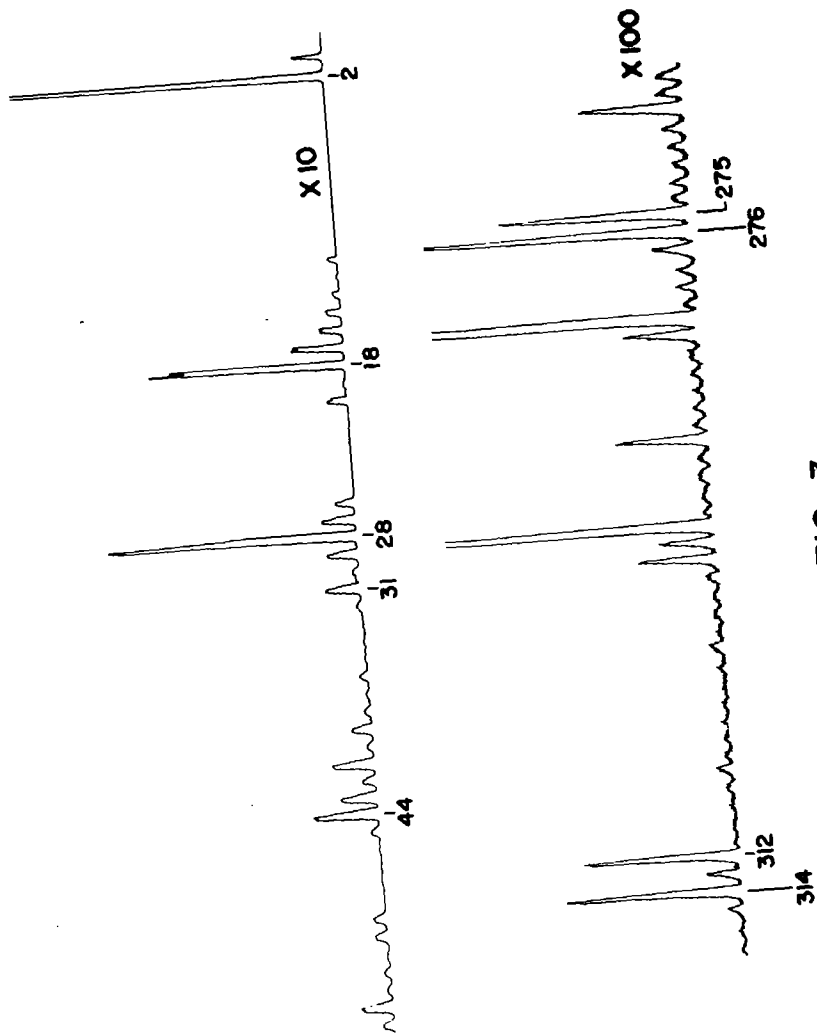


FIG. 3.

$$\frac{U}{V} \approx .16784 - .126 \frac{\Delta m}{m} \quad 1$$

$$V \approx .538 \text{ mf}^2 \quad 2$$

$$U \approx .36119 \text{ m} - .27115 \Delta \text{m} \quad 3$$

FIG. 4.

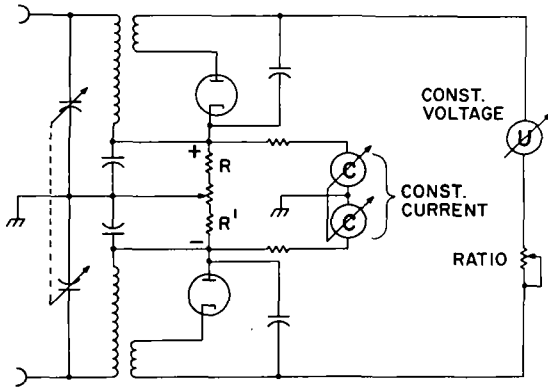


FIG. 5. RF-DC POWER SUPPLY

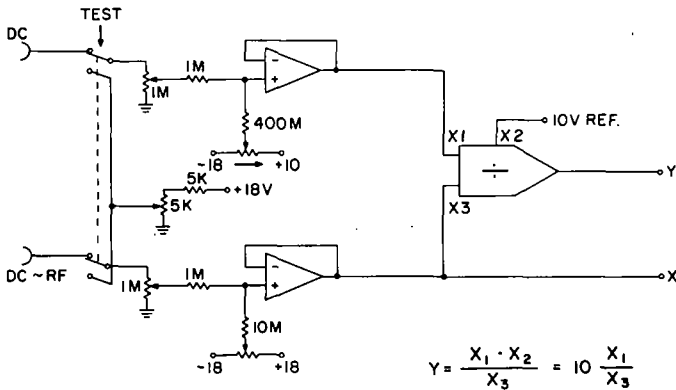


FIG. 6. Analog Divider

The DC does not say that it The total DC

which means that the DC potential at the rods must follow the relation.

$$U \approx .361191 m - .271151 \Delta m \quad (111)$$

To maintain unit resolution, Δm is one, and constant voltage must be added in series with the rectified AC.

Control of the DC/AC ratio requires not only the addition of a constant component to the DC but also that the DC/AC ratio is constant before the constant DC component is added.

I will describe the circuit used in the instrument that produces a DC voltage by rectifying a transformed portion of the RF voltage. Figure 5. Two identical circuits are used to load the RF tank symmetrically. At high DC voltages (10 to 100) the linearity of the rectifier tube is adequate to obtain a linear relationship between the AC and DC potentials. At low voltages < 10 V the contact potential of the rectifier tube used is high enough to upset the linear relationship.

In order to compensate for this contact potential, an adjustable current is added through the dropping resistor ($R_1 R'$). As long as the first portion of formula (111) is satisfied, the second portion, a constant is our case because $\Delta m = 1$, is simulated by adding a fixed voltage source in series with the rectification system. The voltage can be selected from 0 to 1.5 V to obtain the best results over the entire mass range.

In order to measure the ratio of DC to AC voltage in a convenient way and to compare it with the theoretical value an analog divider was used. Figure 6. The feedback signal, which is proportional to the RF peak voltage, and a portion of the DC signal was fed into the divider. The output of this circuit was used as the Y input on a X-Y recorder. The X component was developed from the feedback voltage.

Figure 7. To calibrate the test setup, the X and Y amplifiers of the recorder were adjusted to the calculated values while the quadrupole was adjusted for unit resolutions at m/e 300. Now by scanning the total mass range the ratio variations could be easily observed on the recorder and corrected.

Four traces are shown on the Figure 7.

- 1) Without compensation.
- 2) Current compensation only.
- 3) Voltage compensation only.
- 4) Theoretical compensation.

3. Alignment.

The final subject I want to discuss is the precision of alignment required. Figure 8.

The four cylindrical rods are mounted on three aluminum ^uinsulators. Two more insulators located between the mounting insulators help to keep the ten inch long rods straight. This rod assembly is mounted concentrically in a stainless steel tube.

The ion source was attached to the analyzer tube with intentionally loose tolerance so that it was possible to misalign the source. The individual rods were misaligned by putting thin metal spacers between the rods and the ceramic insulator. A series of experiments were performed to evaluate the criticalness of rod alignment.

4. Starting Conditions.

The axis of the source was aligned to 1/1000 of an inch to the axis of the mounting tube and the axis of the quadrupole assembly was also aligned to the axis of the tube to 1/1000 of an inch, therefore, the maximum total error between the center axis of the two assemblies should be less than 2/1000". The five spacers were selected to agree in X and Y dimensions to 5/10000", while the four rods used were straight to 3 to 5/10000" inch. After assembling and operating under these conditions unit resolution was obtained with this segmented rod assembly over a mass range from 1 to 314. Figure 9. The ion energy in this case was 8 volts. To establish mechanical reproducibility the instrument was disassembled and reassembled three times and the same resolution and ion energy could be obtained each time.

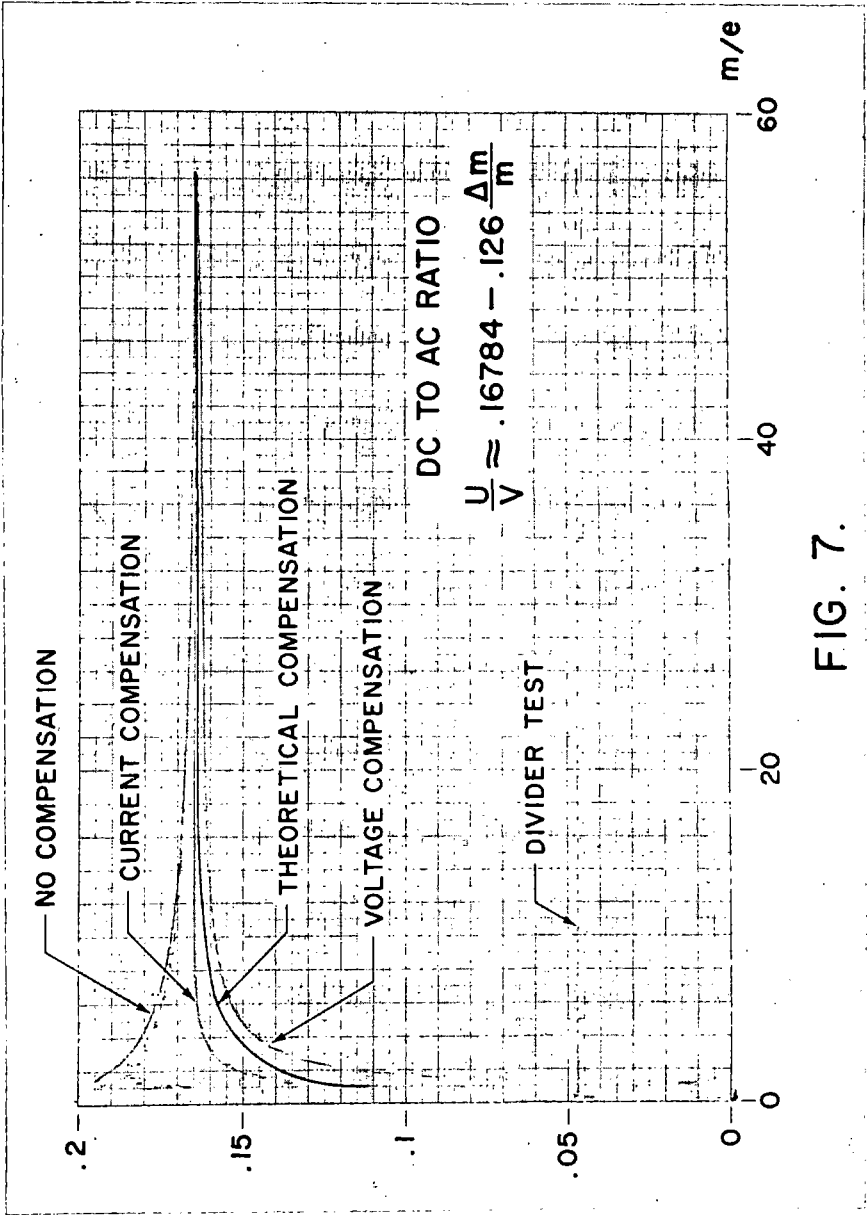


FIG. 7.

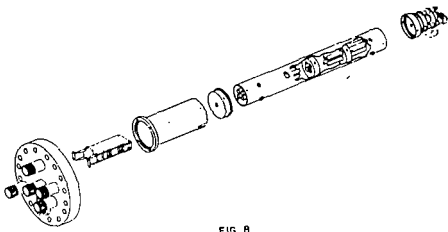


FIG. 8

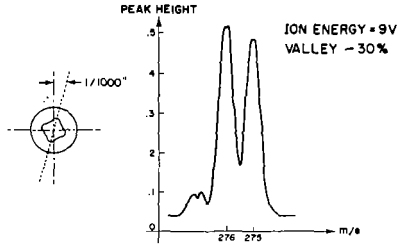


FIG. 11.

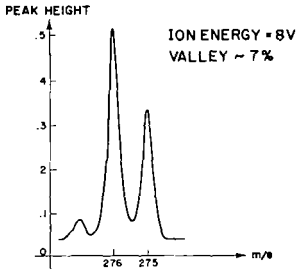


FIG. 9.

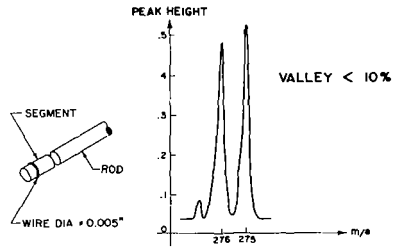


FIG. 12.

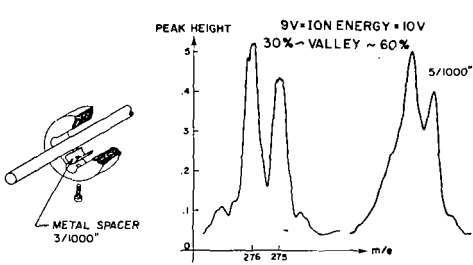


FIG. 10.

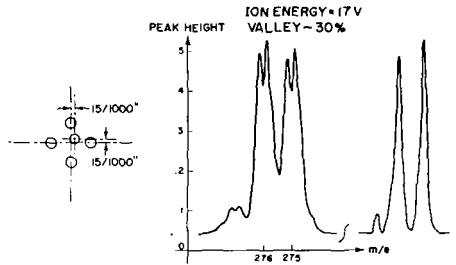


FIG. 13.

5. Rod Misalignment. Figure 10.

- a) One rod was misaligned by inserting a $1/1000''$ thick metal spacer between it and the insulator nearest the source. The center mounting screw was loosened to avoid bending of the rod. Good results were still obtained, but it was still possible that the rod was located $- 5/10000''$ from its ideal location and moved to $+ 5/10000''$.
- b) We misaligned the rod by $3/1000$ in another experiment. Unit resolution could be achieved up to m/e 150. At m/e 275/276 30% valley was all that could be obtained. The ion energy was increased by 9 V also.
- c) We misaligned the rod by $5/1000''$. Unit resolution could be achieved up to m/e 75 at an ion energy of 10 V. At m/e 275/276 60% valley was the best result obtainable. Figure 11.
- d) After restoring the assembly to a well aligned assembly with the shim removed, the rod assembly was then misaligned by rotating two opposite rods from their normal perpendicular position. This was done by changing the insulator which was nearest to the source for one which misaligned this pair of rods. The center lines of the rods were now shifted by $1/1000''$. The resolution at m/e 275/276 was decreased to a 30% valley. Poor peakshape was observed.

6. Misalignment of the Segments. Figure 12.

The relative location of the segments to the rods could not be changed to misalign the segments. Therefore, a $5/1000''$ diameter wire was wound around the segment. Two neighboring segments were treated this way. No change in resolution was observed at m/e 275/276.

7. Axial Misalignment of the Ion Source.

This test was done in three steps.

- a) The source was moved off center by $15/1000''$. The effect on resolution and peakshape are shown in Figure 13. The peakshape was not uniform anymore. Split peaks appeared. The necessary ion energy had to be increased to 17 V.
- b) The source was moved to $10/1000''$ off center. The valley at m/e 275/276 decreased to 15% while the necessary ion energy went back to 11 V. The peakshape was still similar to that of the previous case.
- c) We mounted the source back on center to at least $1/1000''$ and good results were obtained again. A 1% valley could be obtained at m/e 275/276.

In conclusion we have shown that by using segmented rods, varying the DC/AC ratio during the mass scan to keep unit resolution, and mounting the rods so that very high precision of alignment is maintained, we can scan a mass spectrum from mass 1 to mass 300 with good resolution and sensitivity throughout the mass range.

References

1. Wilson M. Brubaker, NASW 1298.
2. W. Paul, H. P. Reinhard, U. von Zahn, Zeitschrift fur Phys. Bd 152, S143-182.

OPERATION OF QUADRUPOLE MASS SPECTROMETER AT HIGH PRESSURE*

W. M. Brubaker[#] and W. S. Chamberlin[#]Earth Sciences, A Teledyne Company
Pasadena, California

An experimental investigation has been made of the operation of a quadrupole mass spectrometer in a high ambient pressure of hydrogen. Three different experiments were performed. First, the hydrogen pressure was raised while the instrument was operated normally, with an electron bombardment ion source. The instrument sensitivity and resolving power for mercury were observed as functions of hydrogen pressure. Second, the experiment was repeated with potassium ions from a thermal ion source. Third, the current at a Faraday cup collector was observed when the transport of ions through the quadrupole was inhibited by one of several means.

When the instrument is operated in the normal manner, with the electron bombardment ion source, the space charge of hydrogen ions becomes quite large at the high pressures. Under the influence of static dc fields, the paths of ions which start at rest are completely independent of their masses. Thus, the beam spreading effect of the positive hydrogen ions causes the paths of the mercury ions to diverge as they travel from the ion source to the quadrupole. Even though this distance is small, the ions move at low average velocities and the effect of space charge on their paths is appreciable. An increase in the radial component of the trajectory as the ion enters the quadrupole decreases the transmission probability, particularly at the higher resolving powers. The experimental data relating transmission efficiency and resolving power at various pressures of hydrogen confirm this hypothesis. At 60% transmission efficiency, the resolving power is 680 at a background pressure of 10^{-6} torr. At 10^{-4} torr, mainly hydrogen, the resolving power for the mercury spectrum has fallen to 530. At a still higher hydrogen pressure of 4×10^{-4} , the resolving power at 60% transmission is 412.

The second experiment was similar to the first, except that the space charge was independent of the pressure. Hence this experiment is concerned with the transmission of ions through the analyzer when their paths of entry are unaffected by the pressure. In this instance, the potassium spectrum was displayed at a constant resolving power of 100 at all pressures below 10^{-2} torr! The transmission efficiency remains constant at 100% for pressures below 5×10^{-4} torr. At 10^{-3} torr, the transmission efficiency is 97%, but at 10^{-2} torr, it has fallen to 20%.

*This research was supported in whole by the National Aeronautics and Space Administration under Contract No. NASW-1736, monitored by Dr. Donald P. Easter and C. E. Giffin, J.P.L.

[#]Present Address: Analog Technology Corporation
Pasadena, California

I have not seen this

In the third experiment, the transmission of ions through the mass analyzer is blocked by placing the working points for all ions in the unstable portion of the stability diagram, or by reducing the ion accelerating potentials to zero. In either case, the current at the detector remains below detection limit (7×10^{-15}) for various combinations of applied potentials when the pressure is below 10^{-6} torr. At higher pressures, the relationship between the background current and the pressure is $I = 2.25 \times 10^{-9} P$ (torr).

This background current sets a limit to the dynamic range of the instrument. When the pressure in the ion source is 5×10^{-4} torr and the source sensitivity is 10^{-5} amperes per torr, the related uncertainty in the measurement of a low pressure is

$$\delta p = 4.2 \times 10^{-11} (t_1)^{-0.5}$$

In this instance, t_1 is the time duration of the measurement, seconds. If t_1 is one second, the dynamic range is $5 \times 10^{-4} / 4.2 \times 10^{-11}$, or 1.2×10^7 .

SUMMARY

The quadrupole mass spectrometer has been operated at hydrogen pressures below 10^{-2} torr. In the absence of high space charge of hydrogen ions (accomplished by the use of a thermal source of potassium ions), the resolving power of the device shows no deterioration at the highest pressure, 10^{-2} torr. Transmission efficiency suffers at pressures above 5×10^{-4} torr, apparently by collisions of ions with the neutral gas. When ionization is produced by electron bombardment, the space charge of the hydrogen ions distorts the trajectories of heavier ions in the source-entrance regions to degrade the resolving power of the instrument. Photon-induced electrical noise at the detector limits the dynamic range (of the system used for these tests) to several million, for a one-second observation of the peak heights.

A NEW MASS SPECTROMETER FOR MEASUREMENTS OF VERY SMALL ISOTOPIC
DIFFERENCES BETWEEN TWO URANIUM SAMPLES
G. NIEF, M. LUCAS, R. BIR (*)

INTRODUCTION -

The precision of the isotopic measurements by mass spectrometry is chiefly limited by the finite number of collected ions. Thus, increasing the precision involves reducing all delays as well as increasing analysing time.

Another cause of error lies in the fact that the measures performed with the mass spectrometer are not absolute : the ratios of two given isotopes ion beams is not equal to the abundance ratios of these two isotopes.

A bias does exist lying in various parts of the apparatus. This bias depends on time (drift) as well as on samples introduction processus, pressure, temperature, chemical purity of samples and so on.

These propertiss of the mass spectrometer leads to the classical measurement conditions, say : double collection of ion currents, amplifiers the drift of which is as low as possible, frequent switching of samples and reference material.

Direct ions counting is, up to now , not possible for high precision work.

To obtain on ratio of isotopic abundance a standard deviation of 10^{-5} , at least $2 \cdot 10^{10}$ ions of the less abundant isotope must be collected, for both sample and standard.

In the case of natural uranium, this means $5 \cdot 10^{12}$ ions for 238 isotope. Counting devices cannot work at such a rate.

After these considerations we have more especially studied the following points :

- 1 - Stabilisation of ion beams positions
- 2 - Inlet system
- 3 - Measuring circuit

1 - STABILISATION OF ION BEAMS POSITIONS -

We use a device, firstly designed by R. BOYER (**), working as follow : in addition to the UF_5^+ ions, UF_4^+ ions are collected and the magnet current is automatically adjusted to keep constant a part of the UF_4^+ ion current.

A scheme of the collector device is showed on fig.1.

The plate A is set to collect the half of the UF_4^+ current if the UF_5^+ beams are correctly positionned. So, any variation of the ion beams position leads to a very important change of the collected UF_4^+ current.

An auxiliary electromagnet coil is fed via a control system, including a conventional potentiometer pen recorder, the differential amplifier of which is connected to output of UF_5^+ and UF_4^+ ion currents amplifiers.

The potentiometer gives the error signal to control the magnet current.

(*) - Commissariat à l'Energie Atomique - Services des Isotopes Stables - Service de Spectrométrie de Masse - BP N° 2 - GIF-sur-YVETTE (91) France.

(**) - R. BOYER - Dispositif d'asservissement en position des faisceaux d'ions dans un spectromètre de masse (Rapport CEA - R. 3268 - 1967) .

With this device, the image position is fixed with an accuracy of ± 2 microns. At the same time, the error signal is permanently recorded and an alarm circuit can be easily put in if the limits of control are to be reached.

The excellent stabilisation of image position in our spectrometer makes possible to use a symmetric double collector (see fig.2).

Both parts include a defining slit, where falls only one ion beam, $^{235}\text{UF}_5^+$ or $^{238}\text{UF}_5^+$, and a Faraday box. So most of the troublesome phenomena, as ions scattering and electron secondary emission, are suppressed.

2 - INLET SYSTEM -

Inlet system is a fundamental part of the apparatus.

The gas is introduced through a metallic capillary tube, the low pressure side of which lying in the ionisation chamber. The high pressure region of the system is so designed that the gases flow permanently in front of the leak. The pressure of gases is kept constant by a cold trap ; in any case the pressure can vary, even if no sample is connected (for example during samples switching). After samples switching, the flow rate is high enough to be sure that the gas flowing has reached the new composition in a few seconds. So the UF_5^+ ion current is constant and not altered during permutation of samples . This feature is very benefic for permanent working conditions of the mass spectrometer.

A principle scheme of the system is described on the fig.3.

The flow of gases is adjusted by the central capillary and takes place between sample connection device A and the cold trap C .

The temperature of C is fixed to 0°C and defines the constant pressure in the vessel B above the inlet of the leak.

The value is so that in normal working conditions, the amount of trapped UF_6 is about constant. More precisely, this value is about .3g par hour that is 500 times the flow into the mass spectrometer. The consumption of product is very similar to that observed with conventional systems.

Our experiments showed that the flow characteristic of the capillary leak remains unchanged for several months and that the ion currents are proportional to the pressure in B, that is on the only dependence of C temperature.

3 - MEASURING CIRCUIT -

An overall scheme of the circuits is showed on fig. 4 .

Voltage-to-frequency converters are in F and K . B and D are pulse shapers. A, C and E represent three pulses counters. J is the master clock, G and H define two delays from the output of J.

At the beginning of a cycle, G opens the gates of A, C and E. When C has reached a fixed number of pulses (say 10^6), the gate of A is closed, its content proportional to the ratio to be measured is print. The delay fixed by H is slightly less than the cycle duration. During this constant time, the gate of E is open. Its final content proportional to the high current intensity, is print too. During the delay defined by G, all gates are closed and samples switching may take place. Then G opens again the gates and the procedure is resumed.

Two informations are available: one is proportional to the isotopic ratio, the other to the high ion current. The last one permits to make sure that the flow of gas is constant or eventually to correct for " pressure effects ".

BEAMS POSITIONS CONTROL

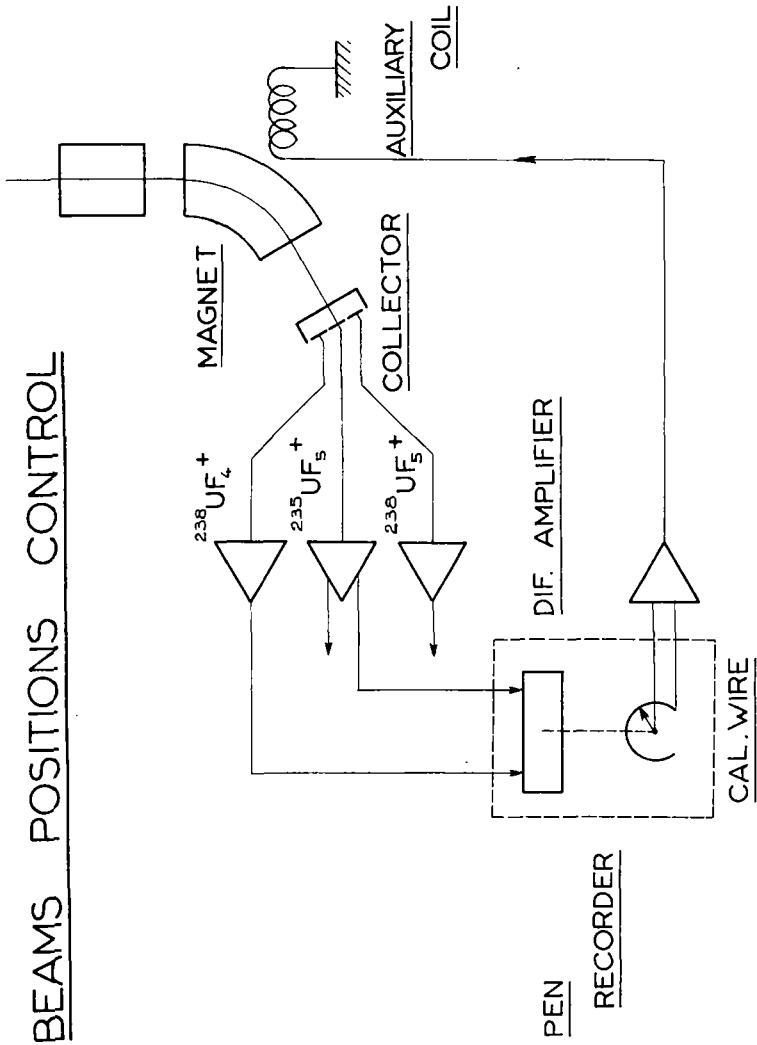


Figure 1

COLLECTOR

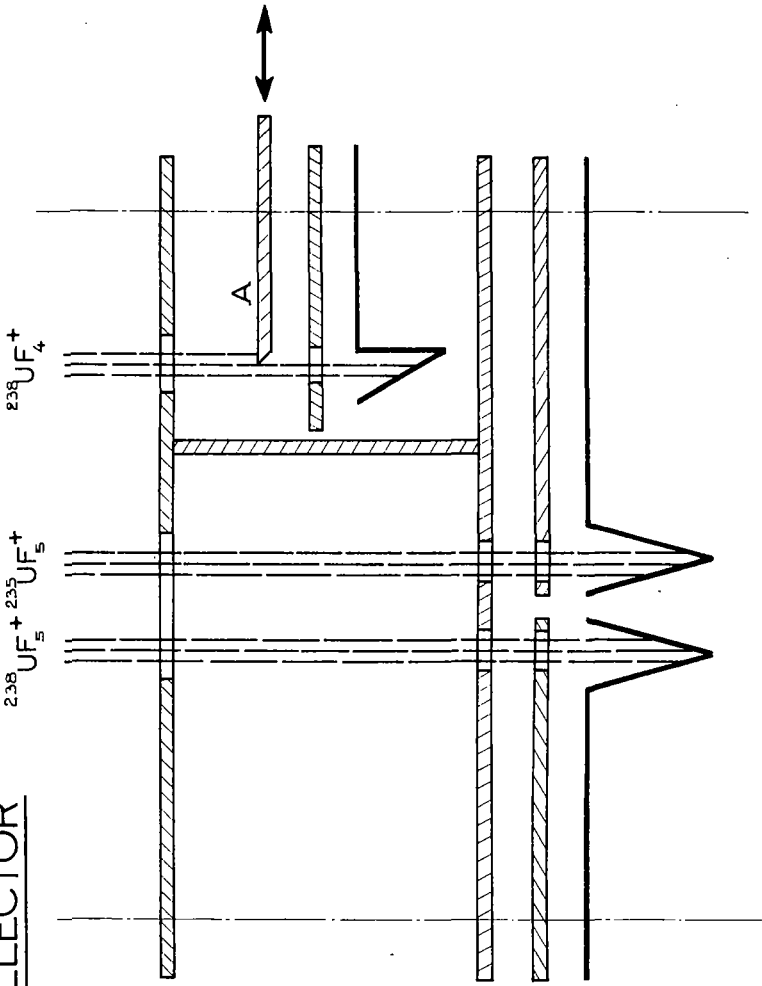


Figure 2

DIGITAL RATIOS MEASURING CIRCUIT

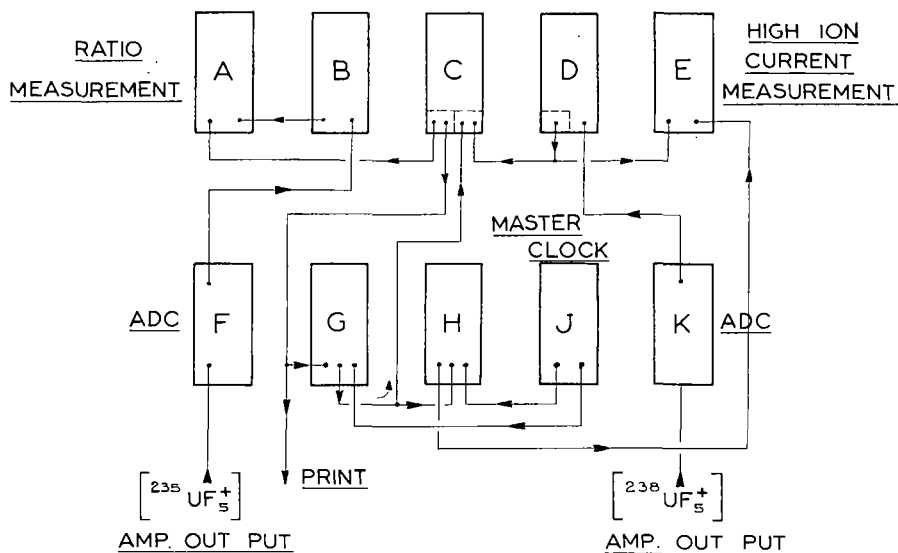


Figure 4

INLET SYSTEM

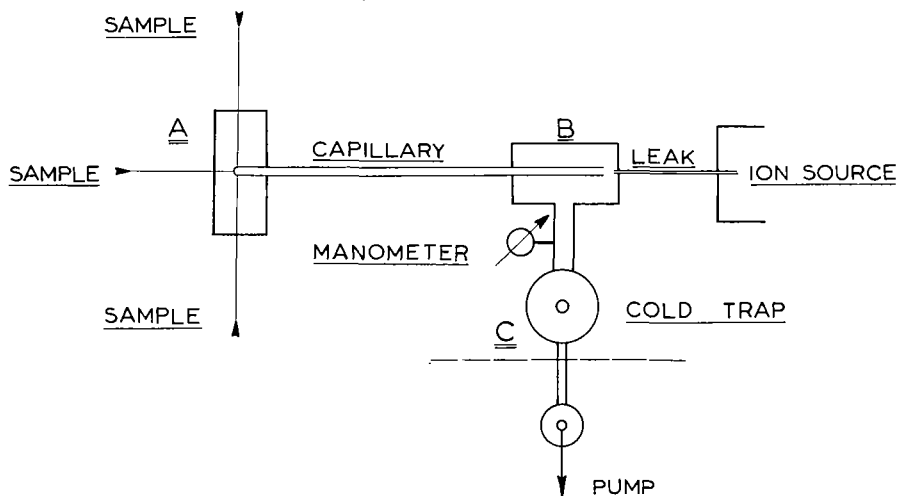


Figure 3

ANALYTICAL PROCEDURE -

We chose the following analytical cycle :

Samples switching : 10 seconds

Recording of ratio : 20 seconds

that is 1 minute to get an enrichment value.

The running is fully automatic with digitized output. It is easy to determine the number of elementary cycles - i.e. the analysis time - to reach a given precision.

In the present state of our experiments, the relative precision of an one minute cycle is $3 \cdot 10^{-4}$ (2 times the standard deviation), that is 10^{-4} for a 10 minutes analysis.

Further experiments will deal with longer analysis (1 or 2 hours) .

AN ELECTRONIC DETECTION SYSTEM UTILIZING INTEGRATION TECHNIQUES
FOR A SPARK SOURCE MASS SPECTROMETER*

by

Arthur J. Socha, C. William Baker, Eleanor M. Masumoto
Electronic Materials Division, Bell & Howell Company, Pasadena, California 91109

I. INTRODUCTION

The electronic detection system described here utilizes the output from an electron multiplier which is first amplified and then the charge integrated. This system can handle all ion pulses without saturating but is only capable of detecting ions to a few parts per billion for most impurities. Below that level the noise becomes a serious problem because no rejection system is used. Also described is a simple yet practical method for locating a particular m/e at the electron multiplier slit.

II. ION BEAM LOCATION

A. Magnetic Scanning. The initial problem in electronic detection is that of locating at the entrance slit of the electron multiplier the ions of the element of interest. Magnetic scanning was chosen as the means to bring the ions of a specific m/e to the slit. A teslameter with minimal temperature sensitivity was devised using an ultrapure epitaxial GaAs Hall probe. Figure 1 is a schematic of the Hall probe and associated equipment. The power supply used is a 0 - 50 volt supply and has a regulation of 0.005%. The digital voltmeter has 100 microvolt sensitivity. The Hall probe is shunt-mounted onto the magnet. The Hall voltage produced in the GaAs chip by the magnetic field is read by the digital voltmeter.

The current through the Hall probe may be adjusted so that the numerical value of the Hall voltage is equal to the numerical value of the magnetic field strength, i.e. one volt equals one tesla. This is accomplished by the power supply and a simple bias voltage system consisting of a potentiometer, battery, and limiting resistor (Figure 1). Figure 2 indicates the change in a tesla vs. m/e curve by changes in the power supply and by the bias voltage system. The power supply changes the slope of the curve whereas the bias voltage changes the intercept. With this system the magnetic field can be determined to better than one part in ten thousand.

Using a variety of samples an instrument calibration curve was prepared. The magnetic field strength was varied to locate the ion beam of the selected m/e at the entrance slit of the electron multiplier. The resultant curve relating mass to magnetic field strength in tesla is given in Figure 3. The curve shows a slight deviation from a straight line due to minor non-uniformity in the Hall voltage at various field strengths. The curve allows rapid selection of the magnetic field necessary to analyze for selected impurities.

The procedure for locating a peak is as follows: the magnet is first saturated and the mass in question is approached by lowering the magnetic field strength. A gold standard is always available in the source of the mass spectrometer. The teslameter is then calibrated such that Au⁺ at mass 196.967 is located at 0.7924 tesla. The gold also provides a series of reference points which may be used from mass 28 to 197. This may be seen in Table I.

TABLE I. Gold Reference Points

<u>Ion</u>	<u>Mass</u>	<u>Tesla</u>	<u>Ion</u>	<u>Mass</u>	<u>Tesla</u>
Au ⁺	196.96	0.7924	Au ⁺⁵	39.39	0.3702
Au ⁺²	98.48	0.5786	Au ⁺⁶	32.83	0.3376
Au ⁺³	65.66	0.4767	Au ⁺⁷	28.14	0.3120
Au ⁺⁴	49.24	0.4138			

B. Electrical "Tuning". A certain amount of fine tuning of the beam position is necessary and is accomplished by adjusting the field plate voltage with a helipot over a range of about ± 15 volts. The field plate voltage is related to the accelerating voltage with a constant 1:10 ratio such that the instrument focus is not affected by this adjust-

*Supported in part by the United States Air Force under Contract No. F33615-68-C-1635.

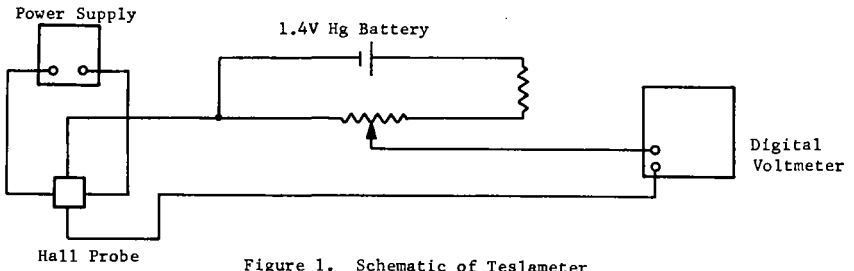


Figure 1. Schematic of Teslameter

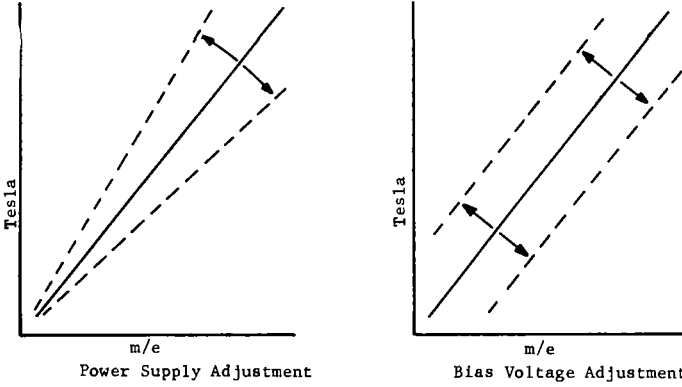


Figure 2. Effect of Teslameter on Tesla vs. m/e Curve

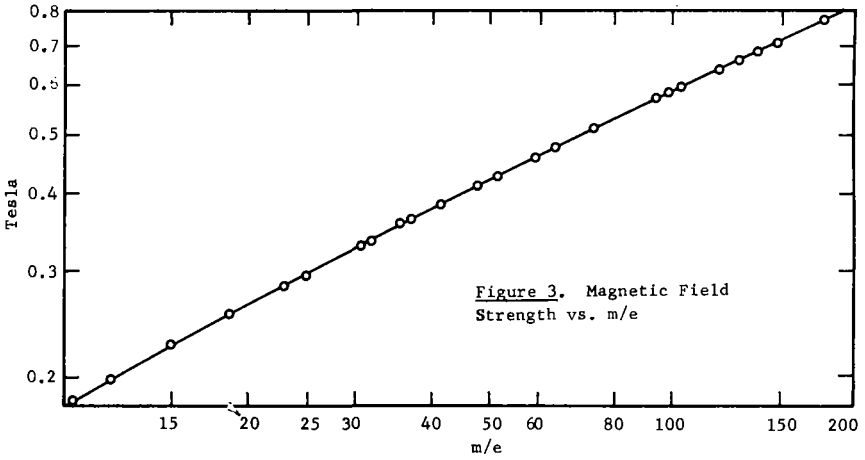


Figure 3. Magnetic Field Strength vs. m/e

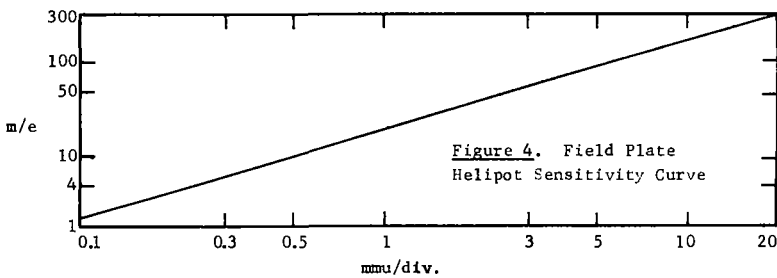


Figure 4. Field Plate Helipot Sensitivity Curve

ment. Nevertheless the amount of adjustment used is restricted so that changes in the accelerating voltage are no more than 0.1%. The helipot used is divided into 150 divisions. Figure 4 shows the effect of each of the helipot divisions at various m/e positions. The general procedure is to locate the m/e of interest from the tesla vs. m/e curve and obtain this by varying the magnetic field strength. After locating the general position of the m/e in question the centering of the ion beam in front of the slit would be achieved by adjusting the helipot.

III. ELECTRONIC DETECTION SYSTEM

Figure 5 is a schematic of the electronic detector used. The slit is a variable slit which is located about 13 inches from the energy slit of the magnetic sector. The electron multiplier is a commercially available CEC electron multiplier commonly used on gas mass spectrometers. The amplifier and integrator sections are actually another beam monitor where current and coulomb readings may be obtained. The output from the integrator is read by the digital voltmeter-printer.

The electronic detector is controlled by an automatic exposure control.¹ In typical operation most readings are made with a total beam monitor charge of 10^{-10} coulombs. When this charge is reached, the automatic exposure control shuts off the spark and triggers the digital voltmeter to read and print the electronic detector's integrator voltage. Following the printing of the readout the beam monitor and the integrator are reset to zero by the automatic exposure control and the spark started for the next exposure. In this manner a series of exposures may be made in quick succession all being printed automatically by the digital voltmeter.

IV. STANDARDIZATION AND SOME RESULTS

A. Use of Standards. Samples are sparked in the usual way. The beam monitor of the mass spectrometer is used to determine the total beam charge. Normally, at least five to ten analyses, at a total beam monitor exposure (T) of 1×10^{-10} coulombs each, is made for each impurity. The impurity ion charge (I) is determined with the electron multiplier system. The nominal impurity concentration for a given analysis is then obtained from the ratio of the impurity ion charge to the total beam charge, I/T.

Actual concentrations cannot be determined directly without making corrections for various parameters (beam width, absolute multiplier gain, elemental sensitivity, etc.) affecting the electronic detection output. Since these effects are not all known standards are used to obtain accuracy in the analysis. The impurity concentrations are determined using the following equation:

$$\text{Impurity concentration in ppma (parts per million atomic)} = S \times \frac{I_U}{I_S} \times \frac{T_S}{T_U} \times \frac{G_S}{G_U}$$

Where S = Impurity concentration in the standard in ppma
 I_S = Electronic detection reading for standard in coulombs
 I_U = Electronic detection reading for unknown in coulombs
 T_S = Beam monitor reading for standard in coulombs
 T_U = Beam monitor reading for unknown in coulombs
 G_S = Gain of the electron multiplier used for standard
 G_U = Gain of the electron multiplier used for unknown.

The terms T and G deal with the total gain of the system. If all the analyses are performed with the same total beam monitor charge, then the ratio T_S/T_U drops out of the equation. For most work this is usually the case. The total gain of the system is usually regulated by changing the gain of the electron multiplier "G" only.

B. Carbon and Sodium in Cadmium Sulfide. Table II shows a typical electronic analysis of a cadmium sulfide sample. The sample was one of a series analyzed for carbon and sodium. It had previously been analyzed using photographic plate detection, so comparison between techniques could be made. The second column shows the total beam charge (T_U) for each analysis made for each impurity. Note that the last analysis for each impurity has a total beam charge (T_U) ten times that of the other analyses. The third column shows the impurity beam charge (I_U) at each exposure. The averages of the short exposures agree well with the values for the longer exposures.

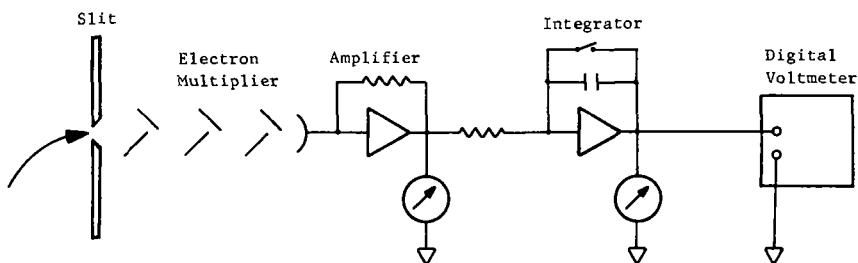


Figure 5. Schematic of Electronic Detector

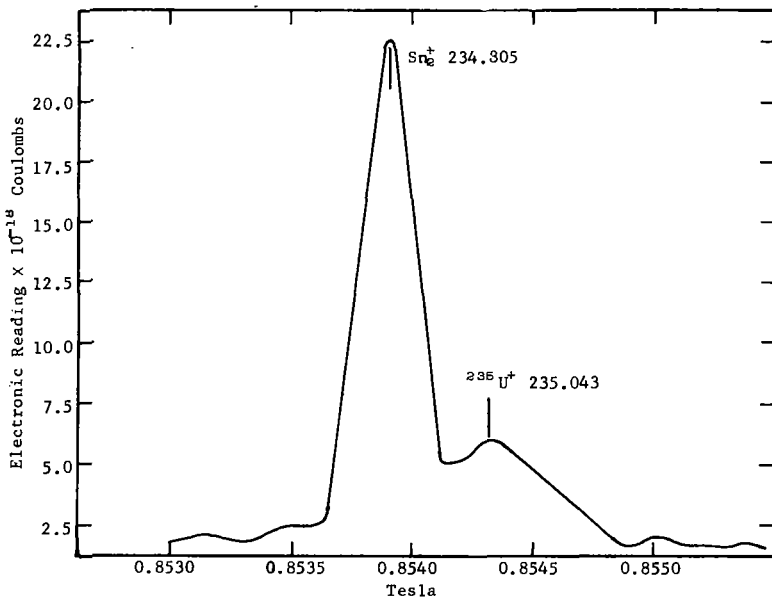


Figure 6. Determination of U^{235} in NBS Zr No. 1215

Lot 315 Impurity	Total Beam Charge, T	Impurity Beam Charge, I	Concentration, ppma		
			Standardized Electronic	Photographic Plate	
Carbon	1.00×10^{-10}	0.496×10^{-16}	1.79	Average 1.48	1.7
	1.00	0.394	1.41		
	1.00	0.504	1.80		
	1.00	0.444	1.59		
	1.00	0.230	0.82		
	10.0	4.01	1.35		
Sodium	1.00	0.485	0.0296	Average 0.028	0.036
	1.00	0.326	0.0200		
	1.00	0.539	0.0329		
	1.00	0.490	0.0299		
	10.0	4.57	0.0278		

Table II. Analysis for Carbon and Sodium in Cadmium Sulfide Using Electronic Detection

Using the above equation impurity concentrations were determined utilizing another cadmium sulfide sample whose carbon and sodium concentrations were known. The results are given in the fourth column. The average values can be compared with the results of the photographic detection in the last column. The agreement is good especially for carbon. Note that the total beam charge for all analyses add up to only 1.5×10^{-9} coulombs. Routine photographic plate analyses are made with a total beam charge of 3×10^{-7} coulombs. Also notice the difference in sensitivity between the sodium and carbon. For approximately the same beam charge I_{U} the sodium level is 1/40 the carbon level.

C. Uranium in NBS Zirconium. A study was made of National Bureau of Standards zirconium alloy 1215, which has a certified uranium concentration of 3.5 ppma. Since ^{238}U has a normal abundance of 0.72%, the concentration of ^{235}U should be 0.024 ppma. One of the difficulties with this sample is that it contains 0.95% tin. After locating m/e 235, the peak intensity found was inconsistent with the small concentration expected.

A helipot scan of the region, taking a set of 5 readings at each 0.0001 tesla from 0.8530 to 0.8550 tesla produced the peaks shown in Figure 6. The larger peak was identified as a tin dimer of $m/e = 234.80$. Since ^{238}U has a mass of 235.04, the two peaks were easily separated (1 part in 1000). The ^{238}U peak was used as a standard to determine the concentration of ^{235}U after the latter had been corrected for the background level, that is:

<u>Mass</u>	<u>Electronic Reading (10^{-18} coulombs)</u>	<u>PPMA</u>
^{238}U	558	3.5
^{235}U	6.0 - 2.0 (Background) = 4.0 (Natural Abundance $^{238}\text{U} = 0.024$)	0.025

An estimate of the detection limit can be made at about 10 ppba in a sample with a similar tin content. With no tin, the detection limit would be much lower because the many tin dimers in the region of the uranium produced a background about 5 times that normally experienced. This type of background noise is believed to be from ions which bounce off of the slit with just the right radius to enter the slit.

V. CONCLUSION

The teslameter is a simple device but has been very accurate in locating a given m/e . Standards must be used if a high degree of accuracy is desired in the analysis. This electronic detection system offers accuracy of $\pm 5-10\%$ when standards are used. Linearity has also been found in calibrating the electronic detector. That is, the standard may be orders of magnitude different in concentration from that of the impurity in question. In addition the detector is capable of handling elemental concentrations which vary over ten orders of magnitude.

VI. REFERENCE

1. A. J. Socha, R. K. Willardson, "Analytical Techniques for the Determination of Trace Impurities in Cadmium Sulfide," Aerospace Research Laboratories Technical Documentary Report ARL 68-0132, Wright-Patterson Air Force Base, Ohio, July 1968.

84. THE STUDY OF A MASTER EMULSION-CALIBRATION CURVE FOR QUANTITATIVE
SPARK SOURCE MASS SPECTROMETRIC ANALYSIS

by

Ping-Kay Hon
Argonne National Laboratory
9700 South Cass Avenue
Argonne, Illinois 60439

ABSTRACT

Preparation of a master emulsion calibration curve useful for a complete batch of photo plates has been attempted. Pure tin is used because it consists of ten isotopes of wide abundance. In a limited exposure range there will be many lines of various intensities. Four plates were run and in each plate the exposures were from 2×10^{-4} to 1.0 nanocoulombs in steps of two or less. There were more than 100 lines with intensities from about 10% to over 95% transmittance and evenly distributed. Absorbance of the lines vs its logarithmic exposure was plotted as usual. All four curves showed good agreement in the low intensity region when they were normalized at $A=0.434$ absorbancy unit. The master emulsion-calibration curve was obtained by averaging these four curves.

As a test of the accuracy of this emulsion calibration curve for quantitative analysis, a pure antimony sample was run on a plate from the same batch. The isotopic ratio of ^{121}Sb and ^{123}Sb was determined to be 1.348 as compared to the true value of 1.339. The relative standard deviation was 8.8% for 16 pairs of measurements. Good accuracy, about 1%, was also obtained when the curve was used to determine the ^{63}Cu isotopic abundance in a copper standard. For impurity concentration determination, the accuracy and precision were as good as those from an individual on-plate calibration curve shown by a uranium sample.

ROUTINE ANALYSIS USING A SPARK SOURCE MASS
SPECTROGRAPH WITH ELECTRICAL DETECTION
C. A. Evans, Jr., R. J. Guidoboni and F. D. Leipziger
Ledgemont Laboratory
Kennecott Copper Corporation
Lexington, Massachusetts, 02173

At the 1968 Pittsburgh Conference on Spectroscopy and Analytical Chemistry, Bingham, Brown and Powers^{1,2} described an electrical detection system for the AEI MS-7 spark source mass spectrograph. The system is designed to be operated in either a peak switch or scanning mode. Leipziger and Evans³ discussed preliminary results with the high accuracy peak switch mode of the AEI system at the Montreal Electrochemical Society meeting. This paper will present an analytical method which permits the use of the peak switch system for rapid, accurate, routine analyses.

Electrical Detection System

The mass spectrograph is converted to electrical detection by the addition of a high gain electron multiplier with its accompanying electronics, as well as modifications to the electrostatic field and magnetic field power supplies. In the peak switch mode the magnetic field is held constant and the desired mass is switched onto the multiplier using the electrostatic analyzer voltage. In order to maintain high speed and sensitivity, electrostatic peak switching is limited to a range of M to 2M in mass at any one magnetic field. Therefore the magnetic field is changed if elements outside of this range are to be analyzed. While the desired mass is focused on the multiplier, a measured total ion beam exposure is made and the electron multiplier current amplified and integrated. With a constant monitor exposure for both a standard and an unknown, the concentration of element i is determined by the relationship:

$$\frac{\text{integrated multiplier current}_i^{\text{unkn.}}}{\text{integrated multiplier current}_i^{\text{std.}}} = \frac{\text{concentration}_i^{\text{unkn.}}}{\text{concentration}_i^{\text{std.}}}$$

Analytical Procedure

As has been suggested from use of the photographic plate as a detector, numerous parameters must be held constant in order to obtain accuracy in the analysis. Because the electron multiplier is a more accurate detector and the data is instantly available, the importance of these parameters is much more apparent. It has been found that electrode positioning is the most important parameter and has been the most neglected in work using the photographic plate. In order to maintain electrode positioning uniform from sample to sample, a rigorous mounting procedure has been established. Using a sample positioning jig, each of the electrodes is mounted either 4 or 8 mm from the accelerating plate depending on whether the electrodes are to be vibrated or rotated during the analysis. Both electrodes must be the same distance from the accelerating plate so that there is no self-shielding with its deleterious change in extraction efficiency. The electrode gap is reproducibly positioned on the ion axis, using an inexpensive 6X microscope mounted onto the instrument. The electrode overlap is always set to 1 mm with the aid of a graduated microscope eyepiece. The effects of a changing spark gap are alleviated by vibrating or rotating the electrodes after a preliminary visual adjustment using the microscope. In addition to maintaining a more

uniform spark, rotation of the electrodes samples over a larger area reducing the effects of inhomogeneity in the sample. Little additional time is required for proper mounting of the electrodes and the resulting analysis is well worth this small effort.

A critical test of this procedure and the electrical detection system as a whole is the precision of repetitive loadings of a given sample. Johnson-Matthey CA6 was loaded seven times according to the above procedure. Then ten 0.3 nC exposures were taken while integrating the $^{107}\text{Ag}^+$ line. The isotopic concentration of the $^{107}\text{Ag}^+$ isotope is about 1.5 ppma in CA6. The precision for each loading averaged 2.7% and the average of the seven loadings had a relative standard deviation of $\pm 1.9\%$. This 1.9% represents the overall accuracy and precision attainable with the system since the experiment was analogous to the analysis of a standard and six unknowns where all seven sets of electrodes happen to have the same Ag concentration.

To test the system against actual analytical standards several elements in the NBS 460 iron series were analyzed. The concentrations of 100 ppm to 1% in these standards are higher than generally encountered with the spark source mass spectrograph but there are few standards available which are certified to the 2% accuracy of which the system is capable. Each set of electrodes was machined to 0.035" in diameter and rotated using two small battery-powered motors mounted in the source of the instrument. Table I shows the analytical results obtained using the spark source mass spectrometer and compares these results to the NBS values. The overall deviation of the mass spectrometric values from those certified by NBS is 7.6% with precisions of $\pm 2\%$ generally encountered for repetitive exposures of the same sample. A working curve obtained using electrical detection is shown in Figure 1. As can be seen the curve is linear over several orders of magnitude and the excellent fit holds even at the 40 ppm level. Unfortunately, accurate, broad-coverage standards such as the NBS 460 series are not available for concentrations below 100 ppm. However, analysis of the Johnson-Matthey series of copper standards demonstrates the validity of this method at ppm levels.

Analytical Time

In addition to being a highly accurate method of analysis, the electrical detection method provides a more rapid analysis than is available with the photographic plate. About 15 minutes is required for sample turnaround, including mounting as described above, pump-down and presparking. An additional 1-2 minutes for each peak is required for 3-5 exposures. Since a mass range of only M to 2M is covered at each magnetic field setting, analyses for elements lying outside this range require that the magnetic field be changed and the new peaks set up. For this reason, it is easiest to analyze all the samples for the elements in a given mass range and then to change the magnet and peak-settings for the analysis of the remaining elements in all the samples. If all the elements lie within the same M to 2M range, one sample can be analyzed for five impurities every 20-25 minutes with approximately 20 samples analyzed per day.

With its ease of operation, electrical detection lends itself to automated operation and data acquisition. A Wang Laboratories Model 370 Programming Keyboard and its peripheral equipment has been interfaced to the mass spectrometer. The interface not only acquires data automatically but can also control peak switching, initiate exposures and sense their completion.

In summary we feel an electrical detection system is now a reliable means of performing precise and accurate routine analyses for minor and trace element impurities. The system has been proven reliable and now the analyst must assume the

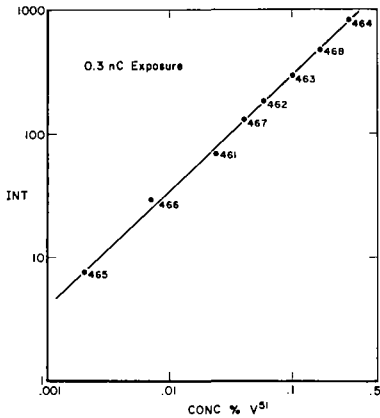
responsibility of providing a reproducible sample to the spectrometer. Methods must be developed for the special types of samples such as thin films and compactions. A more detailed discussion is in preparation for publication.

References

1. R. A. Bingham, R. Brown, and P. Powers, 1968 Pittsburgh Conference on Analytical Chemistry and Applied Spectroscopy, March 3-8, 1968.
2. R. A. Bingham and P. Powers, Sixteenth Annual Conference on Mass Spectroscopy and Allied Topics, May 12-17, 1968, Pittsburgh, Pa.
3. F. D. Leipziger and C. A. Evans, Jr., 134th National Meeting of the Electrochemical Society, Montreal, October 6-11, 1968.

Table I
 Analysis of NBS 460 Series Steels
 (Concentration Percent by Weight)

	461	462	463	464	465	466	468
Zr							
SSMS	--	0.062	Std.	0.010	--	--	--
NBS	--	0.063		0.010			
Nb							
SSMS	0.009	0.089	Std.	0.033	--	--	--
NBS	0.011	0.096		0.037			
Mo							
SSMS	0.26	0.084	Std.	0.025	--	--	--
NBS	0.30	0.080		0.029			
Sn							
SSMS	0.024	0.068	Std.	0.037	--	--	--
NBS	0.022	0.066		0.043			
Cr							
SSMS	0.133	0.85	0.275	Std.	0.0038	0.012	0.58
NBS	0.13	0.74	0.26		0.004	0.011	0.54
Mn							
SSMS	0.38	0.94	1.13	Std.	0.0024	0.0075	0.47
NBS	0.36	0.94	1.15		0.002	0.007	0.47
V							
SSMS	0.025	0.068	0.105	Std.	0.035	0.107	0.18
NBS	0.024	0.058	0.10		0.032	0.113	0.17



Intergrate Multiplier Current vs Concentration of V

Figure 1

R.A. Bingham, P. Powers and W.A. Wolstenholme
AEI Scientific Apparatus Division,
Manchester, England.

Introduction

The use of electrical detection techniques for the analysis of solids by spark source mass spectrometry is now firmly established.^{1,2,3,4} In this laboratory we employ two basic complementary procedures: Peak scanning to obtain an overall survey analysis of the spectrum and peak switching to obtain more accurate quantitative analysis on selected peaks.

Peak scanning employs an exponential magnet scan to sweep each peak of the spectrum across the electron multiplier detector whereas peak switching employs voltage switching by a decade control to switch several peaks in turn onto the collector so that their signals can be integrated and the effects of ion and spark statistics are essentially removed.

This paper discusses some of the more recent improvements in the peak scanning mode of operation, in particular the use of 'Autospark', an automatic spark control system, and the addition of computer processing of the data.

Peak Scanning

Sequential scanning of all peaks in the spectrum will produce quantitative analyses only if the inherent fluctuations of the r.f. spark discharge are corrected or removed. As has already been explained in previous papers^{2,3} we normalise the collector signal by reference to a signal proportional to the total ion current passing through the spectrometer. Such a reference signal is obtained from the monitor electrodes on the AEI MS702 used for this work. Figure 1 shows the principle diagrammatically. The two signals (of opposite polarity) are passed through logarithmic amplifiers of appropriate time constant and of 1000:1 dynamic range and their outputs are summed. The resultant output is proportional to the logarithm of the ratio and this is displayed on an ultra violet chart recorder. Figure 2 shows the tin-antimony region of such a ratio-scan from a copper sample.

A concentration "window" of range 1000:1 is displayed. In Figure 2 the lower horizontal level (the detection limit) represents 0.2 ppm and the upper level 200 ppm. Concentrations below the detection limit do not of course appear, but the concentration window can be shifted from matrix level down to the ppb (part per billion) level simply by adjustment of multiplier gain. Impurity concentrations above the range in use will still appear as saturated peaks on the chart and again the concentration window can be shifted to cover the higher concentrations. The entire concentration range can thus be covered in 3 scans. This technique has now been improved and extended by the addition of the Autospark control and by computer processing of the output data. Figure 3 shows a block diagram of the system.

Autospark

The automatic spark control system uses electrode vibration to allow a sensing element situated close to the r.f. generator to detect the magnitude of the electrode gap, and a feedback circuit then arranges for the vibrated electrode to be adjusted accordingly. The electrode gap can thus be maintained to within a typical tolerance of approximately ± 0.00025 inch (0.01 mm). In this way the discharge will run unattended for long periods and variations of analysis during the period of a scan are minimised. Figures 4 and 5 illustrate the use of 'Autospark' when sparking tungsten and aluminium samples. The upper trace in each case shows the monitor signal obtained under manual conditions and the lower trace shows the same signal when Autospark is used. Each trace shows a one hour run and is recorded from right to left.

The vertical ticks on the manual control traces show

above the trace - points where electrode readjustment was needed
below the trace - points where the signal fell to zero.

It will be seen that under automatic control no manual electrode adjustment was required and that the signal never fell to zero for a period long enough for the recorder to respond.

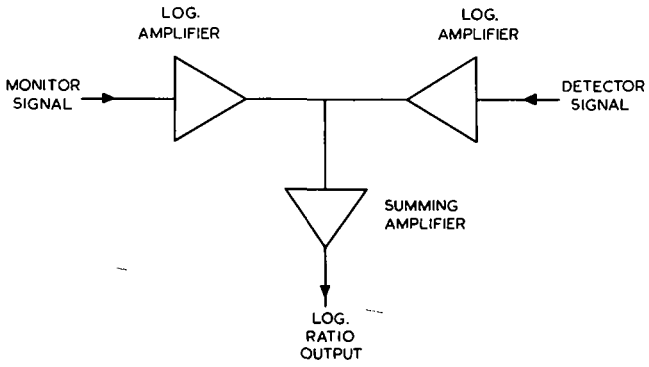
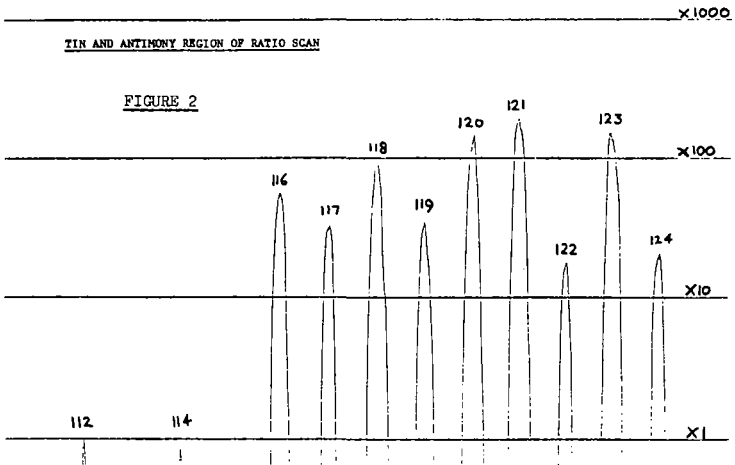


FIGURE 1 BLOCK DIAGRAM OF SPARK SOURCE LOG. RATIO SYSTEM.



SPARK SOURCE DATA PROCESSING.

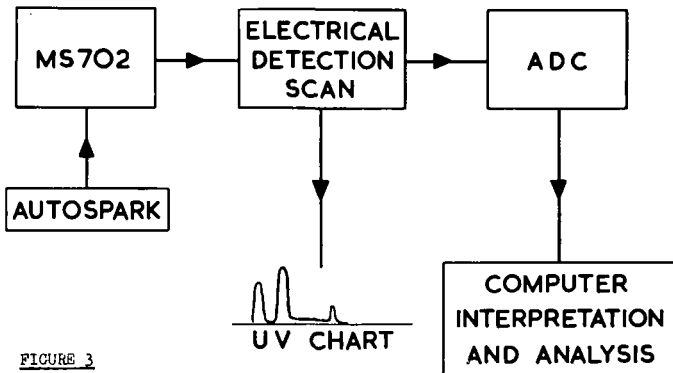


FIGURE 3

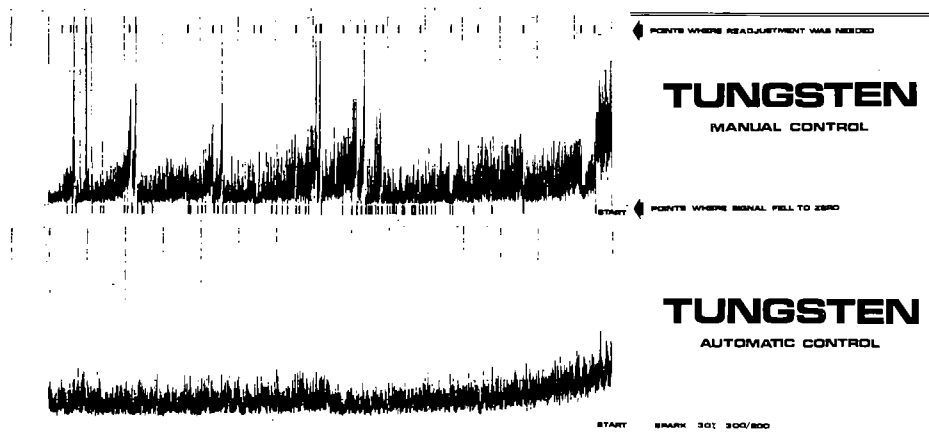


FIGURE 4

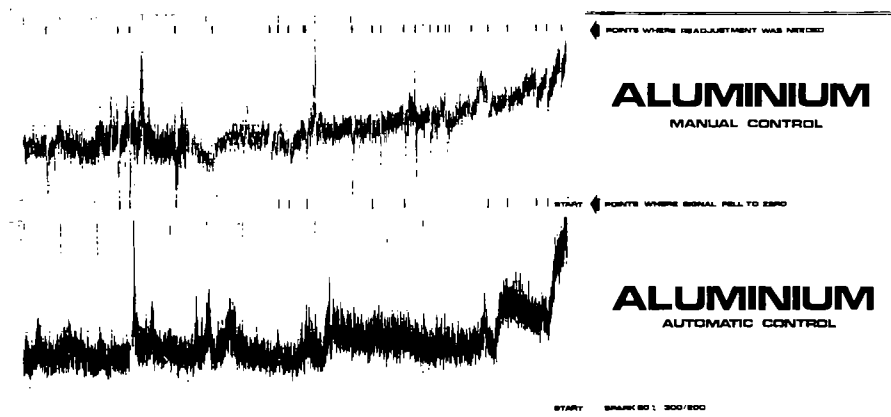


FIGURE 5

Using automatic electrode control samples of copper and steel have been sparked for more than eight hours without operator intervention.

Data Acquisition

The ratio signal produced from the summing amplifier is passed to the data acquisition system after antilogging. This is tested against a threshold level to separate peaks from background, the peaks are digitised, the time of the centroid of each peak calculated on the fly by the computer and this centroid time together with the peak area is stored in the computer memory. A PDP8 computer was used and the data were outputted on paper tape so that it could be processed further using an IBM 360/40 computer. This procedure was followed to allow easy development of the processing algorithm although the algorithm itself is designed to be used on a small computer like the PDP8. All the data given in this paper have been obtained from a PDP8 system on line to the spectrometer and processed on the 360/40.

The first step in the processing algorithm is to convert the peak centroid times into a list of masses. At this time the operator must identify six peaks down the spectrum. The computer then uses this information to calculate by interpolation the accurate masses of all the other peaks in the spectrum. The table below shows the mass measurement accuracy achieved when two reference peaks are 50 mass units apart. The data are from a copper spectrum where a total of 6 peaks were identified between m/e 209 and m/e 27. The reference peaks used were ^{209}Bi , ^{208}Pb , ^{120}Sn , ^{109}Ag , ^{61}Ni , and ^{27}Al . The accuracy of mass measurement is much better than the 0.1 amu required by the elemental analysis program described below.

<u>PEAK TIME</u>	<u>MEASURED MASS</u>	<u>PEAK AREA</u>	<u>ERROR</u>	
35620.74	108.910	81397		(AG 109) REFERENCE
36393.94	106.926	80505	+0.021	(AG 107)
37345.90	104.530	54827	+0.040	(BI 104.5)
37546.49	104.031	39770	+0.042	(PB 104)
37750.44	103.526	26147	+0.038	(FB 103.5)
37952.38	103.029	24233	+0.042	(FB 103)
53422.37	70.962	101321	+0.037	(GA 71)
54161.23	69.695	7422	+0.035	(BI 69.66)
54604.31	68.946	100071	+0.020	(GA 69)
55180.04	67.984	2806	+0.059	(ZN 68)
56416.63	65.960	25486	+0.034	(ZN 66)
57080.88	64.896	201346	-0.032	(CU 65)
57686.37	63.941	40421	+0.012	(ZN 64)
57960.82	63.512	1475	-	-
58341.06	62.922	259070	-0.008	(CU 63)
58637.82	62.466	1004	-	-
58758.61	62.281	1395	-	-
58990.44	61.928	12598	0	(NI 62)
59315.99	61.435	36928	-0.017	(SB 61.5)
59651.68	60.930	2430		(NI 61) REFERENCE

MASS MEASUREMENTS FROM MS702 SPARK SOURCE EXPONENTIAL SCAN

Elemental Analysis

The algorithm for identifying and calculating the concentration of each element is derived from the basic thought process which the chemist normally employs in interpreting a spark source mass spectrum. Rather than attempting to place an identification onto each peak in the spectrum each element is searched for in turn. Every element has its characteristic isotope and if a peak is present at this mass in the mass list then that element is assumed to be present and its concentration is assessed from the area of that peak relative to a previously specified internal standard. Figure 6 shows this process in block schematic form. Several checks are then made to confirm the identification.

The program is written so that the same type of routine can be used for each element. The basic data for all the elements from uranium to lithium (with the exception of the rare gases) is read sequentially during execution of the program; each element being printed as and when its characteristic isotope is found. This arrangement makes it easy for the operator to search for all elements or only for those he has specified.

BASIC OPERATIONS.

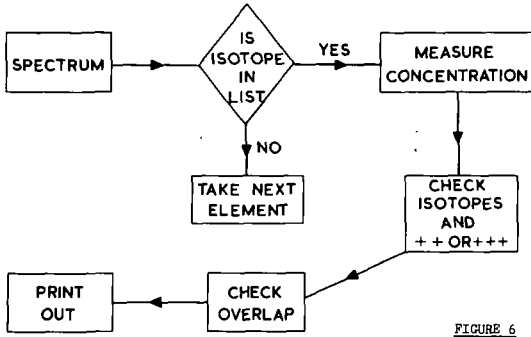


FIGURE 6

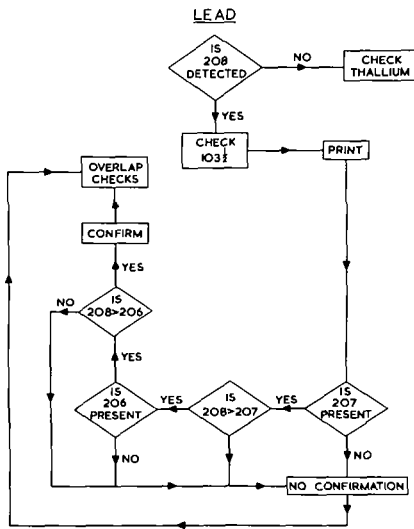


FIGURE 7

MANGANESE

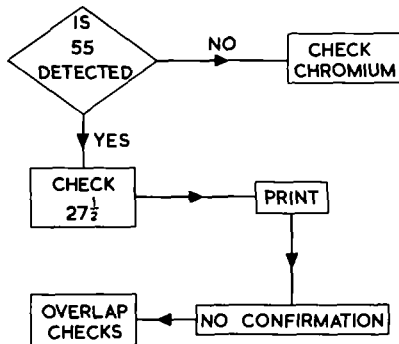


FIGURE 8

AEI-INORGANIC MASS SPECTRAL DATA ANALYSIS PROGRAMME-AEI

MASS	ELEMENT	PPM (AT)	M/CHARGED SPECTRUM	CONFIRMATION ISOTOPE	OVERLAP	COMPLEX IONS
209	BISMUTH	61.24	2+	NO		
208	LEAD	102.71	2+	YES		
121	ANTIMONY	84.82	2+	YES		
118	TIN	156.67	2+	YES		
115	IODINE	1.47	NO	NO		
107	SILVER	STANDARD				
103	RUBIDIUM	14.26	NO	NO	206(103)	
80	SELENIUM	1.55	NO	NO		
69	GALLIUM	102.10	2+	YES		CU OH (80)
66	ZINC	53.98	NO	NO		CU N (77)
63	COPPER	MATRIX				CU C (77)
60	NICKEL	88.43	NO	NO		
59	COBALT	12.60	NO	NO		
56	IRON	52.92	3+	YES		
55	MANGANESE	40.69	NO	NO		
52	CHROMIUM	69.70	NO	NO		
34	SULPHUR	90.36	NO	NO		
31	PHOSPHORUS	20.91	2+	NO		
28	SILICON	58.32	NO	NO		
27	ALUMINIUM	5.72	2+	NO		
					120(60)	
					122(61)	
					124(62)	
					118(59)	
					54(27)	

FIGURE 9

END OF RUN

For some elements (notably nickel), the isotope by which they are recognised is chosen only after a search for possible interference from other major isotopes. In the case of nickel m/e 58 is used as the characteristic isotope if Fe_{57} is absent, otherwise m/e 60 is used.

If the characteristic isotope is found in the spectrum, i.e. a peak is found in the mass list such that its mass is within a specified tolerance (± 0.1 amu) of the characteristic isotope, then the element name is printed, its concentration in ppm atomic is calculated and printed and the presence of the element is confirmed by looking for other relevant isotopes. If they are all found then their relative abundances are checked. Absolute agreement of relative abundance is not required since the accuracy of a single scan will not necessarily give such agreement. The actual criterion used depends on the element being analysed. Figure 7 shows the process for lead. Checks are also made for either doubly or triply charged peaks according to whichever element is being examined. S and Fe are examples where the triply charged spectrum is preferable to the doubly charged one in this respect. Figure 9 shows the print-out format - in this case for analysis of a copper sample. 'YES' is only printed under Confirmation Isotopes if all relevant isotopes are found in roughly the correct ratio. In the event of any doubt 'NO' is printed.

Overlap checks are then made of all higher mass peaks in the spectrum to see if doubly or triply charged ions of those elements would cause overlap with any of the relevant isotopes of the element under consideration. Checks are also made to see whether the more common polyatomic and complex ions involving the matrix element (identified separately by the operator), e.g. combinations of C, N, O and OH with the matrix would interfere with any of the isotopes used for the interpretation process. This is repeated for multiples of each matrix isotope up to a factor 4.

Figure 7 shows the interpretation process in more detail for lead. The characteristic isotope is m/e 208. If it is not found then the next element is looked for - in this case thallium. If it is found then doubly charged 207 is checked and this is followed by the series of rough checks on isotope abundance.

Figure 8 shows the process for a monoisotopic element, manganese. m/e 55 is the characteristic isotope, its doubly charged peak is checked but clearly no isotope checks are possible.

Figure 9 shows the complete print out for the analysis of a copper sample. Silver was used as the internal standard. Bismuth, rhodium, cobalt, manganese etc. are unconfirmed because they are monoisotopic and the possibility of overlap from lead 206 is recognised in the case of rhodium. Selenium tentatively identified at mass 80 is unconfirmed and the entry in the complex ion column indicates that in reality m/e 80 is probably $CUOH$. Notice that since iron is present nickel has been assessed by the use of m/e 60. In this case there is clear indication of overlap from tin.

A total of 53 seconds computer time was required for the elemental interpretation process using the 360/40. The corresponding time using a small computer with teletype output might be 5 minutes.

Conclusion

The addition of computer processing and automatic spark control have brought the peak scanning method to the point where quantitative analysis of inorganic samples by spark source mass spectrometry can be made with reasonable precision (12% standard deviation) covering the entire range of elements in a single run and with a minimum of operator intervention and interpretation.

Acknowledgement

The authors wish to thank Dr. J.D. Waldron, Manager, AEI Scientific Apparatus Division for permission to publish this paper.

References

1. H.J. Svec, R.J. Conzemijs, International Mass Spectrometry Conference, Berlin Sept. 1967.
2. R.A. Bingham, R. Brown and P. Powers paper 210 Pittsburgh Conference on Analytical Chemistry and Applied Spectroscopy March 1968.
3. R.A. Bingham, P. Powers paper 111 ASTM E.14 Meeting Pittsburgh May 1968
4. R.A. Bingham (to be published).

Multiple Specimen Holder for the
Spark Source Mass Spectrometer

Lewis Fergason, John Dowdy and Emile Pierron

A multiple specimen pair holder has been built for the CEC 21-110 solid-state spark-source mass spectrometer. The design allows eight specimen pairs to be analyzed without venting the source region.¹

The efficiency of carbon, nitrogen, and oxygen determination in semiconductor materials has been increased by a factor of three or four because only one source conditioning for each set of eight specimens is required. A more consistent background, obtained by exposure of eight samples under similar conditions, results in more reliable comparisons of volatile element abundances.

The basic mechanism of the Bell and Howell single specimen holder has been retained with the exception of few alterations. The moveable specimen support rod has been replaced by a hollow tube. A one eighth inch rod, inserted through the hollow tube, actuates a Geneva like mechanism which permits selection of sample pairs.

Viton A "O" rings at each end of the tube form rotary vacuum seals. Differential pumping is applied to the seals. All degrees of freedom of movement of the original sample holder have been retained so that the selected electrodes can be aligned with reference to the entrance slit. Stainless steel drafting pens are used for specimen clamps.

No measureable cross contamination of impurities has been detected for levels up to 100 ppm. Higher impurity concentrations have not been investigated.

The machining operation, exclusive of the CEC parts used, cost about \$1,500.

1. Socha, A. J. and Willardson, U.S. A. F. 33(615)-2761, Project No. 7885, July, 1968.

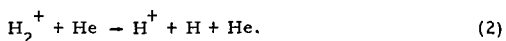
Photoionization Yields and Cross-Sections of H_2O and D_2O

R.E. Huffman, D.H. Katayama, and Capt. C.L. O'Bryan
Air Force Cambridge Research Laboratories (CAR), Bedford, Mass. 01730

The photoionization yield, total absorption cross-section, and photoionization cross-section have been measured for H_2O and D_2O over the wavelength range 580-1050Å. The Hopfield helium continuum was used as background, with a bandwidth of 0.5Å (0.0062 to 0.018 eV). The total ion current was measured using a parallel-plate ionization cell at the exit slit of a vacuum monochromator. The cell was calibrated with xenon. The ionization yields of D_2O and H_2O are approximately equal from the threshold near 983Å to 830Å, but toward shorter wavelengths the D_2O value is definitely larger in accordance with theoretical predictions for isotopically-substituted molecules. For example, at 795Å the D_2O yield is 0.88 and the H_2O yield is 0.80. A number of diffuse bands are observed. From the ionization cross-sections, it is apparent that some of these bands are not autoionized. This is confirmed by the neutral-product cross-section, which is the difference of the total and photoionization cross-sections. The results are in general agreement with the photoionization mass spectrometry and photoelectron spectroscopy results; however, the present measurements give the absolute cross-sections. The electron impact (electron energy loss) spectrum and the present results are in general agreement in the location of stronger diffuse bands. There is a difference in the relative intensities of the underlying continua. It is planned to submit this work for publication in the Journal of Chemical Physics.

A Study of Some Reactions of H_2^+ in Selected Vibrational States,* W. A.

Chupka, J. Berkowitz, and M. E. Russell, Argonne National Laboratory, Argonne, Illinois—Photoionization¹ with photons of narrow band width (0.14 Å) was used to produce H_2^+ ions in specific vibrational states from $v = 0$ to $v = 5$. The reactions of these ions with helium has been studied as a function of kinetic energy in the range 0–10 eV. The reactions studied were



Earlier work² had shown that reaction (1), which is endoergic by about 0.80 eV, occurs for H_2^+ ions with $v \geq 3$. The cross section at thermal kinetic energies increases rapidly with increasing vibrational excitation of the reactant ion. In the present study, the kinetic energy of the reactant ion was varied from 0 to 10 eV by varying the repeller voltage in the ionization chamber. Values of the phenomenological cross section Q were measured with high relative accuracy as a function of kinetic energy by a repetitive scanning technique which employs a multichannel scalar. Microscopic cross sections as a function of kinetic energy were then obtained from the data by use of the expression given by Light.³ The final results for H_2^+ with $v = 0$ and $v = 3$ are shown in Figs. 1 and 2. Similar curves have been obtained for H_2^+ in all vibrational states from 0 to 5, inclusive. The following conclusions are immediately apparent from the data. H_2^+ in any vibrational state will react according to both (1) and (2). The threshold for the reaction occurs at the calculated value, i. e., there is no evidence for excess activation energy. Even well above threshold the cross section for both reactions is strongly dependent on the vibrational energy of the H_2^+ ion. The form of the cross-section curves (e. g., Figs. 1 and 2) are very similar to the analogous curves calculated by Karplus *et al.*⁴ for the isoelectronic reaction



In order to assess the relative effectiveness of vibrational energy and kinetic energy in causing reaction (1) to occur, the cross sections for this reaction were displayed (Table I) for H_2^+ in the vibrational states with $v = 0-5$ and for total center-of-mass internal energy $E_t = 1.0, 2.0, 3.0,$ and 4.0 eV. The values shown have been corrected for the variation of the Langevin cross section—though this correction is very much less than the differences shown in the table. If vibrational and kinetic energy

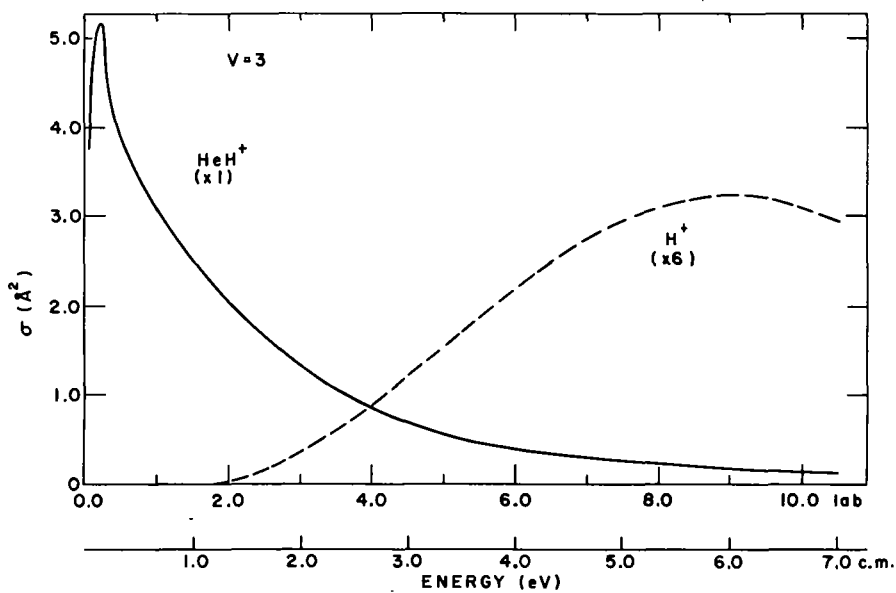
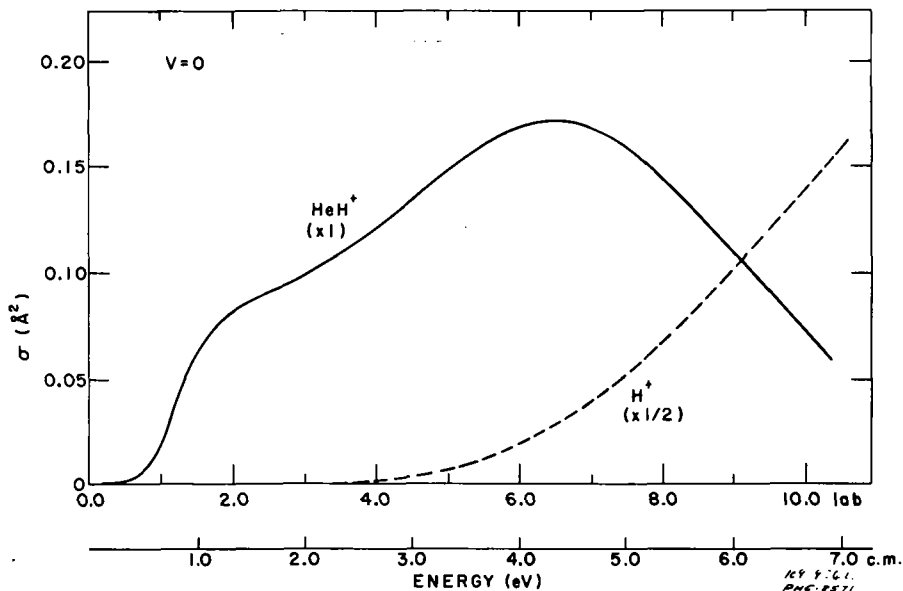
*Work performed under the auspices of the U. S. Atomic Energy Commission.

¹J. Berkowitz and W. A. Chupka, *J. Chem. Phys.* **45**, 1287 (1966); W. A. Chupka and J. Berkowitz, *J. Chem. Phys.* **47**, 2921 (1967).

²W. A. Chupka and M. E. Russell, *J. Chem. Phys.* **49**, 5426 (1968).

³J. C. Light, *J. Chem. Phys.* **41**, 586 (1964).

⁴M. Karplus, R. N. Porter, and R. D. Sharma **45**, 3871 (1966).



Figs. 1 and 2. Cross section vs. kinetic energy for reactions (1) and (2) using H_2^+ , $v = 0$ (top) and H_2^+ , $v = 3$ (bottom).

were equally effective in causing reaction, the values of cross section within each column would be equal. The large variation actually observed shows that vibrational energy is much more effective than translational energy in causing reaction (1). Part of this variation can be attributed to the large values of angular momentum associated with higher translational energies of reactant ions.

TABLE I. Cross section values for reaction (1) as a function of total energy content and vibrational quantum number.

v	Cross Section (\AA^2)			
	$E_t = 1.0 \text{ eV}$	$E_t = 2.0 \text{ eV}$	$E_t = 3.0 \text{ eV}$	$E_t = 4.0 \text{ eV}$
0	0.06	0.10	0.13	0.17
1	0.49	0.35	0.31	0.25
2	1.95	0.93	0.55	0.34
3	—	1.70	0.99	0.56
4	—	2.35	1.22	0.68
5	—	2.49	1.70	0.89

RECENT EXPERIMENTS IN PHOTOELECTRON SPECTROSCOPY

BY G.R. Branton, D.C. Frost, T. Makita*, C.A. McDowell and I. Stenhouse
The Department of Chemistry,
University of British Columbia,
Vancouver 8, B.C. Canada.

Abstract

Photoelectron spectroscopy has been shown to be a means of obtaining accurate information on molecular ionization potentials and the vibrational frequencies with which ions are formed. This data is of great use in the formulation of molecular orbital theories of electronic structure.

The design of a 180 degree spherical electrostatic spectrometer is described, with the photoelectron kinetic energy spectra for a variety of molecules. The resolution and sensitivity of the instrument have been enhanced by incorporating a 1000 channel Fabritek signal averager.

In many cases the spectra have been obtained not only with the usual helium 21.21 eV source, but also using gas discharges in argon (11.61, 11.82 eV doublet) and neon (16.65, 16.83 eV doublet).

Using the neon source the $O_2^+ X^2\Pi_g$ ground state ion spectrum consists of a vibrational progression of 21 members with at least two maxima. A tentative explanation involving a long-lived super-excited state of the neutral molecule is presented. High resolution spectra are given for C_2H_4 , C_2D_4 , NH_3 , ND_3 , PH_3 , C_2H_2 , C_2D_2 and several substituted acetylenes. The orbital energies and vibrational progressions derived from the spectra are compared and correlated with theory.

A description of the apparatus and the work on C_2H_4 and C_2D_4 has been submitted to the Journal of Chemical Physics and that on NH_3 and ND_3 to Chemical Physics Letters.

* Permanent Address: Department of Chemistry, Faculty of Science, Kyoto University,
Kyoto, Japan

Photoionization of Cesium Halides: Chemical Shift of Autoionization.*

J. Berkowitz, Argonne National Laboratory—Several autoionization peaks have been observed in the photoionization efficiency curves of the cesium halides, somewhat displaced in energy from their positions in atomic cesium. In particular, the $(5p)^6 6s \rightarrow (5p)^5 (6s)^2$ transition, which occurs at 12.306 eV in atomic cesium, is shifted to 12.1, 12.4, 12.5, and 12.6 eV for CsF, CsCl, CsBr, and CsI, respectively. These peaks are also present in the ionization efficiency curves of the dimer ions.

Siegbahn and collaborators¹ have proposed a modified free-ion model to predict the effect caused by various ligands on the binding energy of core electrons. This energy shift has the simple form

$$\Delta E = \left(\frac{1}{r} - \frac{1}{R} \right) q,$$

where (in this case) R is the internuclear distance of CsX, r is the radius of a 6s orbital in Cs, and q is one electron charge.

It is suggestive that the magnitude of the shifts observed, as well as the change of sign between CsF and the heavier cesium halides, is predicted by this equation. It should be borne in mind, however, that the equation purports to predict a change in one state whereas the autoionization peaks reflect a relative change in binding energy between the ground state and first excited state.

A detailed account of this work will appear in the *Journal of Chemical Physics*.

* Work performed under the auspices of the U. S. Atomic Energy Commission.

¹K. Siegbahn, C. Nordling, A. Fahlman, R. Nordberg, K. Hamrin, J. Hedman, G. Johansson, T. Bergmark, S.-E. Karlsson, I. Lindgren and B. Lindberg, *Electron Spectroscopy for Chemical Analysis; Atomic, Molecular and Solid State Structures Studied by Means of Electron Spectroscopy* (Almqvist and Wiksells Publishing Co., Stockholm, 1967).

Chemical Ionization Mass Spectroscopy Using a Modified Source with the MS-9

H. M. Fales,¹ G. W. A. Milne,¹ and Marvin Vestal²Section on Chemistry, Molecular Disease Branch, National Heart Institute, Bethesda, Md.¹
and Scientific Research Instruments Corporation, Baltimore, Md.²

The normal source and pumping system of the AEI-MS-9 spectrometer has been replaced by a source ‡ embodying a "closed" ion chamber equipped with a direct insertion probe and reactant gas inlet. The electron beam is admitted at 500 eV through a .013" hole and the ion exit slit is only .003" x .125"; all gas is exhausted through these exits to a housing pumped at 500 l/sec. Pressures of 1 mm of CH₄ were attained at 8 KV and the ion intensity-pressure relationships established by Field and Munson # were duplicated.

A variety of natural products including steroids, alkaloids, peptides, and sugars were studied using CH₄ as the reactant gas. In general, alkaloids such as ephedrine and O-methylpeltoline give abundant ions of mass (M + H) in the chemical ionization mode while giving negligibly small molecular ions under electron impact. Deoxyribose shows ions of mass (M + 1) - H₂, (M + 1) - H₂O, (M + 1) - 2H₂O, (M + 1) - 3H₂O. Cleavage at the C₂-C₃ bond also occurs. Alanyl valine gives intense ions corresponding to the alanyl and valine components; 17-ketoandrostande but not 3-cholestanone loses water with this reagent gas.

‡ Details available from Scientific Research Instruments, Baltimore, Md. 21207

F. H. Field, Accounts of Chemical Research, Vol. 1, American Chemical Society, Washington, D. C., 1968, p. 42.

Photoionization and Dissociation of Fluorine.*

Vernon H. Dibeler, James A. Walker, and K. E. McCulloch

Institute for Materials Research
 National Bureau of Standards
 Washington, D. C. 20234

Abstract

Photoionization yield curves from threshold to 600Å for the fluorine molecular and atomic ions, the latter produced both by dissociative ionization and ion-pair processes, have been obtained with a combined vacuum ultraviolet monochromator-mass spectrometer. The F_2^+ yield curve shows a very sharp onset at 15.69 ± 0.01 eV, preceded by a weak hot band, and followed by partially resolved autoionization peaks. The observed threshold for the process $F_2 + h\nu \rightarrow F^+ + F + e$, 18.76 ± 0.03 eV, is estimated to be not appreciably affected by hot bands. From this threshold is calculated the dissociation energy $D_0^0(F_2) = 1.34 \pm 0.03$ eV, or 30.9 ± 0.7 kcal mol⁻¹. Identical yield curves are observed for $^-F^+$ and F^- ions formed by the ion-pair process, but the adiabatic threshold is not observed for this spin-forbidden process.

The photoionization of hydrogen fluoride was studied in order to achieve a consistent set of values for $D_0^0(F_2)$, $D_0^0(H_2)$, $D_0^0(HF)$, and $\Delta H_f^0(HF)$. The HF^+ yield curve has a slightly tailing onset at 15.92 ± 0.01 eV. No $^0F^+$ ion is observed. The onset of dissociative ionization yielding H^+ occurs at 19.34 ± 0.03 eV. The corresponding dissociation energy is $D_0^0(HF) = 5.74 \pm 0.03$ eV. Results of the present study thus indicate that $\Delta H_f^0(HF) = 65.3 \pm 0.7$ kcal mol⁻¹, in agreement with accepted thermochemical values. Identical yield curves for H^+ and F^- formed by the ion-pair process have a threshold at 15.87 ± 0.02 eV, indicating that $EA(F) = 3.47$ eV.

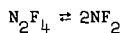
* Work supported in part by the U. S. Atomic Energy Commission.

Mass Spectrometric Study of the Photoionization of
Nitrogen Trifluoride and Trifluoroamine Oxide*

Vernon H. Dibeler and James A. Walker

National Bureau of Standards
Washington, D. C. 20234

Electron impact studies have been reported¹⁻⁴ for a number of nitrogen-fluorine molecules and ionization threshold data used to derive N-F and N-N bond dissociation energies. The thermodynamic values thus obtained are generally in fair agreement for several molecules, although the ordering of some N-F bond strengths is uncertain and rather broad limits of error must be assumed for some values. Furthermore, in the case of at least one molecule, tetrafluorohydrazine, the ambient temperature of the electron impact source affects the equilibrium



and results in ambiguous interpretation⁵ of the NF_2^+ ion yield of the molecule.

Recently, a new highly-stable nitrogen-fluorine molecule, trifluoroamine oxide, was discovered and produced independently by several research groups⁶ and a thorough investigation of its physical and chemical properties is in progress in at least one laboratory⁷. Elsewhere, a determination of the heat of formation of ONF_2 has been reported⁸ as the result of a high temperature and high pressure kinetics³ study. The value, $\Delta\text{Hf}^\circ(\text{ONF}_2) = -34.1 \pm 0.5 \text{ kcal mol}^{-1}$, suggests that the bond dissociation energy $D(\text{O}-\text{NF}_2)$ is considerably less than that of nitric oxide and is nearly the same as the first N-F bond in NF_3 . This is contrary to conclusions reached by Fox, et al.⁷.

Experimental Section

The photoionization yield curves and ionization threshold data were obtained by means of the combined vacuum ultraviolet monochromator and mass spectrometer described previously in some detail⁹. The means of sample introduction, the continuum photon sources, the photon and ion detection systems, and the probable uncertainties in measurements of the ion and photon intensities are essentially as reported in a preceding paper¹⁰.

The nitrogen trifluoride was a commercial sample of research-grade material obtained through Dr. G. T. Armstrong of the Thermochemistry Section. The trifluoroamine oxide was very kindly supplied by Dr. W. B. Fox of Allied Chemical Corporation, through Dr. Armstrong.

Results and Discussion

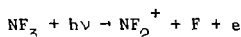
NF_3 -- The relative intensities of the positive ions in the mass spectrum of NF_3 produced by 584Å photons are given in Table I. No negative ions were observed and it is estimated that the relative abundance of any ion-pair process is less than 0.001. These data are consistent with the electron impact mass spectrum¹ obtained at 70 eV. The absence of N^+ and F^+ ions in the photoionization mass spectrum indicates that the thresholds for those ions must be greater than 21.22 eV, a conclusion that is also consistent with the published electron impact data.

The definite onset of the NF_3^+ ion occurs at 954Å (13.00 ± 0.02 eV). This agrees with the electron impact value^{1,2} of 13.2 ± 0.2 eV within the estimated uncertainty of that value. Apparently, no Rydberg series converging to an ionization limit of NF_3 has been reported. However, LaPaglia and Duncan¹¹ have obtained the ultraviolet absorption spectrum and observe a very strong absorption below 960Å. They ascribe that wavelength limit to the lowest ionization threshold of the molecule and our value of 954Å clearly supports their interpretation.

Two independent, careful determinations of the heat of formation of NF_3 have been reported recently¹², the results of which are in agreement within the experimental uncertainties. We have selected the value^{12b} obtained by the combustion of sulfur in NF_3 and, taking the enthalpy difference between zero and 298.15K for NF_3 as tabulated by Wagman, et al.¹³, we obtain $\Delta\text{Hf}^\circ(\text{NF}_3) = -30.38 \pm 0.20 \text{ kcal mol}^{-1}$ (-1,317₄ ± 0.008₇ eV). Adding the threshold energy of the NF_3^+ ion results in 11.68₃ ± 0.02 eV (269.4 ± 0.5 kcal mol⁻¹) for the heat of formation of the ion. Threshold energies and derived thermodynamic values for this and subsequently-treated ions are summarized in Table II.

* Supported in part by the U. S. Atomic Energy Commission. Condensed from a paper accepted for publication by Inorganic Chemistry.

The principal ion in the mass spectrum, NF_2^+ , exhibits a weak but definite onset at 878\AA (14.12 ± 0.01 eV). The ion-yield curve gives evidence of some step structure with intervals of about 8\AA (1000 cm^{-1}) in the wavelength region above 850\AA . The threshold at 14.12 eV is interpreted as the heat of reaction, ΔH_0 for the process



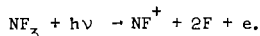
From the ΔH_0 and the heats of formation of NF_3 and F we can calculate the heat of formation of NF_2^+ . A recent study of the photoionization of fluorine¹⁴ has resulted in a new, more accurate value of $\Delta H_f^0(\text{F}) = 0.67 \pm 0.015$ eV (15.45 ± 0.35 kcal mol⁻¹).

This value, together with the heat of formation of NF_3 results in $\Delta H_f^0(\text{NF}_2^+) = 12.13 \pm 0.02$ eV (279.7 ± 0.5 kcal mol⁻¹). Walker^{13b} has combined second and third law evaluation of data on the thermal dissociation of N_2F_4 with a newly-derived value for the heat of formation of N_2F_4 to calculate $\Delta H_f^0(\text{NF}_2) = 8.5 \pm 2$ kcal mol⁻¹, or applying the enthalpy difference for temperature¹⁹, $\Delta H_f^0(\text{NF}_2) = 9.1 \pm 2$ kcal mol⁻¹. We combine the heats of formation of the ionized and neutral NF_2 species to redetermine $I(\text{NF}_2) = 11.73 \pm 0.09$ eV, or 270.6 ± 2 kcal mol⁻¹. Although more accurate, this is probably within the total range of previously reported electron impact values.

The new heat of formation of NF_2 also permits a more accurate calculation of the bond dissociation energy, $D_0(\text{NF}_2-\text{F}) \approx 2.39 \pm 0.09$ eV (55.1 ± 2 kcal mol⁻¹). Again, although more accurate, this is essentially in agreement with the results obtained by electron impact^{2,7b} and further improvement in derived values must await support from improved thermal or spectral data.

A second onset for NF_2^+ at 15.0 eV is difficult to interpret. Mader and Loughran¹⁵ observed an upward break about 0.7 eV above threshold in their electron impact ionization curve for NF_2^+ under experimental conditions which very likely produced NF_2 radicals from the N_2F_4 introduced into their ion source. Thus they suggested the possibility of an electronically-excited state of the NF_2^+ ion 0.7 eV above threshold. Assuming that our somewhat greater energy interval (0.9 eV) results from the more favorable means of determining the photoionization thresholds, the interpretation seems reasonable; particularly as there is no possibility of thermal decomposition in the present experiments and as no known excited state of the product fluorine atom exists within $100,000\text{ cm}^{-1}$ of the ground state. A low-lying singlet, excited state of the NF_2^+ ion would not be surprising.

The NF^+ ion curve exhibits a sharp rise at about 707\AA (17.54 ± 0.02 eV), shows some evidence for step structure in the region 700 to 675\AA , and possibly for unresolved autoionization in the region 675 to 600\AA . The photoionization threshold which is just outside of the reported range of electron impact values (17.9 ± 0.3 eV), is ascribed to ΔH_0 for the reaction



From observations on NF^+ from N_2F_4 reported by Herron and Dibeler², we assume $I(\text{NF}) \approx I(\text{NF}_2)$, and calculate $\Delta H_f^0(\text{NF}) \approx 3.2 \pm 0.2$ eV, or 74 ± 5 kcal mol⁻¹.

ONF₂: The relative intensities of the positive ions in the mass spectrum of trifluoramine oxide produced by 584\AA photons (21.22 eV) are listed in Table I. The two principal ions, NO^+ , and ONF_2^+ and the very weak molecule ion are consistent with the relative abundances in the 70 -V electron impact spectrum reported by Fox, et al.⁷. The higher energy of the latter spectrum produced additional fragment ions, including NF_2^+ . As indicated in the Experimental Section, our observation of NF_3^+ and NF_2^+ ions by photon impact is ascribed to impurity. No negative ions have been reported or observed here.

As the NO^+ ion provides a means of determining the heat of formation of the ONF_2 molecule, it is convenient to discuss first the results for that ion. The definite³ and rapidly-rising onset of the NO^+ ion of ONF_2 first appears at 815\AA (15.21 ± 0.02 eV). The curve exhibits some evidence for unresolved autoionization in the region 715 to 650\AA , and then a nearly constant yield to 600\AA . Aside from the questionable interpretation of autoionization, there is no evidence for thresholds of electronically-excited states of the ion and we can make no contribution to the recent discussions¹⁶ on that matter.

Assuming negligible excess energy in the process, the threshold is taken as the ΔH_0 for the reaction $\text{ONF}_2 + h\nu \rightarrow \text{NO}^+ + 3\text{F} + \text{e}$. The heat of formation of NO^+ is 234.8 kcal mol⁻¹, or 10.18 ± 0.01 eV. Thus we calculate $\Delta H_f^0(\text{ONF}_2) = -3.02 \pm 0.05$ eV (-69.6 ± 1.2 kcal mol⁻¹).

Compared with a dissociation energy of 63 kcal mol⁻¹ derived from the experimental results of Bougon, et al., our value indicates a much stronger O-N bond and is quite consistent with the observations by Fox, et al.⁷ on the relative chemical and thermal stabilities of the N-O and N-F bonds. On the other hand, King and Armstrong¹⁷ report preliminary calculations from a flame calorimeter study of ONF₃ resulting in $\Delta H_f(\text{ONF}_3) = -44.7$ kcal mol⁻¹. If this value is correct, the dissociative ionization process forming the NO⁺ ion must include about 1 eV of excess energy. There is no indication of that in the ion-yield curve.

The molecule ion (ONF₃⁺) has an abrupt onset at 935Å (13.26 ± 0.01). No other determination of the ionization energy has been reported. The $\Delta H_0 = 13.26$ eV for the reaction, ONF₃ + hν → ONF₃⁺ + e added to the heat of formation of the molecule results in $\Delta H_f^0(\text{ONF}_3^+) = 10.24 \pm 0.05$ eV, or 236.1 ± 1.2 kcal mol⁻¹. The summation of the appropriate heats of formation indicate that $D(\text{O-N}^+\text{F}_2) = 4.00$ eV or about 92 kcal mol⁻¹. Thus the O-N bond dissociation energies in the ion and the molecule are similar.

The ONF₂⁺ ion, the second principal ion of ONF₃, has a definite onset at 912Å (13.59 ± 0.01 eV). In the absence of excess energy³ in the dissociation process, the threshold is assumed to be $\Delta H_0 = 13.59$ eV for the process, ONF₃ + hν → ONF₂⁺ + F + e. The usual summation of heats of formation results in $\Delta H_f^0(\text{ONF}_2^+) = 9.90 \pm 0.05$ eV (228.3 ± 1.2 kcal mol⁻¹). Assuming the ionization energies of the ONF₂ and NF₂ radicals are approximately equal, we estimate a $\Delta H_f(\text{ONF}_2) = -1.8$ eV and, consequently, a bond dissociation energy $D(\text{ONF}_2 - \text{F}) = 1.9$ eV or 44 kcal mol⁻¹. Although speculative, this value is quite consistent with conclusions drawn and assumptions made in previous sections and with observations reported by Fox et al.⁷.

References

1. R. M. Reese and V. H. Dibeler, J. Chem. Phys., 24, 1175 (1956).
2. J. T. Herron and V. H. Dibeler, J. Res. NBS, 65A, 405 (1961).
3. C. B. Colburn and A. Kennedy, J. Am. Chem. Soc., 80, 5004 (1958).
4. E. D. Loughran and C. Mader, J. Chem. Phys., 32, 1578 (1960).
5. (a). C. B. Colburn and F. A. Johnson, J. Chem. Phys., 33, 1869 (1960).
(b). A. Kennedy and C. B. Colburn, J. Chem. Phys., 35, 1892 (1961).
6. (a). W. B. Fox, J. S. MacKenzie, N. Vanderkooi, B. Sukornick, C. A. Wamser, J. R. Holmes, R. E. Eibeck, and B. B. Stewart, J. Amer. Chem. Soc., 88, 2604 (1966).
(b) N. Bartlett, J. Passmore, and E. J. Wells, Chem. Commun. 1966, 213.
(c) E. C. Curtiss, D. Pilipovich, and W. H. Moberly, J. Chem. Phys., 46, 2904 (1967).
7. W. B. Fox, J. S. MacKenzie, E. R. McCarthy, J. R. Holmes, R. F. Stahl, and R. Juurik, Inorg. Chem., 7, 2064 (1968).
8. R. Bougon, J. Chatelet, J.-P. Desmoulin, and P. Plurien, C. R. Acad. Sci. Paris, 266C, 1761 (1968).
9. V. H. Dibeler and R. M. Reese, J. Res. NBS, 46A, 409 (1964).
10. V. H. Dibeler and J. A. Walker, Inorg. Chem. 8, 50 (1969).
11. S. R. LaPaglia and A. B. F. Duncan, J. Chem. Phys., 34, 1003 (1961).
12. (a). G. C. Sinke, J. Phys. Chem., 71, 359 (1967).
(b). L. C. Walker, *ibid.* p. 361.
13. D. D. Wagman, W. H. Evans, V. B. Parker, I. Halow, S. M. Bailey, and R. H. Schumm, NBS Tech. Note 270-3 (Jan. 1968).
14. V. H. Dibeler, J. A. Walker, and K. E. McCulloch, To be published in J. Chem. Phys. See also the preceding paper of this Conference.
15. See footnote No. 3, Reference 5.

References (Continued)

16. (a). H. Sjogren and I. Szabo, *Arkiv. Fys.*, **37**, 551 (1968).
 (b). K. P. Huber, *Can. J. Phys.*, **46**, 1691 (1968).
17. R. King and G. T. Armstrong, private communication.

Table I. Mass Spectra of Nitrogen Trifluoride and Trifluoramine Oxide by Photon Impact.

Molecule	Ion	Rel. Abundance ^{a/}
NF ₃	NF ₃ ⁺	0.29
	NF ₂ ⁺	1.00
	NF ⁺	0.21
ONF ₃	ONF ₃ ⁺	0.003
	ONF ₂ ⁺	1.00
	ON ⁺	0.55

^{a/} Measured at the 584Å helium resonance line (21.22 eV).

Table II. Summary of Threshold Energies and Thermodynamic Properties of Ions and Radicals from Nitrogen Trifluoride and Trifluoramine Oxide.

Ion Process	Threshold, eV	Thermodynamic Property
NF ₃ + hν → NF ₃ ⁺ + e	13.00 ± 0.02 ^{a/}	ΔHf ₀ ⁰ (NF ₃ ⁺) = 11.68 eV (269.4 kcal mol ⁻¹).
→ NF ₂ ⁺ + F + e	14.12 ± 0.01	ΔHf ₀ ⁰ (NF ₂ ⁺) = 12.13 eV (279.7 kcal mol ⁻¹).
		I(NF ₂) = 11.73 eV
	15.01 ± 0.02	ΔHf(NF ₂ * ⁺) = 13.02 eV (300.2 kcal mol ⁻¹).
→ NF ⁺ + 2F + e	17.54 ± 0.02	ΔHf ₀ ⁰ (NF ⁺) = 14.88 eV (343.1 kcal mol ⁻¹).
		I(NF) = 11.7 eV
ONF ₃ + hν → ONF ₃ ⁺ + e	13.26 ± 0.01	ΔHf ₀ ⁰ (ONF ₃ ⁺) = 10.24 eV (236.1 kcal mol ⁻¹).
→ ONF ₂ ⁺ + F + e	13.59 ± 0.01	ΔHf ₀ ⁰ (ONF ₂ ⁺) = 9.90 eV (228.3 kcal mol ⁻¹).
		ΔHf(ONF ₂) = -1.8 eV (-42 kcal mol ⁻¹).
		D(O-NF ₃) = 4.26 eV (98 kcal mol ⁻¹).
		D(ONF ₂ -F) = 1.9 eV (44 kcal mol ⁻¹).
→ NO ⁺ + 3F + e	15.21 ± 0.02	ΔHf ₀ ⁰ (ONF ₃) = -3.02 ± 0.05 eV (-69.6 ± 1.2 kcal mol ⁻¹).

^{a/} Estimated uncertainties.

MOLECULAR BEAM STUDIES USING A QUADRUPOLE MASS SPECTROMETER

T. C. Ehlert

Chemistry Department, Marquette University
Milwaukee, Wisconsin 53233

Introduction

A commercially available quadrupole mass spectrometer (1) has been adapted to the study of molecular beams originating in an effusion cell source. Although the total cost of the apparatus is less than one-third that of complete systems available commercially, performance characteristics are comparable. For example, it is possible to detect partial pressures in the cell as low as 10^{-12} atm and to determine ionization/appearance potentials to within a few tenths of a volt. In addition to the details of the adaptation described earlier (2), attempts have been made to sharpen ionization onset measurements, to lower noise levels and to define the ion discrimination properties of the quadrupole analyzer. An internal calibration has been devised which permits accurate determination of the absolute vapor pressure and its temperature dependence for low vapor pressure substances in a single experiment.

Description of Work

As others have reported (3) there appears to be a very large spread in energy in the ionizing electron beam even though the electron energy power supply is regulated to better than 0.02 volts. Although it is possible that this is due to field penetration it seems more likely that the wide beam entrance slit and high filament temperature used in order to achieve high sensitivity are the causes. We have been able to obtain quite satisfactory appearance potential curves by halving the width of this slit to prevent entrance of electrons from the extremes of the filament potential and by using a thoriated tungsten filament operated at significantly lower temperatures thus reducing the voltage drop across the filament and narrowing the Boltzmann distribution of energies. For example, Mn^+ from $Mn(g)$ was found to appear at 7.4 ± 0.2 eV (7.43 eV accepted value) with the energy scale calibrated on the ionization potential of O_2 . The data also clearly showed the contributions of the 5D states of Mn^+ appearing at 9.1 eV.

Considerable effort was devoted to reducing the output noise levels in order to increase the dynamic range of the instrument, a very important consideration for thermodynamic studies. Signal routing switches were eliminated, detector output leads were shortened and stiffened, and the multiplier dark current was lowered to about 20 cpm by baking in oxygen (4) and then in vacuum at $400^\circ C$. However, with the ionizer and the analyzer also turned on one finds about 10^{-10} amperes of noise consisting of random pulses throughout the spectrum. Possible sources peculiar to the quadrupole and/or the in-line ionizer-analyzer-detector geometry used here include a) photons emitted by metastables, b) unfiltered ions, and c) photons resulting from collisions of ions with the analyzer rods. Because of this it is at the present time necessary to use current suppression techniques in order to measure very small ion currents.

It has long been recognized that the efficiency of ion transmission by a quadrupole analyzer drops considerably with increasing ion mass to charge ratio. The nature of this form of discrimination must be known if one wishes to normalize ion current data as in fragmentation pattern work to those obtained with nondiscriminating analyzers or to make partial pressure measurements without laboriously calibrating the entire system for each gas. A technique has been devised which gives the relative transmission efficiency of any discriminating analyzer under actual operating conditions (5). Essentially the method consists of comparison of measured and known isotope abundances in order to determine the slope of the transmission - m/e function. We have found that the transmission is a non-linear function of m/e which initially increases then decreases nearly one hundred fold as the spectrum is scanned upward in m/e (by scanning the RF voltage in our instrument). The initial increase appears to be a result of non-linearity in the RF detection circuit and may be compensated for by an electronic bias in the circuit so as to increase the transmission for low m/e ions (6).

The decreasing transmission efficiency for heavy ions appears to be due to fringe field effects at the entrance to the quadrupole analyzer. Two means of increasing the transmission for heavy ions are to a) use a segmented rod structure so as to expose the ions to the RF fields before the combined RF/DC fields (7) or b) reduce the time spent in the fringing fields by a suitable combination of slits and bias on the

quadrupole structure (8). The transmission efficiency can also be determined by comparing a large number of organic fragmentation patterns with literature values, however this method is very time-consuming and inaccurate due to the considerable variation in reported patterns.

The apparatus described has been applied to studies of the MnF_3 - graphite reaction (9); the sublimation of manganese (10); and the vaporization of magnesium, calcium, magnesium hydride and calcium hydride (2).

In order to improve the accuracy of vapor pressure data and the temperature dependence thereof obtained by the effusion method and monitored mass spectrometrically we have devised an internal calibration method which provides all the necessary data without recourse to a silver calibration as is often done. A semi-continuous record is made of time, the vaporizing sample's temperature, and the observed ion current. The total weight loss is determined experimentally and then the $P = kIT$ (11) and effusion equations are solved by successive approximations to find the unique value of the constant k . Additional details of this method are available (10).

References

- (1) Series 250, Electronic Associates, Inc., Palo Alto, Calif.
- (2) T. C. Ehlert, R. M. Hilmer and Sr. E. A. Beauchamp, *J. Inorg. Nucl. Chem.* 31, 3112 (1969).
- (3) H. Bloom, J. W. Hastie and J. D. Morrison, *J. Phys. Chem.* 72, 3041 (1968).
- (4) J. R. Young, *Rev. Sci. Instr.* 37, 1414 (1966).
- (5) T. C. Ehlert, submitted to *Rev. Sci. Instr.*
- (6) G. Nelson, Electronic Associates, Inc., Palo Alto, Calif., private communication.
- (7) W. Brubaker, in ADVANCES IN MASS SPECTROMETRY, Vol. 4, E. Kendrick, editor, Elsevier Publishing Co., New York (1968).
- (8) R. Lehotsky, Aerospace Systems, Pomona, Calif. 91767, private communication.
- (9) T. C. Ehlert, *J. Phys. Chem.* 73, 949 (1969).
- (10) T. C. Ehlert, accepted by *J. Inorg. Nucl. Chem.*
- (11) W. A. Chupka and M. G. Inghram, *J. Chem. Phys.* 21, 371 (1953).

THE DISSOCIATION ENERGY AND IONIZATION
POTENTIAL OF SILICON MONOXIDE

by

Donald L. Hildenbrand
Advanced Research Laboratory, McDonnell-
Douglas Corp., Huntington Beach, Calif. 92646

and

Edmond Murad
Air Force Cambridge Research Laboratories (OAR)
L. G. Hanscom Field, Bedford, Mass. 01730

ABSTRACT

The dissociation energy of SiO(g) has been determined mass spectrometrically by measuring the heat of reaction of the isomolecular equilibrium $\text{Ge(g)} + \text{SiO(g)} = \text{GeO(g)} + \text{Si(g)}$. Third law calculations lead to $\Delta H_{298} = 26.6 \pm 2$ kcal/mole for the reaction, which leads to a $D_0^\circ[\text{SiO(g)}] = 182.8 \pm 3$ kcal/mole or 7.93 ± 0.13 eV. The ionization potentials of SiO and GeO were measured and found to be 11.6 ± 0.2 eV and 11.5 ± 0.5 eV, respectively. From the measured $D_0^\circ(\text{SiO})$, $\text{IP}(\text{SiO})$ and $\text{IP}(\text{Si}) = 8.15$ eV, a value of 4.5 ± 0.2 eV is derived for $D_0^\circ(\text{SiO}^+)$. From the known $D_0^\circ(\text{GeO}) = 6.77 \pm 0.8$ eV, the measured $\text{IP}(\text{GeO})$ and $\text{IP}(\text{Ge}) = 7.88$ eV, a value of 3.2 ± 0.5 eV is derived for $D_0^\circ(\text{GeO}^+)$.

NOTE: A detailed paper on the subject of this abstract is scheduled to appear in The Journal of Chemical Physics (probably 15 July 1969).

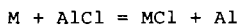
Dissociation Energies of the Group IIA Metal Chlorides
from Equilibrium and Electron Impact Measurements

D. L. Hildenbrand

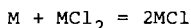
Douglas Advanced Research Laboratories
Huntington Beach, California 92647

Although the band spectra of the Group IIA monochlorides have been known for many years, the dissociation energies of these molecules are very uncertain. In the work reported here, high-temperature gaseous equilibria involving the mono- and dichlorides were studied by mass spectrometry, and the desired dissociation energies, along with information about the chemical bonding, were derived. In addition, the bond dissociation energy $D(\text{MCl}-\text{Cl})$ was obtained from electron impact threshold measurements, and the results were compared with the equilibrium data as an internal check.

Measurements were made with a 12" radius, 60° sector mass spectrometer equipped with a Nier-type electron bombardment source. Effusion beams containing the species of interest were generated by vaporizing the metal dichlorides in the presence of a reducing agent; neutral beam species emanating from the effusion oven were identified by means of appearance potential studies. From ion intensities measured a few volts above the respective ionization thresholds, equilibrium constants were calculated for isomolecular gaseous reactions of the type



and



over a range of temperatures. Thermodynamic analysis then gave the reaction enthalpies and derived dissociation energies listed in Table I; primary reliance was placed on third law calculations since the molecular constants of all species are fairly well established. D_0° values obtained from the diatomic exchange reactions are felt to be more reliable than those obtained from the dihalide reactions, but the agreement is reasonable in all cases.

As a check on the equilibrium measurements, the $\text{MCl}^+/\text{MCl}_2$ fragment ion appearance potentials and the MCl vertical ionization potentials were measured with an estimated accuracy of ± 0.15 eV, and the bond dissociation energies $D(\text{MCl}-\text{Cl})$ were derived. Ionization efficiency curves were plotted automatically on an X-Y recorder and the thresholds evaluated by the extrapolated voltage difference method, using background Hg^+ or the M^+ parent ion signals as calibrants. The electron impact and equilibrium data are compared in Table II. Except for Ba, the agreement is within the combined experimental errors. Ion beam half-width measurements, however, give some indication of excess kinetic energy in the fragmentation process producing MCl^+ , especially for the heavier halides, and this may account for part of the discrepancy. All things considered, the comparison indicates that there are no serious systematic errors in the equilibrium data. This is particularly important since the mass spectrometric equilibrium method remains the most generally applicable method for obtaining dissociation energies of "high-temperature" molecules.

When compared with the predictions of the Rittner electrostatic model, the measured $D_0^\circ(\text{MCl})$ values show, as expected, that the degree of ionic character increases markedly in progressing from the lighter to the heavier monochlorides. Agreement between measured and calculated values of D_0° is good for BaCl , SrCl and CaCl , but the calculated values are increasingly too low on going to MgCl and BeCl . Further, the results show that dissociation energies inferred from the electronic band spectra (Birge-Spencer extrapolation) can be brought into accord with the equilibrium data if the degree of ionic-covalent character is considered. A full account of the work will be submitted to the Journal of Chemical Physics.

TABLE I
REACTION ENTHALPIES AND DISSOCIATION ENERGIES

<u>M</u>	<u>Reaction</u>	<u>ΔH_{298}^*, Kcal</u>	<u>$D_0^0(\text{MCl})^*$, Kcal</u>
Mg	Mg + AgCl = MgCl + Ag	-0.3	74.6
	Mg + CuCl = MgCl + Cu	14.1	75.6
	Mg + MgCl ₂ = 2MgCl	34.6	75.6
Ca	Ca + AlCl = CaCl + Al	24.1	94.2
	Ca + CaCl ₂ = 2CaCl	21.0	97.5
Sr	Sr + AlCl = SrCl + Al	22.5	95.9
	Sr + SrCl ₂ = 2SrCl	16.5	97.2
Ba	Ba + AlCl = BaCl + Al	13.4	105.0
	Ba + BaCl ₂ = 2BaCl	6.9	106.6

*all \pm 2 Kcal

TABLE II
COMPARISON OF EQUILIBRIUM AND ELECTRON-IMPACT
VALUES OF D(MCl-Cl)

<u>M</u>	<u>D(MCl-Cl), Kcal</u>	
	<u>Elec. Impact</u>	<u>Equil.</u>
Mg	112.1 \pm 4.6	110.0 \pm 3.0
Ca	116.2	115.8
Sr	119.9	112.5
Ba	122.2	112.3

High Density Effects Associated with
Pulse Vaporization in a Time-of-Flight
Mass Spectrometer*

Richard T. Meyer
Sandia Laboratories
Albuquerque, New Mexico 87115

INTRODUCTION

The techniques of capacitor-discharge resistive-heating and time-resolved mass spectrometry are being applied to high temperature Langmuir vaporization of solids.¹ Pulse heating releases large quantities of contaminant vapors from various refractory metal, metal oxide and carbon filaments. These high density vapors produce several perturbations upon the experimental measurements of vapor-density and surface temperature versus time. This paper describes the observation and understanding of these high density effects.

EXPERIMENTAL

A detailed description of the experimental methods has been published.¹ A Bendix time-of-flight mass spectrometer provided successive mass spectra of the evolved vapors at 50- μ sec intervals.² A resistive heating pulse of 400- μ sec duration was obtained from a high energy capacitor bank. Measurements of the energy dissipated in the sample as a function of time were obtained from oscilloscope records of current and voltage waveforms. Surface temperature measurements were made with photomultipliers (RCA 8645 with 6500A interference filter). The samples were located within a few millimeters of the ionization zone of the mass spectrometer. The sample materials included wires of Ag, Mo, Zr, Ti, Ta, W, Hf, commercially prepared from high purity, zone-refined raw stocks, and spectroscopic grade graphite rod.

RESULTS AND DISCUSSION

Contaminant Vapor Release - Time resolved mass spectral records revealed that large quantities of hydrocarbons and hydrocarbon decomposition products were released when most solid samples were resistively pulse heated from 300°K to just below the melting points. The contaminant vapors dominated the mass spectra from mass 12 through about mass 200. The individual ion intensities due to the contaminants all equaled or exceeded those due to the background gases (e.g., N₂, O₂) and those due to the vapor of the metal sample. The contaminant spectra persisted for many milliseconds as the sample cooled by radiative energy loss. As the maximum temperature achieved was increased by increasing the input energy pulse, the higher masses diminished and the lower masses increased in relative abundance. This result appears to correspond to thermal decomposition of the higher molecular weight contaminants. Graphite rod produced a high abundance of H₂, CO and CO₂ as well as other hydrocarbon masses.

In most pulse heatings, the amount of contaminant released was proportional to the average temperature of the sample; in some experiments, however, it appeared that localized hot spots developed which released larger quantities of vapor and produced a melting of the sample.

Mass Spectrometer Interferences - The quantity of contaminant released with some pulse heatings caused perturbations to the spectrometer operation. A major effect was a transient increase in the time-of-flight of the ions from the ion source to the electron multiplier. This apparently resulted when the number density of ions produced in the ionization zone was large enough to overload the ion gun power supply, which temporarily decreased the ion accelerating voltages. In some instances, dense pockets of vapor were rapidly released during the pulse heating cycle; the overloading of the ion source was severe enough to render the spectrometer inoperable for several milliseconds.

*This work was supported by the United States Atomic Energy Commission.

Another interference was a transient diminution of spectrometer sensitivity. This perturbation resulted from saturation of the electron multiplier and from scattering of ions in collisions with neutrals in the flight tube.

The time dependent behavior of these various spectrometer responses correlated roughly with the expansion of a cloud of contaminant vapor from the sample surface to the ionization zone and into the flight tube, followed by cryogenic pumping of the spectrometer volume to normal vacuum.

Energy Dissipation in Gaseous Discharge - A consequence of the release of a high density cloud of contaminant vapor during a resistive heating pulse was that electrical arcing through the vapor occurred. The arcing was definitely attributable to the heating pulse of energy and was not associated with the operation of the mass spectrometer. Independent evidence substantiating these conclusions consisted of current and voltage waveforms, photomultiplier records and visual observations obtained for samples located in a separate high vacuum chamber as well as in the spectrometer ion source.

The current and voltage waveforms for a Ta sample which was pulse heated in the spectrometer showed discontinuities at the same point in time that the spectrometer interference occurred. The voltage decreased and the current increased rapidly; both effects correlate with a decreased resistance path which is characteristic of a gaseous discharge.

Arcing for a Ti sample, pulse heated in a high vacuum chamber, was identified by a ringing of the current waveform through several half cycles of discharge; normally, the energy was discharged completely in one half cycle. The formation of the gaseous discharge decreased the circuit resistance and converted the system from an overdamped to an underdamped LCR circuit.

Photomultiplier records of graphite rods showed various degrees of energy dissipation between the solid and the gaseous discharge. Visual observations indicated an incense blue emission when arcing occurred; the emission may have been associated in part with excited C_2 species,³ since C_3 vapor was positively identified in the mass spectrometer measurements.

Time Delayed Response of Photomultiplier to Surface Temperature - Graphite samples could be sufficiently outgassed by successive pulse and dc heatings in order to prevent the occurrence of gaseous discharges. However, photomultiplier records continued to show a delay to the maximum intensity of about 200 μ sec after the end of the input pulse of electrical energy. Hafnium wires, on the other hand, provided photomultiplier records of the surface radiation which peaked precisely at the termination of the energy pulse (total duration equaled 400 μ sec). It was concluded that contaminant vapor, carbon vapor, carbon particles or a combination of vapors and particles was creating an opaque cloud surrounding the graphite sample; this opaque cloud diminished and delayed the photomultiplier response to the surface radiation until the cloud expanded to a sufficiently low density so as to interfere no longer with the optical path. Tveekrem has reported a similar pyrometry error due to soot formation from high temperature graphite.⁴

Origin and Cleanup of Contaminants - Evidence exists that the hydrocarbon contaminant vapor arose both from the surface and the bulk volume of the samples. DC heating of a refractory metal wire or a graphite rod at 1000 to 1500°K in high vacuum (10^{-7} torr) did provide some outgassing of a sample; but when a pulsed current was superimposed on the dc level to raise the sample to a higher temperature, larger amounts of contaminant were released. Successive pulse heatings diminished the amount released per pulse, but a minimum was achieved after only a few pulses. The addition of a liquid N_2 cooled surface surrounding the sample greatly enhanced the cleanup procedure. It not only provided a higher ultimate vacuum, hence a cleaner sample surface, but also trapped a large fraction of the desorbed condensable vapors before readsorption on the sample could occur.

Quantitative measurements on vapors evolved from graphite samples showed numbers of molecules comparable to the impurity specifications. A fresh graphite rod, 0.25 mm diameter by 10 mm long, was found to release enough contaminant vapor, during a single pulse heating to about 2300°K,

to raise the pressure of a 1.5 liter volume from 2×10^{-7} torr to about 1×10^{-4} torr. In such cases, the instantaneous vapor pressure surrounding the sample was apparently great enough to cause a gaseous discharge.

CONCLUSIONS

High purity refractory materials in fabricated forms contain hydrocarbon contaminants in sufficient quantity to interfere with quantitative measurements of the vaporization properties when the material is resistively heated to high temperatures by a capacitor discharge energy pulse. The high density cloud of contaminant vapor can cause mass spectrometer interferences, energy dissipation in gaseous discharges, and, in the case of graphite samples, time delays and radiation intensity errors in the measurement of surface temperatures with photomultipliers. Possible ways of circumventing these problems include extended high temperature outgassing of the samples in a very high vacuum chamber, utilization of high purity single crystals, and localized vaporization with laser beams.

REFERENCES

1. R. T. Meyer and L. L. Ames, in "Mass Spectrometry in Inorganic Chemistry" (J. L. Margrave, editor) pp. 301-324, American Chemical Society, Washington D.C., 1968.
2. R. T. Meyer, J. Sci. Instr., 44, 422 (1967).
3. G. Herzberg, "Molecular Spectra and Molecular Structure III. Electronic Spectra and Electronic Structure of Polyatomic Molecules," p. 591, D. Van Nostrand Company, Inc., Princeton, N.J., 1966.
4. J. O. Tveekrem, J. Chem. Phys., 49, 2878 (1968).

A Mass Spectrometric Study of the Positive
and Negative Ions from Carbon Vapors*

C. Herndon Williams
Sandia Laboratories
Albuquerque, New Mexico 87115

The purpose of this work was to investigate the electron-molecule interactions in the carbon vapor system producing both positive and negative ions. The ion yield for 0 - 30 eV electrons was measured for each species (C_1^+ , C_2^+ , C_3^+ and C_2^-) and used to determine the ionization-fragmentation energetics (ionization potentials, appearance potentials and electron affinity).

The electron-molecule collisions took place in the ion source of a Bendix Model 3015 mass spectrometer, with the molecular beam, electron beam and ion beam mutually orthogonal to each other. The carbon molecular beam was obtained from a Knudsen cell, consisting of a resistively heated tantalum tube with a 1-mm orifice in the side wall. A temperature of $3000 \pm 100^\circ\text{K}$ was used to produce $C_1(g)$, $C_2(g)$ and $C_3(g)$ from pyrolytic graphite powder and $C_1(g)$ from TaC powder. The molecular beam was defined by two sets of slits and manually interrupted by a shutter to distinguish condensable species from the residual gases.

The ion yield curves exhibited a number of linear regions interspersed with upward "breaks", indicating ionization by different processes. For C_1^+ , breaks were observed at 18.4, 19.8 and 21.4 eV (± 0.2 eV); the two lower breaks are associated with fragmentation of $C_2(g)$ and $C_3(g)$, respectively. For C_2^+ , breaks were seen at 19.9 and 22.8 eV (± 0.2 eV); the first break is the threshold for the fragmentation of $C_3(g)$ to give C_2^+ . For C_3^+ , the ion yield curve had breaks at 13.9 (± 0.3 eV) and 17.4 (± 0.2 eV), neither of which should be associated with fragmentation since C_4^+ and C_5^+ were $< 1\%$ of C_3^+ . These and the upper breaks in the C_1^+ and C_2^+ curves are currently not identified, but may be associated with ionization into excited electronic states.

The semi-log method for measuring appearance potentials was used, with Xe^+ as reference for all of the positive carbon ions. Results are given in Table I and compared with literature values.

The negative ion C_2^- was seen in appreciable intensity in the electron impact spectra, and C_1^- about two orders of magnitude lower in intensity. Ion yield measurements indicate that these ions are formed by the dissociative attachment of a electron to $C_3(g)$. The appearance potential of the C_2^- was determined to be 5 ± 0.7 eV, yielding an electron affinity for $C_2(g)$ of 3 ± 0.7 eV, assuming that there is negligible kinetic energy and electronic excitation energy in the products of the dissociative attachment: $C_2 + C$. These measured values are compared with literature values in Table I.

*This work was supported by the United States Atomic Energy Commission.

TABLE I.

SPECIES	APPEARANCE POTENTIAL (AP) or ELECTRON AFFINITY (EA)	
	Literature	This Work
Ag ⁺	AP 7.574 eV (a)	Used as a Standard
Hg ⁺	AP 10.43 eV (a)	"
Xe ⁺	AP 12.127 eV (a)	"
SF ₆ ⁻	AP <0.1 eV (b)	"
SF ₅ ⁻	AP 0.1 eV (b)	"
C ₁ ⁺	AP 11.3 ± 0.2 eV (c)	AP 11.35 ± 0.15 eV from C ₁ (g)
	AP 11.256 eV (a)	AP 11.30 ± 0.15 eV from C _n (g)
C ₂ ⁺	AP 12.0 ± 0.6 eV (c)	AP 12.00 ± 0.15 eV from C _n (g)
C ₃ ⁺	AP 12.6 ± 0.6 eV (c)	AP 12.25 ± 0.15 eV from C _n (g)
C ₁ ⁻	EA 1.25 ± 0.03 eV (d)	
C ₂ ⁻	EA 4.0 eV (e)	AP 5.0 ± 0.7 eV
	EA 3.1 eV (e)	EA 3.0 ± 0.7 eV
C ₃ ⁻	EA 2.5 eV (e)	
	EA 1.8 eV (e)	

- a) R. W. Kiser, Introduction to Mass Spectrometry and Its Applications, Prentice-Hall, Inc., N. J., (1965) p. 302 ff.
 b) W. M. Hickam and R. E. Fox, J. Chem Phys. 25, 642 (1956).
 c) J. Drowart, R. P. Burns, G. DeMaria and M. G. Inghram, J. Chem. Phys. 31, 1131 (1959).
 d) M. L. Seman and L. M. Branscomb, Phys. Rev. 125, 1602 (1962).
 e) R. E. Honig, J. Chem. Phys. 22, 126 (1954).

A MASS SPECTROMETRIC STUDY OF HIGH TEMPERATURE SPECIES IN THE W-O-I SYSTEM

By

Suresh K. Gupta

Lamp Research Laboratory, General Electric Co., Nela Park, Cleveland, Ohio 44112

Abstract

An examination of the evaporation behavior of solid WO_2I_2 and the reaction of gaseous I_2 with condensed WO_2 has been conducted by mass spectrometric and Knudsen effusion techniques. I_2 , WO_2I_2 , and WOI_3 in order of decreasing partial pressures have been established as the vapor species over solid WO_2I_2 by the appearance potentials and temperature dependence measurements. Minor quantities of atomic iodine as an additional species in the cell arise from the dissociation of molecular iodine. The observed strong orifice dependence of I_2 pressures over solid WO_2I_2 in a Knudsen cell has led to an estimate of 10^{-6} for the condensation coefficient for iodine. WOI_3 is present to only about 0.1% of the WO_2I_2 pressures at $500^\circ K$.

The mass spectrometrically determined enthalpy of WO_2I_2 sublimation is 45.2 ± 1.0 kcal/mole at $298^\circ K$. For the enthalpy of the dissociation of solid WO_2I_2 to $I_2(g)$, a value of 40 ± 3 kcal/mole at $550^\circ K$ is obtained by the mass spectrometric and effusion measurements. The decomposition reaction has been assumed as:
 $2WO_2I_2(s) = 2WO_2I(s) + I_2(g)$ on the basis of the reported existence of condensed WO_2I phase, and the heat of formation of solid WO_2I is derived as -136 ± 5 kcal/mole at $550^\circ K$. The present data suggest that $WO_2I(s)$ is only a transient species which further dissociates to the stabler $WO_2(s)$ phase.

The equilibrium data for the reaction: $WO_2(s) + I_2(g) = WO_2I_2(g)$ have been treated by the second and third law methods, which yield -102.8 ± 2.0 kcal/mole and 90.1 ± 2.0 eu for the ΔH_f° and S° , respectively, of gaseous WO_2I_2 at $298^\circ K$.

Details will be published in the Journal of Physical Chemistry.

SPARK SOURCE MASS SPECTROMETRIC ANALYSIS
OF THE LUNAR SAMPLE

G. H. Morrison and A. T. Kashuba
Department of Chemistry
Cornell University
Ithaca, N.Y. 14850

Among the most important types of information desired from the lunar material to be returned by the Apollo Mission is the characterization of its chemical composition. The composition of the lunar surface reflects at least three major processes: chemical fractionations during accretion of the moon from the solar nebula, magmatic differentiation, and infall of meteorites and cosmic dust. Thus, one can construct at least the major outlines of the chemical history of a lunar sample from a study of its trace element abundance pattern.

The Lunar Sample Analysis Program of NASA has included in its selection of essential experiments in the category "Chemical and Isotopic Analysis" all of the important presently available techniques for bulk compositional analysis. Of these, spark source mass spectrometry offers the possibility of the most complete survey of the elements present in a given limited sized sample.

Based on the results of the alpha scattering analysis of the top layer of the moon's surface at the landing sites of Surveyors V, VI, and VII, the chemical composition resembles that of terrestrial basalts. Consequently, a number of basaltic samples have been examined by spark source mass spectrometry and the capability of determining 60 elements in a given sample has been demonstrated. Special interference and/or insufficient limits of detection in this complex rock matrix prevents the determination of additional elements; however, those that can be determined include many of great potential geochemical interest.

The rock samples in powdered form were blended with spectrographic grade graphite or high purity silver powder and briquetted to form conducting self electrodes. A 60kv r.f. discharge between the electrode pairs resulted in volatilization and ionization of the sample constituents. A Nuclide GRAF - 2 spark source mass spectrograph was employed.

For accurate quantitative measurements to be made, a comparative standard must be employed to obtain elemental sensitivity factors to correct for differences in behavior of the various elements in a given matrix. Therefore, experiments have been run using the U.S.G.S. Diabase Standard W-1 as one possible standard for obtaining sensitivity factors. Another U.S.G.S. standard, BCR-1 Basalt, has also been analyzed and treated as an unknown in order to assess the capability of the spark source mass spectrometric method. Neutron activation analysis of these two samples has also been performed as a check on the validity of the results. At present the method results in a relative standard deviation of $\pm 5-25\%$ and an average accuracy of 10% for most elements, but experiments are in progress to improve this.

(This paper is to be submitted for publication in ANALYTICAL CHEMISTRY)

METEORITE DATING WITH THE INERT GASES

by

D. Heymann

Depts. of Geology and Space Science
Rice University
Houston, Texas

Several of the pioneering papers written on meteorite ages began on a hopeful note: that the study of meteorite chronology might in time lead to the complete understanding of the origin of these objects. Today, some 10-15 years later one has learned that meteorites are among the oldest rocks in the solar system; that it takes them from millions to billions of years to reach the Earth; but the question of their origin is still as elusive today as it was one decade ago.

My talk is about inert gases in meteorites and the related calculations of radiation ages and gas-retention ages. Together with Rb-Sr, Os-Ir, and Pb-Pb ages they still represent the most extensive information on solar system chronology. Soon lunar chronology will be added to meteorite chronology, and while the studies of the lunar samples may not resolve the question of meteorite origin, a new and exciting field will be opened for investigation.

Figure 1 shows the basic experimental apparatus used by most of the investigators. The meteorite samples, usually weighing several tens of milligrams are melted and outgassed in a vacuum-furnace which consists of a molybdenum crucible in a water-cooled glass enclosure. Temperatures greater than 1700°C are normally required. The crucible is induction- or resistance-heated. Induction heating has the advantage that the load coil is outside the vacuum, but considerable gas-loss may occur in case of a gas-discharge in the furnace.

The liberated gas contains impurities which must be removed; normally this is done with hot Ti or Pd-Ti getters, but more rigorous cleaning is sometimes required such as "cracking" of hydrocarbons on hot W filaments, the removal of H₂ through a hot Pd barrier, the oxydation of impurities with Cu-CuO.

One cannot admit all the inert gases together into the mass spectrometer. For example doubly ionized Ar⁴⁰ appears on mass-20 together with Ne²⁰. However, He and Ne can be admitted together; likewise Kr and Xe. In order to achieve the fractionation of the gases, Ar, Kr, and Xe are adsorbed on charcoal immersed in liquid N₂ while He and Ne are measured. Then Ar containing a small fraction of Kr is released at about -120°C. Finally, the remainder of Kr and Xe are liberated at or slightly above room temperature.

The mass spectrometer which I use is a 4.5 inch radius 60° sector typed with Nier-source. The ion beam can be detected either on a Faraday cup or on a nine-stage secondary electron multiplier. Because of the extremely small quantities of gas available, typically some 10⁻⁶ ccSTP or less, the spectrometer is operated in the static mode, that is to say: the gas flows from the extraction line directly into the ion source through a tube several mm. wide, while the valve between the spectrometer and the pump remains closed. The scanning is magnetic and the read-out is on chart paper.

Normal operating conditions of the spectrometer and typical sensitivities are listed in Table 1. The sensitivity of the instrument is checked in each experiment by calibration with carefully metered amounts of He³, He⁴, Ne, Ar, Kr, and Xe (the last four gases having atmospheric

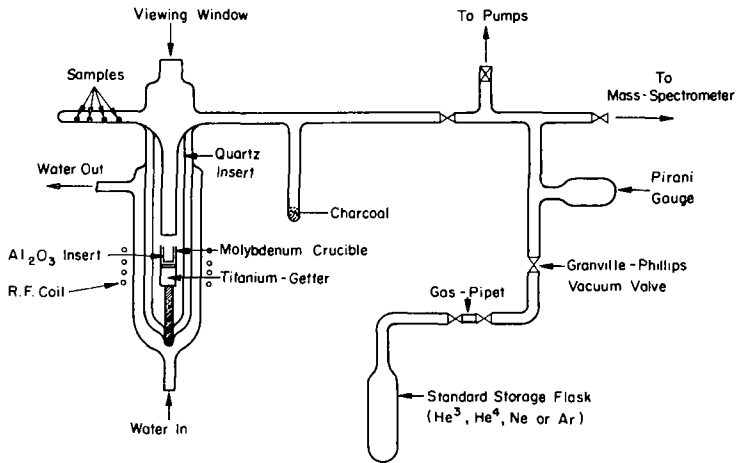


Fig. 1 Gas-extraction and purification line. The samples are dropped into the molybdenum crucible (the insert is used for iron meteorites), which is induction heated by an external load coil. The quartz insert protects the water-cooled enclosure.

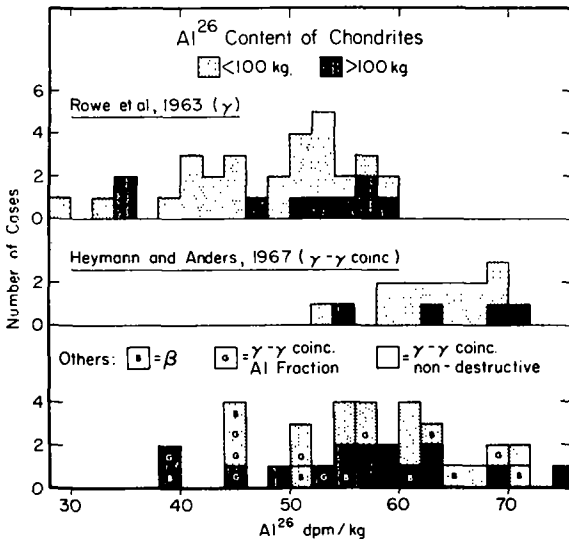


Fig. 2 Al^{26} contents of chondrites reproduced from Heymann and Anders (1967). The systematic difference between the γ - γ coincidence (middle) and the γ -counting results (top) is in part due to a "summing" effect in the γ -results which was not corrected. The γ - γ coincidence results range from about 50-75 dpm/kg.

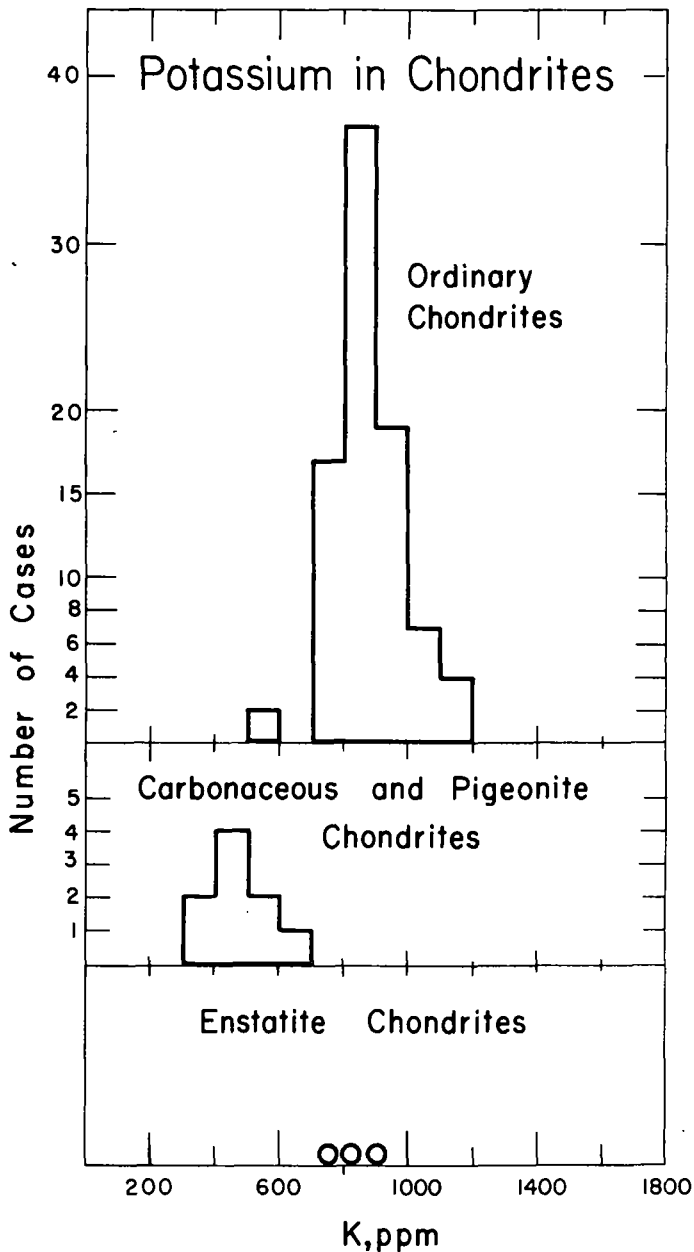


Fig. 3--Potassium contents of ordinary chondrites (top), carbonaceous chondrites (middle), and enstatite chondrites (bottom); data taken from the literature. Note that most of the ordinary chondrites have K between 700 and 1000 ppm.

composition). The gases are stored in containers of several liters which are connected with the spectrometer via all-metal gas pipettes of 0.08 cm³ volume. The "standards" can be admitted at any time during the experiment: before, during, or after the measurement of any sample gas.

I owe you a few remarks concerning precision and accuracy. Under normal operation conditions the precision is a few percent, occasionally one percent or better for isotope ratios of a given element. However, there are complications in the static-mode operation. He⁴ from the atmosphere diffuses through the glass envelope of the spectrometer at a rate of 10⁻⁹ ccSTP/min; memory from preceding samples can be a problem also. Incomplete gas-extraction or gas loss cannot always be detected. Generally speaking, the accuracy of the measurements should be better than 10% for absolute quantities when peak-ratio calibrations are made; possibly 5% or better for isotope dilution work, which is done by a number of investigators.

Let me now turn to the ages themselves. Table 2 shows gas contents of four representative meteorites. The inert gases in the iron meteorite Grant are almost wholly cosmogenic, i.e. cosmic ray produced. The diagnostic features are: He⁴/He³~4; Ne²⁰/Ne²¹/Ne²²~1:1:1; Ar³⁸/Ar³⁶~1.6; He³/Ne²¹~80; and He³/Ar³⁸~15. These gases were produced in situ when the meteorite was exposed to cosmic rays in space. Cosmic-rays also produce radioactive species such as H³, C¹⁴, Al²⁶, Cl³⁶, Ar³⁷, and Ar³⁹. Because the radiation age is known to be much greater than the longest half-life, 0.7 m.y. for Al²⁶, the radioactivities listed above are in secular equilibrium with the radiation at the time of fall of the meteorite. Hence, their specific activities at the time of fall are equal to the average production rate during the last several half-lives, i.e. for Al²⁶ during the last few million years. The stable inert-gas nuclides on the other hand represent the time-integrated radiation rate. In order then to find the radiation age one must know at least one relative production yield σ stable/ σ radioactive. Such relative yields have been obtained by accelerator simulated proton bombardment on targets of appropriate composition.

The basic assumptions that one makes are the following:

- Before time t=0 the meteorite was effectively shielded against cosmic rays on its parent body; no cosmogenic nuclides were formed.
- After the departure of the meteorite from its parent body, its size remained unchanged; and the meteorite was a closed system for the inert gases.
- Exposure to high-energy radiation terminated when the meteorite collided with the Earth; the meteorite remained a closed system.

Every one of these assumptions has been questioned from time-to-time; however, I shall use them now as a working hypothesis.

The next meteorite, Bruderheim, contains substantial amounts of O (~37% by weight), Si (~19%), Mg (~15%) and significant amounts of S (~2%), Ca (~1.5%), and Al (~1.5%) besides Fe (~15%). Yet the effect on the cosmogenic part of the gases is only slight: He⁴/He³~5; Ne²⁰/Ne²¹/Ne²²~1:1:1 and Ar³⁸/Ar³⁶~1.5. The effect of Mg, Si, and Al is seen in He³/Ne²¹~5 and the effect of the decreased content of nuclides A>30 is seen in He³/Ar³⁸~35.

Actually, the measured ratios are not the same as the cosmogenic ones, because Bruderheim contains substantial amounts of radiogenic He⁴ and Ar⁴⁰ which have arisen from the decay in situ of U, Th, and K. The observed Ar³⁸/Ar³⁶ ratio is unity because of the presence of a small amount of trapped Ar with Ar³⁸/Ar³⁶=0.19.

Radiation ages can be calculated for stony meteorites in the same manner as for iron meteorites. However, stony meteorites weigh generally

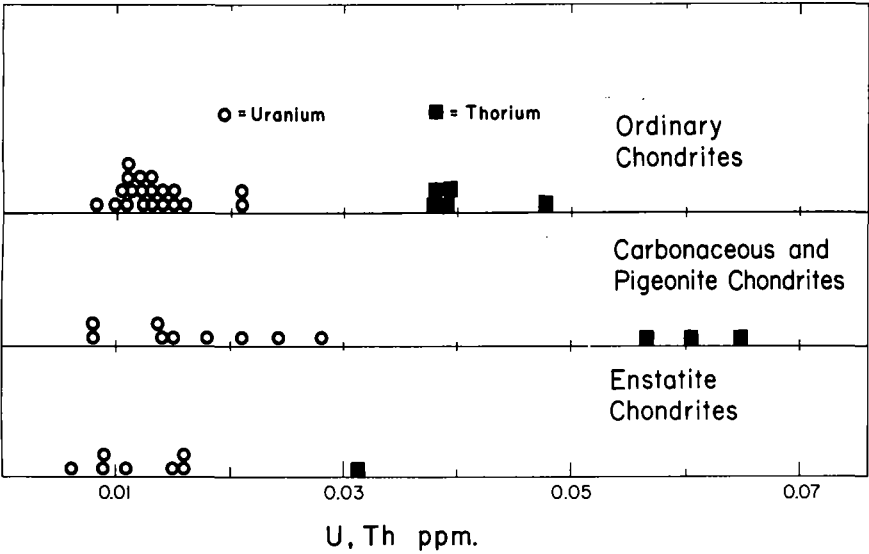


Fig. 4 U and Th contents of chondrites; data taken from the literature. U: open circles; Th: closed circles. Most of the U-values lie between <0.01 and 0.015 ppm.

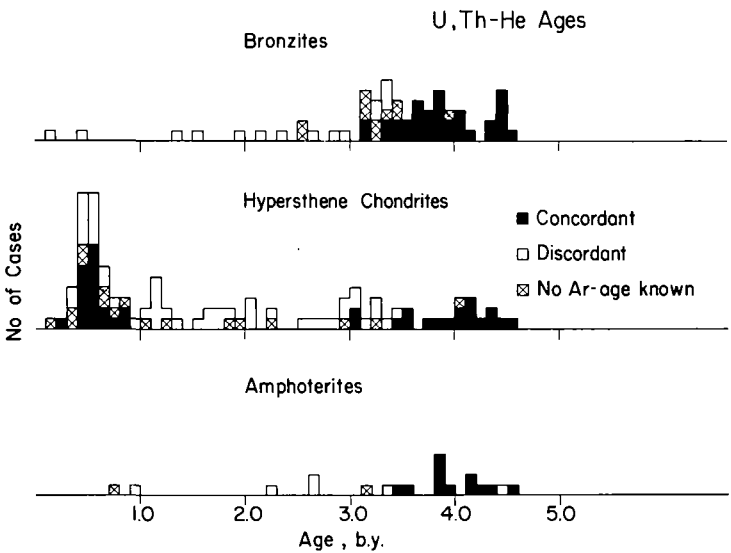


Fig. 5 U, Th-He ages of the bronzite chondrites (top), hypersthene chondrites (middle) and amphoteric chondrites (bottom). The ages range from 1 b.y. to about 4.5 b.y. The "age peak" at about 500 m.y. among the hypersthene chondrites contains moderately and heavily shocked meteorites, many of which have concordant ages, i.e. U, Th-He and K-Ar ages agree within $\pm 20\%$.

much less than iron meteorites such that production rates will not vary as greatly in the stones as they do in the irons. On this ground, several authors have used fixed production rates for He^3 , Ne^{21} , and Ar^{38} such as listed in Table 3. These production rates have to be adjusted when the composition changes significantly. Figure 2 shows to what extent: when $\lambda - \delta$ coincidence measurements of Al^{26} are considered alone, the range is from ~50-75 dpm/kg.

The non-cosmogenic portions of He^4 and Ar^{40} can be used to compute U, Th- He^4 and K- Ar^{40} ages with the usual assumption: That the meteorite became a closed system at time $t=0$ and remained so ever since. The production rates follow directly from the present U, Th, and K^{40} contents and the decay constants. Again, calculations have been made with adopted U, Th, and K contents; Figures 3 and 4 show the extent to which these procedures are justified.

The next meteorite, Orqueil, is listed to show what happens when a meteorite contains vast amounts of trapped gas: the information contained in He^3 , He^4 , Ne^{20} , Ne^{22} , Ar^{36} , and Ar^{38} cannot be used because the cosmogenic and radiogenic components of these nuclides are wholly masked by the trapped component.

Finally, Haraiya is listed because this Ca-rich achondrite resembles the composition of two lunar mare areas as reported by Turkevich, Franzgrote, and Patterson (1967, 1968). The one salient difference with Bruderheim is that $\text{He}^3/\text{Ar}^{38} \sim 7$, reflecting the much greater Ca content of Haraiya (~7.5% Ca).

Let me now turn to certain of the highlights in meteorite dating. Figure 5 shows the U, Th- He ages of the three major chondrite classes. The K- Ar^{40} ages are shown indirectly: a concordant age implies that the K- Ar^{40} age agrees with the corresponding U, Th- He^4 age within $\pm 20\%$. Notice first that the gas-retention ages range from ~0.1 to ~4.6 b.y. Why this great range? Were these meteorites buried deeply within their parent objects such that it required billions of years for them to cool below approximately 450°C where Ar^{40} retention begins? We do not think so. The clue lies in the remarkable "age-peak" near 0.5 b.y. among the hypersthene chondrites. The chondrites in this peak are known to have been moderately to heavily shocked; many of them have concordant gas-retention ages which implies that they were wholly or nearly wholly outgassed 0.5 b.y. ago. Apparently the short ages were caused by one or several impacts on the parent body of the hypersthene chondrites. Vast amounts of rock were shock-heated and totally or partially outgassed such that we now measure short concordant ages in the range 0-1 b.y., discordant ages ~ 4 b.y. and concordant ages again > 4 b.y. This explanation has been widely accepted, although certain specific points such as the accuracy of the 500 m.y. date have been questioned. The implications for the problem of meteorite origin are twofold: The chondrites need not come from the interior of large, lunar-sized or greater, objects where the cooling was slow; and at least one-third of the hypersthene chondrites, perhaps even two-thirds of them come from a single parent object rather than from the tens of thousands of objects known to exist in the asteroid belt.

Figure 6 illustrates another hotly debated issue: the difference in radiation ages of the iron meteorites and the stony meteorites. The radiation ages of the irons are typically hundreds of millions of years, whereas the stones were only millions to tens of million years in space. Urey (1959) concluded that the iron meteorites come from the asteroid belt, the stony meteorites from the Moon. This is grossly consistent with the observed "transit-times". But Eberhardt and Hess (1960) argued that both stones as well as irons could come from the asteroid belt owing to the fact that stones are more fragile than irons such that "secondary collisions" in the asteroid belt after the departure of the meteorites from

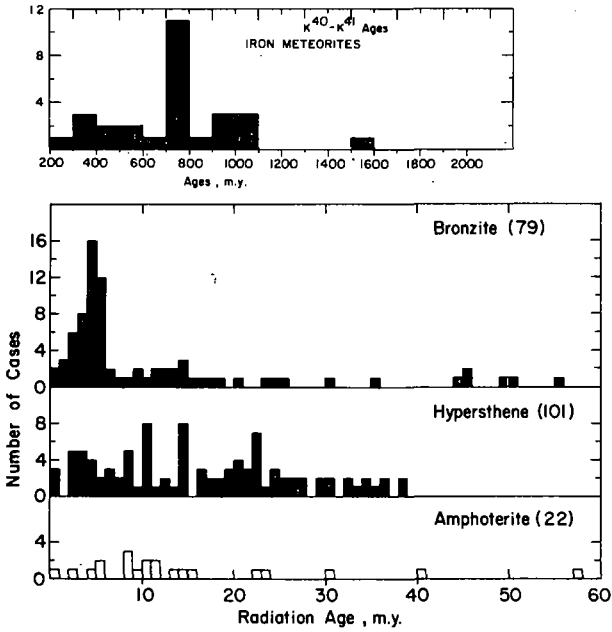


Fig. 6 Radiation ages of iron meteorites (top) and chondrites (bottom) show the systematic difference in ages. Data taken from the literature.

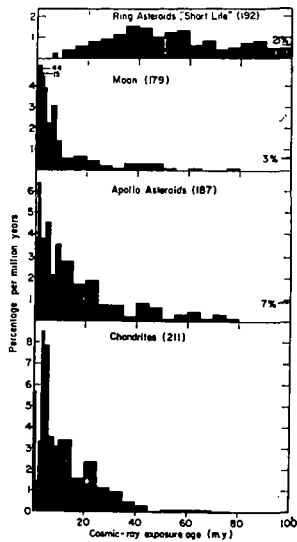


Fig. 7--Radiation ages calculated by Monte Carlo method, taken from Heymann and Anders (1967). Numbers in parenthesis denote number of cases.

their parent objects would destroy the stones at a much faster rate than the irons, hence prevent the survival of "old" stony meteorites. Judging from the age-distributions one requires a mean survival time against destruction of $\sim 10^9$ years for irons and $\sim 10^7$ years for stones which is not unreasonable. Arnold (1965), however, has pointed out that this model requires a space density of dust and rubble in the asteroid belt that is substantially greater than current estimates. Subsequently, Arnold's model-calculations were used by a number of authors in a search for suitable parent objects that would give radiation ages consistent with the observed distribution of the chondrites. Arnold himself had made calculations for the Moon and the ring asteroids. The results of similar calculations by Heymann and Anders (1967) are shown in Figure 7. Objects expelled from the Moon at slightly more than escape velocity find themselves in earth-like orbits with a very high probability of collision with the Earth such that the majority of such ejecta would strike the Earth within the first 2 m.y. The age-distribution calculated for the Moon, while grossly similar to the observed one for chondrites, suffers from an overabundance of cases < 1 m.y. Since stony meteorites with such short ages are uncommon, Arnold proposed that no major impacts have occurred on the Moon in the last 2 m.y.

If the Moon is not quite satisfactory for the origin of chondrites (there are other objections against the Moon which I will not repeat here), then what objects are? From the work of Arnold (1964, 1965) it is clear that the chondrites must have been placed into Earth-crossing orbits initially, because an additional step such as earthward deflection from a Mars-crossing orbit increases the mean collision time with the Earth to such an extent that an embarrassingly large proportion of ages > 100 m.y. is predicted again.

Following private suggestions by Wasson and Anders I proposed (Heymann, 1967) the following scheme: the chondrites were initially on kilometer-sized asteroids, presumably Mars-crossers, a number of which were deflected into Earth-crossing orbits. From then on the object resembles the Earth-crossing Apollo asteroids in its orbital characteristics. Debris broken off from this object will have mean lifetimes against collisions with Earth from 1-10 m.y. Accordingly, the age distributions predicted for Apollo asteroids (Figure 6) is in very good agreement with the observed chondritic case

Wetherill and Williams (1968) and Wetherill (1968) have pointed out, however, that a quantitative study of other aspects such as the time of fall of chondrites during the day and the mass of chondrite influx as compared to the mass of the known Apollo asteroids indicates certain difficulties which must be overcome before the Apollo hypothesis may be considered plausible. Wetherill (1967) has concluded that the morning-afternoon asymmetry (twice as many chondrites are observed to fall in the afternoon) appears to require an aphelion in proximity to Jupiter such as could conceivably be provided by the Hilda or Trojan families of asteroids or by short-period comets.

With these examples I hope to have given you an impression of one of the contributions of mass spectrometry to cosmochemistry. Let me conclude on a hopeful note: meteorite chronology may not have solved the problem of meteorite origin, but as we will learn more about these enigmatic objects the ages will continue to provide an important input for any theory on meteorite origin. Hopefully, one day all the pieces of the puzzle will fit together more coherently than they do at the present time.

References

- Arnold, J. R. (1965), *Astrophys. J.* 141, 1536-1547.
- Arnold, J. R. (1964), *Space Sci. Rev.* 3, 583-714.
- Eberhardt, P. and Hess, D. C. (1960), *Astrophys. J.* 131, 38-46.
- Heymann, D. (1967), *Icarus* 6, 189-221.
- Heymann, D. and Anders, E. (1967), *Geochim. Cosmochim. Acta* 31, 1793-1809.
- Turkevich, A., Franzgrote, E. J. and Patterson, J. H. (1967), *Science* 158, 633-637.
- Turkevich, A., Patterson, J. H. and Franzgrote, E. (1968), *Science* 160, 1108-1110.
- Urey, H. C. (1959), *J. Geophys. Res.* 64, 1721-1737.
- Wetherill, G. T. (1968, *Science* 159, 79-82.
- Wetherill, G. T. and Williams, J. G. (1968), *J. Geophys. Res.* 73, 635-648.

Table 1
Inert Gas Contents of Meteorites

Meteorite	Class	Units 10^{-8} ccSTP/g							
		He^3	He^4	Ne^{20}	Ne^{21}	Ne^{22}	Ar^{36}	Ar^{38}	Ar^{40}
Grant ¹	Of	490	1880	5.89	5.95	6.25	18.8	30.0	27.6
Bruderheim ²	L	52.4	561	8.8	9.90	10.9	1.56	1.56	1155
Orqueil ³	C ₁	6.1	10800	31.2	0.80	4.3	77	15.9	518
Haraiya ⁴	E	40	6500	6.2	6.1	6.4	4.4	5.7	1130

1. Signer and Nier (1960)
2. Eberhardt, Eugster, Geiss, and Marti (1966)
3. Heymann and Mazor (1967)
4. Heymann and Anders (1968)

Table 2

Normal Operating Conditions of RSS Mass-spectrometer

Emission Current	0.5 mA
Trap Current	30 μ A
Electron Voltage	75 V
Accelerating Voltage	2 KV
Voltage across 9-stage Cu-Be multiplier	2 KV
Multiplier Gain	~2000
Input resistor of electrometer	10^{10} Ω

Sensitivity--All on secondary electron multiplier collector.

He ⁴	70 mv/ 10^{-7} ccSTP
Ne ²⁰	100 mv/ 10^{-7} ccSTP
Ar ⁴⁰	400 mv/ 10^{-7} ccSTP

Table 3

Production Rates in Hypersthene Chondrites

Units: 10^{-8} ccSTP/g per m.y.

$$\text{He}^3 = 2.00$$

$$\text{Ne}^{21} = 0.377$$

$$\text{Ar}^{38} = 0.0526$$

STUDIES OF THE COMPOSITION OF THE IONOSPHERE
WITH A SATELLITE MOUNTED MASS SPECTROMETERSEVENTEENTH ANNUAL CONFERENCE ON
MASS SPECTROMETRY AND ALLIED TOPICS

by

John H. Hoffman
Southwest Center for Advanced Studies
Dallas, Texas

Magnetic deflection mass spectrometers have been used by the author since 1964 to study the composition of the ionosphere from rockets and satellites. Such instruments have been successfully flown on four high altitude rockets and one satellite, the Explorer XXXI, which operated for 2-1/3 years in orbit. Basically, the instrument consisted of a 1-1/2" radius 60° sector-field magnetic analyzer (permanent 2200 gauss magnet) with an electron multiplier detector followed by a 6 decade logarithmic electrometer amplifier. An entrance aperture covered by a fine wire screen at -6V with respect to the vehicle skin potential and mounted normal to the vehicle spin axis draws ions from the atmosphere into the instrument, where a negative sweep voltage (-4000 to -200 or -150) produces a mass scan to 1 to 20 amu (satellite) or 1 to 32 amu (rocket) with a period of 2 or 3 sec. An internal calibrator in the log amplifier supplies currents of 10^{-11} , 10^{-9} , 10^{-7} amp to the amplifier input periodically, enabling the amplifier output voltage to be related to input current.

The mass spectra are produced serially by the repetitive high voltage sweep circuit, as is shown in Figure 1, the position of each peak in the spectrum identifying the ion species, and the amplitude of the peak being proportional to the logarithm of the concentration of ions in the vicinity of the entrance aperture of the mass spectrometer, which is dependent on the satellite attitude, velocity, and potential and has a complex relation to the ambient ion concentration. An in-flight calibration, described below, is necessary to obtain absolute ion concentrations.

The data from the satellite experiment shows considerable roll modulation (Figure 1) due to the high vehicle velocity (especially the satellite) with respect to the mean ambient ion velocities and the side mounted (normal to the spin axis) entrance aperture of the mass spectrometer. However since the satellite attitude is known and the spacecraft is in a cartwheel orbit (spin axis normal to orbit plane), it is most practical to use only the data taken in the ram position, when the angle of attack is a minimum, and the sensitivity of the instrument to each ion species is a maximum. The rocket data are also roll modulated and an empirical correction is

made on each ion peak amplitude to 0° angle of attack from a detailed knowledge of the rocket altitude.

An ion mass spectrometer measures relative abundances of the ions it samples from the ionosphere but can be calibrated, as is described below, to give absolute ion concentrations. An in-flight calibration was done by the Explorer XXXI mass spectrometer by comparing the total ion current (the sum of all the peaks) with nearly simultaneously acquired electron density data from the Alouette II topside sounder satellite, (Hoffman, 1969). The Alouette II and Explorer XXXI satellites, launched piggyback into similar orbits, were less than 30 minutes apart over a given latitude for the passes used in this calibration, and it is assumed that both satellites were measuring the same ionosphere for these calibrations. Comparisons were first made in regions of almost pure ($>99\%$) H^+ of various concentrations up to $10^4/cm^3$, then, in regions of greater than 95% O^+ in the range from 10^2 to 5×10^5 ions/ cm^3 . Calibration curves for the two major constituents were thus produced, as are shown in Figure 2. For the other ion species calibration was done by interpolation. The overall precision of the measurements, after applying this calibration procedure, is of the order of 10% as is demonstrated by comparisons with other Alouette II data and the other direct measurements probes on the Explorer XXXI satellite, (Donley et al., 1969).

Since data from a spin stabilized cartwheel orbit type of satellite like Explorer XXXI are highly roll modulated, and only the ram position data are used, the spatial resolution of the data is of the order of 100 to 200 km for spin periods of 2 to 3 rpm. On an oriented satellite such that the angle of attack is maintained near 0° the spatial resolution would be the mass spectrum sweep period times the vehicle velocity, or from 6 to 20 km.

A magnetic deflection mass spectrometer exhibits good mass resolution and sensitivity as is evidenced by the Explorer XXXI data. Ten different ion species have been observed between mass 1 to 20 amu at $1(H^+)$, $2(D^+)$, $4(He^+)$, $7(N^{++})$, $8(O^{++}$ or $He_2^+)$, $14(N^+)$, $15(N_{15}^+)$, $16(O^+)$, $18(H_2O^+$ or $O_{18}^+)$ and $20(Ne^+)$ amu, (Hoffman, 1967). All except mass 15 are shown in Figure 1. The sensitivity of the Explorer XXXI mass spectrometer to H^+ ions is of the order of $0.3/cm^3$ and to O^+ ions of the order of $10/cm^3$.

A summary of recent scientific advances obtained with the magnetic deflection mass spectrometer follows. In general it has been found from the Explorer XXXI data that below 1000 km O^+ is the dominant ion species in the ionosphere (see Figure 3). N^+ varies from 5 to 30% of the O^+ and H^+ is generally a minor constituent,

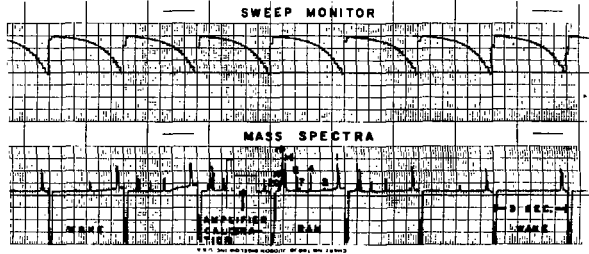


Fig. 1. Portion of Explorer XXXI telemeter record showing sweep monitor in upper channel and mass spectrum below. Downward blips are markers showing recharge of high voltage sweep circuit. Note roll modulation of ion peak amplitudes (labeled in amu).

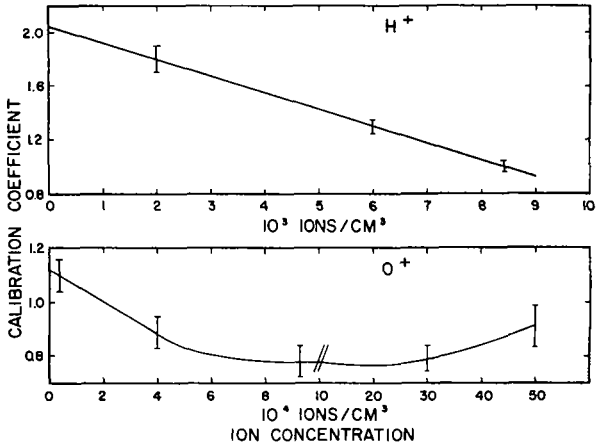


Fig. 2. Calibration coefficients. Ratio of Alouette II electron density to H⁺ and O⁺ concentrations versus ion concentration. Note scale change in abscissa of O⁺ curve.

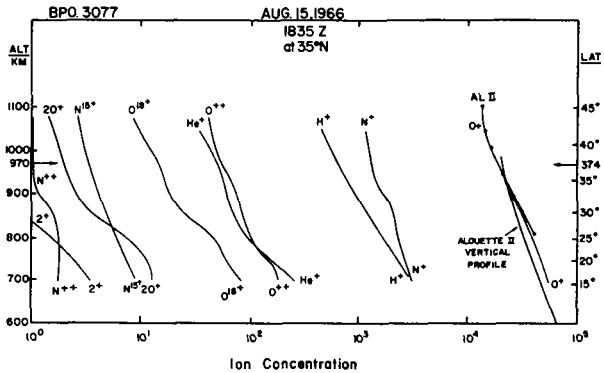


Fig. 3. Typical low altitude data showing ion concentration versus altitude and latitude. Ten different ion species are observed. Alouette II electron concentrations are also given.

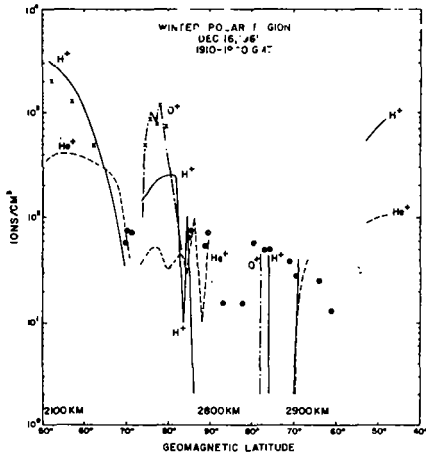


Fig. 4. Ion concentrations versus geomagnetic latitude for northern polar region. X's are Alouette II data reduced by standard method. O's are Alouette II data by Hagg method. In region around 80-85° N H⁺ ions have an upward drift velocity of 10 to 15 km/sec. N⁺ is also observed at concentration of 6% of O⁺, (not shown in figure).

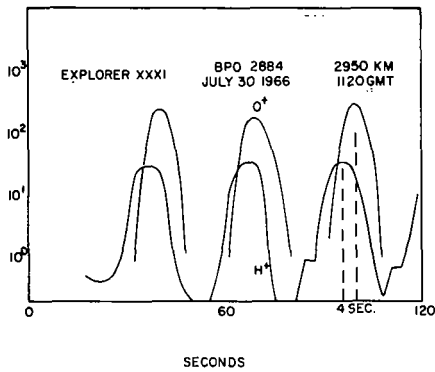


Fig. 5. Ion concentration versus time showing phase difference in the roll modulation maxima of H⁺ and O⁺.

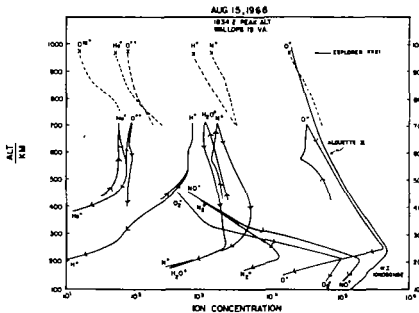


Fig. 6. Ion concentration as a function of altitude showing both the rocket data (solid lines) and the satellite data (broken lines). X's refer to the satellite data at the point of intersection of the two trajectories. The Alouette II electron density from the topside sounder experiment is matched to the Wallops Island ionosonde data at the F maximum.

occasionally, as low as 5% of the O^+ . Above about 2000 km at mid to low latitudes the ionosphere generally consists of the order of 99% H^+ , the remainder being He^+ , D^+ , and S^+ . The cross-over altitude between O^+ and H^+ is quite variable, being a function of several parameters. He^+ is a very minor constituent at all altitudes being of the order of a few % to less than 1%.

An ion peak at mass 8 amu is frequently observed in the data, always at low altitudes and not infrequently above 2000 km. In regions where O^+ is the dominant constituent, the mass 8 ion is identified as O^{++} , formed by photoionization of O^+ . Its relative abundance is of the order of a few $\times 10^{-3}$ of the O^+ . Likewise a peak at mass 7 is identified as N^{++} . These are the first data in which the doubly charged constituents have been observed. From 2200 to 3000 km the mass 8 ion distribution, at a concentration of the order of $1/cm^3$, favors the southern hemisphere in January and February, whereas, in the northern summer, it is more equally distributed. O^+ is found above 2200 km only in the summer northern hemisphere and, then, almost always above $60^\circ N$ geomagnetic latitude. On the other hand, He^+ appears at all times in both hemispheres.

In the winter polar region above 2500 km, O^+ has been observed to become the dominant ion constituent in a highly structured narrow region between 75° and $85^\circ N$ geomagnetic latitude. Figure 4 shows such a situation. The H^+ concentration exhibits 1 to 2 orders of magnitude trough at $70^\circ N$ geomagnetic latitude, whereas, the O^+ region lies to the north, but not to the south, of the trough. There is evidence from the phase difference of the maxima in the roll modulation curves in this structured region, Figure 5, that H^+ ions are flowing upward with a velocity of 10 to 15 km/sec. This is the first experimental evidence for the polar wind (breeze). In the summer, the region of O^+ dominance and the flow of H^+ ions is considerably broader, extending down to 55° or $60^\circ N$ and shows much less structure than in winter.

A Javelin rocket, flown on August 15, 1966 to rendezvous with a pass of the Explorer XXXI satellite, carried a mass spectrometer, identical to that in the satellite, which was calibrated in-flight against the satellite instrument (Hoffman, et al. 1969). The results are shown in Figure 6 and summarized below:

O^+ is the dominant constituent from 200 km to 1000 km with H^+ 5% and He^+ less than 1% of the O^+ . The chemical equilibrium relation between H^+ and O^+ gives a value for the neutral hydrogen concentration of 6.2×10^4 at 250 km and a neutral gas temperature of $940^\circ K$. From the He^+ concentration at 400 km a rate coefficient for the He^+ loss reaction with N_2 of $1.2 \times 10^{-9} cm^3 sec^{-1}$ is calculated. The NO^+ and O_2^+ scale heights from 200 to 300 km agree with those of N_2 and O_2 giving credence

to the ion chemistry involved. In comparing the results from this rocket flight with those of other types of mass spectrometers flown in a similar time period, it is seen that the major discrepancy lies in the $n(H^+)$ measurements, the present result being lowest. The in-flight calibration tends to indicate that a mass spectrometer is more sensitive to light mass ions than to O^+ . This phenomenon may account for the discrepancy noted.

Presently, a second generation magnetic deflection mass spectrometer is being developed for ionospheric composition studies and will be flown on a Javelin rocket in June 1969, and on the ISIS-B satellite in 1971, and the S^3 -B satellite in 1972. It consists of a dual channel analyzer set to simultaneously measure the 1-8 amu and 8-64 amu mass ranges, and a "Peaks" circuit which is an on-board computer that seeks the position and amplitude of each peak in the mass spectra telemetering only this information at an order of magnitude saving in telemetry band width. The dual analyzer will provide an increased mass range, better resolution and sensitivity at the high mass end of the spectrum, and a sweep time of 1 sec per spectrum giving either increased spatial resolution or more precisely defined roll modulation of the data.

BIBLIOGRAPHY

- Hoffman, John H., Composition measurements of the topside ionosphere, Science, 155, 322-324, 1967.
- Hoffman, John H., Ion mass spectrometer on the Explorer XXXI satellite, Proceedings of IEEE, 57, June 1969.
- Donley, J. L., L. H. Brace, J. H. Hoffman, G. L. Wrenn, Comparison of results of Explorer XXXI direct measurement probes, Proceedings of IEEE, 57, June 1969.
- Hoffman, J. H., C. Y. Johnson, J. C. Holmes, J. M. Young, Daytime mid-latitude ion composition measurements, Trans. Am. Geophys. Union, 50, 259, 1969. (To be submitted to J. Geophys. Res.; presented at 12th Plenary Meeting of COSPAR, Prague, May 1969.)

PRECISE MASS DETERMINATIONS FROM HIGH RESOLUTION
SPARK SOURCE MASS SPECTRA OF ORGANIC SUBSTANCES

K.H. Maurer, C. Brunnée and K. Habfast
VARIAN MAT GmbH, Bremen, Germany

Abstract

Using a double focusing mass spectrometer of the Mattauch - Herzog type, equipped with a unipolar low-voltage discharge ion source, high resolution mass spectra of organic molecules are recorded photographically. The evaluation of the mass spectra, recorded with a resolution of more than 25,000, is performed automatically by a precision comparator. The samples are introduced via a new vacuum lock.

1. Introduction

In recent years, a number of authors have published papers on spark source mass spectra of organic compounds. Hodgson, Desjardins and Baun ^{1,2)}, for example, reported on studies which were carried out to investigate whether the spark source could be used as a further means of obtaining information on the structure of a molecule. They studied a larger number of aromatic hydrocarbons and steroids and found that the low-mass fragment ions are much more abundant than the high-mass fragment ions, but that the spectra exhibit quite characteristic features of the molecular structure.

Other authors ^{3,4,5,6)} reported on spark source mass spectra obtained with a spinning electrode. They observed that the spectra were less complex than those obtained with fixed electrodes and attributed this to the fact that undegraded material is brought to the spark continuously. When comparing conventional spark and electron impact spectra of organic substances, Faust and co-workers ⁸⁾ found that, despite the high degree of fragmentation and a far greater number of mass lines, spark mass spectra exhibit many features which suggest that electron impact ionization plays an important part within the spark. They point out that spark source mass spectrometers allowing the correct identification of mass lines by means of accurate mass determinations might provide a possibility to study fragmentation processes, rearrangement and ion-molecule reactions within the spark.

However, to our knowledge, all studies of this type have been performed using high voltage radio frequency spark sources. Thus because of the rather large energy spread of the ions ^{9,10,11)} emitted by the r. f. source the resolving power obtained has not been sufficiently high to permit accurate mass determinations. In contrast to the r. f. source, the energy spread in the case of the unipolar low-voltage discharge source ¹²⁾, is smaller by one order of magnitude so that a very high resolving power can be obtained without reducing the ion beam aperture.

2. Experimental

2.1 Analyzer System

For our measurements, we used a double-focusing VARIAN MAT SM1 B-F mass spectrometer of Mattauch-Herzog geometry, which allows mass spectra to be recorded both photographically and electrically. The instrument is equipped with a low voltage discharge source which has already been reported on in detail earlier ¹³⁾. Image errors are corrected such that the system, at an accelerating potential of 20 kV can cope with the full energy width of about 150 eV of the ions produced and that a resolving power of 20,000 - 30,000 over 80 % of the photoplate length can be obtained.

Fig. 1 shows a portion of a high-resolution spectrum of an iron sample. This spectrum is used as a test for the subsequent measurements on organic substances. To resolve the tungsten/niobium doublet a resolving power of 1,250 is required. The resolution obtained is 27,000.

2.2 Sample Preparation and Introduction

We have used two preparation methods : 1. the organic material was mixed with pure graphite and pressed to electrodes; 2. the sample and PFK as reference substance were placed into boreholes ¹⁴⁾ of the gold electrodes. The highly volatile PFK had been mixed with graphite before.

Fig. 2 shows the introduction of the electrodes by means of a new vacuum lock. At the end of a sample rod there is a tilting device to which the electrode carriers together with the electrodes are mounted with retaining springs. While the sample is being passed through the lock, the electrodes are lying horizontally in the dotted position. After the rod has reached the ion source chamber it is turned by 180°, and the tilting device tilts the electrodes to vertical position due to overweight on one side. The rod is pushed in further, and the electrode adjustment devices take over the electrode carriers together with the electrodes. Then the sample rod is pulled back. Thus change of sample is a matter of a minute without breaking vacuum.

The mass spectra, which were highly resolved for accurate mass determinations and lowly resolved for intensity measurements, were recorded photographically. The high-resolution spectra were evaluated automatically by using the Leitz-MAT precision comparator ¹⁵⁾. The ion accelerating system permits a homogeneous illumination of the object slit and a dilution of the space charge in the ion beam. Therefore, the lines on the low-resolution spectra have rectangular line profiles, as shown in fig. 3b, and the line widths follow the square-root-of-m law, so that the conversion from the measured transparency values to intensities is relatively easy. The transparency values were corrected with regard to background ¹⁶⁾. The dependence of the photoplate sensitivity on the mass was taken into account ¹⁷⁾.

$$\frac{M}{\Delta M} = 27000$$

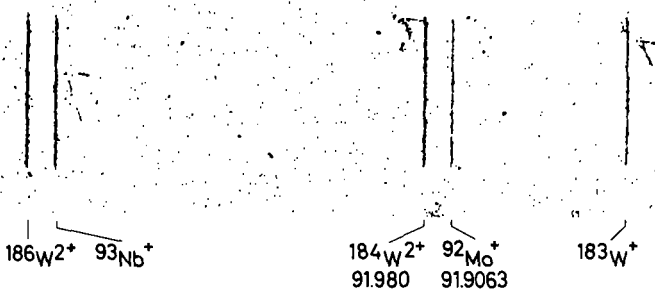


Fig. 1 Portion of a high-resolution spectrum of an iron sample.

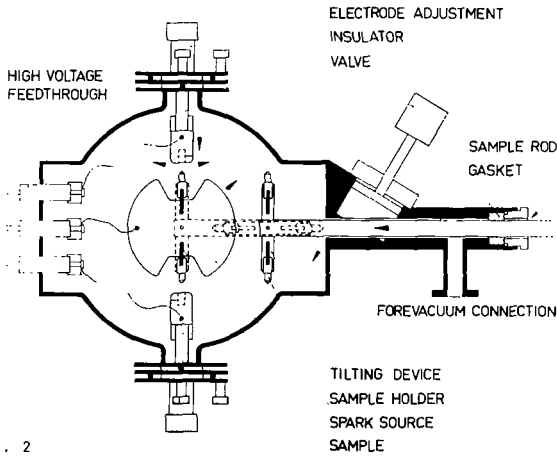


Fig. 2

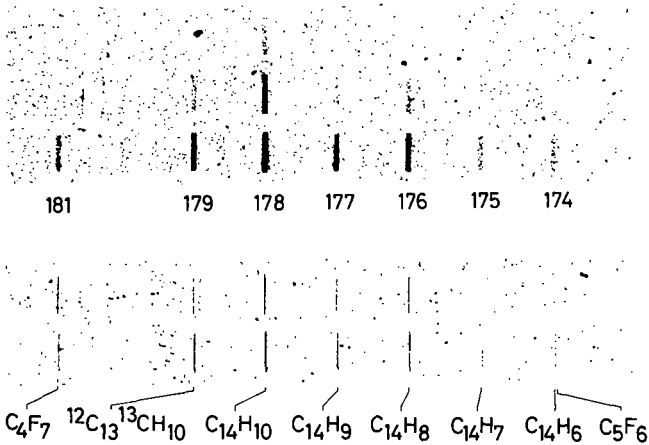


Fig. 3

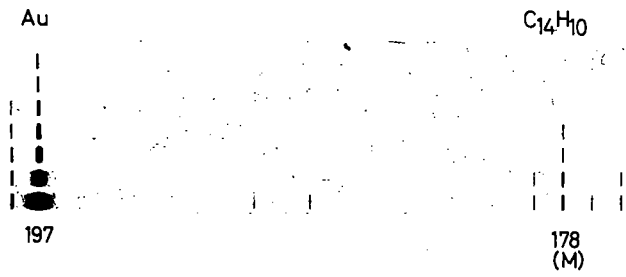


Fig. 4 Parent peak group of anthracene, shown together with the line of the electrode material (gold). Low-voltage discharge ion source.

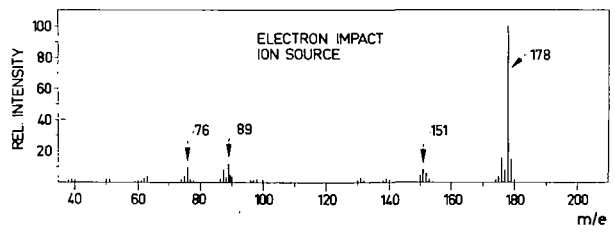
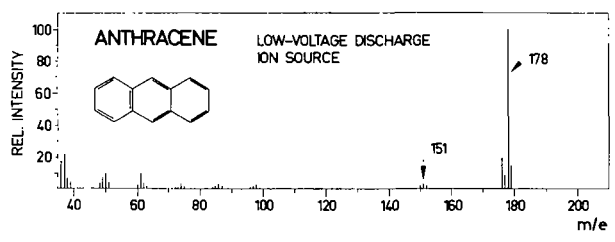


Fig. 5

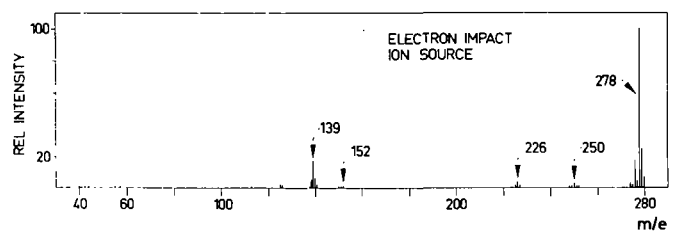
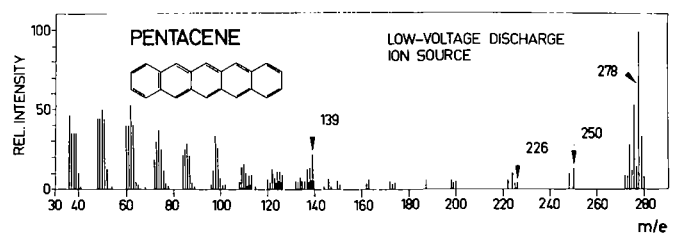


TABLE I. RESULTS OF AN AUTOMATIC EVALUATION WITH A PRECISION COMPARATOR
 SAMPLE : ANTHRACENE
 ION SOURCE : LOW-VOLTAGE DISCHARGE

COMPOSITION	CALCULATED MASS	ERROR*	COMPOSITION	CALCULATED MASS	ERROR*
¹² C ₁₀ ¹³ C ₁ H ₁₀	179.0813	-0.3	C ₁₂ H ₅	149.037	-1.9
¹² C ₁₀ H ₁₀	178.0778	-0.4	C ₁₁ H ₇	139.0526	-2.2
C ₁₄ H ₈	177.0687	-1.7	C ₁₁ H ₃	135.0226	-0.9
C ₁₄ H ₆	176.0613	-1.3	C ₁₁ H ₂	134.0139	-1.8
C ₁₄ H ₇	175.0543	-0.5	C ₁₀ H ₈	128.0513	-1.3
C ₁₄ H ₆	174.0462	-0.7	¹² C ₉ ¹³ C ₁ H ₅	126.0430	+0.6
C ₁₃ H ₇	163.0543	-0.5	C ₁₀ H ₅	125.0392	+0.1
C ₁₃ H ₆	162.0494	+2.4	C ₁₀ H ₃	123.0211	-2.4
C ₁₃ H ₅	161.0376	-1.5	C ₁₀ H ₂	122.0143	-1.3
C ₁₂ H ₈	152.0615	-1.0	C ₁₀ H	121.0064	-1.4
C ₁₂ H ₇	151.0528	-2.0	C ₁₀	118.9997	-0.3
C ₁₂ H ₆	150.046	-0.9	C ₉ H ₇	115.0544	-0.3

TABLE I. CONT'D

COMPOSITION	CALCULATED MASS	ERROR*	COMPOSITION	CALCULATED MASS	ERROR*
C ₉ H ₅	113.0393	+0.2	C ₇	84.0005	+0.5
C ₉ H ₃	111.0207	-2.7	C ₈ H ₄	78.0456	-1.4
C ₉ H ₂	110.0150	-0.7	C ₈ H ₄	77.0386	-0.6
C ₉ H	109.0072	-0.6	C ₈ H ₂	76.0306	-0.7
C ₉	107.9991	-0.9	C ₈ H ₃	75.0227	-0.7
C ₈ H ₆	102.0472	+0.2	C ₈ H ₂	74.0160	+0.4
C ₈ H ₅	101.0381	-1.1	C ₈ H	73.0075	-0.3
C ₈ H ₃	99.0218	-1.7	C ₈	71.9997	-0.3
C ₈ H ₂	98.0148	-0.8	C ₇ H ₂	63.0236	+0.2
C ₈ H	97.0063	-1.5	C ₇ H ₂	62.0155	-0.1
C ₈	95.9992	-0.8	C ₇ H	61.0080	-0.2
C ₇ H ₅	89.0380	-1.1	C ₇	60.0001	+0.1
C ₇ H ₄	88.0301	-1.2	C ₆ H ₃	51.0233	-1.6
C ₇ H ₃	87.0226	-0.9	C ₆ H ₂	50.0161	+0.5
C ₇ H ₂	86.0158	+0.1	C ₆ H	49.0067	-1.1
C ₇ H	85.0077	-0.1	C ₆	47.9999	+0.1

* ERROR IN MILLIMASS UNITS

MEAN ERROR: 0.9

TABLE II. ACCURATE MASS DETERMINATIONS :

MULTIPLY AT MASS 44

COMPOSITION	CALCULATED MASS	ERROR [mu]
Ca	43.9554	- 0.1
CS	43.9718	- 0.2
CHP	43.9814	- 0.2
CO ₂	43.9895	- 0.3
CH ₂ NO	44.0132	- 0.4
C ₂ H ₄ O	44.0257	- 0.5
C ₂ H ₆ N	44.0496	- 0.4

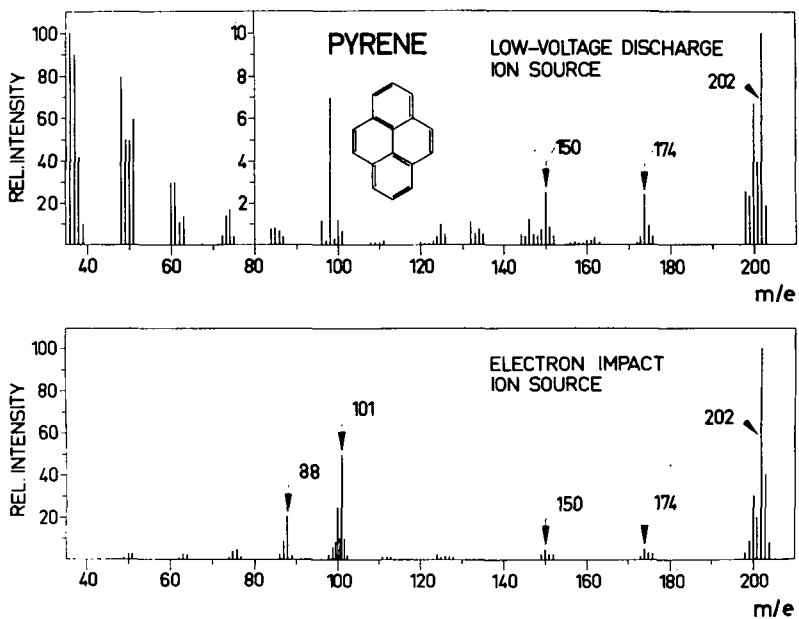


Fig. 7

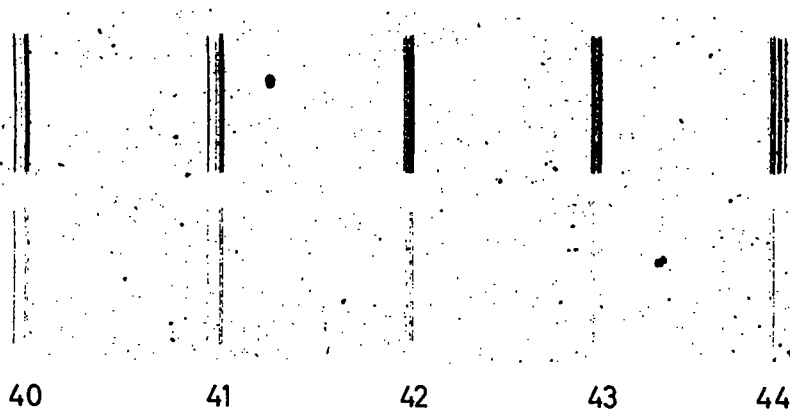


Fig. 8 Portion of a high resolved spectrum of blood plasma.
 Resolution : 22,000
 Ion source : low-voltage discharge.

3. Results

Fig. 3a shows the molecular peak group of anthracene and the lines of the reference sample perfluorokerosene, recorded with high resolution, for accurate mass determinations. The same spectrum, recorded with low resolution for intensity measurements is shown in fig. 3b.

Fig. 4 shows once again the molecular peak group and the line of the electrode material (gold) together with the hydrogen association line.

Spectra of ions produced in the low-voltage discharge source are compared against ions from an electron impact source (fig. 5). The molecular peak is set to 100 %. In the higher mass range, the two spectra are very similar, in the lower mass range the abundance of the fragment ions in the case of low-voltage discharge is considerably higher, whereas the abundance of the doubly - charged molecular ion is below 1 %.

The results obtained by an automatic photoplate evaluation with the precision comparator are shown in table I. It includes lines with abundances of below 1 %. The errors are stated in millimass units.

The mean error of the mass determination of 57 lines is below one millimass unit and, therefore, comes very close to the values obtained so far with electron impact sources.

The low-voltage discharge spectrum of pentacene, shown in fig. 6, is also very similar to the electron impact spectrum. Fragmentation increases noticeably in the lower mass range with decreasing mass numbers. In each case, the first line of each group is a carbon cluster. The doubly charged molecular ion is more abundant than in the case of anthracene.

A high degree of fragmentation can be observed with pyrene (cf. fig. 7).

The molecular peak has only 10 % of the abundance of the carbon cluster at mass 36. Even so, the characteristic fragment ions in the higher mass range are found here, too.

Fig. 8 shows a portion of a high-resolution spectrum of blood plasma. All lines are multiplets. The sample contains impurities and a high resolving power is required for line identification.

To illustrate the resolution, the multiplet at mass 44 is shown in fig. 9, considerably enlarged. It consists of 7 lines. The high resolution obtained permits unequivocal line/mass correlations.

Table II shows a portion of the complete element map of this spectrum, showing the data belonging to this mass number. The errors are in the order of 0.3 millimass units.

4. Conclusions

We have reported here on first results of our measurements on organic materials performed with the low-voltage discharge source. These results show that high resolution and accurate mass determinations, provide a possibility to carry out exhaustive investigations concerning ionization and fragmentation processes of organic molecules in the plasma of the low-voltage discharge.

Over and above this, the high resolution obtained also provides new possibilities in the field of trace analyses of biological materials by direct sparking techniques.

References

- 1) F.N. Hodgson, M. Desjardins, and W.L. Baun
Technical Documentary Report No. ASD-TDR-63-383.
- 2) F.N. Hodgson, M. Desjardins, and W.L. Baun
11th Ann. Conf. on Mass Spectr.,
ASTM Committee E-14, San Francisco (1963).
- 3) W.M. Hickam, and G.G. Sweeney
13th Ann. Conf. on Mass Spectr.,
ASTM Committee E-14, St. Louis (1965).
- 4) L.C. Scala, G.G. Sweeney, and W.M. Hickam
14th Ann. Conf. on Mass Spectr.,
ASTM Committee E-14, Dallas (1966).
- 5) G.G. Sweeney, W.M. Hickam, and L.B. Crider
14th Ann. Conf. on Mass Spectr.,
ASTM Committee E-14, Dallas (1966).
- 6) T. Kessler, A.G. Sharkey Jr., W.M. Hickam, and G.G. Sweeney
13th Ann. Conf. on Mass Spectr.,
ASTM Committee E-14, St. Louis (1965).
- 7) W.M. Hickam, and Y.L. Sandler
Surface Effects in Detection
I. Bregman, and A. Dravnieks
Spartan Books, Inc. Washington, p. 192 (1965).
- 8) R.C. Faust, A.E. Fontaine, B.E. Job, and R.H. Saunders
Z. f. Naturforschung 20 a, 1128-1134 (1965).
- 9) J. Franzen
Z. f. Naturforschung 18 a, 410 (1965).
- 10) J.R. Woolston, and R.E. Honig
Rev. Sci. Instr. 35, 69 (1965).
- 11) J.R. Woolston, and R.E. Honig
12th Ann. Conf. on Mass Spectr.,
ASTM Committee E-14, Montreal (1964).

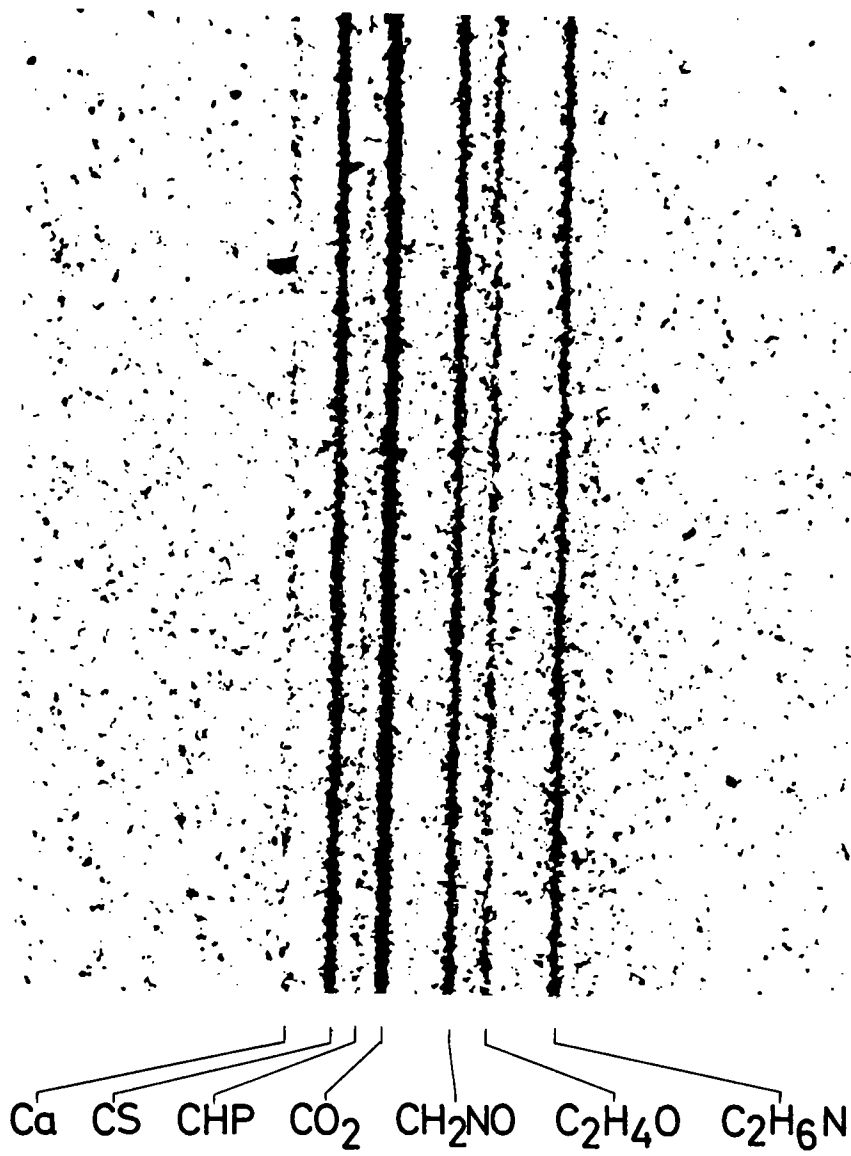


Fig. 9 Multiplet at mass number 44.
Sample : blood plasma
Ion source : low-voltage discharge.

- 12) R.E. Honig, S.S. Glas, and J.R. Woolston
VI th Intern. Conf. Ion. Pl. in Gases, Paris (1963).
- 13) K.D. Schuy, K.H. Maurer, W. Kögler, and P. Winkler
Mass Spectr. Conf., Berlin (1967).
- 14) E.N. Hodgson, M. Desjardins, and J.E. Kuton
Techn. Doc. Report RTD-TDR-63-41-45,
U.S. Air-Force Material Laboratory.
- 15) K. Habfast
Intern. Mass Spectr. Conf., Berlin (1967).
- 16) J. Franzen, K.H. Maurer, and K.D. Schuy
Z. f. Naturforschung 21 a, 37-62 (1966).
- 17) K. Habfast, and K.H. Maurer
14th Ann. Conf. on Mass Spectr.,
ASTM Committee E-14, Dallas (1966).

DETERMINATION OF ORGANIC CONTAMINANTS IN AIR AND WATER
BY HIGH-RESOLUTION MASS SPECTROMETRY

A. G. Sharkey, Jr., J. L. Shultz, T. Kessler,
and R. A. Friedel

U.S. Department of the Interior, Bureau of Mines
Pittsburgh Coal Research Center, Pittsburgh, Pa. 15213

INTRODUCTION

The Pittsburgh Coal Research Center of the U.S. Bureau of Mines is investigating processes to remove various pollutants from flue gases and uses of coal and coal-derived materials to remove organic contaminants from secondary waste water.^{1,2/} As part of this investigation, high-resolution mass spectrometry has been used to study concentrates of organic contaminants in airborne particulate matter and waste water.

Although a wide variety of organic contaminants including chemical carcinogens have been identified in air and water from various sources, little use has been made of modern instrumental techniques such as high-resolution mass spectrometry and nuclear magnetic resonance to further these studies.^{3,4,5,6/} Only recently the Federal Water Pollution Control Administration, Southeast Water Laboratory, reported that mass spectrometry and nuclear magnetic resonance in addition to infrared and ultraviolet spectrophotometry are now being applied to the characterization of organic pollutants in water.^{7/}

Sawicki and co-workers have made extensive studies of organic compounds found in urban atmospheres.^{8/} Because separation and identification of individual components is difficult, the concentrations of 3,4-benzpyrene and one or two other polynuclear aromatics have been used as a basis for comparing organic pollutants in atmospheres.^{9/}

EXPERIMENTAL PROCEDURE

High-resolution mass spectra were obtained using a Consolidated Electroynamics Corp. Model 110 at a resolution of approximately 1 part in 15,000. Precise masses used in determining the elemental compositions were, with few exceptions, assigned with accuracies of 1-3 millimass units.

The solid particulate matter was introduced in the heated inlet system of the mass spectrometer and vaporized at approximately 300° C; about 12 percent was vaporized at this temperature. Concentrates of the organic material in waste water samples were prepared using ether extraction.^{6/}

RESULTS AND INTERPRETATION

Airborne Particulate Matter

Precise mass data were obtained for approximately 750 peaks in the mass 76 to 266 range. Six typical airborne pollutants reported by Sawicki and others are used in table 1 to illustrate the applicability of the high-resolution technique to detecting and determining the elemental composition of polynuclear species in airborne particulate matter.^{3/} The five most intense peaks in the mass spectrum were 178, 202, 228, 252, and 276. Elemental compositions derived from the precise masses and examples of known pollutants corresponding to these formulas are also shown.

The detection of alkyl derivatives is important as it has been shown that in some instances alkyl derivatives are more carcinogenic than unsubstituted aromatic ring structures.^{3/} The presence of alkyl derivatives is possible for three of the ring systems indicated in table 2. Alkyl substituents containing from 2 to 4 carbon atoms were detected.

Effluent from Sewage Treatment Plant

Organics extracted from treated waste water with ether totaled approximately 1 ppm. Contaminants with molecular weights as high as 400 were detected by mass spectrometry. Many multiplets were observed in the mass spectra of the concentrates, indicative of the presence of heteroatoms. Six of the most intense peaks showing multiplets were masses 182, 202, 228, 230, 252, and 276.

Table 1.- High-resolution mass spectrometric data for several organic pollutants in airborne particulate matter

Nominal	Mass, amu		Elemental composition			Examples of possible compounds ^{b/}
	Precise ^{a/}	This work	Δ	C	H	
<u>C,H</u>						
178	.0783	.0775	.0008	14	10	Anthracene
202	.0783	.0774	.0009	16	10	Pyrene
228	.0938	.0930	.0008	18	12	Benzantracene
252	.0938	.0932	.0006	20	12	Benzopyrene
276	.0938	.0943	.0005	22	12	Benzo[ghi]perylene
300	.0938	.0925	.0013	24	12	Coronene

a/ Exact fractional mass for elemental composition shown.

b/ Previously identified air pollutants, see reference 3.

Table 2.- Partial high-resolution mass spectrum of organic contaminants in airborne particulate matter

Nominal mass	Relative intensity	Elemental composition				Examples of possible compounds ^{a/}
		C	H	O	N	
154	6.9	12	10			Acenaphthene ^{b/}
168	6.5	13	12			Methylacenaphthene
	4.0	12	8	1		Dibenzofuran ^{b/}
182	6.2	14	14			Dimethylacenaphthene
	2.7	13	10	1		Benzophenone
196	5.5	15	16			Trimethylacenaphthene
	2.5	13	8	2		Xanthen-9-one ^{b/}
167	12.8	12	9		1	Carbazole ^{b/}
181	5.3	13	11		1	Methylcarbazole

a/ All isomeric variants are possible.

b/ Previously identified air pollutants, see reference 3.

CONCLUSIONS

A major advantage of this type of instrumentation is that the elemental compositions of a wide variety of components can be determined on essentially total samples. Information concerning alkyl derivatives such as carbon number distribution data obtainable by mass spectrometry could be of prime importance in studies of carcinogenic pollutants. A limitation is that particular isomers cannot be determined.

ACKNOWLEDGMENTS

The authors gratefully acknowledge the assistance of Dr. Morton Corn, Graduate School of Public Health, University of Pittsburgh, for supplying the sample of airborne particulate matter, and Dr. Charles Caruso, Water Resources Research Project, Mellon Institute, Carnegie-Mellon University, for assistance in preparing the concentrates of the organic contaminants in the water. G. E. Johnson of the Pittsburgh Coal Research Center obtained the waste water samples and provided helpful discussion during this investigation.

REFERENCES

1. Bienstock, D., J. H. Field, and J. G. Myers, Bureau of Mines Rept. of Inves. 7021, 1967, 52 pp.
2. Johnson, G. E., L. M. Kunka, A. J. Forney, and J. H. Field, Bureau of Mines Rept. of Inves. 6884, 1966.
3. Sawicki, Eugene, Arch. Environ. Health, 14, 46 (1967).
4. Middleton, F. M., and A. A. Rosen, Public Health Reports 71, 1125 (1956).
5. Middleton, F. M., Wallace Grant, and A. A. Rosen, Indus. and Eng. Chem., 48, 268 (1956).
6. Caruso, S. C., H. C. Bramer, and R. D. Hoak, Air and Water Pollution, 10, 41 (1966).
7. FWPCA Team Identifies Organic Pollutants in Water by Wide Variety of Techniques. Chem. and Eng. News, Oct. 14, 1968, p. 56.
8. Sawicki, Eugene, Thomas R. Houser, Walter C. Elbert, Frank T. Fox, and James E. Meeker, Am. Indus. Hygiene Asso. Jour., 23, 137 (1962).
9. Stanley, Thomas W., Myrna J. Morgan, and Ethyl M. Grisby, Environ. Sci. and Tech., 2, 699 (1968).

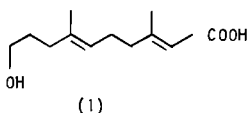
On-Line Computer Analysis of High Resolution
Mass Spectra: Mass Spectrometry of Medium Chain Length Compounds

S.R. Shrader, Wyeth Laboratories, Inc., Radnor, Pa.

A.M. Chalmers, Cornell University, Ithaca, New York

An MS-902 high resolution mass spectrometer PDP-8 computer system has been used to considerable advantage for the structure elucidation of natural products and drug metabolites. The system, as supplied by Picker Nuclear and AEI (England), is schematically described in Figure 1. Centroids and areas of peaks are determined on the fly during a scan, which is typically thirty seconds per decade at a resolution of 10,000-12,000. Following decisions by the operator whether to punch the data and/or repeat the scan, the computer calculates all ion masses by interpolation between reference peaks. The third program phase determines elemental compositions and provides an easily read output. For the composition calculations, the operator has the choice of entering any three heteroatoms in addition to nitrogen and oxygen. Good results are obtained, with very little set-up time required, from quantities of only a few micrograms.

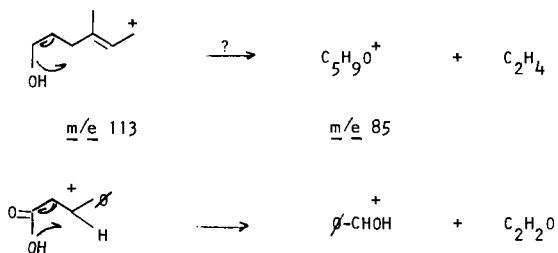
One important application of this tool is the identification of the extremely small amount of materials isolated from biological systems. In particular, the major component of the hairpencils of the monarch butterfly, *Danaus plexippus*, was identified by mass spectrometry and a combination of other techniques including the preparation of several simple derivatives¹. The mass spectra of the natural material (trans, trans-10-hydroxy-3,7-dimethyl-2,6-decadienoic acid, I) and of the derivatives provided not only information leading to the structure, but some interesting observations concerning mass spectral fragmentations.



The mass spectrum (Figure 2) of compound I, with the important high resolution data indicated, contains significant structural information. The molecular ion at $\underline{m/e}$ 212 gives the elemental composition of the compound ($C_{12}H_{20}O_3$) and the M-18 peak is formed by the elimination of water, demonstrating the presence of a hydroxyl function. The M-CH₂O peak at $\underline{m/e}$ 182 is most easily explained as a rearrangement fragmentation involv-

ing the primary alcohol.

Two very significant fragment peaks appear at m/e 100 and 113 ($C_5H_8O_2$ and $C_7H_{13}O$, respectively). These ions are formed by cleavage of the doubly allylic C-4-C-5 bond. The base peak in the spectrum, at m/e 95, is formed by loss of water from the $C_7H_{13}O$ ion. A second fragmentation of this ion is the elimination of ethylene to form the ion at m/e 85 (C_5H_9O , m^+ 63.9). Unfortunately, the scarcity of sample precluded a labelling experiment to determine whether this fragmentation is similar to that observed from certain carboxylic acids².



The mass spectrum (Figure 3) of the methyl ester obtained by reacting I with diazomethane is remarkable in that no elimination of water is observed. This is best interpreted as blockage of 1,4-elimination from the primary alcohol by the C-6 and C-7 double bond. Otherwise, the spectrum exhibits the expected changes in fragmentation behavior. The molecular ion loses methanol, methoxy radical and formaldehyde (from the primary alcohol) to give peaks at 194, 195 and 196, respectively. The base peak remains at m/e 95, as does the fragment at m/e 113, but the fragment corresponding to the other half of the molecule is shifted to m/e 114.

Other compounds which were studied included the O-acyl, O-acyl methyl ester, and the bis-(trimethylsilyl) derivatives. The spectra were not unusual, and as would be predicted from the earlier discussion of the loss of formaldehyde these derivatives do not undergo this fragmentation.

¹J. Meinwald, A.M. Chalmers, T.E. Pliske and T. Eisner, Tetrahedron Letters, 1968 (47), 4893-6.

²H. Budzikiewicz, C. Djerassi, and D.H. Williams, "Mass Spectrometry of Organic

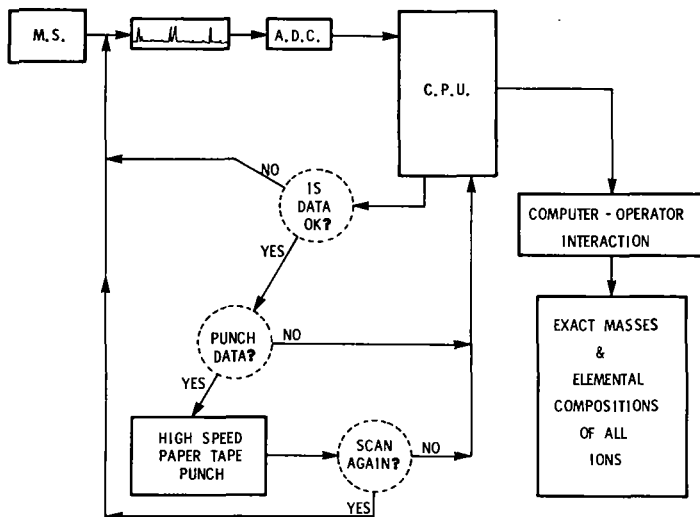


Figure 1

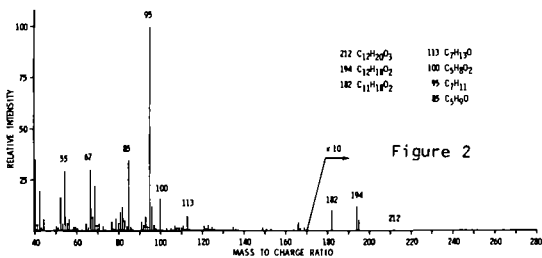


Figure 2

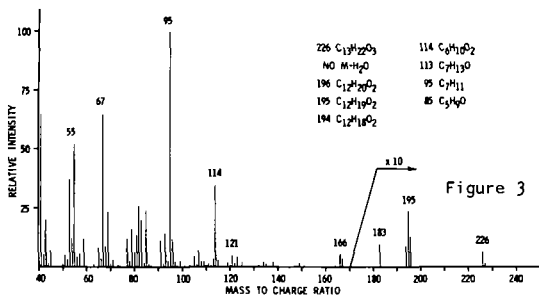


Figure 3

THE ANALYSIS OF SOME MIXTURES USING ULTRA HIGH RESOLUTION AND
FIELD IONIZATION TECHNIQUES

S. Evans, T.R. Kemp and W.A. Wolstenholme, AEE Scientific
Apparatus Division, Manchester, England.

Introduction

The analysis of such complex mixtures as tobacco extracts and petroleum fractions which may contain many components presents many problems, preliminary separation procedures being lengthy and complicated even under ideal conditions. One of the earliest applications of mass spectrometry was the analysis of complex hydrocarbon mixtures. This type of analysis can be performed using low resolution and electron impact as the sole method of ionization. However, for more complex mixtures, where different compound types are present and whose molecular weights are much nearer than, say 14 mass units apart, or even are nominally the same, then a mass spectrometric analysis of the mixture requires the use of high resolution techniques to separate multiplet peaks. Also the use of a combined electron impact-field ionization source is highly desirable so that at least a low resolution study can be made in the field ionization mode in order to facilitate the identification of molecular ion peaks.

This paper presents some results which have been obtained using these techniques. In particular, the petroleum fraction studied was shown to contain sulphur containing compounds which give rise to multiplet peaks in the mass spectrum requiring for separation a resolving power of 70,000.

Experimental

The petroleum fraction studied had a boiling range 355-375°C and a sulphur content of 1.55%. Low resolution spectra were recorded using electron impact at 70eV and field ionization as the source of ions, and then using electron impact, studies were made at resolving powers of 10,000, 30,000 and 70,000.

Preliminary results were obtained on the polycyclic fraction from a tobacco extract using low resolution electron impact and field ionization studies.

All spectra were recorded on a double focusing AEE MS902 instrument. Initial setting up for the very high resolution studies was done using a mixture of xenon and ethylene tetrachloride as the sample since it gives a convenient doublet at m/e 129 with a mass separation of 1 part in 70,000. The performance was also checked using a synthetic mixture of 1,1,3,3,5,6-hexamethyl indane and 7-thiatridecane.

Samples for assessing instrumental performance were admitted via the heated reservoir inlet system and the petroleum fraction and tobacco extract were admitted on the direct insertion probe.

Results

The low resolution electron impact spectra of both the petroleum fraction and the tobacco extract showed the typical pattern for such complex mixtures, namely a peak at every mass number with the intensity generally increasing towards the low mass region. For the petroleum fraction, the field ionization spectrum showed much more clearly the molecular weight range of the compounds present. Peaks were present from about mass 180 to mass 350. Thus, the molecular weight range was established, and a study of high resolution electron impact data was undertaken.

Fig.1 shows part of a scan taken at a resolving power of 10,000 showing the spectrum of the petroleum fraction plus perfluorokerosene. It can be seen that each peak is split into at least two components. The mass range covered in Fig.1 is that which would include the molecular weights of some of the sulphur containing compounds which may be expected to be present, namely mass 202 (7-thiatridecane) and its homologue at m/e 230. There are indications in Fig.1 that some of the peaks are in fact wider than others. Also, any doublets involving C_3-SH_4 differences would remain undetected at this resolution. Some of the peaks were, therefore, examined at higher resolution, and Fig.2 shows the peak at m/e 230 at a resolving power of 30,000. It is now clear that the higher mass component contains at least two different ion species and the lower mass component at least three. Also, it is now clear that a resolving power of the order of 70,000 is required to obtain well resolved spectra in this case.

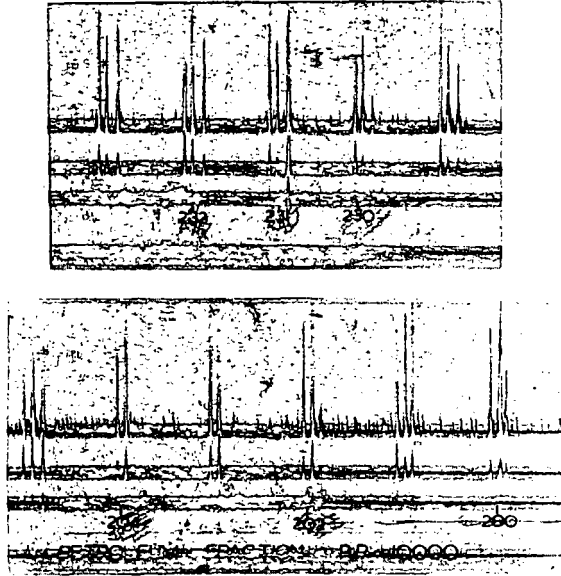


Fig.1 Petroleum fraction and perfluorokerosene.
Resolution 10,000

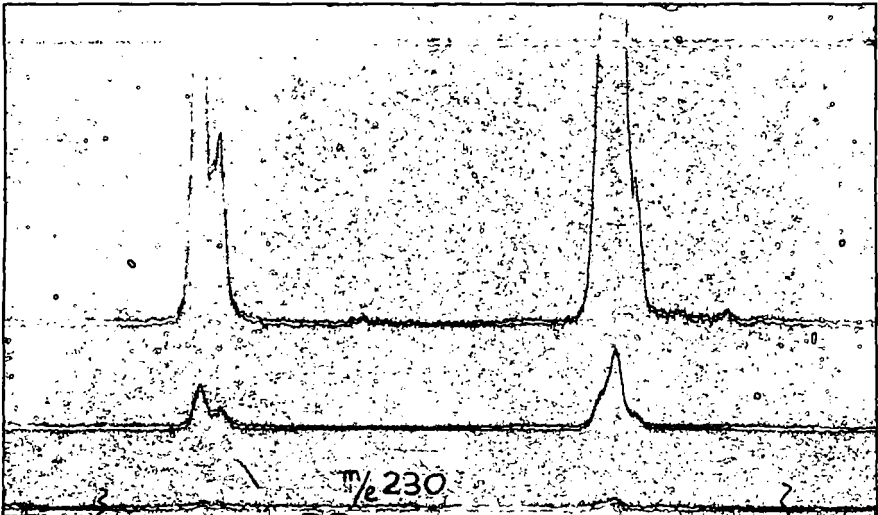


Fig.2 Petroleum Fraction, mass 230. Resolution 30,000

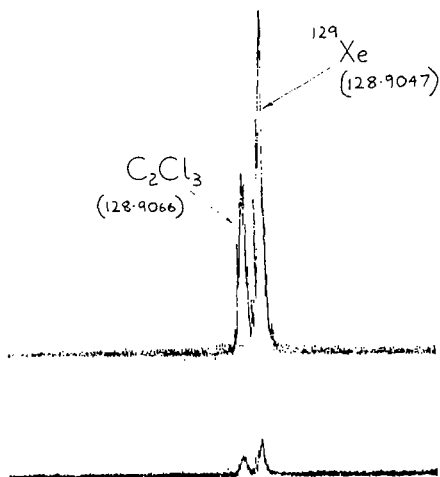


Fig.3 m/e doublet in Xe - C₂Cl₄ mixture. Mass separation 1 part in 70,000. Measured 10% valley resolution 70,000.

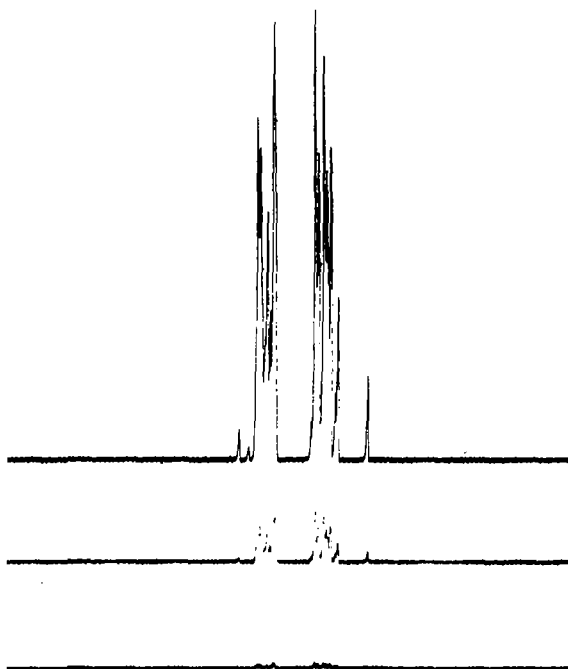


Fig.4 m/e 131 doublet in Xe - C₂Cl₄ mixture. The components are ¹³¹Xe and C₂³⁴Cl³⁵Cl₂, with mass separation of 1 part in 89,000. 10% valley resolution measured from this scan 200,000. Average of 4 repeat scans was 160,000.

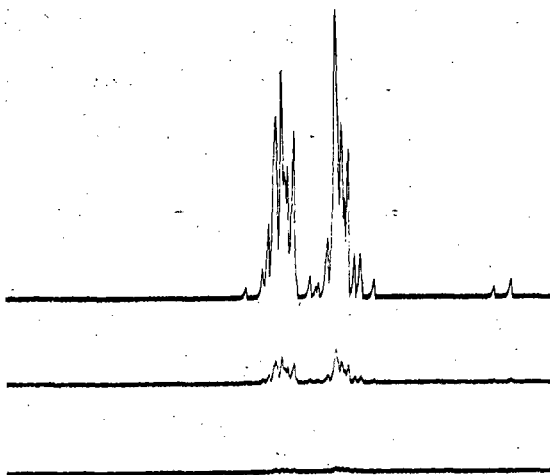


Fig.5 Repeat scan of doublet in Fig.4. 10% valley resolution measured from this scan 140,000. Average of 4 repeat scans was 160,000.

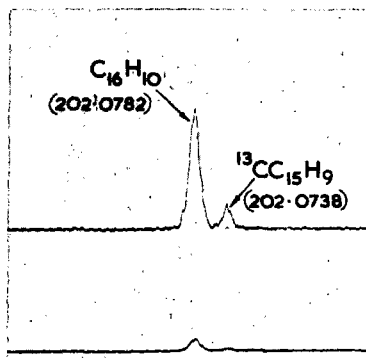
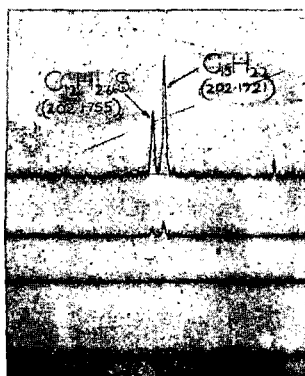


Fig.6 Doublets of the type expected in a petroleum fraction spectrum.

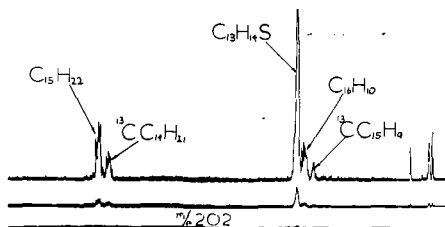
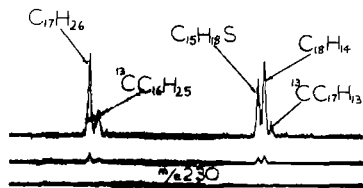


Fig. 7 m/e 202 and 230 from petroleum fraction. Resolution $\sim 60,000$.

PETROLEUM FRACTION

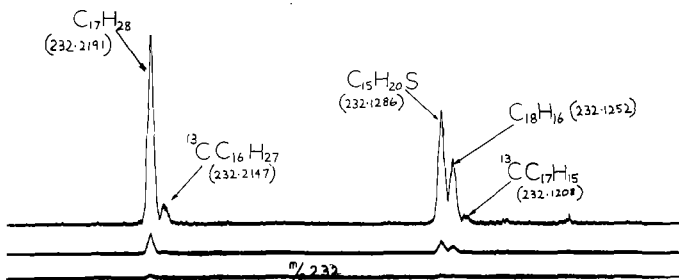


Fig. 8 m/e 232 from petroleum fraction. Resolution $\sim 60,000$

TOBACCO EXTRACT—FIELD IONIZATION.

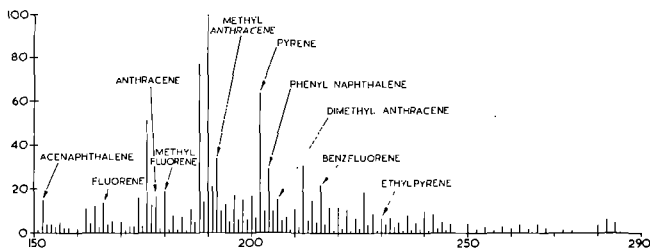


Fig. 9 Line drawing of low resolution field ionization spectrum of tobacco extract.

The MS902 spectrometer in the authors' Laboratory will routinely give a resolution of 70,000 and when required this is set up with the aid of a mixture of xenon and ethylene tetrachloride. This mixture gives a doublet peak at m/e 129 which requires a resolution of 70,000 for separation. Fig.3 shows an example of this doublet recorded during a setting up procedure. It should be pointed out that the other vital parameter to be considered when working under these ultra high resolving power conditions is sensitivity. It is important that the instrument is adjusted to give maximum sensitivity at the required resolving power in order to avoid signal-to-noise ratio or ion statistical problems during the analysis to be performed. Bearing this in mind, it is worthwhile noting that the maximum resolution obtained on the instrument is frequently in excess of 70,000, and this "extra" can then be utilised to allow wider slit settings and, therefore, to give higher sensitivity at 70,000 resolving power.

Figs. 4 and 5 show some of the latest results obtained. These are recordings of the m/e 131 doublet in the spectrum of the xenon tetrachloroethylene mixture. This requires a resolution of 89,000 for separation. The resolving power shown in Fig.4 is in fact over 200,000. However, it should be noted that under these conditions, the rate of arrival of ions is low enough for random variations to be significant, and hence the peak widths observed will vary from one individual scan to another. It is therefore important to run several repeat scans in order to determine a reliable figure for the resolving power of the instrument. Fig.5 is a repeat scan of the m/e 131 doublet which shows a resolution of 140,000. In this particular case, four repeat scans were taken, of which Figs. 4 and 5 are two, and the average value obtained for the resolving power was 160,000.

Fig.6 shows two doublets of the type expected to be present in the spectrum of the petroleum fraction under study. The top trace shows a resolving power of 70,000 (10% valley) and is the molecular ion peaks of 1,1,3,3,5,6-hexamethylindane (C₁₅H₂₂) and 7-thiatridecane. The lower trace is a CH-¹³C doublet at the molecular ion of pyrene. These two known samples served to show that the performance of the instrument was adequate for the problem in hand.

The spectrum of the petroleum fraction was now examined at a resolving power of about 60,000. Fig.7 shows the recorder trace for m/e 202 and 230, i.e. the molecular weight of the two known compounds previously studied and a higher homologue. It can be seen that in each case the two main components have split into a doublet (higher mass) and triplet (lower mass). No peak corresponding to the molecular ion of 7-thiatridecane at m/e 202 or the homologue at m/e 230 was observed. The doublet peak at each mass represents the molecular ion of the methylated indane and the ¹³C isotope peak from one mass unit lower. However, in each case the lower mass component is a triplet. The lowest mass component of this triplet is a ¹³C isotope peak and the other two peaks represent an SH₄-C₃ doublet. Fig.8 shows the trace for m/e 232 which again shows a similar pattern. The table below gives the possible identities of the compounds responsible for these peaks. Those which are underlined are most certainly present in the sample, others are tentative identifications.

PETROLEUM FRACTION

<u>m/e</u>	<u>Formula</u>	<u>Possible Identity</u>	
230	(C ₁₇ H ₂₆ (.2034)	<u>Alkyl indane and/or tetralin</u>	
	(¹³ C C ₁₆ H ₂₅ (.1990)	Isotope Peak	
	{	(C ₁₅ H ₁₈ S (.1129)	Alkyl tetrahydro dibenzothiophene
		(C ₁₈ H ₁₄ (.1095)	Dihydronaphthacene
	(¹³ C C ₁₇ H ₁₃ (.1051)	Isotope Peak	
232	(C ₁₇ H ₂₈ (.2191)	<u>Alkyl benzene</u>	
	(¹³ C C ₁₆ H ₂₇ (.2147)	Isotope Peak	
	{	(C ₁₅ H ₂₀ S (.1286)	<u>Alkyl benzo thiophene</u>
		(C ₁₈ H ₁₆ (.1252)	Tetrahydronaphthacene Tetrahydrochrysene
	(¹³ C C ₁₇ H ₁₅ (.1208)	Isotope Peak	

The tobacco extract studied was the polycyclic fraction which had been previously separated from the heterocyclic fraction of the same extract. In this case, because of the aromatic nature of the compounds present, the low resolution electron impact spectrum was somewhat less complex than that for the petroleum fraction in that it was possible to obtain more information regarding the molecular weight range of the compounds present. However, the field ionization spectrum was further simplified and a line drawing of it is given in Fig.9. Marked on here are the tentative identifications of some of the peaks. The molecular formulae have been confirmed by the complete high resolution spectrum run at a resolving power of about 10,000. However, some of the quite intense peaks are still unidentified and further work on this fraction as well as the corresponding heterocyclic fraction is required before more definite analytical information can be given.

This work has shown the value of field ionization techniques and ultra high resolution studies with electron impact ionization for the study of complex mixtures. The very high resolution has allowed the confirmation of the presence of sulphur containing compounds previously thought to be present in petroleum extracts, but unconfirmed because of the lack of resolving power. It should also be pointed out that the peaks studied were by no means the most intense and yet the instrumental sensitivity was adequate for the doublets involved to be readily measured and identified.

Acknowledgment

The authors would like to thank Dr. J.D. Waldron, Director and General Manager, AEE Scientific Apparatus Division, for permission to publish this paper.

They are also indebted to Mr. M.L. Mead of the British Petroleum Company for helpful discussions regarding interpretation of the results and for supplying the samples of 1,1,3,3,5,6-hexamethylindane, 7-thiatridecane and the petroleum fraction.

Thanks are also due to Dr. K. Rothwell of the Tobacco Research Council, Harrogate, for supplying the tobacco extract.

PYROLYSIS OF NATURAL PRODUCT IV.
Identification of Products from Nucleotide Pyrolysis
by High Resolution Mass Spectrometry

H. G. Boettger and A. M. Kelly

Jet Propulsion Laboratory
Space Sciences Division
4800 Oak Grove Drive
Pasadena, California 91103

During the past years a long series of pyrolysis experiments on biologically important compounds has been carried out at JPL in preparation of proposed life detection experiments on the planets. (1,2,3)

The present study was designed to investigate possible alternate methods to the GC/MS approach for the analysis of pyrolysis products from nucleic acid materials. The main reason for this investigation is to determine whether the lack of characteristic fragments in their pyrograms is due to their inability of being formed under pyrolysis conditions or their inability to pass the gas chromatographic column.

The experimental set up in our laboratory includes a modified MS-902 and the computerized data system described previously. (4,5,6) The modifications on the MS-9 include a high capacity pumping system (700 liter/sec at the diff. pump), a direct coupled capillary or Scot-type GC column for the GC/MS part of the experiments and a new heated probe for the MS-9 direct insertion lock. The oven for the gas chromatographic column is fitted with pyrolyzer and hypodermic injection port. (3) The oven can be operated isothermally and/or programmed from below ambient to 400°C. However, due to limitations on the columns which are suitable for the over-all experiment, maximum operating temperatures did not exceed 220°C.

Figure 1 shows the modified probe for the MS-9 insertion lock. It is fashioned after the one described by Teeter, et al. (7) It is interchangeable with the standard probe. However, it can be heated to approximately 850°C and cooled down to the temperature of liquid nitrogen. A thermocouple is located near the tip of the probe to monitor and/or control the temperature.

During vacuum probe pyrolysis approximately 1 mg is loaded into the probe cavity and pumped down. Spectra are recorded at approximately 30 sec intervals as the probe is heated at a programmed rate continuously or stepwise from ambient to 750°C. The beam monitor output is recorded during the entire run and marked automatically whenever a spectrum is taken. During all experiments spectra are recorded at a resolving power which is never less than that required for mass measurement. We like to operate at a dynamic resolving power of at least 1/5000. However, useful data can be obtained at lower resolving power.

The analysis of the data is carried out by our previously described data system in combination with frequent monitoring by the investigator. The more frequent monitoring of these data in contrast to the usual high resolution processing is carried out to eliminate redundant data and easily identified spectra at an early stage of the processing, and thus reduce the amount of data to be fully processed. Should questions arise at a later date, processing of part or all these spectra can be resumed as required. The presently used system represents a simulation of man-machine interfacing on the remote console of a time shared system such as the Univac 1108.

Figure 2 summarizes the data flow. The recorded spectra are digitized and converted to mass vs. intensity data. We now inspect the data for obvious single component spectra and separate them from suspected multi-component spectra. From the former we eliminate the spectra of readily identified substances, while the remaining single component spectra are submitted to a library search. The results of this search provide identification of the majority of this group. The remainder is submitted for elemental composition calculation and a final identification is attempted by conventional high resolution techniques.

Meanwhile, the obvious mixture spectra are inspected for recognizable components. If these are detected, intensity adjusted reference spectra are subtracted and the residuals are submitted for library search. Spectra which can still not be identified are also processed further by the high resolution mode in order to get a handle on the mixture.

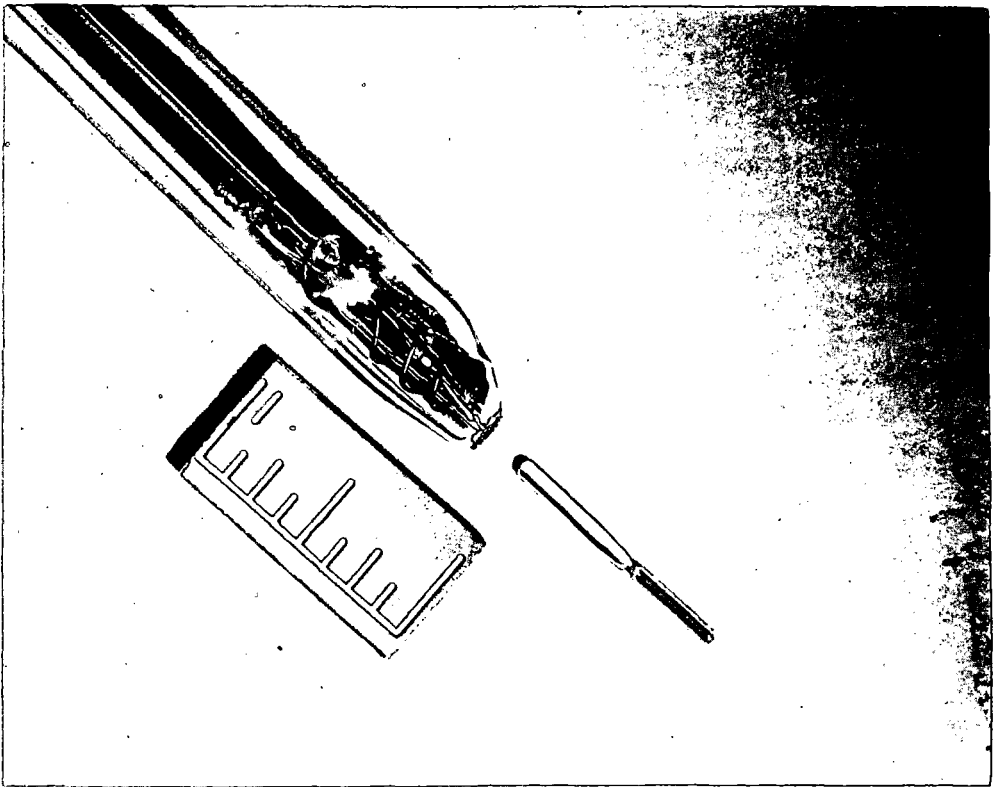


FIGURE 1

DNA - VACUUM - PYROLYSIS

TEMPERATURE, °C	105	175	300	450	600
CYTOSINE	0	6500	450	0	0
METHYLCYTOSINE	0	600	0	0	0
THYMINE	0	102,000	10,000	12,000	12,000
ADENINE	0	80,000	2400	1500	2100
GUANINE	0	0	1600	0	0
ADENOSINE	0	800	0	0	0
ADENOSYL	0	1,700	0	0	0
DEOX ADEN, -2H ₂ O	0	55,000	3900	3400	2900
HCN	800	18,000	56,000	98,000	132,000

FIGURE 3

ANALYSIS OF PYROLYSIS DATA

MAJOR PRODUCTS OF NUCLEIC ACID VACUUM PYROLYSIS

1. RECORD AND DIGITIZE ALL SPECTRA
2. MANUALLY INSPECT PYROGRAM AND SPECTRA
3. SELECT THOSE SPECTRA WHICH APPEAR TO BE DUE TO SINGLE COMPONENTS AND SUBMIT THEM TO A SEARCH OF THE LIBRARY
4. ATTEMPT IDENTIFICATION OF SPECTRA DUE TO MULTIPLE COMPONENTS BY A COMBINATION OF COMPUTER AND MANUAL METHODS
5. PEAKS OR COMPONENTS OF A PEAK STILL UNIDENTIFIED ARE SUBMITTED TO HIGH RESOLUTION MASS ANALYSIS
6. VERIFY ASSIGNMENTS BY CHECKING AGAINST GC RETENTION DATA (IN CASE OF GCMS)

NUCLEIC MATERIAL	PRODUCT
DNA	CYTOSINE, METHYL-CYTOSINE, THYMININE, ADENINE, GUANINE, ADEPHOSINE, DEOXYADEPHOSINE
RNA	SAME
POLYADENYLIC ACID	ADENINE, ADEPHOSINE
POLYCYTIDYLIC ACID	CYTOSINE
FLAVIN-ADENINE DINUCLEOTIDE	ADENINE, FLAVIN
POLYADENYLIC-CYTIDYLIC ACID	ADENINE, CYTOSINE
POLYURIDYLIC ACID	URACIL
ADENYLIC ACID	ADENINE
CYTIDYLIC ACID	CYTOSINE
THYMIDINE-5-TRIPHOSPHATE	THYMININE
URIDINE TRIPHOSPHATE	URACIL
GUANOSINE TRIPHOSPHATE	GUANINE

FIGURE 5

FIGURE 2

DNA - VACUUM - PYROLYSIS
(SMALL FRAGMENTS)

TEMP °C	105	175	275	320	400	450	500	600	640
HCN	800	18,000	15,000	56,000	98,000	51,000	132,000	115,000	14,000
CO	20,000	>125,000	16,000	60,000	60,000	>10,000	35,000	>125,000	>132,000
CO ₂	13,000	>310,000	66,000	144,000	113,000	36,000	115,000	160,000	10,000
CH ₄	800	42,000	9000	12,000	15,000	5000	4000	7000	0
C ₂ H ₂ O	3000	17,000	12,000	15,000	15,000	11,000	8000	7900	0
C ₂ H ₄ O	0	0	37,000	10,000	6000	4000	4000	4000	0
C ₂ H ₂ O	0	0	240,000	-	26,000	7000	4500	4000	15,000
C ₂ H ₄	1800	117,000	18,000	27,000	15,000	4000	5000	5500	0
C ₂ H ₆	400	44,000	1800	3500	3000	900	1000	1800	0
C ₂ H ₄	2000	40,000	2000	4700	5000	2400	3600	3600	0
CH ₃ CHO	900	18,000	1700	20,000	11,000	4700	7300	10,000	0
C ₂ H ₅ N ₃	0	17,000	-	11,000	900	0	0	0	0
ADENINE	0	80,000	4000	2500	1000	1500	1800	2100	1000

DNA - PYROLYSIS - GCMS

(500°C)

HYDROGEN CYANIDE, CARBON DIOXIDE, WATER

ACETONITRILE
ACRYLONITRILE
METHACRYLONITRILE
BUTANENITRILE
PYRIDINE
METHYL-PYRIDINE
METHYL-PYRAZINE

FIGURE 4

FIGURE 6

Finally, assignments are checked against standard spectra and, in case of GC/MS, against retention data.

Typical results are shown in Figures 3 and 4. The nucleic acid bases, e.g., adenine, thymine, etc., are released intact at $\sim 175^{\circ}\text{C}$ and dominate the part of the spectrum above mass 50. As the temperature of pyrolysis continues to rise, only low mass fragments such as HCN, CO_2 , etc., are found in high intensity.

The data show that pyrolysis indeed does yield extremely characteristic fragments, at least under the conditions described above. The bases can be identified readily qualitatively and, hopefully, quantitatively with some refinements of the technique.

The major products of nucleic acid pyrolysis using the vacuum probe technique are summarized in Figure 5. In contrast, Figure 6 shows the products found by GC/MS pyrolysis at 500°C . These products are mostly of minor nature, if one excludes HCN, CO_2 , and H_2O . In addition, they are not characteristic of nucleic acid type materials.

The next question to be answered is whether or not the above technique can be combined with the GC/MS technique to yield an over-all pyrogram of a substance subjected to a search for life related materials. We will report about this phase of the investigation at a later date.

ACKNOWLEDGMENT

This paper presents the results of one phase of research carried out at the Jet Propulsion Laboratory, California Institute of Technology, under Contract No. NAS7-100, sponsored by the National Aeronautics and Space Administration.

REFERENCES

1. Bentley, K. E., Giffin, C. E., Whitten, D. G., Wilhite, W. F., AAS Science and Technology 93, 2 (1964).
2. Whitten, D. G., Bentley, K. E., and Kuwada, D., J. Org. Chem. 31, 322 (1966).
3. Simmonds, P. G., Shulman, G. P., and Stenbridge, C. H., J. Chromatographic Sci., 7, 36 (1969).
4. Boettger, H. G., 15th Annual Conference on Mass Spectrometry and Allied Topics, May 14-19, 1967, Denver, Colorado, N31, p. 90, 1967.
5. Boettger, H. G., American Chemical Society Western Regional Meeting, Anaheim, California, October 30-November 1, 1967, Abstr. #233 (1967).
6. Boettger, H. G., 17th Annual Conference on Mass Spectrometer and Allied Topics, May 19-22, 1969, Dallas, Texas.
7. Private Communication.

COMPUTER ANALYSIS OF HIGH RESOLUTION MASS SPECTRA IV.
 The Influence of Peak Model Parameters Upon
 Mass Measurement Accuracy and Multiplet
 Recognition

H. G. Boettger and A. M. Kelly

Jet Propulsion Laboratory
 Space Sciences Division
 4800 Oak Grove Drive
 Pasadena, California 91103

Two years ago (1,2) we described a new "Peak Analysis" method as part of our data reduction setup for fast scanning high resolution mass spectrometers. The major difference between this method and the methods which had been reported at that time was the attempt to recognize and measure more or less unresolved (threshold $\geq 1\%$ of full scale) multiplets. With only minor changes from the reported version, this program has been in routine operation for the last two years. During this period we have tried to analyze all the factors which might affect the quality of the results. The goal of this study was to improve mass measurement accuracy, peak recognition, and most importantly the over-all confidence in a given set of results.

Figure 1 lists the factors which influence the quality of the processed data:

1. As the resolving power of the mass spectrometer is increased, the quality of the data increases until the point is reached where the loss of sensitivity offsets gains made by greater separation of ionic species. Therefore, the mass spectra should be recorded at a resolving power high enough to make the best possible mass measurement, but not so high that a parent peak of greater than 0.1% would be lost or noise would begin to affect the mass measurement seriously.
2. We investigated the effect of different digital sample rates and recording systems response. We found, that as long as a "normal" peak is represented by about 20 samples and the peak is not significantly distorted, the improvements with increased bandwidth and sample rate are only marginal.
3. Peak model parameters will be discussed in detail in the second part of this presentation.
4. The effect of the data threshold is quite complex and will be studied in more detail elsewhere. At this time I wish to call your attention only to the following facts:

as the thresholds for minimum intensity and minimum numbers of data points are raised, the processing of the data becomes simpler all the time since only large singlet peaks will remain. As a matter of fact, if we raise both values high enough, the peak analysis problems will go away entirely. Unfortunately, that defeats the purpose of running the sample in the first place. Therefore, we provide two chances for thresholding:

- a. during the data logging stage, which accepts all signals resulting from more than 5-10% of the width of a "normal" peak at threshold and greater than 2-3 times rms noise.
 - b. during peak analysis where we accept peak width down to 25% on the first pass and intensities $\geq 1\%$ of full scale. Here we have the option of reprocessing at different levels if desired.
5. The effect of spectra averaging (3) and reasons for it will be discussed in the final part of this presentation.

Figure 2 demonstrates, as pointed out before, any improvements in mass measurement accuracy with increasing clock rate are marginal as long as a sufficient number of points is used to describe the peak. This is due to the fact that at the lower rates a certain amount of noise filtering occurs which is lost at higher rates. Improvements can only be achieved when the data "smoothing rate" is increased proportionately. But this also increases the cost of processing significantly and can be justified only in special cases.

Figure 3 demonstrates several factors. First, increasing the bandwidth does not in itself improve mass measurement accuracy. Secondly, due to the ever present noise in a fast-scan system there are always discontinuities in the relationships because of competing forces. We found that in general the empirical selection of operating parameters leads to the quickest results.

Third, and most comforting, is the fact that the mass measurement accuracy is not critically sensitive to any of these operating parameters as long as one stays within reasonable limits and is willing to accept average errors in the 1-2 milli-AMU range.

Figure 4 shows the variation of the average error with multiplier gain. As expected, as the gain increases, the noise and with it the error increases. But again, there is no critical deterioration as long as one stays within a reasonable range of multiplier gain.

This leads us to the effect of the peak model parameters. Figure 5 presents a list of the ones which are a part of our program:

1. Basewidth (sec.)
2. Filter window (% basewidth)
3. Minimum number of points for slope analysis (% basewidth)
4. Minimum number of points for peak acceptance (samples)
5. Resolution (sec.)
6. Minimum change of slope

It becomes obvious from the relation of items (2) and (3) to (1), that the "basewidth" is the peak model parameter of the greatest importance. If the selected value of (1) is too small, every noise spike and scattered ion is accepted as a peak and produces a spectrum listing which requires as much work to analyze as would have the raw spectrum. On the other hand, if the selected value is too large, multiplets will be treated as singlets. Therefore, peaks will be lost and erroneous mass values and compositions will be calculated. Thus, it is important to determine the basewidth of a normal peak with as much accuracy as possible. The determination of this input value can be made in one or all of the following ways. The spectrum is monitored on an oscilloscope as it is recorded and/or reproduced. The peak width of a number of clean singlets is measured. Alternatively, the determination can be made from raw digital data (PEAK EDIT). The question remains as to how critical is the determination of the basewidth value.

Figure 6 gives us an answer to this question. The true peak width is about 1.5 millisecond. It can be seen that varying the input value from 1.0 to 2.0 produces no significant variation. The optimum filter window was determined in the region of 40-60%. Below 40% insufficient smoothing of the data occurs and above 60% artifacts are produced due to "ringing" of the filter.

The minimum number of points which is required before slope analysis is carried out is normally set at 125-150% of basewidth. 125% is used for good spectra with a minimum of pressure broadening on the peaks. This means that a peak is considered a singlet and treated by the centroid technique unless the width of the peak at the threshold exceeds that of a "NORMAL" peak by 25%. Again, the importance of selecting a good value for the normal peak cannot be over-emphasized.

The remaining three parameters which were listed in Figure 5 are additional safeguards against accepting extraneous peaks due to a noisy spectrum. The "minimum number of points for peak acceptance" limits again the number of signals above threshold that are classified as peaks. The number is usually more restrictive than the one used in the data logging stage. The same is true for the intensity threshold which is used at this point as was mentioned above.

The minimum resolution criterium is derived from resolving power at which the mass spectrum was recorded and eliminates the listing of combinations of ion species which could not have been recognized under the given experimental conditions.

The minimum change of slope guards against introduction of false fragments due to minor distortions in the peak profile. For routine separation this value is set permanently such that the slope must go to zero before a peak is identified.

FACTORS AFFECTING OPTIMUM DATA ANALYSIS

- (1) MASS SPECTROMETER RESOLVING POWER
- (2) DIGITAL SAMPLE RATE
- (3) PEAK MODEL PARAMETERS
- (4) THRESHOLD OF DATA ACCEPTED
- (5) NUMBER OF REPETITIVE SPECTRA THAT CAN BE AVERAGED

MASS MEASUREMENT ACCURACY vs CLOCK RATE

CLOCK (cps)	AVERAGE ERROR (AMU $\times 10^3$)
20,000	0.92
40,000	1.56
80,000	1.15

MASS MEASUREMENT ACCURACY vs BANDWIDTH

BANDWIDTH	AVERAGE ERROR (AMU $\times 10^3$)	
	CLOCK 80,000 cps	CLOCK 40,000 cps
10,000	1.15	1.56
5000	1.15	1.66
2000	1.35	1.23
1000	0.96	0.73
500	—	0.78

MASS MEASUREMENT ACCURACY vs MULTIPLIER GAIN

MULTIPLIER GAIN (DIV)	AVERAGE ERROR (AMU $\times 10^3$)
2000	0.71
3000	0.83
4000	1.15
5000 (10^4)	1.18
6000	1.42

PEAK MODEL PARAMETERS

- (1) BASE WIDTH (sec)
- (2) FILTER WINDOW (% BASE WIDTH)
- (3) MINIMUM NUMBER OF POINTS FOR SLOPE ANALYSIS (% BASE WIDTH)
- (4) MINIMUM NUMBER OF POINTS FOR PEAK ACCEPTANCE (SAMPLING POINTS)
- (5) RESOLUTION (sec)
- (6) MINIMUM CHANGE OF SLOPE

FIG. 5

PEAK AVERAGING MAX ERROR
 (A) ¹²C PEAKS OF HEXACHLOROBADIENE BETWEEN 147 AND 2021

m/e	12.1	12.2	12.3	12.4	12.5	12.3	12.4	AVER	MAX 1"
147	-0.20	0.70	-2.10	-0.50	0.00	0.10	-0.33	-2.10	
151	-0.64	0.50	-0.80	0.20	-1.10	-0.40	-0.37	-1.10	
155	-0.20	-0.70	-0.90	-0.70	-0.10	-1.02	-0.63	-1.70	
157	0.50	-0.30	-0.90	-0.70	-1.30	-1.20	-0.64	-1.20	
159	-0.80	-0.40	-	-	-1.60	-0.40	-0.80	-1.60	
164	-1.00	0.20	-0.20	-1.60	-1.80	0.90	-0.54	-1.80	
166	-2.80	-0.60	-0.90	-0.80	-2.10	-1.90	-1.32	-2.80	
168	-1.10	0.70	-2.00	-	-2.50	-2.80	-1.28	-2.80	
188	0.00	0.30	-0.70	0.50	2.10	-0.10	0.27	2.10	
190	0.40	-1.60	0.30	0.30	1.40	-	0.16	-1.60	
192	-1.50	-1.10	-1.80	-2.10	1.40	0.30	-0.67	-2.10	
194	-1.00	-0.70	-0.30	-0.50	1.50	2.70	0.20	2.70	
196	-0.30	-0.20	-2.10	-	-	-0.70	-0.70	-2.10	
222	-0.90	-0.10	0.60	0.70	-0.80	-0.70	-0.20	-0.90	
223	-2.10	-1.60	0.10	0.80	0.70	-1.30	-0.93	-2.10	
225	-1.00	-0.40	-0.40	-0.40	-0.90	-0.90	-0.90	-1.00	
227	-0.10	0.60	-0.50	-0.50	-1.40	-1.00	-0.57	-1.10	
231	-2.00	2.30	-0.50	-1.40	-0.90	-2.70	-0.84	-2.70	
238	-1.90	0.20	-0.40	0.40	0.80	0.00	-0.07	-1.90	
240	-2.80	0.40	-0.50	-1.10	3.00	1.40	-0.53	-1.90	
262	0.30	1.60	0.40	-1.50	3.70	-0.70	-0.63	-3.20	
AVER	1.20	0.79	0.17	0.79	1.44	0.95	0.60	2.14	

PEAK AVERAGING MAX ERROR

m/e	SINGLE RUN	AVER3	AVER5	AVER10	INTENSITY x WIDTH
32	1.58	0.76	0.95	0.39	0.140
44	1.46	0.75	0.74	0.37	0.018
50	0.98	0.80	0.30	0.20	0.140
69	4.50	2.30	2.30	2.10	100.000
93	2.73	1.60	2.00	1.40	0.720
105	2.79	1.00	1.30	0.30	0.012
133	3.20	1.40	1.30	1.00	0.071
150	2.99	2.30	1.20	1.10	0.200
175	3.00	2.20	1.20	0.90	0.033
224	4.90	3.30	0.70	0.50	0.060
257	7.90	4.30	6.70	1.70	0.010
312	7.50	0.80	1.80	1.10	0.017
412	5.10	5.10	4.70	3.80	0.010
519	6.80	5.30	6.30	3.82	0.012
AVER	3.96	2.28	2.21	1.33	-

FIG. 7

MASS MEASUREMENT ACCURACY AND NPEAK
 VS
 BASE WIDTH AND CLOCK RATE

CLOCK	40 kc						80 kc	
	1.0		1.5		1.8		2.0	
BASE mill-sec	AVER	NPEAK	AVER	NPEAK	AVER	NPEAK	AVER	NPEAK
2.37	35	2.37	35	2.33	40	2.33	38	
	35	2.45	31	1.98	37	2.32	35	
2.35	29	1.97	30	2.57	34	2.37	39	
	33	2.10	32	2.24	37	2.34	38	
2.37			2.26		2.34		2.32	3.5 ppm

FIG. 6

FIG. 8

Having worked out optimized peaklogging and data analysis schemes, we found that in the case of fast scan, high resolution spectra our confidence level in some of the results was less than what we wished it to be. Often mass measurement of an ion did not agree with our preconceived notion of the composition of the ion or the ion of the expected composition showed a larger than usual error. It was obvious from the data that our problems resulted almost exclusively from excessively high random variations due to ion statistics, etc., which occasionally was complicated by unresolved multiplets in a noisy spectrum. An analysis of the available data showed that the solution was to increase the statistical sample. Obviously, the most direct approach would be to scan more slowly and thereby collect more ions. Due to over-all experimental requirements, this approach is not always possible. Therefore, alternate routes were investigated. As a result of this investigation, we concluded that the best solution would be to run as many duplicate spectra as possible, usually 3-5, and average the calculated masses for each peak. The program will also average the intensities. The average intensities, however, are used only when the sample concentration in the ion source stayed reasonably constant during the period when the spectra were taken.

Figure 7 shows the results which are obtained by this technique. It can be seen that typically the mass measurement error is reduced by a factor of three. In addition the confidence in the measured masses is enhanced greatly.

Figures 7 and 8 show the effects of peak averaging as a function of both mass and intensity of the peak.

It has been shown that by optimizing the "PEAK MODEL" and "DATA ANALYSIS" parameters mass measurement errors can be held in the order of $1-2 \times 10^{-3}$ AMU up to $m/e \sim 800$. Further improvement in the order of a factor of 3-5 can be made by "PEAK AVERAGING". In addition, the confidence in the numbers which are generated by the data system is increased significantly by this technique. Finally, by means of the averaging technique, it is possible to extract useful information from relatively poor spectra.

ACKNOWLEDGMENT

The authors wish to thank Mr. D. Locke and Mrs. R. Moor of FSD for their contribution in translating our ideas into computer programs.

This paper presents the results of one phase of research carried out at the Jet Propulsion Laboratory, California Institute of Technology, under Contract No. NAS7-100, sponsored by the National Aeronautics and Space Administration.

REFERENCES

1. Boettger, H. G., 15th Annual Conference on Mass Spectrometry and Allied Topics, May 14-19, 1967, Denver, Colorado, N31, p. 90, 1967.
2. Boettger, H. G., American Chemical Society Western Regional Meeting, Anaheim, California, October 30-November 1, 1967, Abstr. #233 (1967).
3. Burlingame, A. L., Adv. in Mass Spect. Proc. Conf. Berlin, 1967, V. 4, p. 15-35, 1968, Inst. of Petrol. London & Elsevier, Amsterdam and New York.

ANALYSIS OF TRIMETHYLSILYL DERIVATIVES OF
CARBOHYDRATES BY MASS SPECTROMETRY*

Don C. DeJongh and J. D. Hribar

Department of Chemistry,
Wayne State University,
Detroit, Michigan 48202

ABSTRACT

The fragmentations of a number of common monosaccharides and disaccharides have been studied in detail as their trimethylsilyl (TMS) derivatives, using deuterium labeling and exact-mass measurements. It is possible to recognize ring size and degree and position of substitution from the mass spectra. A number of interesting rearrangements are observed, also.

The results obtained from these spectra have been applied to mass spectrometric studies on aminocyclitol antibiotics. These antibiotics, together with model compounds derived from them by various degradative reactions, have been investigated in the form of their N-acetyl-O-trimethylsilyl derivatives. From the mass spectral data, it is possible to recognize the sequential arrangement and gross structures of the units of which the saccharides are comprised.

Minute molecular ion peaks are present in the mass spectra of the N-acetyl-O-trimethylsilyl derivatives of the intact antibiotics. Peaks 15 mass units lower, from loss of CH_3 from a trimethylsilyl group, are more intense. Cleavage of glycosidic bonds is observed. The fragmentations are many and complex.

Although the preparation of TMS derivatives greatly increases the molecular weight, the use of such derivatives is advantageous because of the increase in volatility.

* For previous publications in this area see: a) D. C. DeJongh, J. D. Hribar, S. Hanessian, and P. W. K. Woo, *J. Am. Chem. Soc.*, **89**, 3364 (1967) and b) D. C. DeJongh, T. Radford, J. D. Hribar, S. Hanessian, M. Bieber, G. Dawson, and C. C. Sweeley, *ibid.*, **91**, 1728 (1969).

MASS SPECTRA OF POLYSUBSTITUTED MACROCYCLIC
LACTONES DERIVED FROM MACROLIDE ANTIBIOTICS

by

R. L. Foltz, Battelle Memorial Institute, Columbus Laboratories, Columbus, Ohio
L. A. Mitscher, College of Pharmacy, The Ohio State University, Columbus, Ohio
M. I. Levenberg, Abbott Laboratories, North Chicago, Illinois

The macrolide antibiotics are a clinically important class of compounds which possess as a characteristic feature a substituted macrocyclic lactone system. In order to explore mass spectrometry as an analytical tool for determining the functionality present in specific macrolide molecules, we have obtained mass spectral data on a series of compounds related to the macrocyclic ring system found in erythromycin B.

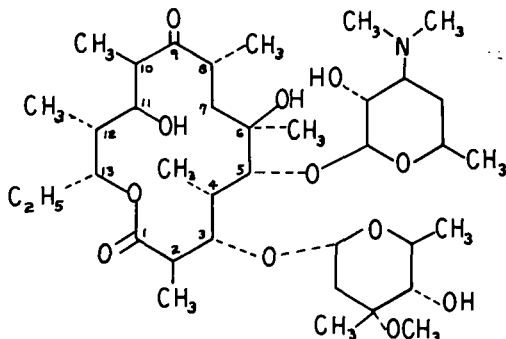


Figure 1. Erythronolide B

Erythronolide B is the aglycone of erythromycin B and is known to be a biological precursor of the antibiotic. Its unit-resolution spectrum is shown in Figure 2. The spectrum is very complex with the stronger peaks at lower masses, making interpretation a definite challenge. The interpretation, however, has been greatly facilitated by our being able to obtain complete high resolution mass spectra on more than twenty compounds related to erythronolide B. The mass spectral data were obtained using the on-line digital data recording system described at last year's conference. As you will see shortly, the high resolution data are nearly essential to the interpretation of these mass spectra.

In this study we have also utilized a semi-automatic metastable scanning system employing the "defocusing technique". With this system it is possible to obtain experimental evidence rapidly and conveniently for precursor ions for nearly every fragment ion in a mass spectrum.

Although there is evidence for many different fragmentation processes occurring in the electron-impact mass spectrum of compounds related to erythronolide B, two specific processes have proven to be particularly useful for structure identification. Both processes are apparently initiated by ring-opening via a McLafferty rearrangement involving the lactone carbonyl. Process A then undergoes rupture of the C₅-C₆ bond as shown in Figure 3. Ions corresponding to retention of the positive charge on either fragment are observed in the mass spectrum of erythronolide B. However, retention of the charge on the fragment containing carbons 6 through 13 (structure II) leads to the more prominent and structurally significant ions. These ions are prominent in the spectra of all of the compounds investigated having a hydroxyl group at the 6-position. The process is completely suppressed in those cases where there is no C₆-oxygen function. In the mass spectrum of erythronolide B, ion II undergoes two consecutive losses of water molecules followed by further C-C bond cleavage. In those compounds in which the C₁₁-OH group is absent or has been acetylated, we see the expected shift in composition of these ions. Also, reduction of the C₉-carbonyl results in the expected ion composition changes.

Fragmentation Process A, therefore, produces ions which are informative in regard to functionality present at carbons 6 through 13.

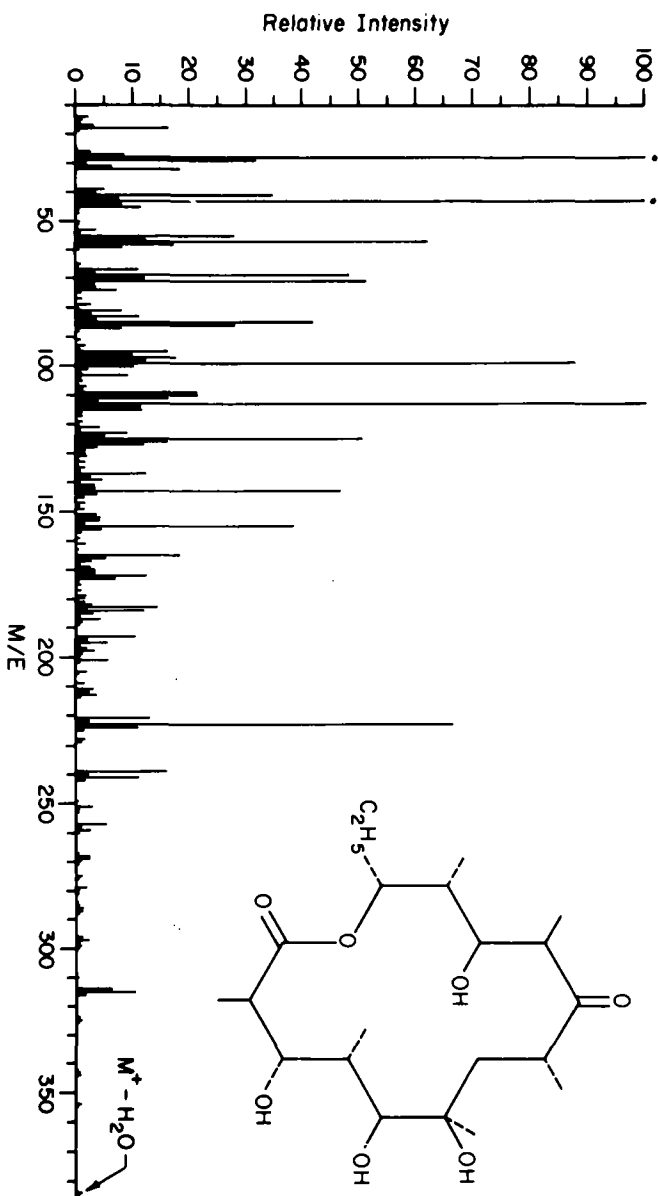


Figure 2. Mass Spectrum of erythronolide B

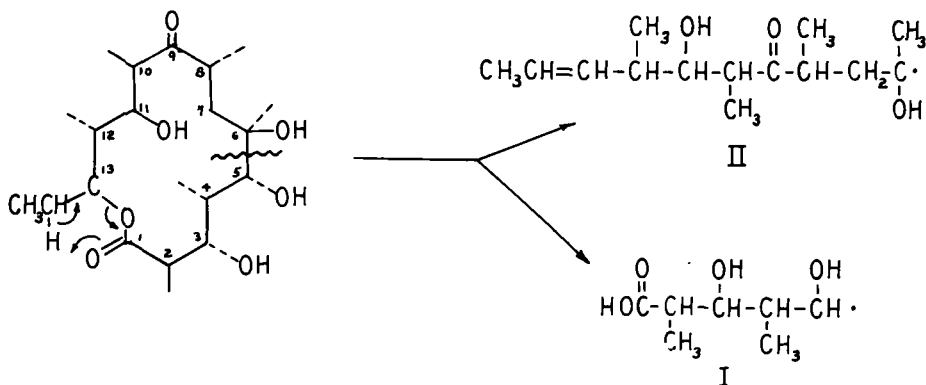


Figure 3. Fragmentation Process A

Fragmentation Process B (Figure 4) is complementary to Process A. Ring opening via the same McLafferty rearrangement is followed by cleavage of the C₉-C₁₀ bond adjacent to the ketone carbonyl. In this case the more prominent ions are due to retention of the positive charge on fragments containing carbons 1 through 9.

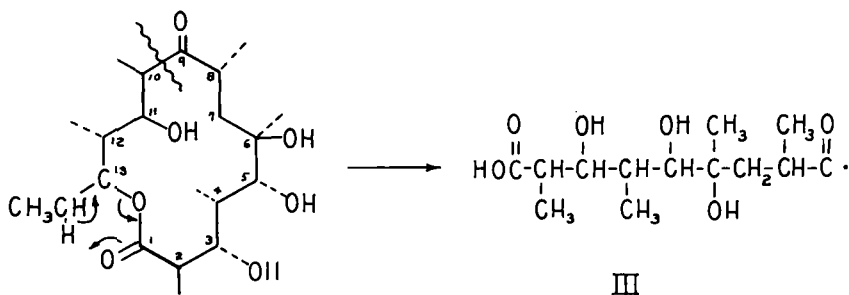


Figure 4. Fragmentation Process B

Fragment ion III then undergoes consecutive losses of 4 water molecules, loss of CO and further C-C bond cleavage. Acetylation or the absence of the hydroxyl groups at the C₃, C₅ and C₆ positions results in the expected ion composition shifts.

In a number of cases the two fragmentation processes lead to ions having the same nominal mass but different elemental composition. A striking example of this is seen in the spectra shown in Figures 5 and 6. Figure 5 shows the spectrum of 3,5,11-triacetyl-erythronolide B. The m/e 223 peak corresponds exclusively to the composition C₁₄H₂₃O₂. This is the ion composition that would result from fragmentation process A with loss of the C₁₁-acetate group as acetic acid.

Figure 6 shows the unit-resolution spectrum of a closely related compound in which the hydroxyl group at C-6 is absent. Again the m/e 223 ion is extremely intense; in fact it is the base peak in the spectrum. However, the high resolution data show that more than 99 percent of the peak corresponds to the composition C₁₃H₁₉O₃. This is the composition that would result from fragmentation process B; that is, ring opening via the McLafferty rearrangement at the lactone carbonyl, α-cleavage at the ketone carbonyl with charge retention on the larger fragment, and loss of two molecules of acetic acid.

Other examples can be cited where the unit resolution spectra by themselves present a confusing picture. Fortunately, complete high resolution spectra, particularly when combined with the metastable scanning data, provides the information necessary to effectively determine the structure of compounds in this series.

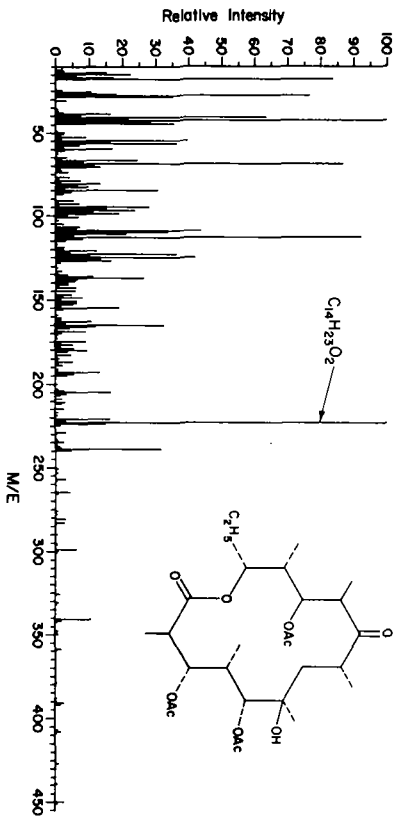


Figure 5.
Mass spectrum of 3,5,11-triacetyl-erythronolide B

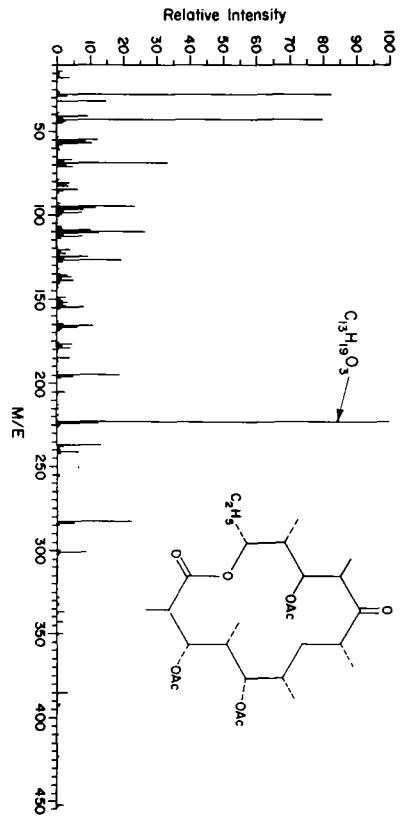


Figure 6.
Mass spectrum of 3,5,11-triacetyl-6-deoxy-erythronolide B

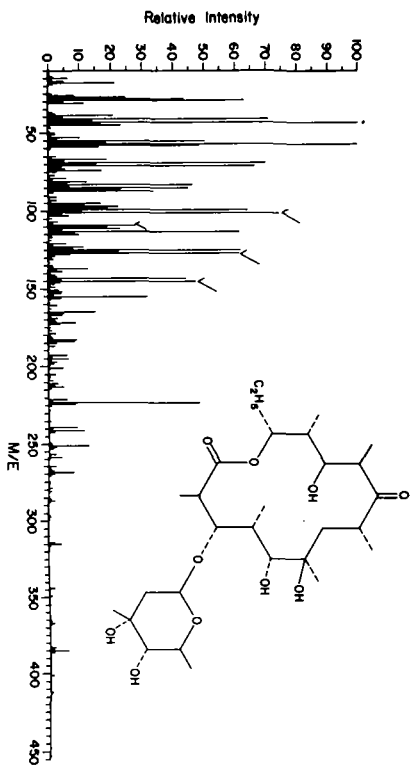


Figure 7.

Mass spectrum of erythronolide B
possessing a sugar substituent

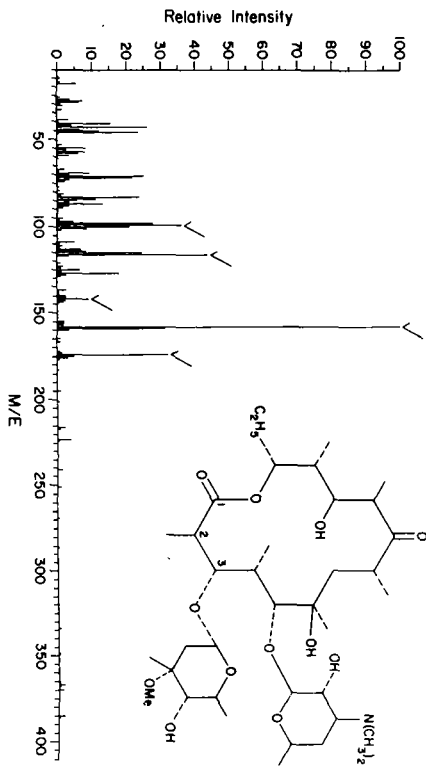


Figure 8.

Mass spectrum of erythromycin B

We therefore turned our attention to an examination of the mass spectra of similar compounds possessing sugar substituents. The mass spectrum of such a compound is shown in Figure 7. This compound corresponds to erythronolide B having one sugar residue attached at the 3 position. Conveniently, the mass spectrum is very similar to that of erythronolide B except for the inclusion of several prominent peaks (indicated by check marks) corresponding to fragments of the sugar residue.

Therefore, in spite of the scarcity of peaks in the high mass region, it is relatively easy to extract important structural information from the high resolution mass spectral data.

Unfortunately, the situation is not quite as satisfactory in the mass spectrum of erythromycin B shown in Figure 8. Erythromycin B contains two sugar substituents, one of which is an amino sugar. Because of the well-known ability of amine nitrogens to stabilize a positive charge, nearly all of the intense peaks correspond to ions containing the nitrogen atom. Furthermore, because of the facility of cleavage of the glycosidic linkage nearly all of these peaks are predominately due to fragments of the amino sugar. These peaks are indicated in the mass spectrum by check marks.

Consequently, in this case, the dominance of the nitrogen-containing fragments seriously interferes with the ability to use the mass spectral data to obtain structural information concerning other portions of the molecule. It may be possible to chemically alter the amino group in order to inhibit this fragmentation-dominating effect.

The study of the mass spectra of compounds related to the macrolide antibiotics is continuing and a more detailed description of the results will be provided in the near future.

Abstract

Uses of C^{13}/C^{12} ratios in biological and biogeochemical research.

P. L. Parker

University of Texas

Marine Science Institute at Port Aransas

Variations in C^{13}/C^{12} ratios which arise from kinetic isotope effects in biological and geochemical systems may be used to gain insight into the chemical processes of these systems. Three problem areas in which C^{13}/C^{12} ratio variations have been used in my laboratory will be discussed.

1. We have found that pure cultures of blue-green algae (BGA) may be grown so that the cells show the same overall fractionation factor (f.f.) to within better than 1 per mil from day to day. Different species of BGA show similar fractionation factors although filamentous forms will vary unless special care is taken. We have found that the f.f. is dependent on the concentration of CO_2 in the air used to grow the organisms.

2. Using BGA and other plants we have found that the "product molecule" normal hydrocarbons may or may not have the same C^{13}/C^{12} ratio as the assumed "precursor molecule". The implications of this approach are discussed.

3. We have found that petrochemical pollution in marine waters may be recognized by C^{13}/C^{12} ratios. We have published on this method (Environm. Sci. & Tech. 2 535 (1968)).

COMPARATIVE MASS SPECTROMETRIC STUDIES ON THE ISOPRENOIDS
AND OTHER ISOMERIC ALKANES IN TERRESTRIAL AND
EXTRATERRESTRIAL SAMPLES

E. Gelpi and J. Oro'
Departments of Biophysical Sciences and Chemistry, University of Houston
Houston, Texas 77004

ABSTRACT

The extractable aliphatic hydrocarbons of numerous meteorite specimens (carbonaceous chondrites and graphite-troilite nodules of iron meteorites) as well as several terrestrial graphites were separated and identified by the combination of gas chromatography-mass spectrometry. Due to the extreme complexity of the hydrocarbons in these samples and the very low levels of concentration in which the individual components are present, unequivocal structural assignments can only be obtained by means of their respective mass spectral features. From the mass spectrometric patterns eleven homologous series of aliphatic hydrocarbons have been identified. These include the n-alkane series, two isoprenoid series of 2,6,10-trimethyl and 2,6,10,14-tetramethyl alkanes, five series of monomethyl substituted alkanes (2-,3-,4-,5-,6-methyl alkanes), one of 4,8-dimethyl alkanes, and two of monocycloalkanes (cyclohexyl and cyclopentyl). From the data thus obtained we can establish interesting correlations between the two types of samples, terrestrial and extraterrestrial, and also determine whether these compounds were derived from biological or abiological sources.

INTRODUCTION

With the advent of the modern chromatographic and mass-spectrometric techniques the organic geochemist has been particularly active in the study of the morphological and molecular records of past life events which are found in terrestrial sediments. It is recognized that the study of these records may provide us with an insight into the evolutionary history of the first living organisms on earth.

The significance of the results obtained in the field of terrestrial bio-geochemistry (1-9) suggests that, from this point of view alone, it would be very interesting to study in detail the extraterrestrial environment. However, although this situation may soon be changed by the NASA Apollo program for the exploration of the moon, the only extraterrestrial samples that are presently available for this kind of work are the meteorites. It follows that an understanding of the nature of the organic matter in meteorites may tell us something about the possible existence of life, past or present, outside of our biosphere.

The chemical approach to the determination of the presence of life processes, on earth or in any other place in the solar system, involves the structural identification of "biological markers" among the organic compounds present either in living systems or in products suspected of bearing or having borne any particular form of life. Because of their chemical and structural properties as well as their stability towards diagenetic changes, the isoprenoid hydrocarbons have often been implicated as biological markers (3-5,9,10). Mass spectrometry has proved of great value in the identification of this type of structures as well as other isomeric alkanes.

EXPERIMENTAL

The analytical techniques used in this type of studies have already been reported in some detail in the literature (9,11). In essence the method is based on the extraction of the powdered samples with organic solvents, fractionation by silica gel chromatography, and analysis of the alkane eluate by gas chromatography and mass spectrometry. Necessary precautions to avoid contamination were taken in much the same manner as previously described (9,11). All the control blanks showed either negative results or negligible amounts of alkanes.

The gas chromatographic analyses were made on an "F and M Model 810" gas chromatograph equipped with a flame ionization detector. Polysev [m-bis-m-(phenoxy-phenoxy)-phenoxy-benzene.] was used as the stationary phase. It was obtained from Applied Science Laboratories, Inc. State College, Penn. Quantative values of the areas under each one of the gas chromatographic peaks were obtained directly from an electronic digital integrator, Infotronics CRS-11AB/H/41. The gas chromatographic-mass

TABLE I
ISOPRENoids AND ALIPHATIC HYDROCARBONS IN METEORITES - GC-MS IDENTIFICATION

	Mo. Mu. O. V.	E. Gr. Mo. Mu. O. V.	E. Gr. Mo. Mu. O. V.
nC ₁₁	1 (19) 2MeC ₁₅	1 1 1 1 1	41 5MeC ₁₈
nC ₁₂	0.1 1 (20) 3MeC ₁₅	1 1 1 1 1	(42) 2,6,10,14 TetraMeC ₁₇
1 Decahydronaphthalene	1 nC ₁₆	1 1 4 6 1 4	43 4MeC ₁₈
2 2,6,10 TriMeC ₁₁	1 0.1 (21) 2,6,10 TriMeC ₁₅	1 1 2 2 2	(44) 2MeC ₁₈
3 2MeC ₁₂	1 (23) 6MeC ₁₆	1 1 1 1 1	(45) 3MeC ₁₈
4 3MeC ₁₂	1 24 5MeC ₁₆	0.1 1 1 1 1	nC ₁₉
5 4,8 DiMeC ₁₂	1 (25) 4MeC ₁₆	1 1 1 1 1	(46) Tridecylcyclopentane
nC ₁₃	1 (26) 2MeC ₁₆	1 1 1 1 1 1	(47) Dodecylcyclohexane
6 2,6,10 TriMeC ₁₂	1 (27) 2,6,10,14 TetraMeC ₁₅	2 1 6 4 1 3	48 4MeC ₁₉
7 2MeC ₁₃	1 (28) 3MeC ₁₆	1 1 1 1 1 1	(49) 2MeC ₁₉
8 3MeC ₁₃	1 1 nC ₁₇	3 1 8 14 3 8	(50) 3MeC ₁₉
9 4,8 DiMeC ₁₅	1 (30) 2,6,10 TriMeC ₁₆	1 1 1 1 1	nC ₂₀
nC ₁₄	1 3 (31) 4,7,11 TriMeC ₁₆	0.1 1 1 1 (51) Tridecylcyclohexane	1 1 1 1
(10) 2,6,10 TriMeC ₁₃	1 1 32 Decylcyclohexane	1 1 1 1	52 2MeC ₂₀
11 4MeC ₁₄	1 (33) 6MeC ₁₇	2 1 (53) 3MeC ₂₀	1 1
(12) 2MeC ₁₄	1 3 (34) 5MeC ₁₇	1 1 1 1	nC ₂₁
(13) 3MeC ₁₄	1 3 (35) 4MeC ₁₇	1 1 1 1	54 Tetradecylcyclohex
14 4,8 DiMeC ₁₄	1 (36) 2MeC ₁₇	1 1 2 1 1 1	55 2MeC ₂₁
nC ₁₅	2 2 1 4 (37) 2,6,10,14 TetraMeC ₁₆	3 1 4 3 1 2	nC ₂₂
(15) 2,6,10 TriMeC ₁₄	1 1 0.1 (38) 3MeC ₁₇	1 1 1 1 1 1	nC ₂₃
17 5MeC ₁₅	1 1 nC ₁₈	6 1 7 9 3 5	nC ₂₄
18 4MeC ₁₅	1 1 (39) Dodecylcyclopentane	1 0.1	nC ₂₅
		(40) Undecylcyclohexane	3 1 1
			nC ₂₆

E.(Essebi); Gr. (Grosnaja); Mo. (Mokota); Mu. (Murray); O. (Orgueil); V. (Vigarano). The amounts given (in ppm) have been obtained by rounding the actual values to the next higher number. Blanks in the columns of the Table do not necessarily indicate the absence of certain alkanes, but rather that no useful mass spectra were obtained. Compounds other than n-alkanes have an identification number corresponding to that given in the gas chromatograms. When this number is placed in parentheses, it indicates that the compound has also been identified in graphite nodules from iron meteorites.

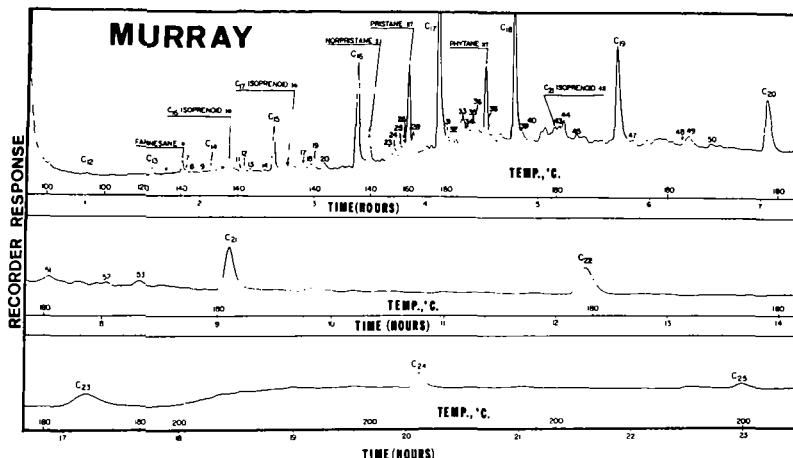


Fig. 1 - HIGH RESOLUTION GAS CHROMATOGRAM OF THE HYDROCARBONS FROM THE MURRAY METEORITE. Stainless steel capillary column (310 m long x 0.076 cm i. d.) coated with Polysev. (See Table I for peak number identification.)

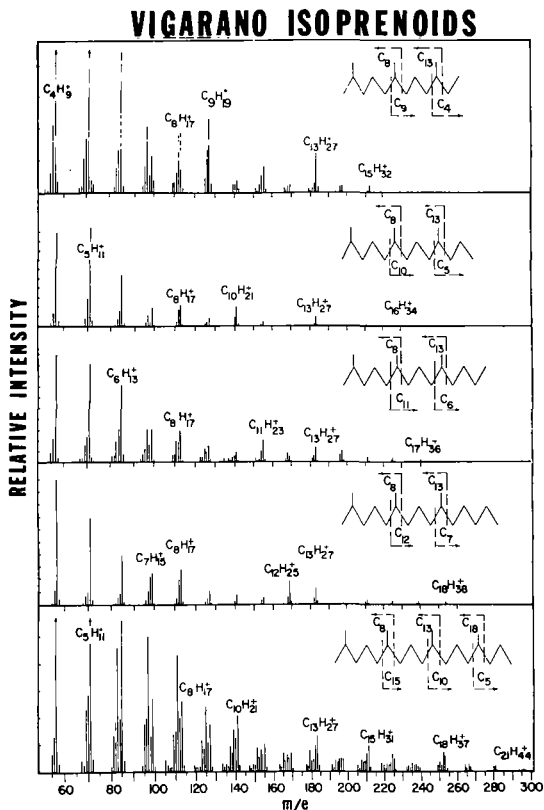


Fig. 2 - Spectra taken as each peak was eluted from a 190m long x 0.076cm/i. d. stainless steel capillary column coated with Polysev. Electron energy, 70 ev. Ionizing current 120 A. Accelerating voltage 3.5 KV.

spectrometric analyses were performed on an LKB 9000 gas chromatograph-mass spectrometer. In the case of the graphitic nodules the samples were secured from the iron meteorites according to the following procedure.

Several meteorite iron pieces were pierced with a carborundum saw until a successful cut was made which showed a nodule divided by the saw in approximately two halves, each one embedded in the corresponding half of the iron meteorite. Tap water was used as a coolant and precautions were taken to avoid contamination. This first operation was carried out at the American Meteorite Laboratory. The cut pieces of iron, containing two halves was then properly identified and considered as an individual specimen out of which three (sometimes only two) portions were taken for analysis. They are the so-called surface, center, and bottom portions. The surface represents material removed from the exposed surface of the cut. After this portion was removed then a second sample of a more internal part of the half-nodule was taken (center) and finally a portion was taken from the deepest part (bottom), that is the part closer to the metal-graphite interface, or the one farther away from the surface of the cut. Equal weights of the three samples were taken for the analyses.

RESULTS

a) Carbonaceous chondrites. The presence of extractable aliphatic hydrocarbons in meteorites has been positively established by their gas chromatographic analyses (9,11,12). An example is shown in Figure 1, which could be taken as the typical gas chromatographic pattern of most meteorite extracts. At this concentration level the complexity of the pattern in terms of the isomeric alkanes eluted in between each n-alkane peak becomes apparent. The identification of the many components detected in meteorites by gas chromatographic techniques would be almost impossible on the basis of GC retention times alone. However, the application of the combined technique of gas chromatography-mass spectrometry affords reliable identifications, even in cases where the gas chromatographic resolution has reached a limit or is rather poor. The peaks shown in Figure 1, whose structural identities have been established by mass spectrometry are numbered for identification purposes according to the system used in Table I. Isoprenoids are indicated by their common name, in Fig.1.

As shown in Table I, a total of 68 individual components have been identified mass spectrometrically in several meteorite extracts. They constitute several homologous series of aliphatic hydrocarbons, such as the n-alkane series, two isoprenoid series of 2,6,10-trimethyl and 2,6,10,14-tetramethyl alkanes, five series of monomethyl substituted alkanes (2-, 3-, 4-, 5-, 6-methyl alkanes), one of 4,8 dimethyl alkanes and two of monocycloalkanes (cyclohexyl and cyclopentyl). The total relative percent composition of the four major hydrocarbon groups is given in Table II.

Mass spectrometric identifications. The members of the isoprenoid series in Vigarano with the exception of pristane and phytane which have already been reported in the literature (12) are shown in Figure 2, arranged from top to bottom according to their increasing molecular weights. Their respective structures are displayed schematically in this figure. The preferred points of cleavage of these molecules (at either side of the methyl substituents due to the formation in each case of a relatively stable secondary carbonium ion) are in all instances reflected in their corresponding maxima within the mass spectral patterns. The C₁₄ isoprenoid, not shown in this figure, was also identified. (see Table I)⁴.

In general the use of high efficiency gas chromatographic columns in this kind of separations enabled us to obtain rather clean isoprenoid mass spectra. However, this was not always the prevailing situation and it must be pointed out here that the utility of the mass spectral data obtained from very complex mixtures of alkanes containing many isomeric forms is limited by the resolving power of the GC columns. In other words if two or more components of the mixture under analysis are eluted together in one single GC peak, the corresponding mass spectrum will represent a combination of their individual fragmentation patterns.

Table III shows an example of the mass spectrometric approach applied in the identification of the components of an unresolved GC peak. This represents an actual case encountered in the analysis of the alkane fraction from the Mokoia meteorite. It has been proved difficult to get

MOKOIA CYCLOALKANES

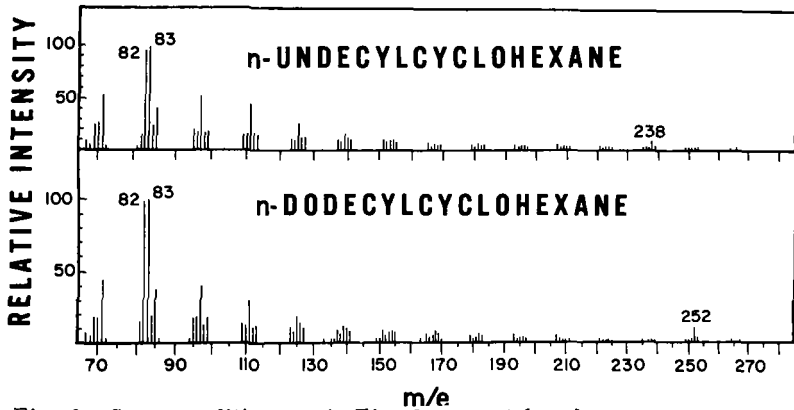


Fig. 3 - Same conditions as in Fig. 2, except for electron energy at 20 eV.

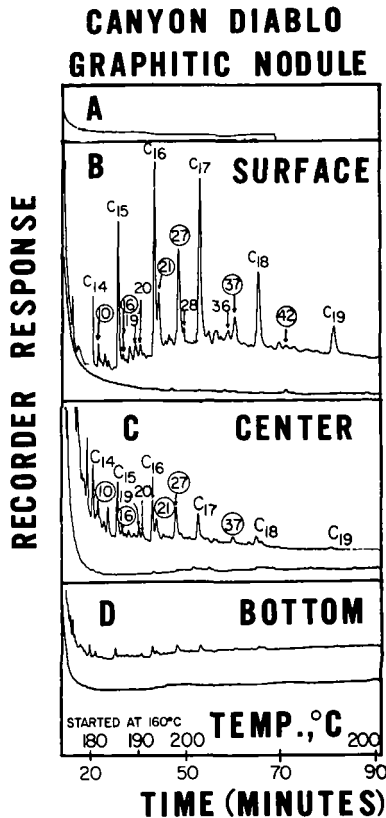


Fig. 4 - GAS CHROMATOGRAPHIC SEPARATION OF THE ALKANES IN DIFFERENT PARTS OF A CANYON DIABLO EMBEDDED GRAPHITIC NODULE. Stainless steel capillary column (195 m long x 0.076 cm i.d.) coated with Poly-sev. (See Table I for peak number identification).

three separate peaks out of the mixture of iso C₁₇, anteiso C₁₇, and pristane (12) (see similar case in Fig. 1, peak labelled 26, 27, and 28), but the mass spectra taken at some points along the upward slope, at the top of the peak and at some points along its downward slope can usually tell each component apart from the others. Careful inspection of Table III shows that the contribution of pristane to the 2-methyl C₁₆ spectra is very low, the spectra being in this case fully representative of the iso-alkane structure as indicated by the parent ion at m/e 240, the M-15 peak at m/e 225 and the high M-43 peak at m/e 197. In the next scan pristane starts to dominate the spectrum as shown by the increase of the intensity of the peak at the m/e 268, the parent ion of pristane, and also by the increase in the intensities of the M-15 peak (m/e 253) and that of the characteristic fragment at m/e 183. Also to be considered are the decrease of the m/e 99 peak and the intensity of the C₁₁ fragment. In the next mass spectrum there is practically no contribution of the iso structure as indicated by the intensity of the iso C₁₇ parent ion. Then, on the last two spectra, taken on the descent of the peak, the anteiso C₁₇ features start to appear on top of the spectrum of pristane. The m/e 99 peak rises, the C₁₁ fragment is no longer higher than the preceding C₁₀ fragment, the intensity of the m/e 240 ion begins to grow again and the characteristic M-29 peak at m/e 211 has increased in intensity. All these features are more pronounced in the last spectrum which has not been labeled as 3-methyl C₁₆ with the purpose to emphasize that the spectrum does still show a relatively high m/e 183 fragment contributed by the fragmentation of pristane.

This illustrates how identification problems which would be very difficult to solve by gas chromatography can easily be resolved with the aid of mass spectrometric techniques.

Another example of the utility of the mass spectrometer in this field is unequivocal identification of several cycloalkane structures. The mass spectrometric patterns of two cyclohexanes are shown in Figure 3.

b) Graphitic nodules in iron meteorites. After having completed our extensive study of the aliphatic hydrocarbons in carbonaceous chondrites, a similar study was carried out on the graphitic nodules that are found embedded in iron meteorites. It was felt that since these nodules had been completely isolated from the terrestrial environment until their release from their surrounding iron matrix, the results would be more reliable than those obtained with the carbonaceous chondrites.

The results of the gas chromatographic-mass spectrometric identification of the hydrocarbons extracted from several specimens of graphite nodules (9,12) indicated that they are essentially of the same type as those identified in carbonaceous chondrites (see Table I), although the amount of alkanes in the nodules was found to be much lower, ranging from 0.32 to 4.1 ppm. The compounds identified in the graphitic nodules are also indicated in Table I by placing their corresponding identification number in parenthesis.

A typical example of the results obtained in this phase of our work is shown in Figure 4. Refer to experimental section for description of the meaning of the words surface, center and bottom. The surface cut shows a distribution of hydrocarbons qualitatively identical to most other meteorite samples. A very clear concentration gradient is readily apparent within the three cuts. That is the part of the nodule best protected from the atmosphere after the cut, the so-called "bottom" shows essentially negligible amounts of extractable hydrocarbons. Mass spectra of four of the isoprenoids and two of the monomethyl alkanes identified in this nodule are shown in Figures 5 and 6, respectively.

An interesting observation is the possible presence of the branched hydrocarbon, 4,7,11-trimethyl hexadecane, in some of the meteorite extracts including the nodules (see Table I). The mass spectrum of this compound is displayed in Table IV in the grid type pattern (13). The different mass series are arranged in columns under their corresponding z value which is taken from the hydrocarbon formula C_nH_{2n+2}. Each row is characterized by a constant carbon number, n. The fragmentation pattern appears to fit very closely the proposed structure. The branching sites are clearly indicated by the rise in the intensities of the ions underlined in the alkyl ion series (z=+1) and the olefin ion series (z=0).

**CANYON DIABLO
SHALLOW EMBEDDED NODULE**

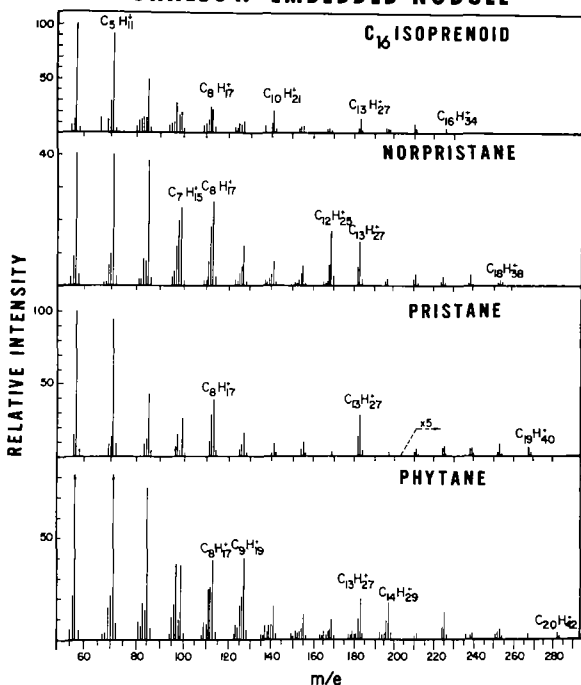


Fig. 5 - MASS SPECTRA OF ISOPRENOID HYDROCARBONS IN GRAPHITIC NODULE. Same conditions as in Fig. 2.

**CANYON DIABLO SHALLOW
EMBEDDED NODULE**

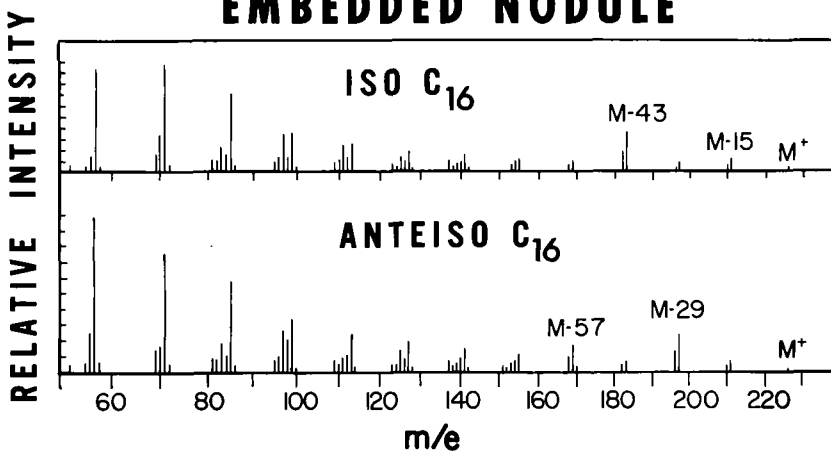


Fig. 6 - MASS SPECTRA OF METHYL BRANCHED ALKANES IN GRAPHITIC NODULE. Same conditions as in Fig. 2.

TOTAL ISOPRENOID DISTRIBUTION
IN THREE GRAPHITIC NODULES

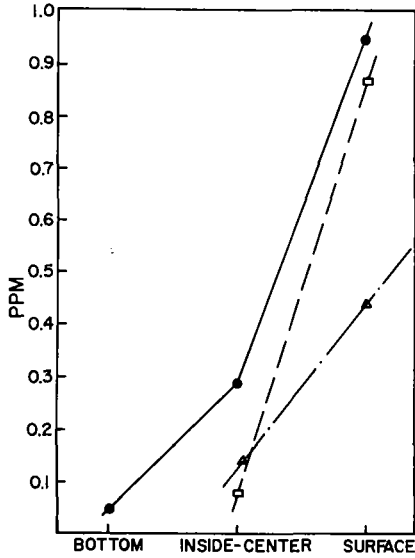


Fig. 7

ALKANE AND ISOPRENOID DISTRIBUTION

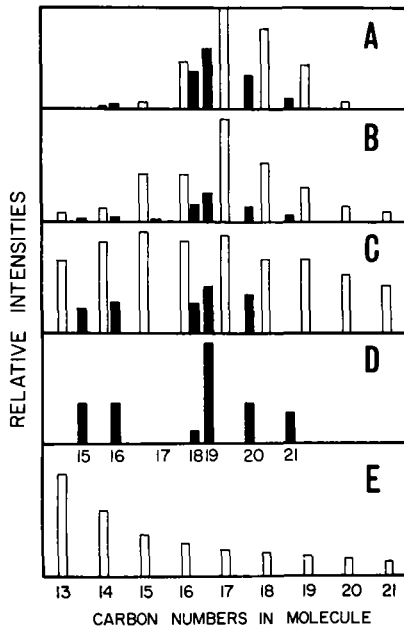
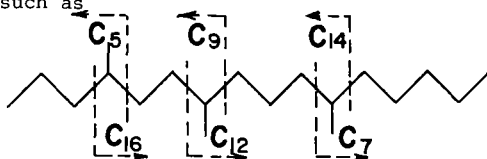


Fig. 8 - Typical alkanes and isoprenoid hydrocarbon distribution in (A) Soudan shale (B) Vigarano meteorite, (C & D) Petroleum crudes, (E) Fischer-Tropsch products. Isoprenoids are shown in black. The positions correspond approximately to the retention time on Polysev GC columns.

Relatively intense C_7 , C_9 , C_{12} , C_{14} , and C_{16} ions would be expected from a structure such as



Nevertheless, this identification must remain tentative until the corresponding standard is synthesized and both spectra are compared.

The observed concentration gradient for the hydrocarbons in the graphitic nodule (Figure 4) is graphically represented in Figure 7 by a plot of the total isoprenoid concentration in three different nodules versus their location within these nodules.

c) Terrestrial graphites. A parallel study of the hydrocarbon composition and distribution of several naturally occurring terrestrial graphites (14) showed essentially identical results as those obtained in the case of the extraterrestrial graphite samples. In some samples (e.g. a graphite schist) we observed a similar concentration gradient between the surface hydrocarbons and hydrocarbons trapped in the interior part of the sample. This work has been presented for publication elsewhere (14).

DISCUSSION

Considering the current criteria of biogenicity (9) frequently applied to the aliphatic hydrocarbons, especially to the isoprenoids which have been considered as suitable biological markers, it turns out that the aliphatic hydrocarbons detected in meteorite extracts can be truly classified as biogenic. This statement can be partially supported by the data condensed in Figure 8. From a comparative point of view the characteristic isoprenoid distribution of sediments, (Figure 8A), and petroleum crudes (Figure 8 C,D) show a great deal of similarity to the distribution of these compounds in the Vigarano meteorite (Figure 8 B), which can be considered representative of most carbonaceous chondrites. This by itself strongly supports the hypothesis that these hydrocarbons may be derived from biological sources. This unique distribution, with a minimum at the C_{17} isoprenoid (9,12) and two maxima at C_{19} (pristane) and C_{16} (methyl farnesane), is considered to be the result of the diagenetic degradation of the phytol in the plant chlorophylls (15). Higher molecular weight isoprenoid precursors, such as the carotenoids, have been suggested as the possible parent substances of the C_{21} isoprenoid (16).

It must be emphasized here that an extensive study of Fischer-Tropsch synthetic processes, implicated in the abiotic synthesis of hydrocarbons within the solar nebula (17), has yielded negative results in terms of the synthesis of isoprenoid structures (9). Although relatively large amounts of normal (Figure 8,E) and monomethyl substituted alkanes are produced in this process no trace of trimethyl or tetramethyl alkanes has ever been detected.

Now if on these grounds we accept the possible biological nature of these hydrocarbons, another question still remains unanswered. That is, whether they are indigenous or not. An answer to such a question can best be given after consideration of the results obtained with the graphitic nodules. The marked concentration gradients of the hydrocarbons found in these samples as well as their nature and unique bimodal distribution of their isoprenoids clearly indicate that besides being most likely of biogenic origin they may be terrestrial contaminants, of the same type found in terrestrial graphites (14), which somehow found their way into the nodules after their exposure to our environment. It would be hard to accept any argument in favor of biological activity within the iron meteorite. Furthermore the very low amounts of hydrocarbons in these nodules are in line with what one would expect from processes of relatively fast terrestrial contamination by contact of the samples with air, dust particles (9,18), petroleum fumes, etc. (9,18).

As a final remark and in support of these observations, it may be pointed out that the analyses recently performed on a freshly recovered

meteorite, the "Pueblito de Allende", show negligible amounts of extractable organic matter. A fact that would be in line with its relatively very short history of terrestrial contamination.

REFERENCES

1. Han, J., McCarthy, E.D., Van Hoesven, W., Calvin, M., and Bradley, W.H. Proc.Nat.Acad. of Science, 59, 29.
2. Oro, J., and Nooner, D.W., Nature 213, 1082 (1967).
3. Oro, J., Nooner, D.W., Zlatkis, A., Wikstrom, S.A., Barghoorn, E.S., Science 148, 77 (1965).
4. Barghoorn, E.S., Meinschein, W.G., and Schopf, J.W., Science 148, 461 (1965).
5. Eglinton, G., and Calvin, M., Scientific Amer. 32, (1967).
6. Gelpi, E., Oro, J., Schneider, H., and Bennett, E.O., Science 161, 700-702 (1968).
7. Gelpi, E., Schneider, H., Mann, J., and Oro, J., Phytochemistry, in press.
8. Schneider, H., Gelpi, E., Oro, J., and Bennett, E.O., Phytochemistry, in press.
9. Gelpi, E., Ph.D. Thesis, University of Houston (1968).
10. Eglinton, G., Scott, P.M., Belsky, T., Burlingame, A.L., Richter, W., and Calvin, M., Advances in Organic Geochemistry, Eds. G.D. Hobson and M. C. Louis, p. 41, Pergamon, London (1964).
11. Nooner, D.W., and Oro, J., Geochim. Cosmochim. Acta, 31, 1359 (1967).
12. Oro, J., Gelpi, E., and Nooner, D.W., J. Brit. Interplanet. Cos. 21, 83 (1968).
13. Clerc, R.J., Hood, A., and O'Neal, M.J., Anal. Chem. 27, 868 (1955).
14. Gelpi, E., Nooner, D.W., and Oro, J., Geochim. Cosmochim. Acta, in press.
15. Bendoraitis, J.G., Brown, B.L., and Hepner, R.S., World Petroleum Congress, Germany (1963).
16. McCarthy, E.D., and Calvin, M., Tetrahedron, 23, 2609 (1967).
17. Studier, M.H., Hayatsu, R., and Anders, E., Geochim. Cosmochim. Acta. 32, 151 (1968).
18. Nooner, D.W., Ph.D. Thesis, University of Houston (1966).

ACKNOWLEDGMENTS

This work was supported in part by research grants NGR-44-005-020, NGR 44-005-002, and contract NAS 9-8012 from the National Aeronautics and Space Administration.

TABLE II
RELATIVE PERCENT COMPOSITION OF PARAFFINIC HYDROCARBONS
IN THE TOTAL n-PENTANE EXTRACT OF METEORITES

Meteorite	Cycloalkanes	me-Alkanes	Isoprenoids	n-Alkanes	Total
Murray	1.54	13.44	11.39	70.52	96.89
Grosnaja	5.00	10.00	11.25	72.50	98.75
Mokoia	2.16	7.92	13.68	40.08	63.84
Vigarano	1.05	7.98	11.55	61.53	82.11

TABLE III
PARTIAL SPECTRA REPRESENTING FIVE SUCCESSIVE SCANNINGS OF A
THREE COMPONENT GAS CHROMATOGRAPHIC PEAK

m/e	ion	2-meC ₁₆	Relative Intensities			
			Pristane +2-meC ₁₆	Pristane	Pristane +3-meC ₁₆	Pristane +3-meC ₁₆
99	C ₇ H ₁₅ ⁺	127 *	62	57	71	106
113	C ₈ H ₁₇ ⁺	100	100	100	100	100
127	C ₉ H ₁₉ ⁺	80.5	41	38	42	71
141	C ₁₀ H ₂₁ ⁺	60	20	18	45	55.5
155	C ₁₁ H ₂₃ ⁺	42 *	22.5	20	24	42
169	C ₁₂ H ₂₅ ⁺	32.5	8	6.5	12	31
183	C ₁₃ H ₂₇ ⁺	25	63	61	55	43
197	C ₁₄ H ₂₉ ⁺	138 *	26	8.5	10	24
211	C ₁₅ H ₃₁ ⁺	13.5 *	4	2.5	12	42.5
225	C ₁₆ H ₃₃ ⁺	42.5	7.5	5.1	8	18
239	C ₁₇ H ₃₅ ⁺	7.5	4	3.5	4	--
240	C ₁₇ H ₃₆ ⁺	13.5	2	1	1.5	15.5
253	C ₁₈ H ₃₇ ⁺	3	5.5	5	4.3	4
267	C ₁₉ H ₃₉ ⁺	4	--	--	--	--
268	C ₁₉ H ₄₀ ⁺	2	5	4.8	3.8	--

TABLE IV

MASS SPECTRUM OF 4,7,11-TRIMETHYL HEXADECANE FROM THE SURFACE OF A
CANYON DIABLO EMBEDDED NODULE

C_n	Z	Mass Series (Z in C_nH_{2n+Z})							
		-5	-4	-3	-2	-1	0	+1	+2
C_5					6.5	11	30	90	6
C_6		12.5	6	16	93	100	23	80	5
C_7			4	15	20	39	<u>37.5</u>	<u>41</u>	3
C_8		3		13	12	28	18	31	3.5
C_9		3.1	3.1	9	9	26	<u>19</u>	<u>35</u>	
C_{10}		5	3	7.5	5	13	13	18.5	
C_{11}				7.5	4	8	7	11	
C_{12}		4	3	6	3.5	6	<u>14.5</u>	<u>28</u>	5
C_{13}		4.8		6	4.5	5	5	8	
C_{14}				6	4.8	5	<u>7.8</u>	<u>17</u>	3
C_{15}				22	6.5	7	6	5	
C_{16}				4	3	3	<u>20</u>	<u>17</u>	4
C_{17}							4.5	6.8	
C_{18}					3		4	5	
C_{19}							3		3

The characteristic fragments originated around the
methyl branches are underlined.

SOME SYSTEMATIC TRENDS IN C^{13} AND O^{18} CONCENTRATION VARIATIONS
IN A CARBONATITE

P. Deines

The Pennsylvania State University
University Park, Pennsylvania

Carbonatites represent a rather peculiar rock type in that they consist largely of carbonates, like sedimentary limestones or marbles, show on the other hand, however, textures and mineral relationships which suggest a formation at high temperatures from a carbonate melt.

The study of the origin of carbonatites derives its importance from a number of sources: (i) it is of basic interest to know what conditions led to the formation of such a peculiar rock type; (ii) carbonatites are genetically closely related to sub-silicic alkalic igneous rocks and kimberlites, hence, formulation of hypotheses on the origin of these rocks necessarily requires some consideration of the processes involved in the formation of carbonatites; (iii) the economic potential of carbonatites and related alkali complexes as reserves for raw materials e.g. rare-earth elements, barium, niobium, uranium, phosphate and agricultural lime is impressive.

The two main problems that have to be considered in the formulation of hypotheses on the origin of carbonatites are: (i) the source of the carbonate, and (ii) the mode of emplacement of the carbonate.

Some authors have suggested that sedimentary limestones should be considered as the source of the carbonate. It was then proposed to test this hypothesis by the study of the carbon isotopic composition of carbonatite carbonates. Since marine limestones show a *restricted isotopic composition range*, they could be ruled out as source, if the carbonatite rocks showed distinctly different isotopic compositions. This assumes naturally that the isotopic composition is not altered in processes that might be involved in a derivation of carbonatite carbonates from sedimentary rocks. Studies by us have shown, however, that under certain geologic conditions the carbon and oxygen isotopic composition of sedimentary carbonates can be altered to approach that considered by some authors as characteristic for carbonatites. Hence it is not unproblematic to base conclusions about the source of carbonatite carbonates on their isotopic composition.

Since physicochemical conditions can influence the isotopic composition systematically, it is logical to inquire whether the conditions of emplacement of the carbonatite have left a record

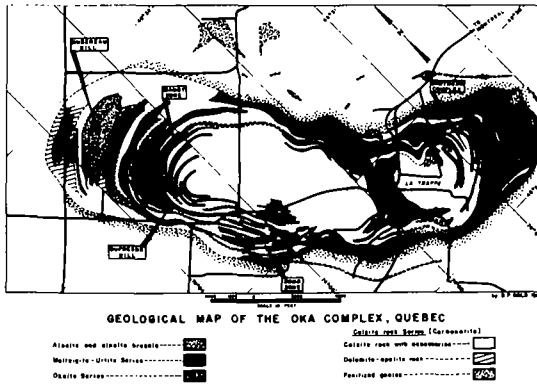


Fig. 1 Geologic Map of the Oka Carbonatite Complex

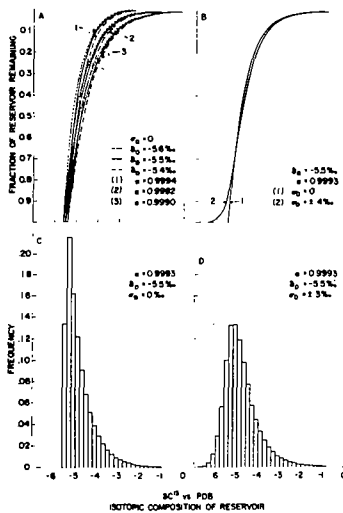


Fig. 2 Examples of Rayleigh-Fractionation Curves and Resulting $\delta^{13}C$ Frequency Distributions

in the isotopic composition of two of the major elements (carbon and oxygen) of the carbonatite rocks. This led us to study in greater detail the carbon and oxygen isotopic composition distribution pattern of a single carbonatite i.e. the Oka carbonatite complex.

The Oka carbonatite lies about 25 miles due west of Montreal, Quebec, Canada. It has geologically the form of a figure eight (Fig. 1) and intrudes a Precambrian inlier of highly, regionally metamorphosed rocks. Through the intrusion of the carbonatite the country rock has been altered, and a zone of fenitization can be noticed around the complex. In the complex itself two major rock units can be distinguished (i) carbonate rocks (calcite rocks and dolomite rocks) and (ii) silicate rocks, i.e. rocks consisting mainly of silicates containing, however, in many cases also considerable amounts of carbonates. The silicate rocks may be divided into the okaite series and the melteigite-urtite series. Alnoites and alnoite breccia pipes, representing the last intrusive phase of the carbonatite cut through the complex and the surrounding country rock.

Accepting as a working hypothesis the crystallization of the carbonatite from a carbonate magma, we consider two points in order to make some general prediction about possible isotopic composition changes in the carbonate melt during the carbonatite formation. (i) The carbonate mass contained in a carbonatite is of limited size. (ii) In the crystallization of a carbonate mineral from a carbonate melt a small difference exists between the isotopic composition of the two carbonate phases.

Statistical mechanical calculations have shown that the solid carbonate might have a slightly lower C^{13} concentration than the CO_2 with which it is in isotopic equilibrium. Continued crystallization of carbonates from a carbonate melt will hence lead to a progressive increase in the C^{13} content of the reservoir. The isotopic composition changes are characterized by a Rayleigh-fractionation process.

In the study of natural isotope variations we are in many cases not so much interested in absolute isotopic abundances but in small changes of isotope ratios. This and the fact that isotopic composition measurements may be made more precisely if the samples are directly compared to a standard has led to the use of isotopic reference standards when measuring and reporting geochemical isotopic composition variations. The variations are expressed as per mil deviations from the reference standard as follows:

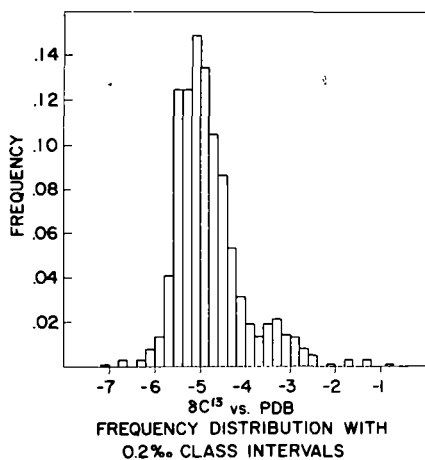


Fig. 3 Carbon Isotopic Composition Frequency Distribution of all Carbonatite Carbonates Analyzed

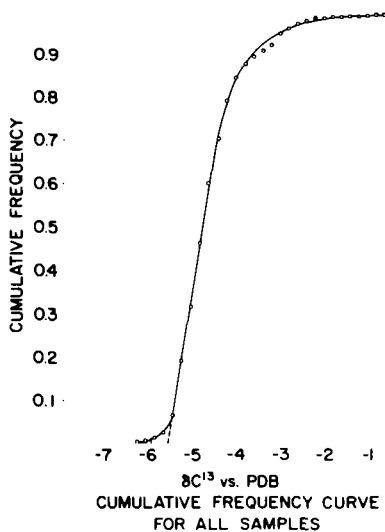


Fig. 4 Observed and Rayleigh-Fractionation Cumulative Frequency Distribution; ooo Observed Frequency, — Calculated Frequency on the Basis of the Modified Rayleigh-Fractionation Model

$$\delta C^{13} = \left(\frac{(C^{13}/C^{12})_{sa}}{(C^{13}/C^{12})_{st}} - 1 \right) \times 1000 \text{ o/oo}$$

$$\delta O^{18} = \left(\frac{(O^{18}/O^{16})_{sa}}{(O^{18}/O^{16})_{st}} - 1 \right) \times 1000 \text{ o/oo}$$

The carbon reference standard commonly used is the C^{13}/C^{12} ratio of the carbonate of a belemnite of the Upper Cretaceous Peedee formation and is called the PDB standard. For oxygen the O^{18}/O^{16} ratio of mean ocean water is used as reference (SMOW).

It can be shown that in a Rayleigh-fractionation process the isotopic composition of a phase removed from the reservoir will change according to:

$$(\delta + 1000) = (\delta_0 + 1000) F^{(\alpha-1)}$$

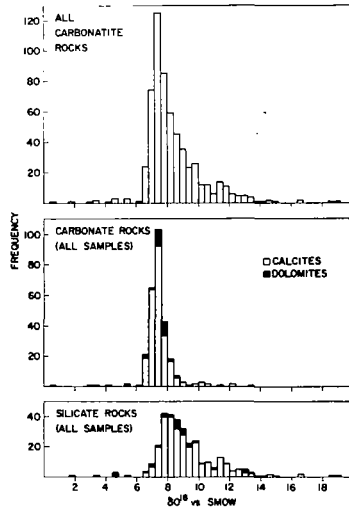
$$\alpha = \frac{\text{fractionation factor,}}{(C^{13}/C^{12})_{\text{removed}} / (C^{13}/C^{12})_{\text{reservoir}}}$$

δ_0 = isotopic composition of the first carbonate removed from the reservoir

δ = isotopic composition of the carbonate removed from the reservoir when the fraction, F , of the reservoir remains.

From this equation we may calculate the isotopic composition of a carbonate crystal forming when the fraction, F , of the reservoir is left. Examples of such calculations are given in Fig. 2A. These curves represent also the cumulative frequency for the isotopic composition of the solid carbonate formed. The ordinate has to be labeled in this case: "amount of carbonate accumulated," and the scale will run from zero to one. From the cumulative frequency distribution we may deduce the relative frequency distribution, an example of which is given in Fig. 2C. This model assumes that the isotopic composition of the reservoir originally is very homogeneous, and that the isotopic composition of a carbonate may be determined with unlimited precision. Both assumptions are somewhat unrealistic. We have hence modified our model and assumed that the isotopic composition of the first carbonate removed would show a measured isotopic composition of mean δ_0 and a variability which is characterized by a standard deviation σ_0 . An example of a cumulative frequency curve and relative frequency distribution derived on the basis of this model is given in Fig. 2B and Fig. 2D.

If we compare this calculated frequency distribution to that actually observed for the rocks of the carbonatite (Fig. 3) we find a considerable similarity in the shape of the two curves. The observed frequency distribution was compared by chi-square



30th FREQUENCY DISTRIBUTIONS OF CARBONATE AND SILICATE ROCKS

Fig. 5 The Oxygen Isotopic Composition Frequency Distributions of Carbonatite Carbonates

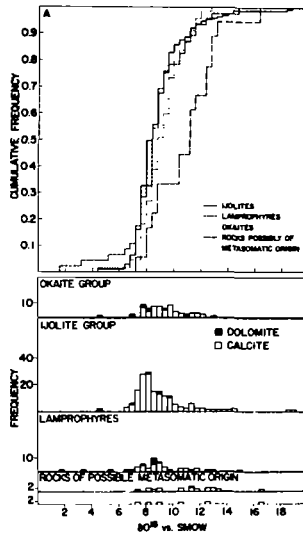


Fig. 6 The Oxygen Isotopic Composition Frequency Distributions of Carbonates from Silicate Rocks

tests with a set of theoretically calculated curves varying in δ_o , σ_o , and α . For a computed distribution based on $\delta_o = -5.5$ o/oo, $\sigma_o = \pm 0.3$ o/oo and $\alpha = 0.9993$ the sum of chi-squares exhibits a minimum and is statistically not significant. Fig. 4 shows the actually observed points superposed on the calculated curve; the excellent fit of the data is taken as evidence that the observed $\delta^{13}C$ frequency distribution could be produced by a Rayleigh-fractionation process characterized by a fractionation factor of $\alpha = 0.9993$, starting with a slightly inhomogeneous reservoir of mean isotopic composition $\delta^{13}C = -4.8$ o/oo and a variability characterized by $\sigma_o = \pm 0.3$ o/oo.

The $\delta^{18}O$ histogram for all carbonatite rocks (Fig. 5) shows some resemblance to the $\delta^{13}C$ frequency distribution, i.e. the limited range of classes with high frequencies, the positive skewness and the sharp decrease in frequencies for light delta values. However, there are two distinct differences: (i) the total range in $\delta^{18}O$ values is about three times as large as that in $\delta^{13}C$, and (ii) there is a peculiar tail of low frequency towards very light oxygen isotopic compositions, which is probably due to isotope exchange with light surface waters.

The $\delta^{18}O$ frequency distributions of carbonate and silicate rocks (Fig. 5) are distinctly different. The histogram of the carbonate rocks shows a steep maximum at 7.4 o/oo, while the distribution of the silicate rocks is platycurtic with a mode of 8.0 o/oo; the median for the carbonate rocks lies at 7.4 o/oo and for the silicate rocks at 8.7 o/oo. The cumulative frequency distribution of the carbonate rocks is too symmetrical to be explained in terms of a Rayleigh-fractionation process, and the variation in the isotopic composition of the carbonates from the silicate rocks are too large to be reasonably interpreted in this fashion.

Significant differences in the oxygen isotopic composition distribution pattern do exist not only between the silicate and carbonate rocks groups, but also within the silicate rock group between rock types (Fig. 6). Ijolites (i.e. rocks belonging to the melteigite-urtite series) show practically the same distribution as the lamprophyres, whereas the okaite cumulative frequency distribution is significantly displaced to higher delta values, the $\delta^{18}O$ distribution of rocks for which a metasomatic origin might be considered (derivation by extremely intense alteration of intruded country rock) is displaced towards still higher $\delta^{18}O$ values. In a broad way the $\delta^{18}O$ concentration in the carbonate minerals associated with the main rock types increases in the following sequence:

carbonate rocks < ijolites and lamprophyres < okaites <
rocks of possible metasomatic origin < fenites

Fig. 7 shows the mean isotopic composition of different rock types and rock groups of the Oka carbonatite. From the cumulative frequency distributions the isotopic composition of the first carbonate crystallized was estimated and is indicated in the figure. If this point is connected with the mean isotopic composition of the carbonate rocks, which represents probably fairly closely the original composition of the carbonatite magma, we obtain very approximately the direction in which the isotopic composition of the carbonates might have changed in the course of crystallization of the carbonatite. Most of the carbonate rocks fall very close to the line or directly on it, and the rocks that are recognized last phases in the petrogenetic sequence i.e. alnoites and related rocks lie close to the heavy-carbon heavy-oxygen end of the fractionation line, and individual alnoite analyses showing the highest C^{13} and O^{18} concentrations fall directly on it.

Further evidence that this is the general trend of δC^{13} - δO^{18} changes in the carbonatite is derived from the fact that the δC^{13} values and δO^{18} values of carbonate rocks, ijolites, and okaites (treated as three separate sample groups) all show significant, positive correlations with slope estimates which are similar to that of the indicated line.

The mean isotopic compositions of the silicate rocks are displaced from this trend towards heavier oxygen isotopic compositions. This, together with the wide variation in the oxygen isotopic composition of these rocks indicates that there was a second source of oxygen involved in their formation. The mean isotopic composition of carbonates from rocks of possible metasomatic origin and from fenites are farthest removed from the trend. In these rocks isotopic exchange with the country rock (which shows considerably higher O^{18} concentrations than the carbonatite) is indicated, and there is the possibility that part of the silicate rocks which are now an integral part of the Oka carbonatite are derived from the country rock by ultrafenitization.

The following working hypothesis could account for the general complexity of the isotopic composition distributions found and explain the larger scale trends that are observed. The carbonate rocks and probably some of the silicate rocks crystallized relatively undisturbed and in isotopic equilibrium from the carbonatite magma. At various stages silicate material from the country rock was fenitized to rocks in which the original texture of the rock can no longer be distinguished. In this process the carbon isotopic composition remained unaffected,

but oxygen exchanged with the country rock. The isotopic composition of the carbonate minerals crystallizing in such a rock would then depend on the amount and isotopic composition of the carbonate and water introduced during the fenitization process, the temperature, and the degree to which isotopic equilibration between the intruding solutions and the altered rock was achieved.

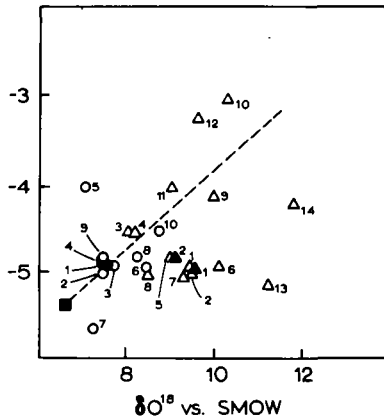


Fig. 7 The Mean Carbon and Oxygen Isotopic Composition of Carbonate and Silicate Rocks: ● Mean of Carbonate Rocks, ▲1 Mean of Okaite Group, ▲2 Mean of Ijolite Group, ■ Estimated Isotopic Composition of the First Carbonate Phases Removed from the Reservoir.

ISOTOPE RATIO MASS SPECTROMETRY AT PHILLIPS PETROLEUM COMPANY

by

T. D. Morgan and R. S. Scalan
Phillips Petroleum Company
Research and Development Division
Bartlesville, Oklahoma 74003

A B S T R A C T

An isotope ratio mass spectrometer facility is described with which routine measurement of carbon isotope ratios are provided with an over-all precision of 0.063 per mil. The system is designed so that carbon and sulfur isotope ratio measurements are made interchangeably without deleterious "memory" effects. This objective was accomplished by providing two identical gas handling systems, and gold plating the inside surfaces of the kovar and copper components of the mass spectrometer. Details of construction are included for solenoid valves where the seal is provided by polished sapphire balls and polished glass seats.

Carbon isotopic data for sediments from British Honduras are included to show dependence on depositional environment. These correlations provide a basis for the interpretation of similar ancient environments.

CHEMICAL IONIZATION MASS SPECTROMETRY OF BIO-ORGANIC COMPOUNDS

G. P. Arsenault

Department of Chemistry
 Massachusetts Institute of Technology
 Cambridge, Massachusetts 02139

Chemical ionization mass spectrometry was discovered by Munson and Field,¹ and was reviewed recently by Field.² Our work differs from all previous work in that we have obtained chemical ionization mass spectra of more complex organic compounds using a direct introduction probe and accurate mass measurements for all ions in these spectra using the photoplate technique.

A CEC 21-110B double focusing mass spectrometer with Mattauch-Herzog type ion optics was modified to make it suitable for chemical ionization as well as electron impact ionization. The modifications are listed in Table I. The opening or closing of a single valve of the ambient temperature reservoir which contains the reactant gas is sufficient to convert from one mode of ionization to the other.

TABLE I
 MODIFICATIONS MADE TO CEC 21-110B FOR USE IN
 CHEMICAL IONIZATION MASS SPECTROMETRY

1. Ion source

0.05 x 1.75 mm electron entrance slit
 0.05 x 5 mm ion exit slit
 400 eV
 gas tight probe-to-ion source connection
 direct pressure measurement with Bourdon gauge

2. Source vacuum system

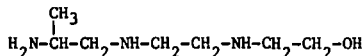
high conductance valve and cold trap
 285 l/sec oil diffusion pump
 165 l/min mechanical pump

3. Inlet system

ambient temperature reservoir

Examples of low resolution chemical ionization mass spectra obtained using the electrical detection system of the modified instrument are shown in Figures 1 and 2. Details of the use of chemical ionization mass spectrometry in determining the molecular weight and elemental composition of the antibiotic botryodiplodin³ will be published elsewhere.⁴

The computer techniques developed earlier⁵ for the conversion of line positions to elemental compositions of ions recorded on photographic plates were used for the analysis of photographic recordings of chemical ionization mass spectra. Table II shows a summary of the extrapolation data produced by the computer. Table III shows the computer-output of the elemental compositions determined for the ions in a weak spectrum of



The ions listed at m/e 85 and 107 originate from the reactant gas and the calibration compound, respectively. The data shows that chemical ionization of polyamino alcohols may yield amino acid sequence information of a different nature than that provided by electron impact ionization.⁶

ACETYSALICYLIC ACID (1 TORR METHANE)

MW 180

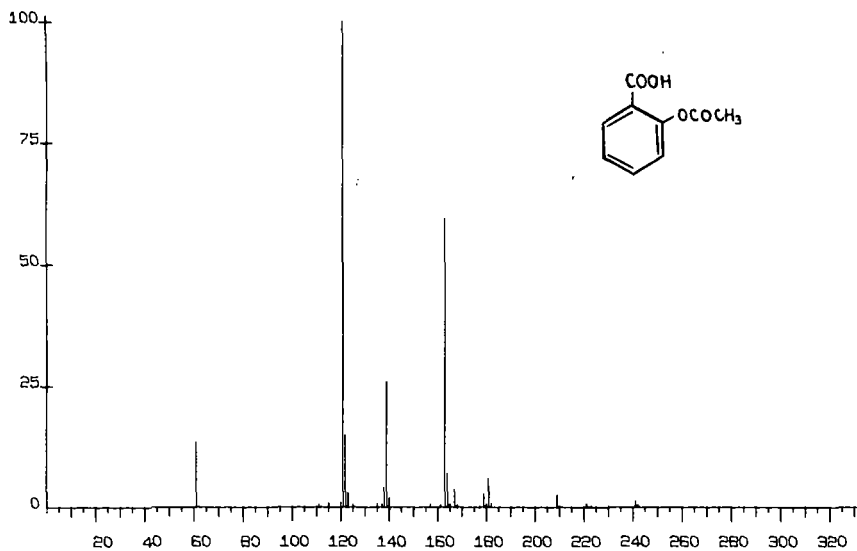


Figure 1. Chemical ionization mass spectrum of acetylsalicylic acid; source temperature: 110°. The spectrum is dependent on source temperature changes. At 90°, m/e 163 and 181 have about the same relative intensity as m/e 139 in the above spectrum.

ADENOSINE (1 TORR METHANE)

MW 267

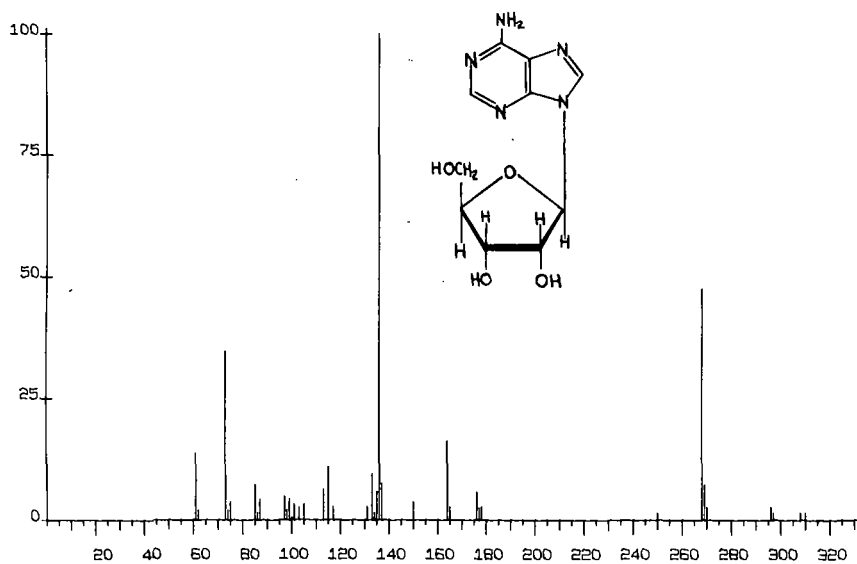


Figure 2. Chemical ionization mass spectrum of adenosine; source temperature: 225°.

TABLE II

B33-03-1 HYDROCARBON MARKER (1 TORR METHANE)

STDM1	DIFF	DIST1	SLOPE	DIFSLO
113.13301	0.00	0.8248	0.0322441	0.00
127.14866	0.00	20.6616	0.0322451	0.09
141.16431	-0.41	39.4315	0.0322236	-2.14
155.17996	9.53	57.3024	0.0322001	-2.35
169.19561	10.48	74.3954	0.0321926	-0.74
183.21126	3.29	90.7977	0.0321910	-0.15
197.22691	0.70	106.5845	0.0321914	0.03
211.24256	-0.13	121.8195	0.0321919	0.05
225.25821	-0.22	136.5567		

TABLE III

B33-17-3 ALA-GLY-GLY POLYAMINO ALCOHOL (1 TORR METHANE)

INT	DETM.	CALC.	DIFF	TOL	C	C'	H	N	O
135	85.09171	85.09277	-1.0	1.7	4	2	11	.	.
166	88.07649	88.07624	.3		4	.	10	1	1
68	101.10826	101.10787	.4		5	.	13	2	.
761	107.08559	107.08607	-.4		8	.	11	.	.
999	162.15934	162.16062	-1.2	2.0	7	.	20	3	1

Acknowledgement: The author is indebted to the National Institutes of Health (Grant No. FR00317) for financial support and to members of the Mass Spectrometry Laboratory directed by Professor K. Biemann for their enthusiastic support.

REFERENCES

1. M.S.B. Munson and F.H. Field, *J. Am. Chem. Soc.*, **88**, 2621 (1966).
2. F.H. Field, *Accounts of Chemical Research*, **1**, 42 (1968).
3. R.S. Gupta, R.R. Chandran and P.V. Divekar, *Indian J. Expe. Biol.*, **4**, 152 (1966).
4. The assigned molecular weight is in agreement with the chemical evidence obtained by Mr. J. Althaus.
5. D. Desiderio and K. Biemann, Twelfth Annual Conference on Mass Spectrometry and Allied Topics, Montreal, June, 1964.
6. K. Biemann, F. Gapp and J. Seibl, *J. Am. Chem. Soc.*, **81**, 2274 (1959).

Studies in Chemical Ionization Mass Spectrometry +

John Michnowicz, Donald Schoengold,* and Burnaby Munson

Department of Chemistry
University of Delaware
Newark, Delaware 19711

Successful modification has been made of a CEC 21-110B mass spectrometer for chemical ionization mass spectrometric studies at pressures up to 0.5 torr. Moderately high resolution and precise mass measurement have been achieved with this instrument.

The instrumental modifications were relatively minor and are as follows: (1) A standard gas manifold for introducing the high pressures of reactant gas has been added. The manifold is very similar to earlier models¹, and is connected through a gold foil leak by a heated glass line into the source. The glass line must presently be maintained at less than 150°C.

(2) A section of Teflon tubing is used to give a tight connection between the entrance port and the ionization chamber. The electron entrance slit was reduced in area from about 2 mm² to 0.8 mm² and the ion exit slit was reduced from about 2.4 mm² to 1 mm². The probe is always inserted into the probe entrance for operation in the high pressure mode.

(3) A quartz spiral gauge (Texas Instruments Precision Pressure Gage, Model 144) was attached to the source by glass and Teflon connections through the port opposite to the probe entrance. Since it is the quartz capillary that is connected to the source, there are no problems with high voltage discharges.

(4) An additional vacuum pump was attached directly to the exit port of the diffusion pump attached to the source housing. No additional diffusion pumps have been added.

The modifications necessary for chemical ionization mass spectrometry have not seriously affected the performance of the instrument for high resolution studies in the conventional low pressure operation. Our instrument is currently being used for both high and low pressure operation without major inconvenience to either mode. If anything, it appears that the sensitivity in the low pressure operation is somewhat higher with the present source design because of the greater source pressures for a given sample size.

Liquid and gas samples may be introduced through the regular oven inlet system of the instrument. Solid samples are introduced through the probe introduction system.

The spectra appear to be normal and show only a slight broadening at the highest pressures and highest resolution. At the highest pressures, the resolution achieved in the chemical ionization studies is somewhat less than the resolution at low pressures, 7000 vs 10,000 (10% valley). This deterioration may be the result of pressure broadening since the chemical ionization peaks appear somewhat wider on the

* On leave, Sun Oil Co., Marcus Hook, Pennsylvania.

+ This work was supported in part by a grant from the University of Delaware Research foundation.

oscilloscope. The precision of mass measurement by the peak matching technique is not affected by the high source pressure. The average error for precise mass measurement is about ± 2 mmu for both high and low pressure operation.

Methane, propane, and isobutane have been successfully used as the reactant gases for chemical ionization studies. The majority of the spectra have been obtained at source pressures of about 0.35 torr. Several compounds have been examined whose spectra have been determined previously with methane at pressures of 1.00 torr.^{1,2} In general, we find the same ions, but their relative abundances are different. For several esters, for example, we find with methane at 0.35 torr less $(MW + 1)^+$ ions and more fragmentation than was reported for methane at 1.00 torr.² This difference may be attributed to more collisional stabilization of $(MW + 1)^+$ ions at 1 torr of CH_4 than at 0.35 torr.

The variation of chemical ionization spectra with the energy of the reacting species is shown in the accompanying table. The major ions of each reactant gas are methane (CH_5^+ , 44%; $C_2H_5^+$, 30%), propane ($C_2H_5^+$, 15%; $C_3H_7^+$, 60%), and isobutane ($C_3H_7^+$, 12%; $C_4H_9^+$, 64%). The pressure of reactant gas was 0.35 torr in each case. Ions of less than 1% abundance have been omitted.

Table 1
Effect of Reactant Ions on Chemical
Ionization Mass Spectra of Acetophenone

m/e	Ion	% of Additive Ionization		
		Methane	Propane	Isobutane
43	CH_3CO^+	69.7	--	--
44	Isotope	2.6	--	--
77	$C_6H_5^+$	4.9	--	--
91	?	1.1	--	--
105	$C_6H_5CO^+$	10.8	18.8	--
121	$(MW + 1)^+$	10.4	74.8	94.3
122	Isotope	1.0	6.3	5.7

Table II shows the chemical ionization mass spectra of a series of aromatic ketones with propane as the reactant gas, P=0.35 torr.

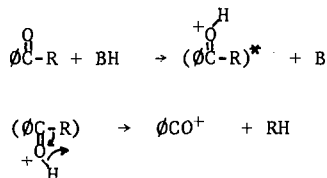
Table II
Chemical Ionization Mass Spectra of Aromatic Ketones

O ØCR R=	% of Additive Ionization			
	$(MW + H)^+$	MW^+	$(MW + H - RH)^+$	RCO^+
CH_3	75	<1	19	Present
CH_3CH_2	47	<1	33	12
$(CH_3)_2CH$	40	<1	50	<1
Ø	60	6	24	$(MW + H - RH)^+$
ØCO	36	<1	55	$(MW + H - RH)^+$

All of the spectra are simple, only two or three major productions.

The protonated molecules are always present. Only one case shows any molecular ion (benzophenone), and that may be the result of a small contribution from the electron impact mass spectrum. The major product ion is the α -cleavage ion, corresponding to the loss of the R group from the molecule. There is also a smaller amount of RCO^+ formed.

We prefer to consider that the O^+C ion, $m/e=105$, which is the major product ion, is formed by a decomposition reaction of the protonated molecular ion,



that is, the reaction is loss of RH from the protonated molecular ion and not loss of R from the molecular ion.

Using $\Delta H_f(\text{O}^+\text{C})=186 \text{ kcal/mole}^3$, we calculate that dissociative proton transfer from C_2H_5^+ is exothermic for acetophenone ($\text{R}=\text{CH}_3$), benzophenone ($\text{R}=\text{O}$), and benzil ($\text{R}=\text{O}^+\text{C}$). Dissociative proton transfer is about 14-20 kcal/mole endothermic for reaction of t-butyl ion in all three cases. Dissociative proton transfer from s- C_3H_7^+ is about thermoneutral: $\Delta H \approx 3 \text{ kcal/mole}$ for acetophenone; +5 kcal/mole for benzophenone; -8 kcal/mole for benzil.

Transfer of the hydrogen to the benzene ring by a similar four-center reaction will give RCO^+ and benzene. A small amount of CH_3CO^+ is formed from acetophenone, but it is difficult to obtain precise amounts in the presence of the large C_3H_7^+ ion current. This dissociation process is less favored. These products (CH_3CO^+ and C_6H_6) are of higher energy than the former pair (O^+C and CH_4). Indeed dissociative proton transfer from C_2H_5^+ is about 7 kcal/mole endothermic, if $\Delta H_f(\text{CH}_3\text{CO}^+)=172 \text{ kcal/mole}^4$. Dissociative proton transfer from s- C_3H_7^+ and t- C_4H_9^+ will be more endothermic. Benzophenone and benzil are symmetrical and give only one product ion.

In addition to these experiments in high resolution chemical ionization mass spectrometry, we have modified a Bendix TOF mass spectrometer for high pressure studies and have attached this directly to a gas chromatograph. In this manner, the carrier gas for the gas chromatograph can be used as the reaction gas in chemical ionization mass spectrometry.

The Bendix high pressure source was modified by the addition of a shield around the filament. The purpose of this modification was to prevent ions formed around the filament from being attracted into the ion sampling region.

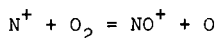
A packed column gas chromatograph is connected to the mass spectrometer through a Nupro valve which is used as a stream splitter.

Chemical ionization mass spectra of several hydrocarbons injected into the GC inlet have been obtained with methane as carrier and reactant gas.

References

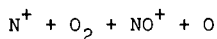
1. M.S.B. Munson and F.H. Field, J. Am. Chem. Soc. 88, 2621 (1966)
2. M.S.B. Munson and F.H. Field, J. Am. Chem. Soc. 88, 4337 (1966)
3. P. Natalis and J.L. Franklin, J. Phys. Chem. 69, 2943 (1965).
4. R.R. Bernecker and F.A. Long, J. Phys. Chem. 65, 1565 (1961).

Crossed Beam Study of the Ion-Molecule Reaction



Zdenek Herman, John C. Tully, Richard Wolfgang
Department of Chemistry, University of Colorado
Boulder, Colorado 80302

The dynamics of the reaction



was studied in the eV range of laboratory energies using a crossed beam apparatus EVA¹: a beam of mass selected ions N⁺ of variable energy and narrow angular and energy spread was intersected by a modulated beam of O₂ of thermal energy. The angular distribution and energy spectra at various angles of the product, NO⁺, were measured. The data are plotted as a contour map showing the distribution of the ionic product in the velocity vector (Newton) diagram.

The product recoils forward with respect to the center of mass. The position of the peak suggests that the prevailing mechanism of the reaction in the energy range studied is a direct, stripping mechanism.

References:

1. Z. Herman, J.D. Kerstetter, T.L. Rose and R. Wolfgang, Rev. Sci. Instr., 40, 538 (1969).

ION-MOLECULE REACTIONS IN METHANE-AMMONIA MIXTURES*

by

W. T. Huntress, Jr.[†] and D. D. Elleman

Jet Propulsion Laboratory
 California Institute of Technology
 Pasadena, California 91103

ABSTRACT

The ion-molecule reactions of ions formed by electron impact in methane-ammonia mixtures have been studied by ion-cyclotron resonance techniques. ICR double resonance experiments on a mixture of ammonia and perdeuteromethane have identified the following reactions: charge transfer between CD_4^+ and ammonia, proton transfer to ammonia from methane parent ion CD_4^+ and from the product ions CD_5^+ and $C_2D_5^+$, and hydrogen atom abstraction by NH_3^+ from neutral CD_4 . A resonant proton transfer process was also observed to take place from the NH_3D^+ product ion to NH_3 , producing NH_4^+ ion. Hydrogen atom abstraction from neutral NH_3 by CD_4^+ ion has been previously observed by Harrison and Thynne at CD_4^+ ion kinetic energies in excess of 3.7 eV. This reaction was not observed by ICR due to faster competing reactions of CD_4^+ .

The most interesting reactions occurring in CH_4 - NH_3 mixtures is a condensation reaction between the fragment ion CH_3^+ and ammonia to form $CH_2NH_2^+$ and a hydrogen molecule. The product ion $CH_2NH_2^+$ is apparently formed initially in an excited state and at low pressures undergoes proton transfer with ammonia to produce the ammonium ion and neutral methylenimine. At higher pressures, the $(CH_2NH_2^+)^*$ is deactivated by non-rearrangement collisions, and the $CH_2NH_2^+$ ion in the ground state will not transfer a proton to ammonia at thermal kinetic energies. At high double-resonance irradiating power, however, the $CH_2NH_2^+$ ground state ion can gain sufficient kinetic energy from the rf field that the process again becomes exothermic and the proton transfer reaction can be forced to occur.

Submitted to the Journal of Chemical Physics

* This paper presents the results of one phase of research carried out at the Jet Propulsion Laboratory, under Contract No. NAS 7-100, sponsored by the National Aeronautics and Space Administration.

[†]NRC Postdoctoral Resident Research Associate, supported by NASA.

Kinetic Analysis of Concurrent Reaction Systems Using Ion Ejection -
Ion Cyclotron Resonance Techniques*

by

Michael T. Bowers, Department of Chemistry
University of California, Santa Barbara, California 93106

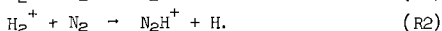
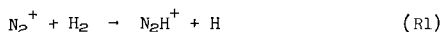
and

Daniel D. Elleman, Jet Propulsion Laboratory
Pasadena, California

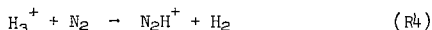
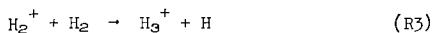
The addition of the ion-ejection capability¹ to the general ICR technique² affords an opportunity for quantitatively determining rate constants in concurrent ion-molecule reaction systems. In an ion-ejection experiment, the ions of a given mass are selectively ejected from the cell in a time short relative to the total reaction time. The non-ejected ions are not affected and proceed to drift through the cell and react. A standard kinetic treatment³ will then yield the rate constant of the non-ejected ions. The ejection field can then be turned off and the increase in intensity of the product ion will be due to reaction of the initially ejected ions. An expression for the relative rates of the ejected and non-ejected species can readily be derived.

$$\frac{k_{ej}}{k_{non}} = \frac{v_{ej} I_{ej} \sigma_{non} L_{non}}{v_{non} I_{non} \sigma_{ej} L_{ej}} \quad (1)$$

where v is the ion velocity, I is the intensity of the product ion, σ is the ionization cross section and L is the zero collision ion path length. The σ 's are known, the I 's are measured, the v 's are proportional to $m^{-1/2}$ and the pathlengths can be calculated from the equation of motion of the ions.⁴ Conveniently, the L 's are very nearly proportional to $m^{-1/2}$ ⁵ and hence to a very good approximation the v 's and L 's cancel. Results are given in Table I for the concurrent reactions in N_2 - H_2 and Ar- H_2 systems. For example, two such reactions are



The treatment can be extended to cover more complex reaction systems. In N_2 - H_2 mixtures, for example,



(R3) and (R4) are also observed and k_4 can be determined using ion-ejection methods.

* To be published in the Journal of Chemical Physics. This research was supported by Contract No. NAS 7-100 extended to the Jet Propulsion Laboratory by the National Aeronautics and Space Administration.

The details are too lengthy to be given here,⁵ but a straightforward kinetic analysis yields k_2/k_4 and hence k_4 . Again the results are summarized in Table I. Similar results have been obtained for the D_2 and HD isotopes.⁵ The reaction of N_2^+ with H_2 has been previously studied⁶ with a value of $k_{N_2^+} = 14.1 \times 10^{-10}$ cc molecule⁻¹sec⁻¹ obtained in exact agreement with the ion-ejection results. The $H_3^+ - N_2$ system has been studied by Aquilanti et al.⁷ who determined a rate constant of 10.0×10^{-10} cc molecule⁻¹sec⁻¹ also in excellent agreement with the ion ejection results. Several studies on the Ar- H_2 system have been made using standard high pressure techniques^{7,8} with the general finding that the rate constants are close to the theoretical. This contrasts with the ion-ejection results. No reason for the discrepancy is obvious.

Table I. Thermal Energy Rate Constants Determined by Ion Ejection Methods.

Reaction	$k \times 10^{10}$ cc molecule ⁻¹ sec ⁻¹		Exptl.	Ratio	
	This Work	Theory ^a		Theory ^a	Theory ^a
$N_2^+ + H_2 \rightarrow N_2H^+ + H$	14.1	15.4	0.72	0.68	
$H_2^+ + N_2 \rightarrow N_2H_3^+ + H$	19.5	22.8			
$[H_3^+]^{*b} + N_2 \rightarrow N_2H^+ + H_2$	10.3	19.0			
$Ar^+ + H_2 \rightarrow ArH^+ + H$	6.83	15.6	0.55	0.69	
$H_2^+ + Ar \rightarrow ArH^+ + H$	12.4	22.5			
$[H_3^+]^{*b} + Ar \rightarrow ArH^+ + H_2$	3.65	19.1			

a) G. Gioumousis and D. P. Stevenson, J. Chem. Phys. 29, 294 (1958).

b) $[H_3^+]^*$ denotes H_3^+ formed from reaction of H_2^+ with H_2 . H_3^+ so formed has up to 2 eV internal energy [J. J. Leventhal and L. Friedman, J. Chem. Phys. 49, 1974 (1968)].

References:

1. J. L. Beauchamp and J. T. Armstrong, Rev. Sci. Inst., 40, 123 (1969).
2. See for example, J. L. Beauchamp, L. R. Anders, and J. D. Baldeschwieler, J. Am. Chem. Soc., 89, 4569 (1967).
3. M. T. Bowers, D. D. Elleman and J. L. Beauchamp, J. Phys. Chem. 72, 3599 (1968).
4. M. T. Bowers, D. D. Elleman and J. King, Jr., J. Chem. Phys. (June 1st Issue-1969).
5. M. T. Bowers and D. D. Elleman, J. Chem. Phys. (submitted).
6. M. T. Bowers, D. D. Elleman and J. King, Jr., J. Chem. Phys. 50, 1840 (1969) and references there-in.
7. V. Aquilanti, A. Galli, A. Giordini-Guidani and G. G. Volpi, J. Chem. Phys. 43, 1939 (1965).
8. D. P. Stevenson and D. O. Schissler, J. Chem. Phys. 29, 282 (1958).

The Reactions of O_2^+ Ions with Simple Alkanes and Ethylene

D. K. Bohme, R. A. Vane, F. C. Fehsenfeld, and E. E. Ferguson

Environmental Science Services Administration

Boulder, Colorado

INTRODUCTION

Reactions between ions and hydrocarbon molecules play an important role in the study of irradiated, ignited, and discharged hydrocarbon gas mixtures. In order to verify these reactions, the gas-phase ion chemistry of hydrocarbons has been investigated extensively in recent years using a number of different experimental techniques. A majority of these investigations have been performed with accelerated ions in suitably modified mass-spectrometer ion sources. With the advent of pulsing techniques and improved source chamber designs which eliminate stray electric fields it has become possible to measure rate coefficients for these reactions near thermal energies. More recently ion-molecule reactions in hydrocarbon systems have been investigated using a tandem mass spectrometer in an attempt to establish unambiguously the product channels in these reactions (1). During the past several years, a flowing afterglow technique has been used extensively to obtain quantitative information on specific rates and product channels of many ion-molecule reactions at thermal energies (2). Most of these studies were concerned with reactions of interest in aeronomy involving atmospheric gases such as N_2 , O_2 , O_3 and NO_2 . It is the purpose of this paper to present some of the first investigations in a flowing afterglow system of reactions of O_2^+ and some positive hydrocarbon ions with hydrocarbon gases such as methane, ethane, propane, butane, and ethylene. The results demonstrate that the flowing afterglow technique provides a valuable method for the study of such reactions.

EXPERIMENTAL

The experiments were performed in the ESSA flowing afterglow system. The details of this experimental apparatus, its operation, and the related data analysis have been described in detail elsewhere (2). In the present experiments either pure O_2 or O_2 in small fractional quantities in a helium or nitrogen buffer gas are introduced into the excitation region. Alternatively O_2 is added just downstream from the electron impact ion source in a helium buffer gas. The O_2^+ ions are then produced either directly by electron impact or indirectly by secondary reactions in the early helium afterglow. Electronically excited O_2^+ ions decay by radiation or collisional quenching before the point of hydrocarbon gas addition further downstream. In the region following the addition of the hydrocarbon reactant gas, the characteristic reactions between O_2^+ and the reactant gas take place. The reaction region is terminated by the sampling orifice of a quadrupole mass spectrometer. In the normal operating mode this spectrometer has a resolution of about 70 for full width at 10% maximum. The decline of the O_2^+ and hydrocarbon ion signals as a function of hydrocarbon gas addition constitute the raw data from which rate coefficients are determined. In the present system the rate coefficients are determined with an estimated absolute accuracy of 30%. The experiments were performed at 22.5°C at a number of total steady state pressures. The hydrocarbon gases used in these studies were standard bottled gases having the following minimum purity in mole %:

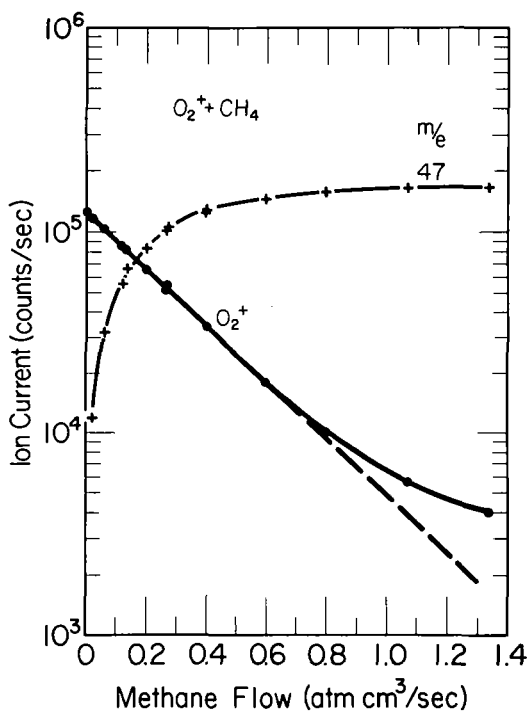


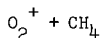
Fig. 1. Ion currents for the reaction of O_2^+ with CH_4 in a helium buffer gas at a steady-state pressure of 0.375 torr.

TABLE I. Reactions of Ions in Methane

Primary Ion	Loss of Primary Ion $k(\text{cm}^3\text{molecule}^{-1}\text{sec}^{-1})$	Secondary Ion	Fraction of Secondary Ion
O_2^+	$7.8 \pm 0.6 (-12)^a$	$CH_3O_2^+$	1
		CH_4^+	< 0.001
		CH_3^+	< 0.001
		CH_2O^+	< 0.001

methane, 99.95, ethane, 99.0; propane, 99.5; n-butane, 99.5; ethylene, 99.5.

RESULTS



An O_2^+ ion loss curve as a function of methane addition is shown in Fig. 1. The only significant product ion observed at the operating pressures and temperature of this experiment had a mass of 47 which was identified by isotope analysis to be the ion $CH_3O_2^+$. No other product ions with an abundance greater than 1% of $CH_3O_2^+$ were observed in the mass range $m/e = 10$ to 100.

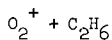
The rate coefficient for the loss of O_2^+ ions due to the reaction



was measured at four different pressures from 0.235 to 0.865 torr with helium as the buffer gas. The rate coefficient was found to be pressure independent and had an average value of $7.8 \pm 0.6 \times 10^{-12} \text{ cm}^3 \text{ molecule}^{-1} \text{ sec}^{-1}$. This value is in fair agreement with the value of $1.26 \pm 0.20 \times 10^{-11} \text{ cm}^3 \text{ /sec}$ obtained by Franklin and Munson (3) in an ion source mass spectrometer experiment in $CH_4 - O_2$ mixtures. The low value for the rate coefficient suggests that only one in about every 140 Langevin collisions completes the above ion-molecule reaction.

The charge transfer reaction and the H abstraction reaction are both endoergic with ground state O_2^+ ions and were not observed in the present experiments. There was also no indication of the formation of CH_2O^+ ions. This result is not in agreement with that of Franklin and Munson who have suggested that CH_2O^+ ions are produced by the reaction of ground state O_2^+ ions with methane with a specific rate of $2.8 \times 10^{-11} \text{ cm}^3 \text{ molecule}^{-1} \text{ sec}^{-1}$. Perhaps there was sufficient uncertainty in their appearance potential measurement of the CH_2O^+ ion to allow for the possibility of CH_2O^+ ion formation by the reaction of CH_4^+ with O_2 or of vibrationally excited O_2^+ with CH_4 .

The results for the reaction of O_2^+ ions with methane are summarized in Table I.



As shown in Fig. 2, the experimental results indicate that the O_2^+ ion reacts rapidly with ethane to produce a variety of secondary ion products. The rate coefficient for the loss of primary O_2^+ ions was measured to be $1.6 \pm 0.2 \times 10^{-9} \text{ cm}^3 \text{ molecule}^{-1} \text{ sec}^{-1}$ with both O_2 and He as a buffer gas. There are three principle products of this reaction. The production of the ion at mass 29 accounts for about 91% of the reactions. About 8% of the reactions give mass 28. Finally about 1% of the reactions result in the formation of mass 47.

The most abundant secondary product ion is mass 29 which, according to stoichiometry, may be either $C_2H_5^+$ or CHO^+ . The formation of the latter ion would however require considerable bond breaking and is not expected on mechanistic grounds. The production of the ethyl carbonium ion $C_2H_5^+$ on the other hand would simply involve the transfer of a hydride ion according to the reaction



The intensity of the mass 30 ion accounts for the isotopic contribution from $C_2H_5^+$. This suggests, but does not prove, that mass 29 is $C_2H_5^+$. The isotope abundance ratio may

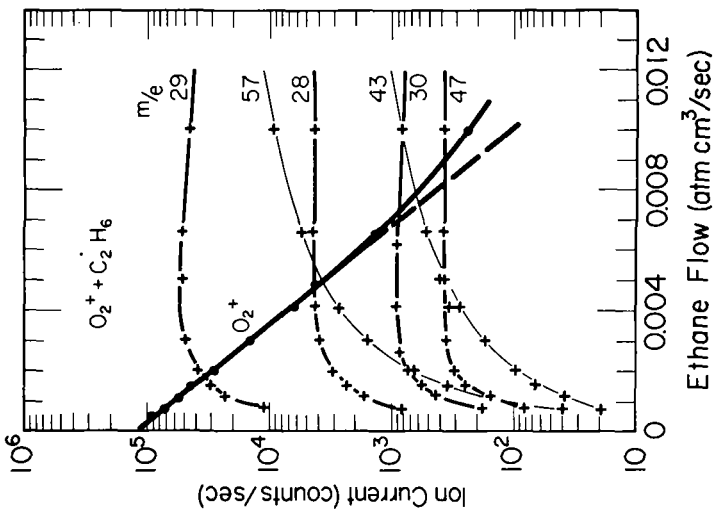


Fig. 2. Ion currents for the reaction of O_2^+ with C_2H_6 in a helium buffer gas at a steady-state pressure of 0.281 torr.

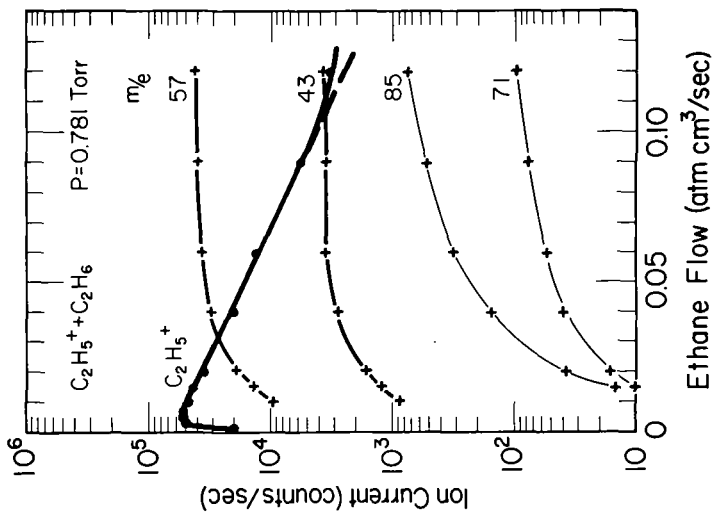
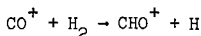


Fig. 3. Ion currents for the reaction of $C_2H_5^+$ with C_2H_6 in a helium buffer gas at a steady-state pressure of 0.281 torr.

indeed be misleading since $C_2H_6^+$, which has $m/e = 30$, is a possible exoergic charge transfer channel. The identity of mass 29 was therefore established from its further reaction with C_2H_6 . As indicated in Fig. 3, the mass 29 ion reacts further with ethane to yield the product ion masses 43 and 57. The CHO^+ ion can be generated in the absence of the $C_2H_5^+$ ion by the reaction



which has a measured specific rate of $2.0 \times 10^{-9} \text{ cm}^3 \text{ molecule}^{-1} \text{ sec}^{-1}$ (4). It was found that CHO^+ reacts rapidly with ethane to yield major product ions with masses 57 and 31 according to the reactions



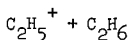
and



The measured rate coefficient for the loss of the CHO^+ ion was about $2 \times 10^{-10} \text{ cm}^3 \text{ molecule}^{-1} \text{ sec}^{-1}$. This specific rate is about four times that for the loss of the mass 29 ion in the O_2^+ , C_2H_6 system. Moreover, the mass 31 ion was not observed as a product ion in the O_2^+ , C_2H_6 system. These results identify the mass 29 ion observed in the O_2^+ , C_2H_6 system as predominantly $C_2H_5^+$. The magnitude of the $m/e = 30$ ion signal now allows an estimation of an upper limit to the rate coefficient for the charge transfer process of $1 \times 10^{-11} \text{ cm}^3 \text{ molecule}^{-1} \text{ sec}^{-1}$.

The second most abundant product ion for the reaction of O_2^+ with C_2H_6 is mass 28 which may be either $C_2H_4^+$ or CO^+ . Here the production of CO^+ is expected to be unlikely on mechanistic grounds. The results of this experiment did not indicate a significant loss process for the mass 28 ion even though exoergic two-body reactions can be written for both the $C_2H_4^+$ and CO^+ ions. It was again expected that an independent investigation into the reaction of CO^+ with C_2H_6 would establish unequivocally the identity of this mass 28 ion. CO^+ did indeed seem to react with C_2H_6 . However, $C_2H_4^+$ appeared to be a product of this reaction so that a rate coefficient for the loss of CO^+ could not be measured. CO^+ has concurrently been found to react rapidly with CH_4 , C_3H_8 and $n-C_4H_{10}$. These results suggest that the mass 28 ion observed in the O_2^+ , C_2H_6 system is $C_2H_4^+$ and that this ion is non-reactive in ethane. The non-reactivity of $C_2H_4^+$ in ethane has been established previously by Munson and Field (5).

Stoichiometry unequivocally identifies the non-reactive mass 47 product ion as $CH_3O_2^+$. This ion was found to be the only significant oxygen-containing product ion. The specific rate for the reaction of O_2^+ with C_2H_6 to yield $CH_3O_2^+$ is equivalent to the ratio of the $CH_3O_2^+$ signal to the total product ion signal times the rate coefficient for the loss of O_2^+ ions. This means that the rate of formation of $CH_2O_2^+$ from the O_2^+ , C_2H_6 reaction is roughly equivalent to the rate of formation of $CH_3O_2^+$ from the reaction of O_2^+ with CH_4 as discussed above.

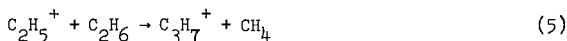


The results of this experiment for the reaction of the ethyl carbonium ion with addition of ethane to the flowing afterglow are shown in Fig. 3. The variations of the ion currents at $m/e = 43$ and 57 suggest that $C_3H_7^+$ and $C_4H_9^+$ are both primary products of the reaction of $C_2H_5^+$ with ethane. The rate coefficient for the loss of $C_2H_5^+$ ions was measured as a function of total pressure in both He and N_2 buffer gases at 20 different

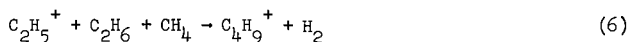
pressures from 0.17 to 0.64 torr. The results suggested that $C_2H_5^+$ is lost by a two-body process with a specific rate of $5.1 \pm 1.0 \times 10^{-11} \text{ cm}^3 \text{ molecule}^{-1} \text{ sec}^{-1}$. In addition $C_4H_9^+$ was found to be the dominant product channel with 10% of the output channel going to $C_3H_7^+$. The overall condensation reaction may be written as



Mass spectrometric studies of gaseous ionic reactions in mixture of $CH_4 + 1\%$ C_2H_6 at pressures up to 2 torr have led Munson and Field (5) to propose the following product channel for the reaction of $C_2H_5^+$ with ethane:



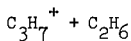
for which they report a rate coefficient of about $6 \times 10^{-11} \text{ cm}^3 \text{ molecule}^{-1} \text{ sec}^{-1}$. Furthermore they conclude that although $C_4H_9^+$ can be formed from a second-order reaction of $C_2H_5^+$ with ethane by an exoergic process, the reaction does not occur to an appreciable extent. Instead they propose that the $C_4H_9^+$ ion may result from a three-body reaction of the type



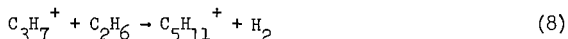
or the equivalent reaction involving a collision complex



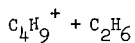
The apparent discrepancy of our observations with those of Munson and Field may be a result of the different states of the $C_2H_5^+$ ion. In the flowing afterglow experiments, the $C_2H_5^+$ ion is produced by the reaction of O_2^+ with ethane whereas in the mass spectrometer ion source experiments Munson and Field attribute the formation of the $C_2H_5^+$ ion from the reaction of CH_3^+ ions with CH_4 and CH_5^+ ions with C_2H_6 . The $C_2H_5^+$ ion in the two experiments may contain different amounts of internal energy which may yield differences in the ratio of product ions.



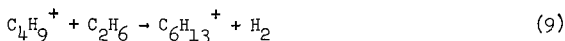
An effective binary rate coefficient of $3 \times 10^{-12} \text{ cm}^3 \text{ molecule}^{-1} \text{ sec}^{-1}$ may be estimated for the condensation reaction



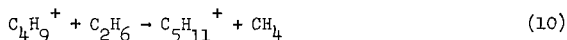
from the production of $m/e = 71$ shown in Fig. 3. We must point out that the order of this reaction has not been experimentally established. It is assumed that this reaction is the only source of $C_5H_{11}^+$. However, the allowance for an additional source of this ion, such as $C_4H_9^+$ reacting with C_2H_6 , will make the above estimate an upper limit to the rate coefficient of reaction (8). To our knowledge this reaction has not been reported previously.



From the production of $m/e = 85$ shown in Fig. 3 an estimated value of the effective binary rate coefficient for the condensation reaction

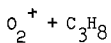


is $6 \times 10^{-13} \text{ cm}^3 \text{ molecule}^{-1} \text{ sec}^{-1}$. In addition, for the condensation reaction



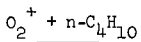
an upper limit estimate to the rate coefficient of $7 \times 10^{-14} \text{ cm}^3 \text{ molecule}^{-1} \text{ sec}^{-1}$ may be made. As was the case with the reaction of $C_3H_7^+$ with C_2H_6 the order of these reactions has not been established. There are no previously reported investigations of these reactions. It is interesting to note that the ratio of the product channels leading to the elimination of H_2 and CH_4 is similar for the condensation reaction of $C_2H_5^+$ and $C_4H_9^+$ with C_2H_6 . The product channel leading to the elimination of CH_4 for the reaction of $C_3H_7^+$ with C_2H_6 could not be observed since the return of the product $C_4H_9^+$ ion of this, no doubt slow, reaction is masked by the $C_4H_9^+$ ion produced by relatively fast reaction (7a).

The results for the reaction of O_2^+ ions with ethane and the further reactions of the fragment hydrocarbon ions with ethane are summarized in Table II.



The rate coefficient for the loss of O_2^+ ions due to the reaction with propane was measured at 5 different total pressures in helium from 0.20 to 0.37 torr. The results suggest that O_2^+ is lost by a fast two-body process having a rate coefficient of $1.8 \pm 0.3 \times 10^{-9} \text{ cm}^3 \text{ molecule}^{-1} \text{ sec}^{-1}$. The dominant product ion was observed at $m/e = 43$. Minor product ions were observed at masses 42, 28, 29, 44 and 61. The mass 28 and 29 ions were lost rapidly upon further addition of propane. Unfortunately, both isotope analysis and secondary reaction studies did not lead to an unequivocal identification of most of the product ions. The intensity of the mass 44 ion accounts for the isotopic contribution from $C_3H_7^+$ and sets an upper limit of about $6 \times 10^{-11} \text{ cm}^3 \text{ molecule}^{-1} \text{ sec}^{-1}$ to the exothermic charge transfer channel. Mass 61 is determined by stoichiometry to be the oxygen containing ion $C_2H_5O_2^+$.

The secondary reactions of hydrocarbon ions in propane are relatively well understood as a result of recent mass-spectrometric measurements (1). The results of this experiment are in fair agreement with these measurements when masses 43, 42, 28 and 29 are assumed to be the hydrocarbon ions $C_3H_7^+$, $C_3H_6^+$, $C_2H_4^+$ and $C_2H_5^+$ and not the oxygen containing ions $C_2H_3O^+$, $C_2H_2O^+$, CO^+ and CHO^+ . Table III is a summary of the reactions and the measured specific rates which are believed to apply in this system.



The rate coefficient for the reaction of O_2^+ ions with n-butane was measured at 5 different steady-state pressures in helium from 0.15 to 0.36 torr. The reaction was found to proceed rapidly in two-body fashion with a rate coefficient of $2.4 \pm 0.6 \times 10^{-9} \text{ cm}^3 \text{ molecule}^{-1} \text{ sec}^{-1}$. The two dominant secondary ions were observed at masses 43 and 58. Minor secondary ions were observed at masses 42, 28, 29 and 41. The mass 43 ion and all the minor ions were found to react rapidly with n-butane to form product ions with masses 57 and 56. Again however, isotope analysis and secondary reaction studies did not

TABLE II. Reactions of Ions in Ethane

Primary Ion	Loss of Primary Ion $k(\text{cm}^3 \text{molecule}^{-1} \text{sec}^{-1})$	Secondary Ion	Fraction of Secondary Ion
O_2^+	$1.6 \pm 2 (-9)$	C_2H_5^+	0.915
		C_2H_4^+	0.078
		CH_3O_2^+	0.007
		C_2H_6^+	<0.01
		$\text{C}_2\text{H}_5\text{O}_2^+$	<0.001
		CHO^+	<0.001
		C_4H_9^+	0.9
C_2H_5^+	$5.1 \pm 1.0(-11)$	C_3H_7^+	0.1
		$\text{C}_5\text{H}_{11}^+$	
C_3H_7^+	$\leq 3(-12)$	$\text{C}_6\text{H}_{13}^+$	
C_4H_9^+	$\sim 6(-13)$	$\text{C}_7\text{H}_{15}^+$	
C_4H_9^+	$\leq 7(-14)$	$\text{C}_9\text{H}_{19}^+$	

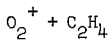
TABLE III. Reactions of Ions in Propane

Primary Ion	Loss of Primary Ion $k(\text{cm}^3 \text{molecule}^{-1} \text{sec}^{-1})$		Secondary Ion	Fraction of Secondary Ion		
O_2^+	This work Munson et al(5,6)					
	$1.8 \pm 0.3(-9)$				$\text{C}_3\text{H}_7^+(\text{C}_2\text{H}_3\text{O}^+)$	0.75
					$\text{C}_2\text{H}_4^+(\text{CO}^+)$	≤ 0.08
					$\text{C}_2\text{H}_5^+(\text{CHO}^+)$	≤ 0.08
					$\text{C}_3\text{H}_6^+(\text{C}_2\text{H}_2\text{O}^+)$	≤ 0.08
					C_3H_8^+	≤ 0.015
					$\text{C}_2\text{H}_5\text{O}_2^+$	~ 0.001
					CH_3O_2^+	<0.001
$\text{C}_2\text{H}_4^+(\text{CO}^+)$			$1.3(-9)$	$6.3 \pm 1.0(-10)$	$\text{C}_3\text{H}_7^+(\text{C}_2\text{H}_3\text{O}^+)$	
	$\text{C}_3\text{H}_6^+(\text{C}_2\text{H}_2\text{O}^+)$					
$\text{C}_2\text{H}_5^+(\text{CHO}^+)$	$8.2(-10)$	$6.2 \pm 1.3(-10)$	$\text{C}_3\text{H}_7^+(\text{C}_2\text{H}_3\text{O}^+)$			
$\text{C}_3\text{H}_7^+(\text{C}_2\text{H}_3\text{O}^+)$	<(-11)	no net reaction				
$\text{C}_3\text{H}_6^+(\text{C}_2\text{H}_2\text{O}^+)$	<(-11)					

TABLE IV. Reactions of Ions in n-Butane

Primary Ion	Loss of Primary Ion $k(\text{cm}^3 \text{molecule}^{-1} \text{sec}^{-1})$		Secondary Ion	Fraction of Secondary Ion
	This work	Munson et al(5)		
O_2^+	$2.4 \pm 0.6(-9)$		$\text{C}_3\text{H}_7^+(\text{C}_2\text{H}_3\text{O}^+)$	0.60
			$\text{C}_4\text{H}_{10}^+(\text{C}_3\text{H}_6\text{O}^+, \text{C}_2\text{H}_2\text{O}_2^+)$	0.25
			$\text{C}_2\text{H}_4^+(\text{CO}^+)$	≤ 0.05
			$\text{C}_2\text{H}_5^+(\text{CHO}^+)$	≤ 0.05
			$\text{C}_3\text{H}_6^+(\text{C}_2\text{H}_2\text{O}^+)$	≤ 0.04
			$\text{C}_3\text{H}_5^+(\text{C}_2\text{HO}^+)$	≤ 0.01
			CH_3O_2^+	< 0.001
			$\text{C}_2\text{H}_5\text{O}_2^+$	< 0.001
$\text{C}_3\text{H}_7^+(\text{C}_2\text{H}_3\text{O}^+)$	$5.1 \pm 0.4(-10)$		$\text{C}_4\text{H}_9^+(\text{C}_3\text{H}_5\text{O}^+)$	≥ 0.9
			$\text{C}_4\text{H}_8^+(\text{C}_3\text{H}_4\text{O}^+)$	≤ 0.1
$\text{C}_3\text{H}_6^+(\text{C}_2\text{H}_2\text{O}^+)$	$1.0(-9)$			
$\text{C}_3\text{H}_5^+(\text{C}_2\text{HO}^+)$	$9.4(-10)$	$8.5(-10)$		
$\text{C}_2\text{H}_5^+(\text{CHO}^+)$	$2.0(-9)$	$6.6 \pm 2.8(-10)$		
$\text{C}_2\text{H}_4^+(\text{CO}^+)$	$1.7(-9)$	$1.2 \pm 0.4(-9)$		

lead to an unequivocal identification of the product ions. The ion-molecule reactions which are believed to apply in this system are summarized in Table IV, together with the measured specific rates.



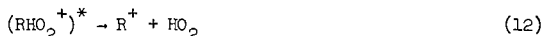
O_2^+ ions were found to react rapidly with ethylene to yield a product ion at mass 28 with an apparent two-body rate coefficient of $1.9 \times 10^{-9} \text{ cm}^3 \text{ molecule}^{-1} \text{ sec}^{-1}$ at 0.182 torr in oxygen. The formation of the reaction products $CO^+ + CH_3OH$ was calculated to be endoergic and thus can be precluded at thermal energies. This identifies the mass 28 ion as $C_2H_4^+$ and the reaction of O_2^+ with ethylene as the charge transfer reaction



No attempt was made to resolve the hydrocarbon ion chemistry initiated by the reaction of $C_2H_4^+$ with C_2H_4 . Such investigations have been reported in detail by several workers (7,8).

CONCLUSIONS

The early mass-spectrometric investigations of Franklin and Munson (3) indicated that O_2^+ ions react only slowly with the hydrocarbon gases methane and acetylene. The present flowing afterglow results corroborate the low reactivity of O_2^+ ions toward methane but indicate that O_2^+ ions react essentially on every spiralling or orbiting collision with ethane, propane, butane and ethylene. The dominant product channel in the reaction of O_2^+ with ethane and propane corresponds to hydride ion abstraction. There was no evidence for an appreciable charge transfer product in these two reactions. This indicates that in these two cases hydride ion abstraction successfully competes with the less exoergic charge transfer for the output channel. The formation of the dominant product ions by dissociative charge transfer is endothermic. Hence the intimate collision can be thought to proceed via the direct breakup of the intermediate ion,



The dissociative charge transfer mechanism is often invoked in the initiation of radiation chemistry by ions of a higher recombination energy than O_2^+ (1).

The reaction of O_2^+ with butane is believed to proceed principally by methide ion abstraction although a significant charge transfer product is observed. The hydride ion transfer channel which in this case is less exoergic than the charge transfer channel was not significant. The reaction of O_2^+ with ethylene has been shown to proceed principally by charge transfer. The hydride ion transfer channel is endoergic.

The hydrocarbon ion chemistry initiated by O_2^+ in ethane was found to be determined by relatively slow condensation reactions accompanied by the elimination of H_2 and CH_4 . In contrast, the postulated hydrocarbon ion chemistry initiated by O_2^+ in propane and butane proceeded principally by H^- abstraction reactions and to a much lesser extent by H_2^- abstraction reactions. These observations are consistent with the earlier measurements in mass-spectrometer ion source experiments in which the hydrocarbon ions are generated in the hydrocarbon gas by secondary reactions involving ions of higher recombination energy than O_2^+ .

In conclusion, the flowing afterglow technique has been applied to the study of reaction sequences initiated by O_2^+ reacting with a variety of simple hydrocarbon gases. The present results indicated the suitability of the method as a tool for the systematic investigation of chemionization in hydrocarbon gases.

REFERENCES

1. L. I. Bone, L. W. Sieck, and J. H. Futrell, *The Chemistry of Ionization and Excitation*, Taylor & Francis, Ltd. London E.C. 4 (1967).
2. E. E. Ferguson, F. C. Fehsenfeld, and A. L. Schmeltekopf, *Advances in Atomic and Molecular Physics*, Vol. 5, Academic Press, New York, 1969; F. C. Fehsenfeld, A. L. Schmeltekopf, P. D. Goldan, H. I. Schiff, and E. E. Ferguson, *J. Chem. Phys.*, 44, 4087 (1966).
3. J. L. Franklin and M. S. B. Munson, *Proc. Tenth Intern. Symposium Combustion*, The Combustion Institute, p.561 (1965)
4. F. C. Fehsenfeld, A. L. Schmeltekopf, and E. E. Ferguson, *J. Chem. Phys.*, 46, 2802 (1967).
5. M. S. B. Munson, J. L. Franklin, and F. H. Field, *J.A.C.S.* 87, 3294 (1965).
6. M. S. B. Munson, J. L. Franklin, and F. H. Field, *J. Phys. Chem.*, 68, 3098 (1964).
7. J. J. Myher and A. G. Harrison, *Can. J. Chem.* 46, 101 (1968).
8. D. A. Durden, Ph.D. Thesis, 1969, Dept. of Chemistry, The University of Alberta, Edmonton, Alberta.

ION-CYCLOTRON RESONANCE STUDY OF THE KINETIC ENERGY
DEPENDENCE OF ION-MOLECULE REACTION RATES

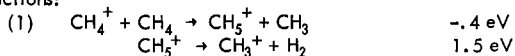
Roger P. Clow and Jean H. Futrell
University of Utah, Salt Lake City, Utah 84112

The method of ion-cyclotron resonance (ICR) mass spectrometry has been utilized to give good qualitative results on mechanisms of ion-molecule reactions and the kinetic energy dependence of reaction rates. However, some characteristics of the standard ICR cell and operating procedures have made quantitative deductions difficult. In particular, "leakiness" of the cell and ion space charge effects are prominent artifacts. By using a newly designed ICR cell and by pulsing the electron gun and irradiating rf oscillator, we are able to eliminate these effects. The energy dependence of reaction rates in methane and argon-deuterium mixtures have been investigated. The results agree well with theoretical predictions and published values which have been obtained through other experimental means.

Figure 1 is a schematic of the modified cell. Its dimensions are those of Varian's conventional bakeable flat ceramic cell except for the addition of a 2 1/2 inch reaction zone between the source and the analyzer region. To reduce the leakiness of the cell, the trapping field plates have been separated between the source and the reaction-analyzer regions. An additional total ion current collection plate was added at the end of the cell to increase collection efficiency. Finally, the various ion drifts can be varied independently.

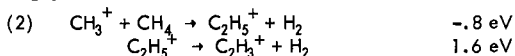
The monoenergetic ions were obtained by pulsing the electron energy from below the ionization potential to above at a frequency of 1.2 kilohertz. This 100-microsecond pulse was followed by activation of the irradiating radio-frequency oscillator at the cyclotron resonance frequency of the ion to be energized. The rf pulse duration was 250 μ seconds and the amplitude was varied to establish the terminal energy. These monoenergetic ions were drifted into the reaction zone and the products detected in the analyzer region with a phase sensitive detector. The various ion drifts and the pulsing frequency were judiciously chosen to insure minimum reaction during acceleration. Ion losses from the cell were reduced by operating at high magnetic fields and by using trapping fields in the reaction-analyzer region which was generally about five times greater than that in the source region.

Figure 2 is a plot of the CH_5^+ and CH_3^+ ion intensities as a function of center of mass energy for the reactions:



The CH_5^+ intensity begins to decrease almost immediately with CH_4^+ energy. This decrease can be attributed in part to more reaction channels being opened up with energy. The formation of CH_3^+ which is endothermic by 1.5 eV is such a case.

The formation of C_2H_3^+ as a function of CH_3^+ energy behaves analogously:

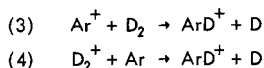


The thermo rate constants for these processes were determined to be

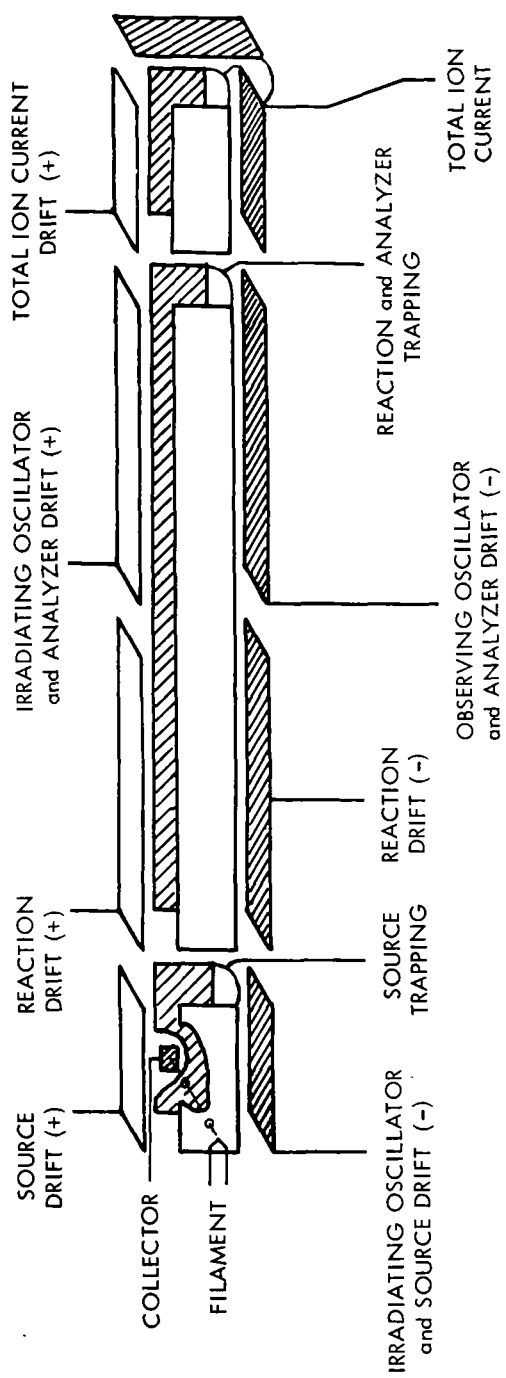
$$\begin{aligned} k_1^{\text{th}} &= 1.2 \pm 0.1 \times 10^{-9} \text{ cm}^3\text{-mol}^{-1} \text{ sec}^{-1} \\ k_2^{\text{th}} &= 1.0 \pm 0.1 \times 10^{-9} \text{ cm}^3\text{-mol}^{-1} \text{ sec}^{-1} \end{aligned}$$

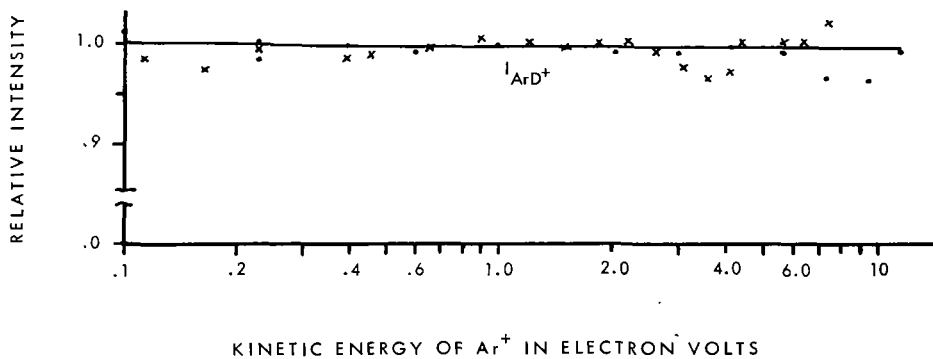
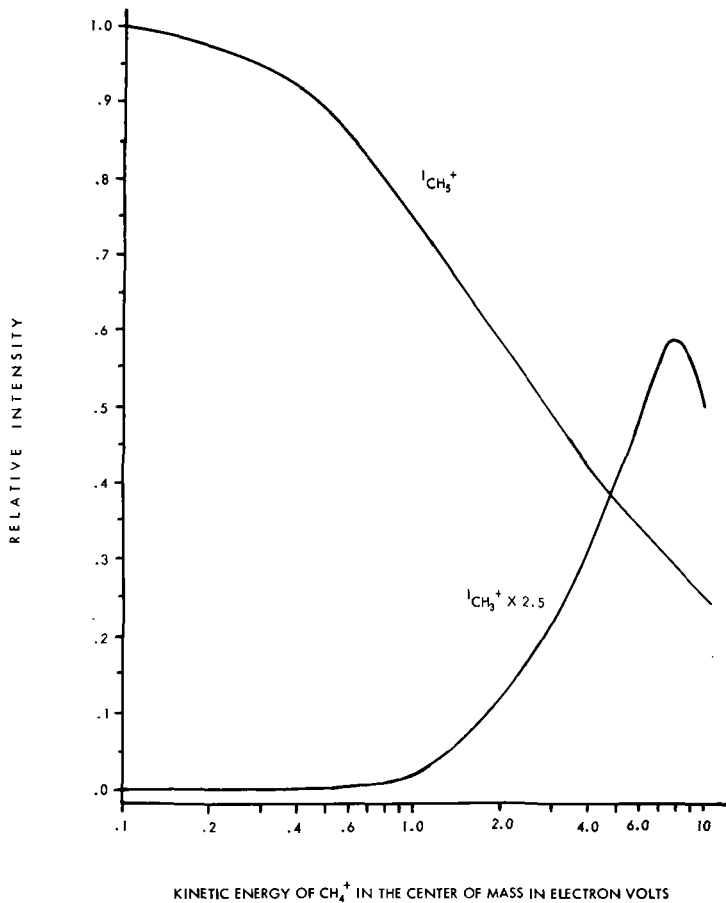
These values are in excellent agreement with published results using other techniques.

The argon-deuterium system (1:3.5 mixture) behaved quite differently from that of methane. The reactions studied were:



As can be seen in Figure 3, the ion intensity of ArD^+ is constant with kinetic energy of reactant ion Ar^+ . This is the behavior predicted by the polarization theory of ion-molecule reactions. Thus, although it proceeds via a stripping mechanism over the energy range investigated, the overall cross-section is apparently governed by long-range ion-induced dipole forces. (It is worth noting that the conventional double resonance





techniques should not confirm the $\text{Ar}^+ + \text{D}_2 \rightarrow \text{ArD}^+ + \text{D}$ channel due to the constancy of ArD^+ intensity with energy of Ar^+ .)

The energy dependence of reaction (4) was not investigated in detail because of experimental complications. Thermal rate constants for the argon-methane systems were found to be

$$k_3^{\text{th}} = 0.9 \pm 0.1 \times 10^{-9} \text{ cm}^3\text{-mol}^{-1} \text{ sec}^{-1}$$
$$k_4^{\text{th}} = 1.6 \pm 0.2 \times 10^{-9} \text{ cm}^3\text{-mol}^{-1} \text{ sec}^{-1}$$

which are in good agreement with both theoretical and previously published results for the argon-deuterium system.

A more detailed account of these results will be submitted to the *Journal of Chemical Physics*.

Figure Captions.

Figure 1. Modified ICR cell permitting separate control of drift and trapping potentials for source, reaction, analyzer, and total ion current regions.

Figure 2. Kinetic energy dependence of reaction rate of CH_4^+ with CH_4 .

Figure 3. Kinetic energy dependence of reaction rate of Ar^+ with D_2 .

COMPOUND IDENTIFICATION BY COMPUTER MATCHING OF MASS SPECTRA

B. Knock⁺, D. Wright⁺, W. Kelly* and R. G. Ridley⁺

Introduction

The GC/MS technique has vastly increased the opportunities for producing large numbers of low resolution mass spectra. In many applications it would be extremely useful to have a preliminary identification of the data by matching the spectra against a library file. Ideally, even where the actual spectrum is not included in the library the output should give some guide to the type of compound being examined.

In a preliminary study of computer matching of low resolution mass spectra presented at Denver it was found that of four methods tried then, two were worth pursuing further.

$$\text{Method 1: } P_1 = \frac{1}{n} \sum_{k=1}^{n_a} (n - |i - j| k)$$

$$\text{Method 2: } P_2 = \frac{1}{R} \sum_{r=1}^R \left[\frac{1}{n} \sum_{k_p=1}^{n_{ar}} (n - |i - j| k) \right]$$

Method 1 is a variation of using the 'n' strongest peaks which takes account of the position, 'i', of each peak compared in the unknown to the position, 'j', of the corresponding peak in the library spectrum. Method 2 was developed in the earlier studies to handle spectra which showed particularly large differences with different instruments and operating conditions. The spectrum is divided into R intervals of 'm' amu and inside each of these the 'n' strongest peaks are compared, as with Method 1. The factor P₁ and P₂ in each case is a measure of the degree of match, being 1.0 for an exact match. Table 1 shows a typical computer output for one of these methods with ten compounds printed out in order of decreasing 'P' value.

Table 1. Method 1 n = 20; 197 spectra in Library M.Wt. 167-173

Ref. No.	Mol. Wt.	'P'	Compound
API 04.04	170	1.00	N-Dodecane C12.H26
API 0023	170	0.87	N-Dodecane C12.H26
API 0981	170	0.83	N-Dodecane C12.H26
API 1028	170	0.82	N-Dodecane C12.H26
API 1598	170	0.80	N-Dodecane C12.H26
AST 2012	170	0.78	2-Methylundecane C12.H26
AST 2013	170	0.75	4-Methylundecane C12.H26
AST 2011	170	0.74	2,5-Dimethyldecane C12.H26
API 1944	170	0.72	2,5-Dimethyldecane C12.H26
API 04.05	170	0.64	2,2,4,4,6,6-Pentamethylheptane C12.H26

Hydrocarbons

In cooperation with MIT, JPL and ICI the Data Centre now has more than 6200 complete spectra from the ASTM, DOW, MCA and API collections on magnetic tape. Together with the first 1000 spectra from the MSDC collection[†] it was possible to extend the earlier work to a much wider range of compound type and molecular weights. Initially 174 hydrocarbons were selected each of which had at least two spectra on these tapes. One spectrum of each compound was run as the 'unknown' using both Method 1 and Method 2, the former using n = 20, and the latter using n = 3, m = 20. Somewhat arbitrarily, a range of ± 3 amu on the molecular weight was selected to define the range of match. The compounds covered a range of chemical type Aliphatic Saturated, Aliphatic Double Bond, Aliphatic Triple Bond, Alicyclic, Aromatic Benzene Rings and Fused Ring. The molecular weight ranges covered and the average number of spectra examined in the library in each range were 56-150 amu (250), 151-200 amu (175), 201-250 amu (100) and 251-506 amu (50).

[†]Mass Spectrometry Data Centre, AWRE, Aldermaston, Berks.

*Unilever Ltd., Colworth Laboratories, Bedford.

[‡]MSDC 1001-2000 are now available on magnetic tape.

Table 1 shows an example where several duplicates are retrieved successfully. Here the chain isomers have been ranked in order of their structural differences from the 'unknown', but in many other cases the spectra were sufficiently similar to rank such isomers or positional isomers above the duplicate.

Table 2 summarises these results for both methods. There is very little to choose between the two methods, both of which show a high degree of success. It is of interest that one apparently bad result was traceable to a tape error, adjacent spectra being interchanged.

Table 2. Hydrocarbons (Percentages)

Mol. Wt. Range	56-150		151-200		201-250		251-506	
	1	2	1	2	1	2	1	2
1st Position	67	59	87	81	78	70	98	98
1st Position or isomer	98	98	100	96	100	100	100	100

Several variations were tried:-

Method 1, n = 10

In this variation only the ten strongest peaks are used, but in general again the results were very good. Of 31 compounds tested, only 3 were worsened by this change, and that marginally. Two were slightly improved with respect to isomers.

Method 2, n = 2, m = 14

This variation gave very similar results. About 6% were improved, and 9% were made worse, in most cases only with regard to isomeric positions. For manual measurement of spectra the 3/20 method is preferable.

Method 2, n = 6, m = 40

This variation was tested for 31 compounds with no significant difference in the results.

Non-Hydrocarbons

A similar set of results was obtained for as many other compound types as possible that still satisfied the requirement of having a duplicate spectrum available. Sulphur, Nitrogen, Halogen and Oxygen compounds were studied. The molecular weight ranges covered and the average number of spectra examined in the library in each range were 78-130 amu (250), 131-190 amu (275) and 191-350 amu (125). The overall results are summarised in Table 3 which gives the percentage matching in this way.

Table 3. Non-Hydrocarbons (Percentages)

Mol. Wt. Range	78-130		131-190		191-350	
	1	2	1	2	1	2
1st Position	84	70	84	84	58	80
1st Position or isomer	95	84	100	100	68	84

The results are very similar to the hydrocarbons, but somewhat less successful. Several exact matches were found where the same spectra have been included in different collections, and these results have not been used. The different starting points used in recording the data, and also impurity peaks, accounted for most of the poorer results. Method 2 has given slightly better results compared to Method 1.

Some of the possible variations were examined.

Method 1, n = 10

Using only the ten strongest peaks, the results were about the same. Out of 75 trials, 5 were worse, and 4 better (not counting isomeric positions) compared to using n = 20.

Method 2, n = 2, m = 14

The 75 spectra were tested with this change, and the results for 7 were worse, and for 3 better.

Range - 20 to +20

The alcohols were re-run at a range of -20 to +20 and, as expected, a match was obtained occasionally with the corresponding unsaturated hydrocarbon.

GC/MS Spectra

The earlier study had indicated that the methods applied encouragingly to terpenes. Since that time a special file of 300 spectra has been assembled from the literature and elsewhere to enable this to be tested more thoroughly. To simulate an actual complete system a geranium oil was run through the GC/MS using a Biemann type separator and an MS12. The spectra were manually measured using the three largest peaks out of 20 and this data was punched on to cards and run as unknowns against the terpene library.

Six of the 'unknowns' were not on the file, and 4 of the other spectra were found to be mixtures from unresolved GC peaks. Table 4 shows that out of the 30 remaining spectra taken, 24 were identified correctly in the 1st position, and the others were all given in the 4th position or better. This is an excellent result when it is considered that none of the library spectra were obtained on the same instrument as used for the GC/MS measurements.

Table 4

Peak No.	Compound	Position	Px100
4	α -Pinene	1	95
5	2,6,6,-Me ₃ -2-vinyl tetrahydropyran	1	76
6	Myrcene	2	93
7	α -Phellandrene	2=	78
11	Limonene	1	93
14	β -Ocimene-X	4	87
16	β -Ocimene-Y	3	82
17	p-Cymene	1	80
18	α -Terpinolene	1	76
21	2-Isobut-1-enyl methyl THP	1	96
23	" (isomer)	1	85
25	cis Linalool oxide	1=	86
26	trans " "	1=	69
27	Menthone	2	79
28	Isomenthone	1	89
29	Linalool	1	85
31	α -Gurjunene	1	86
33	Neomenthol	1	74
36	Citronellyl formate	1	93
38	" acetate	1	76
39	(β -Farnesene (Neryl formate	3 1	58 67
40	α -Terpineol	1=	63
41	Geranyl formate	1	68
42	Citronellyl propionate	1	71
44	(β -Citronellol (δ -Cadinene	1 1	77 70
45	Nerol	1	85
48	Geranyl propionate	1	72
49	Geraniol	1=	89
			Av. = 80

Conclusion

These studies have shown that comparatively simple mathematical procedures can produce an excellent computer identification of low resolution mass spectra. No manual allocation of 'significant' peaks is necessary with these methods. Over a wide range of compound types and molecular weight, and using a library of over 7000 spectra, the retrieval of duplicates was 8%. Counting similar isomers as successes the retrieval was 97%. It can be expected that where exact duplicates are not on file, but closely similar compounds are available, these will be retrieved.

Variations on the basic methods used do not show very significant changes in the results, but it is still likely that in practical applications of the method refinements can be added to improve the retrieval in the particular area of interest. In particular, it is possible that weighting on the larger peaks or the peaks of highest mass to charge ratio may be advantageous. In many cases it will be possible to utilise other chemical or spectroscopic information.

A test of matching of an actual GC/MS run was very successful and there seems no reason why in practical cases the GC/MS and the computer cannot be linked to give useful automatic presorting of mass spectral data.

Acknowledgements

We are grateful to Mr. I. C. Smith for assistance with the earlier development of the computer program, and to Dr. A. Brickstock and Mr. D. C. Maxwell for useful discussions.

This study, and the Mass Spectrometry Data Centre at Aldermaston are supported by the Office for Scientific and Technical Information, Department of Education and Science.

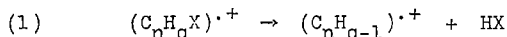
Full details of this study will be published elsewhere.

A DETAILED STEREOCHEMICAL ANALYSIS OF ELECTRON IMPACT INDUCED 1,3
ELIMINATION IN CYCLOHEXANOL AND CYCLOHEXYL CHLORIDE

Mark M. Green and Richard J. Cook
Department of Chemistry
University of Michigan
Ann Arbor, Michigan 48104

This work has been published: J. Amer. Chem. Soc., 91, 2129 (1969).

Electron impact induced elimination reactions (1) are commonly occurring processes in mass spectrometry and various researchers have documented the positions of hydrogen abstraction. The importance of the heteroatom (X) in the site selectivity is dramatically demonstrated



by the behavior of acyclic chlorides and alcohols which show predominant 1,3 and 1,4 elimination respectively. In contradiction to the proposed dominant role of the heteroatom it has been found recently that both cyclohexanol (I) and cyclohexyl chloride (II) show closely similar site selectivities. These results suggested that the hydrocarbon may control the choice of hydrogen abstraction site.

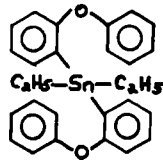
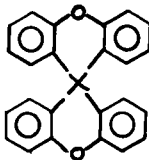
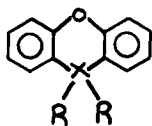
We now report that the apparently similar 1,3 eliminations in I and II occur by different mechanisms, with the eliminations continuing to follow the pattern observed in the acyclic compounds. These results have prompted us to propose a theory which invokes the bonding radius of the heteroatom as the driving force for selection of the hydrogen abstraction site.

MASS SPECTRA OF SOME ORGANOTINS AND ORGANOSILICONS

Istvan Lengyel, Michael J. Aaronson, and James P. Dillon

Department of Chemistry, St. John's University
Jamaica, New York 11432

Conventional ("low resolution") and high resolution mass spectra¹ of the heterocyclic organotin and organosilicone compounds I-IX² were recorded and evaluated. Low voltage studies (at 12eV) were carried out to identify energetically favorable decomposition paths. Comparison with the mass spectrum of diethyl bis(o-phenoxyphenyl)tin (compound X), an analog without heterocyclic ring, showed some unexpected differences. We are unaware of any previous published reports on electron-impact induced reactions of closely related compounds.



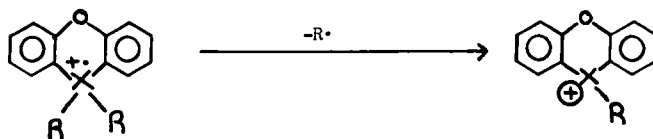
- I, X=Sn, R=CH₃
 II, X=Sn, R=C₂H₅
 III, X=Sn, R=n-C₄H₉
 IV, X=Sn, R=C₆H₅
 V, X=Sn, R=Cl
 VI, X=Si, R=CH₃
 VII, X=Si, R=C₆H₅

- VIII, X=Sn
 IX, X=Si

X

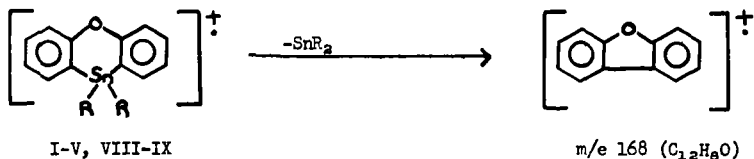
The mass spectra of the tin and silicone derivatives investigated show many common features; the differences observed can be related to the lower ionization potential of tin, compared with silicone, and to the increase in the metal-carbon bond strength when going from tin to silicone. Thus, the 70eV spectra of the dialkyl- and diarylphenoxasilins (VI and VII) exhibit a moderately abundant molecular ion, while in the spectra of the dialkyl- and diarylphenoxastannins (I-IV) the molecular ion is very weak or absent. 10,10'-Dichlorophenoxastannin (V) and the two spiro-compounds, 10,10'-spirobiphenoxastannin and 10-10'-spirobiphenoxasilin (VIII and IX) show abundant molecular ions.

Radical elimination by R-X bond cleavage is the dominant decomposition path for the molecular ions of all compounds investigated (even at 12eV), except the two spiro-compounds. In the latter, fission of at least two bonds is required for any particle, except hydrogen, to be eliminated. The reason for the overwhelming predominance of this fragmentation in the tricyclic systems studied is that the ion formed, (M-R)⁺, contains the metal in the IV oxidation state which is^{3,4} the most stable for both Sn and Si. Radical elimination is also observed from odd-electron fragment ions.



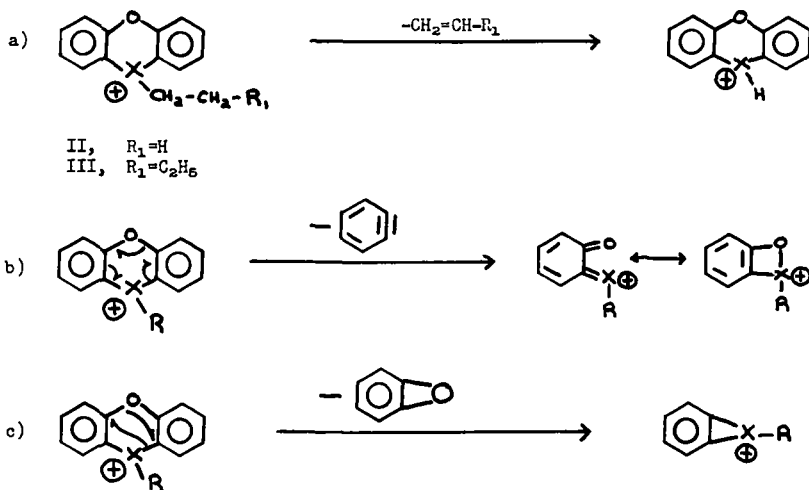
I-VII

Formation of a radical ion at m/e 168 ($C_{12}H_9O$)⁺ by elimination of XR_2 is a significant process in all tin compounds and in the spiro-Si-compound IX. The absence of m/e 168 in the spectra of VI and VII is probably due to the reluctance of silicone to form divalent species SiR_2 , whereas divalent tin is much more stable.

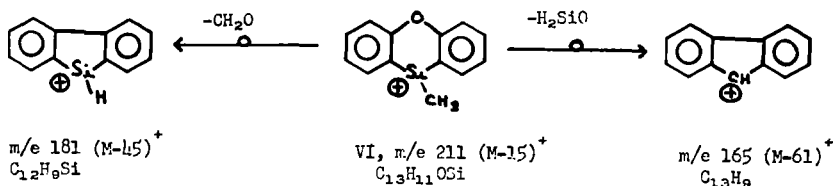


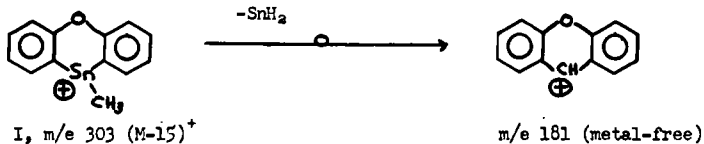
Only a few examples of loss of a neutral particle from the molecular ion leading to an odd-electron fragment ion with tetrasubstituted metal have been observed. The scarcity of this type of fragmentation can be understood, as it would require the metal to be in the V oxidation state, which is known³ to be "abnormal". There is no evidence for the formation of $(XR_2)^+$ type ions, with the exception of a small peak at m/e 182 in the spectrum of VII.

The $(M-R)^+$ ion undergoes at least three different characteristic fragmentations, each involving the elimination of a neutral particle and leading to a metal-containing even-electron ion. Alkene elimination (a) from the $(M-R)^+$ ion is an important process, even at 12eV, for sigma-bonded metal alkyls if R contains two carbon atoms or more (II and III)



In some of the compounds studied, the $(M-R)^+$ ion undergoes additional, more complex fragmentations, involving both skeletal and multiple hydrogen rearrangements. Thus, the $(M-CH_3)^+$ ion in the spectrum of compound VI (m/e 211, $C_{13}H_{11}OSi$) eliminates both CH_2O and H_2SiO to yield m/e 181 ($C_{12}H_9Si$) and m/e 165 ($C_{13}H_9$), respectively. On the other hand, the tin-analog, compound I, shows an ion at m/e 181, which is metal-free ($C_{13}H_9O$), corresponding to elimination of SnH_2 from the $(M-CH_3)^+$ species. Details of the mechanisms of these reactions are under study.





A detailed account of this work will be submitted to Org. Mass Spectrometry.

ACKNOWLEDGEMENT

We thank Professor E. J. Kupchik, Department of Chemistry, St. John's University, New York, for kindly providing the samples used in this investigation and to Professor K. Biemann and his associates, Department of Chemistry, Massachusetts Institute of Technology, for the high resolution data.

REFERENCES

- 1) The low resolution mass spectra were measured on a CEC 21-1030 and a Hitachi RMU-6D instrument. The high resolution data, in the form of "element maps", were obtained on a CEC 21-110C instrument.
- 2) E. J. Kupchik, J. A. Ursino, and P. R. Boudjouk, *J. Organometallic Chem.*, **10**, 269 (1967).
E. J. Kupchik and V. A. Perciaccante, *ibid.*, **10**, 181 (1967).
- 3) M. Gielen and J. Nasielski, *Bull. Soc. Chim. Belges*, **77** (1968).
- 4) D. B. Chambers, F. Glockling, and J. R. C. Light, *Quart. Rev.*, **22**, 317 (1968), and references therein.

STEREoisomERIC EFFECTS ON MASS SPECTRA. II. THE ISOMERIC METHYLDECALINS

Seymour Meyerson and A. W. Weitkamp*

Research and Development Department, American Oil Company, Whiting, Indiana 46394

ABSTRACT

Mass spectra of the four stereoisomeric 1-methyldecals and the four 2-methyldecals have been measured. Intensities of the parent ions do not correlate with relative stabilities of the molecules, but those of the parent-less-CH₃ ions do. For each set of stereoisomers, the order of relative intensity of the parent-less-CH₃ ion parallels the order of relative stability of the molecules. The correlation suggests that loss of the methyl group from the members of each set of stereoisomers leads to a common product, with the differing conformational energies converting into differences in vibrational energy, which in turn lead to differing extents of further decomposition.

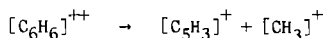
*Research and Development Department, Amoco Chemicals Corporation, Whiting, Indiana 46394

To be published in Organic Mass Spectrometry.

The $[M-15]^+$ Peak in the Mass Spectrum of BenzeneBy: M. A. Baldwin, D. P. Craig^{*} and Allan MaccollWilliam Ramsay and Ralph Forster Laboratories, University
College, Gower St., London, W.C.1.

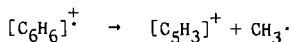
Abstract: By use of deuterium labelling, namely by the study of 1,4-dedeutero- and 1,3,5-trideutero-benzene, it has been shown that over the energy range between 20 and 50 eV, the three hydrogen atoms lost in the production of $[M-15]^+$ come randomly from the benzene nucleus. Mechanisms are discussed which could account for this.

Macdonald and Shannon¹ have shown very elegantly, by examining a number of deuterated benzenes, that the peak in the mass spectrum of benzene at m/e 52, $[M-26]^+$, corresponds to the loss of two carbon atoms with two hydrogen atoms selected at random from the benzene nucleus. They explain this result in terms of a series of 1,2-hydrogen shifts. The mass spectrum of benzene also shows a small peak at m/e 63 (~3%) which formally corresponds to a loss of a methyl group. Jennings² has shown that this peak arises in part through the process



which gives rise to a metastable peak at m^+/e 101.8. Using his metastable defocussing technique³, he was able to collect the ion $[CH_3]^+$ from $[C_6H_6]^+$ at 1.24 E/V. He further showed by a study of deuterated benzenes, using this technique, that the hydrogen atoms involved in the loss of $CH_3\cdot$ come randomly from the benzene nucleus. We thought it of interest further to pursue the mechanism of the production of $[M-15]^+$ from the molecular ion.

In the mass spectrum of benzene, there is a very weak feature at about m/e 51, which is partly hidden by the peaks at m/e 50, 51 and 52, which could correspond to the metastable transition ($m/e = 50.7$, calc.) below. It was decided to run the mass spectra



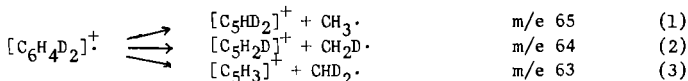
of benzene and a series of deuterated benzenes at electron beam energies between 20 and 50 eV, and analyse the peaks in the region m/e 63.

Commercial samples of benzene(I), 1,4-dideutero-benzene(II), 1,3,5-trideutero-benzene(III) and hexadeutero-benzene(IV) were used without further purification. Low voltage mass spectra (~8 eV) were run to check the isotopic purity. The value obtained for II, III and IV were 94.2%, 91.5% and 96.9% respectively. The mean value of

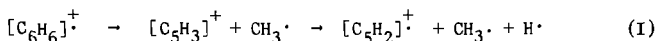
* Present address: Dept. of Chemistry, School of Advanced Studies, Australian National University, Canberra, A.C.T.

$[M + 1]^+ / [M]^+$ for I and IV was 5.35%. The reason for the deviation from the calculated value (6.58%) is not known.

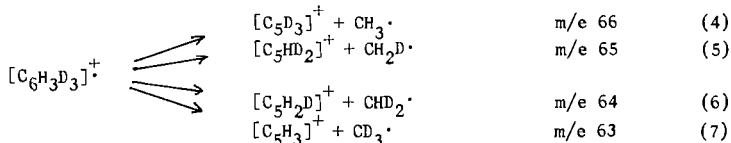
For dedeuterobenzene the processes of interest are



The abundances of these three peaks were measured on the collector meter as a function of electron beam energy, between 20 and 50 eV. Two corrections have to be made to get the true abundances. In the first plan m/e 65 and m/e 64 have to be corrected for the ^{13}C abundances of m/e 64 and m/e 63. And secondly the mass spectrum of benzene shows a peak at m/e 62 of relative abundance 24.2% (50 eV). This peak can arise in either of two ways



The corrections to the measured abundances will differ in cases (I) and (II). For the trideutero compound, the processes of interest are



Corrections to the abundances were made as for the dedeuterio compound. The relative abundances of m/e 62 / m/e 63 in the benzene spectrum from 20-50 eV were measured, in order to enable the correction to be made.

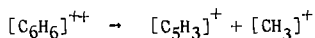
The relevant experimental abundances are set out in the Table, together with the values calculated on the basis of random loss of hydrogen atoms. Values of the experimental results based on corrections I and II are given in the Table.

Table: Comparison of Experiment with Theory.

1:4-dideuterobenzene				
	$[C_5HD_2]^+$	$[C_5H_2D]^+$	$[C_5H_3]^+$	
Random loss (theor.)	33.3	100	33.3	
Correction I (exptl.)	32.6	100	31.8	
Correction II (exptl.)	32.7	100	31.2	
1:3:5-trideuterobenzene				
	$[C_5D_3]^+$	$[C_5HD_2]^+$	$[C_5H_2D]^+$	$[C_5H_3]^+$
Random loss (theor.)	11.1	100	100	11.1
Correction I (exptl.)	10.8	97.4	100	14.5
Correction II (exptl.)	11.0	98.1	100	12.3

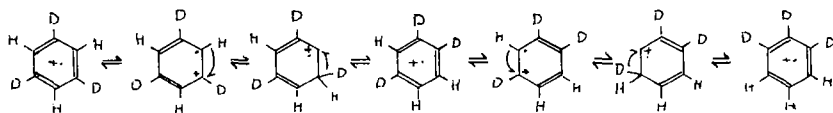
From the data, the unavoidable conclusion is that the loss of hydrogen atoms in forming the ion $[C_5H_3]^+$ from the benzene molecular ion is completely random.

Wacks² and Dibeler⁴ have determined the second ionization potential of benzene by electron impact, as 26.4 eV. Since there is no abrupt change in the ratios reported here in the range 20-50 eV, it would appear that the process

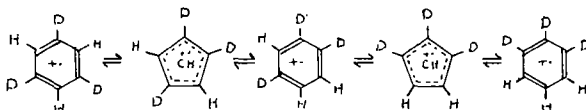


plays only a minor role in the production of m/e 63. An approximate estimate of the contribution of $[\text{C}_6\text{H}_6]^{++}$ to the peak at m/e 39 can be made from the mass spectrum of monodeuterobenzene. For this molecule $[\text{M}]^{++}/e$ occurs at 39.5, $[\text{C}_5\text{H}_3]^+$ at m/e 39 and $[\text{C}_5\text{H}_2\text{D}]^+$ at m/e 40. The abundances are 3.4%, 7.0% and 5.8% respectively⁵. For benzene examined under the same conditions, the abundance of m/e 39 was 14.3%, and from the above figures, about 20% of this comes from $[\text{C}_6\text{H}_6]^{++}$.

Two plausible mechanisms can be written for the random loss of hydrogen atoms. These will be illustrated in the case of trideuterobenzene. The first involves a succession of 1,2-hydrogen shifts which suffice to produce a mixture of all possible isomers¹.



Alternatively the process could be written as



The five membered ring ion can be regarded as a type of distorted resonating pre-fulvene⁶.



Either of these mechanisms suffices to explain the observed results. The second has perhaps the advantage over the first in that it leads naturally to the CH abstracting two H atoms (or H, D or 2D) to yield the ion under discussion.

Experimental.

Measurements were made with an MS9 mass spectrometer, samples being introduced through the cold inlet to give a pressure of about 2×10^{-5} torr. A trap current of 200 μ A was used.

References.

1. C. G. Macdonald and J. S. Shannon, Aust. J. Chem., 15, 771 (1962).
2. K. R. Jennings, J. Chem. Phys., 43, 4176 (1965).
3. Idem, Z. Naturfor., 22A, 454 (1967).
4. M. E. Wacks and V. H. Dibeler, J. Chem. Phys., 31, 1557 (1959).
5. A.P.I. Project 44, Spectrum No. 538.
6. D. Bryce-Smith and H. C. Longuet-Higgins, Chem. Comm., 1966, 593.

by

G. G. Meisels, J. Y. Park, and B. G. Giessner
 Department of Chemistry
 University of Houston
 Houston, Texas 77004

ABSTRACT

$C_3H_5^+$ ion formation from 1-butene-4d₃ and 1-butene-4c¹³ by electron impact has been examined near the ionization threshold. The deuterated compound shows essentially statistical elimination of hydrogens in the dissociation. Fragmentation of the C¹³ labelled compound leads to 75% retention of the label in the $C_3H_5^+$ ion, indicating skeletal rearrangement. A series of 1,3 ring closures and reopenings with simultaneous occurrence of 1,3 hydride or hydrogen atoms shifts is proposed to account for these observations. At higher electron energies both randomizations are decreased significantly, and this is ascribed to competition between rearrangement and fragmentation.

INTRODUCTION

It has long been known that it is difficult to assign the location of the double bond in alkenes on the mere examination of the 70 eV fragmentation patterns. The similarity of spectra can be demonstrated even with C₄H₈ compounds (1), and suggests that part of the fragmentation occurs from a precursor common to all isomers. This argument is essentially substantiated by the observation that the hydrogens in specifically deuterium labelled butene-1 readily randomize before dissociation to allyl ion, first reported by Bryce and Kebarle (2). Later investigations (3,4) suggested series of 1,2 and 1,3 shifts as a mechanism for the hydrogen atom migration. This appeared awkward since it required a three-membered ring intermediate, while most other rearrangements typically involve five or six membered rings (5).

We have recently reconfirmed that hydrogen randomization occurs before fragmentation of butene-1-4d₃ to C₃(H,D)⁵⁺ ion, and have shown that skeletal isomerization must occur near the threshold for the formation of this ion (6). In this communication we report further details of the fragmentation of butene-1 specifically labelled with deuterium or with C¹³.

EXPERIMENTAL

Materials: Unlabelled butene-1 (Matheson Co.) was purified by preparative gas chromatography. CD₃I and C¹³H₃I were obtained from Merck, Sharpe and Dohme (Canada); the former had an isotopic purity (stated by the manufacturer) of 99%, the latter one of 40%. The corresponding labelled compounds were prepared by converting the iodides to the Grignard compounds and reaction with allylbromide (Matheson, Coleman and Bell) following the procedures given by Regier and Blue (7) and references quoted there. The products were purified by preparative gas chromatography. Mass spectrometric scans at low electron energies where fragmentation to other four-carbon ions did not occur showed isotopic purities of 98 and 37%, respectively, for the deuterated and the C¹³ labelled compounds.

Mass Spectrometry: The mass spectra for the unlabelled and one of the labelled 1-butenes were obtained in rapid succession through the use of the dual inlet system of an Atlas CH-4 60°, 20 cm radius of curvature commercial mass spectrometer. The electron energy had a width at half height of 0.55 eV, as measured by differential retarding analysis at the electron trap; this width was slightly dependent on electron energy (8). The distribution could be well represented by convolution of a uniform potential drop across the electron emitting filament, and a Maxwell distribution. Nominal electron energies are reported here; they were not corrected for contact potentials, etc., but were within 0.2 eV of the maximum associated with the distribution function.

RESULTS AND DISCUSSION

The randomization of deuterium atoms in the precursor of $C_3H_5^+$ ion when 1-butene-4d₃ is subjected to electron impact is well known to decrease with increasing electron energy (3,5). The retention of the label in the $C_3H_5^+$ ion from 1-butene-4c¹³ also decreases substantially over a range of ca. 5 eV (Figure 1). This decrease in C¹³ content is well outside experimental error, and continues at higher energies. Unfortunately, it is necessary to correct for the contributions of labelled $C_3H_4^+$ ion to the intensity of the peak at m/e 41. Since the C¹³ content of the $C_3H_4^+$ ion can only be estimated, the correction begins to introduce an appreciable uncertainty at nominal electron energies greater than ca. 17 V. It is clear, however, that skeletal randomization decreases with increasing electron energy.

The decrease in randomization could have two causes. At higher energies it is possible that dissociation occurs from a methylcyclopropane ion structure leaving the

FIGURES

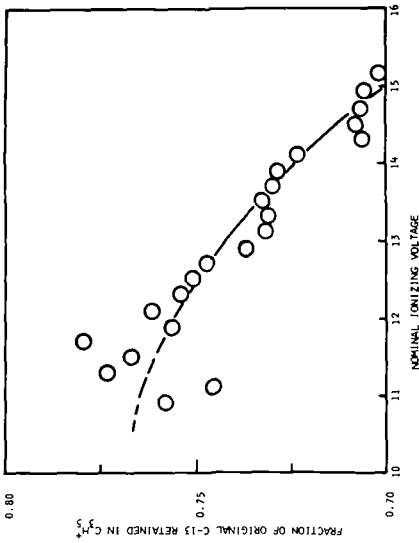


Fig. 1. Fractional retention of C-13 label in $C_3H_5^+$ from 1-butene-4-Cl3 containing 38.5% Cl3. Corrected for contribution of $C_2H_4^+$ to m/e 41 assuming random elimination of carbon. The correction never exceeds .02.

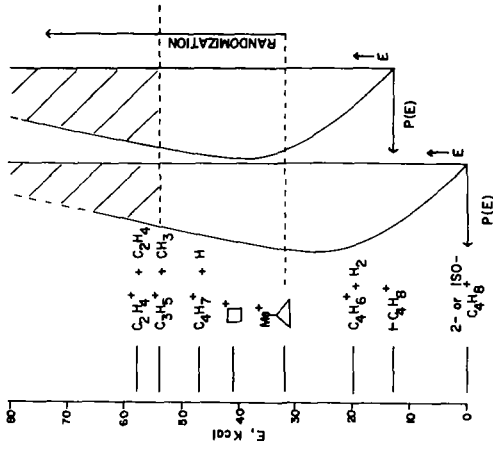


Fig. 2. Schematic representation of relative energy contents of parent and fragment ions with total composition $C_4H_8^+$, with respect to the lowest energy form (butene-2 ion). Also shown are assumed energy deposition probability functions corresponding to ionization of butene-2 and butene-1 by 70 eV electrons. The shaded portion corresponds to the fraction of ions capable of yielding $C_3H_5^+$ fragments.

$C_3H_5^+$ ion in the cyclopropyl structure. The heat of formation of the cyclopropyl ion is approximately 10 kcal/mole greater than that of the allyl ion, however, the appearance potentials of these ions from methylcyclopropane probably differ by ca. 0.9 eV (9). While such a change in product ion structure is certainly possible, the second differential ionization efficiency curves of $C_3H_5^+$ ion from butene-1 show no fine structure corresponding to the formation of cyclopropyl ion (10).

A second and more attractive interpretation invokes competition between rearrangement and fragmentation. Near the threshold of $C_3H_5^+$ formation the intermediate is formed with barely sufficient excess energy to permit dissociation, and the average observable rate constant of dissociation may therefore be assumed to be of the order of 10^7 sec^{-1} , typical of ions no longer detected as metastables. The rearrangement has been suggested to proceed in a methylcyclopropane ion structure, and the process therefore presumably has an activation energy or barrier lower than that of fragmentation and therefore proceeds at a faster rate. As the internal excitation energy of the parent ion is increased beyond the dissociation limit, the dissociation rate constant will increase considerably more rapidly than that for rearrangement because of the disparity in activation energies (11).

While the precursor ion has lost the memory of its original structure near the onset of allyl ion formation, this does not imply that structural information cannot be derived from the mass spectra at higher energies. Even neglecting the decrease in randomization, the ions from different butene isomers will differ in energy content. To a first approximation it may be assumed that the energy deposition distributions as derived from differential photoionization efficiencies or photoelectron spectroscopy (11) are similar for these molecules. Since these are additive to the threshold energy for parent ion formation, a higher heat of formation of the parent ion will increase the fraction of initial parent ions with energies in excess of any given possible fragmentation path. This is demonstrated in Figure 2 where the shaded areas correspond to the fraction of the total ions capable of dissociation to $C_3H_5^+ + CH_3$. It appears, therefore, that characteristic features of a spectrum may appear merely on the basis of available energies and without relation to the ion precursor structure.

ACKNOWLEDGEMENTS

This investigation was supported in part by the U. S. Atomic Energy Commission, for whose assistance we are deeply grateful. This is AEC document No. ORO-3606-12.

LITERATURE CITED

1. Catalog of Mass Spectra Data, American Petroleum Institute Project 44, Texas A & M College, College Station, Texas, 1964.
2. W. A. Bryce and P. Kebarle, *Can. J. Chem.*, **34**, 1249 (1956).
3. G. K. Helmkamp and N. Schnautz, *J. Org. Chem.*, **24**, 529 (1959).
4. B. J. Millard and D. F. Shaw, *J. Chem. Soc. B*, 664 (1966).
5. K. Biemann, "Mass Spectrometry--Organic Chemical Applications," McGraw-Hill Book Co., Inc., New York, N. Y., 1962, p. 83; H. Budzikiewicz, C. Djerassi, and D. H. Williams, "Mass Spectrometry of Organic Compounds," Holden-Day, Inc., San Francisco, Calif., 1967, p. 55.
6. G. G. Meisels, J. Y. Park, B. G. Giessner, *J. Am. Chem. Soc.*, **91**, 1555 (1969).
7. R. B. Regier and R. W. Blue, *J. Org. Chem.*, **14**, 505 (1949).
8. B. G. Giessner and G. G. Meisels, 17th Annual Meeting on Mass Spectrometry, Dallas, Texas (1969), paper No. 62.
9. Critical Data Compilation on Mass Spectrometry; Data as of Jan. 1, 1968. Natl. Bureau of Standards, Washington, D. C.
10. G. G. Meisels, J. Y. Park, and B. G. Giessner, 16th Annual Meeting on Mass Spectrometry, Pittsburgh, Pa. (1968), paper No. 31.
11. For a review and pertinent references, see H. M. Rosenstock, in "Advances in Mass Spectrometry," V. 4, E. Hendrick, ed., Institute of Petroleum, London (1968), p. 523.

BIMOLECULAR REACTIONS OF IONS TRAPPED IN AN ELECTRON SPACE CHARGE

A. G. Harrison and A. A. Herod

Department of Chemistry

University of Toronto

Toronto 181, Ontario, Canada

The technique for ion trapping in pulsed-source mass spectrometry proposed by Bourne and Danby (1) has been applied to the study of ion-molecule reactions at near-thermal energies. In this technique ions produced by a short (~ 1 μ sec) pulse of electrons of 30-50 eV energy are trapped in the space charge created by a continuous low energy (5-8 eV) electron beam. A known and variable time after the ionizing pulse a positive voltage pulse (~ 4 μ sec duration, ~ 8 V amplitude) is applied to the repeller plate to push the ions out for mass analysis. The present work was carried out using a 6 inch 90° magnetic deflection instrument equipped with a Nier type source using a magnetic field of 100-200 gauss to focus the electron beam.

By such a technique ions can be trapped for periods of time up to at least 2 milliseconds and the rates of bimolecular reactions followed as a function of time at pressures in the region of 3×10^{-4} torr. In the present work ion-molecule reactions in methane, ethylene and acetylene were studied. Source pressures were not measured directly but were related to the inlet pressures from observations of the rate of decrease of the CH_4^+ signal in methane using a rate constant (2) of 1.20×10^{-9} cm^3 molecule $^{-1}$ sec $^{-1}$ for the reaction $\text{CH}_4^+ + \text{CH}_4$. The rate constants for disappearance of the CH_3^+ and CH_2^+ primary ions in the methane system were found to be 1.1×10^{-9} cm^3 molecule $^{-1}$ sec $^{-1}$ and 2.0×10^{-9} cm^3 molecule $^{-1}$ sec $^{-1}$ respectively.

The rate constants measured in the ethylene system are summarized in Table I and the relative rates compared with previous results. The $k_{\text{C}_2\text{H}_4^+} = 0.85 \times 10^{-9}$ cm^3 molecule $^{-1}$ sec $^{-1}$ is in good agreement with an earlier measurement (3) of 0.83×10^{-9} cm^3 molecule $^{-1}$ sec $^{-1}$ obtained from pressure studies at 0.85 eV ion exit energy. In addition the relative rates are in reasonable agreement with previous studies particularly the work of Tiernan and Futrell.

TABLE I
REACTION RATES IN ETHYLENE

Reactant Ion	$k \times 10^9$	This Work	Relative Rate Constants			
			<u>a</u>	<u>b</u>	<u>c</u>	<u>d</u>
C_2H_2^+	1.6	1.9	2.2	1.5	3.3	1.1
C_2H_3^+	0.8 ₈	1.0	1.0	0.7 ₆	1.2	0.7 ₄
C_2H_4^+	0.8 ₅	1.0	0.6 ₇	1.0	1.0	1.0
C_2H_5^+	0.3 ₇	0.4 ₄	0.6 ₀	0.4 ₅	0.4 ₇	

^aTiernan and Futrell, J. Phys. Chem. 72, 3080 (1968).

^bKebarle and Hogg, J. Chem. Phys. 42, 668 (1965).

^cWexler et al., Advances in Chemistry 58, 193 (1966).

^dBowers et al., J. Phys. Chem. 72, 3599 (1968).

The rate constants measured in the acetylene system are summarized in Table II and the relative rates compared with those previously reported. Again good agreement with the tandem experiments of Futrell and Tiernan is obtained.

TABLE II
REACTION RATES IN ACETYLENE

Reactant Ion	k x 10 ⁹	This Work	Relative Rate Constants			
			a	b	c	d
C ₂ ⁺	2.6 ₇	1.9	2.4 ₆	1.1 ₆	1.5 ₆	1.4 ₀
C ₂ H ⁺	2.4 ₅	1.7 ₄	1.6 ₈	1.1 ₃	1.4 ₉	1.6 ₈
C ₂ H ₂ ⁺	1.4 ₁	1.0	1.0	1.0	1.0	1.0
C ₄ H ₂ ⁺	0.1 ₃	0.1	0.3 ₉	-	-	0.5 ₀

^aFutrell and Tiernan, J. Phys. Chem. 72, 158 (1968).

^bDerwish et al., J. Am. Chem. Soc. 87, 1159 (1965).

^cMunson, J. Phys. Chem. 69, 572 (1965).

^dWexler et al., Adv. Chem. 58, 193 (1966).

Full details of this work will be published at a later date.

REFERENCES

1. A. J. Bourne and C. J. Danby, J. Sci. Inst. 1968, Series, 2, Vol. 1, Page 155.
2. S. K. Gupta, E. G. Jones, A. G. Harrison and J. J. Myher, Can. J. Chem. 45, 3107 (1967).
3. J. J. Myher and A. G. Harrison, Can. J. Chem. 46, 101 (1968).

MASS SPECTROMETRIC DETERMINATION OF THE PROTON
AFFINITIES OF VARIOUS MOLECULES

Max A. Haney and J. L. Franklin

Department of Chemistry
Rice University
Houston, Texas 77001

Previous mass spectrometric determinations of proton affinities have utilized one of two methods. In the first method, the appearance potential of the protonated species yields its heat of formation, from which the proton affinity can be calculated according to the relation:

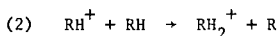
$$(1) \text{ P.A. (M)} = 366 + \Delta H_f(\text{M}) - \Delta H_f(\text{MH}^+)$$

The second method involves the occurrence or non-occurrence of ion-molecule reactions to place limits upon the proton affinity. The original supposition was that if an ion-molecule reaction occurs, it must be exothermic, while if it does not occur, it is endothermic. Neither of these assumptions can be true for ion-molecule reactions in general. Endothermic reactions may occur if the reactant ion is internally excited. Exothermic reactions may not be observed because of competing processes. The latter restriction should not prevail in the special class of ion-molecule reactions involving proton transfer from an even-electron ion to an even-electron molecule. Charge exchange is impossible and the simple process of exothermic proton transfer should occur with a fast rate.

In a recent study¹ of exothermic ion-molecule reactions involving transfer of hydrogenic species, the translational energies of the products were found to be a nearly constant fraction of the heat of reaction, ~0.2. This suggests that the heat of formation of a protonated species may be obtained by estimating the exothermicity of a reaction producing it.

The latter two methods have been used to determine the proton affinities of several simple molecules. All work was performed on a Bendix model 12 time-of-flight mass spectrometer equipped with the ion-molecule reaction source. The procedure for the second method consisted of introducing a pair of gases into the mass spectrometer simultaneously and adjusting the pressure and electron energy so that the only peaks in the spectrum were the two protonated molecules. The relative intensities of these two peaks were then recorded as the reaction time was increased. An example is shown in Figure 1. In some cases, the relative intensities were constant as reaction time increased, indicating nearly equal proton affinities. By comparing the proton affinities in this manner, a consistent relative order was established as listed in the first column of Table I. Several molecules having known proton affinities are included for reference points.

The procedure for the third method involved measuring the translational energies of the products of the following reaction:



The translational energies were multiplied by five as an estimate of the heat of reaction (2). This quantity is listed in column 2 of Table I. The proton affinity estimated by this method is listed in column 3. Except for HCN and CH₃CN, the proton affinity obtained by this method is consistent with the relative order independently established by method 2. The unusually large exothermicity of reaction (2) for these two cases may result in electronic excitation of CH₂CN and CN. The values in column 3

TABLE I. Values in kcal/mole

Decreasing Order	Estimated $-\Delta H^\circ$ (Reaction 2)	Estimated P.A.	Best P.A.
CH ₃ NH ₃	9	211	211±3
NH ₃			207±3 ^a
CH ₃ COCH ₃	6	188	188±2
CH ₃ OCH ₃	12	189	187±1
PH ₃	21	186	186±1
CH ₃ CN	16	135	186±1
CH ₃ SH	10	189	185±1
CH ₃ CHO			185±1 ^b
C ₆ H ₆			183±3
CH ₃ OH	19	182	182±3
HCOOH			179±3 ^e
HCN	22	139	170±3
H ₂ S			170±3 ^a
CH ₂ O			168±1 ^b
H ₂ O			165±3 ^a
CH ₃ Cl	9	164	164±3
HI	0	145	145±3
CO			142±3 ^c
HCl	8	141	141±3
HBr	7	140	140±3
CH ₄			126±1 ^d

^a reference 2

^b reference 3

^c reference 4

^d reference 5

^e Due to unknown $\Delta H_f^\circ(\text{HCO}_2)$, this proton affinity could not be determined by method 3. This value comes from appearance potential of HCOOH_2^+ from ethyl formate, corrected for excess energy.

TABLE II. Values in kcal/mole

X	P.A. (HX)	P.A. (CH ₃ X)	Difference
NH ₂	207	211	4
CN	170	186	16
SH	170	185	15
HCO	168	185	17
OH	165	182	17
Cl	141	164	23

were compared with the relative order in column 1 and with the reference values to arrive at the "best" proton affinities in column 4.

Table II illustrates the difference between the proton affinities of HX and CH_3X molecules. Note that methyl substitution has a more pronounced effect the lower the proton affinity.

Conclusions: The consistency of this data with previously determined proton affinities indicates that both of these methods are valid.

References

1. J. L. Franklin and M. A. Haney, J. Phys. Chem., to be published.
2. M. A. Haney and J. L. Franklin, J. Chem. Phys. 50, 2028 (1969).
3. K. M. A. Rafeay and W. A. Chupka, J. Chem. Phys. 48, 5205 (1968).
4. M. A. Haney and J. L. Franklin, Trans. Faraday Society, to be published.
5. M. S. B. Munson and F. H. Field, J. Am. Chem. Soc. 87, 3294 (1965).

A complete paper will be submitted for publication to the Journal of Physical Chemistry.

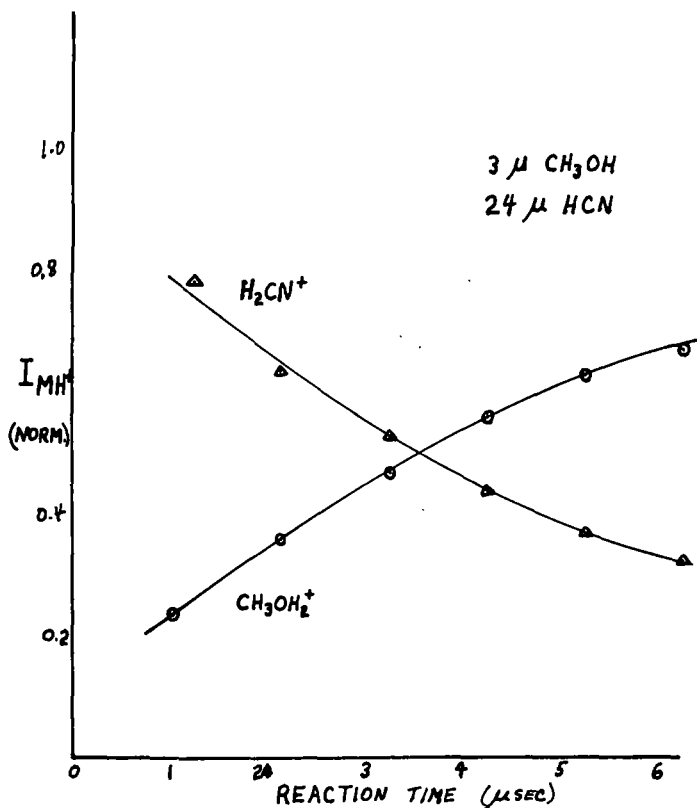


Figure 1. Illustration of Method 2.

Steven M. Schildcrout and J. L. Franklin

Department of Chemistry
Rice University
Houston, Texas 77001

Positive ion mass spectra of CO_2 have been obtained at pressures from 10^{-3} to 1 torr using an electron bombardment ion source with a quadrupole mass filter. The translational energy of ions in the source is determined by the potential applied to an ion repeller grid. From consideration of the dependence of ion intensities upon pressure, repeller potential and electron energy, the occurrence of certain ion-neutral reactions is established and their rates are determined.

Bombardment of CO_2 at low pressures by 150 eV electrons produces significant abundances of the fragment ions C^+ , O^+ and CO^+ , as well as the parent ions CO_2^+ and CO_2^{2+} .

The process



accounts for loss of C^+ at higher pressures and proceeds with a rate constant of about $1.4 \times 10^{-9} \text{ cm}^3 \text{ molecule}^{-1} \text{ sec}^{-1}$, which is close to a thermal rate constant previously reported.¹ There is evidence that at a sufficiently high repeller potential C^+ is formed by collision-induced decomposition of excited CO_2^+ .

While it has been assumed in other studies^{2,3} that O^+ reacts only to give O_2^+ ,



it is found here that the energy imparted to O^+ by the field of the repeller permits the charge transfer



to compete with (2). When (3) is energetically allowed, $k_3 = 1.0 \times 10^{-9} \text{ cm}^3 \text{ molecule}^{-1} \text{ sec}^{-1}$ and $k_2 = 2.5 \times 10^{-10} \text{ cm}^3 \text{ molecule}^{-1} \text{ sec}^{-1}$.

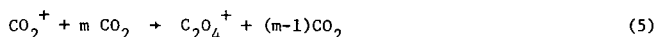
While (1) creates CO^+ , this ion is destroyed by the charge transfer



whose rate constant is found to be $2.0 \times 10^{-9} \text{ cm}^3 \text{ molecule}^{-1} \text{ sec}^{-1}$, somewhat greater than that for the thermal reaction.¹

The ion CO_2^{2+} is destroyed by reaction with CO_2 with a rate constant of $3 \times 10^{-9} \text{ cm}^3 \text{ molecule}^{-1} \text{ sec}^{-1}$ but the reaction products are not known.

The most abundant of the primary ions is CO_2^+ . Also, this ion is formed by secondary processes 3 and 4. At pressures above several tenths of a torr, however, CO_2^+ reacts with CO_2 to yield C_2O_4^+ and near 1 torr this dimer ion is the most abundant in the mass spectrum. The reaction is

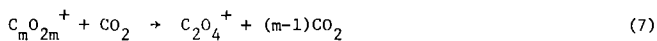


where m takes on apparent values from 3 to 5 as the repeller potential goes from 1.4 V to 12.4 V. The reacting CO_2^+ is in the ground state. A suggested mechanism consists of a sequence of steps



where $x = 1, 2, \dots, (m-1)$ and where the product ion is unstable with respect to

spontaneous decomposition. The sequence is terminated by



where now $C_2 O_4^+$ is in a long lived state. With the repeller at 5.9 V, $m = 4$, and k_5 is calculated as $1.0 \times 10^{-59} \text{ cm}^{12} \text{ molecule}^{-4} \text{ sec}^{-1}$, which seems reasonable for the suggested mechanism.

* This work was sponsored by Project SQUID, which is supported by the Office of Naval Research, Department of the Navy, under Contract N00014-67-A-0226-0005, NR-098-038. Reproduction in full or in part is permitted for any use of the United States Government.

A full paper has been submitted for publication to Journal of Chemical Physics.

References

1. F. C. Fehsenfeld, A. L. Schmeltekopf, and E. E. Ferguson, J. Chem. Phys. 45, 23 (1966).
2. J. F. Paulson, R. L. Mosher, and F. Dale, ibid., 44, 3025 (1966).
3. F. C. Fehsenfeld, E. E. Ferguson, and A. L. Schmeltekopf, ibid., 44, 3022 (1966); D. B. Dunkin, F. C. Fehsenfeld, A. L. Schmeltekopf, and E. E. Ferguson, ibid., 49, 1365 (1968).

OF INTERMEDIATE COMPLEX LIFETIMES

by

H. F. Tibbals and G. G. Meisels
 Department of Chemistry
 University of Houston
 Houston, Texas 77004

ABSTRACT

The collision model for higher ion-molecule reactions has been applied to the ethylene system, and a fit of Myher and Harrison's experimental data at low terminal ion energies is obtained readily. When the reaction parameters derived therefrom are used to calculate ion abundances at higher terminal energies, poor agreement with other experimental results is observed. Various complications such as symmetrical charge transfer and the contribution of hard-sphere collisions were examined. Only allowance for dependence of the first order dissociation rate constant of intermediate adduct ions such as $C_4H_8^+$ and $C_5H_9^+$ on incident ion kinetic energy could approach an adequate account of the experimental observations. Such a variation with energy arises from conversion of translational energy to internal energy in the formation of a strongly bonded intermediate. It was found impossible to assign a simple reaction order to an ion participating in such competitive reactions. This is consistent with a change of reaction order reported for $C_5H_9^+$ formation even at low terminal ion energies.

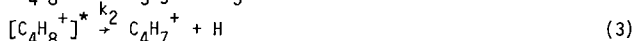
INTRODUCTION

A theoretical description of ion-molecule reactions applicable to higher order processes in the ion source of a mass spectrometer has recently been reported (1). This treatment is based on a simplified classical description of the trajectories of individual ions and integrates the reaction probability as a function of position over the ion path in a conventional ion source. Reaction probabilities are calculated using energy dependent collision cross sections and invariant unimolecular dissociation rate constants of intermediate complexes.

In this paper we present a comparison of the model with the experimental results for ethylene reported by three groups of investigators, and demonstrate that some previous discrepancies can be accounted for by the energy dependency of unimolecular dissociation rate constants.

COMPARISON WITH EXPERIMENT

The model (1) was used to calculate curves of normalized ion current versus pressure for various path lengths and draw-out or repeller fields in the ion source. The following reaction mechanism, suggested by a number of investigations (2,4), was assumed:



Fourth and higher order reactions were neglected. Simple unimolecular dissociation of complexes with invariable rate constants and with reaction cross sections proportional to the inverse square root of the relative kinetic energy (5) were used in the calculations. Good agreement with the experimental results reported by Myher and Harrison (2) could be obtained (Figure 1) when the following parameters were used:

$$k_1 = 9 \times 10^6 \text{ sec}^{-1} \quad \sigma_1 = \sigma_2 = 37 \times 10^{-16} (\sqrt{E_{\text{rel}}}) / \sqrt{E_{\text{rel}}} (\text{eV})$$

$$k_2 = 8 \times 10^5 \text{ sec}^{-1} \quad \sigma_3 = 0.15 \sigma_1$$

The same treatment was applied to the data of Wexler and Marshall (3) and those of Tiernan and Futrell (4). Although parameters were varied extensively no fit was obtained, even when allowance was made for the additional production of $C_2H_4^+$ by charge transfer for acetylene



Figure 2 gives a comparison between Tiernan and Futrell's data and ion intensity curves calculated for their conditions using the parameters derived from Harrison's data. The major discrepancy is the appearance of secondary and tertiary ions at pressures much higher than expected.

It is possible that the assumptions of the model do not hold at the high ion energies employed in the earlier studies. An obvious refinement is to replace simple induced dipole cross sections by energy independent cross sections at higher ion energies (6). However, insertion of reaction cross sections of the form suggested by Hamill and co-workers (6), which are constant above a critical energy, leads to variations of ion currents only slightly different from those calculated using the simple cross sections, and do not improve the fit to experimental data (Figure 3). The similarity of the variations calculated for the two functional forms of the cross section indicates that reactions at low energies dominate the observed distribution in the mass spectrometer at higher pressures and moderate draw-out fields (up to 10 v/cm).

An additional factor of possible importance is the range of pressures used by Futrell and Tiernan and by Wexler and Marshall, which substantially exceeds that employed by Myher and Harrison. The shorter ion paths and higher repeller fields employed in these investigations necessitated the use of higher pressures in order to obtain appreciable yields of higher order ions. Under these conditions one of the basic assumptions of the model, that ions travel in two dimensional freely accelerated trajectories, may have been invalid. A deviation may be in fact indicated from Warneck's studies of drift times of nitrogen molecular ions in air (7), which were found to increase threefold over a pressure range of 0 to 0.2 torr. However, nitrogen readily undergoes charge exchange with N_2^+ ion, a process in which all momentum of the charge carrier is lost. The condensation reaction 1 occurs very nearly with collision efficiency, and reactant ions are therefore not as readily retarded in the ethylene system.

Apparently a more complicated mechanism must be invoked in order to interpret the experimental results within the assumptions of the model. It is plausible (3) that the deficit of C_5Hg^+ with regard to the calculated quantities at low pressures is a result of redissociation:



$C_5H_9^+$ observed at higher pressures would then be a result of collisional stabilization of excited $C_5H_9^+$



with reaction 7 competing with reaction 8 and withdrawal of the ion from the source. $C_3H_5^+$ formation may thus be calculated by summing the dissociation paths of $C_4H_9^+$ and of $C_5H_9^+$, and C_5Hg^+ intensity is calculated as the sum of the component which survives without undergoing collision or decomposition, and that which is stabilized with collision efficiency. Dissociation rate constants were again taken as invariant with ion energy. However, even when such a mechanism was assumed, it was not possible to find a set of parameters which would give satisfactory fits to the experimental data, although an "induction" interval could be obtained. Typical results are shown in Figure 4.

In view of the inherent plausibility of redissociation, and the ability to obtain a pressure range where C_5Hg^+ is not formed, it appeared advisable to remove the most injudicious remaining approximation: the immutability of the rate constant. Such an assumption is, in fact, excluded by the known existence of a long-lived complex of $C_4H_8^+$. The relative kinetic energy of the collision within the center of mass system must be converted to internal modes. The internal energy of the collision complex therefore increases rapidly as the point of collision moves toward the exit slit, and this effect will be more important when terminal ion energies are larger such as in the investigations whose results could not be fitted by our model. Since the average distance through which the ion beam has been accelerated prior to reaction decreases with increasing pressure, one would expect less dissociation at higher pressures. At the low ion energies used by Myher and Harrison (2), such processes would be much less important.

The effect of pressure and source fields on the unimolecular dissociation rate constant and hence on ion abundances can be calculated by noting that the internal energy (E_c) of a complex will be given by the sum of initial (thermal) kinetic and electronic excitation energies of the primary reactant ion (E_x), the heat of reaction (E_b) associated with the complex formation (such as in reactions 1 and 5), and the contribution from the ion translational energy, or:

$$E_c = E_x + E_b + E_k(1 - m_1/(m_1 + m_2))$$

where E_k is the relative translational energy and m_1 and m_2 are the masses of the ion and neutral species, respectively. E_b for reaction 1 can be estimated from thermodynamic data to be 58 kcal (this volume, paper no. 62). By the assumptions of the model, E_k is expressible as a function of the field strength and a set of parameters L_1, L_2, \dots, L_x which represent positions of primary, secondary, etc. ions in the source.

FIGURES

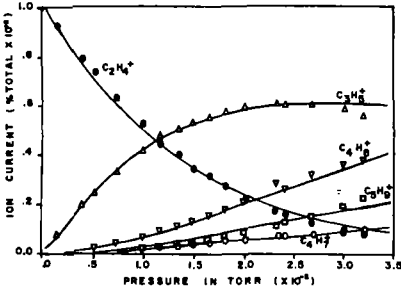


Fig. 1. Comparison between calculated and experimental variations of ion abundance (ref. 2) for reactions of C₂H₄⁺

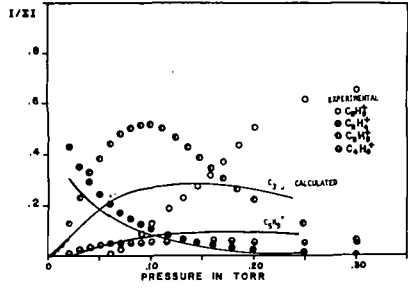


Fig. 2. Comparison between calculated and experimental variations of ion abundance (ref. 4) in the C₂H₄ system: simple model

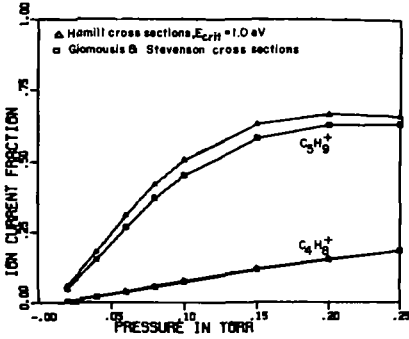


Fig. 3. Comparison between calculated results for G.&S. (ref. 5) and for Hamill (ref. 6) cross sections for tertiary ions; experimental conditions of Futrell and Tiernan's (ref. 4) C₂H₄ system

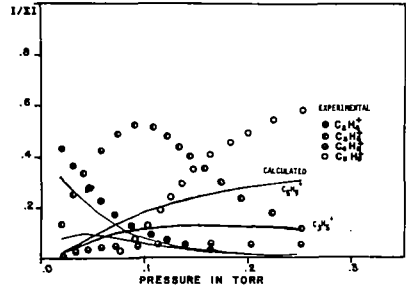


Fig. 4. Comparison between experiment and calculations for Futrell and Tiernan's C₂H₄ system (ref. 4): allowance for C₅H₉⁺ dissociation with energy independent rate constant.

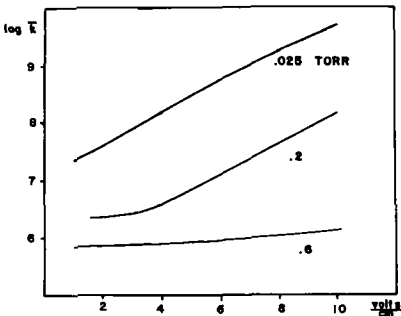


Fig. 5. Calculated average rate constant for C₄H₈⁺ dissociation

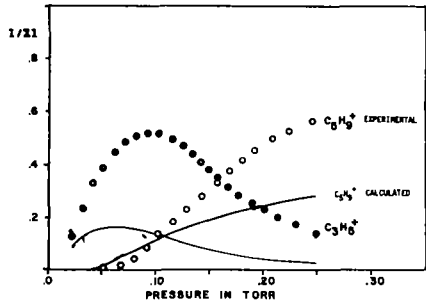


Fig. 6. Comparison of calculated ion abundances: allowing for energy dependence of unimolecular dissociation rate constants with results of Futrell and Tiernan (ref.4)

Recent advances in unimolecular dissociation rate theory (8,9,10) permit calculation of $k(E_c)$ for limited ranges of E_c provided information on vibrational frequencies and thermodynamic data on the dissociating molecule are known. Accurate application of this theory to ionic species is prevented by the lack of vibrational data and by the inadequacies of the theory at low energies (11). As an approximation to the behavior of the rate constant for dissociation of $[C_4H_8]^+$ (reaction 2), quasi-equilibrium calculations were carried out using slightly modified vibrational frequencies of 2-butene and the state density equation given by Haarhoff (8). The threshold for fragmentation was taken as the difference between the ionization potential of 2-butene and the appearance potential of $C_3H_5^+$ from 2-butene, or about 1.3 eV. The excitation energy, E_x , was taken as 0.1 eV, obtained as an estimated average of the first band in the photoelectron spectrum of ethylene (13). The range of rate constant values centered about 10^7 sec^{-1} , the value which gave the best fit to Myher and Harrison's data (2) for low ion energies when an invariable rate constant was assumed.

In order to illustrate the effect of the draw-out field on unimolecular dissociation rates, the average value of the rate constant,

$$\bar{k} = \frac{\int_0^{L_x} k(E_c) [M]^\sigma (L_1) \cdot \exp(-\int_0^{L_1} [M]^\sigma (L') dL') dL_1}{\int_0^{L_x} [M]^\sigma (L_1) \cdot \exp(-\int_0^{L_1} [M]^\sigma (L') dL') dL'}$$

was calculated as a function of pressure for various field strengths, as shown in Figure 5. The curves shown here cannot be truly representative of the true physical behavior of the complex because σ goes to infinity at low energies. However, they provide an insight into the rate constant range of interest here since the model is sensitive only to rate constant changes in the range of $10^6 - 10^8 \text{ sec}^{-1}$.

The threshold for the redissociation of $C_5H_9^+$ (reaction 7) was taken as 1.54 eV using thermodynamic data (14). As a rough approximation, it was assumed that the mean vibrational frequency and the mean square vibrational frequency of $C_5H_9^+$ equalled those of $C_4H_8^+$.

When calculations are carried out using energy dependent rate constants for the unimolecular dissociation of $C_4H_8^+$ and $C_5H_9^+$, and allowing for competition with collisional stabilization for both species, it is possible to reproduce the shape of the pressure dependency, but not the intensities, of the experimental data reported by Wexler and Marshall (3) and those of Tiernan and Futrell (4) (Figure 6). The same parameters fit Myher and Harrison's results (2), including intensities. The failure to reproduce the intensities of the former experimental curves is probably due at least in part to participation of reaction 6, charge exchange of $C_2H_2^+$ with ethylene, and an inadequate selection of parameters which must be selected by trial and error.

In conclusion, the experimental results obtained under widely differing conditions can be interpreted consistently on the basis of a simple kinematic model, provided allowance is made for the dependence of unimolecular dissociation rate constants on ion kinetic energy.

ACKNOWLEDGEMENTS

This investigation was supported in part by the National Science Foundation; computer time was made available by the Robert A. Welch Foundation. We are deeply grateful for this assistance.

LITERATURE CITED

1. G. G. Meisels and H. F. Tibbals, *J. Phys. Chem.* **72**, 3746 (1968).
2. J. J. Myher and A. G. Harrison, *Can. J. Chem.* **46**, 101 (1968).
3. S. Wexler and N. Jesse, *J. Amer. Chem. Soc.* **84**, 3425 (1962).
4. J. H. Futrell and T. O. Tiernan, *J. Phys. Chem.* **72**, 158 (1968).
5. G. Giomousis and D. P. Stevenson, *J. Chem. Phys.* **41**, 117 (1964).
6. D. A. Kubose and W. K. Hamill, *J. Amer. Chem. Soc.*, **85**, 125 (1963).
7. Peter Warneck, *J. Chem. Phys.* **46**, 502 (1967).
8. P. C. Haarhoff, *Mol. Phys.* **7**, 101 (1963/4).
9. Everett Thiele, *J. Chem. Phys.* **39**, 3258 (1963).
10. H. M. Rosenstock, *Advan. Mass Spec.* **4**, 523 (1968).
11. W. Forst, Z. Prasil and P. St. Laurent, *J. Chem. Phys.* **46**, 3736 (1967).
12. Critical Data Compilation on Mass Spectrometry; Data as of Jan. 1, 1967. Natl. Bureau of Standards, Washington, D. C.
13. A. D. Baker et. al., *J. Mass Spec. and Ion Phys.* **1**, 285 (1968).
14. F. H. Field and J. L. Franklin, "Electron Impact Phenomena," Academic Press, New York (1957).

HIGH-RESOLUTION CHEMICAL IONIZATION MASS SPECTROSCOPY

Leonard Wojcik and Jean H. Futrell
University of Utah, Salt Lake City, Utah 84112

Since Field and Munson introduced chemical ionization mass spectroscopy in 1966, much interest has been shown in this lower energy method of generating mass spectra via ion-molecule reactions. The basic technique has been well documented elsewhere, so we shall describe briefly only unique construction details of our high-pressure source and sample-handling equipment along with some preliminary results.

A CEC model 21-110B mass spectrometer was substantially modified to ensure high pressure differential between the source and analyzer. A standard gas source was equipped with an ion exit slit 1.25 by .062 mm, and an electron entrance mask .25 mm in diameter, while all other obvious leaks in the source were eliminated. Inlet source connections were made with ball joints and a stainless steel bellows assembly welded to the source to reduce leakage.

Among additional modifications, a 500-volt power supply was installed to supply electrons with sufficient energy to penetrate the gas in the source when at 1 mm pressure, and the filament regulation circuit was changed to regulate on total filament emission. The latter modification was required since under operating conditions the electron current is totally attenuated and little anode current was expected. A 680-liter-per-second pumping system (T. M. Vacuum Corporation) was installed directly below the source housing. A MKS Baratron was used to monitor the source pressure, and its output was connected to a Granville-Phillips Automatic Pressure Controller which kept the source pressure constant by means of an automatically adjusted variable leak.

Since pressures of approximately 1 Torr are very prone to electric discharge when high voltages are applied across it, we built an inlet line which contained a voltage divider network consisting of glass-encapsulated resistors, alternating with balls of stainless steel wool gauze to control the voltage gradient. By this system, it is possible to control the gradient at a magnitude which will not sustain a discharge. The total system operates over the pressure range of 10^{-7} - 5 Torr at 10 KV potential. A resolution check at 1 Torr demonstrated a resolving power $M/\Delta M = 56,000$ with 20% valley, which was at least equal to our best resolution with conventional operation.

Chemical ionization spectra of some primary alcohols were studied using both methane and isobutane as reagent gases. With methane as reagent gas, the smaller alcohols through propanol show protonation with little fragmentation. The longer chain length alcohols exhibit hydride abstraction as the preferred reaction pathway for formation of the pseudomolecular ion. Considerable fragmentation occurs in the longer chain length alcohols, especially loss of water (which is still much less than that observed with electron impact). The site of hydride abstraction in alcohols was shown by deuterium labeling to include both alpha and chain positions. The amount of abstraction from the chain became larger with increasing chain length. No abstraction occurs from the hydroxyl position.

Chemical ionization spectra with isobutane as the reagent gas resulted in less fragmentation than with methane. This is reasonable since a tertiary ion (t-butyl) is thermodynamically more stable than the methane reagent ions (CH_5^+ , C_2H_5^+). Hence, exothermicity of the initial reaction will be less. More interesting, perhaps, is the observation of condensation products between the alcohols and the t-butyl ions. Ions observed were: $M+1$, $M+t\text{-butyl}$, $M+C_3H_7$, $2M+1$, and $2M+t\text{-butyl}$. A plausible mechanism for forming the protonated monomer and dimer is the decomposition of the t-butyl adduct of the alcohol and of the t-butyl adduct of the dimer of the alcohol. The suggested mechanism was substantiated by observing metastable transitions for these processes. This was done by defocusing the electric sector to allow the metastables to pass.

In addition, a pronounced temperature effect on distribution of chemical ionization products was observed. At higher temperatures the t-butyl adduct of the dimer disappeared and the amount of monomer t-butyl adduct decreased substantially. Further studies of chemical ionization mechanisms for alcohols with several reagent gases are in progress.

The metastable defocusing technique and source modifications will be described in the Review of Scientific Instruments. The chemical ionization study of the alcohols will be submitted to the Journal of the American Chemical Society.

COLLISION INDUCED DISSOCIATION OF NO^+ IONS AT LOW KINETICS ENERGIES*

Ronald E. Marcotte[†] and Thomas O. Tiernan
 Aerospace Research Laboratories
 Office of Aerospace Research
 Wright-Patterson Air Force Base, Ohio 45433

The observation of the dependence of ion-neutral cross sections on the properties of the reactant ion beam is a powerful method for deducing the role of excited species in these processes. It has previously been demonstrated that conversion of translational energy into internal energy is a rather efficient process in many ion-neutral interactions¹. It has further been shown that kinetic energy can be utilized as the effective driving force for endothermic ion-neutral processes such as the collision induced dissociation processes described above. The participation of internal excitation energy of the ionic reactant in such processes is a topic which has received much less emphasis. The present study was undertaken in an effort to assess the role of internal ion energy in collision-induced dissociation reactions. It was further expected that these and related charge transfer experiments would lead to the identity of the excited states present in the reactant ion beam.

The experiments reported here were accomplished using a double mass spectrometer of in-line geometry which has previously been described in some detail². The mass and energy analyzed reactant ion beam enters the collision chamber with a kinetic energy spread of only 0.3eV under the operating conditions employed. In these studies, the population of states in the ion beam was changed by varying the ionizing electron energy in the first stage of the mass spectrometer. The effectiveness of this technique has been demonstrated in studies by McGowan and Kerwin³. The time required for an ion of m/e 30 to traverse the path from the first stage ion source to the collision chamber in our instrument is of the order of 38μsec. Consequently, the only excited states which will survive for a sufficient time to reach the collision chamber are relatively long-lived metastable electronic states. Vibrational excitation in such an ion beam is also quite probable. The electron energy in these experiments was calibrated by determining the ionization efficiency curve of argon and comparing it to that obtained by Rapp and Englander-Golden⁴. For the studies reported here, the cross-sections for various collision-induced dissociation reactions of NO^+ and O_2^+ were measured as a function of both kinetic energy and electron energy forming the ion beam. The effect of changing the population of excited ionic states on the dissociation thresholds could thus be observed directly.

The observed cross section dependence for the presumed reaction,
 $\text{NO}^+ + \text{NO} \rightarrow \text{N}^+ + \text{O} + \text{NO}$ (1)

is displayed by the family of curves shown in Figure 1. The bottom curve, which was obtained using 13 eV electrons, shows the kinetic energy dependence of the cross section for a beam of predominately ground state (X^1E^+) NO^+ ions. As expected of an endothermic reaction, an energy threshold is observed after which the cross section increases rapidly. For NO^+ ions formed at successively higher energies, the threshold shifts to lower kinetic energies suggesting that the ions are being formed with greater amounts of internal energy. At the highest electron energy used, 20 eV, structure appears which can be related to the presence of excited states of NO^+ . Before making a detailed interpretation of the curves, it was necessary to demonstrate that the observed production of N^+ was actually occurring by collision induced dissociation rather than an alternative ion-molecule reaction channel. The reaction was therefore studied using argon as the target gas. In this case, a similar family of curves, shown in Figure 2, was obtained. While the cross section is somewhat larger, the reaction exhibits the same functional dependence upon the ion kinetic energy. The curve for $E_e = 20$ eV was also essentially duplicated using neon as the target gas. Taken together, these facts seem to indicate that the reaction producing N^+ here is really a simple collision-induced dissociation.

*A more detailed account of this investigation will be submitted for publication in the Journal of Chemical Physics.

[†]Research performed at the U. S. A. F. Aerospace Research Laboratories while in the capacity of an Ohio State University Research Foundation Visiting Research Associate under contract F33615-67-C-1758.

Figure 1. Cross sections for the production of N^+ from the NO^+/NO reaction as a function of kinetic energy of the reactant ion at various ionizing electron energies.

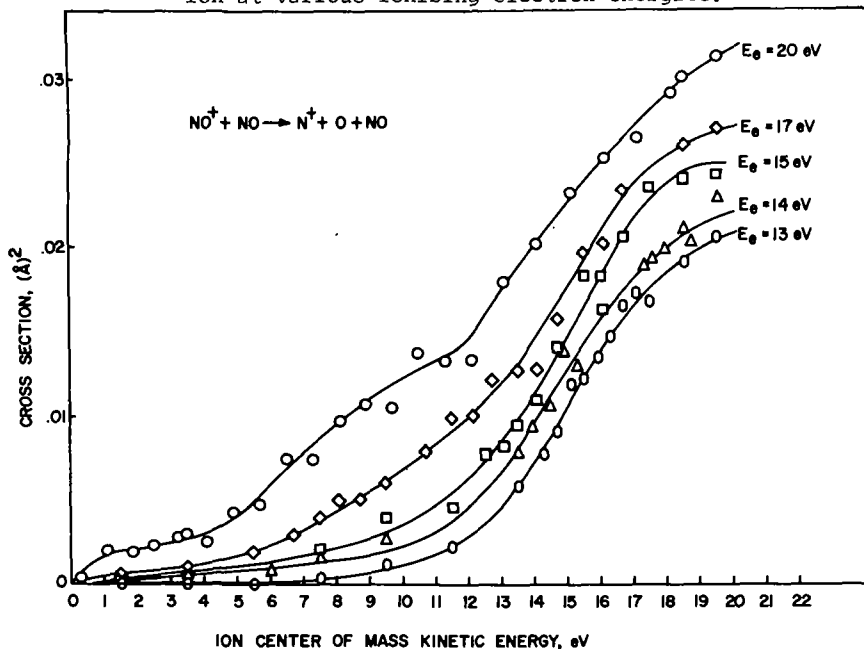


Figure 2. Cross sections for the production of N^+ from the NO^+/Ar reaction as a function of kinetic energy of the reactant ion at various ionizing electron energies.

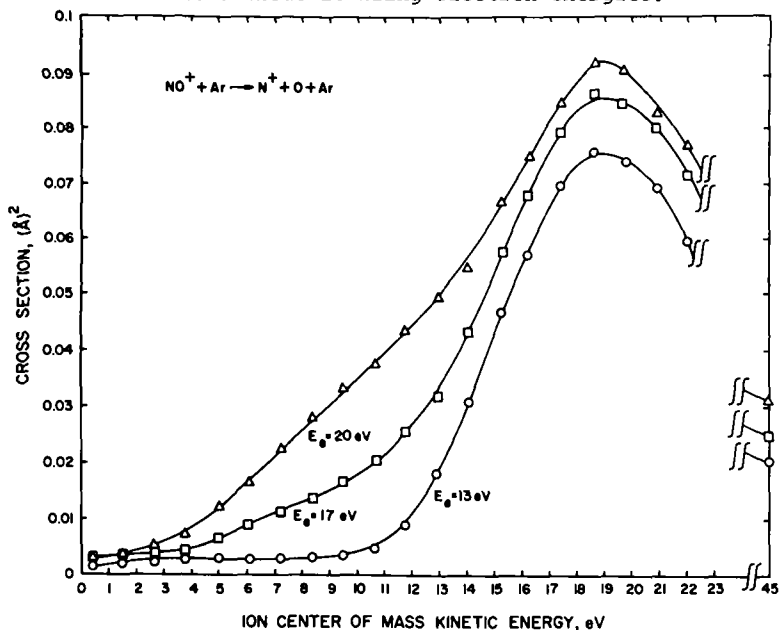


Figure 3. Cross sections for the production of N^+ from collision of excited NO^+ with argon as a function of ion kinetic energy.

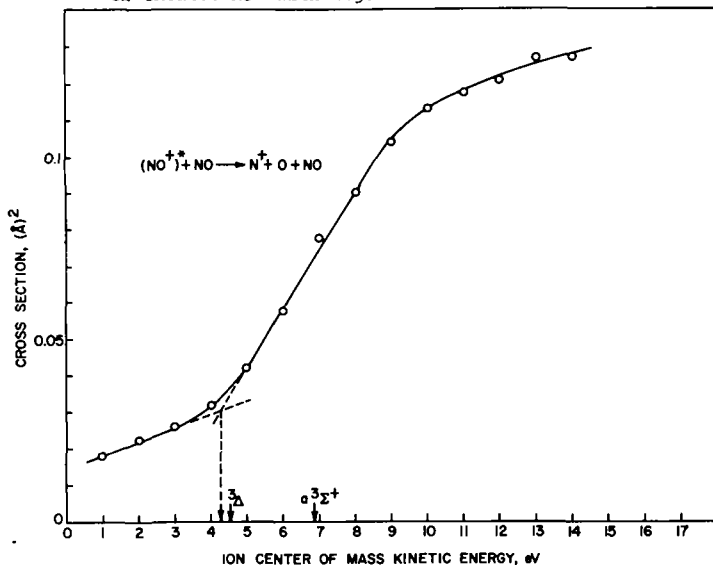
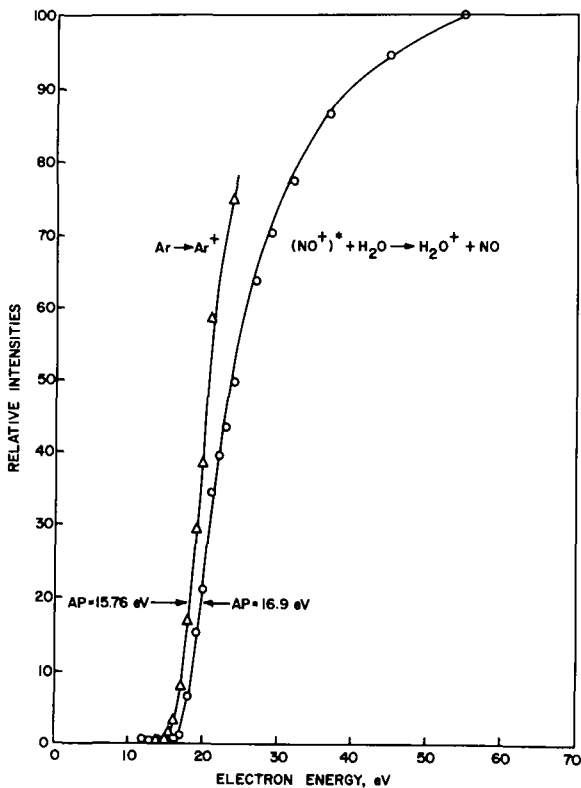


Figure 4. Appearance potential of excited NO^+ .



From the 13 volt electron energy curve of Figure 1, one can get an approximate value for the dissociation energy of the ground state ($X^1\Sigma^+$) ion by extrapolating the straight portions of the curve before and after the threshold region. This gives a value of 11.6 eV which is comparable to the value of 11.77 eV which can be obtained from the potential curves reported by Gilmore⁵. Similar methods were applied to several other reactions examined and the results are summarized in Table I.

Table I. Comparison of Measured Thresholds for Collision-Induced Reactions with Known Dissociation Energies.

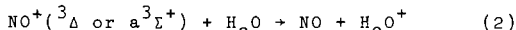
Ground State Reaction	Measured Threshold(eV)	Reported ⁵ Dissociation Energies(eV)
$\text{NO}^+(\text{X}^1\Sigma^+) + \text{NO} \rightarrow \text{N}^+ + \text{O} + \text{NO}$	11.6	11.77
$\text{NO}^+(\text{X}^1\Sigma^+) + \text{Ar} \rightarrow \text{N}^+ + \text{O} + \text{Ar}$	11.8	11.77
$\text{NO}^+(\text{X}^1\Sigma^+) + \text{Ar} \rightarrow \text{O}^+ + \text{N} + \text{Ar}$	10.7	10.8
$\text{O}_2^+(\text{2}\Pi_g) + \text{Ar} \rightarrow \text{O}^+ + \text{O} + \text{Ar}$	6.9	6.6

The excellent agreement with known dissociation energies was taken as an indication of the validity of the method and this treatment was extended to the curves obtained at higher electron energies. Metastable electronic states are known to exist in NO^+ , but there is some disagreement in the recent literature as to whether the long lived excited state present under these experimental conditions is the $^3\Delta$ state⁶ or the $a^3\Sigma^+$ state.⁷ To obtain the cross-section dependence for excited states from our data, the ground state curve ($E_e = 13$ eV) was subtracted from the curve for 20 eV electrons. The resultant curve (Figure 3) shows a break which closely approximates the reported dissociation energy of the $^3\Delta$ state.⁵ In a similar manner, curves and dissociation energies were obtained for the remaining systems studied. The results, which are summarized in Table II, show that in all the NO^+ dissociations observed, the measured dissociation energy most closely approximated that of the $^3\Delta$ state.

Table II. Comparison of Measured Thresholds for Collision-Induced Dissociation Reactions with Known Dissociation Energies.

Excited State Reaction	Measured Threshold(eV)	Reported ⁵ Dissociation Energies(eV)
$\text{NO}^+(\text{3}\Delta) + \text{NO} \rightarrow \text{N}^+ + \text{O} + \text{NO}$	4.3	4.49
$\text{NO}^+(\text{3}\Delta) + \text{Ar} \rightarrow \text{N}^+ + \text{O} + \text{Ar}$	3.9	4.49
$\text{NO}^+(\text{3}\Delta) + \text{Ne} \rightarrow \text{N}^+ + \text{O} + \text{Ne}$	4.4	4.49
$\text{NO}^+(\text{3}\Delta) + \text{Ar} \rightarrow \text{O}^+ + \text{N} + \text{Ar}$	3.2	3.56
$\text{O}_2^+(\text{4}\Pi_u) + \text{Ar} \rightarrow \text{O}^+ + \text{O} + \text{Ar}$	2.7	2.60

Another method of detecting the presence of excited ionic states involves the observation of charge transfer reactions which are endothermic for ground state ions but exothermic for ions in excited states. The reaction,



which is a reaction of this type, was observed as a function of the electron energy used to produce the NO^+ ions. Argon was added to the first stage ion source to act as an internal standard for the electron energy. As shown in Figure 4, the appearance potential of H_2O^+ from the above reaction was found to be 16.9 eV. This is close to the estimated appearance potential of $\text{NO}^+(\text{3}\Delta)$ of 16.55 eV. Production of H_2O^+ from the $a^3\Sigma^+$ state would be expected to show a threshold at an electron energy of 14.2 eV. Similarly, when argon was used in the collision chamber, the A. P. of the excited state was found to be 17 eV. Again, these results indicate that under our experimental conditions the principal excited electronic state present in the NO^+ beam is the $^3\Delta$ state.

A study of the low kinetic energy collision-induced dissociation reactions of NO^+ has recently been reported by Moran and Roberts⁹. A single source mass spectrometer operating in the Cermak-Herman mode⁹ was utilized in this investigation. The cross section dependences on ion kinetic energy reported by Moran and Roberts were quite different than those observed in the present study and showed quite sharp thresholds. Since the Cermak-Herman technique necessarily yields an ion beam of rather broad kinetic energy distribution, such sharp thresholds are somewhat surprising. A possible explanation of the dependences observed by Moran and Roberts may be found from a consideration of the limitations of the experimental technique employed which requires that the ion kinetic energy and the electron energy be simultaneously varied. On the basis of our data reported in Figures 1 and 2, it can be seen that such a simultaneous

variation of these parameters would yield cross section points which effectively step across the family of curves. Artificial thresholds would therefore be expected and it is not surprising, therefore, that the thresholds observed by Moran and Roberts were in much poorer agreement with known dissociation energies than those determined in the present study. The single source methods seem to be clearly inadequate for detailed study of collision-induced dissociation phenomena such as those under consideration

References.

1. Such topics are discussed at some length in a review article by J. H. Futrell and T. O. Tiernan, "Ion-Molecule Reactions" in "Fundamental Processes in Radiation Chemistry", P. Ausloos, ed., John Wiley-Interscience Publishers, N. Y., 1968.
2. J. H. Futrell and C. D. Miller, Rev. Sci. Instr. 37, 1521 (1966).
3. J. W. McGowan and L. Kerwin, Can. J. Phys. 42, 972 (1964).
4. D. Rapp and P. Englander-Golden, J. Chem. Phys. 43, 1464 (1965).
5. F. R. Gilmore, J. Quant. Spectroc. Radiat. Transfer 2, 369 (1965).
6. D. W. Vance, Phys. Rev. 169, 263 (1968).
7. R. F. Mathis, B. R. Turner and J. A. Rutherford, J. Chem. Phys. 49, 2050 (1968).
8. T. F. Moran and J. R. Roberts, J. Chem. Phys. 49, 3411 (1968).
9. V. Cermak and Z. Herman, Nucleonics 19, 106 (1961).

157. ION-POLAR MOLECULE REACTIONS: ENERGY DEPENDENCY OF HYDROGEN ATOM
AND ION TRANSFER IN THE METHANOL-ACETALDEHYDE SYSTEM

by

L. J. Leger and G. G. Meisels
Department of Chemistry
University of Houston
Houston, Texas 77004

and

T. O. Tiernan
Aerospace Research Laboratories
Office of Aerospace Research
Wright-Patterson Air Force Base, Ohio 45433

ABSTRACT

A tandem mass spectrometer has been employed to investigate hydrogen atom, hydrogen ion, and charge transfer in collisions involving specifically deuterium labelled methanol and acetaldehyde and their molecular ions at energies between 1 and 7 eV (laboratory system) ions. At the lowest incident ion energies, hydrium transfer is preferred from the electronegative group, while randomness is approached at higher energies. Ion transfer is the most important process at all energies, and transfer of the hydrogen ion from the electronegative group is always favored. The non-randomization of equivalent atoms in a possible complex suggests that the ion retains its identity in the reaction. Both the atom and the ion transfer show a marked isotope effect. These results are interpreted by charge localization in the reactant ion and a stripping mechanism in which long range forces are important.

INTRODUCTION

Ion-molecule reactions have been studied extensively during the past decade. Giomousis and Stevenson (1) provided a quantitative theory based on the interaction between a point charge and an isotropic polarizable neutral point molecule (2), which showed agreement with experiment in simple systems. For more complex molecular reactants, however, deviations from the Giomousis and Stevenson theory occurred even at very low ion energies. One possible explanation for such deviations takes into account the effect of a permanent dipole on the forces of the system. Moran and Hamill proposed (3) that the dipole of the neutral molecule aligns with the ion in a minimum energy configuration, that is, with the negative end of the dipole closest to the positive ion. This would lead to an increase in the reaction cross section $\sigma(E)$ over that derived from the simple model; moreover, $\sigma(E)$ would not simply vary as $E^{-1/2}$. The "lock-in" suggested by such a treatment neglects the rotational energy of the neutral species.

A complete evaluation of the classical dynamics of a system containing an ion and a rotating permanent dipole was reported by Dugan and Magee (4,5), who demonstrated that conservation of angular momentum prevents complete alignment. Their conclusion that the permanent dipole increases the total reaction cross section only slightly was confirmed experimentally by Harrison (6).

Another manifestation of the effect of a permanent dipole may be its preferred orientation in an atom or ion transfer reaction. This effect should be particularly large if a long lived reaction complex is involved, but may also be expected when a stripping mechanism applies (7). For a pure spectator stripping mechanism no preference for transfer due to the dipole moment would be expected (8).

Meisels and Leger (9,10) have investigated the effect of the permanent dipole moment on hydrogen atom transfer in the methanol-acetaldehyde system, using a conventional mass spectrometer and the ratio plot technique (11-15). The use of appropriately deuterated compounds demonstrated that H atom transfer occurred predominately from the electronegative end of the molecule. This earlier study was performed at one terminal ion energy and the results therefore represent an average over a range of ion energies. The present investigation was undertaken in order to obtain further insight into the nature of ion-polar molecule reactions from an analysis of the effects of ion energy on the preferred transfer. This is facilitated by the beam instrument utilized in these experiments in which the reactant ion energy has an energy spread of approximately ± 0.3 eV.

EXPERIMENTAL

Materials: Unlabelled methanol and acetaldehyde (Matheson Coleman and Bell research grade) were purified by repeated bulb-to-bulb distillations. CD_3OH , CD_3CDO , CD_3CHO were

obtained from Merck Sharpe and Dohme of Canada and CH_3CDO was prepared as described by Leitch (16).

Instrumentation and Procedure: The tandem mass spectrometer used for these studies has been described elsewhere (17). The pressure in the collision chamber of the mass spectrometer was maintained at 5 millitorr by a Granville Phillips Series 213 automatic pressure controller using an MKS Baratron model 77H1 pressure transducer as a reference sensor. Pressure in the ion source was adjusted initially to provide a primary ion beam of approximately 10^{-9} amps. Most experiments were performed with the collision chamber at room temperature, but a few runs were made at 198°C to determine the effect of temperature on the reactions.

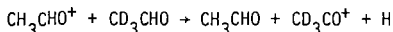
A particular set of experiments was performed by introducing the gases into the collision and ion chambers, adjusting their pressures, and maximizing the primary ion intensity at a selected energy. The appropriate peaks were then scanned and their intensity measured using pulse-counting techniques. The energy of the primary beam was then increased, the instrument parameters again optimized, and the appropriate mass peaks recorded again. This procedure was repeated for impacting ion beam energies ranging from 0.3 to 7 eV (lab).

RESULTS

(1) **Relative reaction cross sections.** Reaction cross sections were approximately proportional to reciprocal ion energy. Typical variations of secondary to primary ion current ratios are shown in Figure 1 for the impact of CD_3OH^+ on CH_3CDO . The mass to charge ratios shown correspond to the possible hydron (proton or deuteron), hydrium (hydrogen or deuterium atom) and charge transfer reactions. These are the most important processes in all mixtures.

(2) **Preferential Transfer.** The dipole effect can be examined with greater clarity if secondary ion intensity ratios are examined relative to each other. The variation with ion energy of the ratio of hydrium transfer from the methyl group to that from the functional group is shown in Figures 2 and 3. In all the reactions studied the probability of hydrium transfer from the methyl group increases with increasing energy.

The ion current ratio i_{46}/i_{45} observed for the reaction of CH_3CHO^+ with CD_3CHO (Figure 3) exhibits a stronger dependence on energy than the relative transfer probabilities in other systems. This is probably the result of a simultaneous contribution to m/e 46 from the dissociative charge transfer reaction,



This could be expected since it is well known that the relative importance of charge transfer increases at higher energies (18); fragment ions were indeed also observed in other reactions in this study. Even a small contribution from such a process would have a sizable effect since the cross section for atom transfer from the methyl group is small. A similar ambiguity is possible for the impact of CH_3OH^+ on CD_3OH , however, its effect would be small because of the large secondary ion currents resulting from atom transfer. Contributions from dissociative charge exchange in other systems would not lead to products identical in mass with those resulting from the reactions of interest.

The variation with energy of hydron transfer from the methyl group relative to that from the functional groups is summarized in Figure 4. Most of the ion transfer processes also show a preference for transfer from the methyl group at higher ion energies. Only the hydron transfer reactions from methanol to acetaldehyde display much smaller variations with energy.

(3) **Temperature Dependence.** Since rotational energy may be expected to decrease the preferential orientation if it occurs at any one ion kinetic energy, a series of runs were also carried out with the collision chamber maintained at 198°C . The corresponding results are shown in Figures 2 and 4.

(4) **Comparison with Earlier Experiments.** An earlier investigation (9,10) reported a threefold preference for atom transfer from the hydroxyl group to that from the methyl group for the reaction of CH_3CHO^+ with CD_3OH . This investigation was carried out in a conventional mass spectrometer so that reactions were averaged between thermal energies and a terminal ion energy of 1.20 eV. In order to carry out a comparison it is necessary to average the present results over the range 0 - 1.20 eV, using an appropriate reaction probability function $P(E)$. Such a calculation can only be approximated from the present investigation since the energy dependence of the ratio is uncertain at the lowest energies. Assuming that the transfer ratio is linear with energy as suggested by the dashed line in Figure 2 and taking the reaction cross section, and therefore $P(E)$, to be proportional to $E^{-1/2}$, one obtains

$$\langle \text{CH}_3\text{CHOH}^+ / \text{CH}_3\text{CHOD}^+ \rangle = \int_0^{1.19 \text{ eV}} (\text{CH}_3\text{CHOH}^+ / \text{CH}_3\text{CHOD}^+) P(E) dE = 0.4$$

FIGURES

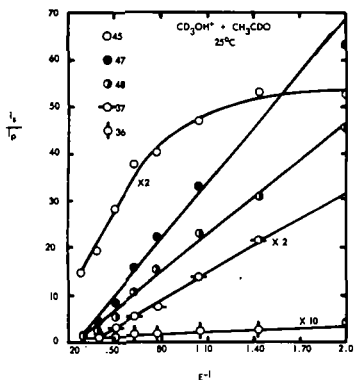


Fig. 1. Relative cross sections for hydron and charge transfer in the reaction of $CD_3OH^+ + CH_3CDO$ at $25^\circ C$ as a function of E^{-1} .

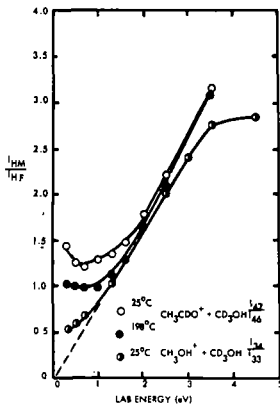


Fig. 2. Ratio of hydrium transfer from the methyl to the functional group for methanol using methanol and acetaldehyde ions.

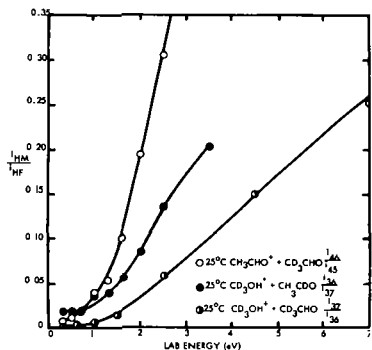


Fig. 3. Ratio of hydrium transfer from the methyl to the functional group for acetaldehyde using methanol and acetaldehyde ions.

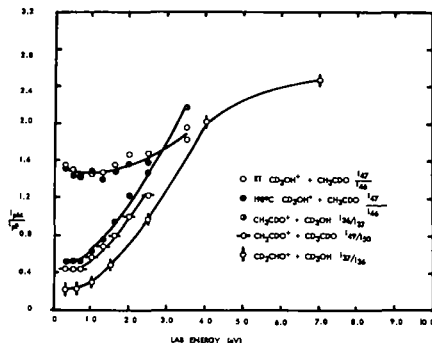


Fig. 4. Ratio of hydron transfer from the methyl to the functional group for various systems.

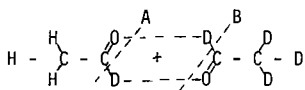


Fig. 5. Possible structure for long-lived complex in acetaldehyde self-reactions.

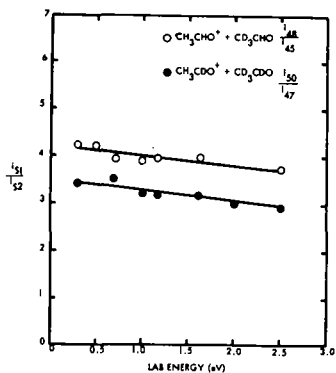


Fig. 6. Ratios of secondaries produced by scission of long-lived complex for the acetaldehyde self-reactions.

This is in acceptable agreement with the value of 0.33 reported previously.

Earlier studies of methanol using the same instrument (19) led to a ratio of i_{34}/i_{33} of 1.08 for the reaction of CH_3OH^+ with CD_3OH at 0.3 eV. This is in disagreement with our value of 0.54 at that energy, which was reproducible over several months. The previous value may have been affected by isotopic impurities. It is also worthwhile noting that the ratio is strongly temperature dependent (Figure 2), possibly offering an alternate explanation of the discrepancy.

DISCUSSION

(1) Evidence for participation of the permanent dipole. The earlier suggestion that the permanent dipole effects preferential atom transfer is supported by the results of this investigation. It is difficult, if not impossible, to extrapolate results showing preferential transfer to zero ion kinetic energy. If one disregards data at the lowest ion energies because instrument adjustment and tuning are difficult below 1 eV, and if one extrapolates the results at higher energy linearly, one could argue that atom transfer to thermal ions occurs only from the functional, electronegative group. Since the alignment of the dipole must be in competition with its rotation, a decrease in the preferential transfer may be expected at increased temperature, which will substantially increase the average rotational energy, and indeed higher temperatures reduce the apparent dipole effect (Figure 2). The approach to random (statistical) atom transfer at higher ion energies is also consistent with the participation of the permanent dipole in the reaction mechanism, since at higher ion energies the collision encounter should be shorter.

(2) Evidence for the effect of ion structure. At the lowest ion energies hydron conveyance from the functional group from acetaldehyde predominates just as in the atom transfer reactions. The simple picture that transfer occurs preferentially from the negative end of the molecule because this species aligns itself with the ion cannot be applied for the hydron transport. The ion transfer from the aldehyde group is by far the most dominant process at all energies, and conveyance from the methyl group never exceeds approximately 20%. A possible complication is the existence of charge transfer preceding the reaction, followed by hydrium transfer of the now neutralized original incident species. The likelihood of such a reaction is quite small for the impact of acetaldehyde ions on methanol since charge transfer is endothermic by 14.3 kcal in this case.

The preferential ion transfer in the reactions of methanol ion with acetaldehyde shows only a very small energy dependency, and the relative probabilities of conveyance from the hydroxyl group never substantially decreases. While such a decrease is apparent in the reactions of aldehyde ion with acetaldehyde, under no circumstances is a nearly statistical ratio observed. While these results may indicate that at least at the lower energies the rotation of the ion may also affect the transfer probability from the functional group, this is not consistent with the absence of an effect of temperature on the transfer ratio (Figure 4). We prefer therefore to ascribe the preferential hydron transfer to a weakening of the bond being broken. The charge should be localized near the oxygen atom, therefore primarily lengthening and weakening the O-H bond.

(3) Reaction mechanisms. The data discussed up to this point cannot distinguish between a mechanism involving a long-lived complex or a stripping process in which the long range forces are effective. Additional evidence can be obtained for a stripping mechanism by considering the acetaldehyde self-reactions. A simplified consideration of a possible long-lived intermediate in acetaldehyde self reactions is instructive. One might expect a complex for the reaction of CH_3CDO^+ with CD_2CDO to attain a minimum energy configuration. When CD_3CDO is "aligned" with CH_3CDO^+ a reasonable structure may well be that shown in Figure 5. Assuming essentially complete redistribution of energy in the complex, scission should occur with equal probability at A or B. This would lead to a ratio of $\text{CD}_3\text{CDO}^+/\text{CH}_3\text{CDO}^+$ (50/47) of approximately unity while the observed ratio is 3.5. The similar reaction of CH_3CHO^+ with CD_2CHO leads to a value of 4.0 for the ratio of 48/45 ($\text{CD}_3\text{CHO}^+/\text{CH}_3\text{CHO}^+$), and not one of unity as predicted from the complex. Moreover, the ratios remain nearly invariant throughout the energy range studied (Figure 6). It is clear that the ion retains its identity during the reaction. Hydrogen atom transfer, where preferential conveyance would be most probable, is a relatively minor channel of reaction at the lowest ion energies. The characteristic which dominates the overall reaction appears to be the bond strength of the entity to be transferred from the incident ion. Clearly the majority of the encounters do not yield products through a long-lived intermediate complex.

(4) Isotope effects. The existence of an appreciable isotope effect on the hydrium or hydron transfer was demonstrated for two systems (Figures 2 and 4). Such phenomena have been reported in the past, and have been ascribed to several effects: a) the change in the reduced mass of the colliding pair and its effect on the Langevin cross section (1,2); b) changes in the displacement of the center of mass from the center of charge and its effect on the "activation energy" of the dissociation process (20);

c) the kinetic isotope effect on the first order dissociation process (21); and d) the dissociation of product ions when the internal energy deposited in the product ion exceeds its dissociation energy (8). The first three are of primary concern for long-lived complexes surviving numerous vibrations, while the last is the source of the large effect associated with stripping reactions.

The first two factors cannot readily make a noticeable difference in systems of this complexity, even though one is seeing the product of two isotope effects, one for transfer from the methyl, and the other for transfer from the aldehyde group. The reduced mass of the colliding pair is altered by only 2%, while the major cause of the displacement effect is the original asymmetry of the compound, and would be only little affected by the isotopic substitution. The explanation may therefore be sought either in phenomena associated with further decomposition of the ion, or in the greater availability of the hydrium atom in the aldehyde group when it is not labeled.

Simplified analysis of the further dissociation of the product ion using rate theory suggests that the deuterated compound should be longer-lived and therefore more abundant if the two complexes are formed with the same energy content, the exact reverse of the present observation. However, if the transfer occurred by a stripping mechanism, whether one takes such a model in its original idealized form or in the modification which allows for attractive potentials, the larger internal energy when deuterium atom is abstracted would lead to just such an isotope effect.

CONCLUSIONS

The retention of ion identity during the reaction and the considerable isotope effect suggest that in the 1 - 7 eV (laboratory system) energy range the dynamics of ion-polar molecule reactions cannot be described purely in terms of long-lived intermediates. However, rotation of the molecule and the dipole moment clearly play an important part in determining the position from which atom transfer occurs. These observations are consistent with a stripping model in which long-range forces are effective.

ACKNOWLEDGEMENTS

We are deeply grateful to the National Science Foundation for partial support of this investigation.

LITERATURE CITED

1. Giomousis, G., Stevenson, D. D., J. Chem. Phys. 29, 294 (1958).
2. Langevin, P., Ann. Chim. Phys. 5, 245 (1905).
3. Moran, R. F., Hamill, W. H., J. Chem. Phys. 39, 1413 (1963).
4. Dugan, J. V., Magee, J. L., J. Chem. Phys. 47, 3106 (1967).
5. Dugan, J. V., Rice, J. H., and Magee, J. L., Chem. Phys. Letters 2, 219 (1968).
6. Gupta, S. K., Jones, E. G., Harrison, A. G., Myher, J. J., Can. J. Chem. 45, 3107 (1967).
7. Herman, Z., Kerstetter, J. D., Rose, R. L., Wolfgang, R., Discussions of Faraday Soc., 44, 123 (1967); J. Chem. Phys. 46, 2844 (1967).
8. Henglein, A., Advan. Chem. Ser. 58, 63 (1966).
9. Leger, L. J., Meisels, G. G., Chem. Phys. Letters 1, 661 (1968).
10. Meisels, G. G., Leger, L. J., Advan. in Chem. 82, E. Hart, ed., Am. Chem. Soc., Washington, D. C. (1968) p. 133.
11. Hutchison, D., Pobo, L., Proc. Meeting Mass Spectrometry, 9th, Chicago, June, 1961.
12. Harrison, A. G., Can. J. Chem. 41, 236 (1963).
13. Harrison, A. G., Tait, J. M. S., Can. J. Chem. 40, 1986 (1962).
14. Shannon, T. W., Harrison, A. G., J. Chem. Phys. 43, 4201 (1965).
15. *Ibid.*, p. 4206.
16. Leitch, L. C., Can. J. Chem. 33, 400 (1965).
17. Futrell, J. H., Miller, D. C., Rev. Scie. Instr. 37, 1521 (1966).
18. Futrell, J. H., Abramson, F. P., Advan. in Chem. Ser. 58, 107 (1966).
19. Sieck, L. W., Abramson, F. P., Futrell, J. H., J. Chem. Phys. 45, 2859 (1966).
20. Reuben, B. G., Friedman, L., J. Chem. Phys. 37, 1623 (1962).
21. Stevenson, D. P., Schachtschneider, J. Am. Chem. Soc., Div. Phys. Chem., University of Utah, Salt Lake City, Utah, Summer 1963.

Robert H. Shapiro and James W. Serum
Department of Chemistry
University of Colorado
Boulder, Colorado 80302

The molecular ions of nitrobenzoic acid derivatives initially cleave alpha to the carbonyl group to yield mass 150, nitrobenzoyl cations (Figure 1). This mass 150 ion further decomposes by expulsion of NO and NO₂ (both of which are odd electron species) to yield odd electron ions, a process which is usually energetically unfavorable.

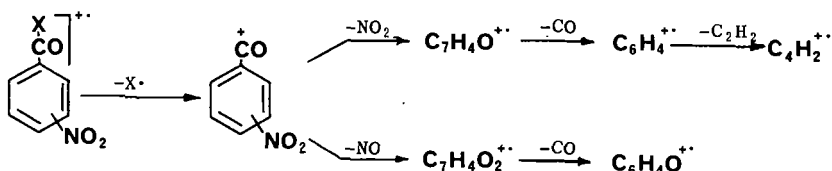


Figure 1

A problem arises in an attempt to kinetically investigate these two decomposition modes, in that although the expulsion of NO must arise from a rearranged nitrobenzoyl cation, the expulsion of NO₂ can in principle arise from either a rearranged or an unrearranged nitrobenzoyl cation. It was therefore necessary to determine the mechanism of NO₂ expulsion, and nitrobenzene was chosen for initial investigation.

The mass spectrum of nitrobenzene has been thoroughly studied,¹ and, as in the case of the nitrobenzoyl cation, the expulsion of NO₂ may arise from two possible pathways.

In 1959 Chupka reported that a rearrangement process will show a more abundant metastable ion than a simple cleavage process,² and recently McLafferty and Fairweather³ have provided additional evidence for this using nitrobenzene as an example. The metastable ion for expulsion of NO was found to be much more abundant than the metastable ion for the loss of NO₂. These results may be interpreted to mean that most of the C₆H₅⁺ ions are formed by simple cleavage of the C-N bond in the unrearranged molecular ion.

Another method for determining the occurrence of a rearrangement process is based on the quasi-equilibrium theory. This method, originally stated by Chupka² and recently employed by Williams and Cooks⁴, is based on a simplified form of the basic rate equation of the quasi-equilibrium theory (equation 1). For two competing reactions, one

$$k(E) = \nu \left[\frac{E - \epsilon}{E} \right]^{s-1} \quad (\text{equation 1})$$

being a simple cleavage and the other a rearrangement process, the terms E and s-1 will be constant for the two reactions. The frequency factor (ν_r) for a rearrangement reaction is lower than the frequency factor (ν_s) for a simple cleavage, and it has been experimentally determined that the activation energy (ϵ_r) for a rearrangement process is generally lower than the activation energy (ϵ_s) for a simple cleavage. At high ionizing energies then, the simple cleavage would be expected to dominate because the frequency factors will be most significant; however, at lower ionizing energies the activation energies control the reactions, and the rearrangement process should become progressively more important.

This method was used to interpret the data for nitrobenzene, and

the results (Figure 2) showed that as the ionizing energy is lowered, the $(M-NO)^+ / (M-NO)^+ + (M-NO_2)^+$ ion abundance ratio progressively increases.

These results provide additional evidence that the $(M-NO_2)^+$ ion from nitrobenzene is being generated from an unrearranged molecular ion.

Using the same method, data were examined for the loss of NO and NO_2 from the nitrobenzoyl cation, and, as in the case of nitrobenzene, the $(150-NO)^+$ ion became progressively more abundant as the ionizing energy was lowered. It was therefore concluded that the $(150-NO_2)^+$ ion from the nitrobenzoyl cation was formed via a simple cleavage and that the $(150-NO)^+$ ion was formed via a rearrangement process.

In an attempt to study other even-electron nitroaromatic systems to determine if they behaved in an analogous manner, the expulsion of NO and NO_2 from the mass 136 ions ($C_7H_8NO_2^+$) generated from *m*- and *p*-nitrobenzylbromide was investigated. Although it had recently been reported that decomposing $C_7H_8NO_2^+$ ions produced from *m*- and *p*-nitrobenzylphenyl ethers possessed the nitrotropylium ion structure,⁵ the values obtained for the dependence of the $(136-NO)^+ / (136-NO)^+ + (136-NO_2)^+$ abundance ratio on ionizing energy were quite different for the *m*- and *p*- isomers (Figure 2). It would be expected that these values would be the same if the 136 ion does indeed rearrange to a nitrotropylium structure.

Dependence of $(136-NO)^+$ and $(136-NO_2)^+$ from Nitrobenzyl Compounds on Ionizing Energy

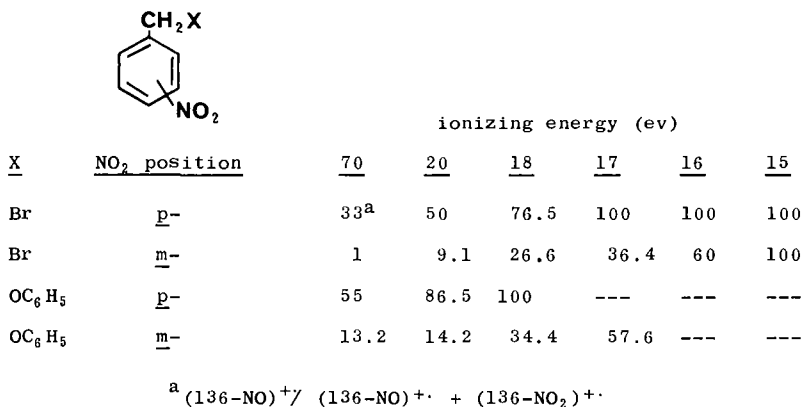


Figure 2

It appears that the driving force for expulsion of NO is much stronger for the *p*- isomer than for the *m*- isomer. These results can be rationalized by examination of contributing structures of the $C_7H_8NO_2^+$ ion, using the nitrobenzyl ions as models. In the unrearranged *p*- $C_7H_8NO_2^+$ ion, there are contributing structures which violate the adjacent charge rule, and these can be relieved by rearrangement to a nitro ion. There are no such direct interactions in the contributing structures of the *m*-isomer.

Additional evidence to support the existence of different structures for the *m*- and *p*- isomers is that metastable ions are observed for both loss of NO (m/e 82.6) and NO_2 (m/e 59.5) in the mass spectra of the *p*- isomers, whereas only the metastable ion corresponding to the loss of NO_2 (59.5) is observed in the mass spectra of the *m*- isomers.

It is concluded from these results that the decomposing mass 136 ions generated from *m*- and *p*- nitrobenzylbromides and *m*- and *p*-nitrobenzylphenyl ethers do not have the same structure and therefore do not both decompose as nitrotropylium ions.

REFERENCES

1. J.H. Beynon, R.A. Saunders and A.E. Williams, Ind. Chem. Belge., 311 (1964).
2. W.A. Chupka, J. Chem. Phys., 30, 191 (1959).
3. F.W. McLafferty and R.B. Fairweather, J. Am. Chem. Soc., 90, 5915 (1968).
4. D.H. Williams and R.G. Cooks, Chem. Commun., 663 (1968).
5. P. Brown, J. Am. Chem. Soc., 90, 2694 (1968).

LOSS OF LARGE AND SMALL RADICALS FROM
ACETALS AND KETONES*

R. G. Cooks,† A. N. H. Yeo, and D. H. Williams
University Chemical Laboratory
Lensfield Road, Cambridge, U.K.

Metastable transitions have been used in an investigation of the relative ease of loss of small vs large n-alkyl radicals from ethylene acetals and ketones. The low energy parent ions in each case exhibit the more abundant metastable ion for loss of the smaller radical, which indicates that the process M^+-R_S has a lower appearance potential than the M^+-R_L process. Both processes apparently involve a simple bond cleavage yet the relative daughter ion abundances are reversed at 70eV. Such a "cross-over" in daughter ion yield appears to be a general phenomenon in compounds where competitive loss of n-alkyl radicals can occur (e.g. phenylalkanes, ethers, imines).

That this unexpected result is not due merely to the fact that the M^+-R_S ion possesses a greater average internal energy and has more decomposition pathways open it than has the M^+-R_L ion was shown by studies at electron energies at which further decomposition of both daughter ions was negligible. The result was also not due to the more extensive decompositions of the M^+-R_S ion during its slower passage through the analyser, although this factor had a small effect as seen by the effects of varying accelerating voltage on ion abundances.

Surprisingly, it was observed for both the ketones and ketals studied, that neither the M^+-R_S nor the M^+-R_L ions formed in the first field free region necessarily arose only from the molecular ion. For example, loss of the larger radical from n-butyl n-propyl ethylene ketal resulted equally from transitions $M^+ \rightarrow M^+-C_4H_9$ and $(M-C_2H_5)^+ \rightarrow M^+-C_4H_9$, while the smaller radical was largely formed directly from the molecular ion. While it is impossible to extrapolate quantitatively from processes occurring in the metastable region to those occurring in the source, this observation does provide a possible explanation for the "cross-over" behavior. Thus, the greater number of routes by which M^+-R_L may be formed relative to M^+-R_S , means that in high energy parent ions (from which multistep decompositions are possible) M^+-R_L should increase relative to M^+-R_S as is observed.

* Submitted for publication in Org. Mass Spectrom.

† Present address, Department of Chemistry, Kansas State University, Manhattan, Ks.

In ketones the McLafferty rearrangement and the loss of an alkyl radical exhibit metastable peaks of similar intensity and daughter ions of at least comparable abundances, yet one process is a rearrangement and the other ostensibly a simple cleavage. This observation leads to the suspicion that both the M^+-R_S and the M^+-R_L ions are each formed by two processes, one favored in ions of high and the other in ions of low internal energy. Thus it is suggested that at the threshold, M^+-R_S and M^+-R_L are formed by a low frequency factor reaction which favors M^+-R_S formation, that is by a rearrangement process. At higher internal energies the higher A. P., higher frequency factor α -cleavage process will be dominant.

ABSTRACT

FRAGMENTATION PROCESSES IN THE MASS SPECTRA
OF THE BENZO(b)THIENYLTHIAALKANES

by

Norman G. Foster, Julie Pei-min Liao and Robert W. Higgins*

Contributed by the Chemistry Department
Texas Woman's University
Denton, Texas 76204

The mass spectra of five 1-[2-benzo(b)thienyl]-1-thiaalkanes, five 1-[3-benzo(b)thienyl]-1-thiaalkanes, and 4,5,6,7-tetrahydro-1-[2-benzo(b)thienyl]-1-thiapentane are reported.

Fragmentation-structure correlations are outlined and some pathways to prominent ions established by means of low-voltage and metastable ion data. In all cases, the most intense ion is formed by cleavage of the C-S bond in the thienyl chain. The sulfur atom and a rearranged hydrogen atom remain with the fused ring moiety. Expanded ring structures and "propellane" like intermediates are proposed to explain the fragment ions observed. Evidence supporting the ring expansion and other structures is considered.

Other cleavage processes are shown to be parallel to those expected from the alkylbenzenes, alkylthiophenes and the thienylthiaalkanes. An m/e 147 ion appears that contains only one sulfur atom and which requires either a carbon skeletal rearrangement or the formation of an additional fused ring system followed by ejection of a neutral sulfur containing moiety. Beta cleavage accompanied by the hydrogen atom rearrangement was found to be an energetically more favorable process than the loss of a neutral ethylene group from the tetrahydrobenzene ring for the one compound of this type. The mass spectrum of this molecule showed fragments corresponding to all the functionalities originally present.

Throughout this study it was found that the sulfur containing moieties preferentially held the charge in competitive fragmentation.

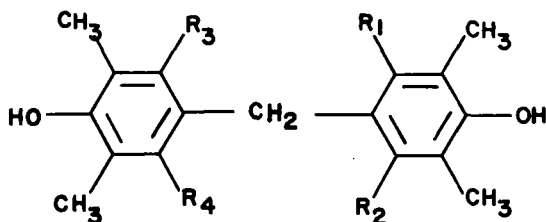
This work was supported by The Robert A. Welch Foundation of Houston, Texas, and by the Texas Woman's University Institutional Research funds.

*Deceased

163. MASS SPECTROMETRIC INVESTIGATION OF SUBSTITUTED DIARYLMETHANES

W. M. Scott, M. E. Wacks, J. D. Fitzpatrick and C. Steelink
 Department of Chemistry, The University of Arizona
 Tucson, Arizona 85721

The mass spectra of a number of ortho substituted diarylmethanes (listed below) were presented and several interesting aspects of fragmentation modes were discussed.



- I:- $R_1, R_2, R_3, R_4 = H$
 II:- $R_1 = CH_3; R_2, R_3, R_4 = H$
 III:- $R_1, R_2 = CH_3; R_3, R_4 = H$
 IV:- $R_1, R_3 = CH_3; R_2, R_4 = H$
 V:- $R_1, R_2, R_3 = CH_3; R_4 = H$
 VI:- $R_1, R_2, R_3, R_4 = CH_3$

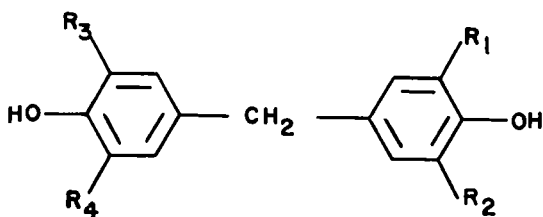
Meyerson, Drews and Fields¹ noted that when an OH, SH, CH₃, etc. group is present in the ortho-position of one or the other of the two aryl moieties in substituted diphenylmethanes, a characteristic even mass fragment ion is observed in the mass spectrum due to decomposition of the molecular ion by "ortho-rearrangement." In the mass spectrum of I, which has no ortho substituents, an ion was observed at m/e 134. Many related diphenylmethane mass spectra were examined but no other "pseudo" ortho rearrangement ions were observed. Investigations as to the origin of this ion are continuing via deuterium labelling techniques.

However, the ortho-rearrangement was examined in the mass spectra of compounds II-VI. Steric interactions between ortho methyl groups on each aryl moiety cause the planes of the two rings to twist to a more strain-free configuration in which these planes are mutually perpendicular. This is the geometry which most favours ortho-rearrangement. The intensity of the rearrangement ion (I_R) is expressed as a function of the total ion current (Σ_{39}) in

Table 1, which gives an indication of steric interactions between these ortho methyl groups.

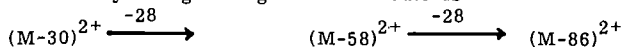
Compound	Rearrangement Ion (m/e)	$I_R / \sum_{39}(\%)$
II	148	8.2
III	162	11.0
IV	148	23.2
V	162	18.4
V	148	14.7
VI	162	38.2

Abundant doubly-charged ions were particularly evident in the mass spectra of several t-butyl substituted diphenylmethanes, whose structures are listed below.



- VII:- $R_1, R_2, R_3, R_4 = t\text{-butyl}$
 VIII:- $R_1, R_2 = \text{CH}_3; R_3, R_4 = t\text{-butyl}$
 IX:- $R_1, R_2 = \text{OCH}_3; R_3, R_4 = t\text{-butyl}$
 X:- $R_1, R_3 = \text{CH}_3; R_2, R_4 = t\text{-butyl}$

When there is a t-butyl group located on each "half" of the molecule, i.e. in VII and X, the doubly-charged fragmentation route is



but when both t-butyl groups are on the one aryl moiety, the doubly-charged fragmentation route is



There are metastable ions which indicate stepwise loss of these molecules, each of 28 mass units. An explanation of these phenomena, based on the deuteration studies of Rylander and Meyerson² of the mass spectrum of t-butyl benzene, has been proposed³.

Finally, the mass spectrum of the triphenylmethane analogue of this system was examined and a few of the abundant multiply-charged ions are listed below.

Ion	(M-30) ²⁺	(M-58) ²⁺	(M-45) ³⁺	(M-73) ³⁺	(M-101) ³⁺	(M-129) ³⁺
Rel. Ab.	25.6	9.2	2.1	1.3	0.9	2.5

While the intensities of the triply-charged ions are indeed low, it is hoped that by defocusing the normal ion beam and looking at the focused metastable ion spectrum, there will be found the first evidence of stepwise decomposition of ions in the triply-charged state, by elimination of small neutral molecules. The energetics of these and related systems of multiply-charged ions are currently under further investigation in this laboratory.

EXPERIMENTAL

All spectra were obtained on an Hitachi RMU-6E double-focusing mass spectrometer via the direct insertion probe, at temperatures in the range 100-150°C.

ACKNOWLEDGEMENTS

The authors wish to acknowledge the helpful advice of Dr. S. Meyerson during this investigation, and to thank Mr. J. Teets for aid in obtaining the spectra.

REFERENCES

1. Meyerson, S., Drews, H. and Fields, E.K., J. Am. Chem. Soc., 86, 4964 (1964).
2. Rylander, P.N. and Meyerson, S., J. Am. Chem. Soc., 78, 5799 (1956).
3. Fitzpatrick, J.D., Scott, W.M., Steelink, C. and Wacks, M.E., Int. J. Mass Spectrom. Ion Phys., 1, 415 (1968).

ELIMINATION OF SMALL NEUTRAL MOLECULES IN THE IONIZATION-DISSOCIATION
OF SALICYLIC ACID AND ITS ESTERS

by
Clemond D. Eskelson, Jack C. Towne, and C. Cazee
Veterans Administration Hospital, Tucson, Arizona 85713
and

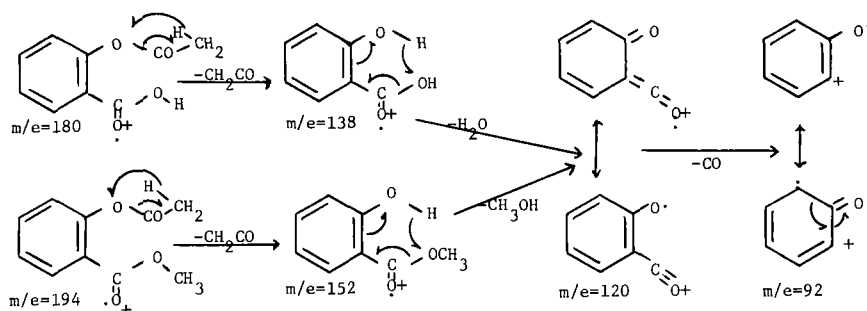
Morton E. Wacks and Ward M. Scott
University of Arizona, Tucson, Arizona 85721

In the mass spectra of salicylic acid and some of its simple esters,^{1/} it was noted that the primary dissociative ionization processes involved the consecutive loss of the elements of small neutral molecules. If the ions having the same value of m/e formed from each of the compounds, salicylic acid (SA), methyl salicylate (MeSA), 2-acetoxy benzoic acid (AcSA), and methyl 2-acetoxy benzoate (MeAcSA), were assumed to have the same structure, then positive identification of the neutral species lost in these processes as the corresponding unexcited molecules could be made through energetic considerations.

TABLE I
RELATIVE ABUNDANCE OF PRINCIPAL IONS IN THE MASS SPECTRA
OF SUBSTITUTED SALICYLIC ACIDS

COMPD	m/e 92	120	138	152	180	194
SA	80.2	100.0	52.4			
MeSA	45.1	100.0		45.4		
AcSA	28.7	100.0	59.5		2.9	
MeAcSA	27.3	100.0		64.3		2.7

The principal ions in the mass spectra of these compounds (Table I) correspond to the parent ion (small in the acetylated compounds); loss of C_6H_5O from the acetylated compounds followed by loss of H_2O or CH_3O (from the methylated compounds) giving the base peak in all these compounds (at $m/e = 120$). This fragmentation is in turn followed by loss of CO to give an ion at $m/e = 92$. These fragmentation pathways are shown in Scheme 1. If the structure for the ions of $m/e = 120$ and $m/e = 92$ are indeed common to all the compounds, then the heats of formation of these ions calculated from thermochemical data and measured ionization and appearance potentials should be the same. In order to calculate the heats of formation of the ions in question, it is necessary only to know the heats of formation of the gaseous compounds, the neutral molecules assumed to be formed, the ionization energies of the compounds, and the appearance potentials of the ions in question. It is not necessary in this series to approximate any ionic heats of formation since these are all measurable within the group.



Scheme 1. Fragmentation pathways for salicylic acid and derivatives.

The basic equations describing these processes are Eq. 1 which describes the dissociative ionization process,



Eq. 2 which describes the energetics of this reaction in terms of the measured appearance potential of ion R_1^+ , $[A(R_1^+)]$, and any excitation energy (electronic, vibrational, rotational, and kinetic), E , associated with the dissociative ionization process (1)

$$A(R_1^+) = \Delta H_{\text{Reaction}} = \Delta H_f(R_1^+) + \Delta H_f(R_2) - \Delta H_f(R_1R_2) + E \quad (2)$$

and Eq. 3 which relates the ionization energy to the heat of formation of the ion and the

^{1/}W. M. Scott and M. E. Wacks, OMS 1, 847 (1968).

molecule

$$I(R_1) = \Delta H_f(R^+) - \Delta H_f(R_1) \quad (3)$$

As an example, the heat of formation of the salicylic acid ion (SA^+) formed by the loss of CH_2CO from AcSA is given by

$$\Delta H_f(SA^+) = A(SA^+) - \Delta H_f(CH_2CO) + \Delta H_f(AcSA) \quad (4)$$

If the basic assumptions that (1) the neutral fragments lost in the dissociative ionization are the neutral molecules, ketene, water, methanol, and carbon monoxide, and (2) the ions formed having the same value of m/e have the same configuration, then the value of $\Delta H_f(SA^+)$ from Eq. 4 should correspond to that found for this ion from the measurement of the ionization energy of salicylic acid as shown in Eq. 3. The heats of formation of the neutral molecules used in these calculations are given in Table II. These are accurate values for the gaseous molecules involved. The only estimate is for MeAcSA and is estimated to be within ± 2 kcal.

TABLE II
HEATS OF FORMATION (KCAL/MOLE) OF NEUTRAL MOLECULES

CMPD	H ₂ O	MeOH	CO	CH ₂ CO	SA	MeSA	AcSA	MeAcSA
ΔH_f (g)	-57.8	-48.1	-26.4	-14.6	-118.1	-113.8	-157.2	-152.9*

* Calcd.

The measured ionization and appearance potentials for these compounds are given in Table III. These values show the expected differences between appearance potentials for similar ions [e.g., AP(m/e 120 - m/e 92) = 3.3 eV] indicating that the assumption of common ionic structures for these compounds is indeed valid. If it is assumed that there is very little or no excess energy associated with the dissociative ionization and that the neutral species formed are unexcited, then it is possible to calculate a value (or at least an upper limit) for the heats of formation for these ions. These calculated values

TABLE III
IONIZATION AND APPEARANCE POTENTIALS (eV)

m/e	92	120	138	152	180	194
SA	14.02	10.60	9.03			
MeSA	14.30	11.00		8.90		
AcSA	14.45	11.16	9.50		8.80	
MeAcSA	15.05	11.74		9.52		8.90

are presented in Table IV. The heats of formation for the ions for the unacetylated species confirm the assumptions, i.e., that the ionic structures are the same and the neutral fragments lost are the molecular species, essentially unexcited, of water, methanol, and carbon monoxide. The data for the acetylated compounds do not yield values as close to the values of the unacetylated as expected in view of the precision of the experimentally measured ionization and appearance potentials. However, the mean value for the heat of formation of the m/e 120 ion is 100.6 kcal/mole ± 0.35 eV (the experimental uncertainty for the appearance potentials was approximately one half of this value). This spread in the values of the ionic heat of formation is undoubtedly due to the difficulty of measuring ionization energies for the low abundance molecular ions and the small amount of thermal cracking occurring in the acetylated compounds.

TABLE IV
HEATS OF FORMATION OF IONS (KCAL/MOLE)

M/e	92	120	138	152	180	194
SA	292.2	184.4	90.3			
MeSA	290.7	188.2		91.6		
AcSA	275.1	172.8	76.7		45.9	
MeAcSA	283.5	180.8		81.5		52.5

In conclusion, the measured ionization energies and appearance potentials of the ions formed in these substituted salicylic acids by loss of small neutral fragments confirms the fact that these fragments are the molecules, water, ketene, methanol, and carbon monoxide. In addition, the fragmentation of these molecules leads to the formation of ions at m/e 120 and m/e 92 which have the same structure and give rise to the observed similarities in the fragmentation pattern for these and related salicylic acids.

The authors are indebted to Dr. Daniel R. Stull of the Dow Chemical Company and Dr. William H. Evans of the National Bureau of Standards for supplying from their files pertinent data on the heats of formation of molecules used in calculating the ionic heats of formation.

THE MASS SPECTRA OF SOME HALOGENATED PHENOLS AND NAPHTHOLS

Theodore L. Folk

Research Division, The Goodyear Tire & Rubber Company
Akron, Ohio, 44316

A competition observed in the mass spectra of halophenols has recently been reported from this laboratory.¹ The two processes in competition are loss of halogen atom (and HX) and loss of CO (and CHO) from the molecular ion. In the mass spectrum of o-chlorophenol loss of [Cl] plus loss of [HCl] was noted to be twice the loss of [CO] plus the loss of [CHO]. This ratio was reversed for p-chlorophenol. The proximity of the chloro group to the labile hydroxyl hydrogen probably accounts for this unexpected reversal. In contrast to the chlorophenols, the bromo- and iodophenols all showed much greater loss of halogen than [CO] from the molecular ion.

We have begun investigation by mass spectrometry of several halonaphthol and substituted halophenol compounds. With only two exceptions, the mass spectra were divided into two types: (1) those with [M-X] ion as the base peak* and (2) those with the molecular ion as the base peak.

The mass spectra in the first category were those of 2-chloro-4-methylphenol, 4-chloro-2-methylphenol, 4-chloro-3-methylphenol, 2-bromo-4-methylphenol and 4-chloro-3,5-dimethylphenol. The mass spectra with the molecular ion as the base peak were than of 2-chloro-4-phenylphenol, 4-chloro-1-naphthol, 6-bromo-2-naphthol and 4-bromo-2,6-dimethyl phenol.

The fragmentation pattern for 1-bromo-2-naphthol has not as yet been rationalized. The base peak is formed by loss of [BR+CHO] from the molecular ion.

2-Bromo-4-t-butylphenol showed a base peak due to loss of a methyl radical from the molecular ion. Once again a competition between loss of [CO] and [Br] existed. However, these losses were from the base peak, not the molecular ion. Several other dimethylhalophenol and halonaphthol compounds are being investigated. When these investigations and possibly labelling studies are completed, the results will be submitted for publication in Organic Mass Spectrometry.

We thank James R. Boal, Carnegie-Mellon University, for running the mass spectra on the MS-9 mass spectrometer.

1. T. L. Folk and L. G. Wideman, Chem. Commun., 491 (1969).

* In all cases the base peak is the largest peak.

This is Goodyear Contribution No. 432.

QUANTITATIVE ANALYSIS OF TRIGLYCERIDE MIXTURES BY MASS SPECTROMETRY

Ronald A. Hites

Northern Regional Research Laboratory, Peoria, Illinois 61604

Vegetable and animal fats have considerable commercial importance--several billion dollars per year worldwide. Furthermore, edible fats and oils form a large portion of the human diet. It is, therefore, remarkable that there are few methods for the quantitative analysis of these naturally occurring triglyceride mixtures. Existing methods such as thin-layer chromatography and lipase hydrolysis (Ref. 1), either are time consuming, somewhat inaccurate, or require relatively large samples. A new semi-automated mass spectrometric method has been developed in this Laboratory for measuring the triglyceride composition of fats that is both rapid (~1 hour per sample) and sensitive (less than 100 micrograms of fat).

The mass spectra of triglycerides show a small molecular ion peak (Ref. 2) and an M-18 peak which decreases in intensity as unsaturation increases. The base peak is due to the loss of an acyloxy group. Since few peaks are within at least 200 amu. of the molecular ion, it was felt that the molecular weight distribution of a triglyceride mixture could be accurately measured.

The following procedure was, therefore, evolved: (1) The fat is placed into the mass spectrometer on the probe inlet and heated at a fixed, known temperature (~250° C.) until the total ion current is constant. (2) The mass spectrum is recorded from M/e = 700 to 900 several times while the data (magnetic field readings and intensities) are acquired and punched on paper tape by an Infotronics CRS-160 digitizer. (3) An IBM 1130 computer reads the paper tape, converts magnetic fields to masses, corrects for heavy isotopes, sums the M⁺ and (M-18)⁺ intensities, averages replicates, applies the corrections (see below), and prints the molecular weight distribution. It should be emphasized that since various structurally different triglycerides have the same molecular weight, no molar sensitivity corrections can be applied.

Because an inlet system is used that is equivalent to molecular distillation, a correction must be made for the consequent fractionation. For a small range of molecular weights and at a constant temperature, the rate of molecular distillation for a given substance is directly proportional to its vapor pressure (Ref. 3). Since the logarithm of the vapor pressure of triglycerides is proportional to the total number of carbon atoms regardless of unsaturation or carbon distribution within the three alkyl chains (Ref. 4), the logarithm of the fraction correction factor should be directly proportional to the carbon number of the triglyceride.

To test this hypothesis, a mixture of known composition was analyzed by this mass spectral procedure and correction factors were calculated. The results, shown in Figure 1, confirm the feasibility of this type of fractionation correction. The datum point for 1,2-dipalmitoyl olein (PPO), however, lies far from the line. This deviation is attributed to different molar intensities of the molecular ion peaks of fully saturated and unsaturated triglycerides. Data for oils of known composition (see Table I) show that a simple saturated-unsaturated correction as well as the carbon number fractionation correction, gives reasonably accurate values.

The procedure was used to analyze cocoa butter (see Table I). The mass spectrometric values are compared to values calculated on the basis of the 1,3-random (saturates) 2-random (unsaturates) theory of triglyceride distribution (Ref. 1). This theory assumes that unsaturated acids are esterified preferentially at the beta-position of glycerol. The good agreement between theoretical and observed values, shown in Table I, supports this model of triglyceride distribution and validates the saturated-unsaturated and carbon number corrections.

Because a single fat does not have the correct properties for many applications, new fats are made by chemically scrambling the fatty acid moieties among all glycerol positions. Because this process produces a random distribution of triglycerides, it is called randomization or interesterification.

As an example of the mass spectral technique described here, natural and randomized cocoa butter and natural and randomized tallow (beef fat) were analyzed (see Figure 2). Note the great change in the cocoa butter composition upon randomization; there is a corresponding change in physical properties as well. This large change is a result of the nonrandom structure; namely, the preferential esterification of unsaturated fatty acids at the beta-position.

The corresponding data for a partially hydrogenated tallow having about the same fatty acid composition as cocoa butter are also given in Figure 2. As expected, the randomized distribution is similar to that of randomized cocoa butter. Unlike cocoa butter, however, the difference between the natural and randomized distributions is small. Therefore, we conclude that there is less specificity for unsaturated acids in the beta-position of tallow than in cocoa butter. Other data from lipase hydrolysis confirm that animal fats have less beta-unsaturated specificity than do vegetable fats (Ref. 1).

Acknowledgment. The assistance and encouragement of W. K. Rohwedder, H. J. Dutton and J. C. Cowan are gratefully acknowledged.

References

1. M. H. Coleman, *Advan. Lipid Res.* (1963) 1.
2. M. Barber, T. O. Menen and W. Kelley, *Tetrahedron Lett.* (1968) 1063.
3. E. W. Berg, "Physical and Chemical Method of Separation," McGraw-Hill, New York (1963) p. 40.
4. E. S. Perry, W. H. Weber, and B. F. Daubert, *J. Amer. Chem. Soc.* 71, 3720 (1949).

A laboratory of the Northern Utilization Research and Development Division, Agricultural Research Service, U.S. Department of Agriculture.

Mention of the names of firms or trade products is made for your information only and does not imply that they are endorsed or recommended by the U.S. Department of Agriculture over other firms or similar products not mentioned.

Table I. Triglyceride composition of natural cocoa butter

Triglyceride ¹	Distribution ²	
	Theory	Observed
POP ³	12.3	13.3
POO + PLS	11.1	10.1
POS	32.1	30.5
OOS + SIS	12.2	11.2
SOS	20.8	20.3

¹P = palmitic, O = oleic, S = stearic, L = linoleic

²Mole percent of total

³Order of letters is not significant

Figure 1. Semi-logarithmic plot of the fractionation correction factor versus carbon number for triglycerides (see Table I for explanation of point labels)

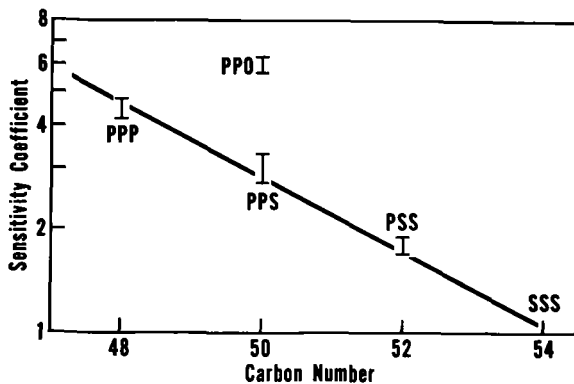
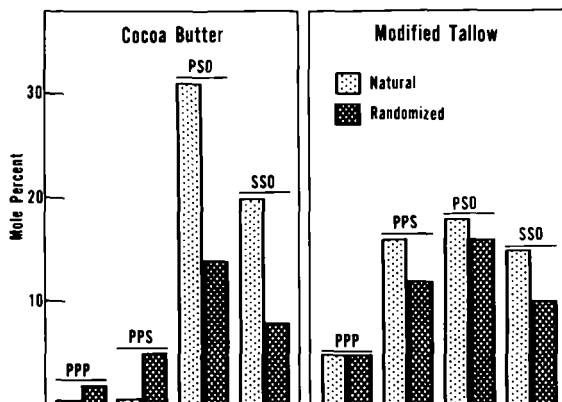


Figure 2. Partial triglyceride composition of natural and randomized cocoa butter and tallow. Only selected triglycerides are shown. The order of the letters is not significant (eg. PSO = POS = OPS).



CARBON-HETEROATOM BOND CLEAVAGE IN THE FRAGMENTATION
OF N-ACETYLPIRROLIDINE AND HOMOLOGUES

J. Tesarek, W. J. Richter and A. L. Burlingame
Space Sciences Laboratory, University of California, Berkeley, California 94720

Carbon-heteroatom bond rupture may be expected to result from multi-step rather than from single-step fragmentation, e.g., as terminating event in sequences where a radical site has been generated adjacent to the heteroatom during molecular rearrangement. In cyclic amine systems, simple α -cleavage produces radical sites at beta- rather than alpha-carbon atoms, and excludes carbon-nitrogen bond rupture as a direct result. Skeletal rearrangement effecting ring contraction of molecular ions has recently been suggested as a cause of C-N bond cleavage in acylated cyclic amines, particularly in N-acetyl morpholine and related systems (1). In this case, the radical center required for C-N bond cleavage is generated by the formation of a "new" bond by cyclization of the α -cleavage product. An alternative and more obvious mode of generating a radical site at the appropriate position is abstraction of hydrogen from positions adjacent to nitrogen by N-acyl substituents. Certain features of the fragmentation of N-acetyl-pyrrolidine provide evidence for the actual occurrence of C-N bond cleavage as a direct consequence of such hydrogen abstraction. In contrast to the formation of α -radical sites by skeletal rearrangement as exemplified by the N-acetyl morpholine system, the hydrogen-abstraction step in the fragmentation of the pyrrolidine analog reflects a much more amide-like behavior in suppression of α -cleavage and even more so in rapid hydrogen abstraction by the carbonyl function as the initial step of fragmentation.

N-acetylpyrrolidine represents a relatively small and simple system in which the radical-induced ring contraction of the N-acetylmorpholine type seems to be precluded, since a strained four-membered cyclic intermediate would have to be traversed (see Fig. 1). A previous study reported several years ago included N-acetylpyrrolidine in a series of acylpyrrolidines, investigated to establish the source of hydrogen retained in the loss of acyl substituent as ketene or its higher homologs. This study required the introduction of deuterium only into the alkyl portion of the acyl moiety, and fragmentation of the ring atoms was inferred in this context largely from analogy to processes which were elucidated for pyrrolidine and its N-methylated derivative; this projection, however, appears inadequate in several respects, requiring major revision.

The compounds studied in our laboratory include N-acetylpyrrolidine together with its 2,2-d₂, 3,3-d₂, 7,7,7-d₃, 2,2,3,3-d₄ and 2,2,5,5-d₄ derivatives.

The mass spectrum of N-acetylpyrrolidine (Fig. 1) shows four major peaks: a molecular ion peak at m/e 113 and peaks at m/e 43, 70 and 85.

M-28 Ions: These ions are unusual with respect to their genesis rather than their composition. Accurate mass measurement establishes that these ions are formed by loss of C₂H₄, as already inferred by the previous study (1). An analysis of the spectra of the ring-labeled compounds demonstrates, however, that in contrast to earlier suggestions adjacent α - and β -carbon atoms (2 and 3, or 4 and 5, respectively) rather than beta and beta are expelled, a fragmentation which requires C-N bond rupture. Thus, the spectra of 2,2-d₂- and 3,3-d₂-N-acetylpyrrolidine display a clear split of the M-28 peak at m/e 85 peak between m/e 85 and 87 (now representing losses of 28 and 30 mass units). Correspondingly, the 2,2,5,5-d₄ analog shows a clear loss of 30 mass units, while--as would have to be expected from symmetry--the 2,2,3,3-d₄ compound shows an approximately equal distribution of ion current between M-28 and M-32 fragments, indicating loss of either all or none of the deuterium labels.

These data clearly exclude a fragmentation process analogous to that encountered in the free amine pyrrolidine, where exclusively carbon atoms 3 and 4 are implicated in the expulsion of ethylene. In view of this striking difference, some allowance for operation of amide--rather than amine--characteristics in governing the fragmentation of acylated derivatives appears mandatory. Amide-like behavior, for instance, would be reflected in hydrogen abstraction by the carbonyl function, preferably from positions adjacent to the C-N bond to be broken. Abstraction from this position might also be favored by resonance stabilization of the resulting isomeric molecular ion. Substantial driving force for the C-N bond cleavage should arise from generation of an extended conjugated system. Ejection of a stable ethylene moiety from the isomeric molecular ion can be interpreted as a consequence of the preceding or concomitant C-N bond cleavage, which produces a radical center at a site favorable for terminal decomposition. Of course, totally or at least partially concerted alternatives with C-N bond cleavage as a terminating rather than a preceding event of ethylene elimination must also be considered. This concerted type of reaction would apply, however, solely to the particular five-membered ring systems of pyrrolidine, in contrast to the higher homologs.

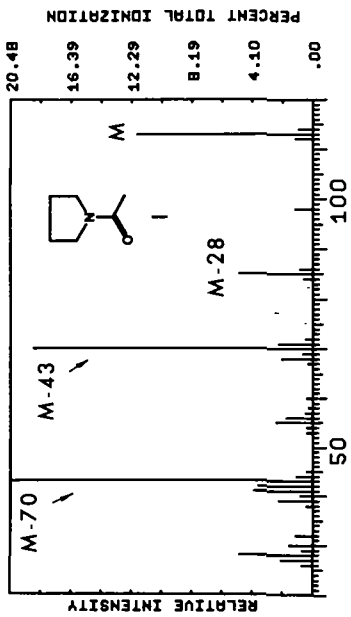
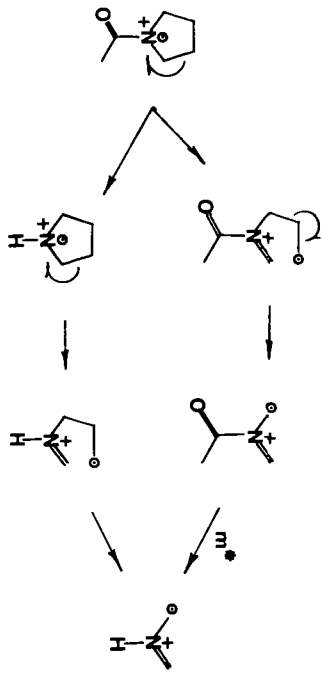
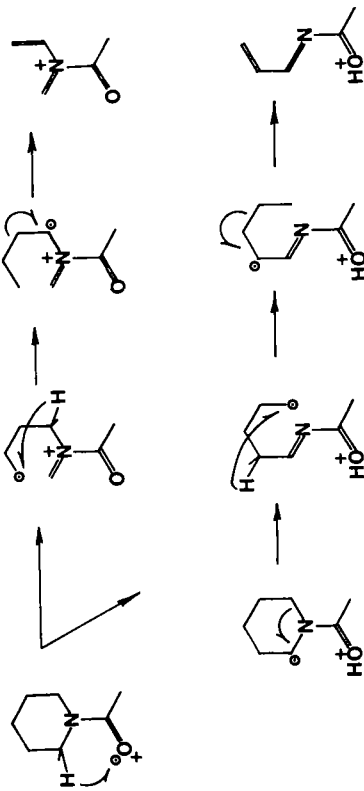


Fig. 1. Mass spectrum of N-acetylpyrrolidine



Scheme 1



Scheme 2



Structures

M-43 ions, formed by the previously established expulsion of ketene and hydrogen, arise via either ordering of the sequence, as substantiated by metastable peaks. Data from deuterated compounds establish that the hydrogen atoms lost originate in this case predominantly from α -positions.

The M-70 peak (at m/e 43) corresponds to three distinguishable components, a nitrogen-containing species which dominates, an acetyl ion and a hydrocarbon fragment. Loss of ethylene together with ketene appears strongly indicated from the composition of the major component, particularly since both losses are observed also as single processes. Two sequential processes (Scheme 1) have been considered, with the upper being supported by observation of an appropriate metastable peak. That ethylene loss in this particular instance does indeed, as previously proposed, involve the two β -carbon atoms follows from the spectra of the deuterated derivatives, where the appropriate shifts are observed. It becomes apparent that the overwhelming majority of M-28 ions observed as such (Structure 1) cannot serve as precursors for the generation of M-70 ions or fail--in other words--to eliminate ketene in subsequent decomposition. The fact that ions resulting from loss of both β -carbon atoms (Structure 2) exhibit significantly shorter lifetimes and escape detection due to rapid further ketene elimination appears qualitatively understandable. Its protonated isomer (Structure 1) would require transfer of two hydrogen atoms in loss of ketene and, consequently, exhibit enhanced lifetime leading to its almost exclusive detection.

Extrapolation of the mechanistic concept abstraction-induced C-N bond cleavage to both expanded ring systems and extended acyl substituents is compatible with the following observations (Scheme 2):

Loss of ethyl radicals incorporating α -carbon atoms can be ascertained in the case of N-acetylpiperidine; however, the operation of an additional competing process of comparable importance and the simultaneous production of M-C₂H₄ ions of similar abundance impedes an exact evaluation of the relative contribution of the process. N-acetylhexamethyleimine, the seven-membered ring homolog, exhibits distinct peaks for losses of 29 and 43 mass units, both hydrocarbon fragments, as established by precise mass measurement. These peaks are shifted in part to M-33 and M-47 in the 2,23,3-d₄ derivative, a finding very well compatible with abstraction-induced C-N bond rupture.

To probe the influence of extended acyl side-chains upon this mode of fragmentation, N-n-butyl pyrrolidine was analyzed together with variously deuterated derivatives. In this case, the alkyl portion of the acyl moiety is sufficiently large to permit a McLafferty rearrangement, which does indeed account for the main portion of the M-28 fragments. Abstraction-induced α,β -carbon loss can be inferred from the spectrum of the deuterated analogs chiefly as a mode of secondary decomposition of these M-28 ions generated via McLafferty rearrangement, rather than as a primary process involving molecular ions. This follows from an inspection of the spectrum of 2,2,5,5-d₄ compound, which exhibits primary loss of 28 mass units followed by distinct loss of 30 mass units, as documented by the appropriate metastable peaks. No evidence exists for a reverse ordering of the steps.

The evidence presented lends support to the interference of a novel mode of fragmentation which more genuinely reflects amide-properties of N-acyl functionalities than their otherwise apparent amine-governed behavior. However, while these amide-type properties are conspicuously retained in the modified systems considered, their relative importance seems to diminish within the framework of the over-all fragmentation. The occurrence of these processes in the fragmentation of N-acetylpyrrolidine might be considerably favored by the geometry of the five-membered ring, which could, for instance, enhance the importance of the contribution of a concerted process. On the other hand, the availability of additional competing pathways of fragmentation due to the larger molecular size of the homologs might diminish the relative importance of the abstraction-induced process. Projection of the concept of amide-dominated fragmentation to simple non-cyclic acylated amines appears to have limited applicability, as can be concluded from a preliminary study (2) of suitably labeled tertiary acetamides. However, it might be expected that the observed inhibition of secondary ketene loss from certain fragment ions can provide a convenient diagnostic means for facile recognition of abstraction-induced processes.

Acknowledgement. Financial support was provided by National Aeronautics and Space Administration Grant NGL 05-003-003 and Contract NAS 9-7889.

REFERENCES

- (1) J. M. Tesarek, W. J. Richter and A. L. Burlingame. *Organic Mass Spec.* 1, 139 (1968).
- (2) W. J. Richter, unpublished results, this laboratory.

INTRAMOLECULAR HYDROGEN REARRANGEMENT PRIOR TO FIELD-INDUCED DISSOCIATION

P. Schulze, W.J. Richter and A.L. Burlingame

Space Sciences Laboratory, University of California, Berkeley, California 94720

When a molecule is subjected to a sufficiently high, static electric field ($\sim 10^7$ V/cm) perturbation of its potential barrier permits the tunneling of a valence electron to the emitter anode to form a molecular ion-radical (1). Since the residence time of this molecular ion in the high field region is less than 10^{-12} seconds, Beckey and co-workers (2,3) have claimed recently that rearrangement processes prior to field-induced dissociation occur too slowly to yield appreciable abundances ($> 0.1\%$ of base peak) of positively charged fragment species, excepting as decomposition processes taking place during or after acceleration for mass analysis, i.e., metastable ions, or as ion-molecule reactions occurring in the condensed phase, i.e., the adsorption layer on the field anode (4).

During recent investigations of carboxylic esters by field ionization, we found, however, a number of fragment ions of surprising prominence which can arise only from field-induced dissociation of rearranged molecular ions. That the processes represented by these peaks are genuine unimolecular gas phase reactions has been deduced from an analysis of the kinetic energies of species in question. The techniques employed were similar to the decoupling techniques which have been employed for the detection of metastable transitions during acceleration (5).

Of particular prominence were $C_nH_{2n}^+$ ions formed by several aliphatic esters, e.g., n-propyl acetate, propionate and n-butyrate (Fig. 1). In these compounds, the field-induced rearrangement ions at m/e 42 ($C_3H_6^+$) even represent the base peaks of the FI mass spectra. The process itself corresponds formally to a McLafferty rearrangement with charge retention on the olefinic moiety thus formed. The equivalent rearrangement in electron impact induced fragmentation is of only little importance, as is the complementary process with opposite charge retention on the acyl portion of the molecule ($M-42$ ions). Suppression of this latter process is probably due to competing double hydrogen transfer prior to dissociation. In this case a protonated carboxylic acid fragment is produced as the more stable species. These ions are also observed with remarkable abundance in the FI spectra.

For the elimination of neutral carboxylic acid moieties from alkyl alkanoates under electron impact, it is known that hydrogen transfer prior to O-alkyl cleavage proceeds with little specificity. The abstraction takes place mainly from alpha and beta positions of the alkyl substituent involving favorable six- as well as five-member transition states (6).

Employing deuterium-labeled derivatives of n-butyl acetate, it could be shown that field induced rearrangement proceeds with almost exclusive transfer of beta hydrogen atoms, i.e., with specific involvement of cyclic six-membered transition states.

This preference for charge retention by the olefinic rather than the carboxylic acid fragment is in obvious contrast to the behavior of the model compounds under electron impact. This phenomenon, which seems, in addition, to pertain to related classes of compounds, can be rationalized by considering the different kinds of processes involved as well as the different sources of energy available to the decomposing species. Thus, sufficient excess energy is transferred to the molecule during ionization by electron impact to permit almost any kind of bond rupture, whether of ionic or radical nature. Radical and ionic processes will occur depending upon the thermodynamic properties of the possible products. Field ionization, however, provides almost no excess energy for the molecular ion, thus limiting fragmentation possibilities to processes promoted by interaction of positively charged, or at least of sufficiently polarized, bonds with the very strong electric field. Consequently, the typical mode of fragmentation to be expected would reflect heterolytic rather than homolytic reaction. For the present case, the rearranged molecular ion M_1 would more probably undergo ionic dissociation to m/e 42 much more readily than a radical-triggered cleavage to m/e 60 (Fig. 2). The rate-accelerating effect of the electric field on the rupture of polarized bonds in the course of ionic (i.e., non-radical) processes could be viewed as an analogy to the promotion of heterolytic reactions by polar media in solution chemistry. Measurements yielding information about the time elapsed between ionization and fragmentation show that these rearrangement ions are not formed instantaneously with ionization, i.e., in less than 10^{-12} sec. These short times are only observed for such single bond cleavages normally observed in field dissociation.

Although some rearrangement ions are observed within 10^{-12} sec. as shown by their occurrence in the normal FI mass spectrum, the majority was found to be formed 10^{-11} to

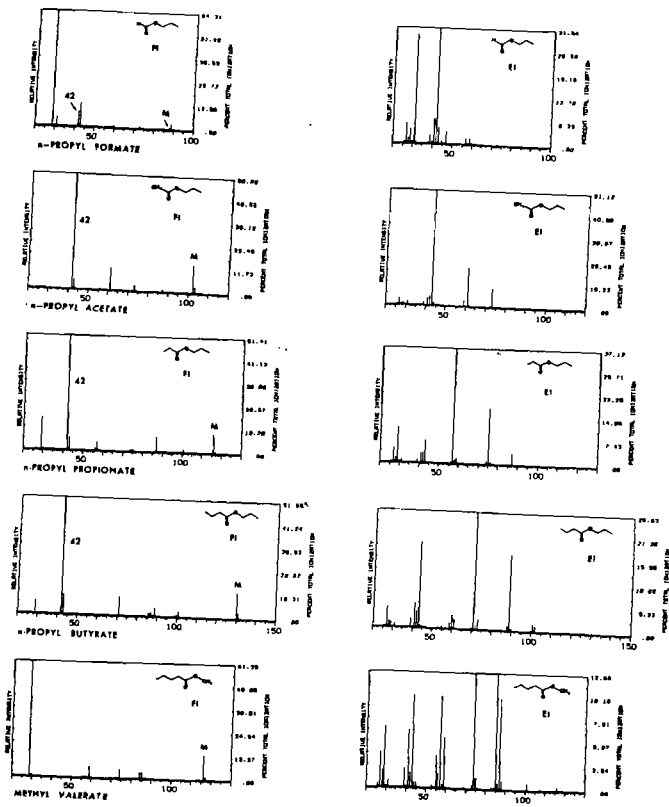


Figure 1

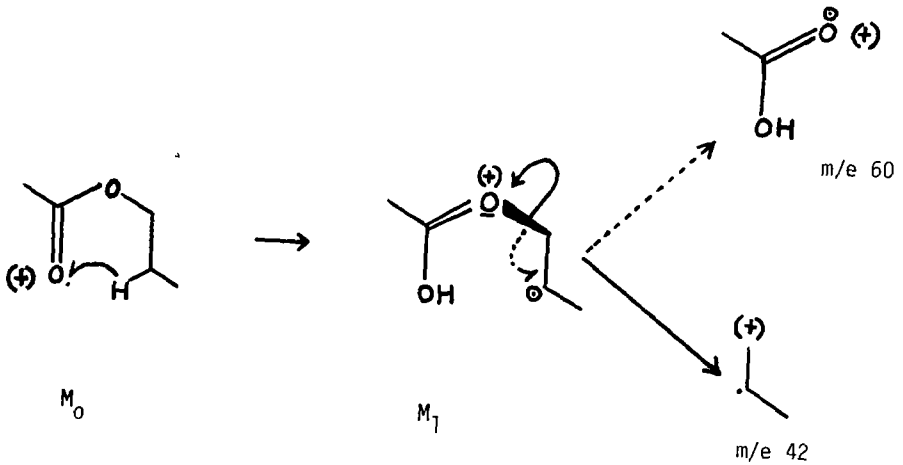


Figure 2

10-10 sec. after ionization. These data appear compatible with a concerted as well as sequential course of the process as long as both steps are sufficiently fast. In view of potential applications for distinguishing between two major classes of fragmentation reactions, the scope and limitations of abstraction induced field dissociation are currently being explored in further detail.

Acknowledgement. The authors are indebted for financial support of this research to the National Aeronautics and Space Administration, Grant NGL 05-003-003 and Contract NAS 9-7889.

References

- (1) J. Block, in Advances in Mass Spectrometry Vol. 4 (E. Kendrick, Ed.), The Institute of Petroleum, London, 1968, p. 791.
- (2) H. D. Beckey, H. Key, K. Levson and G. Tenschert, J. Mass Spectrometry and Ion Physics, 2, 101 (1969).
- (3) H. D. Beckey, J. Mass Spectrometry and Ion Physics, 1, 93 (1968).
- (4) H. D. Beckey and P. Schulze, Z. f. Naturforschung, 21a, 214 (1966).
- (5) P. Schulze and A. L. Burlingame, J. Chem. Phys., 49, 4870 (1968).
- (6) W. Benz and K. Biemann, J. Am. Chem. Soc., 86, 2375 (1964).

MECHANISTIC STUDIES IN THE FRAGMENTATION
OF SUBSTITUTED BENZYL COMPOUNDS.

Peter Brown

Department of Chemistry, Arizona

State University, Tempe, Arizona 85281

In studies intended to elucidate the energy/structure characteristics of daughter ion A^+ produced directly from a molecular ion, e.g., $M^+ \longrightarrow A^+ + Y$, two types of information may be obtained.

- (i) From decomposition of A^+ . This includes fragmentation pattern, especially isotope distribution in labelled compounds, metastable ion peaks, and ion/molecule reactions. Such data refers to the activated complex for A^+ decomposition, and gives information only about those daughter ions energetic enough to decompose.¹
- (ii) From formation of A^+ . This includes ionization and appearance potentials, reaction rates, and isotope effects. Such data reflect the transition state for formation of all A^+ ion from M^+ .

It is suggested that formation rather than decomposition data will be more useful in characterizing the energy/structure of A^+ because (a) according to Hammonds Postulate, the transition state resembles the product rather than the reactant for an endothermic reaction (e.g., bond cleavage); (b) the daughter ion A^+ may possibly rearrange before decomposing.

The importance of conducting both kinds of experiments is emphasized.

Traditionally, isotope labelling and appearance potential measurements have been used for decomposition studies, and ionization and appearance potentials for formation investigations. In an attempt to extend the somewhat limited range of experimental methods available, simple kinetic methods² for estimation of ion formation activating energies (i.e., AP-IP) and metastable ion peak relative intensities³ for ion decomposition have been evaluated.

In order to overcome certain severe objections to the original simple steady state kinetic treatment,² it is suggested that the effect on activation energy for the smallest feasible structural change in isomers be compared, for the one major reaction $M^+ \longrightarrow A^+$. Thus m- and p-X substituted isomer pairs of aromatic compounds with the same substituent X have been employed, and the relative rate parameter Z_p/Z_m determined as a function of electron energy.^{4,5} In addition, metastable ion peak relative abundances for isomeric M^+ and isomeric A^+ ions have been recorded.

As test systems, compounds that have been studied by conventional techniques were selected, to allow critical comparison and evaluation of the newer techniques. These included the $M \longrightarrow M-Y$ reaction of a series of m and p-X substituted benzyl phenyl ethers ($Y = OC_6H_5$), ethyl benzenes ($Y = CH_3$) and toluenes ($Y = H$).

The correlations possible and the limitations of this approach will be discussed in papers submitted to Organic Mass Spectrometry.

References

1. S. Meyerson, P. N. Rylander, E. L. Eliel and J. D. McCollum, J. Am. Chem. Soc., **81**, 2606 (1959).
2. M. M. Bursey and F. W. McLafferty, ibid., **88**, 529 (1966).
3. T. W. Shannon and F. W. McLafferty, ibid., **88**, 5021 (1966).
4. P. Brown, ibid., **90**, 4459 (1968).
5. P. Brown, ibid., **90**, 4461 (1968).

Franck-Condon Factors for the Ionization of Nitrous Oxide

H. M. Rosenstock

Institute for Materials Research
National Bureau of Standards
Washington, D. C. 20234

Previous work on calculation of polyatomic Franck Condon factors has emphasized the determination of geometry changes on the basis of experimentally observed Franck Condon factors, using simple valence force fields to determine normal modes. The results obtained on acetylene and water were rather insensitive to the choice of force field. In the case of N_2O , there are available experimental Franck Condon factors for two ionizing transitions for which the geometries are known. These make possible a determination of the vibrational force field. It is found that it is possible to determine the value of the Bond-Bond interaction constant in the valence force fields of the two ion states. The physical basis for this is discussed. It is shown that simplified considerations relating vibrational excitation to changes in a given bond length are invalid.

PEAK HEIGHT DISTRIBUTION OF ORGANIC MASS SPECTRA

S. L. Grotch
 Jet Propulsion Laboratory
 Pasadena, California

INTRODUCTION

The gas chromatograph-mass spectrometer (GC/MS) is an instrument being considered for a Mars lander as part of Project Viking. Because of the large amount of mass spectral data produced by this instrument, there is a significant incentive to investigate the digital encoding of these data.

One important aspect of the data problem is the distribution of peak heights in mass spectra, i.e., the relative frequencies of occurrence of peaks within specified peak height ranges. This distribution is important in digital encoding for two reasons:

1. For most encoding schemes the average number of bits required to encode a mass spectrum (for a given mass and dynamic range) requires an estimate of the expected number of peaks which lie above a specified threshold.
2. Based on concepts of information theory⁽¹⁾ one would expect that, if mass spectral peak height information is to be encoded with maximum information content, the transitions between digital levels should be set so that equal numbers of peaks lie in each level. To make this transition assignment optimally, it is necessary to know the distribution of peak height.

Although these two considerations provided the primary impetus for this work, it is believed that these results may prove to be of more general interest. Two potentially important areas of application are those of pattern recognition⁽²⁾ and compound identification⁽³⁾

MASS SPECTRAL DATA

The approach adopted in this study was the use of a large library of mass spectral data to serve as a statistical model of spectral behavior. Four sources of low resolution mass spectral data were utilized:

1. The Dow Chemical Co. uncertified collection⁽⁴⁾ (1967 spectra).
2. A collection provided by Prof. K. Biemann⁽⁵⁾ of MIT, consisting of the ASTM collection and other spectra measured in his laboratory (2004 spectra).
3. A collection of 500 spectra provided by the Mass Spectrometry Data Centre⁽⁶⁾.
4. A group of 2261 certified spectra from the API collection and 150 spectra from the Manufacturing Chemists Association (MCA), provided by the MSDC.

For purposes related to Project Viking the spectra from sources 1 and 2 above were merged, redundancies removed, and the resultant collection was divided into two groups called Category I and Category II. Category I consisted of 1164 compounds thought to be particularly relevant to a proposed GC/MS experiment for a Mars lander. Compounds specifically excluded from Category I were: (a) all compounds containing halogens or deuterium, and (b) all non-hydrocarbons with molecular weight greater than 175. Category II consisted of all remaining non-redundant spectra from sources 1 and 2 (2234 spectra). The primary purpose of this division was to provide the spectra of a group of compounds relevant to the Viking GC/MS experiment which could be studied in more detail in future studies (Cat. I), while also providing a second group (Cat. II) to assess the sensitivity of results to the choice of library. The spectra from sources 3 and 4 will eventually be merged into Categories I/II, but in this study they were considered as two additional groups. Several characteristics of the four groups (Cat. I, Cat. II, MSDC, API/MCA) are summarized in Table I.

It should be emphasized that the somewhat arbitrary divisions imposed by the Viking application did not affect the basic conclusions of this study. A number of other compound groupings were also studied, all yielding the same general conclusions regarding the peak height distribution.

PEAK HEIGHT DISTRIBUTION OF COLLECTIONS OF SPECTRA

The mass spectral data used in this study were stored on digital magnetic tape, and an IBM 7094 computer was used for all calculations. Each spectrum was normalized so that the maximum intensity peak (base peak) was assigned a value of 100.0. The minimum peak

TABLE I. MASS SPECTRAL LIBRARY

GROUP	NUMBER SPECTRA	AVERAGE MOL. WT.	MOLECULAR WEIGHT RANGE	AVG. NUMBER PEAKS/SPECTRUM
CATEGORY I	1164	132.1	16-536	71.2
CATEGORY II	2234	171.3	18-536	94.3
MSDC	500	234.0	59-862	102.7
API/MCA	2411	177.2	2-1318	111.8

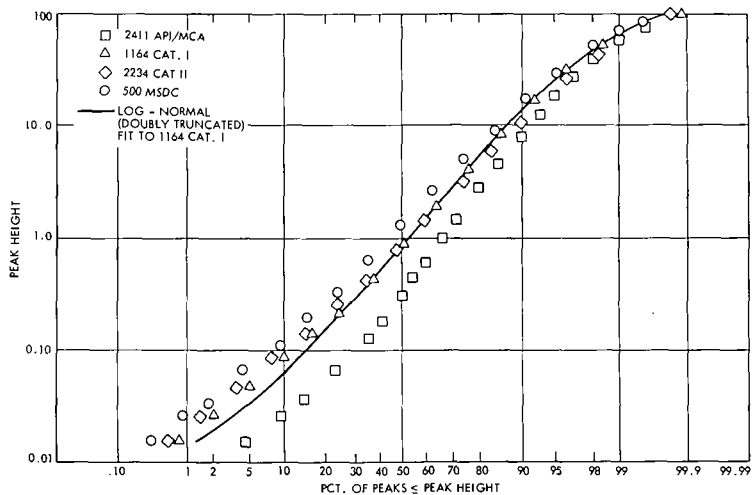


Fig. 1. CUMULATIVE PEAK HEIGHT DISTRIBUTION FOR FOUR GROUPS OF SPECTRA PEAKS ≥ 0.01

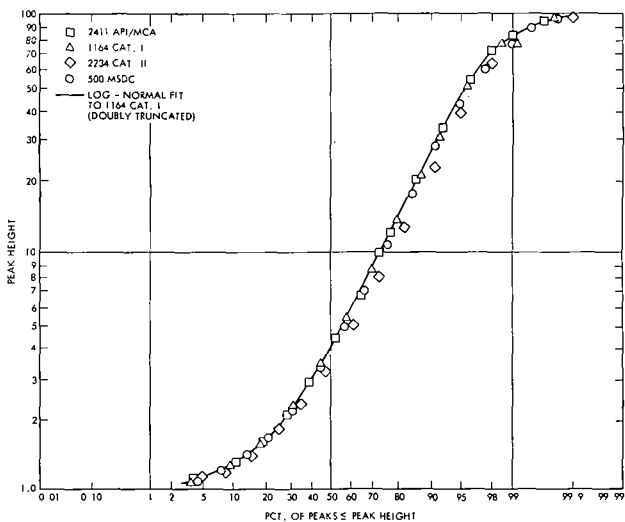


Fig. 2. CUMULATIVE PEAK HEIGHT DISTRIBUTION FOR FOUR GROUPS OF SPECTRA PEAKS ≥ 1.0

height reported for any of the spectra was 0.01% of the base peak. However, approximately 25% of the spectra used contained no peaks with heights less than 0.1% of the base peak. Only low resolution spectra (integral mass) were used.

For the calculation of the group peak height distribution, the combined distribution was considered to be the aggregate sum of all of the individual spectral peaks in the collection. Peaks at the same mass number in different spectra were considered as distinct peaks.

A convenient means for presenting these results is in terms of a cumulative peak height distribution plot, i.e., the fraction of all peaks less than or equal to a given peak height vs. peak height. In Figure 1 are given the cumulative peak height distributions for the four groups of spectra. These results are plotted on a log-probability grid which has the property that, if the logarithm of a variable is distributed normally, the cumulative distribution will plot on this grid as a straight line.

Several observations are apparent from these plots:

1. From the near linearity of these data in the central portion of the curve when plotted on a log-probability grid, it appears that the logarithm of the peak height is in fact distributed normally for each group of spectra. (The curvature observed near peak heights of 0.01 and 100.0 will be discussed in more detail shortly.)
2. For each grouping of spectra the distribution of peak heights is highly non-linear. For example, for all of the groups, approximately one-half of the reported peaks lie below a peak height of only 1% of the base peak.
3. Three of the four groupings show similar peak height distributions over the entire range of peak heights (0.01-100.0). The API/MCA group, however, appears to have a significantly larger number of smaller peaks than do the other groupings. This is probably due to the fact that the API spectra were derived for purposes of quantitative analysis and hence a greater emphasis was placed on the determination of smaller peaks.

Each of the cumulative distributions shown in Figure 1 exhibits an asymptomatic curvature towards peak heights of 0.01 and 100. This results from the truncated nature of the distributions under consideration. That is, no peak heights less than 0.01 are reported in these data, and by the nature of the normalization procedure, no peaks greater than 100.0 can exist.

Also presented in Figure 1 is a true log-normal curve truncated at both 0.01 and 100.0 fitting the data of Category I. This truncated curve was obtained by calculating a log-normal distribution of specified mean and variance and considering the distribution of only those peaks in the range of $.01 \leq \text{peak height} \leq 100.0$. The truncated log-normal curve and the calculations of chi-square (7), indicate that excessively large disagreements occur in the lower range of peak heights ($< 1\%$). Most likely this is due to the experimental difficulty in accurately measuring small peak heights as evidenced in the fact that many spectra did not report any peaks with height $< 0.1\%$. The addition of only 1-3 peaks/spectrum in this lower range causes the data to agree well with the log-normal fit.

The cumulative peak height distributions for the four groups, considering only the larger peaks (i.e., only those peaks with heights $> 1\%$ base peak), are given in Figure 2. Here it can be seen that the distributions for the groups are more nearly the same than when the smaller peaks were included. These data also appear to follow a log-normal distribution (truncated at peak heights of 1 and 100) as can be seen in Figure 2 where the solid curve is such a doubly truncated log-normal distribution fitting the Category I data. This suggests that the "average" peak height distribution for the larger spectral peaks is probably insensitive to the choice of compounds forming the aggregate. In Project Viking it is likely that only the larger peaks will be encoded and this result provides assurance that the peak height distribution should not be sensitive to the choice of library.

PEAK HEIGHT DISTRIBUTION OF INDIVIDUAL SPECTRA

The data presented thus far represent the average peak height distributions for large collections of mass spectra. It is also interesting to examine the corresponding distributions for individual pure compound spectra.

The peak height distribution for propane⁽⁴⁾ is presented in Figure 3. A log-normal distribution (not truncated) with a log mean and variance calculated from the propane distribution is also shown. Since the propane spectrum contains only 29 peaks, the

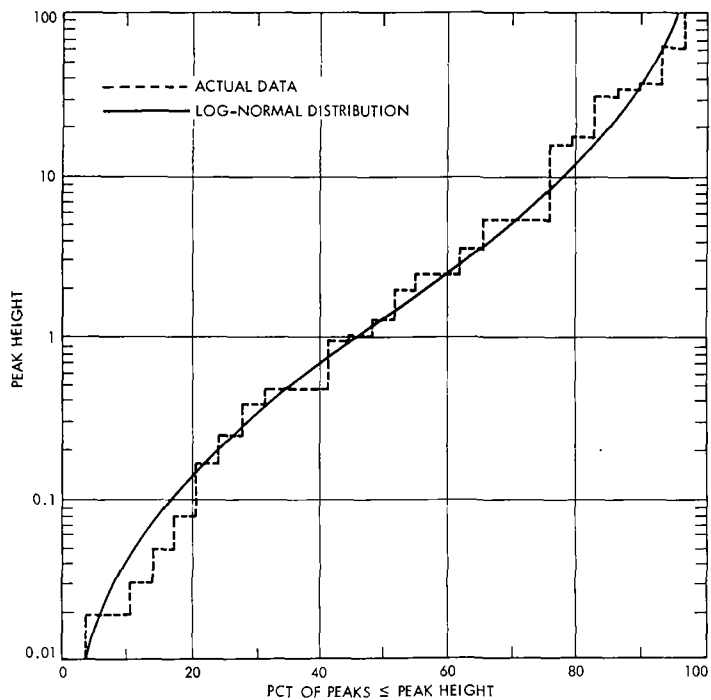


Fig. 3. CUMULATIVE PEAK HEIGHT DISTRIBUTION OF PROPANE (REF. 1)

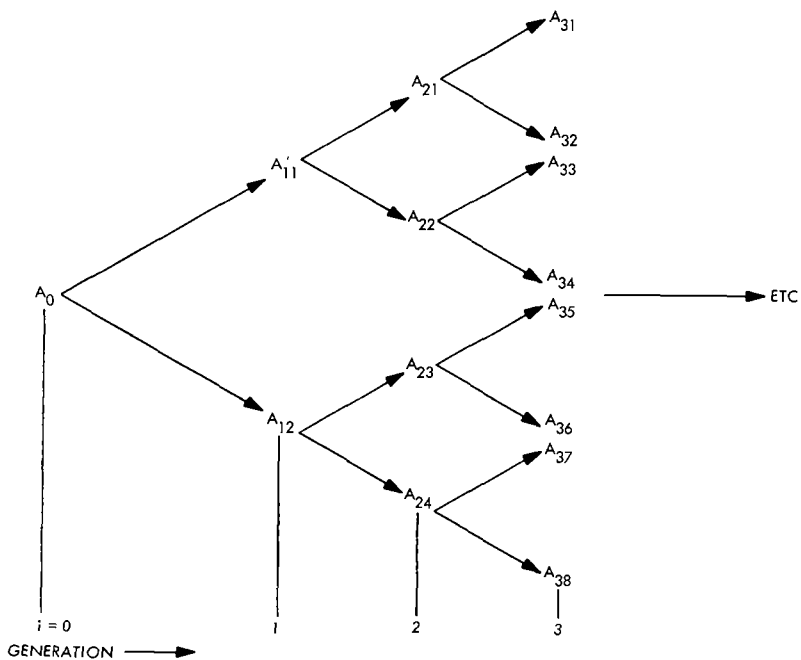


Fig. 4. CASCADE REACTION SCHEME

discontinuous nature of the cumulative distribution is more apparent than for the larger spectral groupings. It can be seen that the data are reasonably well fit by a log-normal curve. Approximately one hundred individual spectra were compared in the manner of Figure 3 and all could be approximated by a log-normal distribution.

It appears that the underlying cause of the log-normal distribution for large groups of spectra is that each individual spectrum conforms to a log-normal distribution. Calculations show that the mean and the variance of log height of individual spectra are each distributed approximately normally. In these distributions, moreover, the variance of the variance is much less than the variance of any individual spectrum. It can be shown that, if this is the case, the resultant heterogeneous mixture of distributions will be distributed normally.

The log-normal distributions found for individual spectra can probably be ascribed to a common origin of such distributions; namely, that "if the change in magnitude corresponding to a given cause is proportional to the intensity of that cause and further to the size of the element, the distribution obtained will be log-normal" (Ref. 7, pg. 197).

It should be mentioned that the distribution of peak heights will remain log-normal if the spectra are normalized in terms of the total ion current rather than the maximum peak height, since this merely involves a linear operation on each spectrum.

REACTION KINETIC MODEL

An attempt has been made to describe the observed peak height distribution for groups of spectra in terms of a simplified reaction kinetics model. Since the model describes a very complex system, it was felt that a gross characteristic such as peak height distribution would provide a first test of model validity. In order to obtain sufficient statistics for this test, each of a group of 600 spectra from Category I was fit using the model and the resultant peak height distribution was compared with the actual experimental data.

The formation of ionized species in a mass spectrometer is assumed to proceed in a cascade process as illustrated in Figure 4. For each generation i ($i = 0, 1, 2, \dots$), the j^{th} distinct ion A_{ij}^+ , is assumed to disintegrate further into m_{ij} daughter products. (In Figure 4, all $m_{ij} = 2$). If all reactions are assumed to be first order, and irreversible, with rate constant k_i for the i^{th} reaction, the kinetic equation describing the system is:

$$\frac{dC_{ij}}{dt} = -k_i m_{ij} C_{ij} + k_{i-1} C_{i-1,n} \quad (i > 0) \quad (1)$$

C_{ij} is the concentration of species A_{ij}^+ at time t , and $C_{i-1,n}$ is the concentration of the species n in the $i-1^{\text{st}}$ generation which disintegrates into A_{ij}^+ .

If it is assumed that only the first ionic species A_0^+ is initially present, the appropriate initial condition is:

$$\begin{aligned} \text{at } t=0 \quad C_0 &= C_0^0 \\ \text{at } t=0 \quad C_{ij} &= 0 \text{ for } i > 0 \end{aligned} \quad (2)$$

To make the problem tractable in terms of only a few parameters, it is assumed that all rate constants are equal to a constant, k . If it is further assumed that the increase in moles in each generation also is a constant (i.e., all $m_{ij} = m$), the resulting solution of differential equation (1) subject to boundary condition (2) is:

$$\frac{C_{ij}}{C_0} = \frac{(ktm)^i e^{-ktm}}{m^i i!} \quad j = 1, 2, \dots, m^i \quad (3)$$

This solution is a slightly modified form of the classical Poisson process with Poisson parameter $\lambda = ktm$ (7). For $m=1$ (no increase in moles as the reaction proceeds) the resultant distribution is a true Poisson process (Reference 8, pg. 38).

The interpretation of Equation 3 in physical terms is as follows. It is assumed that in the i^{th} generation of ions ($i=0, 1, 2, \dots$) there are m^i independent species, each having a concentration given by Equation 3 (i.e., $C_{i1} = C_{i2} = C_{i3}$, etc.). It is seen that this concentration is a function of the two model parameters, m and λ .

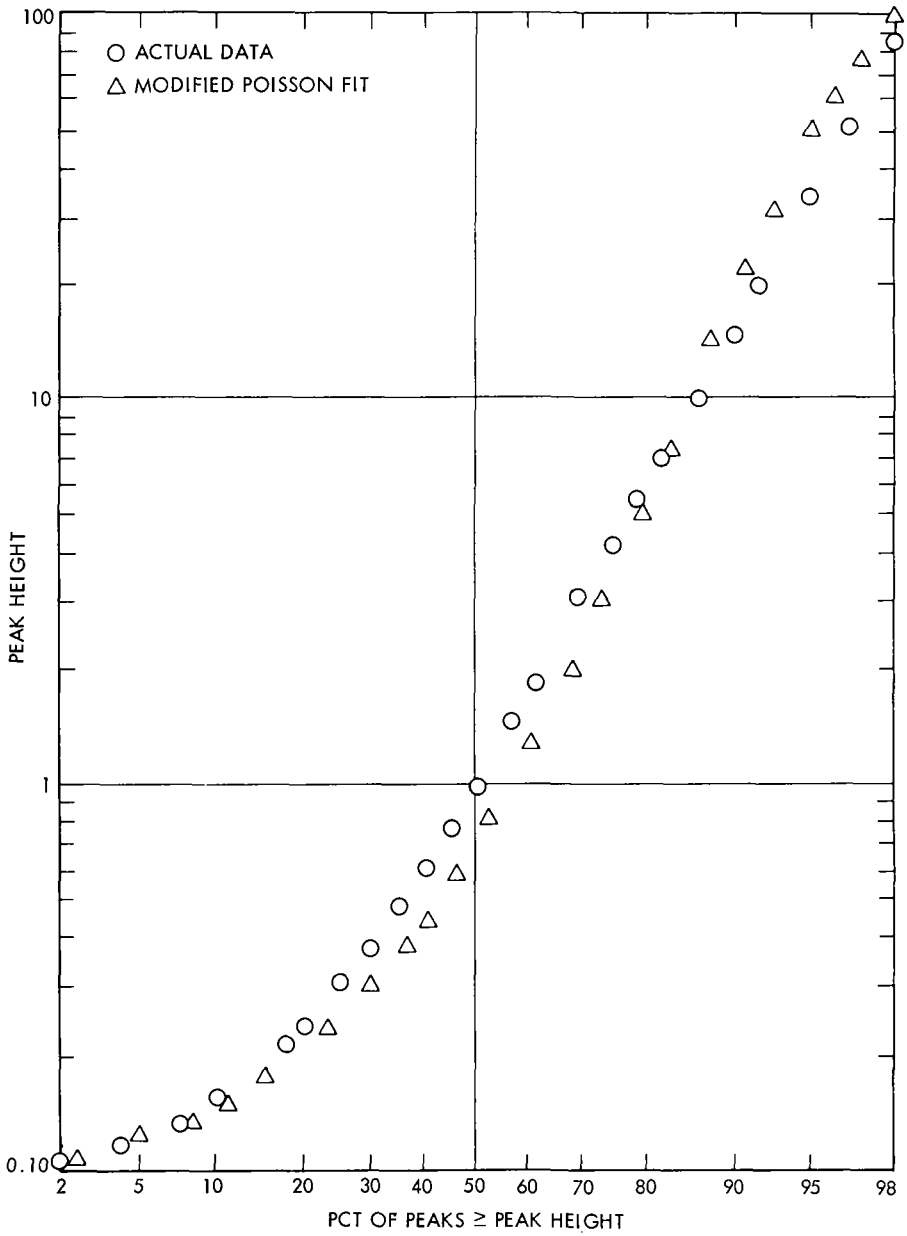


Fig. 5. CUMULATIVE PEAK HEIGHT DISTRIBUTION - 600 SPECTRA ONLY ≥ 0.10

It should be noted that even for $m=1$, where the right hand side of Eq. 3 is of the Poisson form, the distribution of concentration is not statistically Poisson. The reason for this apparent paradox is that Eq. 3 describes the magnitude of the random variable, whereas in the statistical view, the right hand side is the probability that the random variable will be equal to a given value. Thus, the statistical distribution of concentration resulting from Eq. 3 will not be Poisson but will be highly skewed to smaller peaks.

DETERMINATION OF MODEL PARAMETERS

In order to fit the proposed kinetic model to actual mass spectral data, the following procedure was followed for each of 600 different organic mass spectra (mol. wts. 16-157). The resultant individual fits were then combined to generate a group peak height distribution which was compared with the actual data for the same spectra.

1. The modified Poisson distributions generated from Eq. 3 were normalized in the same manner as the experimental data.
2. Since the available spectra reported peak heights only above 0.01, only heights greater than this value were considered.
3. A maximum of 6 generations ($i \leq 6$) was assumed to occur in the cascade process. Calculations show that the restriction of a minimum peak height of 0.01 (step 2) cuts off most spectral distributions before $i=6$. It is obvious that the cascade model must break down in a finite number of generations due to the finite divisibility of compounds.
4. The multiplication factor for ionic species, m , is calculated by fitting the total number of peaks predicted by the model (with heights ≥ 0.01) with the experimental data. (The average value of m found for the 600 spectra was 2.4.)
5. The remaining Poisson parameter λ , was determined by fitting the total ion current (i.e., the sum of all of the peak heights) of the model with the experimental data.

In summary, then, for each individual spectrum the two model parameters were determined by: (1) fitting the total number of peaks, and (2) fitting the total ion current.

COMPARISON OF THE MODEL WITH ACTUAL DATA

The model predictions from the individual fits were combined into larger aggregates and the peak height distributions were compared with the corresponding experimental data as shown in Figure 5. It is seen that the simple cascade model predicts the observed peak height distribution reasonably well for peaks > 0.10 .

However, the model described here is obviously too crude to predict other important details of mass spectra. For example, when fit as above, the height of the second highest peak predicted by the model agrees only qualitatively with that observed experimentally. Nevertheless, the scheme proposed here may prove to be a valuable starting point for a more refined model (probably in terms of more free parameters). It may prove possible to predict additional spectral details or to suggest relationships between spectral and chemical parameters.

CONCLUSIONS

1. The mass spectral peak height distributions of individual pure compounds and large groups of compounds appear to be log-normal. Since the peak height distribution is known in analytical terms, further studies of digital encoding will not necessitate the time-consuming use of individual spectra or selected spectral libraries.
2. The peak height distribution of the larger peaks (height $> 1\%$) for large collections of compounds appears to be insensitive to the choice of compounds. Since it is generally these peaks which are of most interest, certain encoding schemes can be made relatively insensitive to the choice of library.
3. When fit to pure compound spectral data, a very simple cascade reaction scheme yields a peak height distribution agreeing with that experimentally observed.

REFERENCES

1. "The Mathematical Theory of Communication," C. E. Shannon, W. Weaver, The University of Illinois Press, Urbana, Illinois (1963).
2. B. R. Kowalski, P. C. Jurs, T. L. Isenhour, C. N. Reilley, Analytical Chemistry, 41 496 (1969).
3. L. R. Crawford, J. D. Morrison, Analytical Chemistry, 40 1469 (1968).
4. "Uncertified Mass Spectral Data" Ed. R. S. Gohlke, Eastern Research Laboratory, Dow Chemical Co., Framingham, Mass., October 1963.
5. K. Biemann, personal communication, June 1968.
6. Mass Spectrometry Data Centre (MSDC), Aldermaston, Great Britain, (Spectral serial numbers MSDC-1 to MSDC-500).
7. "Statistical Theory with Engineering Applications," A. Hald, J. Wiley, New York (1952).
8. "The Foundations of Chemical Kinetics," S. W. Benson, McGraw-Hill, N.Y., 1960.

VARIATIONS IN U^{234} CONCENTRATION OF NATURAL URANIUM*

R. F. Smith and J. M. Jackson
Union Carbide Corporation, Nuclear Division
Paducah Gaseous Diffusion Plant
Paducah, Kentucky 42001

ABSTRACT

Uranium ore concentrates from sixteen world sources have been analyzed to determine variations in the U^{234} content of natural uranium. A spread of approximately 7.5% of the U^{234} content was apparent among the various sources. The lowest concentration, 0.00500 ± 0.00002 Wt.% U^{234} , was obtained on ore concentrate from Mines Development in Edgemont, South Dakota. The highest concentration, 0.00539 ± 0.00002 Wt.% U^{234} , was obtained on Belgian Congo Pitchblende. The latter is in substantial agreement with "best values" quoted by Glenn T. Seaborg.

Of the sixteen world sources, five showed significant U^{234} differences between independent lots. The maximum spread between lots from the same source was about 1.5% of U^{234} assay. Independent lots from the remaining eleven sources were not significantly different.

- * This work was supported by the United States Atomic Energy Commission. The report (KY-581) will be available from:
Clearinghouse for Federal Scientific and Technical Information
National Bureau of Standards, U. S. Department of Commerce
Springfield, Virginia 22151

Mass Spectrometric Determinations of
2200 m/s Neutron Cross Sections of Fissile Nuclides

M. Lounsbury, R.W. Durham and G.C. Hanna
Atomic Energy of Canada Limited
Chalk River, Ontario, Canada

INTRODUCTION

Most measurements of alpha, (the ratio of the neutron capture to fission cross section,) for thermal neutrons have been made in reactor spectra with an appreciable contamination of epithermal neutrons and with some uncertainty in the neutron temperature. This makes the interpretation of the experimental measurements, in terms of the standard 2200 m/s cross sections, difficult.

This paper describes an experiment designed to yield 2200 m/s values of alpha for U-233, U-235 and Pu-239 with little ambiguity in the spectral conditions. For this work, thermionic emission mass spectrometry was combined with isotope dilution, using U-238 and Pu-242 as internal spikes for uranium and plutonium, to determine the destruction of the fissile nuclides and the growth of the capture products.

EXPERIMENTAL PROCEDURE

Samples were prepared by mixing together pairs of the fissile nuclides. Series A samples consisted of 3.5 mg each of fissile U-235 and Pu-239 and 0.35 mg each of U-238 and Pu-242 spikes, diluted with 20 times their weight of aluminum to reduce neutron self-shielding. Series B samples were similar except that the fissile pair was U-233 and Pu-239.

The samples were accompanied by cobalt-aluminum spectrum monitors and irradiated inside a light-water annulus in a thermal pit in a bismuth rod position between the core and the graphite thermal column of the NRU reactor. This provided a well-thermalized neutron spectrum with a very low Westcott epithermal index, r , of $(2.4 \pm 0.2) \times 10^{-4}$. The temperature of the water was maintained at $37.5 \pm 0.5^\circ\text{C}$ throughout the one year irradiation. Thermalization and self-shielding calculations indicated that the effective neutron temperature was $51 \pm 3^\circ\text{C}$. The integrated neutron flux was 0.7 n/kb, (0.701 n/kb for Sample A, 0.710 n/kb for B).

After a cooling period of one year, the samples were separated into uranium and plutonium fractions and analyzed with a Consolidated Electro-dynamics triple-filament mass spectrometer Model 21-703. The mass spectra were scanned magnetically, and the ion currents measured with a Faraday cage detector, vibrating reed electrometer and pen recorder.

EXPERIMENTAL RESULTS

The isotopic analysis results are summarized in Table 1. In all cases, the standard error is quoted; it ranges from about $\pm 10\%$ for the minor isotopes to about $\pm 0.1\%$ for the major isotopes.

The results obtained for the 2200 m/s parameters are summarized in Table 2. The 2200 m/s absorption cross sections of U-233 and U-235 were taken to be 575.64 ± 3.28 b and 679.48 ± 2.54 b respectively, from published transmission data. The Westcott g factors and their uncertainties were taken from Westcott's latest tables (AECL-3255, in press).

TABLE 1

Sample A (235/239)					
Uranium Fraction			Plutonium Fraction		
Mass	Initial	Final	Mass	Initial	Final
234	0.062±0.002	0.091±0.002	238	0.057±0.002	0.112±0.002
235	100.	100.	239	100.	100.
236	0.065±0.003	8.728±0.009	240	1.214±0.002	32.861±0.030
238	9.529±0.009	15.099±0.012	241	0.290±0.002	3.235±0.004
			242	6.210±0.005	13.945±0.012

Sample B (233/239)					
Uranium Fraction			Plutonium Fraction		
Mass	Initial	Final	Mass	Initial	Final
233	100.	100.	238	0.057±0.002	0.110±0.002
234	0.056±0.002	4.090±0.004	239	100.	100.
235	0.100±0.002	0.225±0.002	240	1.215±0.003	32.926±0.030
236	0.000±0.000	0.017±0.002	241	0.291±0.003	3.255±0.003
238	9.622±0.008	14.424±0.014	242	6.197±0.005	13.932±0.010

TABLE 2

QUANTITY	2200 m/s VALUE	ERRORS			
		M.S.	OTHER σ 's	SPECTRUM	σ FACTOR
α (233)	0.0899	± 0.0004	0	0	± 0.0017
σ_Y (234)	96.1 b	± 2.0	± 0.4	?	?
α (235)	0.1702	± 0.0007	0	0	± 0.0020
α (239)	0.3594	± 0.0009	± 0.0011	± 0.0015	± 0.0046
σ_a (239)	1017.7 b	± 4.0	± 1.3	± 4.8	± 2.9
σ_Y (240)	289.3 b	± 0.6	± 1.1	± 0.6	?

DISCUSSION

The results obtained for α (U-233) and α (U-235) are slightly lower than those recommended by Westcott et al in 1965 (At.En.Rev. 3 (2), 3-62), but not outside their errors. For Pu-239, the result for α agrees with Westcott et al's value, but is more accurate. The σ_a value is higher than the recommended 1008.1 ± 4.9 b, though hardly significantly. It agrees satisfactorily with the best value from transmission measurements which is 1012.0 ± 6.3 b.

The authors gratefully acknowledge the contributions of their colleagues at Chalk River: C.B. Bigham, F.W. Molson, J.A. Schruder, Miss C.M. Sprague and S.A. Kushneriuk. A complete description of this work will be given in the AECL series of publications.

A DIFFUSION-THERMAL IONIZATION SOURCE
FOR THE ASSAY OF TRACE METALS

W. G. Myers and F. A. White

Division of Nuclear Engineering and Science
Rensselaer Polytechnic Institute
Troy, New York 12181

Introduction

A new thermal ionization source has been developed for the mass spectrometric assay of trace metals. Previous attempts to enhance the ion emission of such sources have involved changes in source design and/or treatment of the sample and ion emitting surface. However, sample evaporation and chemical reactions on the surface have either retarded the ionization process or restricted the operation of these sources to temperatures well below optimum.

The concept of this new source is to utilize a diffusion mechanism in addition to thermal (surface) ionization, in order to obtain a higher ionization efficiency and a mass spectrum which is not obscured by impurities or superposed molecular spectra. The sample element together with its isotopic "spike" is "encapsulated" within an appropriate "filament" that is made of a refractory metal of high work function. After insertion in the mass spectrometer, the filament is operated at a high temperature, which causes the sample atoms to diffuse to the exterior surface and become ionized by thermal ionization. High temperature operation of this source provides the following potential advantages over conventional ion sources: (1) prompt loss of the sample in the form of neutral vapor is minimized, (2) the diffusion time required for the sample atoms to reach the ionizing surface allows this surface to become free of impurities and to stabilize with a work function that is characteristic of the pure metal, (3) the diffusion controlled release of the sample provides a longer time to focus the spectrometer and conduct the analysis, (4) the elevated filament temperature minimizes the "mean residence time" and reduces the probability that atoms of the sample will undergo surface recombination prior to ionization, and (5) the diffusion process promotes the generation of an "atomic" ion beam as the diffusion process dissociates virtually all the sample molecules. Therefore, the chemical form of the sample plays a minor role.

Experimental Results

A number of techniques or filament configurations were investigated to test the sample encapsulation condition including; physical vapor deposition, spot-welding, and tubular containment. The ion filament material used was high purity rhenium, while enriched NBS uranium isotopes were employed as the diffusant atoms. The fabricated filaments were operated over a temperature range of 3500 to 4000°F (2200-2480°K)⁻³ brightness, using rhenium cover thicknesses from 5×10^{-6} to 8.75×10^{-3} centimeters. In connection with this ion source development, measurements were also made of the diffusion coefficients of uranium in rhenium, in order that a comparison could be made of experimental results with theoretical calculations. A number of determinations were made over the temperature interval of 2530-2840°K (absolute) using the mass spectrometric procedure developed by Schwegler and White⁽¹⁾. This data indicated a dilute impurity diffusion coefficient equation for uranium in polycrystalline rhenium of:

$$D = (0.78 \pm 0.78) \exp\left(\frac{-107,000 - 20,000}{RT}\right) \text{ cal/mole}$$

Figure 1 shows the U^{235} ion emission profile from four different filaments having the same sample size ($\sim 3 \times 10^{-8}$ gm U^{235} , NBS U930) but rhenium "cladding" thicknesses deposited by a physical vapor deposition process. Filament temperatures were maintained at approximately 3700°F for all four runs. Curve A clearly demonstrates the result of operating an ordinary "canoe" filament (no metal cladding) at high temperatures. Here, most of the uranium sample is promptly lost by evaporation, leaving only a fraction of the sample on or impregnated within the surface of the filament. Curves B, C, and D show the effects that an increasingly thicker vapor deposit covering has on the retention and ultimate ionization efficiency of the sample. The shape of these ion emission curves requires an explanation which includes both sample diffusion mechanisms and changes in the ionization efficiency of the source. However, there does appear to be an optimum cladding thickness (Curve "C") for this type of encapsulation technique. This thickness, estimated in the order of 500 Å, is apparently heavy enough to retain and prevent most of the sample from evaporation, yet thin enough to evaporate away before too much of the sample can diffuse deep into the crystalline lattice of the substrate filament. At these operating temperatures (3700°F), uranium atoms would diffuse into the rhenium filament to a depth of 0.0001" ($\sim 25,000$ Å) in this period of time (4 minutes), producing a shallow "doped" filament. The experimentally observed ion emission decay from those filaments having vapor deposits of 500 Å or thicker (Curves C and D), followed a rate characteristic of the depletion of a doped, thin plate.

Satisfactory results were obtained also when uranium samples were sandwiched between thin (0.0005") rhenium ribbons and fused together with a spot welder. Limited success was found using 0.002" walled x 0.015" O.D. rhenium tubing formed by chemical vapor deposition. Two additional encapsulation methods which appear to merit consideration are: (1) electron-beam welding, and (2) sputtering. An electron-beam welder permits the welding together of very thin ribbons of refractory metals under high vacuum. The sputtering process is capable of laying down heavy deposits in a very short period of time. In addition, the energy of the sputtered atoms are higher than those created by physical vapor deposition, and are known to produce coatings having better substrate adhering properties. The ability of the process to deposit alloys and non-metallics suggests the possible deposition of materials having ionization properties (high work function, melting point, etc.) superior to those of the substrate.

Conclusions

An improved thermal ionization source for the mass spectrometric assay of trace metals has been developed, based on the concept of "implanting" sample and tracer atoms within the crystalline lattice of a refractory material. There is some latitude in the method or technique that is employed to achieve this "implanted" or "doped" condition, for subsequently, the temperature dependent diffusion and thermal ionization processes can be controlled to provide both desired source characteristics as well as optimum ionization efficiencies. The diffusion controlled release of the "spiked" sample, regardless of its original chemical form, from within the source material, provides ion emission currents that allow precise isotopic ratio measurements to be made. On the basis of the experimental results obtained, it would appear that all the advantages of high temperature operation of thermal ionization sources were achieved, while either reducing or eliminating their inherent disadvantages. The sample encapsulation techniques investigated in this work, while not always fulfilling theoretical boundary conditions, did function to retain most of the sample long enough so that crystalline lattice "impregnation" conditions could be achieved before prohibitive loss, via evaporation, had occurred. For highest sensitivity, the encapsulation or covering thickness should be kept to minimum values to reduce diffusion times and maintain most of the sample close to the ionizing surface. At the same time, the cover thickness should be great enough to allow a thorough cleaning of its surface to take place before

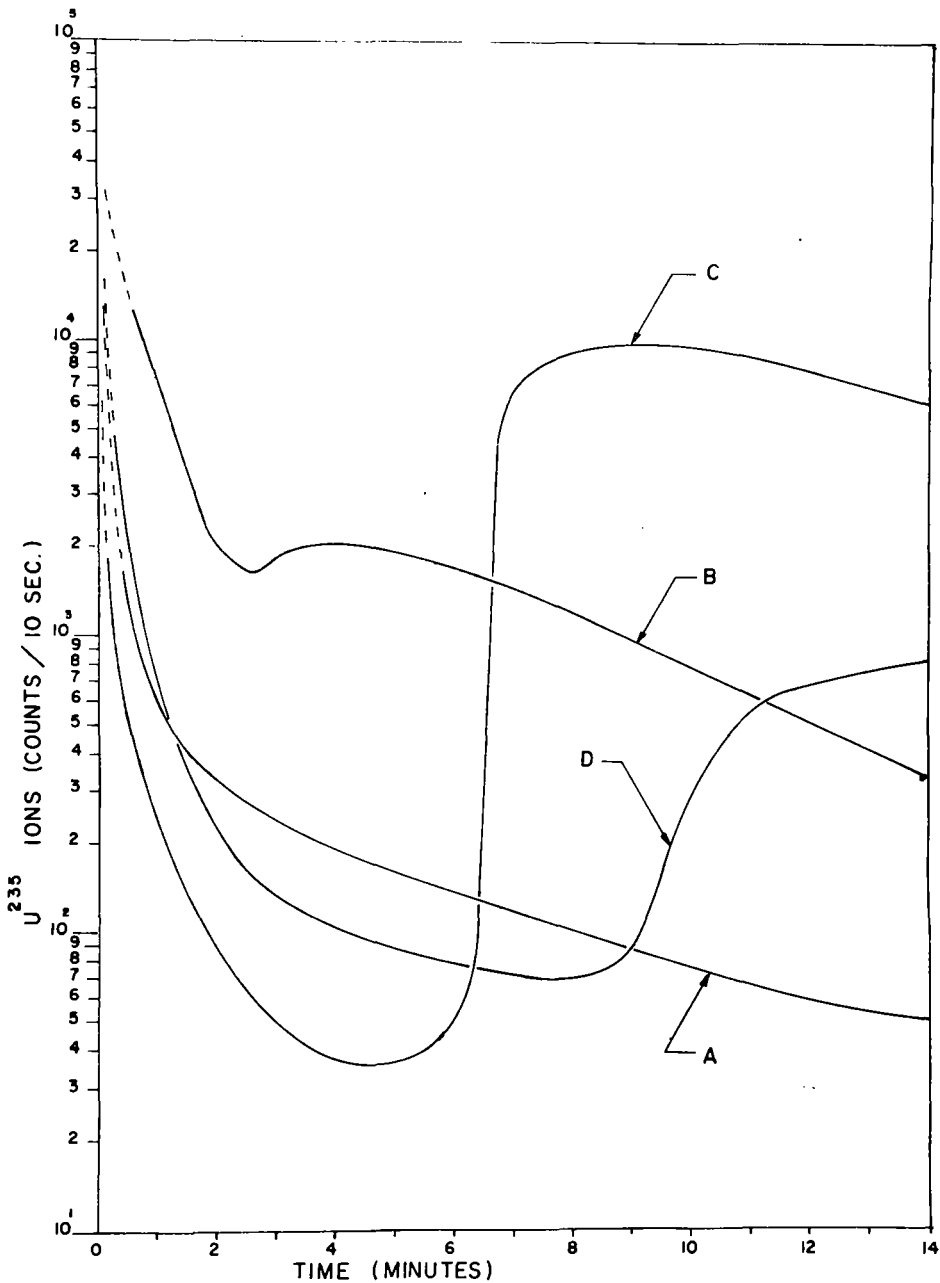


Figure 1. Ion Emission Rates of Uranium Samples ($\sim 3 \times 10^{-8}$ g) Having Different Rhenium Vapor Deposited "Cladding" Thicknesses.

the appearance of the sample atoms. This cleaning of the surface ensures the maintenance of a high and constant work function; essential for high ionization efficiencies. For uranium diffusion in rhenium, this thickness should be a maximum of 0.0005" when operating in the temperature range of 3500 to 3900°F. When analyzing lighter elements, their faster diffusion rates will allow the use of considerably thicker coverings.

Reference

- (1) Schwegler, E. C., Jr. and White, F. A., International J. Mass Spectr. & Ion Physics, 1, 191, (1968).

The Observation of UH^+ and PuH^+ Produced During the Thermal Ionization
of Uranium and Plutonium*

P. E. Moreland, Jr., D. J. Rokop, and C. M. Stevens

Argonne National Laboratory, Argonne, Illinois 60439

Following an initial observation of PuH^+/Pu^+ ion concentrations of about 3 ppm during analysis of ^{239}Pu having ppb concentrations of ^{240}Pu , brief studies have been made of the UH^+ , UD^+ , PuH^+ , and PuD^+ ions produced in a triple-filament thermal ionization source when H_2 , D_2 , H_2O , or D_2O is admitted to the source chamber, at ion gauge pressures up to 10 μTorr . A tandem magnetic sector mass spectrometer with a retarding potential energy filter¹ at the detector was used.

For H_2 and D_2 , the hydride ion yield, relative to the metal ion, appears to increase as the 1.1 power of gas pressure. Since ion gauge linearity was not calibrated, this slight deviation from linear pressure dependence may be instrumental. At the same indicated source pressure, the UD^+ ion yield is 4 times the PuD^+ yield, and UH^+ has 60% greater yield than UD^+ , including any mass discrimination effects for these ions at the electron multiplier detector. The hydride ion yields, at constant gas pressure, are independent of ionizing surface material (Re, W, and Ta were used) and surface temperature over the range 2200–2500°K. Variation of the electric field gradient near the ionizing surface does affect the hydride yield. These effects indicate that gas-phase ion-molecule reactions of the form $\text{U}^+ + \text{H}_2 \rightarrow \text{UH}^+ + \text{H} + \Delta E$, rather than surface phenomena, are the source of the observed hydrides.

In each case, the hydride and deuteride ions have a distribution of kinetic energies somewhat lower than that of the metal ions. Both retarding-potential energy analysis and a de-convolution analysis of the UH^+ and UD^+ ion peak shape versus the shape of the U^+ ion peak indicate that this energy distribution is roughly Maxwellian. For hydride ions produced in H_2 or D_2 , the distribution has a threshold about 1.5 eV below the metal ion energy, a maximum 1.1 eV below this, and a tail of still lower energy ions extending some 13 eV below threshold. These results seem consistent with an endothermic ion-molecule reaction process.

The 1.5 eV energy difference between metal ions and the most energetic hydride ions allows the latter to be very effectively discriminated against with the retarding potential analyzer. In this way we have successfully determined ^{240}Pu concentrations of 24 ± 5 ppb in ^{239}Pu , despite a large background of ^{239}PuH ions.

A complete report of this work is being submitted to the International Journal of Mass Spectrometry and Ion Physics.

* Work performed under the auspices of the U. S. Atomic Energy Commission.

¹ Kurt A. Kaiser and Charles M. Stevens, Argonne National Laboratory Report ANL-7393, "Ion-Retarding Lens to Improve the Abundance Sensitivity of Tandem Mass Spectrometers."

FIELD-IONIZATION MASS SPECTROMETRY - FRAGMENTATION AND METASTABLES*

Contribution No. 1584, Central Research Department
E. I. du Pont de Nemours and Company, Wilmington, Delaware 19898

E. M. Chait

Field-ionization (FI) mass spectrometry is an established method for obtaining abundant molecular ions of a variety of compounds, and has recently been used in conjunction with exact mass measurements.¹ Very little, however, has been reported on the value of the normal fragment ions and metastable ions appearing in the field ion spectrum as a source of structural information. We report here the observation of normal ion peaks in the FI mass spectrum corresponding to the mass spectral rearrangements commonly observed in electron impact spectra for several compounds. Such rearrangements are unexpected from previous literature reports that rapid acceleration of molecular ions in FI prevented the observation of relatively slow rearrangement processes as normal ions.^{2,3} Experiments show that these rearrangements are at least in part a surface phenomenon on the FI anode as observed for the rearrangement loss of ethylene in the FI spectrum of n-butyrophenone.^{4,5} Metastables accompanying these reactions were examined using the defocusing technique in the double focusing mass spectrometer.⁶

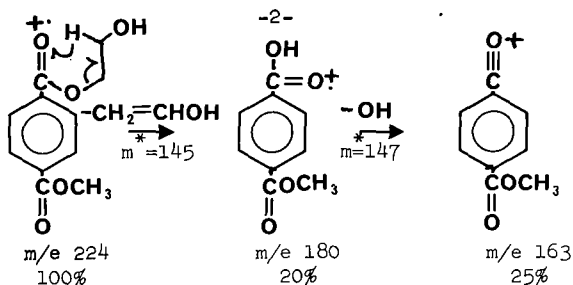
Experimental

Spectra were obtained using the dual FI/EI source designed and constructed for the CEC21-110B high-resolution mass spectrometer and described previously.^{1,4} Commercially available chromium-plated razor blades were used as FI anodes. With these blades, no conditioning procedure was required to reach full sensitivity as with other types of anode materials. Defocusing of normal ions to observe metastables was accomplished by variation of electrostatic sector potential⁷ so that the magnitude of the ionization field would not be disturbed.

Observation of Rearrangements and Multistep Processes in FI Spectra

Mass spectral rearrangements have been observed as normal ions in field ion spectra. Most common among these are the McLafferty rearrangements of 2-alkanones to give ions at m/e 58, the consecutive hydrogen rearrangements in 4-octanone to give ions at m/e 86 and 58, and the double rearrangement in sec-butyl acetate to give an ion at m/e 61. Other rearrangements are observed as part of multistep decomposition processes. Note that although such multistep processes are

* A full account of this research will be submitted for publication in the Journal of Mass Spectrometry and Ion Physics.

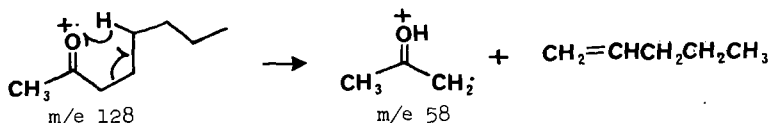


relatively slow mass spectral reactions with low frequency factors,⁸ they are still observed as abundant normal ions as well as metastables in the FI mass spectrum.

Origins of FI Rearrangement Ions

Observation of rearrangements as abundant normal ions leads to the conclusion that these reactions must occur primarily in the ion source. They cannot occur exclusively in the gas phase or they would be observed as metastable ions.^{2,3}

The conclusion that these rearrangements occur in part on the surface of the anode is supported by the effect of increasing temperature on the abundance of the m/e 58 ion in the spectrum of 2-octanone. As the temperature of the anode is increased from 80 to 250°C, the abundance (relative to the molecular ion at m/e 128) drops from 8 to 4%. This may be interpreted as the evaporation of the condensed phase from the surface of the anode. It is apparent that hydrogen transfer to the carbonyl oxygen occurs in this condensed phase prior to field-dissociation loss of olefin from the molecular ion.^{4,5}



The component of the rearrangement reaction occurring in the gas phase is observed both as a low mass tail on the m/e 58 peak corresponding to the "fast metastables" (10^{-11} sec) described by Beckey⁵ and as a typical metastable transition at m/e 26.3. The m/e 58 ion from 4-octanone formed by a consecutive rearrangement process does not show the temperature effect of the surface reaction and is of lower abundance. This reaction occurs exclusively in the gas phase and is too slow to give an abundant normal ion in the FI mass spectrum.

Use of FI Fragmentation and Metastables for Organic Structure Determination

The rearrangement ions in field ion spectra are a source of additional structural information. Metastable ions observed in FI spectra are valuable for identifying isomers. In the case of the isomers, camphor and trans-8-methylhydrindanone, which give identical electron impact spectra, the abundances of FI metastables for the processes $M-CH_3$, $M-OH$, $M-C_2H_4$, and $M-CH_2C=O$ may be used to distinguish the compounds.³

1. E. M. Chait, T. W. Shannon, J. W. Amy, and F. W. McLafferty, Anal. Chem., 40, 835 (1968).
2. H. D. Beckey, J. Mass Spectrometry Ion Phys., 1, 93 (1968).
3. H. D. Beckey and H. Hey, Org. Mass Spectrometry, 1, 47 (1968).
4. E. M. Chait, T. W. Shannon, W. O. Perry, G. E. Van Lear, and McLafferty, J. Mass Spectrometry Ion Phys., 2, 141 (1969).
5. H. D. Beckey, H. Hey, K. Levsen and G. Tenschert, ibid, 2, 101 (1969).
6. M. Barber and R. M. Elliott, ASTM E-14 Conference on Mass Spectrometry, Montreal, Canada, May, 1964.
7. M. L. Gross, R. B. Fairweather, W. F. Haddon and F. W. McLafferty, ASTM E-14 Conference on Mass Spectrometry, Pittsburgh, Pa., 1968.
8. W. A. Chupka, J. Chem. Phys., 30, 191 (1959).

dew
5/23/69

Electron Microscopic Study of the Surfaces of Wires
Used in Field Ionization Mass Spectrometry*

James C. Tou and L. B. Westover
Chemical Physics Research Laboratory

E. J. Sutton
Microscopy Laboratory

The Dow Chemical Company
Midland, Michigan 48640

Introduction

After years of development^{1,2}, field ionization mass spectrometry, a complement to electron impact mass spectrometry, has now become available to laboratories as a routine analytical tool for the elucidation of organic molecular structure. Wollaston wires^{1,2}, sharp metal tips¹, razor blades^{3,4} and metal foils⁵ have been used in field ionization mass spectrometry for generating the necessary high electric fields (on the order of $1\text{V}/\text{\AA}$). Their surfaces^{4,6} have been studied using transmission electron microscopes in an attempt to understand the role of the surfaces in the field ionization process. However, few surface details have been reported. In this paper, two Wollaston wires, used in a MAT CH4 mass spectrometer and with different sensitivities, have been studied using a Cambridge scanning electron microscope and a Cameca electron microprobe.

Experimental

The two wires studied had a field ionization sensitivity ratio of about 70 as shown in Figure 1. The sensitivities of the wires were measured as multiplier output voltage produced by the acetone molecular ion, $m/e = 58$, with 9 KV applied between the wire and its counter electrode. The ion source pressure was adjusted to 2×10^{-6} torr, which was also the pressure used in conditioning the wires. The wire having higher sensitivity is designated as Wire C in the text and that having lower sensitivity as Wire B. The average sensitivity of the conditioned wires used so far has been found between 5 and 40 volts. Wire C had a preconditioned sensitivity of about 16 volts as contrasted to 10-20 millivolts for an average wire. Both wires had been exposed to organic molecules containing C, H, N, O, halogens, As and S in the mass spectrometer before the investigation was initiated. However, field ionization analysis had been performed on only one sample containing S using Wire C and on no samples containing S using Wire B.

Figure 2 shows the mountings, H_1 and H_2 , used to support the wire and the wire holder for the studies with the scanning electron microscope and the electron microprobe spectrometer respectively. In the case of the electron microprobe analysis, the wire was suspended above a hole drilled in the center of the mounting, H_2 . The bottom of the hole was lined with graphite to avoid any back scattering of X-rays.

In the Cambridge scanning electron microscope used in this study, the energy of the bombarding electrons was maintained at 15 KV and the pressure of the spectrometer at about $10^{-6} - 10^{-7}$ torr. The electron probe microanalysis of the wire surfaces was done using a Cameca/CEC electron microprobe spectrometer. The samples were bombarded by 15 KV electrons and the X-rays emitted were analyzed. A liquid-nitrogen cold plate was used just a few centimeters above the samples to avoid the deposition of C on the wire surface during electron impact. For the purpose of quantitative comparison, the specimen current was adjusted to 100 na at maximum X-ray emission. Because of the round shape of wires, it was impossible to obtain a quantitative determination of elements present⁸. The results obtained can only be treated as a semiquantitative comparison of a particular element between the two wires studied. The electron beam, $1\mu \times 25\mu$, was scanned over the wire in order to get an average element distribution. Vibration of the wire was observed when the electron beam bombarded an area located 90μ or greater away from the end of the wire. The experiment was carried out on an area, $60\mu - 90\mu$ from the end where no

*Submitted to the Journal of Mass Spectrometry and Ion Physics for publication.

vibration occurred. The X-rays emitted were diffracted by different crystals and their intensities were recorded either with a Polaroid Land Camera or as counts per second with a gas fluid proportional counter containing 90% Ar and 10% CH₄. A search was made for the possible elements with atomic number larger than 5 on the surface of Wire B. However, no effort was made to detect the presence of elements on the surface of Wire C, other than those observed on Wire B.

Results and Discussion

Figure 3 shows the general features of the wire surface near the center of Wire C. The magnification is 4,750X. Several interesting phenomena can be seen from the picture: 1) Whiskers grow on the wire, 2) Whiskers appear to be longer and denser on the side toward the wire holder than on the side toward the counter electrode containing the ion exit slit, 3) Ridges are observed on the surface of the wire, 4) Small amounts of deposits are seen on the surface. These observations can be seen more clearly on Figures 4-6 where higher magnification was used. Figure 4 shows the upper portion as shown in Figure 3, but with magnification of 19,000X. Similarly, Figure 5 shows the lower portion of the section of the wire shown in Figure 3. Comparing Figures 3 and 4, it is obvious that the whiskers appear longer and denser on the side toward the wire holder. One of the possible explanations might be as follows. The ion draw out rate would be faster at the side facing the slit than the side facing the holder, because the ions must travel around the wire. Hence, the partial pressure of the ions must be higher on the side of the wire away from the slit and so the partial pressure of the neutral molecules must be lower if the total pressure remains the same. The gaseous neutral molecules at high temperature (200°C) and high electric field might interact strongly with the whiskers removing some materials from the whiskers. In this case, the materials would be removed faster from the side facing the slit because, from the above argument, there are more neutral molecules present on this side of the wire. The possible explanation is consistent with the earlier report of Beckey⁵ that the whiskers were found to be shorter after a sample had been run and is also supported by the fact that the sensitivity of the wires were observed to have decreased after a sample had been run. More interesting is the growth of whiskers along the wire ridges. This is shown in Figure 6 with a magnification of 47,500. This phenomena might not be too surprising considering the higher catalytic activity and the higher field strength at the ridges than on the flat portion of the surface. Figure 7 shows the end portion of the wire. It is obvious that there are not as many whiskers as observed on the center portion of the wire. Figure 8 shows the bending portion of the wire, which is approximately the area investigated by electron microprobe spectrometry. The general features of this area are about the same as those near the center of the wire. Figures 9-12 show the surface features near the center portion of Wire B before and after conditioning with acetone. Deposits of various sizes on the wire surface are clearly demonstrated in Figures 9 and 10. The deposits tend to cover the wire surface more evenly after the wire was conditioned, as shown in Figures 11-12. Generally speaking, few whiskers were found on such a coated surface, which is in contrast to what was observed for Wire C, a wire with much higher sensitivity.

Figure 13 shows the X-ray pictures of pt-M_{L1} and S-K_{α1} emitted from Wire B and Wire C. It is obvious that the intensity of the S-K_{α1} signal from Wire B is much stronger than that from Wire C. All the elements with atomic number larger than 5 detected by electron microprobe spectrometry on Wire B and Wire C, after conditioning, are summarized in Table I. The significant differences between the two wires are the contents of C and S. Wire B contained more C and S than Wire C. This is consistent with the observation from the scanning microscopy than Wire B has more deposits than Wire C. However, the compounds themselves were not specifically identified.

Conclusion

From our study of the two wires with quite different sensitivities, the following points might be concluded:

- 1) The sensitivity of the wire depends upon not only the cleanness of the wire surface but also on the population of whiskers.
- 2) The deposits on the wire tend to prevent the growth of the whiskers.
- 3) A deposit appeared to cover the surface of Wire B after conditioning

as contrasted to the observed agglomerates before conditioning.

- 4) Pure platinum metal induced field ionization can be seen at the beginning of the sensitivity curve of the wire, where whiskers might not be present.
- 5) The whiskers tend to appear in greater density and to be longer on the side of the wire facing the holder rather than on the side facing the counter electrode consisting of the ion exit slit.
- 6) The whiskers tend to grow along the ridges on the wire, probably because the ridges have higher catalytic activity and higher field strength than the flat part of the wire.

Acknowledgment

The authors would like to express their sincere appreciation to Dr. D. R. Beaman, Mr. T. M. Hess and Mr. L. Solosky for their helpful discussions and assistance.

References

1. H. D. Beckey, H. Knöppel, G. Metzinger and P. Schulze, *Advances in Mass Spectrometry* (The Institute of Petroleum, London, 1966), Vol. 3, p. 35.
2. G. G. Wanless and G. A. Glock, Jr., *Anal. Chem.* 39, 2 (1967).
3. E. M. Chart, T. W. Shannon, J. W. Amy and F. W. McLafferty, *Anal. Chem.* 40, 835 (1968).
4. P. A. Blenkinsop, B. E. Job, D. F. Brailsford, C. M. Cross and A. J. B. Robertson, *J. Mass Spectry. and Ion Phys.*, 1, 421 (1968).
5. H. D. Beckey, reported on Sixteenth Annual Conference on Mass Spectrometry and Allied Topics, 1968, Pittsburgh, Pennsylvania.
- 6a. L. S. Birks, "Electron Probe Microanalysis", Interscience Publishers, 1963.
- 6b. Private communication with Dr. D. R. Beaman, Metallurgical Laboratory, The Dow Chemical Company, Midland, Michigan.

Table 1: Intensities of X-rays Emitted by Elements Detected in Wire C and Wire B

Elements	Diffraction Crystals	X-rays	Wire C I X-ray (cps)	Wire B I X-ray (cps)
Pt	KAP	M α_1	1104	1268
S	PET	K α_1	2	61
C	LSD	K α	22	238
Si	KAP	K α	10	7
Ag	PET	L α_1	10	20
O	LSD	K α	7	23
K	PET	K α	6	5

Captions for Figures

- Figure 1: Sensitivities of Wire B and Wire C.
- Figure 2: Wire mounting used in the scanning electron microscope (H_1) and the electron microprobe spectrometer (H_2).
- Figure 3: General surface features near the center of Wire C (4,750X).
- Figure 4: Surface facing the counter electrode of Wire C (19,000X).
- Figure 5: Surface facing the wire holder of Wire C (19,000X).
- Figure 6: Detail of whiskers on the surface of Wire C (47,500X).
- Figure 7: End portion of Wire C (1,900X).
- Figure 8: Bending portion of Wire C (19,000X).
- Figure 9: Surface detail of the central portion of Wire B before conditioning showing crystal-like deposit (11,000X).
- Figure 10: Surface detail of the central portion of Wire B before conditioning showing large deposit (11,000X).
- Figure 11 and 12: Surface detail of two areas near the central portion of Wire B after conditioning (11,000X).
- Figure 13: X-ray pictures of Pt-M α_1 (.5 min. exposure) and S-K α_1 (5 min. exposure) emitted from Wire B and Wire C.

Figure 1

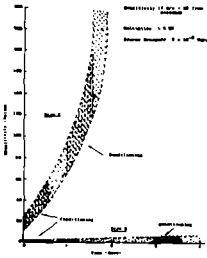


Figure 2

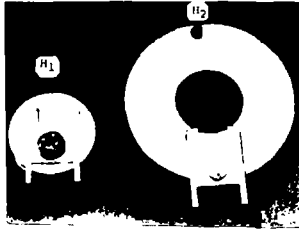


Figure 3

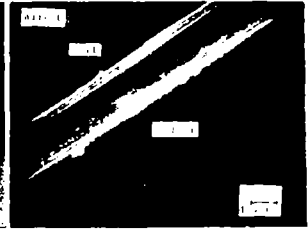


Figure 4

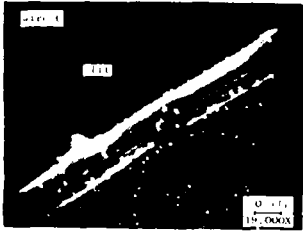


Figure 5



Figure 6



Figure 7

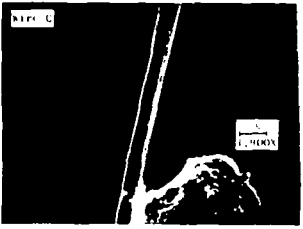


Figure 8



Figure 9

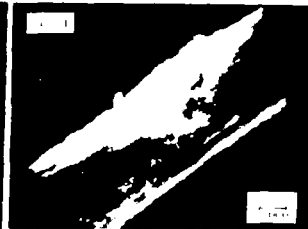


Figure 10



Figure 11

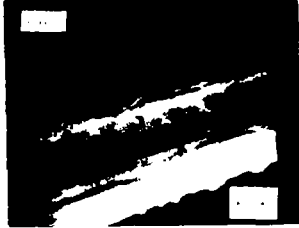


Figure 12

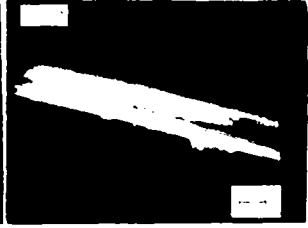


Figure 13



Author Index

Name	Paper No.	Name	Paper No.
Aaronson, M. J.	140	Evans, S.	114
Arnold, W.	78	Fales, H. M.	93
Arsenault, G. P.	129	Fehlner, T. P.	56
Arshadi, M.	149	Fehsenfeld, F. C.	41, 134
Aspinal, M. L.	52	Fenn, J. B.	53
Bailey, C. A.	6	Ferguson, L. A.	87
Baker, C. W.	83	Ferguson, E. E.	134
Baldwin, M. A.	142	Field, F. H.	128
Ban, V. S.	22	Fitzpatrick, J. D.	163
Beauchamp, J. L.	148	Flesch, G. D.	96
Beachey, J.	59, 60	Folk, T. L.	165
Benz, W.	158	Foltz, R. L.	119
Berkey, E.	25	Foster, N. G.	144, 162
Berkowitz, J.	89, 92	Fowler, R. G.	144
Berry, R. S.	38	Franklin, J. L.	68, 152, 153
Biemann, K.	43	Freedman, C. M.	51
Bingham, R. A.	86	Friedel, R. A.	112
Bir, R.	81	Friedman, H. L.	74
Blue, G. D.	64, 98	Frisch, M. A.	11
Boettger, H. G.	115, 116	Frost, D. C.	90
Bohme, D. K.	134	Futrell, J. H.	27, 135
Botnick, E. M.	12		155
Bowers, M. T.	133	Gallegos, E. J.	120
Branton, G. R.	90	Garcia, N.	138
Bridges, J. C.	8	Gelpi, E.	125
Brion, C. E.	61	Giessner, B. G.	62, 143
Brown, C. L.	47	Gilland, J. C., Jr.	50
Brown, P.	169	Gingerich, K. A.	64, 98
Brubaker, W. M.	79	Glow, R. P.	135
Brunnee, C.	46, 110	Good, A.	150
Bultemann, H. J.	46	Goodlett, V. W.	50
Burke, R. R.	54	Goshgarian, B. B.	49
Burlingame, A. L.	15, 167, 168	Gradsztajn, E.	109
Cazee, C.	164	Green, M. M.	137
Cermak, V.	37	Greene, F. T.	58, 59
Chait, E. M.	176		60
Chalmers, A. M.	113	Grigsby, R. D.	161
Chamberlin, W. D.	79	Grotch, S. L.	171
Chupka, W. A.	89	Guidoboni, R. J.	86
Clampitt, R.	32	Gunduz, D. H.	65
Cook, R. J.	137	Gupta, S. K.	103
Cooks, R. G.	160	Haddon, W. F.	76
Coutant, J. E.	16	Hanley, M. A.	152
Craig, D. P.	142	Hanna, G. C.	173
Crawford, C. K.	5	Harrison, A. G.	147
Dale, F.	69, 151	Harrison, B. H.	51
Damoth, D. C.	44	Heckendorn, R. H.	47
Davis, D.	57	Heymann, P.	106
Deines, P.	126	Herman, Z.	131
DeJongh, D. C.	118	Herod, A. A.	147
Delmore, J. E., Jr.	24	Herron, J. T.	57
Denholm, A. S.	18	Herzog, L. F.	104
Dibeler, V. H.	94, 95	Higgins, R. W.	144, 162
DiEdwardo, A. H.	76, 77	Hildenbrand, D. L.	99, 100
Dillon, J. P.	140	Hills, L. P.	27
Dollimore, J.	51	Hinds, S.	161
Doolittle, P. H.	91	Hites, R. A.	166
Dougherty, R. C.	138	Hoffman, J. H.	108
Dowdy, I. D.	87	Hribar, J. D.	118
Dowell, J. T.	3	Habfast, K.	110
Dunn, G. H.	4	Huffman, R. E.	88
Dupzyk, R. J.	6	Hughes, B. M.	70, 71
Durden, A.	150	Hute, R. E.	57
Durham, R. W.	173	Huntress, W. T., Jr.	132
Dzidic, I.	149	Itagaki, Y.	111
Ehlert, T. C.	97	Jackson, J. M.	172
Elleman, D. C.	132, 133	Jennings, K. R.	35
EskeIson, C. D.	164	Jones, S.	35
Evans, C. A.	85		

Author Index

Name	Paper No.	Name	Paper No.
Judson, C. M.	19	Morrison, G. H.	25, 105
Kappus, G.	46	Morrison, J. D.	17
Kashuba, A. T.	105	Mosharrafa, M.	80
Katayama, D. H.	88	Muenow, D. W.	72
Kebarle, P.	149, 150	Munson, B.	130
Kelly, A. M.	115, 116	Murad, E.	99
Kelly, W.	136	Naito, M.	111
Kemp, T. R.	114	Neiswender, D. D.	55
		Newton, A. S.	30
Kessler, T.	112	Nief, G.	81
Kieffer, L. J.	1	Norman, J. H.	66
Kinneber, K.	161	Nounou, P.	28
Kilmowski, R. J.	16	O'Bryan, C. L.	88
Kinneberg, K.	14	Occolowitz, J. L.	33
Knock, D.	136	Olsen, L. A. R.	61
Knox, B. E.	22	Olsen, R. W.	15
Kohout, F. C.	55	Olson, P. D.	9
Krueger, P. M.	45	Oro, J.	125
Kubicek, W. G.	80	Osheim, D. L.	13
Lampe, F. W.	40	Ottinger, Ch.	29
Langer, H. G.	73	Park, J. Y.	143
Leger, L. J.	157	Parker, P. L.	124
Lengyel, M. J.	140	Patterson, R.	80
Levenberg, M. I.	119	Paulson, J. F.	69, 151
Lewis, J. S.	50	Peterson, J. R.	39
Lewis, R. K.	19	Peterson, R. L.	6
Li, H-Y.	14	Pierron, E. D.	87
Liao, J. Pei-min	162	Ping-Kay Hon	84
Liepziger, F. D.	85	Pinson, W. H.	121
Lincoln, K. A.	21	Powers, P.	86
Linnarson, A.	42	Rapp, D. R.	2
Lipsky, S. R.	10	Redfern, J. P.	52
Livingston, L. H.	65	Reed, R. I.	139
Lohle, U.	29	Reinhold, V. N.	43
Lounsbury, M.	173	Reynolds, W. E.	8
Lucas, M.	81	Richter, W. J.	168
Luchte, A. J.	44	Ridley, R. G.	136
Maccoll, A.	142	Rinehart, K. L.	47
Major, H. W., Jr.	36	Ritcher, W. J.	167
Makita, T.	90	Robertson, D. H.	139
Mappes, G. W.	56	Rokop, D. J.	175
Marcotte, R. E.	156	Rosenstock, H. M.	170
Margrave, J. L.	72	Rovner, L. H.	66
Masumoto, E. M.	83	Russell, M. E.	89
Maurer, K. H.	110	Ruth, J. M.	13
McAdams, D. R.	7	Saalfeld, F. E.	67
McAdoo, D. J.	31	Saunders, R.	14
McCloskey, J. A.	45	Scalan, R. S.	127
McCrea, J. M.	23	Schaeffer, O. A.	122
McCulloh, K. E.	94	Scheppele, S. E.	161
McDowell, C. A.	90	Schildcrout, S. M.	153
McDowell, M. V.	67	Schilling, K. J.	47
McLafferty, F. W.	16, 31	Schoen, R.	91
McMurray, W. J.	10	Schoengold, D.	130
Meisels, G. G.	62, 143	Schroeder, J. M.	26, 65
	154, 157	Schuddemage, H. D. R.	31
Melton, C. E.	63	Schulze, P.	168
Meyer, R. T.	101	Sciamanna, A. F.	30
Meyers, W. G.	174	Scott, W. M.	163, 164
Meyerson, S.	141	Searles, S. K.	149
Michnowicz, J.	130	Serum, J. W.	159
Miller, W. J.	54	Shannon, T. W.	34
Mills, L.	14	Shapiro, R. H.	159
Milne, G. W. A.	93	Sharkey, A. G.	112
Milne, T. A.	58, 59, 60	Shino, M.	111
Mitscher, L. A.	119	Shrader, S. R.	113
Moorman, C. J.	44	Shultz, J. L.	112
Moreland, P. E.	175	Siemens, P. D.	6
Morgan, T. D.	127	Simpson, D.	14

Author Index

Name	Paper No.	Name	Paper No.
Smith, D. H.	15		
Smith, J. S.	31		
Smith, R. F.	172		
Smyth, K. C.	34		
Socha, A. J.	83		
Stapleton, W. G.	48		
Steelink, C.	163		
Stenhouse, I.	90		
Stevens, C. M.	175		
Stillman, R. A.	8		
Struck, A. H.	36		
Studniarz, S. A.	151		
Sutton, E. J.	177		
Svec, H. J.	96		
Tesarek, J. N.	167		
Thomas, C. E.	61		
Tibbals, H. F.	154		
Tiernan, T. O.	70, 71, 156		
	157		
	177		
Tou, J. L.	164		
Towne, J. C.	52		
Treherne, B. L.	8		
Tucker, R. B.	131		
Tully, J. C.	58		
Vandegrift, A. E.	134		
Vane, R. A.	75		
Vaughan, H. P.	15		
Venkataraman, R.	93		
Vestal, M.	163, 164		
Wacks, M. E.	27		
Wahrhaftig, A. L.	14		
Walden, J.	94, 95		
Walker, J. A.	14		
Waller, G. R.	15		
Walls, F. C.	13		
Wasserburg, G. J.	123		
Watanabe, E.	111		
Weikamp, A. W.	141		
Westover, L. B.	177		
Whitaker, D.	161		
White, F. A.	174		
Williams, C. H.	102		
Williams, D. H.	160		
Witsoe, D.	80		
Wojcik, L.	155		
Wolfgang, R.	131		
Wolstenholme, W. A.	52, 86,		
	114		
Woodley, F. A.	21		
Woolston, J. R.	12		
Wright, D.	136		
Yamadagni, R.	149		
Yeo, A. N. H.	160		
Yergey, A. L.	68		
Zahringer, J.	107		
Zitomer, F.	76, 77		
Zschau, E. V. W.	9		

QIP 235
243

Spore
rtact p 251

A.S.T.M. Publications on Mass Spectrometry*

A. Recommended Practices and Methods of Test**

Title and Citations in 1968 Book of ASTM Standards

Designation

D1137-53	Analysis of Natural Gases and Related Types of Gaseous Mixtures by the Mass Spectrometer, Part 19, pp. 213-223.
D1302-61T	Analysis of Carburetted Water Gas by the Mass Spectrometer, Part 19, pp. 288-294.
D1658-63	Carbon Number Distribution of Aromatic Compounds in Naphthas by Mass Spectrometry, Part 17, pp. 599-602.
D2424-67	Hydrocarbon Types in Propylene Polymer by Mass Spectrometry Part 18, pp. 574-582.
D2425-67	Hydrocarbon Types in Middle Distillates by Mass Spectrometry, Part 17, pp. 875-884.
D2498-66T	Isomer Distribution of Straight-Chain Detergent Alkylate by Mass Spectrometry, Part 18, pp. 622-627.
D2567-66T	Molecular Distribution Analysis of Monoalkylbenzenes by Mass Spectrometry, Part 18, pp. 751-753.
D2601-67T	Low-Voltage Mass Spectrometric Analysis of Propylene Tetramer, Part 18, pp. 779-782.
D2650-67T	Chemical Composition of Gases by Mass Spectrometry, Part 18, pp. 796-804.
E137-65	Evaluation of Mass Spectrometers for Use in Chemical Analysis, Part 30, pp. 339-342.
E244-64T	Atom Percent Fission in Uranium Fuel, Mass Spectrometric Method, Part 30, pp. 767-772.
E304-66T	Use and Evaluation of Mass Spectrometers for Mass Spectro-chemical Analysis of Solids, Part 30, pp. 1003-1009.

Title and Citation in Other ASTM Publications

Proposed	Hydrocarbon Types in Olefinic Gasoline by Mass Spectrometry ASTM Standards on Petroleum Product and Lubricants, App. VIII, Vol. I, p. 1128 (October, 1961). (Published as information only.)
Proposed	Hydrocarbon Types in Low Olefinic Gasoline by Mass Spectrometry: App. VII, Report of Committee D-2, 1961; republished for information.
Proposed	Carbon Number Distribution of Saturate and Aromatic Classes in Distillate Waxes by Mass Spectrometry: App. III, Report of Committee D-2, 1967; published for information.

B. Other ASTM Mass Spectrometric Information

DS27	Index of Mass Spectral Data, published Sept., 1964, 248 pages (Initially published as STP No. 356).
DS27-1a	Mass Spectral Data - Punched Card Index—3200 cards
DS27-1b	Mass Spectral Name Formula - Punched Card Index—3500 cards
STP No. 149	Chemical Analysis of Inorganic Solids by Means of Mass Spectrometer, published 1951.

* Prepared by Subcommittee VI, ASTM Committee E-14, June, 1968.

** Committee jurisdiction for the mass spectrometric practices and methods is as follows:

Committee D3 - D1137 and D1302
Committee E10 - E244
Committee E14 - E137 and E304
Committee D2 - all others listed.